NASA SP-59

.57

ff 653 July 65

MARINER-VENUS 1962
FINAL PROJECT REPORT

FACILITY FORM 602

N 66 14702 (ACCESSION NUMBER) (THRU)

380 (PAGES) 1 (CODE)

(NASA CR OR TMX OR AD NUMBER) 31 (CATEGORY)

NATIONAL AERONAUTICS AND SPACE ADMINISTRATION

MARINER-VENUS 1962
FINAL PROJECT REPORT

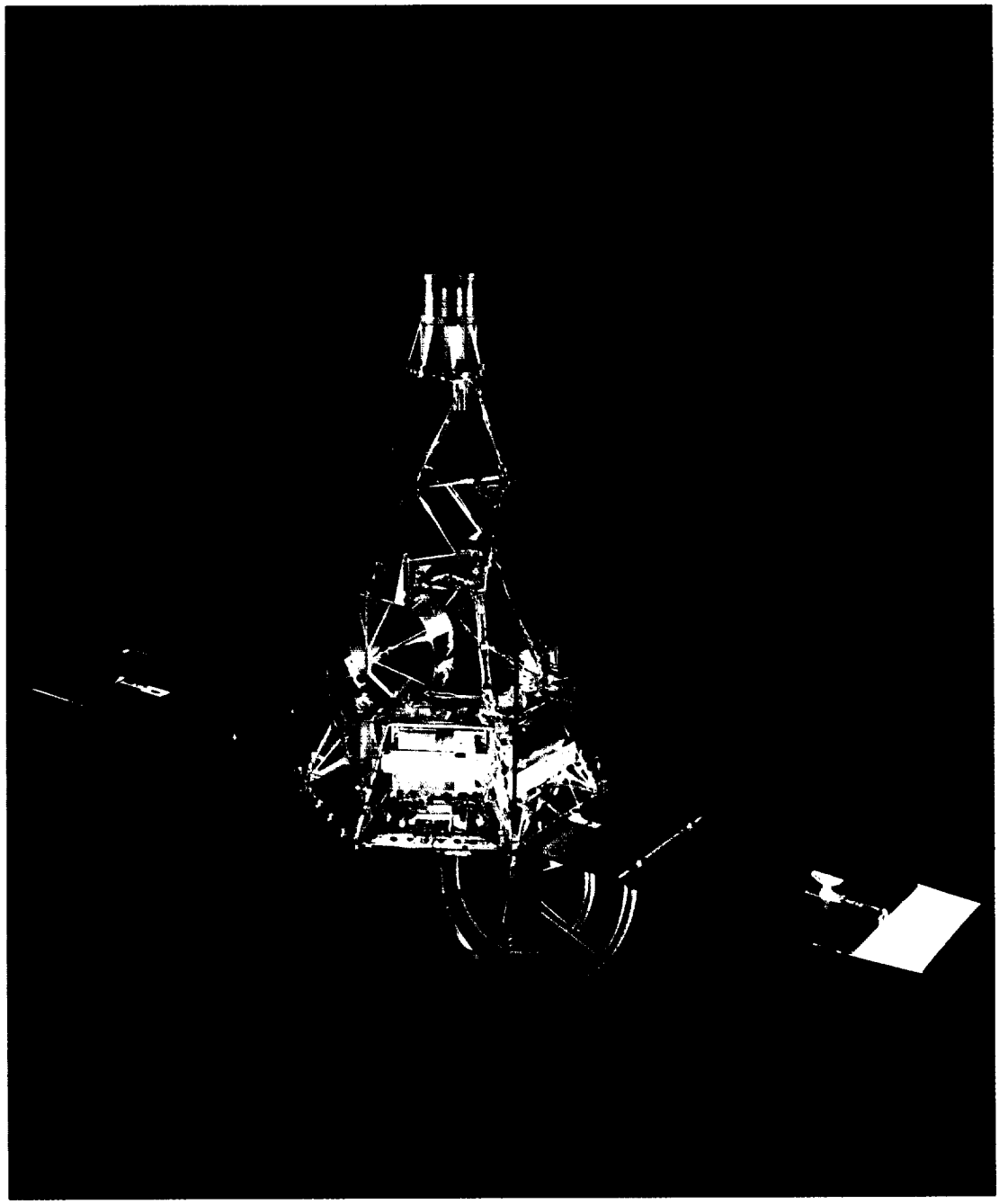

MARINER II

NASA SP-59

MARINER-VENUS 1962
FINAL PROJECT REPORT

Prepared under contract for NASA by
Jet Propulsion Laboratory
California Institute of Technology

Scientific and Technical Information Division 1965
NATIONAL AERONAUTICS AND SPACE ADMINISTRATION
Washington, D.C.

FOR SALE BY THE SUPERINTENDENT OF DOCUMENTS, U.S. GOVERNMENT PRINTING OFFICE
WASHINGTON, D.C. 20402 - PRICE $2.50

Foreword

The flight of Mariner II to the planet Venus represents the first time that man has sent his instruments close to another planet and received meaningful data from them back on Earth. The following pages describe the Mariner R project and its problems, solutions, difficulties, and successes. Perhaps a part of the drama and some of the tensions associated with this kind of mission will be felt and understood.

From the successful launching of Mariner until its arrival at the planet 109 days later, the spacecraft was under continuous observation as it transmitted data back to Earth. In the control room in Pasadena, men who designed and built the instruments hovered over its readings as anxiously as any parent. As the days grew into weeks and the distances into millions of miles, the tensions in the control room mounted steadily. Finally, the spacecraft flew past the planet and its instruments made the first closeup observation of Venus. Three weeks later, on January 3, 1963, with the spacecraft 9 million km (6 million miles) beyond Venus and 87 million km (54 million miles) from Earth, the signals stopped.

The journey of Mariner was a spectacular achievement of modern science and technology. It was made possible by the coordinated efforts of many people and many organizations. The National Aeronautics and Space Administration selected the Jet Propulsion Laboratory to manage the project. The spacecraft was designed and built by JPL with the assistance of numerous industrial subcontractors. The launch vehicle was the responsibility of the Marshall Space Flight Center of NASA and the launchings were conducted at the Atlantic Missile Range with the support of the United States Air Force. Tracking of the Mariner was assigned to the Deep Space Network, operated by the Jet Propulsion Laboratory. The scientific experiments were selected from proposals by scientists from many universities.

Several thousand men and women had a direct part in the Mariner R project. It would be impossible to list all of those who made some special contribution in their specific task, but every member of the project performed his job accurately, on time, and in a superior manner. The failure of any one of the many thousands of components would have invalidated the mission. Design, manufacture, and testing all demanded the very highest standards to achieve the necessary reliability.

While Mariner is the first interplanetary spacecraft and has opened a new era of planetary exploration, it is only a beginning. Soon there will be spacecraft flying by other planets, then orbiting the planets, and finally landing instruments on their surfaces. Exploring the solar system, becoming acquainted with the planets, answering questions about extraterrestrial life—these are the challenges that lie ahead.

W. H. PICKERING,
Director, Jet Propulsion Laboratory,
California Institute of Technology.

Contents

Introduction

Five lunar and planetary spacecraft were launched from Earth in 1962; of these, one mission can be considered an outstanding scientific and engineering success. This was the United States' Mariner II, which on December 14, 1962, made history by flying on a predetermined trajectory to an encounter point 34 833 km (21 645 miles) from planet Venus and 57 934 800 km (36 000 000 miles) from Earth and returning scientific data on both interplanetary space and the planet itself.

The Mariner R project was an unmanned deep-space program of the National Aeronautics and Space Administration (NASA), managed and carried out under contract (NAS7–100) by the Jet Propulsion Laboratory (JPL), California Institute of Technology. Marshall Space Flight Center (MSFC) at Huntsville, Ala., was responsible for launch vehicle procurement and for launch operations. JPL engineers and scientists planned and designed the spacecraft and scientific experiments (in collaboration with NASA and the scientific community), industrial contractors built many of the subassemblies of the spacecraft (see appendix B), and the United States Air Force supplied the launch vehicle.

This report describes the history-making flight of the Mariner II spacecraft to the vicinity of Venus. The chronology begins with the activation of the project as a means for meeting the 1962 Venus launch opportunities. Chapters include historical background on Venus, project organization and management, the space vehicle system, and the trajectory and orbit. Other chapters cover operational events describing the Mariner II mission, evaluation of the subsystems, the tracking network, the data-recovery and processing system, and findings of the scientific experiments.

Abbreviations used in this book are defined in appendix A.

CHAPTER 1

History of Knowledge About Planet Venus

Our solar system comprises one star (the Sun) and nine principal planets that move around the Sun in orbital paths which are elliptical. However, early man had different ideas; to him the Earth was the center of all things and the celestial bodies were divine. Indications are that five planets—Venus, Mercury, Mars, Jupiter, and Saturn—were known to man from nearly the beginning of recorded human history.

Venus appears to have intrigued man for at least 4000 years. The most ancient observations of the planet on record, dating back 2000 years before Christ, seem to come from Babylonia, and are recorded on the famous Venus tablets.

ANCIENT LEGENDS AND BELIEFS

The Egyptians, the Greeks, and the Chinese had thought of Venus as two stars because it was visible first in the morning and then in the evening sky. The Babylonians called Venus "Istar," the personification of woman and the mother of the gods. In Egypt the evening star was known as Ouaiti and the morning star Tioumoutiri; to the Chinese, Venus was known as Tai-pe, or the Beautiful White One. The Greeks called the morning star Phosphorus and the evening star Hesperos, but by 500 B.C. Pythagoras, the Greek philosopher, had realized that the two were identical. As time evolved the Romans changed the name of the planet to honor their own Goddess of Love, Venus.

It was not until the Golden Age of Greece that astronomy as a science was placed upon a firm foundation and the Earth and the planets were regarded as not flat but globes. Had Greek quantitative analysis taken one more step and dethroned the world from its position as the center of the universe, progress of human thought and logic would have been accelerated. The Greek philosopher and mathematician, Aristarchus, held a heliocentric view of the solar system but his ideas were opposed on religious grounds, and the later Greeks reverted to the idea of a central Earth.

Ptolemy, who died about 130 A.D., left a record of the state of the universe at the end of the classic Greek period. In his Ptolemaic system, the Earth lies in

the center of the universe, with the various heavenly bodies revolving around it in perfect circles. First comes the Moon, the closest body in the sky; then Mercury, Venus, and the Sun, followed by the three other planets then known (Mars, Jupiter, and Saturn), and finally the stars.

Finally, Copernicus in 1546 explained that the Sun is the center of the solar system and that the planets, like Earth, circle the Sun. Galileo was a strong supporter of the Sun-centered theory of the planetary system, and was the first to look at the heavens through a telescope and to prove the Earth was not the center of all orbits of heavenly bodies. Kepler, the German mathematician and astronomer, through his studies and the observations made by the Danish astronomer Tycho Brahe, was able to formulate the famous laws of planetary motion. The first of these laws states that the planets revolve around the Sun in elliptical paths with the Sun occupying one of the foci of the ellipse. Sir Isaac Newton's work on universal gravitation put the whole matter beyond doubt, and thenceforth the Ptolemaic and other Earth-centered systems were relegated to the past. In 1776, Venus was tracked across the face of the Sun, from which event the presence of an atmosphere about the planet was deduced because of the fuzzy edges of the image visible in the telescope. Throughout the 18th and 19th centuries, Venus continued to excite growing scientific curiosity in Europe and America.

By the year 1962, scientists had determined a number of facts about the apparent orbit of Venus but very little, if any, indisputable knowledge about the surface of the planet. Venus was apparently covered by clouds which even the most powerful telescopes could not penetrate. The clouds of Venus, as inferred from radioastronomical observations made from Earth, indicated to some scientists that the surface of Venus was probably very hot, possibly 600° K (620° F = 600° K) or more, while the temperature of the tops of the clouds was estimated by others at several hundred degrees, with a cool surface. The result was that no one knew for certain what the surface temperature of Venus might be.

STATISTICS

Venus, called by scientists the Earth's twin, approaches the Earth closer than any other celestial body except the Moon, some vagrant comets, and asteroids. The diameter of Venus is estimated at approximately 12 198 km (7580 miles), compared with Earth's 12 713 km (7900 miles). The amount of polar flattening of Venus is difficult to determine because of the permanent cloud mantle. In the case of the Earth, this flattening is appreciable, so that the polar diameter is

41.84 km (26 miles) shorter than the diameter as measured through the Equator. Venus' orbit is almost a perfect circle, with an eccentricity of only 0.0068, the lowest of all the planets. Venus rides this orbital path at a mean distance from the Sun of approximately 108 million km (67 million miles) compared to Earth's orbital path of approximately 149 million km (93 million miles). While Venus has a mean orbital speed of 125 808 km/hr (78 300 miles/hr), Earth's is 107 179 km/hr (66 600 miles/hr).

The mean density of Venus is slightly less than that of Earth—0.92, or 5.1 times that of an equal volume of water, as compared with 5.5 for Earth. The mass of Venus is 0.81 that of Earth and the volume is 0.88 that of Earth.

Venus appears particularly brilliant, not merely because of its size, but because of its closeness and high reflectivity. Venus has an albedo, or reflective factor, of 85% of the light from the Sun falling upon it, as compared with only 7% for the Moon. Venus receives about twice as much solar light and heat as Earth.

Since Venus is closer to the Sun than Earth and moves faster, it has a shorter yearly or annual orbital revolution period. The sidereal period is estimated at 224 days, 16 hours, and 48 minutes, according to Earth's calendar.

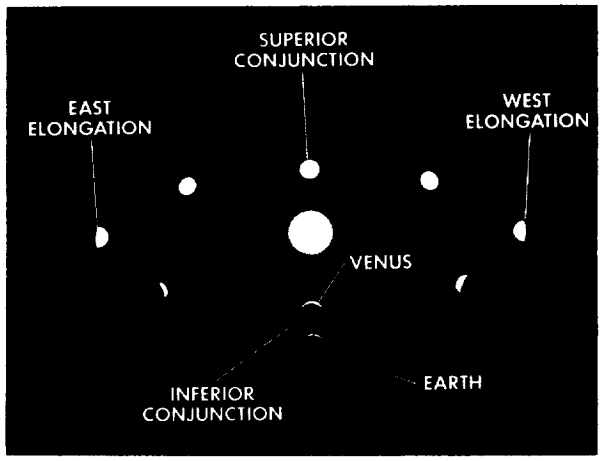

FIGURE 1-1.—Venus at inferior and superior conjunction.

Venus approaches within 40 million km (26 million miles) of Earth at inferior conjunction, when the planet is between Earth and the Sun, and is as far away as 260 million km (160 million miles) at superior conjunction, when Venus is on the opposite side of the Sun (fig. 1-1). When Venus reaches the two positions marked "elongation" in figure 1-1, it has reached its greatest angular distance from the Sun, approximately 47°. At eastern elongation, Venus is an evening star, at western elongation a morning star. The "synodic period" of Venus, the interval between successive inferior conjunctions, is about 584 days. Approximately 144 days elapse between evening and morning elongation, while 440 days are required for the planet to rotate around the Sun and return again to evening elongation.

788-025 O—65——2

FIGURE 1–2.—Visualized Venusian mountain peak.

The escape velocity (that velocity required to free an object from the gravitational pull of a planet) on Venus is 10.29 km/sec (6.4 miles/sec) compared with Earth's escape velocity of 11.26 km/sec (7 miles/sec). The gravity of Earth is sufficient to trap an oxygen-bearing atmosphere near the terrestrial surface. Because the escape velocity of Venus is about the same as that of Earth, men have long believed that planet might hold a similar atmosphere and, thus, be favorable to the existence of living organisms as known on Earth.

PRE-MARINER II THEORIES

Before Mariner II, Venus probably caused more controversy than any other planet in our solar system with the possible exception of Mars. Observers have visualized Venus as anything from a wet steaming abode of Mesozoic-like creatures, such as were found on the Earth millions of years ago, to a dead, noxious, and Sunless world constantly ravaged by winds of incredible force.

Conjectures about the Venusian atmosphere have been inescapably tied to theories about the Venusian topography. Because the clouds forming the Venusian atmosphere, as viewed from the Earth through the strongest telescopes, appear opaque and almost featureless, this relationship between atmosphere and topography has posed many problems.

Impermanent light spots and certain dusky areas were believed by some observers to be associated with Venusian oceans. One scientist believed he identified a mountain peak, as visualized in figure 1–2, which he calculated as rising more than 43.45 km (27 miles) above the general level of the planet.

FIGURE 1–3.—Venus visualized as a hot, wet world.

Another school of thought speculated that Venus was covered entirely by vast oceans, one theory being that Venus was covered with a seltzer ocean because of carbon-dioxide measurements obtained through Earth spectrographic analysis. Other observations concluded that these great bodies of water have long since evaporated and that the winds, through the Cytherean ages, have scooped up the remaining chloride salts and blasted them into the Venusian skies, thus forming the clouds.

Related to the topographic speculations were equally tenuous theories about its atmosphere. It was reasoned that if the oceans of Venus still exist, then the Venusian clouds may be composed of water droplets; if Venus were covered by water, it was suggested that it might be inhabited by Venusian equivalents of Earth's Cambrian period of 500 million years ago, and the same steamy atmosphere and topography could be a possibility as visualized in figure 1–3.

Other theories respecting the nature of the atmosphere, depending on how their authors viewed the Venusian terrain, included clouds of hydrocarbons with perhaps droplets of oil, or vapors of formaldehyde and water. Finally, the seemingly high temperature of the planet's surface, as measured by Earth-bound instruments, was credited by some to the false indications that could be given by a Venusian ionosphere heavily charged with free electrons.

However, the consensus of pre-Mariner scientific thinking seemed generally to indicate no detectable free oxygen in the atmosphere; this fact inveighed against the probability of surface vegetation because Earth-type vegetation, at least, uses carbon dioxide and gives off oxygen into the atmosphere. On the other hand, a preponderance of carbon dioxide in the Venusian atmosphere was measured, which could create a "greenhouse effect," in which the heat of the Sun would be trapped near the surface of the planet, raising the temperature to as

high as 600° K. If the topography were in truth relatively flat and the rate of rotation slow, as many believed, the heating effect might produce winds of 400 miles per hour or more, and create sand and dust storms beyond any Earthly experience. And so the controversy continued.

SCIENTIFIC EXPERIMENTS IN MARINER II

The Mariner II spacecraft carried six scientific experiments representing the efforts of scientists at nine institutions: the Army Ordnance Missile Command, the California Institute of Technology, the Goddard Space Flight Center of NASA, Harvard College Observatory, the Jet Propulsion Laboratory, the Massachusetts Institute of Technology, the State University of Iowa, the State University of Nevada, and the University of California at Berkeley. Table 1–I lists the original experimenters and their affiliations.

The two primary planetary experiments were a microwave radiometer and an infrared radiometer. They were designed to operate during a period of about 45 minutes while the spacecraft passed the planet at distances ranging from approximately 12 874 to 64 372 km (8000 to 40 000 miles). These radiometers obtained information about the planet's temperature and the nature of its atmosphere.

The other four experiments made scientific measurements during the cruise through interplanetary space and in the near vicinity of Venus. They were: a magnetometer; charged-particle detectors, including an ionization chamber and several Geiger-Mueller counters; a cosmic dust detector; and a solar plasma detector. They also gathered data in the immediate vicinity of Venus.

One of the important considerations in choosing these experiments was the compromise between what scientists would like to measure during the mission and what was technologically possible. For example, of the 447 pounds that could be placed in a Venus trajectory with the available launch-vehicle thrust, only about 40 pounds could be allocated to scientific experiments. In addition, engineers and scientists designed Mariner II to convert electrical power from the sunlight, report its findings from as far as 57 934 800 km (36 000 000 miles), and, although sensitive and unattended, remain in precise working order for 3 to 5 months in outer space. Another restricting factor was time. Venus is in a favorable position for the launching of a Mariner-type spacecraft only during a period of a few weeks every 19 months.

Several theories concerning the nature of Venus' atmosphere and surface

have already been advanced in this chapter. One of the missions of Mariner II was to make scientific measurements in the vicinity of the planet which might substantiate one of these theories, or call for the formulation of a new one.

Table 1-I.—Mariner experimenters

Experiment	*Description*	*Experimenters*
Microwave radiometer...	Determine the temperature of the planet surface and details concerning its atmosphere.	Dr. A. H. Barrett, Massachusetts Institute of Technology; D. E. Jones, JPL; Dr. J Copeland, Army Ordnance Missile Command and Ewen-Knight Corp.; Dr. A. E. Lilley, Harvard College Observatory.
Infrared radiometer.....	Determine the structure of the cloud layer and temperature distributions at cloud altitudes.	Dr. L. D. Kaplan, JPL and University of Nevada; Dr. G. Neugebauer, JPL; Dr. C. Sagan, University of California, Berkeley, and Harvard College Observatory.
Magnetometer.....	Measure planetary and interplanetary magnetic fields.	P. J. Coleman, NASA; Dr. L. Davis, Caltech; Dr. E. J. Smith, JPL: Dr. C. P. Sonett, NASA.
Ion chamber and matched Geiger-Mueller tubes.	Measure high-energy cosmic radiation..	Dr. H. R. Anderson, JPL; Dr. H. V. Neher, Caltech.
Anton special-purpose tube.	Measure lower radiation (especially near Venus).	Dr. J. Van Allen and L. Frank, State University of Iowa.
Cosmic dust detector.....	Measure the flux of cosmic dust particles in space.	W. M. Alexander, Goddard Space Flight Center, NASA.
Solar plasma spectrometer.	Measure the spectrum of low-energy positively charged particles from the Sun.	M. Neugebauer and Dr. C. W. Snyder, JPL.

During the cruise and Venus encounter phase of the mission, Mariner II telemetered information to Earth. As the sensors of the six experiments received information, they fed it to a data conditioning system (DCS) which was located in one of the modules in the hexagonal base of the spacecraft. The DCS prepared information for transmission to Earth in the form of a digital code.

Since all of the data collected by Mariner II could not be transmitted at the same time, an electronic clock was built into the DCS. This clock controlled the equipment so that the receiver "listened" to one experiment at a time for about 1 second. After 20.16 seconds, the DCS switched off the scientific data and then the telemetry system sent spacecraft engineering data for 16.8 seconds. This cycle was continued during the cruise in interplanetary space. When the spacecraft was switched to the encounter mode, however, the spacecraft devoted its telemetry system to the full-time transmission of scientific information from its six experiments.

CHAPTER 2

Project Organization and Management

EARLY MARINER PROJECTS

The Mariner A and B projects were intended to launch spacecraft in the 1250-pound class that were designed to make scientific investigations in interplanetary space and in the vicinity of Venus and Mars, respectively, during the 1962–1964 launch opportunities. Both types of spacecraft were to be launched by a vehicle consisting of a modified Atlas D first stage, and a Centaur liquid-hydrogen/liquid-oxygen, high-energy second stage.

The Centaur vehicle, under development by General Dynamics/Astronautics at San Diego, Calif., had two gimbal-mounted engines, each capable of generating 15 000 pounds of thrust. Ten small hydrogen peroxide monopropellant engines were provided for attitude control, consolidation of main propellants, and final velocity correction.

The Mariner A configuration was scheduled to fly the NASA P-37 and P-38 missions to Venus in the summer of 1962 as a developmental spacecraft on Centaurs 7 and 8. However, slippages in the Centaur schedule began to compromise the Venus launches and the missions were forced into rescheduling.

By the second week of August 1961, it was generally recognized that the Centaur would not be available for the 1962 Venus launch period. Consequently, in mid-August, JPL discussions with NASA explored the possibility of using lightweight, attitude-stabilized spacecraft for the P-37 and P-38 missions, since it was considered most important that the United States launch probes to the planets in 1962 if at all possible.

On August 28, 1961, in a letter to NASA Headquarters, JPL proposed the feasibility of a 1962 Venus mission, based on an Atlas-Agena launch vehicle and the use of a hybrid spacecraft combining features of the Ranger and Mariner A designs. This proposed Mariner R spacecraft could carry 25 pounds of instruments (later increased to 40 pounds). Only one launch could be guaranteed, but two were possible within the July–September 1962 period if the Agena weight could be reduced. The project would not require significant changes in the Ranger schedule, but would necessitate the transfer of certain launch vehicles.

In addition to the activation of a Mariner R project, JPL would proceed with the design and development of the Mariner B spacecraft, scheduled for launch by Atlas-Centaur with dual Mars-Venus capability in 1964 and beyond. Coincidental with the implementation of the Mariner R project and the shift of emphasis in Mariner B, the Mariner A project was to be canceled.

Accordingly, NASA authorized cancellation of Mariner A, activation of the Mariner R project, and establishment of the dual capability for the Centaur-based Mariner B in 1964.

MARINER R (1962) PROJECT

The purpose of the Mariner R (1962) project was to perform the National Aeronautics and Space Administration's P–37 and P–38 missions to Venus during the third-quarter launch opportunities in 1962.

The primary objective of the Mariner R (1962) project was to develop and launch two spacecraft to the near-vicinity of the planet Venus in 1962, to establish and maintain two-way communication with the spacecraft throughout the flight, to obtain interplanetary data in space and during the Venus encounter, and to perform scientific surveys of the planet's characteristics. The launch vehicle used in this project was to be the Atlas D-Agena B (fig. 2–1),

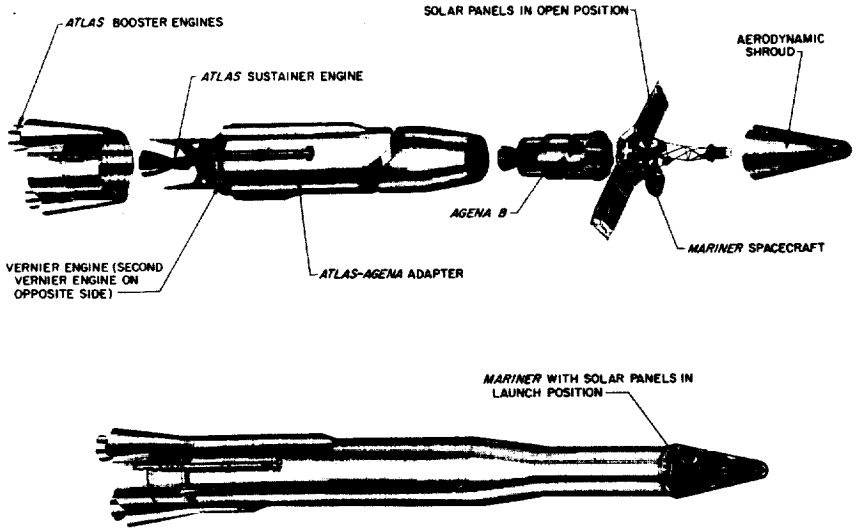

FIGURE 2–1.—Flight configuration of Atlas D–Agena B–Mariner II spacecraft.

permitting a spacecraft weight of approximately 460 pounds and including about 25 pounds of scientific instruments.

Two spacecraft were scheduled for launch in order to increase the probability that at least one would accomplish its objective. Launch schedules for the two probes were arranged to take maximum advantage of the limited 56-day launch period available from July 18 through September 12, 1962. By June 11, 1962, the firing dates had been established and both spacecraft were ready for launching. The minimum separation between the two launch dates was established as 21 days.

Since the time from the first consideration of the Mariner R mission to the initial launch date was less than a year (mid-August 1961 to mid-July 1962), to achieve the objectives in the limited time available it was necessary to make decisions quickly, to "freeze" the design at the earliest feasible point, and to meet all schedule milestones on time.

An all-out effort was initiated to design, develop, and procure components, and to test and launch the two spacecraft in an 11-month period. The many associated activities, such as trajectory work, preparation for launch and flight operations, and design and fabrication of ground support equipment, were pursued on a "crash" basis, concurrently with a major launch-vehicle effort involving design and manufacturing changes.

To take advantage of experience already gained, use was made of existing Mariner A and Ranger hardware and procedures wherever possible. The resultant design, limited by the many time and weight restrictions, produced a spacecraft with little or no redundancy.

Project planning specified delivery of two spacecraft (Mariners R–1 and R–2)[1] and one set of spares (later assembled and designated as Mariner R–3), two sets of system test complex equipment and one set of spares, and two sets of launch complex equipment in support of the spacecraft.

All major milestones were met on time, including arrival of equipment at Atlantic Missile Range and the subsequent launches on July 21 and August 27, 1962, respectively, for the P–37 and P–38 missions.

Because of a launch-vehicle deviation from the planned flight path, Mariner R–1 was destroyed by the range safety officer after approximately 290 seconds of flight. Measures taken to correct the difficulties experienced in this launch included a more rigorous checkout of the Atlas rate beacon and a revision of the

[1] Mariner R–1 and R–2 are spacecraft serial numbers, which are used in all prelaunch references and until injection into planetary transfer trajectory. Thereafter, the references become Mariner I and Mariner II.

data-editing equation, designed as a precaution against acceptance of faulty data by the ground guidance equipment.

FIGURE 2–2.—Liftoff of Mariner II.

The subsequent launching of Mariner R–2 on August 27, 1962 (fig. 2–2) initiated a space flight in which the project objectives were met with a high degree of success. A vast quantity of valuable scientific and engineering data was telemetered to Earth from the spacecraft throughout its flight, up to the time of its final communication on January 3, 1963.

Because of the high quality and great amount of the data transmitted by Mariner II, it was decided to terminate activity on the Mariner R spacecraft schedule for the 1964 Venus attempt—a spacecraft which would have carried a nearly identical set of scientific experiments. The cancellation decision was made in January 1963, and all Mariner R effort after that time was directed toward termination of the project. Much of the work underway was directly or partially applicable to the Ranger or Mariner Mars 1964 programs, and appropriate transfer of effort in these areas was made.

MANAGEMENT STRUCTURE

The National Aeronautics and Space Administration was created by the Space Act of 1958. To NASA was given the main job of creating and providing a broad capability of launching large loads into space, of surviving there, of taking new knowledge of nature from the more unobstructed view of the universe, and of operating in space as required by the national interest. Military space activities peculiar to the defense of the United States were left with the Department of Defense.

The responsibility for the Mariner R project at National Aeronautics and Space Administration Headquarters was assigned to the Office of the Director of Lunar and Planetary Programs, under the overall direction of the Office of Space Sciences. The organization chart shown in figure 2–3 indicates the relationship of these offices.

The Jet Propulsion Laboratory was assigned project management responsibility for the Mariner R project. JPL was also assigned system management responsibility for the Mariner R spacecraft system, including the associated complex for postinjection space-flight operations. Figure 2–4 shows an organization chart of the Jet Propulsion Laboratory during the period of the Mariner project. A summary of the responsibilities under the project manager structure is presented in figure 2–5.

The George C. Marshall Space Flight Center was assigned responsibility for the overall management and conduct of the launch vehicle portion of the Mariner

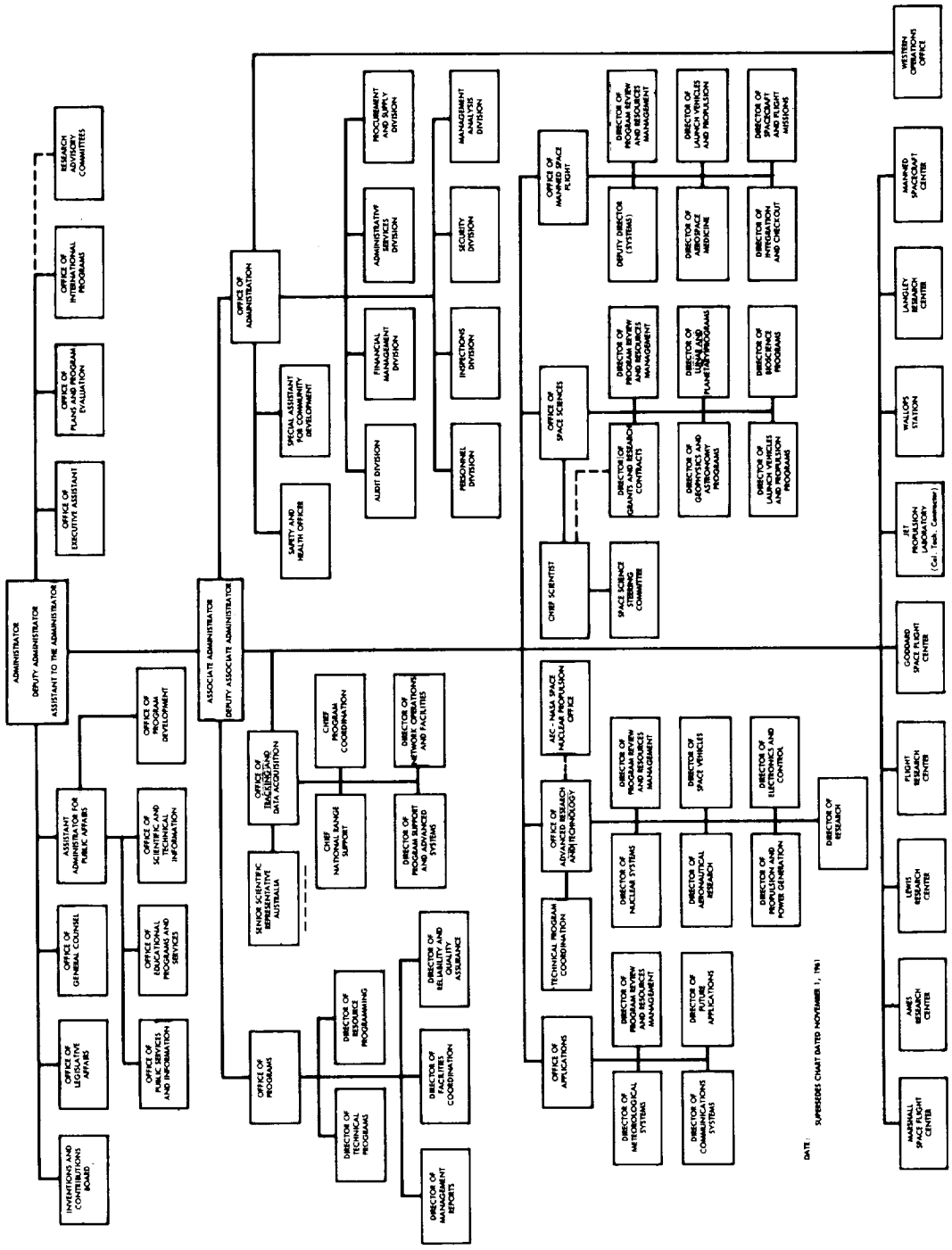

FIGURE 2–3.—NASA functional organization chart.

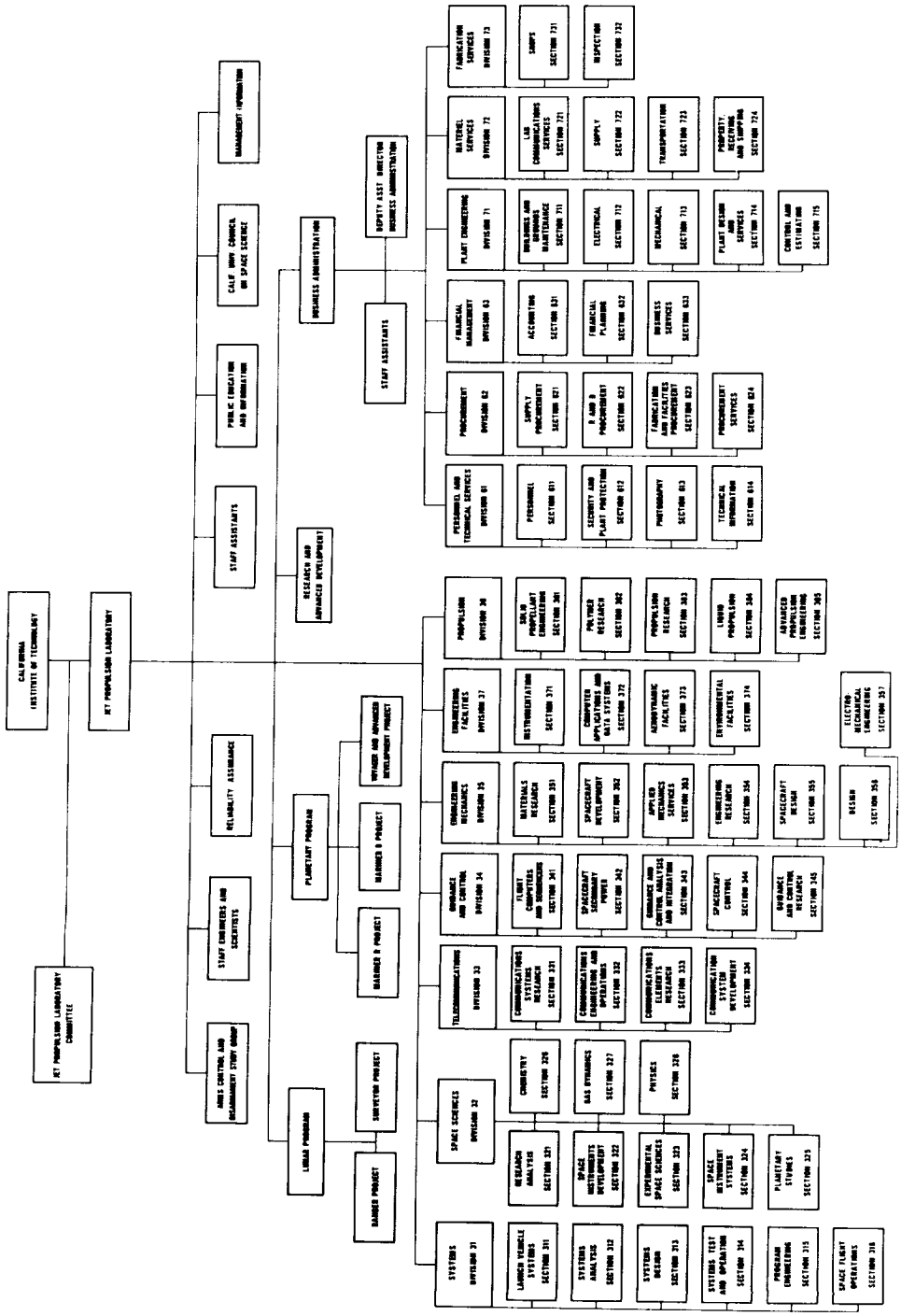

FIGURE 2–4.—JPL functional organization chart, September 10, 1962.

R project. In particular, this assignment included administrative and technical responsibility from vehicle procurement through launch and tracking to spacecraft injection.

The Director, MSFC, in order to assume management cognizance of the Agena B and Centaur projects, established as his principal agent a Light and Medium Vehicle Office. This office was responsible for assuring proper vehicle support to the several space projects, including Mariner R, which utilize these vehicles along with procurement and coordination with the Air Force Atlas boost vehicle. In order to support the Mariner R project, a systems manager was appointed within the MSFC organization. He was responsible for the planning and execution of the approved launch vehicle projects, including procurement and modification; GSE; planning and implementation of launch-to-injection tracking and instrumentation; and certification of performance and reliability analysis. The assigned responsibility included insuring the integrity, performance and proper mating of the launch vehicle and spacecraft systems. This effort included facilities and ground support equipment for the various phases of manufacturing, testing, and launch preparation. In view of the contractual arrangements for launch vehicles, the activities of the prime contractors and subcontractors were directed by the systems manager through the Air Force Space Systems Division.

Within Marshall Space Flight Center, a Launch Operations Directorate (LOD) was assigned responsibility for NASA launches. For the projects assigned to the Light and Medium Vehicle Office, LOD was to perform the launch operations in response to program requirements and objectives as specified by the Agena B systems manager. On July 1, 1962, LOD was redesignated as the Launch Operations Center. There was no need, however, to renegotiate agreements reached earlier with LOD relating to the Mariner R project.

Responsibility for procurement of launch vehicles, together with logistic and management support to meet NASA Agena launch schedules, was assigned to the USAF. The Air Force Space Systems Division (AFSSD) was responsible for operational, administrative, and technical support for NASA Agena launch vehicles. This assignment included personnel and facilities in support of launch operations. AFSSD acted as agent for MSFC in contract procurement of launch vehicles in accordance with USAF procedures, except as modified by NASA regulations and policy or by law. The SSD director for NASA Agena projects was the normal USAF contact for SSD operations associated with the NASA Agena project.

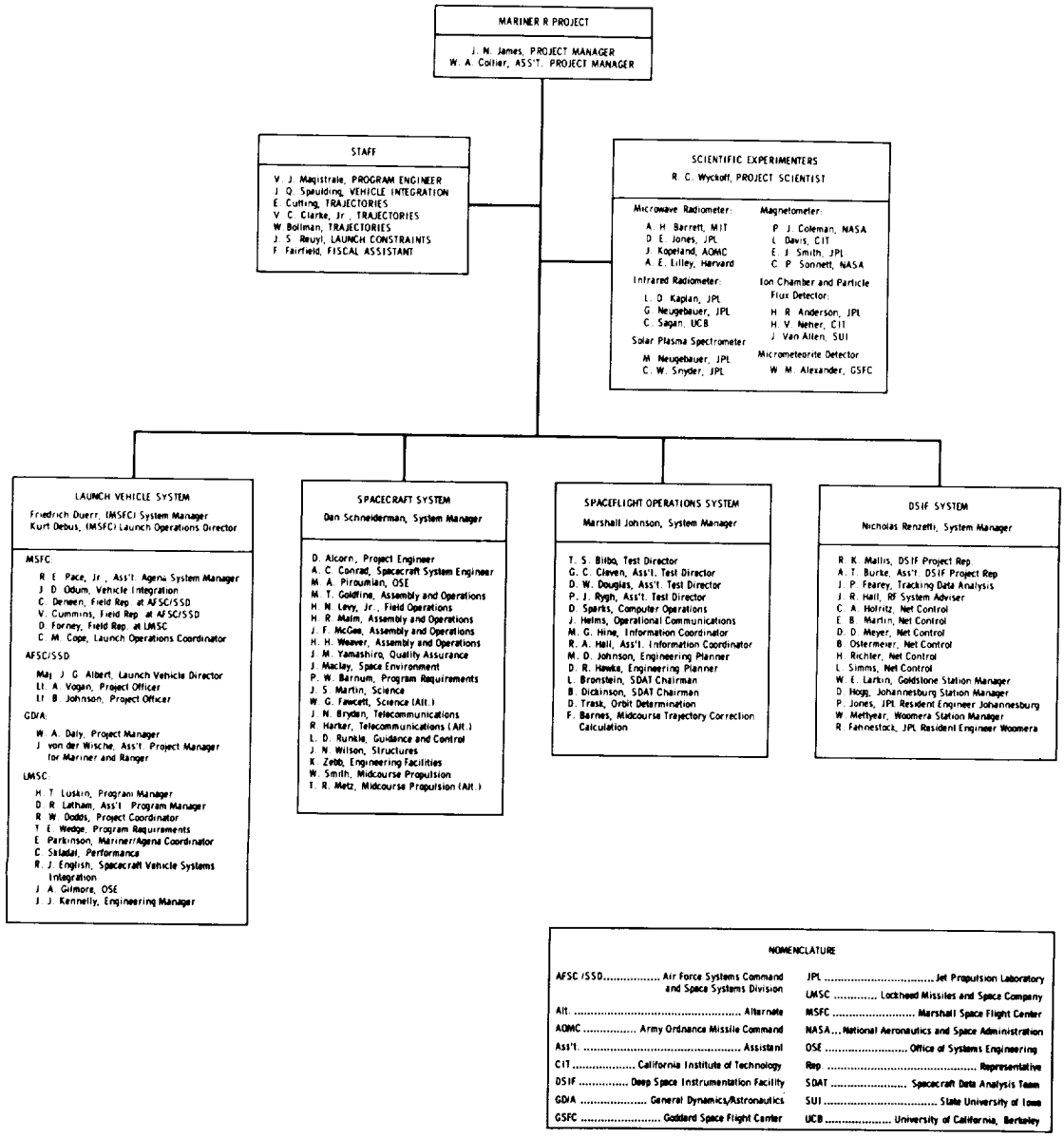

FIGURE 2–5.—Mariner R project organization chart.

MAJOR CONTRACTOR SUPPORT

Within Lockheed Missiles and Space Company, the NASA Agena project was managed by a program office. The MSFC representative's office and a portion of the LMSC staff active on the project were located in close proximity for ease of communications. In 1960, LMSC "projectized" its organization to increase the responsiveness of the various technical groups contributing to the program.

The Atlas launch booster for the Mariner R project was procured for NASA by the United States Air Force from General Dynamics/Astronautics. The GD/A organization consisted of a program office which reported directly to the project engineer for Atlas D, who in turn reported to the vice president and program director of Space Launch Vehicles.

PERMANENT PROJECT-WIDE BODIES

In order to utilize the relationships developed on Ranger to the maximum, the same board and panels that existed in the Ranger project were used for Mariner R, serving as technical advisers to the project and system managers.

The Agena B Coordination Board was appointed at the beginning of the Ranger project to coordinate the vehicle requirements of the various users of the Agena B vehicle and to provide a mechanism for the settlement of interagency problems.

The Vehicle Integration Panel continually monitored, compiled, and evaluated the structural, network, and configurational problems as they related to the interface between the spacecraft and vehicle with shroud. The panel was also responsible for the interface aspects of the launch checkout procedure.

The Performance Control Panel continually monitored, compiled, evaluated, and coordinated data relating to performance, trajectories, guidance and control, and flight dynamics as they interacted with the vehicle, the shroud, and the spacecraft interface.

The Tracking, Communication, In-Flight Measurements and Telemetry Panel continually monitored, compiled, evaluated, and coordinated data relating to tracking, communications, in-flight measurements, and telemetry as these items interacted with the vehicle, the shroud, and the spacecraft.

The Atlas/Agena B Flight Test Working Subgroup acted as the prime mechanism for coordinating flight preparations. Members participated in vehicle and

range readiness meetings, culminating on launch − 1 day, at which time the Launch Operations and Test director assumed overall control with AFSSD assistance.

LAUNCH VEHICLE RELATIONS

A major concern of the Mariner R project management was to control, coordinate, and remain aware of the many activities of the project, since five separate organizations had areas of prime technical cognizance in the project. To assist in the resolution of problems, to keep channels of communications open, and to inform and unite the different organizations for achieving the objectives of the Mariner R project, numerous person-to-person contacts were made.

To facilitate coordination, a series of status reviews was held. At these reviews, project policies and orientation were presented and all agencies involved in the project were represented. Consensus was that the status meetings promoted better understanding of organizational interfaces within the project.

JET PROPULSION LABORATORY ACTIVITIES

In addition to project management responsibility for the Mariner R project, JPL was responsible for: (1) the design, fabrication, and testing of the spacecraft and its associated ground support equipment; (2) the space flight operations from spacecraft injection to planetary encounter; and (3) the Deep Space Instrumentation Facility tracking operations. To implement these responsibilities, the following techniques were developed by the project.

The Project Policy and Requirements document specified the project policy and requirements for the Mariner R project internal to JPL. It established the operational procedures for the project in that it stated mission objectives, system requirements, milestones, and an overall guideline schedule.

Weekly internal JPL project meetings were held with key representatives from each of the JPL divisions. These meetings established the hard core of individuals who had a continuity with the overall aspects of the project. These individuals were assigned from each technical area and formed an organizational matrix to aid in the exchange of information, to monitor progress, and to function as the hub of all project action.

Since Mariner R was an expedited project, requiring shipping of equipment to AMR 9½ months after the go-ahead, it was necessary to freeze the design as early as possible, with mandatory changes handled through an engineering change

788-025 O—65—3

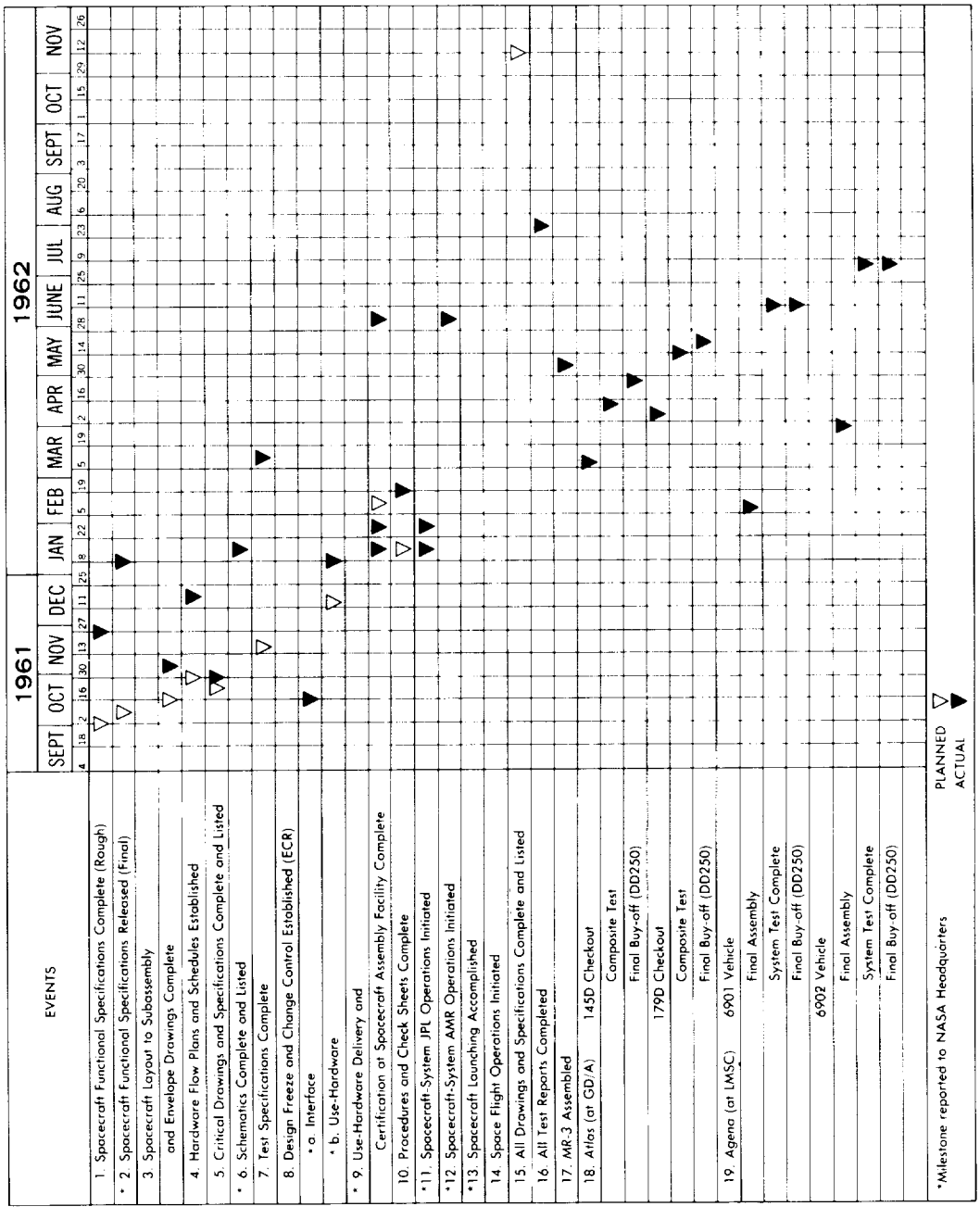

FIGURE 2–6.—Spacecraft schedule.

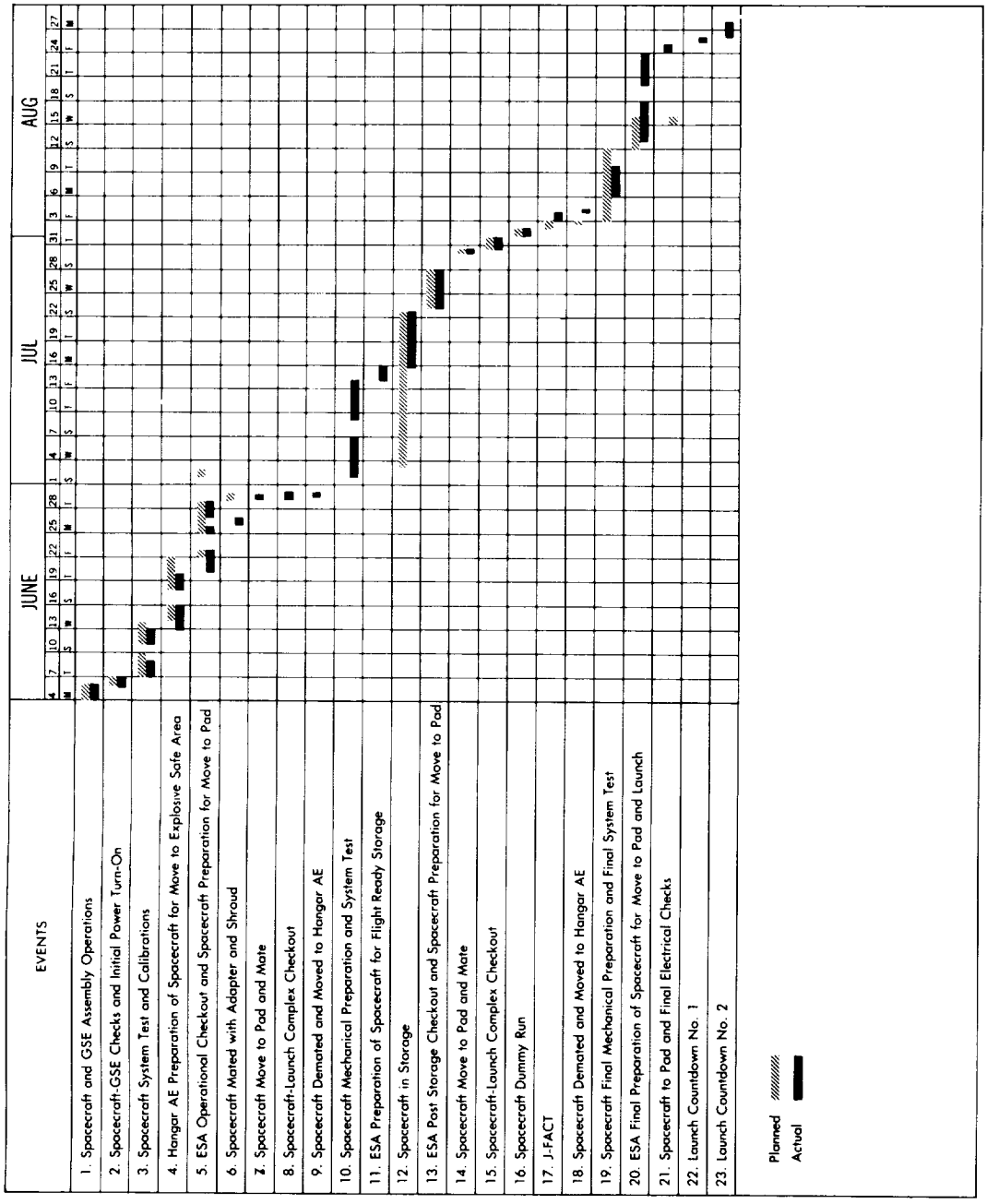

FIGURE 2–7.—Mariner R launch base operations schedule.

requirement (ECR) system. Thus, the Mariner R project was able to institute a progressive freeze concept while maintaining flexibility of operation by scheduling major interface freezes.

An initial survey of the subsystems was conducted to determine when to freeze and in what order. Major interfaces were scheduled first. Thereafter, any individuals who desired to freeze their particular subsystems, in whole or in part, could do so by referencing the appropriate control documents on the freeze list. A list, "Mariner R Change Freeze," was published periodically and any changes to the listed drawings and specifications required an ECR. A complete freeze was instituted January 15, 1962.

The evolution of schedules continued during the project so that two agencies, JPL and MSFC, were providing a continuous flow of detailed functional schedules. Figures 2–6 and 2–7 show the concurrent activity that existed in a number of the more significant areas of the Mariner R project.

It was project policy to accept the schedules as being at all times dynamic in nature and, therefore, subject to change. However, it was also project policy to insist that all phases of the project be scheduled with the best available information, and to use the schedules as a measurement of planning efficiency.

From the schedules, periodic project management plans were prepared, and submitted to NASA Headquarters.

CHAPTER 3

Space Vehicle System

As a result of the program change to adapt the Mariner spacecraft to the Atlas-Agena B launch vehicle for the 1962 Venus mission, an essentially new spacecraft design was initiated. This design relied heavily on hardware and techniques that had been developed for Ranger and Mariner A. The design of the configuration, the detail design of the spacecraft, and the fabrication of prototype and flight hardware progressed rapidly and with a minimum of problems. The first flight structure was delivered a little over 3 months from the start of preliminary design.

DESIGN PARAMETERS OF MARINER R SPACECRAFT

Reevaluation of the Agena vehicle capability showed that certain hardware could be removed without compromising the objectives, resulting in an allowable spacecraft weight of 460 pounds. The Mariner R preliminary design was initiated in early September 1961, using this new weight constraint. It was then possible to include the weight of a midcourse propulsion system to increase the probability of approaching near enough to Venus to perform the planet-oriented scientific experiments. The initial weight allocations of the Mariner R spacecraft are shown in table 3–I.

Certain design characteristics served as guidelines in the preliminary design phase. These included:

1. The capability of two-way communications until the spacecraft passed Venus.

2. Reasonable assurance (1:1000) of not impacting the planet with an unsterilized spacecraft.

3. The capability of performing planetary and interplanetary experiments.

4. Performance of a midcourse maneuver to correct for miss components and time of arrival in the vicinity of Venus; planet encounter to occur within view of the Goldstone, Calif., tracking station.

5. Maintenance of Sun and Earth lock by the spacecraft to permit the reception of telemetry through the directional antenna, to assist in the environ-

mental control of the spacecraft, and to enable continuous generation of power by the solar panels.

6. Use of two data rates: a high rate (33⅓ BPS) early in the flight and a second rate (8⅓ BPS) from Earth acquisition to encounter.
7. Derivation of power primarily through use of solar cells.
8. Transmission of science data in real time.

Table 3–I.—Initial Mariner R spacecraft weight allocations

Subsystem	Initial allocation weight, lb	Final weight, lb
Transponder	41.07	39.0
Command	10.00	8.8
Power	108.39	105.3
CC&S	9.96	11.2
Data encoding	15.50	13.6
Attitude control	57.40	53.3
Structure	82.30	77.2
Actuators	3.40	3.3
Pyrotechnics	3.75	4.3
Motion sensors	1.33	1.4
Spacecraft wiring	33.00	37.8
Propulsion	31.18	33.9
Thermal control	17.00	10.1
Science	40.00	49.5
Contingency	5.72	.....
Total	460.00	448.7

A Spacecraft Design Specification Book was prepared and published to provide a single source of information about the spacecraft; it served as a design tool and a control document defining the system in general terms. The book was used in the establishment of systems, subsystems, and overall spacecraft design, and in the dissemination of design changes to all persons concerned with the program. It encompassed only the spacecraft flight systems and associated ground equipment.

DESIGN COORDINATION MEETINGS

A series of meetings was held in which the electrical interfaces between the subsystems were defined. As a result, circuit data sheets were generated

for each signal. These sheets provided information useful to the cable designers, as well as a record of the circuit characteristics for signals between every source and user. The telemetry channels were assigned as shown in table 3–II.

Table 3–II.—Telemetry channel assignments

Battery voltage, v	23 to 40
Yaw control gyro, deg/hr	1800
Pitch control gyro, deg/hr	1800
Roll control gyro, deg/hr	1800
Battery current drain, amp	0 to 25
Pitch Sun sensor, deg arc	±0.2
Yaw Sun sensor, deg arc	±0.2
Roll Sun sensor, deg arc	±1.25
Spacecraft events	Not applicable
Command detector monitor	Frequency error
Earth brightness	Not defined
Antenna reference hinge angle, deg arc.	0 to 180
Antenna hinge position, deg arc	0 to 180
L-band AGC, dbm	−70 to −15
L-band phase error, deg phase	+30
Propellant tank pressure, psia	0 to 500
Battery charger current, amp	0 to 1
Midcourse motor N_2 pressure, psia	0 to 4000
Science experiments data	Not applicable
L-band phase error, deg	±3
L-band direct power, w	0 to 3
Louver position, deg arc	0 to 90
Low reference	Not applicable
Solar panel 4A11 voltage, v dc	20 to 60
L-band omni power, w	0 to 3
Attitude control N_2 pressure, psia	0 to 3500
Panel 4A11 current, amp	0 to 5
Panel 4A12 voltage, v dc	20 to 60
Panel 4A12 current, amp	0 to 5
High reference	Not applicable
Reference temperature, ohm	500
Booster-regulator temperature, °F.	70 to 200
Midcourse motor nitrogen tank temperature, °F.	0 to 170
Propellant tank temperature, °F.	−25 to +165
Earth-sensor temperature, °F	−40 to +150
Battery temperature, °F	20 to 170
Attitude control nitrogen temperature, °F.	35 to 165
Panel 4A11 front temperature, °F.	70 to 250
Panel 4A12 front temperature, °F.	70 to 250
Panel 4A11 back temperature, °F.	−300 to +300
Electronic assembly I temperature, °F.	20 to 170
Electronic assembly II temperature, °F.	20 to 170
Electronic assembly III temperature, °F.	20 to 170
Electronic assembly IV temperature, °F.	20 to 170
Electronic assembly V temperature, °F.	20 to 170
Lower thermal shield temperature, °F.	−100 to +100
Upper thermal shield temperature, °F.	10 to 300
Plasma electrometer temperature, °F.	15 to 160
Antenna yoke temperature, °F	−50 to +150

Another series of meetings defined the mechanical configuration, packaging layout, cabling, and thermal-control aspects of the spacecraft. The interface definitions, both mechanical and electrical, were determined so that the subsystem design could proceed.

Since time did not permit a proof test model (PTM) of the spacecraft, particular attention was paid to the interface between subsystems and the system test complex. This interface was defined in terms of the signal characteristics on either side of the interface. Furthermore, intensive preplanning made it

possible to achieve a maximum result from the comparatively short period allocated to spacecraft system and environmental testing.

DESIGN VERIFICATION

The design verification tests normally performed on the PTM were performed on the assembled flight spacecraft. Required design changes were immediately incorporated into the other spacecraft and the spares.

The system test complex (STC) was the basic equipment used for system design verification of the spacecraft. It had the capability to:

1. Operate the entire spacecraft in a manner simulating the countdown and flight sequence.
2. Monitor system functions as well as subsystem inputs and outputs for quantitative evaluation of spacecraft performance.
3. Exercise all elements of the spacecraft through their dynamic range for the purpose of evaluating their performance under influences produced by the presence of the complete spacecraft.

DESIGN UTILIZATION

Full use was made of the Mariner A and Ranger design experience. Some of the benefits derived from the Ranger program were:

1. Basic hex structures were available from Ranger test programs for use as temperature control, mockup, separation test, and structure test models.
2. The solar-panel actuators and hinge geometry were the same.
3. The high-gain antenna feed was very close mechanically to that used on the early Ranger flights.
4. The Sun-sensor mounting locations, as well as mechanical alinements, were the same as on Ranger.
5. The basic ground-handling dollies were the same as the Ranger units.

Many of the design and fabrication techniques developed for Mariner A were either used directly or were applied to the new design. Among these items were:

1. The high-gain antenna dish similar to that designed for Mariner A.
2. The Earth-sensor package, mechanical alinement, and mounting provisions defined during the Mariner A design period.
3. The Mariner A type of construction used on the solar panels.
4. The temperature-control louvers used on one of the hex electronic boxes designed, built, and tested during the Mariner A program.

5. Much of the electronic packaging and hardware similar to those built for Mariner A.

6. The superstructure stress configuration and fabrication techniques evolved directly from Mariner A experience.

7. The integration of the radiometer, including the type and method of articulation, expedited by the Mariner A design experience in relation to the trajectory passes in the vicinity of Venus.

Many new items and concepts, yet untried on Ranger or Mariner A, had to be designed and built. Among the larger new efforts on Mariner R were:

1. The cable trough relocated below the hex to facilitate the midcourse motor insertion. The assembly cabling connected directly into connectors hard-mounted to the trough.

2. The Ranger-Agena adapter structure which dictated that the Mariner A long-range Earth sensor be mounted on a redesigned high-gain antenna and be inclined at an angle with respect to the antenna pointing direction. A mirror mounted on the yoke allowed the sensor to "see" in the antenna "look" direction.

3. After several tests, it was found that stray light reflecting off spacecraft components, such as the high-gain antenna feed, affected the Earth-sensor performance. A light baffle box was installed around the mirror assembly to reduce the amount of stray light entering the Earth sensor.

DEVELOPMENT AND TEST

Five different types of spacecraft structure were assembled and used during different phases of the testing program:

1. *Mockup.* While the spacecraft was still in the preliminary design stage, work commenced on building a full-scale mockup. As the mechanical design was firmed up, the mockup was constantly updated. This mockup was used in a match-mate test with a prototype Lockheed-Agena adapter. The early completion of this test allowed the interface incompatibilities to be corrected without a schedule delay. After the match-mate test, the mockup was delivered to the cabling group for use as a cabling mockup. When the cabling function had been completed, the mockup was used for measuring the spacecraft antenna patterns.

2. *Structural test model.* Various vibration tests and modal surveys were performed on prototype and type-approval component parts. Tests were conducted to verify the adequacy of the superstructure and the radiometer structure and

their methods of attachment. Type-approval test levels verified the adequacy of the solar panel structure and the high-gain antenna when subjected to a greater-than-normal vibration environment.

A structural-test prototype spacecraft was fabricated from flight-worthy components. This spacecraft was used in a second match-mate test as a final verification of the mechanical interface with a flight-type adapter structure. After match-mate, the structural test model was successfully subjected to a modal vibration test and type-approval vibration tests. This structure was used throughout the program for developmental and prototype work. Among the items tested on this structure, to be later added to the flight units, were: (a) the Earth-sensor damper system, (b) the solar panel extension, (c) the solar sail, and (d) the high-gain antenna vibration damper.

3. *Temperature control model.* Thermal tests were conducted in the 6-ft vacuum chamber with a complete thermal mockup of the spacecraft, and later on the basic hex structure in the 6-ft vacuum chamber. Electric strip heaters were placed on the exterior of the spacecraft to simulate the solar load. The power dissipation load in the hex boxes was also simulated with heaters. The tests supplied valuable information as to the proper temperature control surfaces and techniques that were applied to the flight units.

4. *Separation test model.* A primary hex structure was ballasted to the proper weight, center of gravity, and moment of inertia. This structure was taken to Lockheed, where a separation test was conducted using a test setup similar to that developed for Ranger. Specifically, Lockheed checked the effects of:

(a) The lighter-than-Ranger spacecraft on the separation rates.
(b) The location and forces of the pyrotechnic arming switches on the separation.
(c) The Earth-sensor baffle box and the adapter on the separation clearance angles.
(d) The removal of the Ranger sterilization diaphragm from the adapter.
(e) The forces applied to the spacecraft as a result of the Earth-sensor damper installation.

5. *Flight spacecraft structures.* Three complete sets of flight equipment were fabricated: Mariner R-1 and R-2 and the spare Mariner R-3.

MARINER R-3

The original plans for the Mariner project stated a requirement for two flight-ready spacecraft and one set of unassembled spares. When the delivery

of the three sets of spacecraft parts was complete, it was decided that the incorporation of the set of spares into an assembled and tested spacecraft would be beneficial and useful to the project. Subsequent events showed this decision to be wise. The resulting Mariner R-3 spacecraft was used for problem detection at AMR while Mariner R-1 was in launch condition.

LAUNCH VEHICLE DESCRIPTION

The mission of the Atlas D booster was to lift the second-stage Agena B and the Mariner R spacecraft into the proper position and altitude at the right speed so that the Agena could enter Earth orbit, preliminary to injection into a Venus transfer trajectory. The Atlas D, as developed by Convair for the Air Force, develops 360 000 pounds of thrust, has a range of 10 138 km (6300 miles) and reaches a top speed of 25 748 km/hr (16 000 miles/hr).

The Atlas D has two main sections: a body or sustainer section, and a jettisonable aft or booster-engine section. The vehicle is approximately 100 feet long and has a diameter of 10 feet at the base. The weight is approximately 275 000 pounds. No aerodynamic control surfaces such as fins or rudders are used, as the Atlas is stabilized and controlled by "gimbaling" or swiveling the engine thrust chambers by means of a hydraulic system. The direction of thrust can be altered to control the movements of the vehicle.

The aft section mounts two 154 500-pound-thrust booster engines and the entire section is jettisoned or separated from the sustainer section after the booster engines burn out. The 60 000-pound-thrust sustainer engine is attached at the centerline of the sustainer section. Two 1000-pound-thrust vernier (fine steering) engines are installed on opposite sides of the tank section in the yaw or side-turn plane. All three groups of engines operate during the booster-powered phase. Only the sustainer and the vernier engines burn after staging (when the booster-engine section is separated from the sustainer section).

All of the Atlas engines use liquid oxygen and a liquid hydrocarbon fuel (RP-1). Dual turbopumps and valves control the flow of these propellants. The booster-engine propellants are delivered under pressure to the combustion chamber, where they are ignited by electroexplosive devices. Each booster thrust chamber can be swiveled a maximum of 5° in pitch (up and down) and yaw (from side to side) about the missile centerline. The sustainer engine is deflected 3° in pitch and yaw. The outboard vernier engines gimbal to permit pitch and roll movement through 140° of arc, and in yaw through 20° toward the missile body and 30° outward.

All three groups of engines are started and develop their full rated thrust while the vehicle is held on the launch pad. After takeoff, the booster engines burn out and are jettisoned. The sustainer engine continues to burn until its thrust is terminated. The swiveled vernier engines provide the final correction in velocity and attitude before they shut down.

The propellant tank is the basic structure of the forward or sustainer section of the Atlas. It is constructed of thin stainless steel and is approximately 50 feet long. Pressure of helium gas is used to support the tank structure, thus eliminating the need for internal bracing, saving considerable weight, and increasing overall performance. The helium gas used for this purpose is expanded to the proper pressure by heat from the engines.

Equipment pods on the outside of the sustainer section house the electrical and electronic units and other components of the vehicle systems. The Atlas uses a flight programmer, an autopilot, and the gimbaled-engine thrust-chamber actuators for flight control. The attitude of the vehicle is controlled by the autopilot, which is set for this automatic function before the flight. Guidance commands are furnished by a ground radio guidance system and computer. The airborne radio inertial guidance system employs two radio beacons which respond to the ground radar. A decoder on board the vehicle processes the guidance commands.

Launching Mariners R–1 and R–2 to Venus required a second-stage vehicle capable of driving the spacecraft out of Earth orbit and into a proper flight path to the planet. The Agena B used for this purpose weighs 1700 pounds, is 60 inches in diameter, and has an overall length of 25 feet, in the Mariner R configuration. The Agena B fuel tanks are made of 0.080-inch aluminum alloy. The liquid-burning engine develops more than 16 000 pounds of thrust. The propellants are a form of hydrazine and red fuming nitric acid.

The Agena can be steered to a desired trajectory by swiveling the gimbal-mounted engine on command of the guidance system. The attitude of the vehicle is controlled either by gimbaling the engine or by ejecting gas from pneumatic thrusters. The Agena B has the ability to restart its engine after it has already fired once to reach an Earth orbital speed. This feature makes possible a significant increase in payload and a change of orbital altitude. A velocity meter ends the first and second burns when predetermined velocities have been reached.

After engine cutoff, the major reorientation of the vehicle is achieved through gas jets controlled from an electronic programming device. This system can turn the Agena completely around in orbit, or pitch it down for reentry into the

atmosphere. The orbital attitude is controlled by an infrared, heat-sensitive horizon scanner and gyroscopes.

The principal modification to the Agena vehicle for the Mariner R mission was an alteration to the spacecraft-Agena adapter in order to reduce weight.

SPACECRAFT DESCRIPTION

As discussed earlier in this chapter, the Mariner R spacecraft (fig. 3–1) utilized many of the design principles and techniques developed for the Ranger program. The basic structural unit of Mariner R was a hexagonal frame made of magnesium and aluminum to which was attached an aluminum superstructure, a liquid-propelled rocket engine for midcourse trajectory correction, six rectangular chassis mounted one on each face of the hexagonal structure, a high-gain directional antenna, the Sun sensors, and gas jets for control of the spacecraft's attitude. The spacecraft configuration is shown in figures 3–2 and 3–3.

The tubular, truss-type superstructure extended upward from the base hexagon. It provided support for the solar panels while latched under the shroud during the launch phase, and for the radiometers, the magnetometer, and the omnidirectional antenna, which was mounted at the top of the structure. The superstructure was designed to be as light as possible, yet be capable of withstanding the predicted load stresses. The six magnesium chassis mounted to the base hexagon housed the following equipment: The electronics circuits for the six scientific experiments, the communications system electronics; the data encoder and the command electronics; the attitude control and CC&S circuits; a power control and battery charger assembly; and the battery assembly.

The Mariner R spacecraft was self-sufficient in power. It converted Sun radiation into electrical energy through the use of solar panels composed of photoelectric cells which charged a battery installed in one of the six chassis on the hexagonal base. The control, switching, and regulating circuits were housed in another of the chassis cases. The battery operated the various spacecraft subsystems during the period from launch until the solar panels were faced into the Sun. In addition, the battery supplied power during trajectory maneuvers when the panels were temporarily out of sight of the Sun, and shared the demand for power when the panels were overloaded. The battery furnished power directly for switching various equipment in flight and for certain other heavy loads of brief duration, such as the detonation of explosive devices for releasing the solar panels. The Mariner R battery used sealed silver-zinc cells and had a capacity

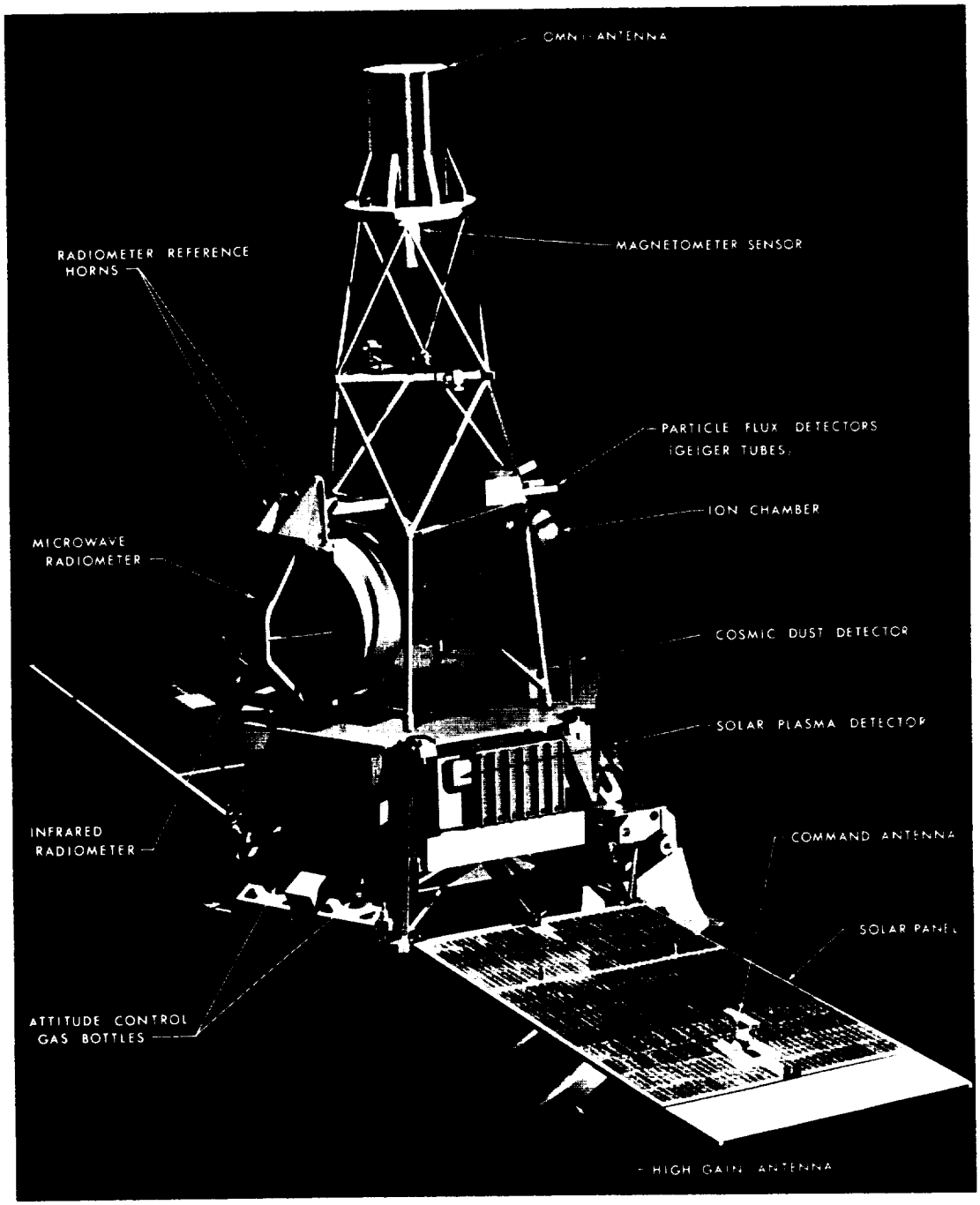

FIGURE 3–1.—Mariner R spacecraft.

of 1000 watts/hr. It weighed 33 pounds and was recharged in flight by the solar panels. The two solar panels, as originally designed, were each 60 in. long by 30 in. wide and each panel contained about 4900 cells, or approximately 9800 solar cells in a total area of 27 sq ft. Each solar cell produced only about 230 one-thousandths of a volt. The entire array was designed to convert the Sun's energy to electrical power in the range between 148 and 222 watts. When a later design change required a 2.5-sq-ft extension of one panel in order to add about 910 more solar cells, it was necessary to add an extension (Dacron impregnated with silicone rubber) to the other panel in order to balance the solar pressure on the spacecraft. In order to protect the solar cells from the infrared and ultraviolet radiation of the Sun, which would produce heat but no electrical energy, each cell was shielded from these rays by a glass filter that was transparent to the light which the cells converted into power. The power subsystem electronics circuits were housed in another of the hexagonal chassis cases. This equipment was designed to receive and switch power either from the solar panels, the battery, or a combination of the two, to a booster-regulator.

Mariner R was stabilized in space by the attitude-control subsystem. The roll axis was pointed at the Sun, providing stability about the pitch and yaw axes. Roll stability was achieved by keeping the Earth sensor, mounted on the directional antenna, pointing at Earth, in order to maintain continuity of communications. Pointing the roll or longitudinal axis at the Sun allowed the maximum amount of solar energy to strike the solar panels and aided the thermal control of the spacecraft by maintaining the Sun at a constant known attitude relative to the spacecraft.

The beam width of the high-gain antenna was 16.3° at half-power and, consequently, the antenna had to be pointed at Earth. This requirement was used to roll-stabilize the spacecraft, thus providing a stabilized platform for the science experiments. The Sun and Earth acquisitions were achieved through a series of sensors, gyros, and internal logic circuits which caused actuation of cold-gas valves. Expulsion of gas in preferential directions provided desired rates about the various axes to bring the spacecraft into the desired stable attitude.

The central computer and sequencer (CC&S) subsystem supplied timing, sequencing, and computational services for other subsystems of the Mariner R spacecraft. All events of the spacecraft were implemented in three distinct sequences or "modes": (1) the launch sequence controlled events which occurred during the launch phase; (2) the propulsion sequence controlled the events necessary to perform the midcourse maneuver; (3) the encounter sequence in-

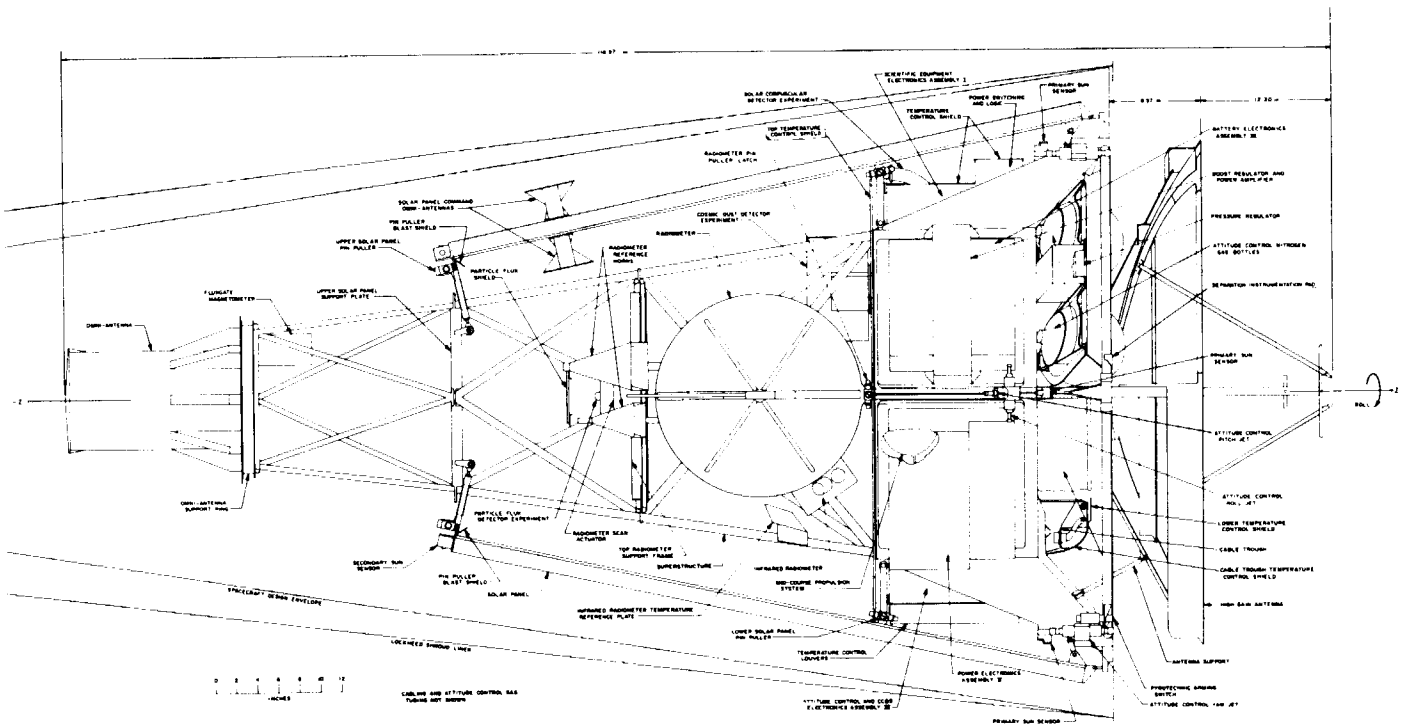

FIGURE 3–2.—Mariner R spacecraft configuration, side view.

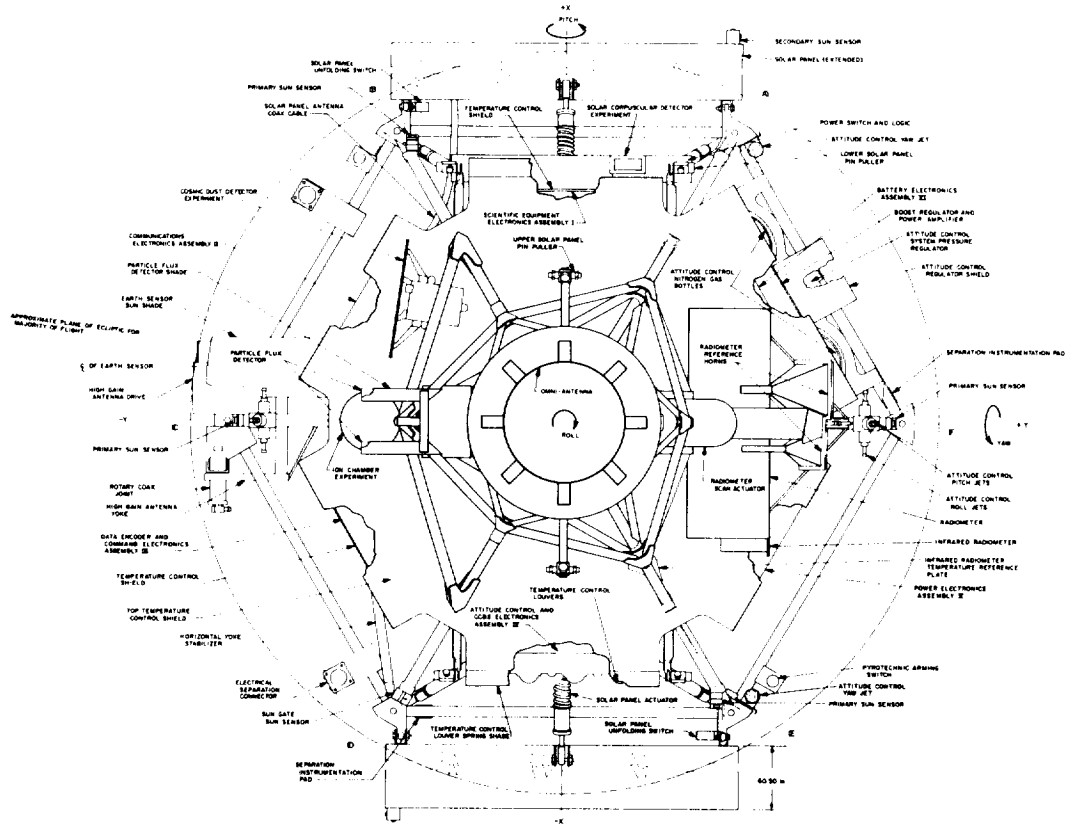

FIGURE 3–3.—Mariner R spacecraft configuration, end view.

cluded all CC&S commands required in the vicinity of Venus. A highly accurate electronic clock (crystal-controlled oscillator) scheduled the operations of the spacecraft subsystems. The oscillator frequency of 307.2 kc was reduced to the 2400- and 400-cps output required for the power subsystem. The control clock also timed the issuance of commands by the CC&S in each of the three operating modes of the spacecraft.

Mariner R used a technique for modulating its radio carrier with telemetry data known as phase-shift keying. In this system, the coded signals from the telemetry measurements displaced another signal of the same frequency but of a different phase. These displacements in phase were received on Earth and

then translated back into the codes, which indicate the voltage, temperature, intensity, or other values measured by the spacecraft telemetry sensors or scientific instruments. A continually repeating code was used for synchronizing the ground receiver decoder with the spacecraft. The decoder then deciphered the data carried on the information channel.

This technique was called a two-channel, binary-coded, pseudo-noise communication system and was used to modulate a radio signal for transmission.

Radio command signals transmitted to Mariner R were decoded in a command subsystem, processed, and routed to the proper using devices. The subsystem was used to receive the commands, send back confirmation of receipt to the Earth, and distribute them to the spacecraft subsystems.

Mariner R used four antennas in its communication system. A conelike nondirectional (omni) antenna was mounted at the top of the spacecraft superstructure and was used from injection into the Venus flight trajectory until Earth acquisition and during the midcourse maneuver (the directional antenna could not be used until it had been oriented on the Earth). A dish-type, high-gain, directional antenna was used following Earth orientation, and after the trajectory correction maneuver was completed. The directional antenna was located beneath the hexagonal frame of the spacecraft while it was in the nose-cone shroud. Following the unfolding of the solar panels, it was swung into operating position, although it was not used until after the spacecraft locked onto the Sun and the Earth. The directional antenna was equipped with flexible coaxial cables and a rotary joint. It was moved in two directions; one motion was supplied by rolling the spacecraft around its long axis. In addition, two command antennas, one on either side of one of the solar panels, received radio commands from the Earth and were used for measuring spacecraft velocity and angular position in the two-way Doppler mode.

The Mariner R propulsion subsystem for midcourse trajectory correction employed a rocket engine that weighed 37 pounds with propellant and a nitrogen pressure system, and developed 50 pounds of thrust. The system was suspended within the central portion of the basic hexagonal structure of the spacecraft, with the thrust axis parallel to the roll axis of the spacecraft. The rocket engine used a type of liquid propellant known as anhydrous hydrazine and it was so controlled that it could burn from as little as 0.2 of a second to a maximum of 57 seconds, and increase the velocity of the spacecraft from as little as 0.7 ft/sec to as much as 200 ft/sec. The hydrazine was stored in a rubber bladder inside a doorknob-shaped container. At the ignition command, nitrogen gas under a

pressure of 3000 lb/sq in. was forced into the propellant tank through explosively activated valves. The nitrogen then squeezed the rubber bladder, forcing the hydrazine into the combustion chamber. (Hydrazine, a monopropellant, requires ignition starting for proper combustion.) In the Mariner subsystem, nitrogen tetroxide starting or "kindling" fluid was injected into the propellant tank by a pressurized cartridge. Aluminum oxide pellets in the tank acted as catalysts to control the speed of combustion of the hydrazine. The burning of the hydrazine was stopped when the flow of nitrogen gas was halted, by explosively activated valves.

The spacecraft's temperature control system was made as thermally self-sufficient as possible. Paint patterns, aluminum sheet, thin gold plating, and polished aluminum surfaces reflected and absorbed the amounts of heat necessary to keep the spacecraft and its subsystems at the proper temperatures. Thermal shields were used to protect the basic hexagonal components. The upper shield, constructed of aluminized plastic on a fiber-glass panel, protected the top of the basic structure and was designed for maximum immunity to ultraviolet radiation. The lower shield was installed below the hexagon: it was made of aluminum plastic faced with aluminum foil where it was exposed to the blast of the midcourse rocket-engine exhaust.

The six electronics cases on the hexagon structure were variously treated, depending upon the power dissipation of the components contained in each. Those of high power were coated with a good radiating surface of white paint; assemblies of low power were provided with polished aluminum shields to minimize the heat loss. The case housing the attitude control and CC&S electronics circuits was particularly sensitive because the critical units might fail above 130° F. A special assembly was mounted on the face of this case; it consisted of eight movable, polished aluminum louvers, each activated by a coiled, temperature-sensitive bimetallic element. When the temperature rose, the elements acted as springs and opened the louvers. A drop in temperature would close them.

Structures and bracket assemblies external to the basic hexagon were gold plated if made of magnesium, or polished if aluminum. Thus protected, these items became poor thermal radiators as well as poor solar absorbers, making them relatively immune to solar radiation. External cabling was wrapped in aluminized plastic to produce a similar effect. The solar panels were painted on the shaded side for maximum radiation control properties. Other items were designed so that the internal surfaces were as efficient radiators as possible, thus conserving the spacecraft heat balance.

CHAPTER 4

Trajectory and Orbit

TRAJECTORY DESIGN AND SELECTION

Interplanetary travel of even the most elementary nature is a complex ballistics problem involving the "three M's" of celestial mechanics: Moments, masses, and motions. Until recently, interplanetary travel was not possible, owing to lack of sufficient vehicle energy to boost a meaningful payload out of the Earth's gravitational sphere of influence and into an interplanetary transfer solar orbit; however, the development of high-energy rockets has made Earth escape and planetary exploration possible.

The Ballistics Problem

For best utilization of the rocket energy available, the relative motion and positions of the planets about the Sun must be considered, since the spacecraft itself (once freed from the Earth's gravitational pull) will become a member (planetoid) of the solar system and, therefore, subject to the same inertial forces. As a result of the changing planetary relationships, the available time of departure (launch date), speed of travel, time of flight, and flight path change continually.

Of prime significance in scheduling an interplanetary trip is the knowledge that a free-falling (orbiting) body travels in an imaginary plane which passes through the center of a controlling body (figs. 4–1 to 4–3). For an Earth-Venus interplanetary spacecraft, this controlling body is first the Earth, then the Sun, then Venus, and again the Sun.

Within each of these planes of motion, the spacecraft will follow certain geometric paths that are mathematically definable and predictable. The trajectory path describes various conic figures: Earth orbit—ellipse, Earth escape—hyperbola, Sun-centered transfer orbit—ellipse, Venus encounter and escape—hyperbola, Sun-centered permanent orbit—ellipse.

The energy required to escape the Earth and effect a ballistic transfer from Earth to Venus is at a minimum approximately every 19 months. This time sequence is the synodic period and results from the harmonic relationship of the Venus and Earth orbital periods of revolution about the Sun.

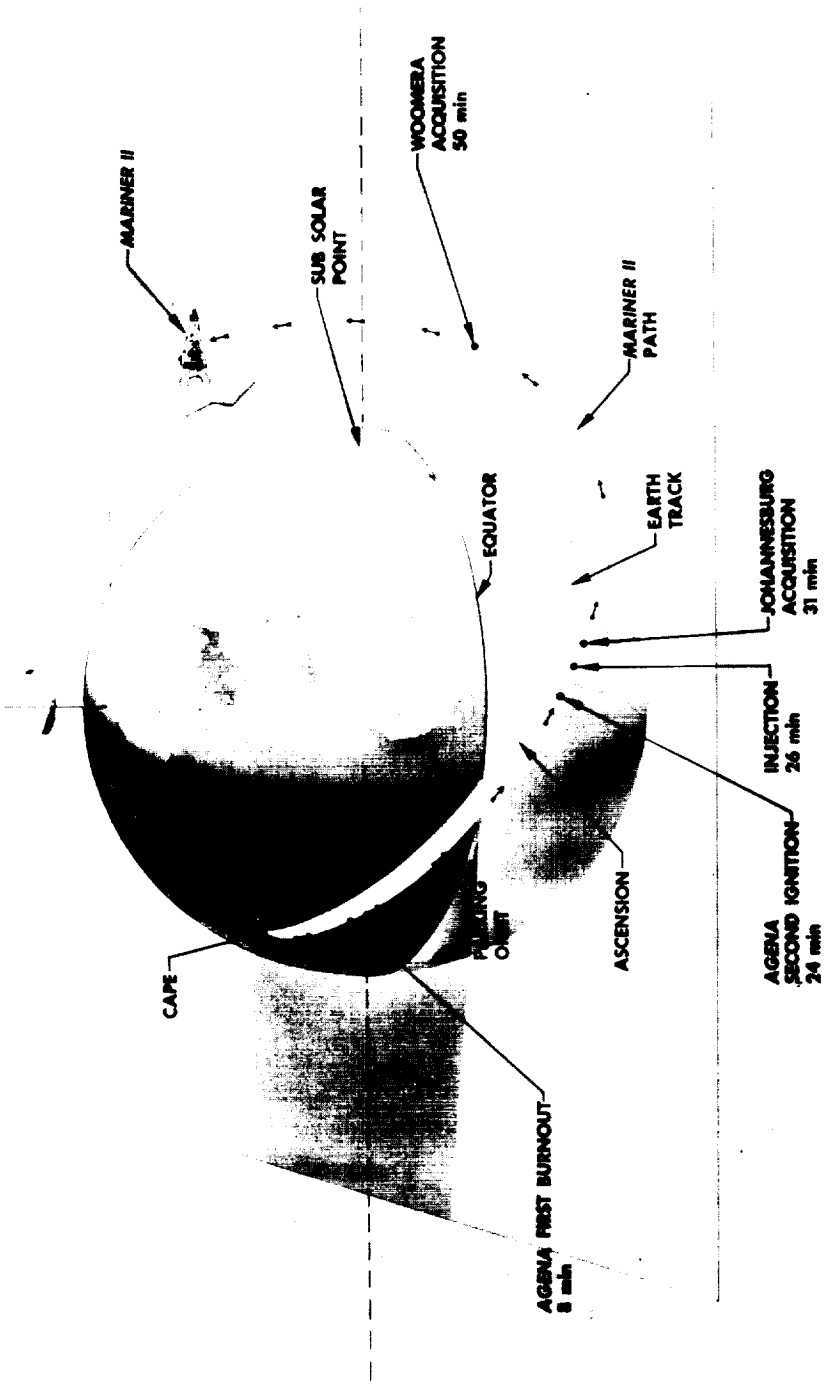

FIGURE 4–1.—Early flight of Mariner II showing plane of spacecraft motion.

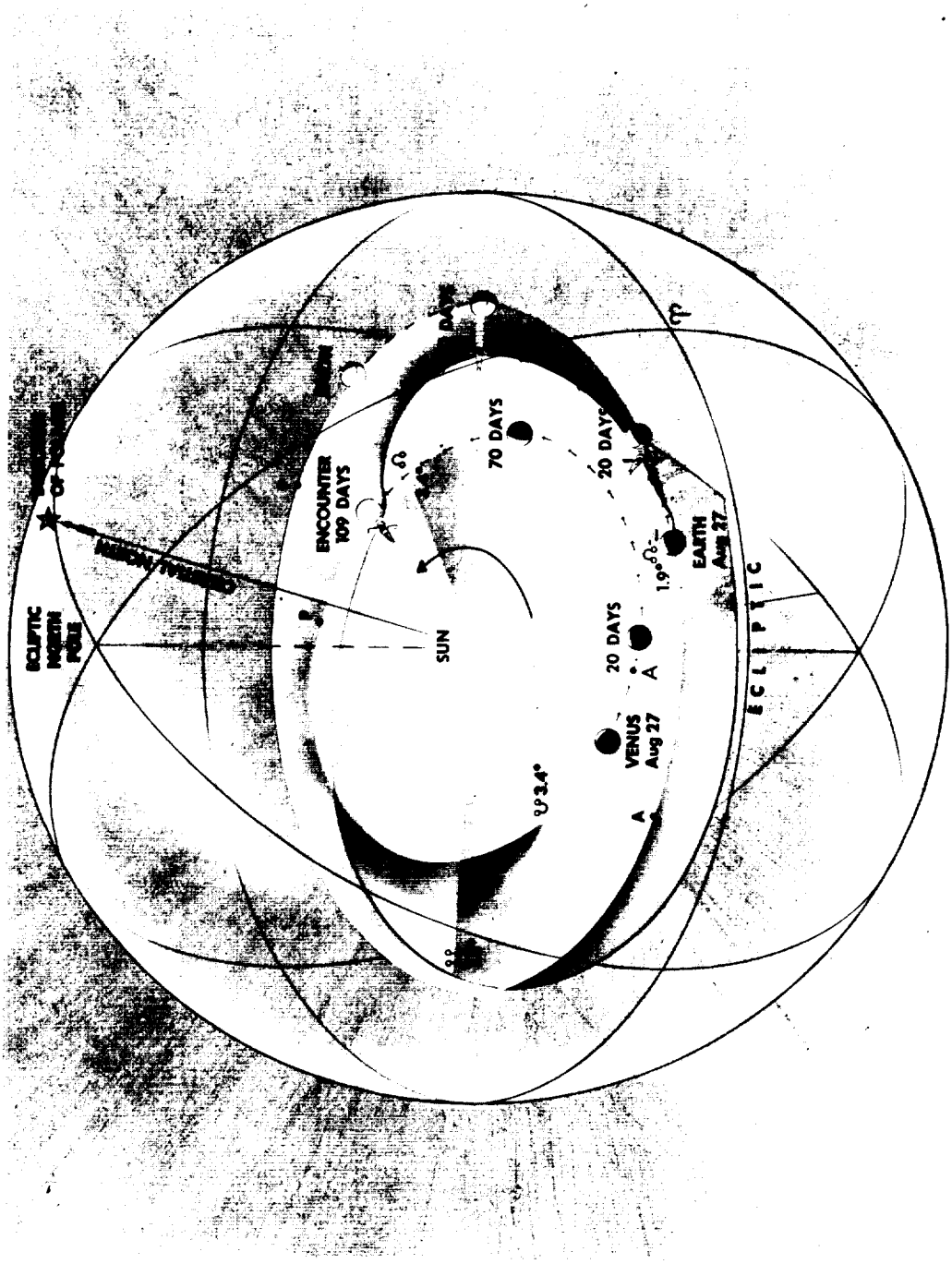

FIGURE 4–2.—Orientation of Earth, Venus, and Mariner II orbit planes in the celestial sphere.

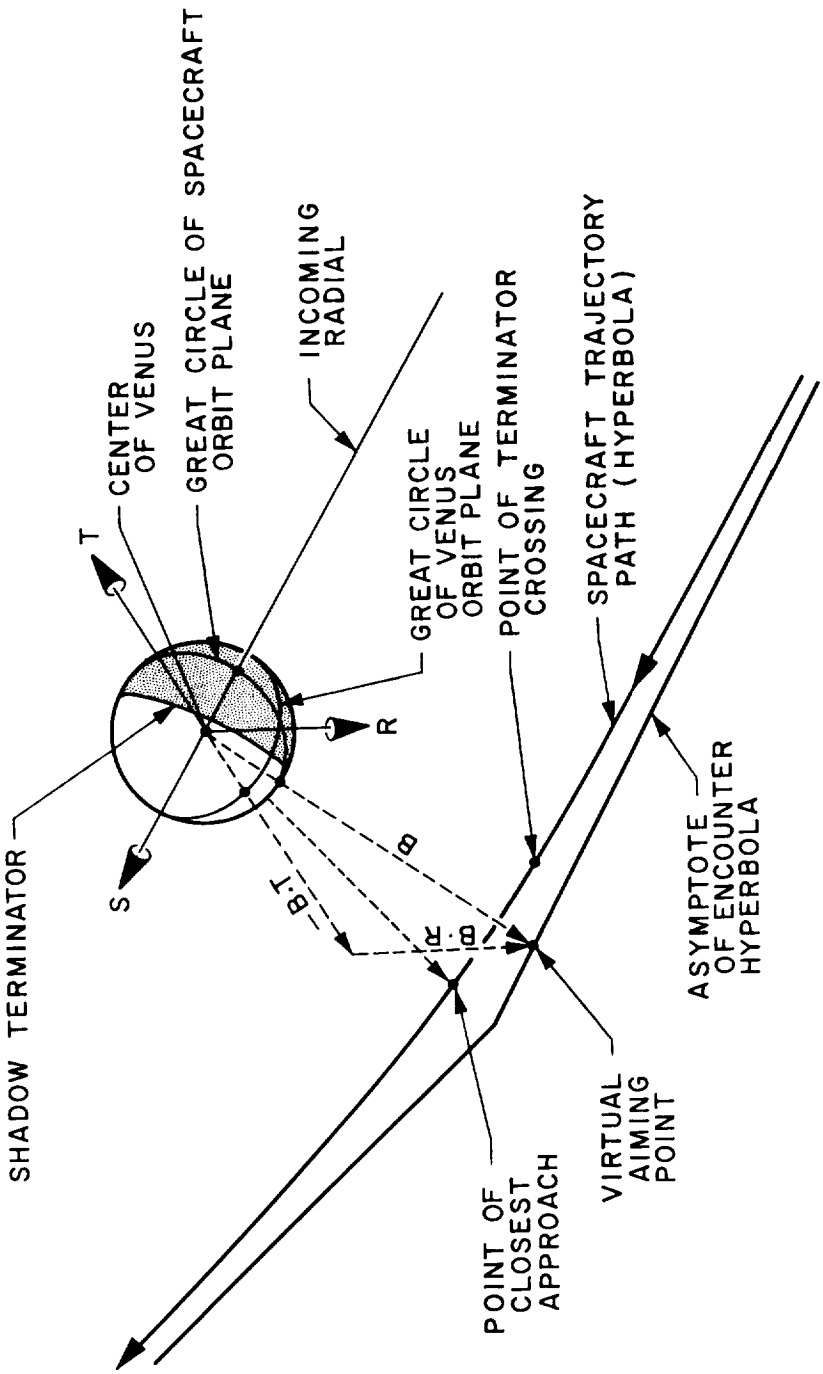

FIGURE 4–3.—Mariner II aphrodiocentric (Venus-centered) encounter geometry and aiming point coordinate system.

The minimum velocity required just to escape the Earth's gravitational sphere of influence is approximately 11 km/sec (6.8 miles/sec); the actual velocity required to reach Venus is greater than 11 km/sec. This additional velocity is necessary in order to move the spacecraft in closer to the Sun and to displace the spacecraft from the ecliptic plane to the Venus celestial latitude of planet encounter. (The Mariner II opportunity permitted encounter to take place near the intersection of the Venus and Earth orbit planes—the Venus ascending node—and, therefore, the displacement from the ecliptic plane was near a minimum.)

The position of the Earth at launch for an optimum rendezvous trajectory to Venus occurs when Venus is trailing the Earth around the Sun by approximately 60° in celestial longitude. (In 1962 this most efficient trajectory had a launch date of August 22 and a total flight time of 114 days; consequently, the maximum spacecraft weight could be placed on top of the launch vehicle for this trajectory.) As launch dates and flight times are selected which deviate from this optimum trajectory, the energy required to effect the interplanetary transfer increases, thereby decreasing the allowable spacecraft weight. For a given spacecraft weight there is a corresponding value of injection [1] energy which will be achievable by the booster vehicle. Also, for a given fixed energy above the absolute minimum, there is a corresponding "launch interval" (number of days) in which the spacecraft can be launched.

Each day (in a launch opportunity of several weeks) has its own launch period or "window" of only several hours or minutes. This launch window is created by several interrelated restrictions and conditions:

1. The geographically fixed launch site on the surface of the Earth.
2. The Earth center point
3. The geocentrically referenced place and direction of injection into an Earth-escape hyperbolic orbit. (The range of locations and directions varies with the Venus celestial latitude at encounter and with the Earth's own orbit position and, therefore, does not change greatly for any given day.)
4. The Earth's rotation on its axis.
5. The 90° to 114° S. lat. geographic launch corridor (fig. 4-4). (This is an AFETR range safety restriction in the event of a booster malfunction.)

[1] Injection occurs when the final Agena thrust period is terminated and, consequently, when the spacecraft is "injected" into its hyperbolic orbit away from the Earth.

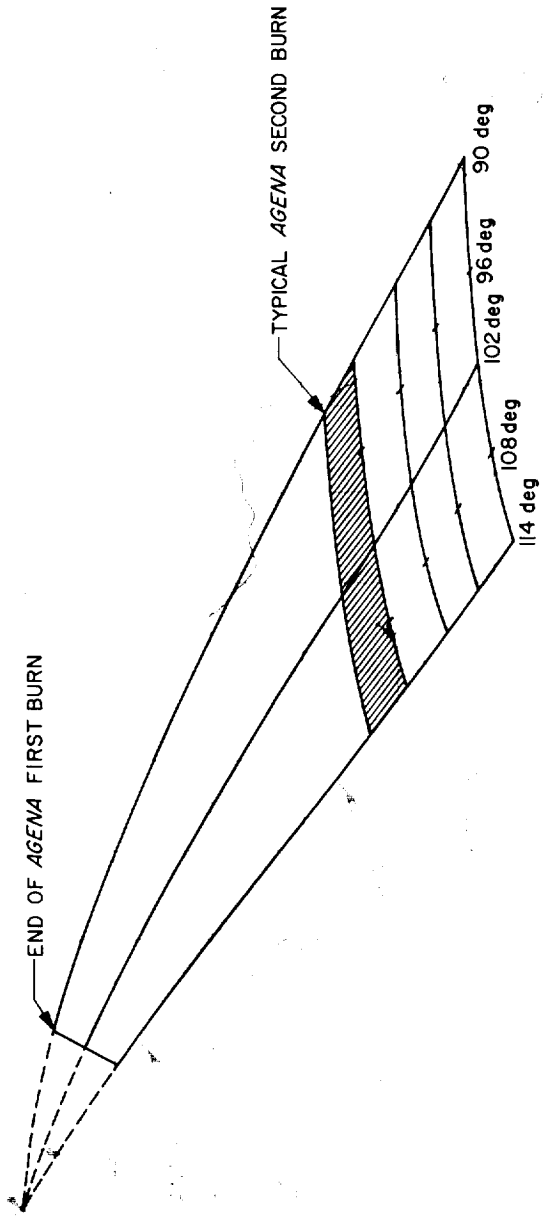

FIGURE 4–4.—Typical injection loci for a Mariner Venus flight.

The launch site, Earth center, and asymptote of the escape hyperbola [2] will all be in the spacecraft's orbit plane when the place and direction conditions of injection are satisfied. The effect of the Earth's rotation is to move the launch site eastward 15 deg/hr and continuously to change the required launch azimuth to coincide with the continuously inclining spacecraft orbit plane. For each day, the period of time is limited during which the range of azimuth headings is available. This period of time defines the launch window.

Mission Constraints on Trajectory Design

Interplanetary trajectory design requires early consideration of the mission objectives and their resulting constraints. For the Mariner R mission these constraints fell into five broad classes:

1. *Communications.* The maximum distance at which communications might be achieved between Earth and spacecraft was estimated to be approximately 1×10^8 km (6×10^7 miles). Each spacecraft (Mariners R–1 and R–2) had to encounter Venus near the middle of the Goldstone tracking day. A 2-day separation in arrival dates for each spacecraft was required to prevent simultaneous reception of planet-encounter data.

2. *Equipment life.* The travel time to Venus had to be kept at a minimum to enhance the probability of survival of the electronic equipment, which was to operate continuously during the nearly 110-day nominal flight period.

3. *Atlas-Agena guidance system.* The booster vehicle guidance system design determined the preinjection trajectory characteristics and, therefore, the initial conditions for planning the interplanetary transfer trajectory.

4. *Launch facility.* The two spacecraft were to be launched with the use of a single launch facility, requiring a substantially long firing opportunity.

5. *Instrumentation considerations.* These included such general factors as spacecraft distance from planet at encounter, planet lighting, spacecraft mechanical-pointing and view-angle limitations, and the probability of impacting the planet with the spacecraft. The following specific constraints were used to establish the design aiming point for the Mariner Venus encounter:

---

[2] The asymptote of the escape hyperbola is a straight line that is parallel to the outgoing radial; the outgoing radial is a straight line connecting the center of the Earth and the geocentric point in space at which the spacecraft finally escapes Earth's gravitational sphere of influence. The spacing between these two lines is determined by the eccentricity of the hyperbola; this eccentricity is in turn determined by the spacecraft's velocity at the time of injection.

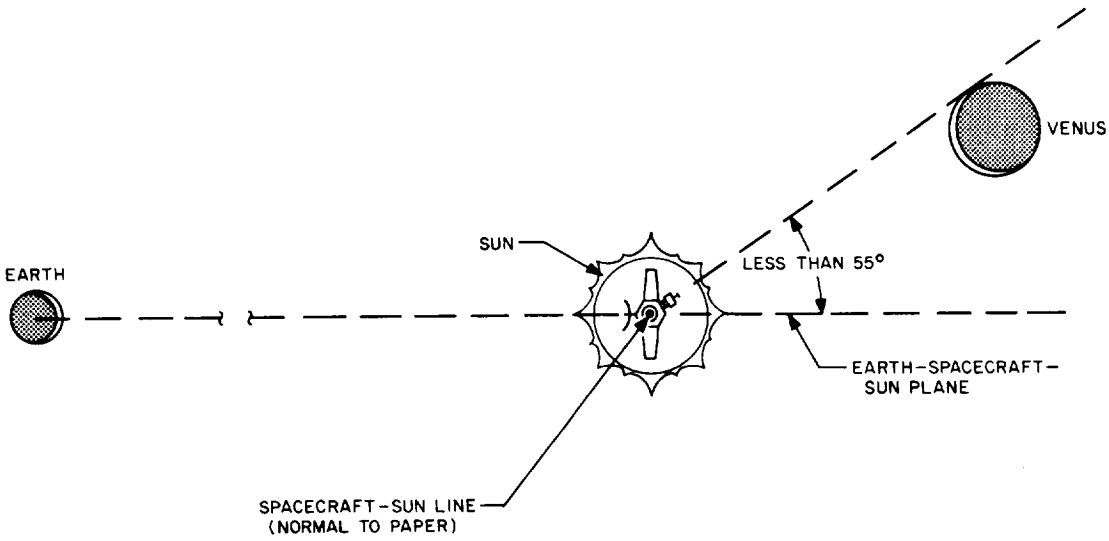

FIGURE 4–5.—Encounter geometry constraint resulting from radiometer limitations.

(a) The probability of Venus impact was to be less than one part in a thousand to avoid having to sterilize the spacecraft.
(b) When the spacecraft was to cross the Venus terminator plane, the planet (as viewed from the spacecraft) was to subtend an angle between 10° and 45° for magnetometer and radiometer considerations.
(c) The angle to be measured at the spacecraft between the Earth-spacecraft-Sun plane and the far edge of Venus, in the plane normal to the spacecraft-Sun direction, was not to exceed 55° because of radiometer limitations (fig. 4–5).
(d) Venus was not to occult the Sun from the spacecraft because of attitude control and power considerations.
(e) Because of Earth-sensor limitations (fig. 4–6), the angle between Earth, probe, and near limb of Venus was to remain greater than 60° until the radiometer scan went off Venus.

Four Phases of the Mariner R Trajectory

1. *Near-Earth ascent.* The ascent phase is divided into three portions: the powered-flight ascent, the parking-orbit coast, and postinjection ascent (fig. 4–7).

The first part of the ascent phase consists of an Atlas and Agena thrust period. At the end of the Agena thrust period, the spacecraft/Agena stage is placed in a

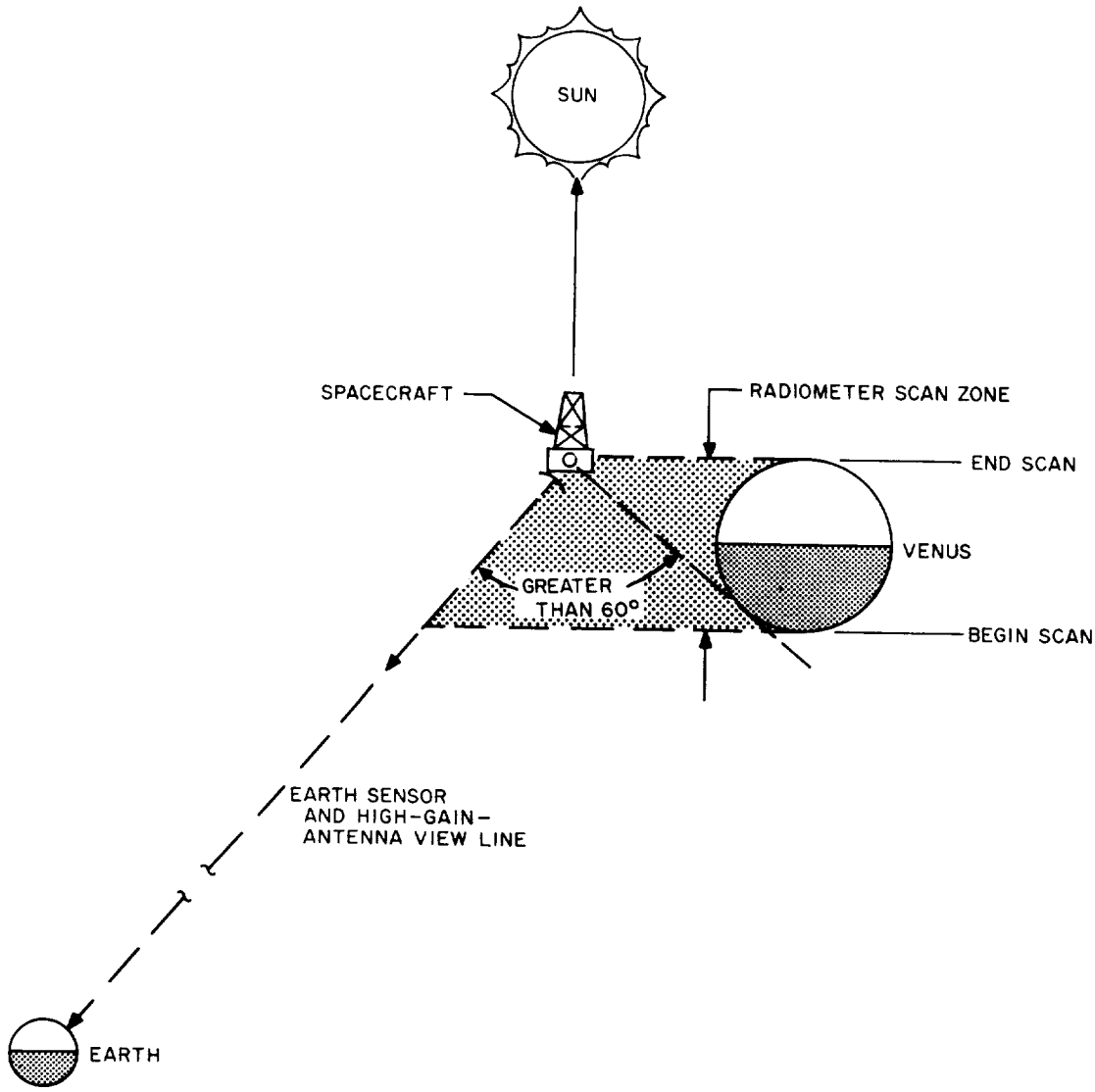

FIGURE 4-6.—Encounter geometry constraint resulting from Earth-sensor limitations.

187-km (116-mile) circular orbit. The spacecraft/Agena stage "coasts" in this orbit until the optimum point is reached for a final thrust phase (near perigee of the required escape hyperbola) at which time the Agena engine is restarted. Injection takes place upon termination of this final Agena thrust period.

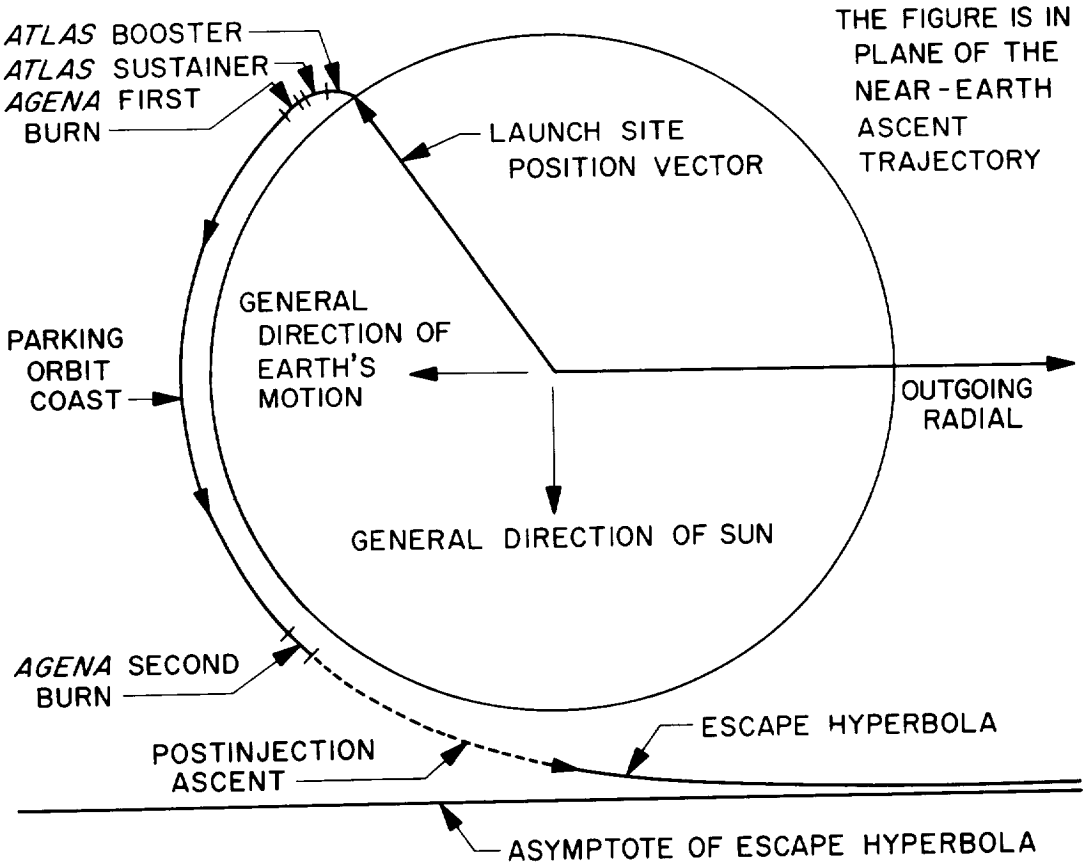

FIGURE 4–7.—Typical near-Earth Mariner Venus ascent trajectory profile.

The postinjection portion of the near-Earth ascent phase describes an escape hyperbola with the Earth center at the principal focus. A characteristic of the escape trajectory is that after a few hours the spacecraft travels essentially radially away from the Earth along the outgoing asymptote of the escape hyperbola. The direction of the outgoing radial is defined by its celestially referenced right ascension and declination. The value of the right ascension and declination is determined from the relative positions of the Earth at launch and Venus at encounter, and remains essentially fixed for a given launch date.

Since the launch site location remains at a fixed geographic latitude, the requirement of the near-Earth ascent phase is to match the powered-flight

portion (which begins at the launch site) to the required escape velocity vector. The escape velocity vector has a direction determined by the asymptote of the escape hyperbola. The hyperbolic excess speed is the geocentric speed which the spacecraft attains a few days after launch as it leaves the Earth's gravitational sphere of influence. (The magnitude of this hyperbolic excess speed is given by the square root of the injection energy.)

The line (outgoing radial) through the Earth's center, parallel to the asymptote of the escape hyperbola, and the geocentric position of the launch site define the plane of the near-Earth ascent trajectory.

As a result of AFETR range safety constraints, there is only a certain number of minutes in a given day of the launch opportunity during which the spacecraft can be launched, and this period varies throughout the launch opportunity. As the daily launch time increases, the launch azimuth also increases—from approximately 90° to 114° (fig. 4–4).

In addition to the launch azimuth change due to launch time delays, the parking-orbit coast time decreases as time increases through the daily launch window. The coast time decreases since the angle between the launch-site position vector and the outgoing radial (projected backward) gets smaller as the Earth rotates.

The change in both launch azimuth and parking-orbit coast time results in a wide geographic range of the injection locations. This variation of the injection location for a given launch date and arrival date, when projected onto the Earth's surface, describes the injection loci. As the launch and arrival dates change, different injection loci are generated.

2. *Heliocentric transfer.* The heliocentric transfer orbit is an ellipse that essentially intersects the Earth at launch and the planet Venus at encounter, with the Sun at one focus. The spacecraft escapes the Earth along its outgoing radial and at a speed determined by the specific energy imparted to the spacecraft. The hyperbolic excess velocity vector, plus the Earth's velocity vector about the Sun, add vectorially to determine the velocity at which the spacecraft enters the heliocentric orbit. Since the spacecraft is launched "backward" from the Earth's orbital velocity (fig. 4–8), the magnitude of the resultant velocity vector is smaller (relative to the Sun) than the Earth's, and the spacecraft falls in gradually toward the Sun (fig. 4–9).

As the probe falls in toward the Sun, it picks up speed and finally passes the Earth. The spacecraft goes through a very slow roll as it passes the Earth in order to keep its high-gain antenna and Earth sensor pointed toward the Earth. At this

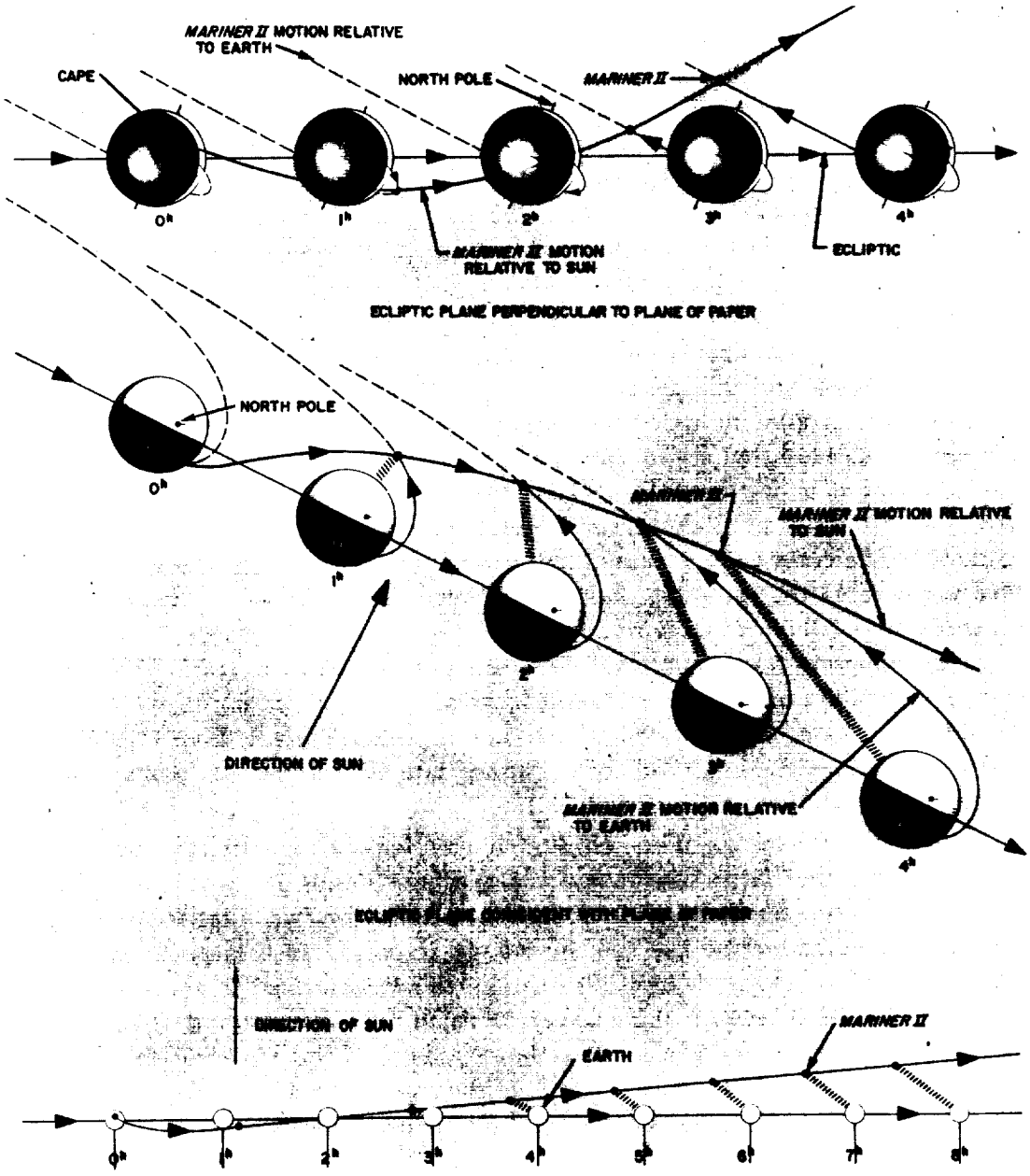

FIGURE 4–8.—Mariner II flight path relative to Earth and Sun.

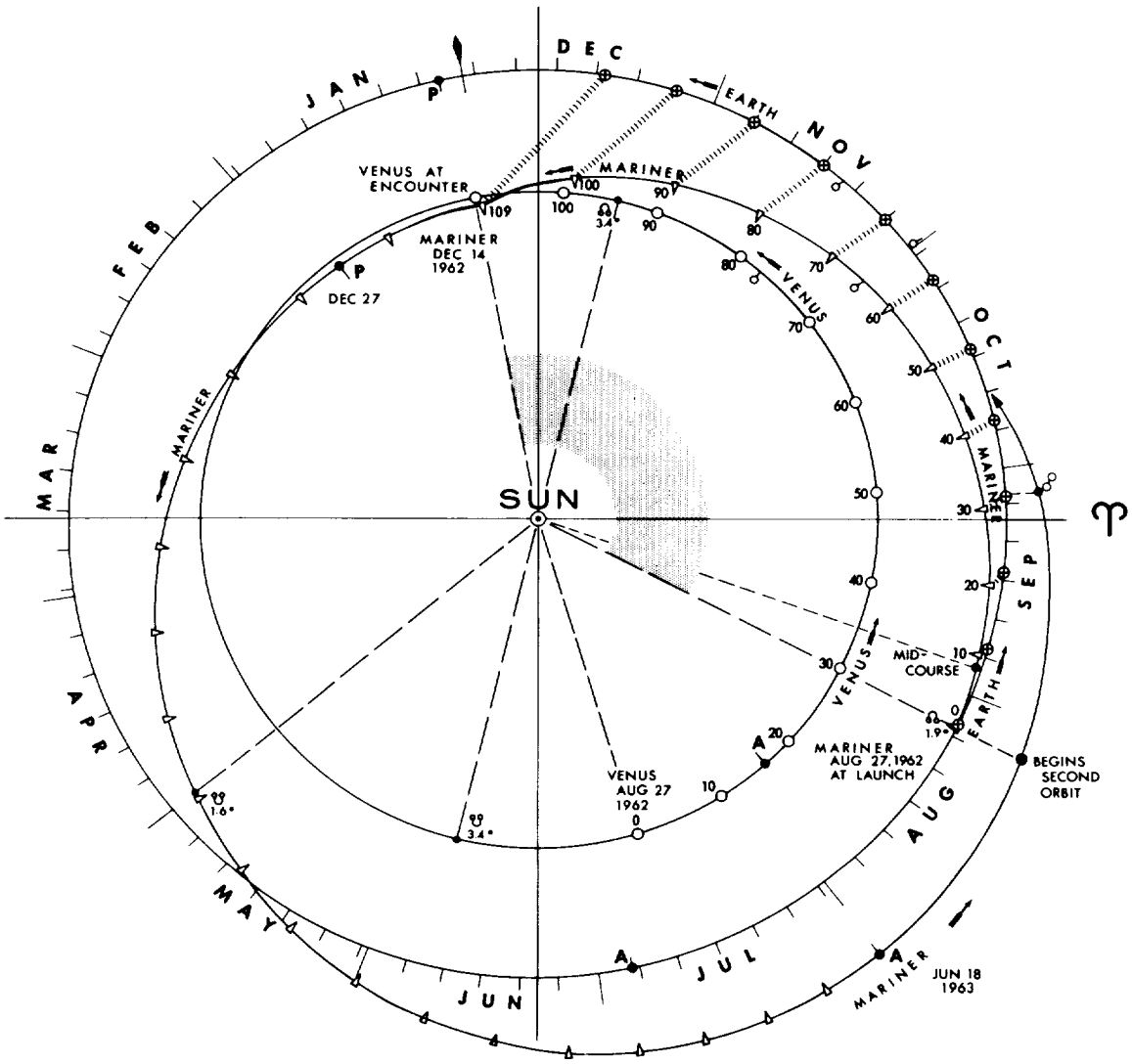

FIGURE 4–9.—Heliocentric plan view of Mariner II trajectory projected on the ecliptic plane.

time the Earth-spacecraft-Sun angle reaches a maximum which is less than 180°. The reason this angle does not reach 180° is that the probe is not in the ecliptic plane on its path to Venus. If this angle were to come too close to 180°, there

would be an attitude-control problem since the Mariner R spacecraft uses the Sun and the Earth for its attitude references.

3. *Venus encounter.* The third phase of the spacecraft's trajectory is the encounter phase when the primary source of gravitational attraction is the planet Venus. The trajectory of the spacecraft during the encounter phase is similar to the Earth ascent phase—both described by hyperbolas—except that during the encounter phase the spacecraft travels along an incoming hyperbolic path. Also, the altitude of the closest approach is several times greater for the Venus encounter phase than for the Earth ascent phase.

4. *Heliocentric orbit.* After Venus encounter and the hyperbolic escape from its sphere of influence, the spacecraft takes up a new heliocentric orbit (fig. 4–9). The parameters of the new elliptic orbit differ greatly from those of the pre-encounter orbit due to the large inertial perturbations introduced during the Venus encounter. The spacecraft acquires additional energy and has a greater heliocentric speed after encounter since the spacecraft approaches from "behind" Venus and travels in the same general orbital direction prior to encounter.

Basic Trajectory Characteristics

Studies of the relationship between flight time, launch date, and injection energy were made to reveal the acceptable launch intervals during the Venus-encounter launch opportunity in 1962.

Since there is a direct relationship between injection energy achievable from the booster and the weight of the spacecraft, a trade-off between the length of the firing period and spacecraft weight is evident. A design goal for the spacecraft of 450 pounds was finally established, allowing an approximate 55-day firing period for the two launchings. A decision was made that if the weight of the spacecraft after construction should be greater or less than the nominal 450 pounds, the firing period would then be altered accordingly. Changes in the performance of the Atlas-Agena boost vehicle would also reflect upon the length of the firing period. In order to include all feasible launch days, a firing period of 69 days was utilized in the trajectory design. This firing period extended from July 10 to September 15, 1962. Subsequent to spacecraft completion, however, the scheduled launch date of Mariner R–1 was established as July 21, 1962. The nominal launch date for Mariner R–2 was then to be 21 days after Mariner R–1 was launched.

Results of these studies are illustrated in figures 4–10 and 4–11. Two sets of closed contours, denoted types I and II, are presented. The characterizing dif-

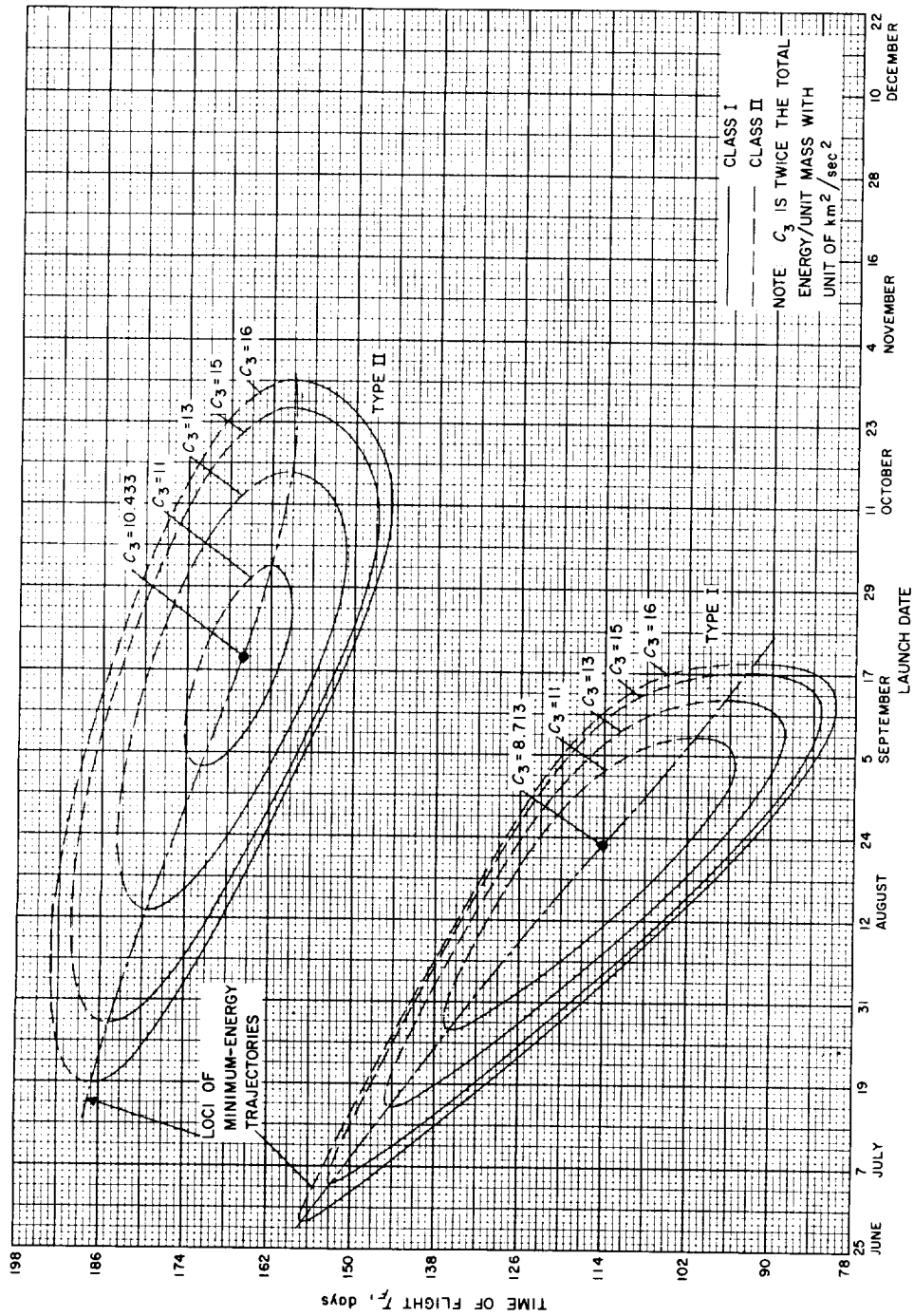

FIGURE 4–10.—Time of flight vs launch date.

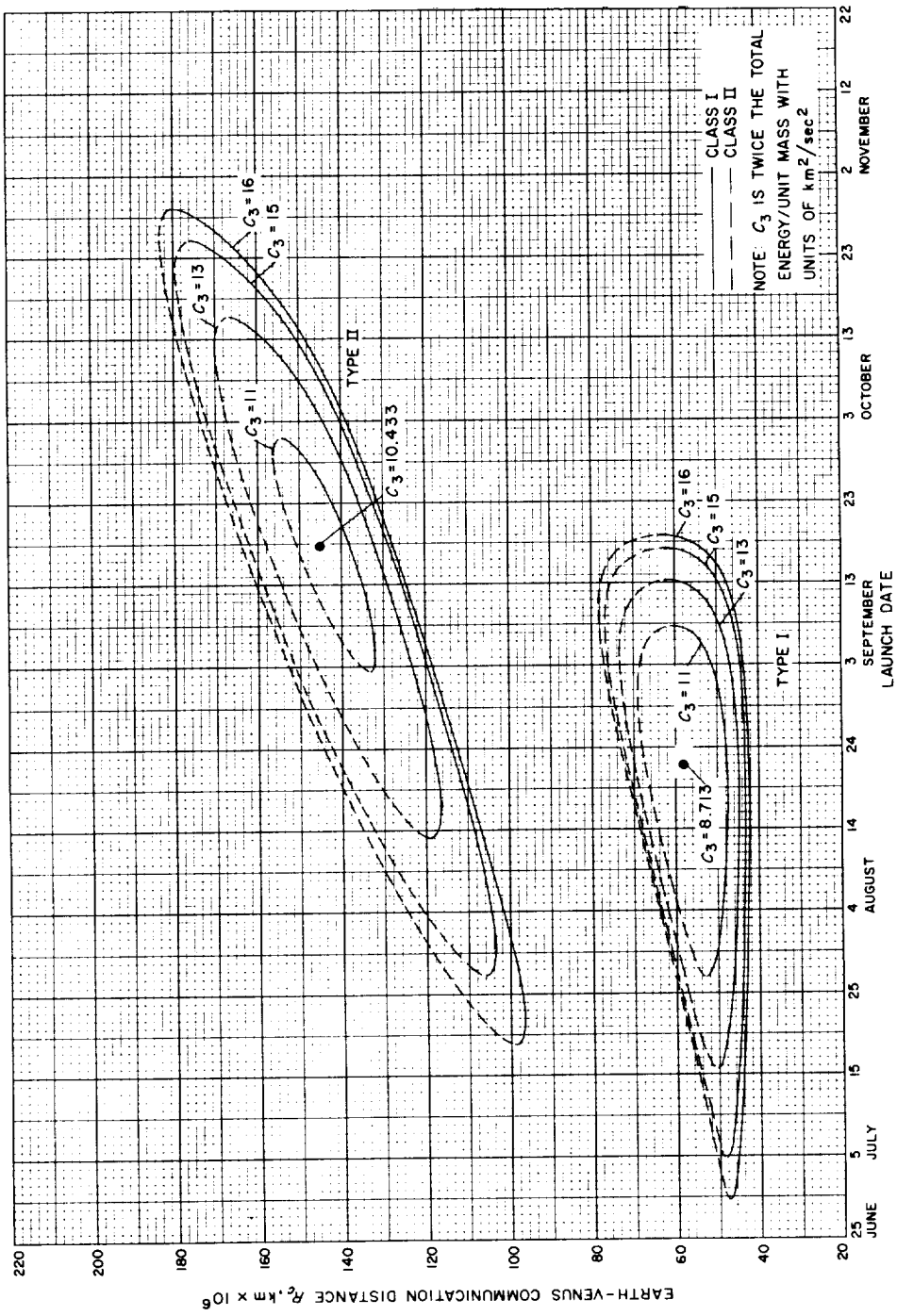

FIGURE 4–11.—Earth-Venus communication distance vs launch date.

ference between type I and type II trajectories was the heliocentric transfer angle that the spacecraft was to traverse from launch to encounter:

Type I: Less than 180°

Type II: Between 180° and 360°

Several important properties of these trajectories are as follows:

1. Type II trajectories have longer flight times and communications distances at encounter than type I.

2. For a given injection energy (C_3) and launch date, up to four different trajectories can be used.

3. For both type I and type II, there are minimum-energy transfers for each launch date (with absolute minimums occurring on August 23, 1962, for type I and on September 19, 1962, for type II).

4. For a given fixed energy above the absolute minimum, there is a corresponding launch interval or permissible firing period.

Type I transfers with their relatively short flight times and distances at encounter were selected for the Mariner R mission; type II trajectories were immediately discarded because of their long flight times and communications distances. After checking all type I transfers, it was decided to use a trajectory near minimum energy for each launch date. Such transfers (a) satisfied all constraints mentioned proviously, (b) assured that a maximum firing period would ultimately be available once the spacecraft was built and the maximum injection energy attainable by the Atlas-Agena launch vehicle was calculated, and (c) produced hyperbolic excess speeds at Venus (and relative to Venus) which were almost a minimum, thereby maximizing the time which the spacecraft would spend in the near vicinity of the planet.

The arrival dates of the minimum-energy trajectories which were selected for the Mariner R missions varied with the day of launch and time of flight (table 4–I); the trajectories essentially followed the minimum-energy loci of the type I trajectories. For these trajectories, the Earth-Venus communication distance at encounter varied from 51.7×10^6 to 58.9×10^6 km (32.1×10^6 to 36.6×10^6 miles), which was safely less than the 1×10^8 km (6×10^7 miles) maximum distance permitted by communication system constraints. The time of closest approach to Venus for each selected arrival date was chosen to correspond to the middle of the Goldstone daily viewing period.

Targeting studies were conducted of the near-Venus trajectories to choose the aiming point. The aiming point for Venus encounter was determined principally by space-science-instrumentation, communication, and spacecraft

constraints. Subject to these constraints, a design aiming point on the trailing edge of Venus was selected within the acceptable region shown in figure 4–12. The plane of the coordinate system in figure 4–12 is normal to the incoming asymptote and passes through the center of Venus.

Table 4–I.—Schedule of launch and arrival dates

Launch date, 1962	Flight time, days	Arrival date, 1962: GMT
July 10–July 17	149–142	Dec. 6; 18:14
July 18–July 27	143–134	Dec. 8; 18:08
July 28–Aug. 6	135–126	Dec. 10; 18:03
Aug. 7–Aug. 16	127–118	Dec. 12; 17:57
Aug. 17–Aug. 31	119–105	Dec. 14; 17:55
Sept. 1–Sept. 15	106–92	Dec. 16; 17:53

In order to facilitate error analysis and other trajectory computations, a virtual aiming point is selected (fig. 4–3). The virtual aiming point is defined by using three orthogonal unit vectors **R, S,** and **T**. The unit vector **S** coincides with, and is in the direction of, the incoming radial (i.e., through the planet center and parallel to the asymptote of the encounter hyperbola); the unit vector **T** lies in the ecliptic plane and points in a direction generally away from the Sun; the unit vector **R** completes the right-handed orthogonal set. The aiming-point (or miss [3]) parameter **B** is divided into components along **T** and **R** which are called **B·T** and **B·R**. The components **B·T** and **B·R** define the virtual aiming point in the plane normal to the incoming asymptote and passing through the center of Venus.

The nominal Mariner R design aiming point had components $\mathbf{B}\cdot\mathbf{T} = -29\,545$ km ($-18\,358$ miles) and $\mathbf{B}\cdot\mathbf{R} = +5210$ km ($+3237$ miles). The magnitude of the closest approach distance (not **B**) to the center of Venus was 20 000 km (12 427 miles) for this aiming point.

Trajectory Ephemerides, Targeting Criteria, and Firing Tables

The Mariner R trajectory ephemerides and targeting criteria were developed to satisfy strict mission objectives and their constraints. Studies of the relation-

[3] By definition of **B**, values of "miss distance" refer to the distance from the center of the planet and not to the distance from the surface of the planet nor to the distance from an aiming point.

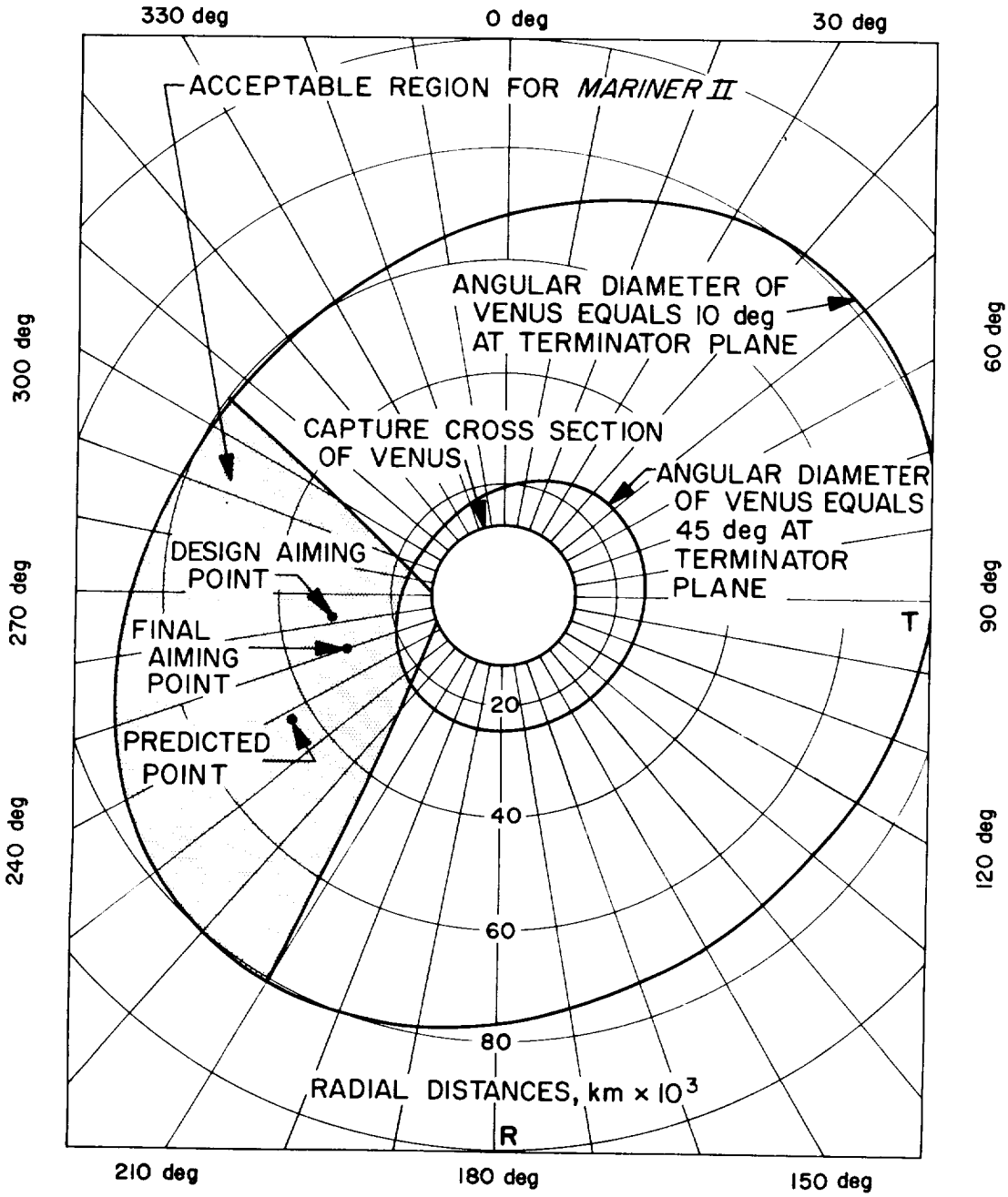

FIGURE 4–12.—Mariner II aiming zone chart.

ship between the various ballistic conditions were first conducted to reveal the acceptable launch intervals and characteristics of the various trajectories. Preparation of the trajectory ephemerides and targeting criteria required detailed simulation of: (1) the Atlas-Agena boost (ascent) trajectory as constrained by the guidance system parameters (equations) and (2) the free-flight trajectory from injection to target, under the influence of the Earth, Moon, Venus, Jupiter, Sun, and solar wind (plasma) pressure.

Then, after considering all mission constraints that would be placed upon the flight path, the families of Mariner trajectories were selected and their ephemerides computed precisely on the IBM 7090 computer. A targeting criteria specification was also prepared for the boost-vehicle contractor's use in generating the firing tables.

Computations were made for a 93° to 111° launch azimuth corridor, an approximate 2-hour daily firing window, and injection locations that were confined to a region of about 6° in latitude and 35° in longitude, in the South Atlantic Ocean off the coast of Africa and near Ascension Island.

ORBIT DETERMINATION

Tracking Data Editing and Orbit Determination Programs

The Mariner R orbit determination operations were centered around two digital computer programs: the tracking data editing program (TDEP) and the orbit determination program (ODP). These programs and their relationship to each other are depicted schematically in figure 4–13.

The TDEP functioned as a service program to the ODP; its principal functions were to:

1. Remove blunder (error) points from the input data.
2. Use data-compression methods to reduce the amount of data that the ODP was to process.
3. Reduce input data received from different tracking sources to a uniform format for the ODP.
4. Compile ancillary data which the ODP needed to utilize the tracking data.

The TDEP was essentially an elaborate bookkeeping program. It accepted as inputs: the tracking data, portions of the tracking station reports, and computer control cards, which allowed an operator certain options on how the data would be handled.

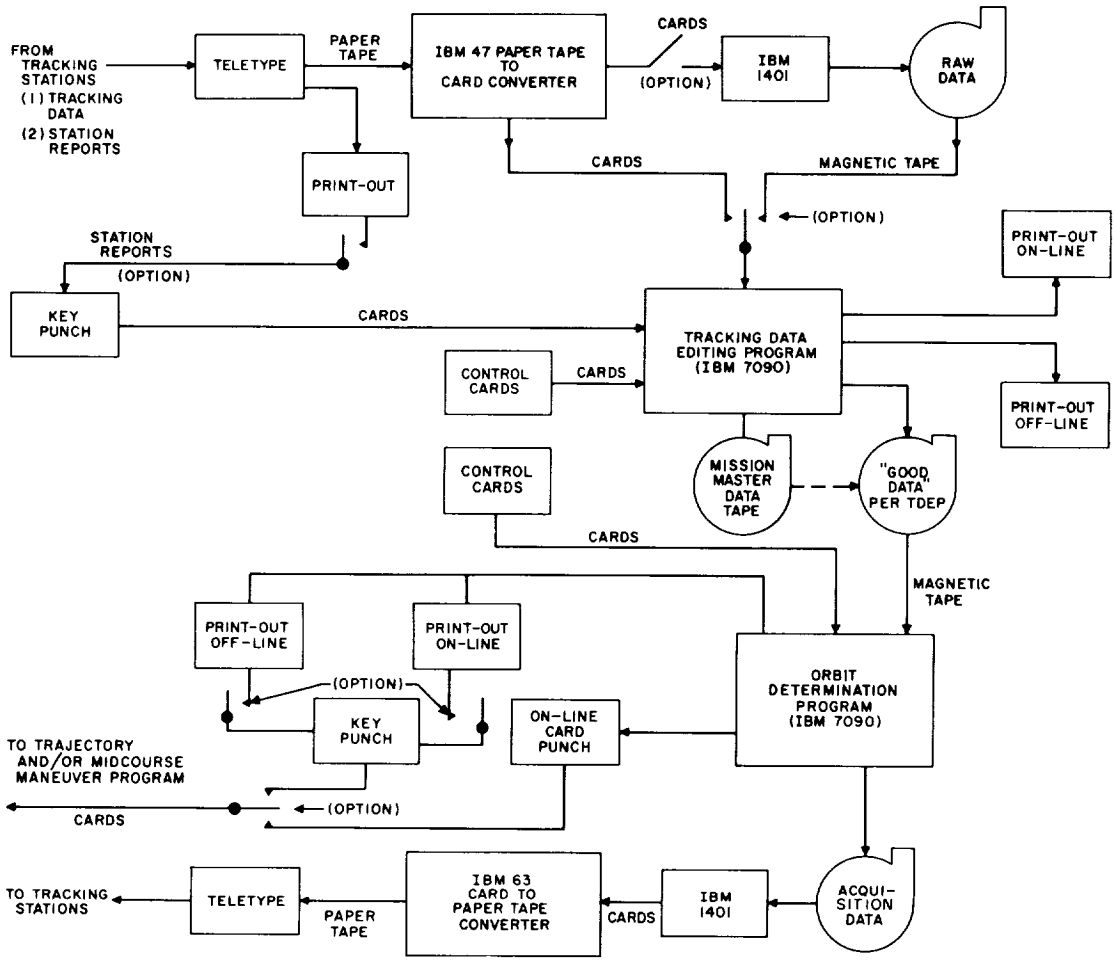

FIGURE 4–13.—Functional block diagram of orbit determination operations.

Aside from the use of the control cards, the editing of the TDEP was limited to removing automatically the blunder points caused by such things as teletype transmission errors (when unrecognizable characters occurred) or out-of-limit values. This editing was most important during the early phase of the mission because of the relatively small amount of data available. At that stage, gross blunders have a strong effect on the "least squares" solution to the orbit as determined by the ODP.

All Deep Space Instrumentation Facility (DSIF) tracking data had to be

converted into a format that the ODP was equipped to handle. As an example, the ODP assumed that all counted Doppler data were labeled with the event time which occurred at the middle of the Doppler count interval. This meant that all DSIF-counted Doppler data which were tagged with the time occurring at the end of the count had to be "re-time-tagged" by the TDEP. In addition, the ODP needed to know the duration of the sample time interval, Doppler count, tracking station identification, and transmitter frequency. The TDEP compiled all this information from the tracking data messages, station report messages, and control card inputs, and either labeled the appropriate tracking data or passed the information on to the ODP in tabular form.

The TDEP provided both "on-line" and "off-line" print-outs for a visual record of the data state, amount of data discarded (and why), and the systems the operator had selected. In addition, it compiled a mission master data tape which included all tracking data that might be useful; that is, the master tape included certain data which were currently considered "bad" but which the operator might want to use on option. A separate data tape (which contained a subset of the data from the master tape) was prepared as an input tape to the ODP. This data tape contained only "good" data which the operator had selected to determine the orbit.

The ODP accepted the mission master data tape from the TDEP and proceeded to determine the orbit, using the trajectory program in subroutine form as a model for a least-squares solution. A "3-times-standard deviation" (3σ) option allowed the ODP to edit statistically the input tape from the TDEP and to construct its own "good data" records for future use.

The orbit determination method was based on the fact that computed values of the Doppler observables may be obtained by integrating the equations of motion of the spacecraft and by taking into account the observation times, station coordinates, and speed of light. Partial derivatives of observables with respect to initial conditions were also available. Initial conditions were used here in the sense of any parameter that affects the trajectory. These partial derivatives were obtained by solving a set of variational differential equations in addition to the usual equations of motion. Finally, the partial derivatives with respect to nondynamical constants, such as station locations, were easily available.

The observable and partial derivative quantities were used in an iterative weighted least-squares procedure which adjusted the values of the initial condi-

tions and station locations so that the weighted sum of squares of residuals between observed and computed data points was a minimum. *A priori* information about the initial conditions was also treated as data and formed part of the quantity to be minimized.

The output of the ODP included: acquisition data for the tracking stations (which were transmitted via teletype), data cards used as inputs to the midcourse maneuver program, and print-outs which described the characteristics of the predicted spacecraft trajectory.

Effects of Tracking Data Accuracy

The quality of the tracking data received from the DSIF constituted a significant factor in the success of the Mariner II mission (fig. 4–14). Special calibration, maintenance, operating, and analytical procedures were performed by the DSIF in recognition of the following relationships:

(1) The manner in which tracking measurements are obtained, and also the equipment used to produce them, establish the quality of the tracking data.

(2) The quality of the tracking data has a direct effect on the accuracy of orbit determination.

(3) Establishing and maintaining such accuracy is of paramount importance, since the midcourse maneuver and the trajectory are determined directly from orbital data.

The performance of the DSIF insured successful fulfillment of the data accuracy requirements.

Values of Mariner II Target Parameters

The Mariner II premidcourse orbit was determined on the basis of data received from the DSIF tracking stations in Johannesburg, Woomera, and Goldstone. Values of the target parameters derived from the premidcourse orbit determination are given in table 4–II. The primary data types were coherent pseudo-two-way Doppler from Goldstone and coherent two-way Doppler from the other two stations. Angle data were also used for the first 15 hours of flight.

The Mariner II postmidcourse orbits were determined on the basis of data received from the DSIF tracking stations in Johannesburg and Goldstone. The target parameters corresponding to various solutions are given in table 4–II. Coherent two-way Doppler data from the Johannesburg and Goldstone Echo

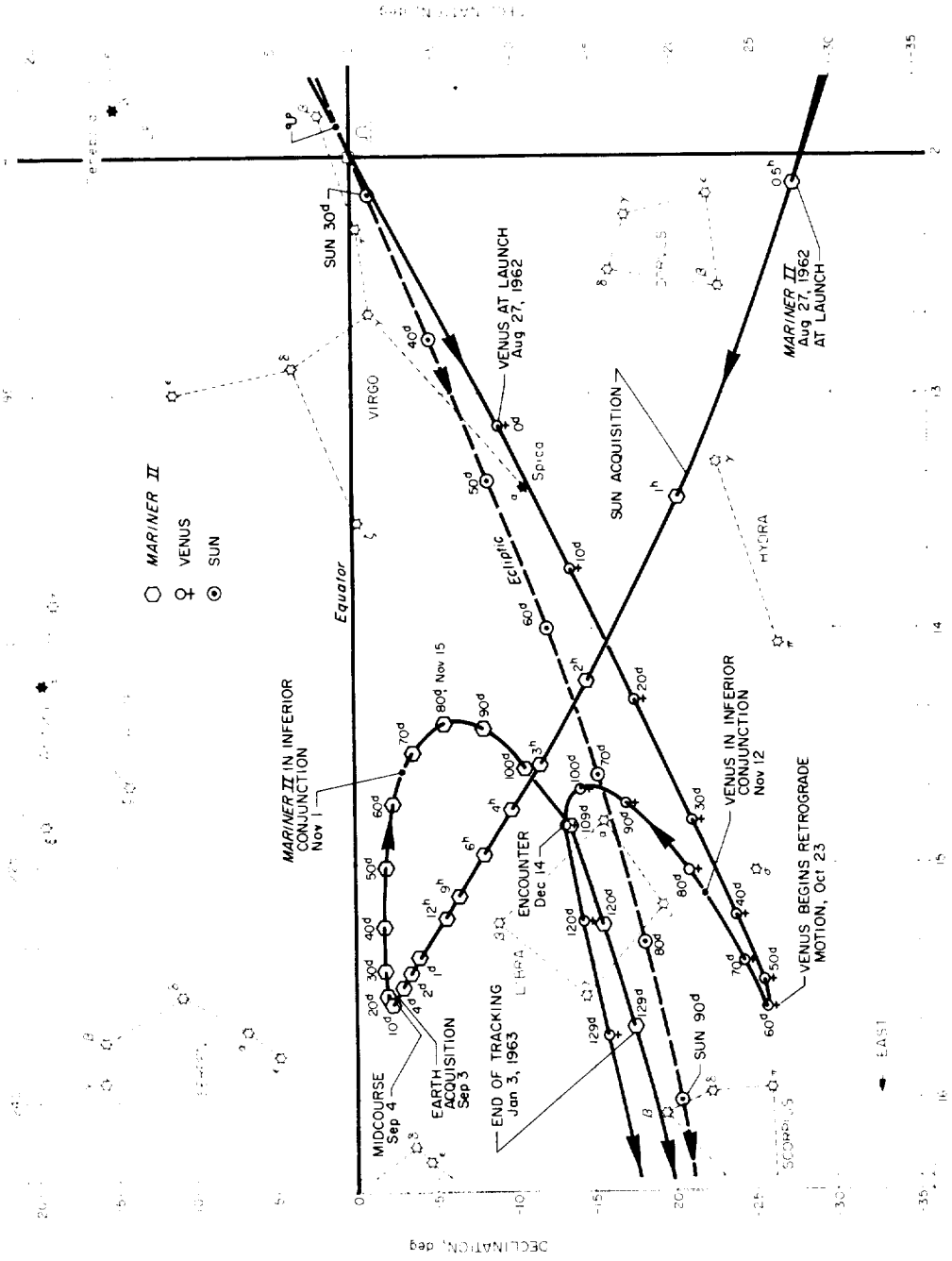

FIGURE 4–14.—Celestial path of Mariner II.

Stations and coherent pseudo-two-way Doppler from the Goldstone Pioneer Station were used. After September 9, the DSIF stations normally tracked only 1 day per week. No angle data were used in the postmidcourse-orbit determinations.

Values of the postmidcourse-orbit target parameters in table 4–II changed with additional data from each weekly pass. The effects of inaccuracies in station locations and in the astronomical unit were not considered in arriving at the results.

Table 4–II.—Values of the Venus target parameters prior to December 7, 1962

Condition	B, km	B·T, km	B·R, km	Radius of closest approach, km	Time of closest approach (Dec. 14, 1962), GMT
Premidcourse orbits: no advance information,[a] epoch of Aug. 27 at 07:19:19.000 GMT	394 293	291 715	−265 272	384 180	
Postmidcourse orbits: advance information,[a] epoch of Sept. 5 at 00:23:32.000 GMT					
Data used from epoch to					
Sept. 9	53 159	−42 655	31 725	43 314	19:31:46
Sept. 15	49 921	−39 768	30 176	40 153	19:12:59
Sept. 24	49 850	−39 722	30 120	40 083	19:14:47
Oct. 7	50 839	−41 473	29 404	41 042	19:47:05
Oct. 15	50 869	−41 590	29 291	41 071	19:50:35
Oct. 25	50 690	−41 581	28 992	40 895	19:55:12
Oct. 28	50 549	−41 543	28 798	40 756	19:56:50
Nov. 5	50 177	−41 351	28 420	40 392	19:59:18
Nov. 11	50 050	−41 282	28 298	40 269	19:59:53
Nov. 17	49 931	−41 189	28 223	40 152	20:00:05
Nov. 26	49 712	−41 068	28 012	39 938	20:00:32
Dec. 1	49 709	−41 066	28 009	39 935	20:00:32

[a] The advance information consisted of a covariance matrix corresponding to a set of nominal position and velocity components at epoch. This matrix expressed the uncertainty assumed to exist in the premidcourse-orbit solution and in knowledge of the midcourse maneuver.

Data covering the period from December 7 to the end of the mission showed that the encounter parameters were:

B·T	41 481 km (25 775 miles)
B·R	29 244 km (18 171 miles)
B	50 753 km (31 536 miles)
Radius of closest approach	40 954 km (25 448 miles)
Time of closest approach (Dec. 14)	19:59:28 GMT

The Mariner II Trajectory

The Mariner II spacecraft was launched at a booster roll azimuth[4] of 107.5° east of north. During the Atlas sustainer and vernier stages, adjustment in vehicle attitude and engine cutoff times was commanded to adjust the altitude and velocity at Atlas vernier-engine cutoff. After the Atlas-Agena separation, there was a short coast period prior to the first Agena ignition. At a preset value of velocity increment, the Agena engine was shut off; then both the Agena and the attached spacecraft were in a circular parking orbit at a distance of approximately 187 km (116 miles) from the Earth's surface and were traveling at a speed of 7.8 km/sec (4.8 miles/sec) (space-fixed). After a total coast time of 16.3 min in the parking orbit, the second Agena ignition was initiated. The parking-orbit coast time was determined after lift-off by the ground guidance computer and transmitted to the Agena during the Atlas vernier stage.

At the end of Agena final cutoff (26 min, 3 sec after liftoff), the Agena with the spacecraft was traveling at a speed of 11.41 km/sec (7.09 miles/sec) (space-fixed). The latitude and longitude of injection (Agena cutoff) into the geocentric hyperbolic orbit were −14.8° and +357.9°, respectively, injection thus taking place over the south Atlantic Ocean. The geocentric characteristics of the Mariner II trajectory are listed in table 4–III.

Within an hour after injection, the spacecraft was receding from the Earth in an almost radial direction with decreasing speed. This reduced the geocentric angular rate of the spacecraft in inertial coordinates until, at 1.3 hours after injection, the rotational rate of the Earth exceeded the spacecraft's geocentric angular rate (fig. 4–15). The direction of the spacecraft's Earth track then reversed from increasing to decreasing longitude over the Earth's surface.

After several hours of continuous tracking, it was estimated that the spacecraft would miss Venus with a closest approach radius of approximately 384 000 km (239 000 miles) on the leading edge, passing slightly above the planet in its

[4] Due to the Earth's rotation, the direction in which the booster vehicle should fly is constantly changing. The Atlas rolled to the proper bearing (107.5°) from its initial bearing of 105°, shortly after lift-off. The Atlas then performed a gradual gravity-pitch maneuver from the vertical in the desired flight direction, 15 sec after lift-off.

orbital revolution around the Sun, and with a flight-time error of approximately −1 day. Comparison of these results with the desired Venus Sun-side pass indicated that the launch-vehicle's injection guidance system had performed within 3σ (three times the standard deviation) of the nominal values. The results indicated, however, that no useful encounter data could be obtained, and that a midcourse maneuver would be required.

Table 4-III.—Geocentric characteristics of Mariner II trajectory

	Geocentric injection	Postmidcourse orbit	Postencounter epoch of Dec. 7, 1962
Parameter			
Radius, R, km	6 581. 582 9	2 408 739. 5	481 240 41
Inertial speed, V, km/sec	11. 410 720	2. 988 012 2	14. 156 288
Earth-fixed speed, v, km/sec	11. 006 321	175. 486 47	3 437. 172 4
Geocentric latitude, ϕ, deg	−14. 843 545	−2. 436 175 6	−11. 330 543
Longitude, θ, deg	357. 855 51	244. 190 18	144. 053 87
Right ascension, H, deg	82. 734 037	233. 708 90	219. 337 85
Path angle of inertial velocity, Γ, deg	1. 830 689 6	89. 366 651	70. 676 903
Azimuth of inertial velocity, Σ, deg	118. 714 12	58. 845 343	127. 429 84
Path angle of Earth-fixed velocity, γ, deg	1. 897 978 1	0. 975 563 59	0. 222 685 51
Azimuth of Earth-fixed velocity, σ, deg	119. 875 11	270. 005 58	269. 952 53
Time of event, T, GMT	07:19:19 Aug. 27, 1962	00:23:32 Sept. 5, 1962	00:00:00 Dec. 7, 1962
Hyperbolic orbital element			
Semimajor axis, a, km	43 910. 177		
Eccentricity, e	1. 149 744 4		
Inclination to Earth's equator, i, deg	32. 031 083		
Longitude of ascending node, Ω, deg	237. 670 91		
Argument of perigee, ω, deg	205. 459 53		
Perigee distance, q, km	6 575. 303 3		
Time of perigee passage, T, GMT	07:18:45 Aug. 27, 1962		

The entire midcourse maneuver took approximately 34 min. At the time of the maneuver, the spacecraft had reached a distance of 2.4×10^6 km (1.5×10^6 miles) from Earth and was moving primarily under the influence of the Sun in an elliptical orbit with the Sun at a focus. Its speed was 2.98 km/sec (1.85 miles/sec) with respect to the Earth and 26.9 km/sec (16.7 miles/sec) with respect to the Sun. Postmidcourse orbit computations indicated that a projected closest approach radius of approximately 41 000 km (25 000 miles) and a flight-time

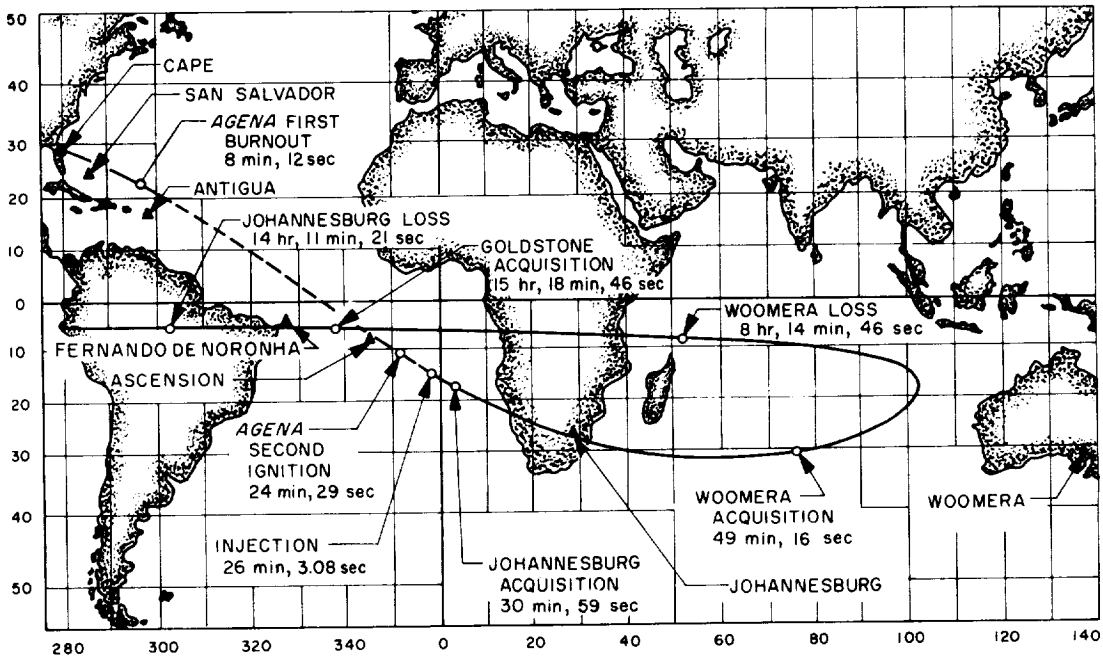

FIGURE 4–15.—Earth track of Mariner II showing turnaround effect caused by Earth's rotation.

error of approximately +0.14 day had been achieved by execution of the maneuver.

As the spacecraft continued out of the gravitational influence of the Earth, it followed the Earth around the Sun, but at a reduced speed (fig. 4–16). Slowly, Mariner II curved in toward the Venus orbit with increasing heliocentric speed, so that, at 65 days after launch, it passed the Earth in its orbital revolution around the Sun. Figures 4–17 to 4–22 present curves of geocentric radius, geocentric speed, heliocentric speed, spacecraft-Venus distance, geocentric declination, and Earth-spacecraft-Sun angle as functions of flight time from launch to Venus encounter. Note in figure 4–22 that the maximum Earth-spacecraft-Sun angle was approximately 167°, rather than 180°, when the spacecraft passed Earth in its orbital revolution around the Sun. (If the inclination of the heliocentric-transfer orbital plane to the ecliptic plane had been 0°, the maximum Earth-spacecraft-Sun angle would have reached 180°.) The heliocentric and aphrodiocentric characteristics of the Mariner II trajectory are shown in tables 4–IV and 4–V.

Sixteen orbital computations were made during the interplanetary phase of the flight, covering the period from the midcourse maneuver on September 5 to December 7, when the mass of Venus caused the first detectable perturbation in the Mariner II trajectory. During the period December 8 to 18 (see fig. 4–23), fourteen computations were made. Of these, eight preceded Venus encounter

Table 4–IV.—Heliocentric orbital elements of Mariner II trajectory

Elliptical orbital element	Pre-encounter orbit	Post-encounter orbit
Semimajor axis, a, km	127 198 500	144 419 000
Eccentricity, e	0. 191 186 1	0. 270 075 7
Inclination to ecliptic, i, deg	1. 850 642	1. 664 805
Longitude of ascending node, Ω, deg	332. 667 2	42. 708 12
Argument of perihelion, ω, deg	172. 158 5	83. 644 02
Perihelion distance, q, km	102 879 900	105 414 900
Time of perihelion passage, T, GMT	12:25:35 Jan. 7, 1963	05:15:46 Dec. 28, 1962

Table 4–V.—Aphrodiocentric orbital elements of Mariner II trajectory

Hyperbolic orbital element	Venus-encounter orbit
Semimajor axis, a, km	10 971. 61
Eccentricity, e	4. 732 749
Inclination to ecliptic, i, deg	134. 899 3
Longitude of ascending node, Ω, deg	216. 745 8
Argument of periapsis, ω, deg	236. 826 7
Periapsis distance, q, km	40 954. 24
Time of periapsis passage, T, GMT	19:59:28. 3 Dec. 14, 1962

and six followed. On the basis of these fourteen computations, it was determined that the closest approach to the surface of the planet was 34 854 km (21 645 miles), occurring at 19:59:28, Dec. 14, 1962. Spacecraft velocity at the time was 6.743 km/sec (4.188 miles/sec) relative to Venus; the heliocentric latitude of Venus and the spacecraft above the ecliptic was 1.43°; the elapsed time from injection to closest approach was 109.546 days. Additional pertinent data are:

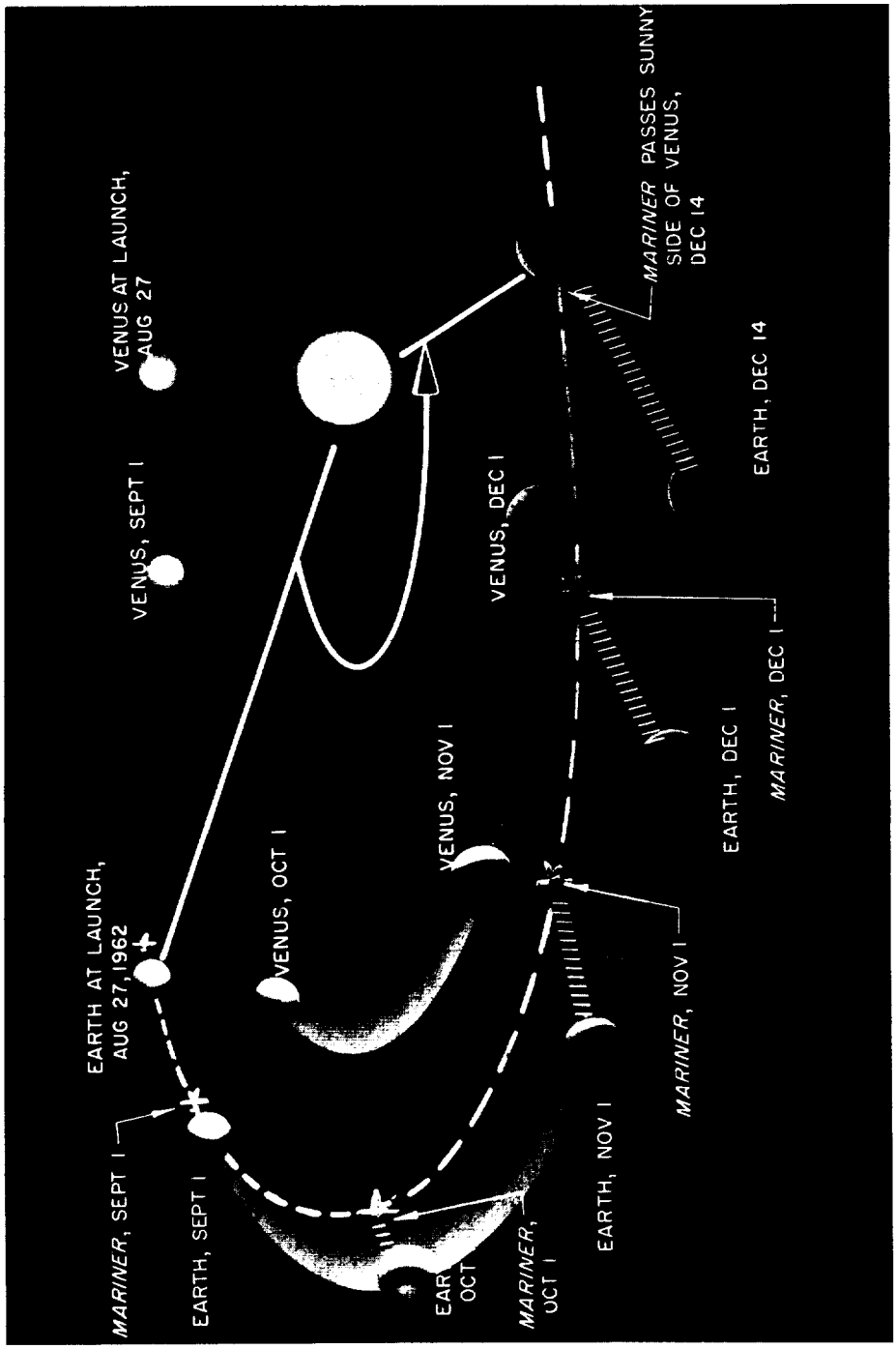

FIGURE 4–16.—General relationship of Earth, Venus, and Mariner II during cruise to encounter.

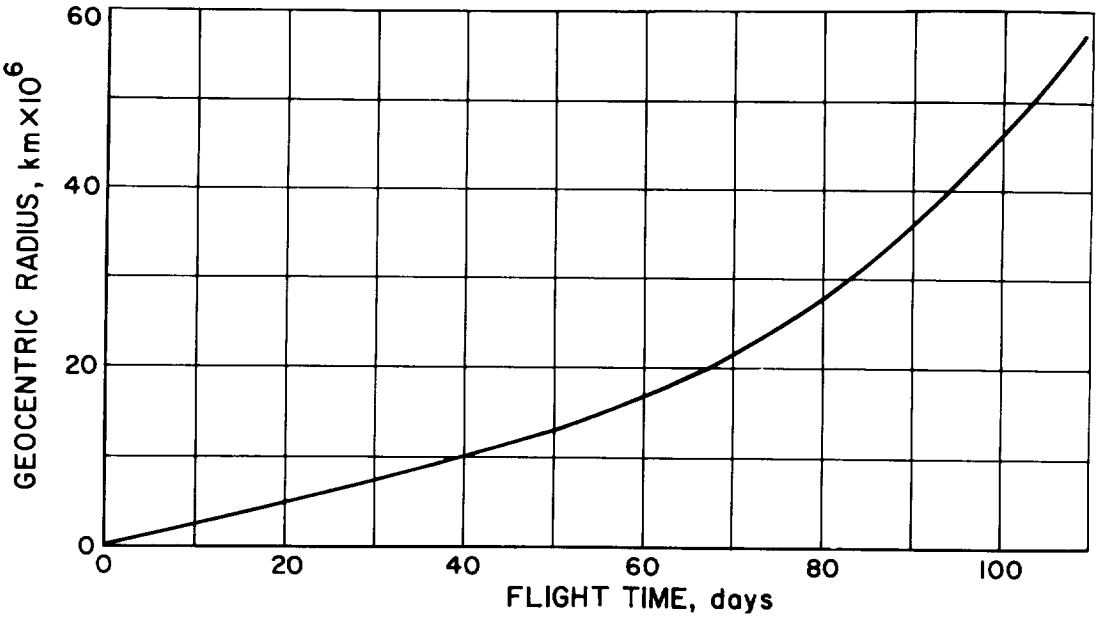

FIGURE 4–17.—Geocentric radius vs flight time.

Distance from Earth	57.785×10^6 km (35.907 million miles)
Distance from Sun	107.557×10^6 km (66.834 million miles)
Velocity relative to Earth	18.115 km/sec (11.256 miles/sec)
Velocity relative to Sun	39.490 km/sec (24.538 miles/sec)

Mariner II approached Venus along the trailing edge and from outside the planet's orbit. Figures 4–24 and 4–25 illustrate the planetocentric geometry of the flight past Venus. At about 65 min before closest approach, or at a distance of about 47 400 km from the planet's center, the radiometer commenced to scan the planet. At a distance of about 41 800 km from the planet's center, 42 min later, the scan moved permanently off the planet because of the angular movement of the spacecraft in its hyperbolic orbit about Venus.

The planet's gravitational pull altered the spacecraft's heliocentric orbit, as it left the vicinity of Venus, to such an extent that the perihelion distance changed from 102 880 000 to 105 415 000 km (63 926 000 to 65 502 000 miles), and the time of perihelion passage changed from Jan. 7, 1963, to Dec. 28, 1962 (fig. 4–9). The aphelion distance changed from about 151 500 000 km (94 100 000 miles) to about 183 423 000 km (113 973 000 miles), and its passage was predicted

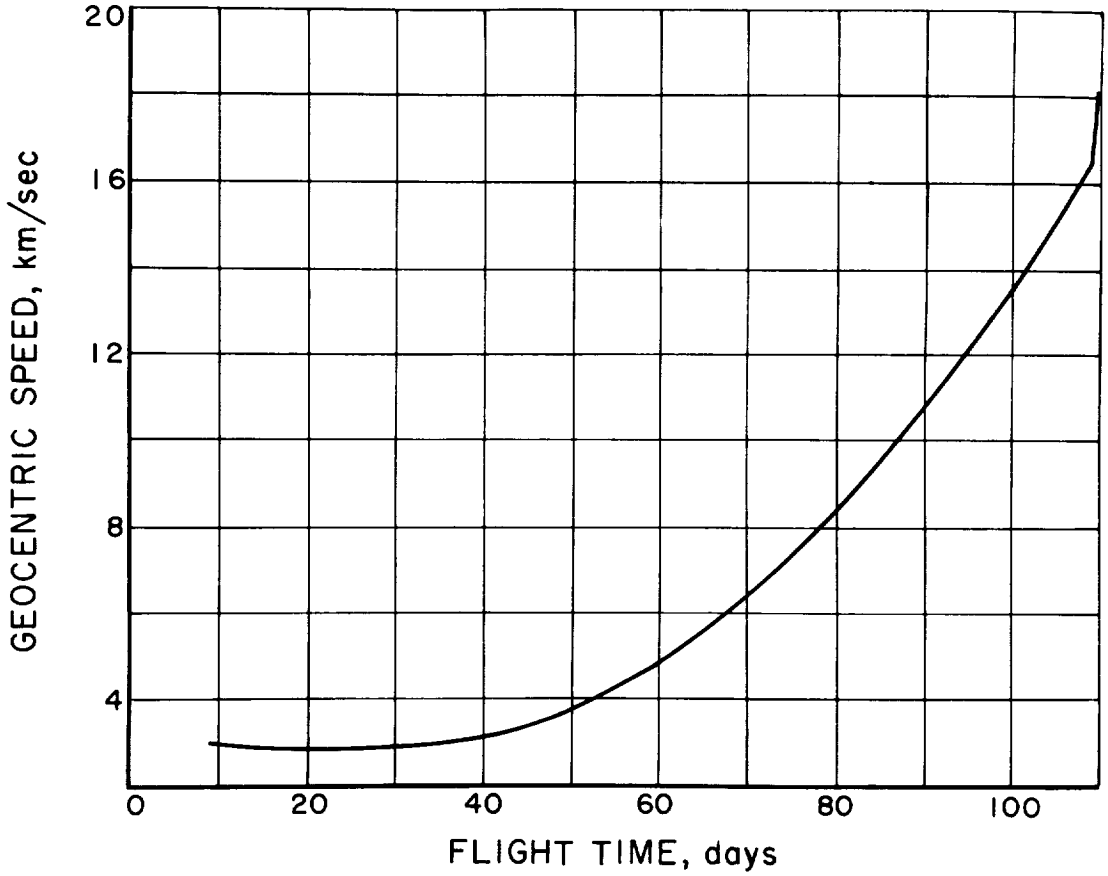

FIGURE 4–18.—Geocentric speed vs flight time.

for June 19, 1963. Curves of additional spacecraft-related parameters near Venus are presented in figures 4–26 to 4–29.

MIDCOURSE TRAJECTORY CORRECTION

Effects of Injection Accuracy

When a spacecraft is actually launched, it will not, in general, be injected precisely into the desired, or standard, trajectory because of small errors in the guidance system components. The accuracy of the Atlas-Agena was such that a midcourse correction was needed to satisfy the Mariner R mission requirements; a statistical description of the coordinate deviations at injection

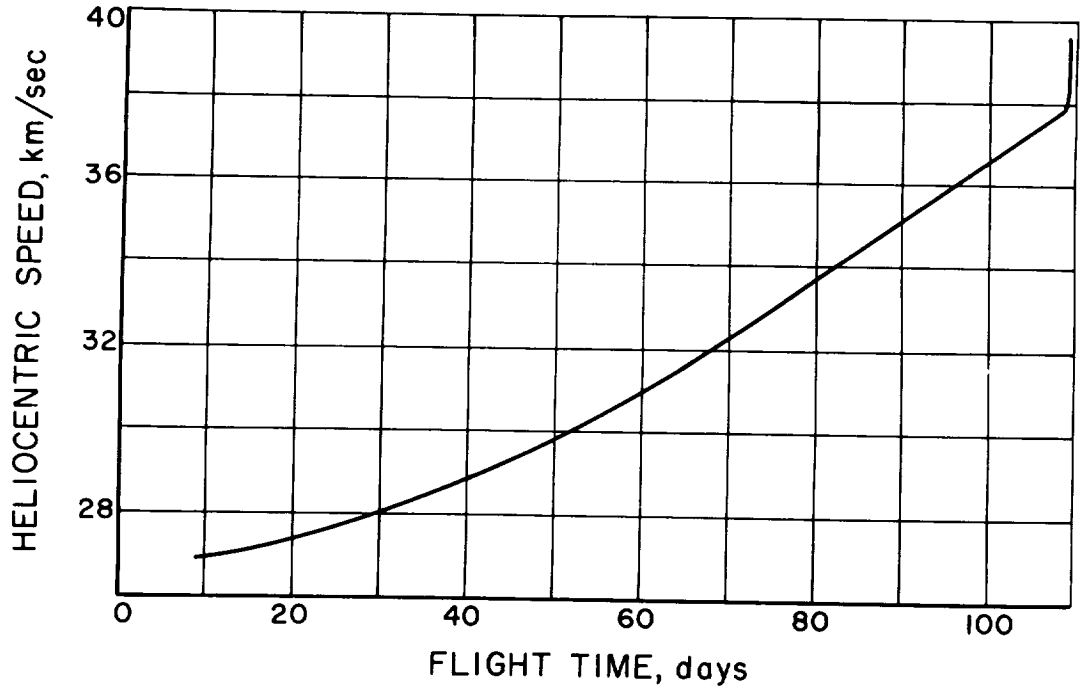

FIGURE 4–19.—Heliocentric speed vs flight time.

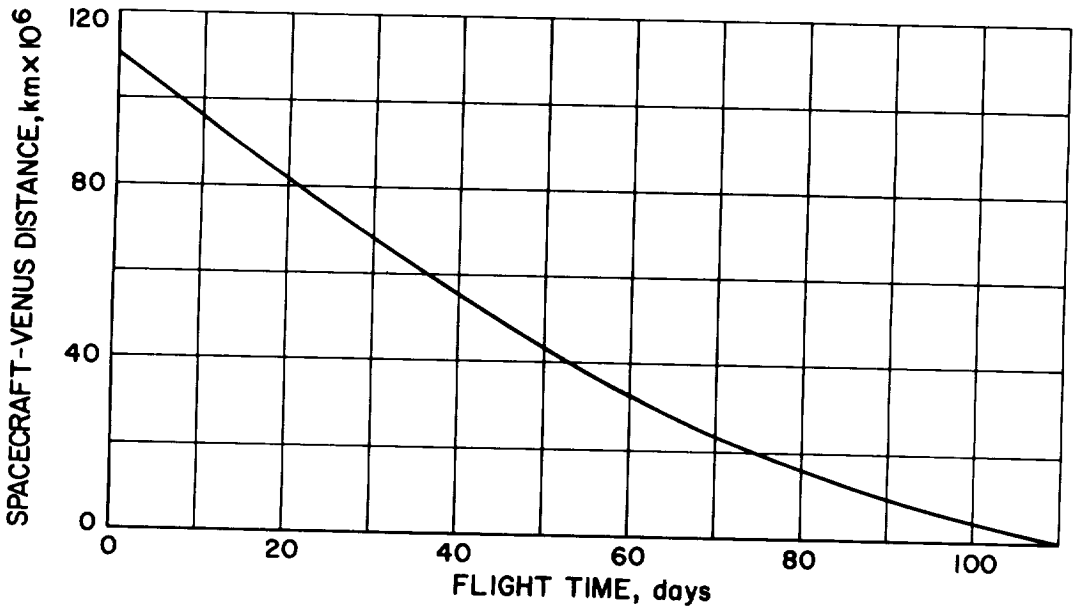

FIGURE 4–20.—Spacecraft-Venus distance vs flight time.

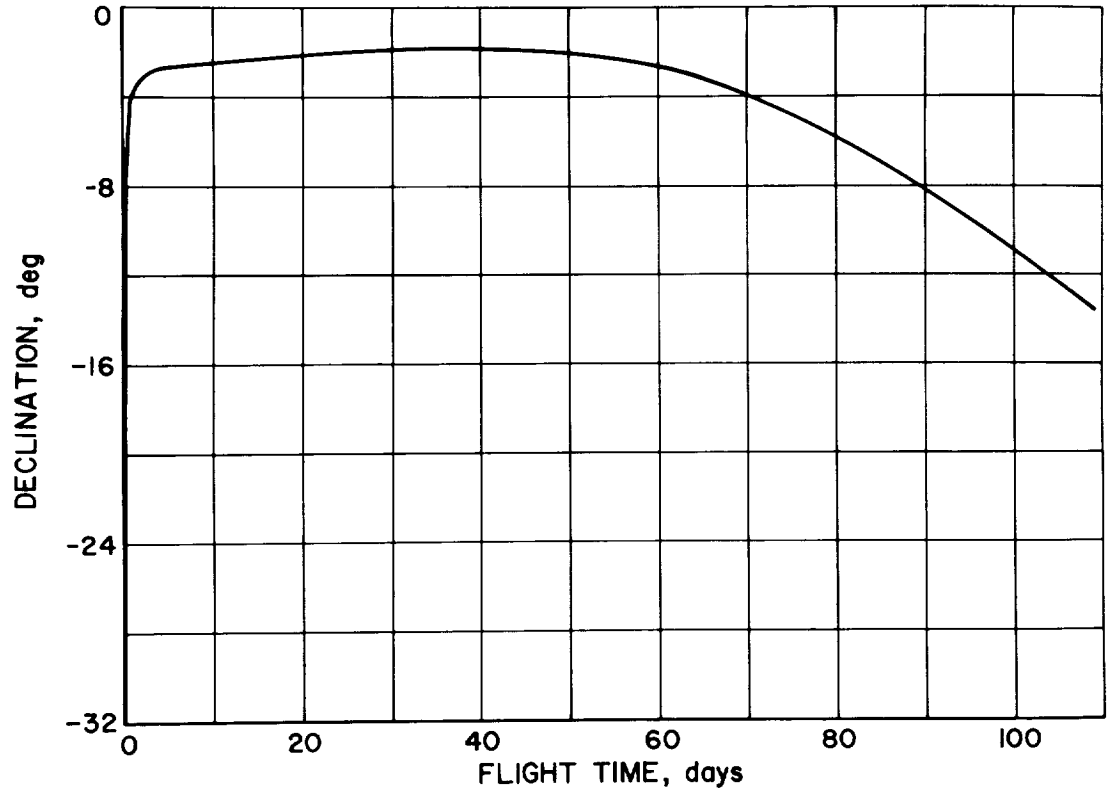

FIGURE 4–21.—Geocentric declination vs flight time.

was necessary to determine the midcourse correction capability needed to assure arrival at the desired aiming point at Venus.

It was not realistic to specify the accuracy of the injection system in terms of the uncertainties in the individual injection coordinates, since there were many combinations of injection errors that would map into the same magnitude of the midcourse correction. The injection accuracy had to be specified in terms of the variance (or the mean squared magnitude) of the midcourse maneuver.

The statistically expected magnitude of the midcourse maneuver was found once a covariance matrix of injection coordinate deviations, the time of the midcourse maneuver, and the sensitivity of the target miss components with the maneuver were known. A units-of-variance analysis was then performed to determine the relationship between the variance of the magnitude of the mid-

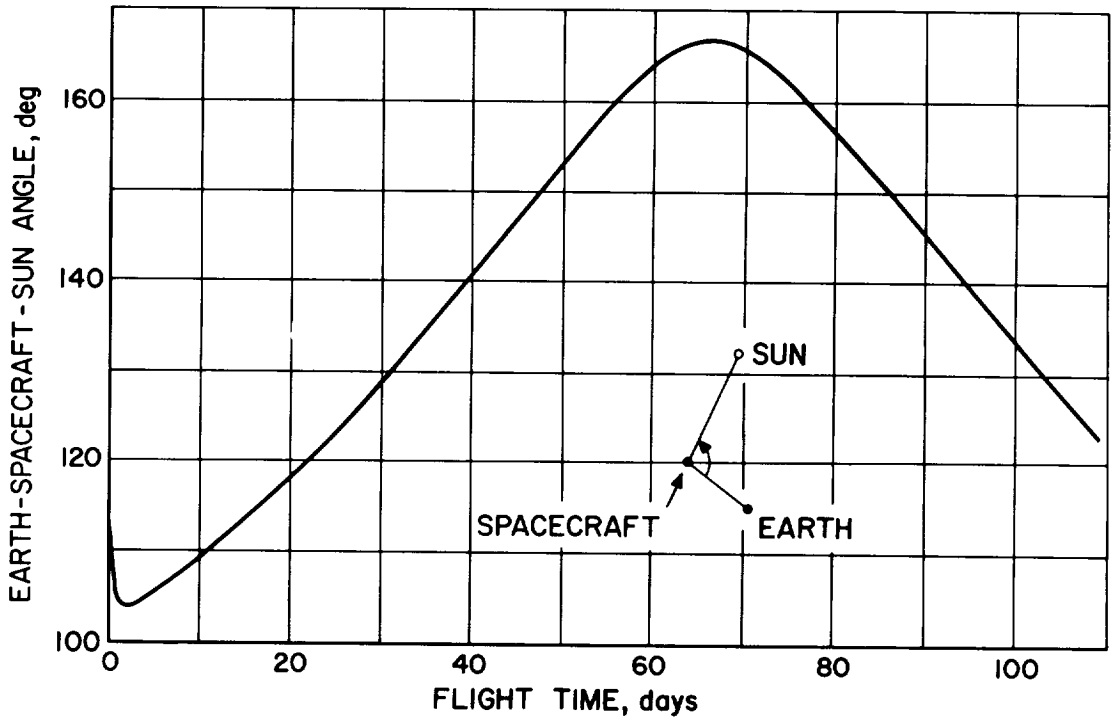

FIGURE 4–22.—Earth-spacecraft-Sun angle vs flight time.

course maneuver and the variance of the individual Atlas-Agena guidance-system-component errors.

The analysis of the Atlas-Agena injection guidance system, to determine the statistical description of the coordinate deviations at injection, was performed as follows:

1. The standard deviation (1σ) value of each independent component error source and the sensitivity of injection coordinates to these errors were obtained from the Agena contractor, Lockheed Missiles and Space Company.
2. The 1σ injection coordinate deviations were then obtained.
3. This information was used to form a noise-moment matrix of injection coordinate deviations.
4. This matrix was used to calculate the target miss components in the absence of midcourse guidance.
5. The matrix was also used to compute the rms midcourse velocity capability needed for the Mariner R.

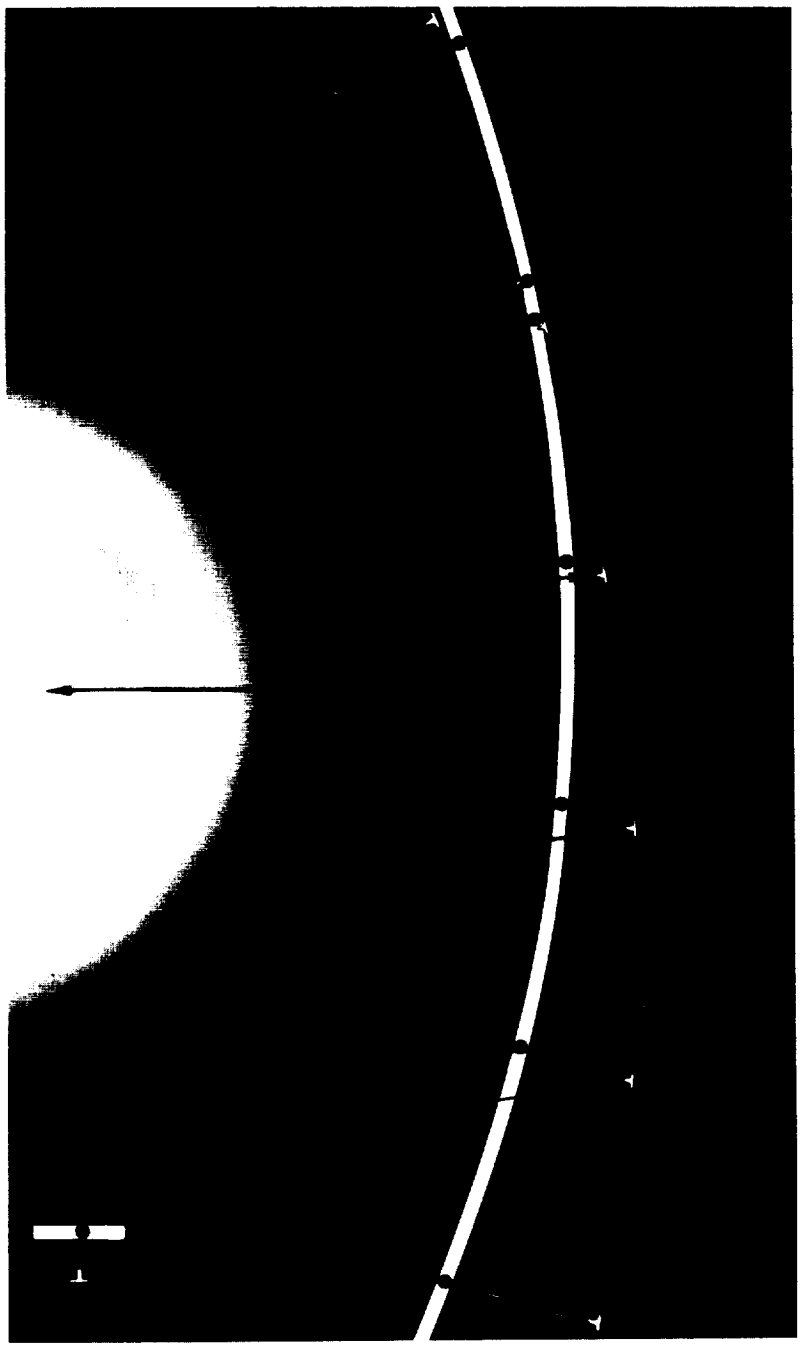

FIGURE 4–23.—Mariner II and Venus orbits near encounter.

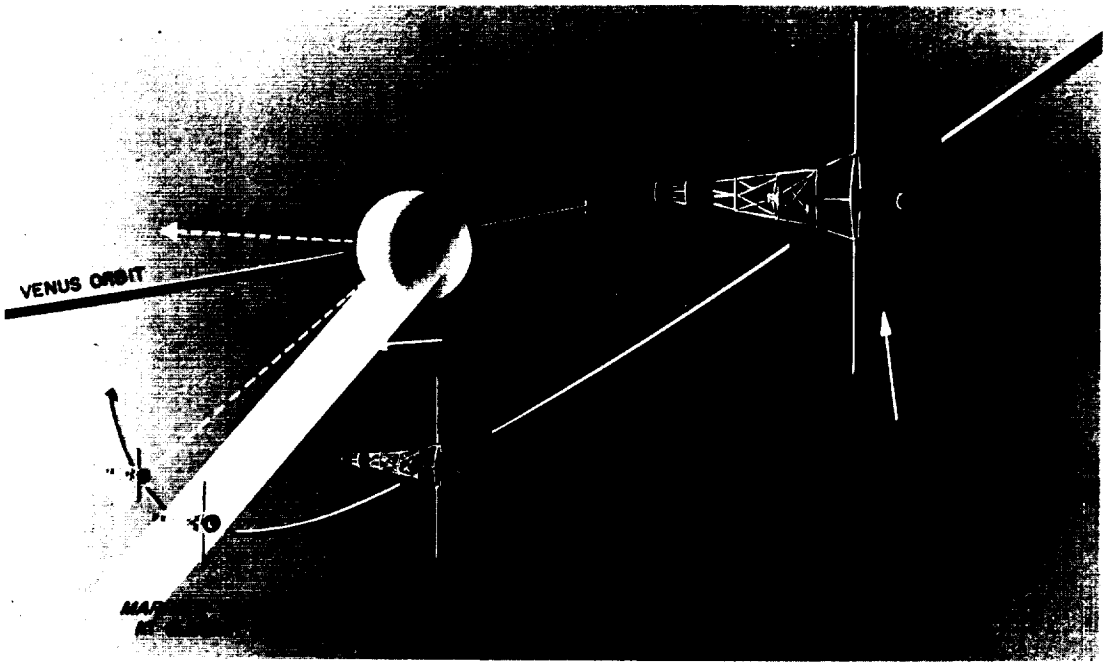

FIGURE 4–24.—Mariner II encounter of Venus as seen from Earth.

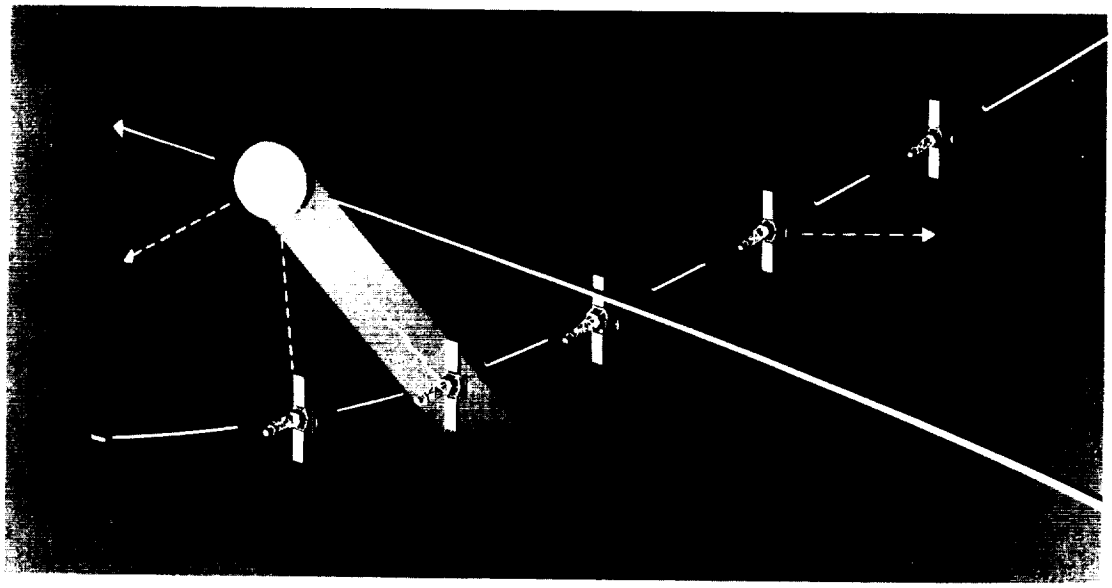

FIGURE 4–25.—Mariner II encounter of Venus as seen from inside Venus orbit.

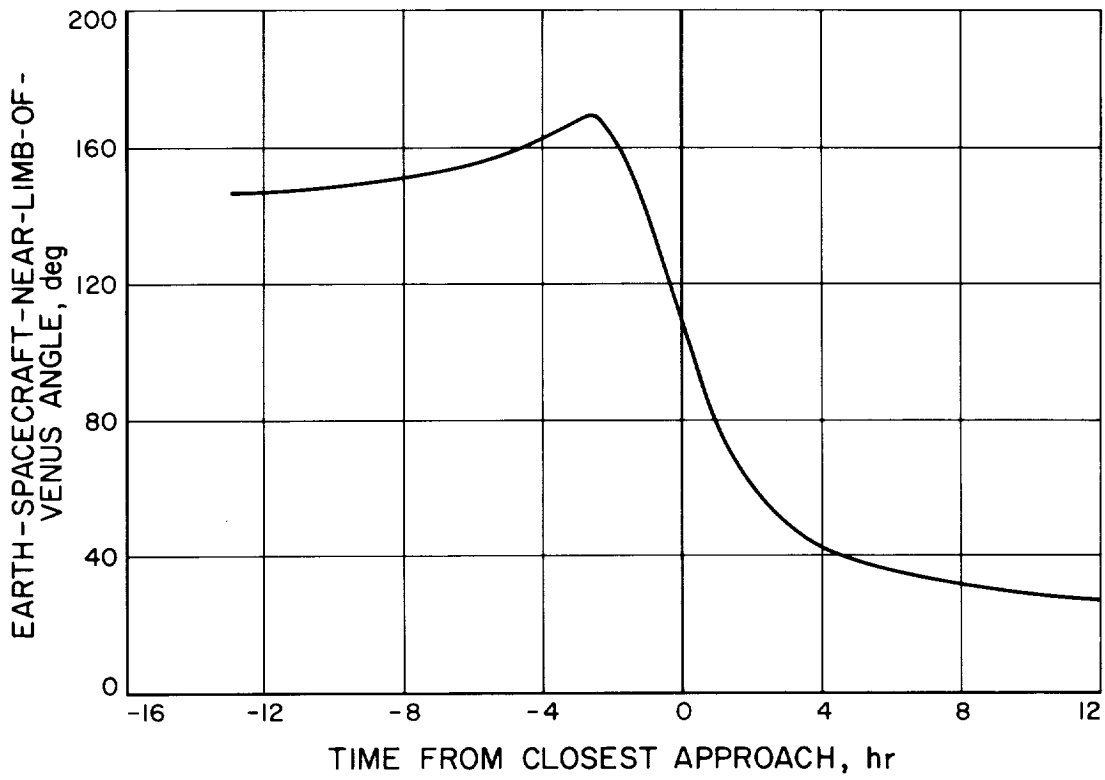

FIGURE 4–26.—Earth-spacecraft-near-limb-of-Venus angle vs time from closest approach.

6. A units-of-variance analysis was performed to obtain the relative effect of each Atlas-Agena guidance-system-component error on the midcourse maneuver.

Capability of Midcourse Correction System

Four types of error existed in the midcourse guidance system:

1. Execution of the commanded maneuver.
2. Radio observations.
3. The mathematical model used for trajectory computation.
4. Disturbances occurring after the maneuver.

Type 1 errors resulted entirely from velocity increment and pointing errors. The velocity error vector depended on component errors in the midcourse system. For Mariner R, the main source of execution error was expected to be the pointing error.

Type 2 errors were caused by random noise in the radio tracking observations.

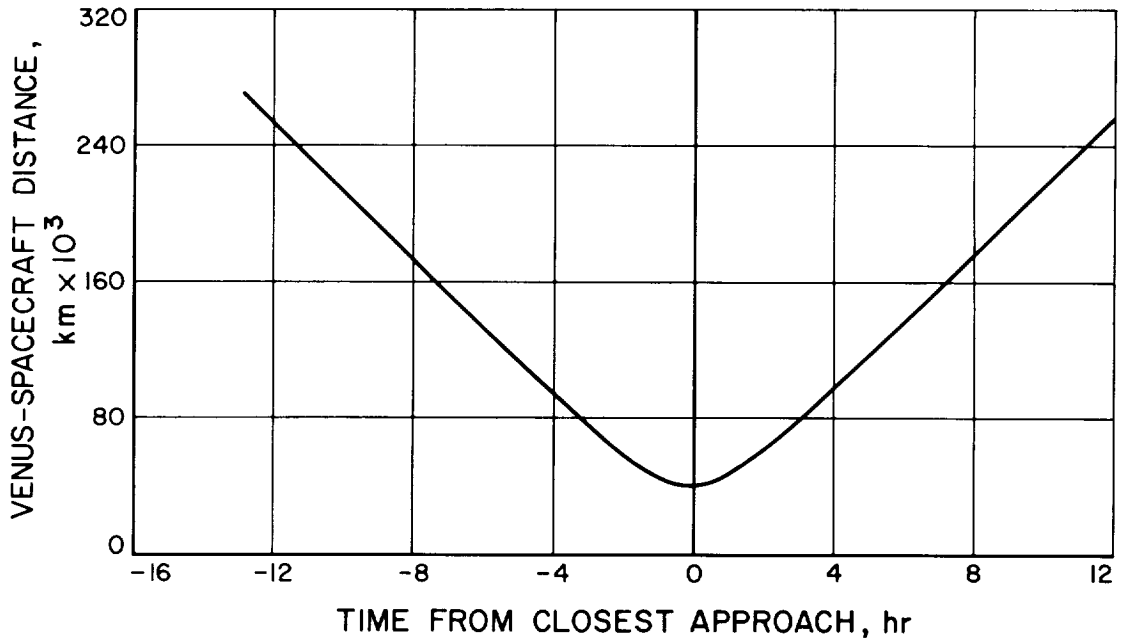

FIGURE 4–27.—Venus-spacecraft distance vs time from closest approach.

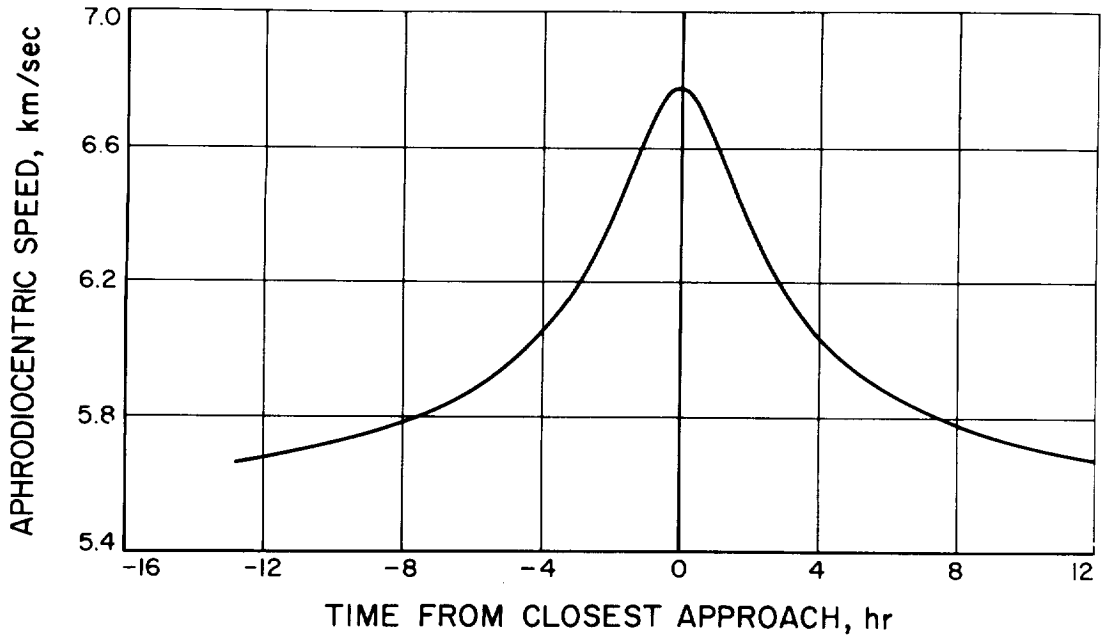

FIGURE 4–28.—Aphrodiocentric speed vs time from closest approach.

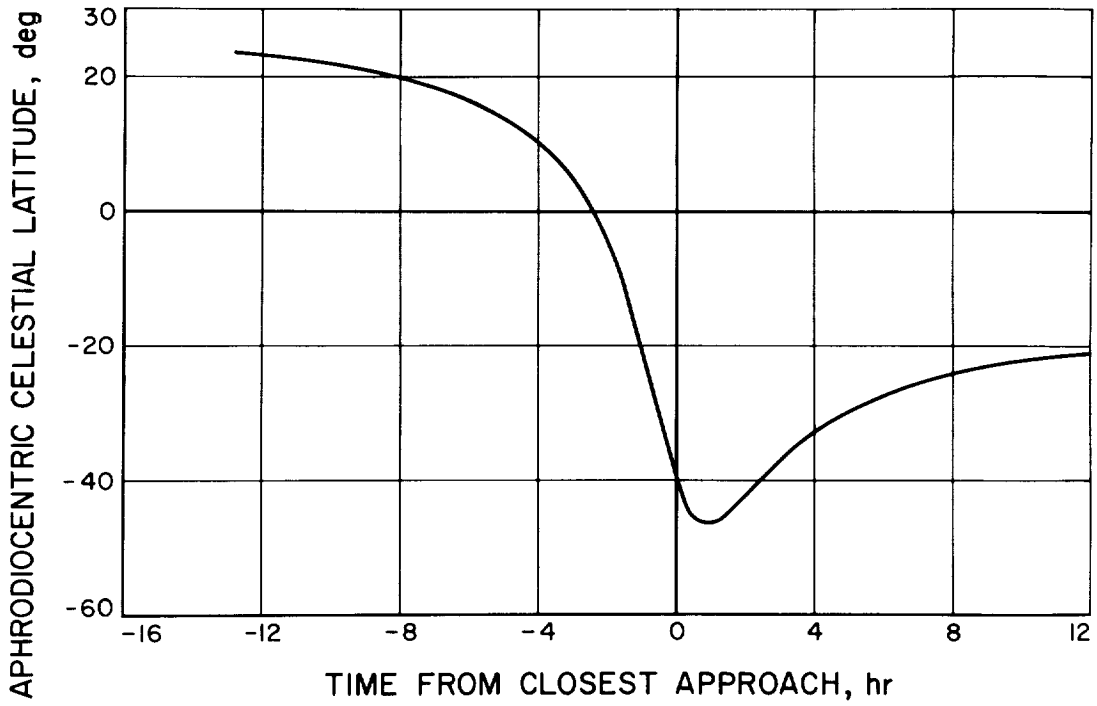

FIGURE 4–29.—Aphrodiocentric celestial latitude vs time from closest approach.

This noise produced an error in the estimate of miss components which in turn caused an error in the computed maneuver. The DSIF takes measurements of Doppler shift and angular information, but for Mariner R the two-way Doppler data were of primary importance in determining the orbit. A typical figure for the Type 2 rms miss was 700 km (435 miles).

Type 3 errors arose from uncertainties in physical constants such as the astronomical unit, gravitational constant of the Earth, tracking station locations, and speed of light. They also arose from uncertainties about the spacecraft such as the area and reflectivity for computing the solar pressure effect, and the translational acceleration caused by attitude-control jets. The total rms miss due to Type 3 errors was estimated to be 1500 km (932 miles).

Type 4 error was the miss caused by such unpredictable factors as solar corpuscular pressure if a solar storm occurred after the maneuver; this type of error was assumed to be negligible.

When the three error sources (Types 1 to 3) were combined, the total rms

possible error after the maneuver was about 8200 km (5095 miles). This was a preflight estimate of the system guidance accuracy, a number that changed once the injection errors had been determined and the required maneuver was known.

In designing the midcourse guidance system, it was assumed that the injection guidance system was accurate enough so that linear perturbation theory could be used with the preflight standard trajectory as the reference trajectory. This approximation was sufficiently accurate for engineering design of the system. The maneuver requirements were primarily the same over the entire firing period, which was convenient from the design viewpoint. In computing the maneuver during actual flight, iterative schemes were used to refine the linear approximation.

To correct for at least 99% of all possible injection errors, a correction capability V of 2.6 times the rms maneuver was required; a capability of about 40 m/sec was required for Mariner R. Actually, to be conservative, the midcourse propellant tanks were loaded to a capability of 61 m/sec (200 ft/sec), the maximum range of the counter for the digital accelerometer. Figure 4–30 shows the 99% dispersion ellipses resulting from the uncorrected injection vehicle errors referenced to the desired aiming point.

Given the correction capability available in the spacecraft, it was useful to know the range of terminal errors which could be corrected. Figure 4–31 shows the capability ellipses for $V=61$ m/sec (200 ft/sec); when the ellipse was centered at the aiming point, it contained all coordinates which could be reached by the midcourse maneuver. The range of capability shown assumed that the flight time was left uncorrected, which was a secondary, though important, consideration.

Operational Computer Program and Sequence

The primary function of the midcourse maneuver operations program was to formulate the three stored commands and one real-time command required to achieve standard operation with the midcourse maneuver. The three stored commands (which specified the parameters of the maneuver desired), when transmitted to the spacecraft, were stored in the memory of the central computer and sequencer (CC&S) prior to performance of the maneuver. The one real-time command initiated the maneuver sequence.

The sequence of events in computing and executing the midcourse maneuver was as follows:

1. The spacecraft was tracked from launch. On about the seventh day of flight, a definitive orbit determination was made.
2. The midcourse velocity impulse required to modify the trajectory of the

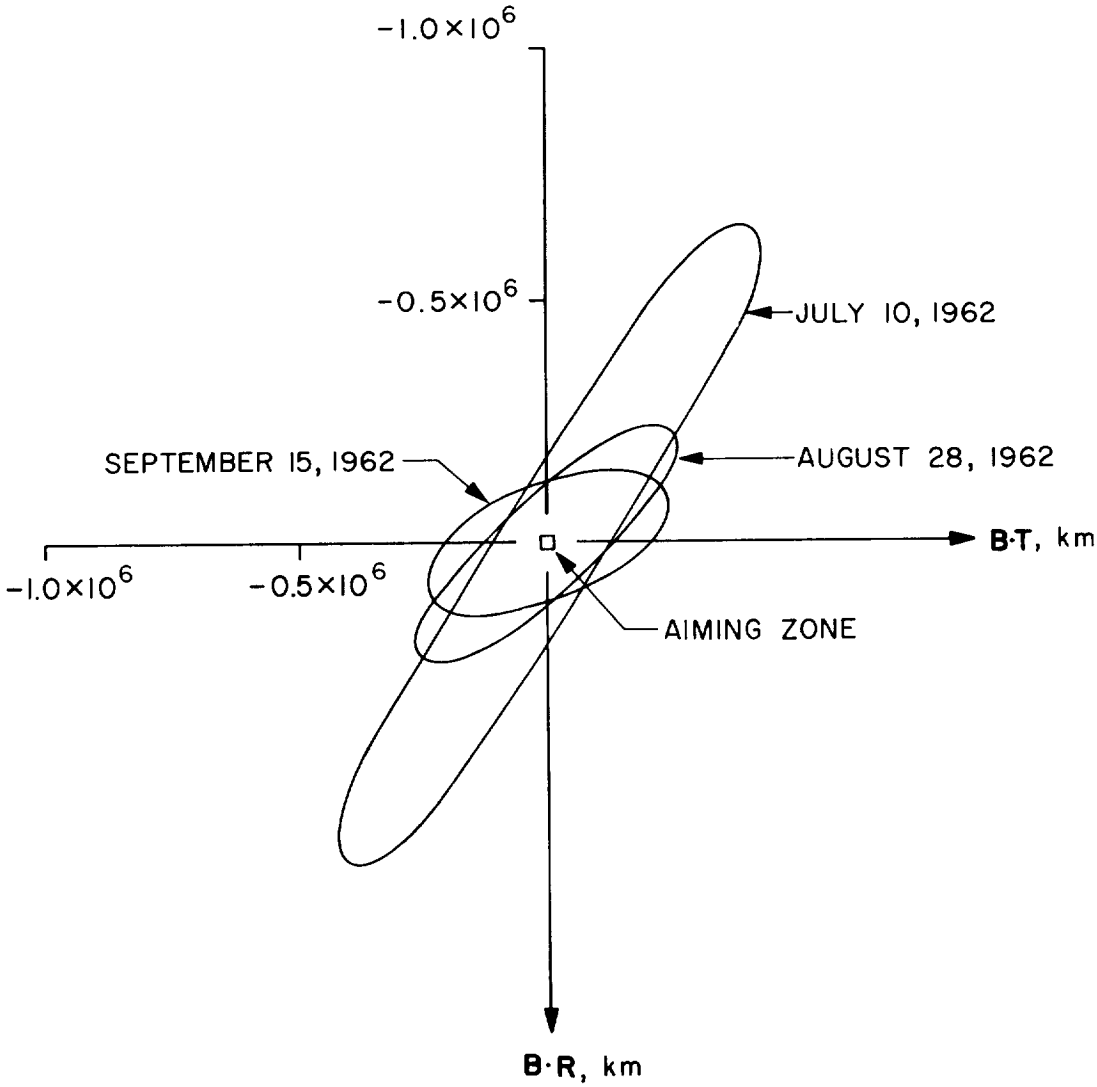

FIGURE 4–30.—99% dispersion ellipses before midcourse maneuver.

spacecraft so that it would fly by Venus in an acceptable manner at a favorable time was computed. If a maneuver could not be found which modified the best-fit (least-squares) orbit so that it passed through the optimum aiming point with an acceptable time of flight, a failure situation would have existed. If the spacecraft was operating properly and was following a trajectory which took it suffi-

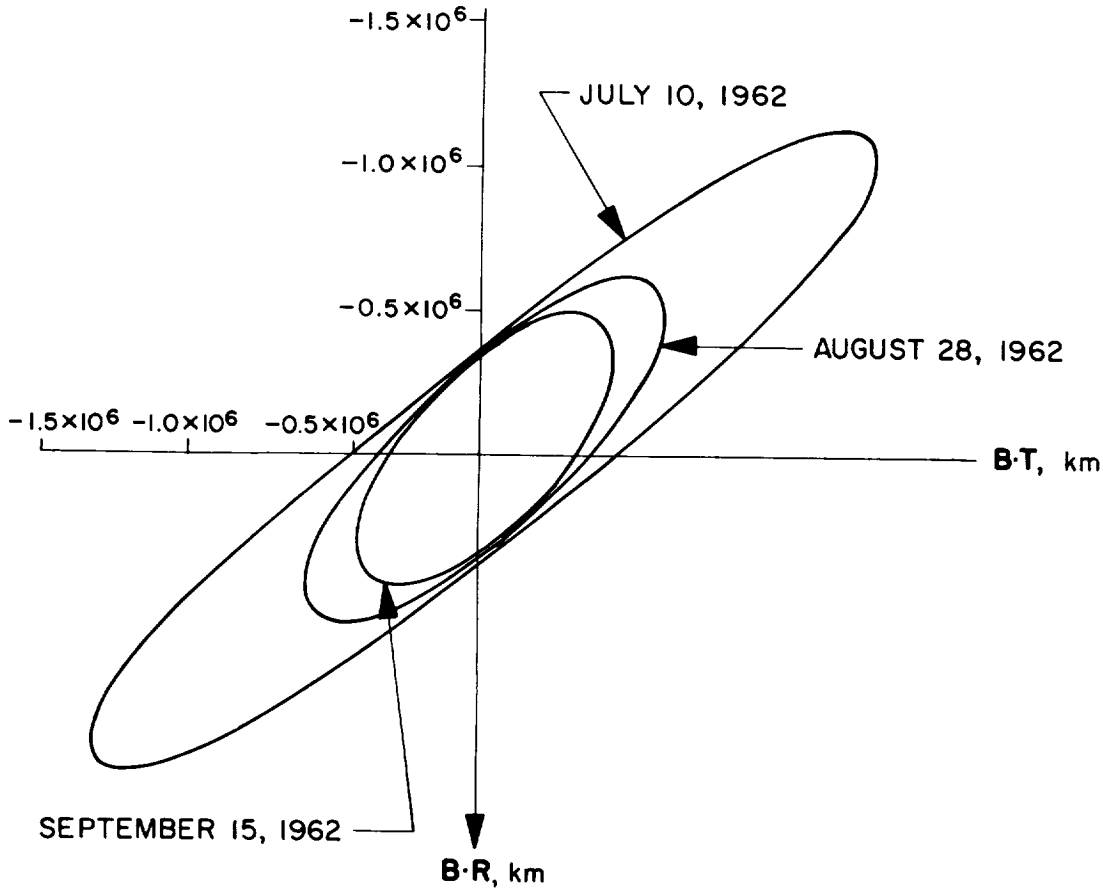

FIGURE 4-31.—Capability ellipses for $V=61$ m/sec.

ciently close to Venus, an attempt would have been made to determine a midcourse maneuver which placed the spacecraft on the most advantageous trajectory available. The trajectory evaluation features of the guidance operations program would have enabled the operations personnel to choose a revised aiming point.

3. The vector impulse was converted to the appropriate coordinates: roll-turn angle, pitch-turn angle, and magnitude of impulse. The two angles and magnitude were then converted to the binary-coded form acceptable to the spacecraft.

4. The three stored commands (roll, pitch, impulse) were transmitted to the appropriate DSIF station where the command operator checked them and sent them to the spacecraft. The spacecraft stored the commands in registers in the CC&S.

5. The real-time command "execute midcourse maneuver" was transmitted.
6. The roll and pitch turns were executed by the spacecraft.
7. The midcourse motor was ignited and burned until the required velocity impulse was measured by the accelerometer and integrator. Digital output from the integrator counted down the register containing "magnitude" each time an increment of 0.03 m/sec (0.1 ft/sec) in the velocity was sensed.

After completing the maneuver, the spacecraft returned to the cruise mode, orienting itself by means of its Sun and Earth sensors.

Execution of Mariner II Midcourse Maneuver

When results of the analysis of uncertainties in the midcourse guidance system were mapped onto the R-T plane, through the planet center (figs. 4–3 and 4–12), they resulted in a standard-deviation ellipse (1σ includes 40% of anticipated dispersions from the nominal) having a semimajor axis of 2300 km, rotated 8° from the T-axis, and a semiminor axis of 1900 km. The standard deviation in the time of flight was estimated to be 13 min. These statistical estimates were conditional, because they were based on the assumption that no failure would take place in the spacecraft system.

The nominal Mariner R trajectory was so designed that the spacecraft would pass between Venus and the Sun, with a closest approach to the center of the planet of about 20 000 km (12 427 miles). The premidcourse orbit showed, however, that the spacecraft would have passed on the other side of the planet, with a closest approach of 384 000 km (238 600 miles). (For comparison with the aiming-zone chart in fig. 4–12, the $\mathbf{B}\cdot\mathbf{T}$ and $\mathbf{B}\cdot\mathbf{R}$ coordinates of the premidcourse orbit were estimated to be: $\mathbf{B}\cdot\mathbf{T} = 291\ 715$ km (181 263 miles) and $\mathbf{B}\cdot\mathbf{R} = -265\,272$ km ($-164\,832$ miles).) This deviation from the nominal was well within the accuracy tolerance of the injection guidance system. The midcourse correction required to alter the trajectory was about one-half of the 61 m/sec (200 ft/sec) propulsion capability of the spacecraft.

When the results of the statistical analysis were considered in conjunction with the aiming-zone chart (fig. 4–12), the final aiming point was selected as: $\mathbf{B}\cdot\mathbf{T} = -28\,000$ km ($-17\,400$ miles), $\mathbf{B}\cdot\mathbf{R} = 10\,000$ km (6214 miles); and time from injection to closest Venus approach = 109.41 days.

Estimates of the postmidcourse orbit, on the basis of tracking data obtained through encounter, indicated that the coordinates in the R-T plane were $\mathbf{B}\cdot\mathbf{T} = -41\,481$ km ($-25\,775$ miles), $\mathbf{B}\cdot\mathbf{R} = 29\,244$ km (18 171 miles); and time from

injection to closest Venus approach = 109.546 days. The aiming point is designated as the "predicted point" in figure 4–12.

The following is an estimate of the accuracy with which the Mariner II spacecraft performed its midcourse maneuver:

The maneuver [5] which the spacecraft was commanded to perform was:

$$\Delta\dot{x} = 28.38 \text{ m/sec } (93 \text{ ft/sec})$$
$$\Delta\dot{y} = 12.07 \text{ m/sec } (40 \text{ ft/sec})$$
$$\Delta\dot{z} = -4.49 \text{ m/sec } (-14.7 \text{ ft/sec})$$

where $\Delta\dot{x}$, $\Delta\dot{y}$, and $\Delta\dot{z}$ are velocity changes in geocentric equatorial coordinates. (The x-axis points to the Vernal Equinox, and the z-axis points to the North Pole.) This maneuver corresponded to:

$$\text{Pitch turn } \theta_p = -139.83°$$
$$\text{Roll turn } \theta_R = -9.33°$$
$$\text{Speed increment } \Delta v = 31.16 \text{ m/sec } (102 \text{ ft/sec})$$

The estimate from tracking data of the maneuver [6] performed was:

$$\Delta\dot{x}^* = 29.34 \text{ m/sec } (93.92 \text{ ft/sec})$$
$$\Delta\dot{y}^* = 13.98 \text{ m/sec } (44.75 \text{ ft/sec})$$
$$\Delta\dot{z}^* = -5.95 \text{ m/sec } (-19.05 \text{ ft/sec})$$

This corresponded to:

$$\theta_p^* = -137.51°$$
$$\theta_R^* = -12.49°$$
$$\Delta v^* = 33.12 \text{ m/sec } (106.20 \text{ ft/sec})$$

Thus the estimated errors in the execution of the midcourse maneuvers were:

$$\delta(\Delta\dot{x}) = \Delta\dot{x}^* - \Delta\dot{x} = 0.96 \text{ m/sec } (3.07 \text{ ft/sec})$$
$$\delta(\Delta\dot{y}) = \Delta\dot{y}^* - \Delta\dot{y} = 1.91 \text{ m/sec } (6.11 \text{ ft/sec})$$
$$\delta(\Delta\dot{z}) = \Delta\dot{z}^* - \Delta\dot{z} = -1.46 \text{ m/sec } (-4.67 \text{ ft/sec})$$

[5] That maneuver which would have been performed by a perfect spacecraft, with gyros at the temperatures observed in the telemetry data, in response to the radio commands which were sent to the spacecraft and verified in the spacecraft telemetry.

[6] The estimated maneuver is the difference between the estimate of the spacecraft velocity vector at the end of the maneuver and the estimate of what the velocity vector would have been at that time if there were no maneuver.

This corresponded to errors in the spacecraft controlled variables θ_p, θ_R, and Δv of:

$$\left.\begin{aligned}\delta\theta_p &= \theta_p{}^* - \theta_p = +2.32^\circ \\ \delta\theta_R &= \theta_R{}^* - \theta_R = -3.16^\circ\end{aligned}\right\}\ \text{Equivalent turn errors required to account for pointing errors}$$

$$\delta\Delta v = \Delta v^* - \Delta v = 1.96\ \text{m/sec}\ (6.27\ \text{ft/sec})$$

The pointing error (the angle between the commanded and estimated maneuver vectors) was 3.11°. This does not necessarily mean that the pitch and roll turns were performed with the above errors, since the pointing error can result from other factors such as angular error in pitch and yaw of the center-of-gravity location with respect to the thrust vector pivot point; pitch, yaw, and roll gyro drift; and electrical and mechanical null offsets in the pitch, yaw, and roll sensors.

On Mariner II the expected contributions to the pointing error due to factors other than roll- and pitch-turn errors were increased by the lack of a path guidance loop. The standard deviation of dispersion in the pointing error due to center-of-gravity offsets alone was about 0.69°. The standard deviation of the overall pointing error was 1.43°; thus, the estimated pointing error was 2.2σ.

The estimation error in determining the accuracy of the midcourse guidance system performance had standard deviations of 0.86° in estimating the pointing error and 0.6 m/sec (1.9 ft/sec) in estimating the shutoff error.

The expected standard deviation of velocity increment error was 0.13 m/sec (0.42 ft/sec).

The error in position at closest approach due to cutoff error was -17.1×10^3 km (-10.6×10^3 miles) in $\mathbf{B}\cdot\mathbf{T}$ and $+13.3\times10^3$ km ($+8.26\times10^3$ miles) in $\mathbf{B}\cdot\mathbf{R}$.

The error due to pointing error was $+7.3\times10^3$ km ($+4.5\times10^3$ miles) in $\mathbf{B}\cdot\mathbf{T}$ and $+1.6\times10^3$ km ($+0.99\times10^3$ miles) in $\mathbf{B}\cdot\mathbf{R}$.

The overall error was -9.8×10^3 km (-6.1×10^3 miles) in $\mathbf{B}\cdot\mathbf{T}$ and $+14.9\times10^3$ km ($+9.26\times10^3$ miles) in $\mathbf{B}\cdot\mathbf{R}$. (Note that the pointing error cancels out some of the effect of the velocity increment error. The semiaxes of the midcourse maneuver dispersion ellipse for Mariner II at Venus were 3.37×10^3 and 0.863×10^3 km (2.09×10^3 and 0.536×10^3 miles) for the 1σ execution errors.)

CHAPTER 5

The Mariner Mission

MARINER R-1 LAUNCH AND ABORT

The countdown for Mariner R–1 began at 11:33 p.m., e.s.t., July 20, 1962, after several delays because of trouble in the range safety command system. Another hold delayed the count until 12:37 a.m., July 21, 1962, when counting was resumed at T minus 165 min. The count then proceeded without incident to T minus 79 min at 2:20 a.m., when uncertainty over the cause of a blown fuse in the range safety circuits caused the operations to be canceled for the night. The next launch attempt was scheduled for July 21–22.

The second launch countdown for Mariner R–1 began shortly before midnight, July 21, 1962. Spacecraft power had been turned on at 11:08 p.m., with the launch count at T minus 200 min. A 41-min hold was required at T minus 130 min (12:17 a.m., July 22, 1962) in order to change a noisy component in the ground tracking system.

When counting was resumed at T minus 130 min, the clock read 12:48 a.m. A previously scheduled hold was called at T minus 60 minutes, lasting from 1:58 to 2:38 a.m. At T minus 80 sec, power fluctuations in the radio guidance system forced a 34-min hold. Time was resumed at 4:16 a.m., when the countdown was set back to T minus 5 min.

The Atlas lifted off the launch pad at 4:21.23 a.m., e.s.t. The booster performed satisfactorily until the range safety officer noticed an unscheduled yaw-lift (northeast) maneuver. By 4:25 a.m., it was evident that, if allowed to continue, the vehicle might crash in the North Atlantic shipping lanes or in some inhabited area. Steering commands were being supplied but faulty application of the guidance equations was taking the vehicle far off course.

At 4:26.16 a.m., after 293 sec of flight and with just 6 sec left before separation of the Atlas and Agena—after which the launch vehicle could not be destroyed—a range safety officer pushed the "destruct" button, which destroyed the vehicle. The radio transponder of the Mariner R–1 continued to transmit signals for 1 minute and 4 seconds after the destroy command had been sent.

MARINER R-2

Prelaunch and Launch Operations

Assembly of the spacecraft designated as Mariner R–2 was started at the JPL Spacecraft Assembly Facility in Pasadena on January 19, 1962. The spacecraft was assembled, subjected to subsystem, system, and environmental tests, and shipped to the Atlantic Missile Range (AMR), Cape Canaveral, Fla. (fig. 5–1), where it arrived on June 3, 1962.

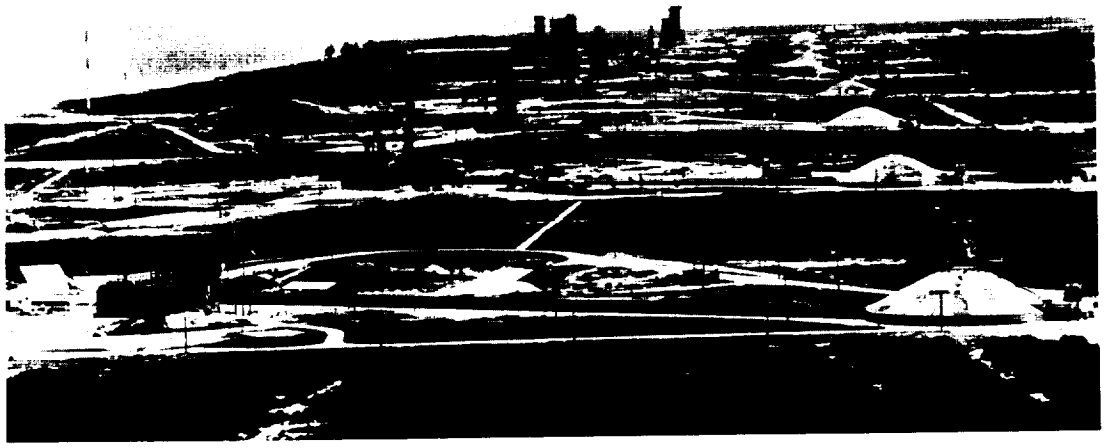

FIGURE 5–1.—Atlantic Missile Range, Cape Canaveral, Fla.

At the end of the scheduled series of AMR prelaunch tests (identical with those applied to Mariner R–1), the Mariner R–2 assembly was stored in a flight-ready condition as a standby spacecraft. After the unsuccessful launching of Mariner R–1 on July 22, 1962, Mariner R–2 was removed from storage, and the AMR prelaunch checks were essentially repeated. The total test time accumulated by the Mariner R–2 spacecraft prior to launch was 690 hours. Figures 5–2 to 5–9 illustrate various phases of the prelaunch and launch operations.

On August 25, 1962, the space vehicle composed of Atlas D–179, Agena

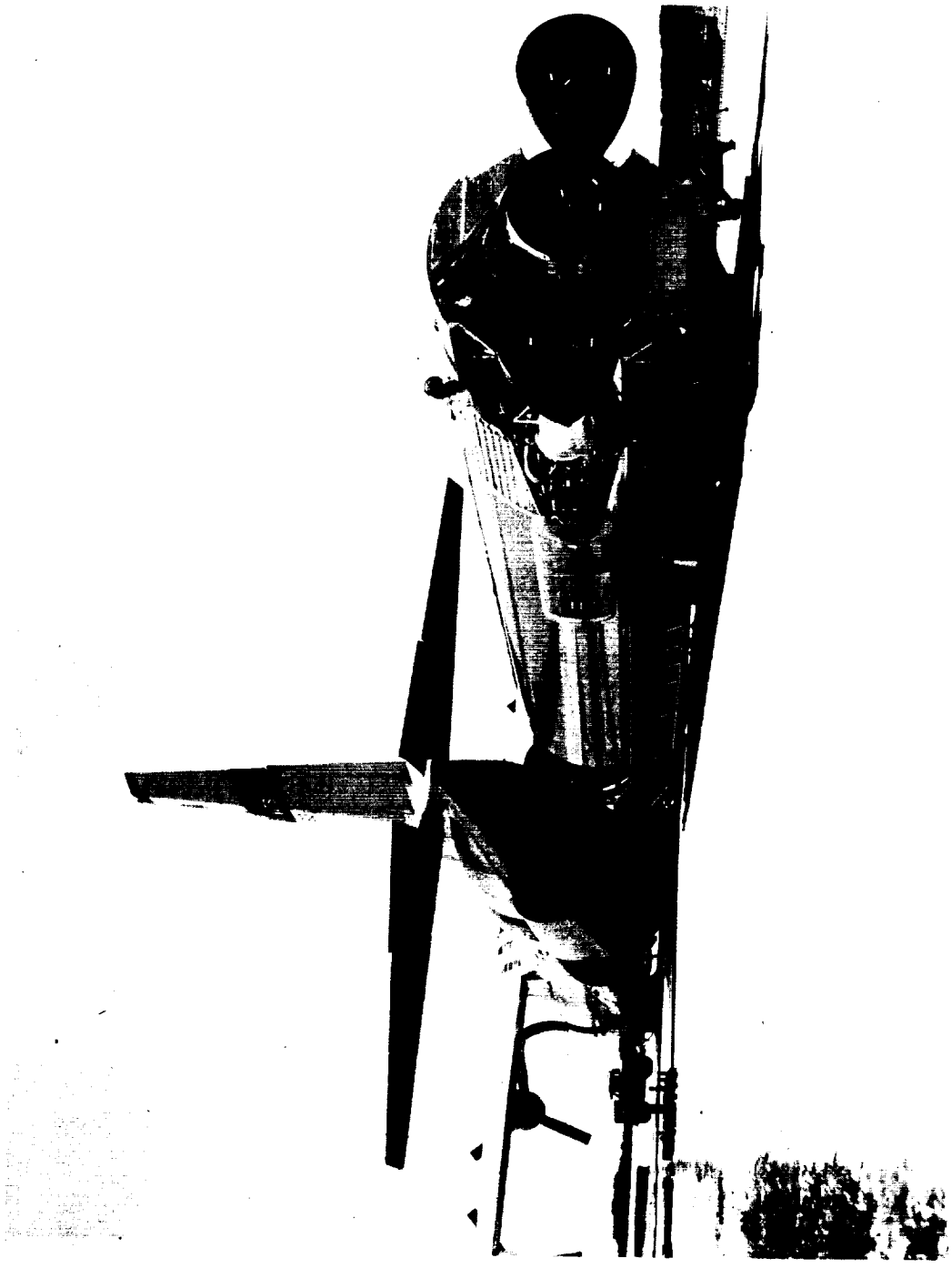

FIGURE 5-2.—Arrival of Atlas D booster at Atlantic Missile Range.

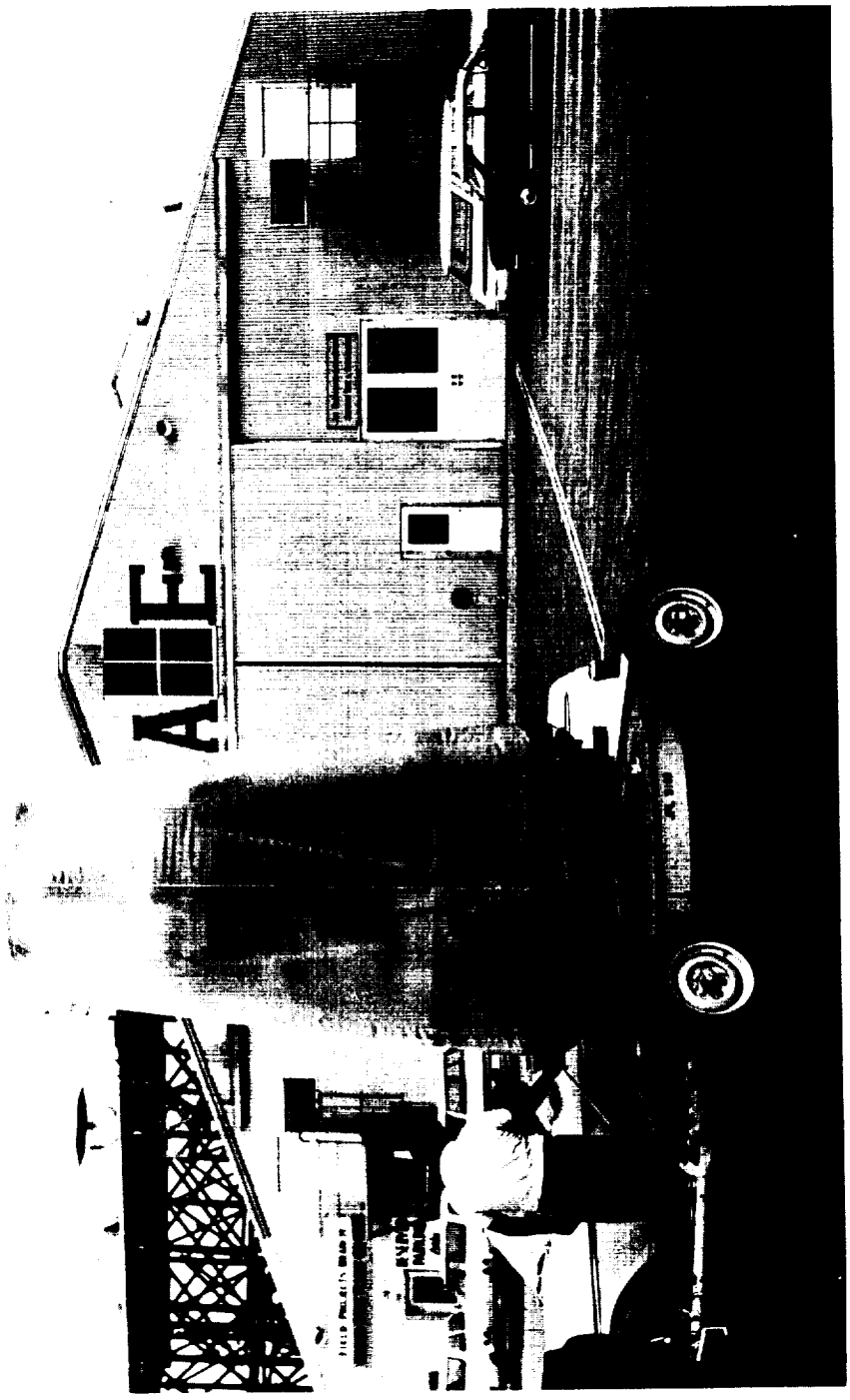

FIGURE 5–3.—Mariner II spacecraft, wrapped in dust cover, awaiting preflight tests at AMR.

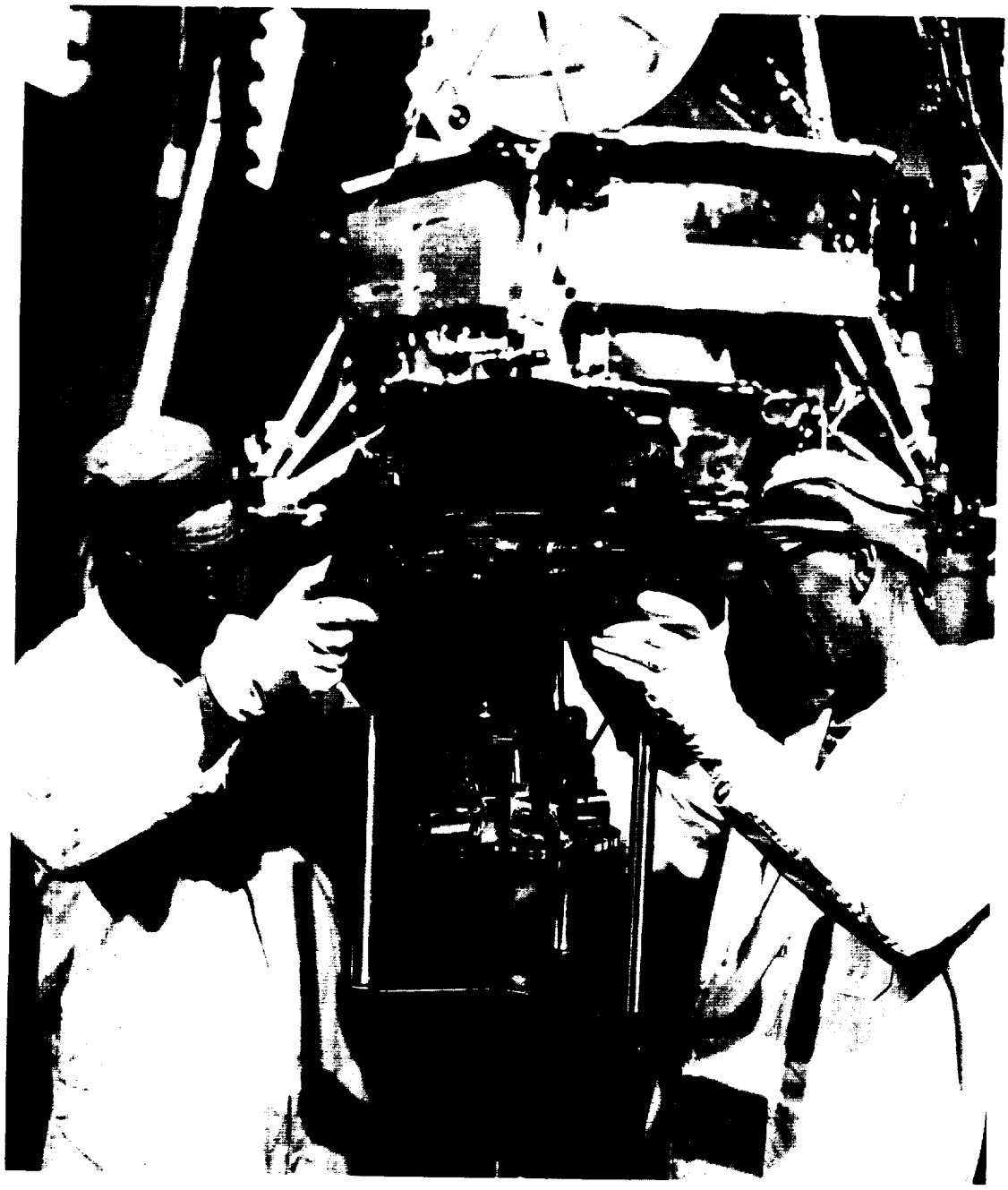

FIGURE 5–4.—Installation of Mariner II midcourse propulsion system at AMR explosive safe area.

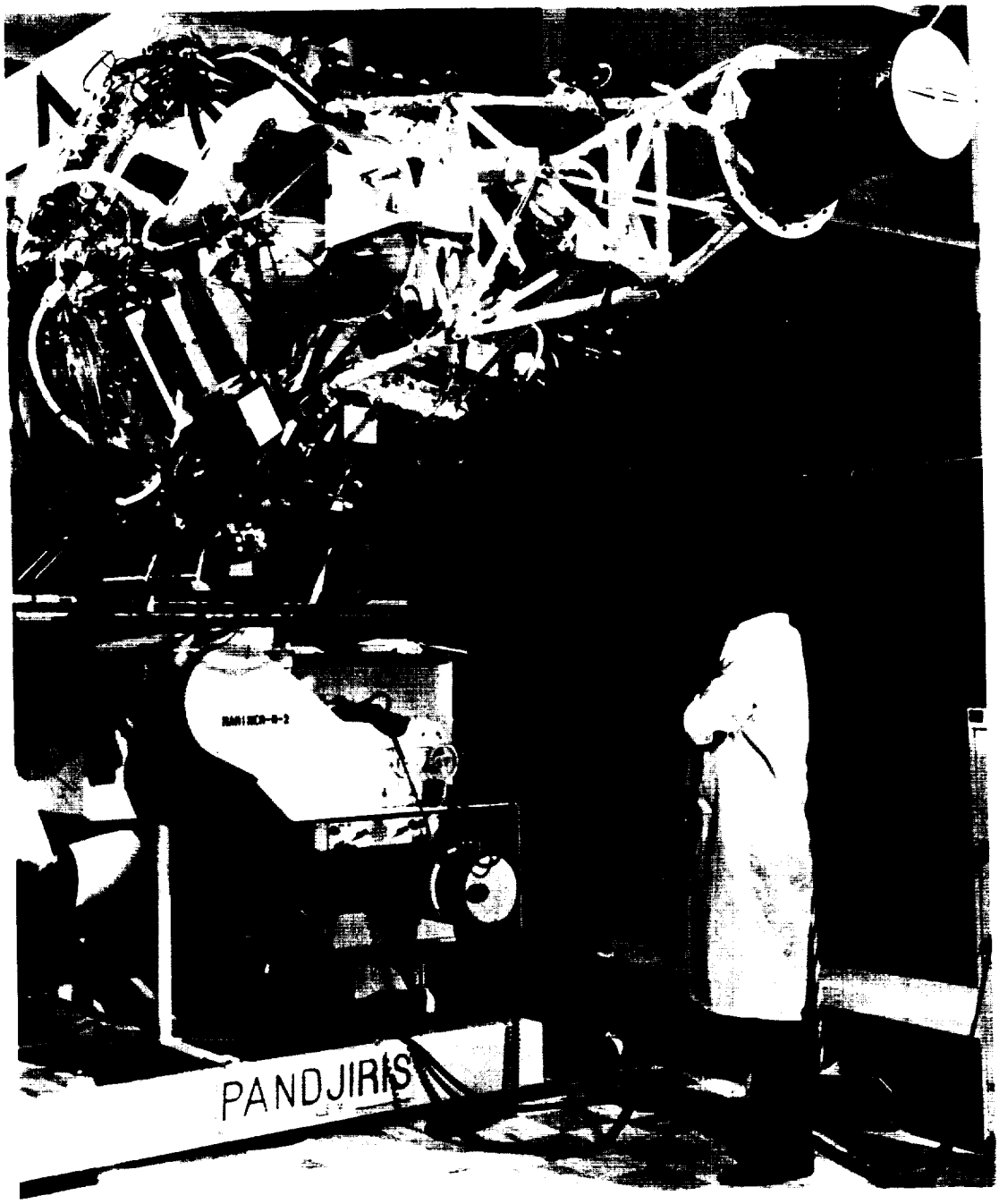

FIGURE 5–5.—System tests in progress at electronic checkout station in hangar AE.

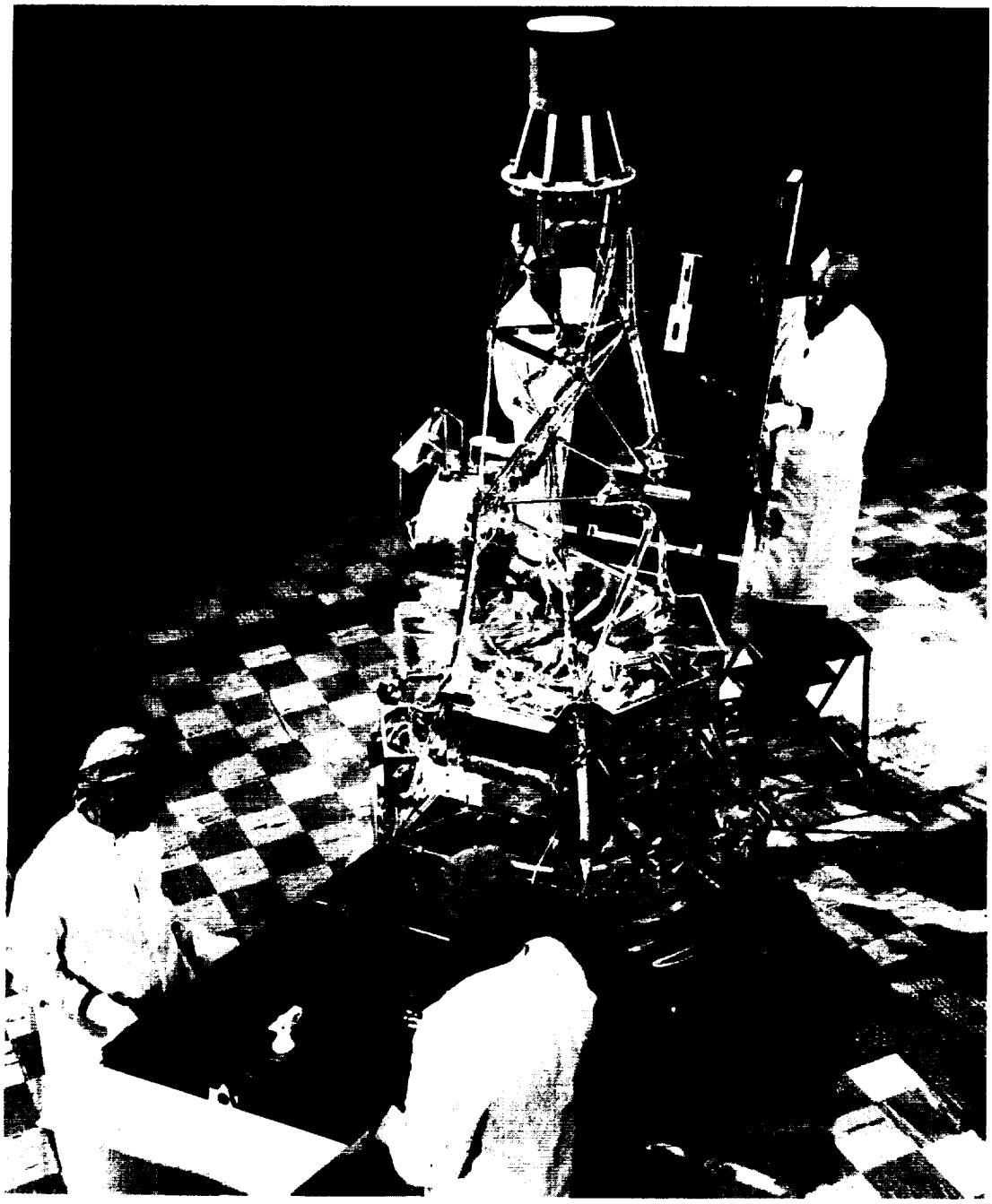

FIGURE 5–6.—Attachment of solar panels, a final step in assembly of Mariner II.

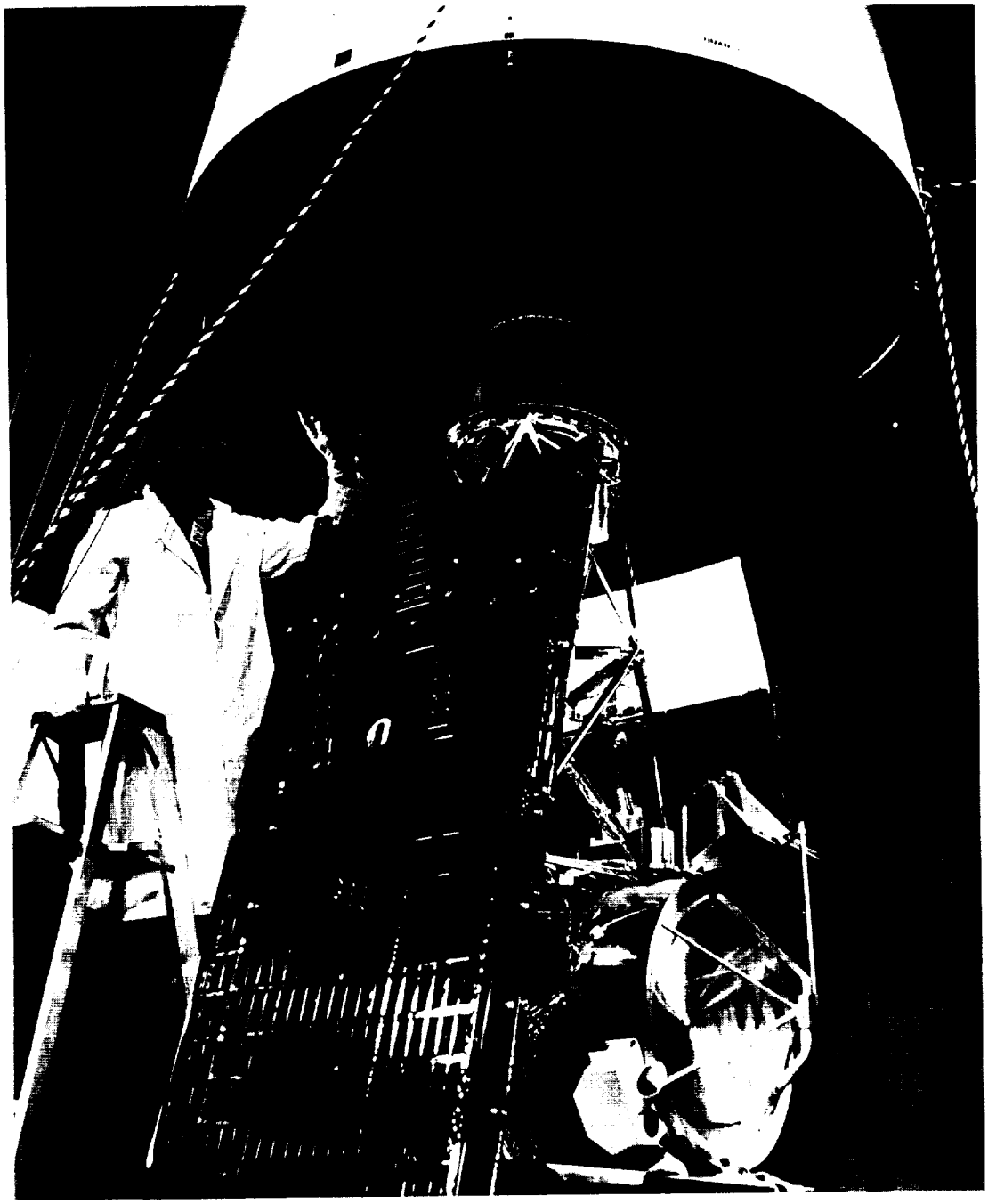

FIGURE 5-7.—Mariner II in nose shroud being lifted to top of gantry.

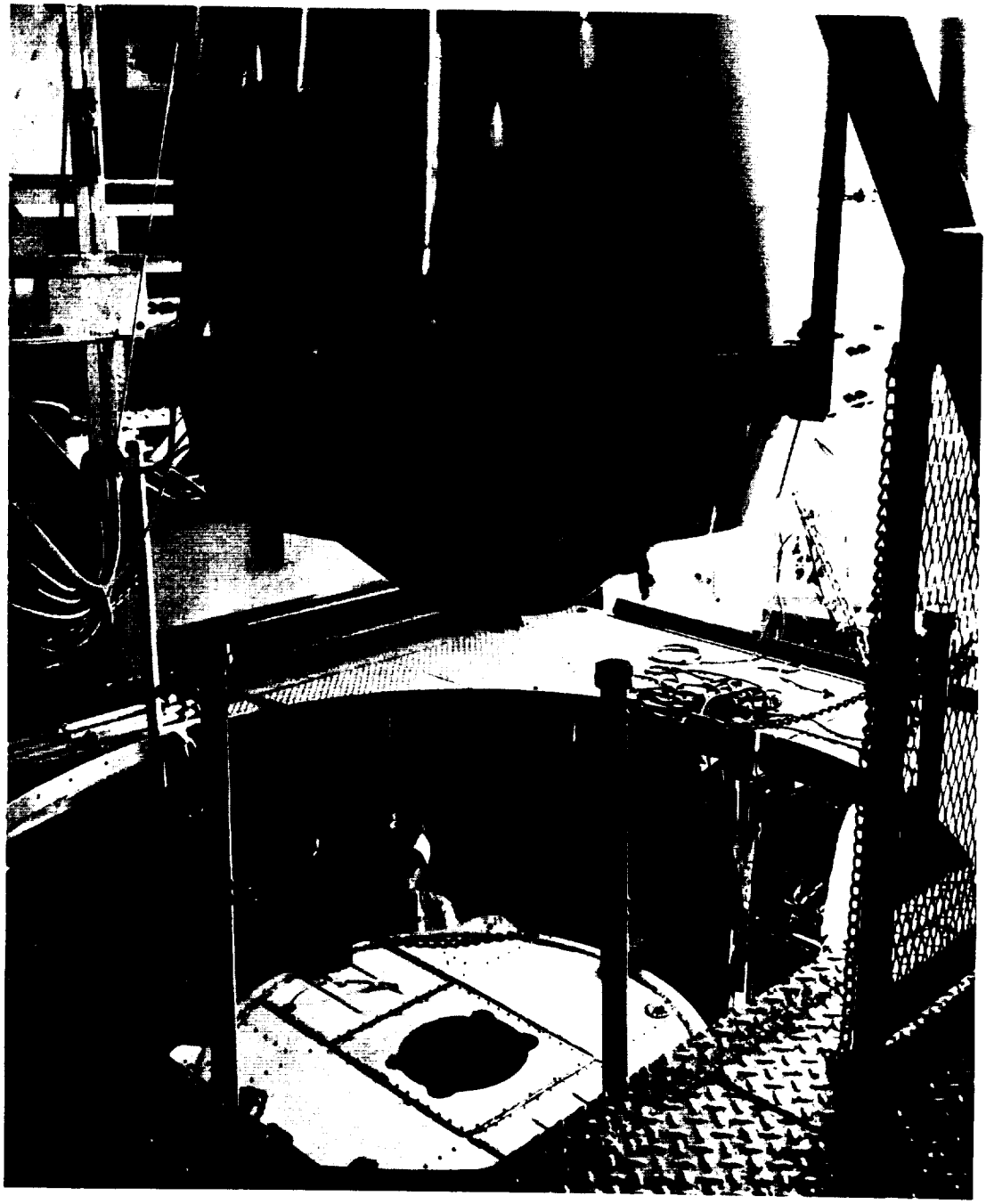

FIGURE 5–8.—Joining of Mariner II and Agena B, atop Atlas D.

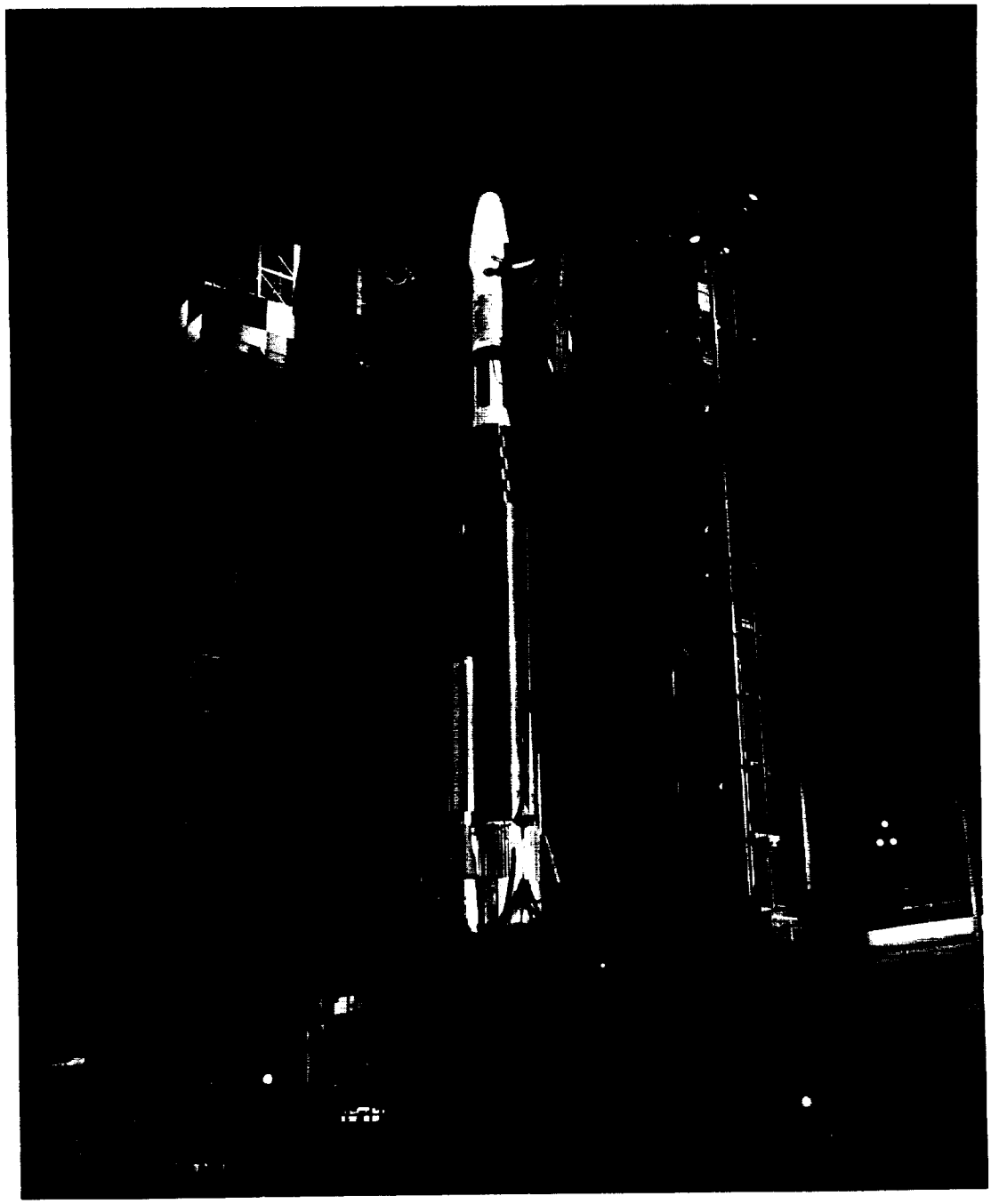

FIGURE 5–9.—Space vehicle on launch pad during countdown operations.

B–6902, and Mariner 2 was started into launch countdown. At launch minus 205 min, the countdown was canceled because of a stray voltage in the Agena destruct batteries.

Countdown 2 was started at 22:37 GMT on August 26, 1962. Table 5–I presents the operations log for the launch countdown. At T minus 200 min in the countdown, external power was applied to the spacecraft and prelaunch checkouts began. Although four unscheduled holds delayed launch for a total of 98 min, none was attributed to the spacecraft. One hold was called to replace the Atlas battery and a second because of loss of radio ground-station power. The other two holds resulted from fluctuations in the radio ground-station beacon signals. At 06:50:07 (GMT) on August 27, 1962, the inhibit on the CC&S counter was released, and approximately 3 min later the Mariner R–2 spacecraft, atop the Atlas D–Agena B vehicle, was launched.

Flight Period From Launch to Injection

The flight history and major events of Mariner II are listed in table 5–II. At lift-off, the space vehicle rose from its pad in the nominal bearing of 105° east of north. Shortly after launch, the vehicle rolled to the programmed booster roll azimuth of 107.5° east of north.

A few seconds prior to booster-engine cutoff (BECO), control of one of the two vernier engines on Atlas was lost for an undetermined reason, and the engine moved to the maximum negative mechanical stop. The main booster engines overrode and maintained the proper roll attitude during this time. At BECO, however, the booster engines were turned off and jettisoned and their roll control was terminated. With one vernier engine at full mechanical stop, the space vehicle began to roll. The companion vernier engine then moved to its electrical stop to oppose the roll; however, the vernier-engine forces remained unbalanced, and the vehicle began a negative roll (counterclockwise when viewed from the rear).

Control of the vernier engine was regained approximately 60 sec after loss of control occurred. At this time, the vehicle was rolling at a rate of about 360 deg/sec. Telemetry data later showed that the motion was arrested in about 10 sec, after a total of 35 revolutions. Even though the vehicle had no provision for maintaining roll reference in such a case, the roll-attitude error in the new null position was approximately 1.5°. This random perturbation has never been fully resolved.

Table 5-I.—Operations log for launch countdown 2 [a]

Time, GMT	Countdown time	Event
23:32	$T-300$ min	Communications with Pasadena established.
23:37	$T-295$ min	Range count started. Range status: All *green* with following exceptions: a. Computer on Twin Falls Victory Ship (TFV) is again inoperative. Uncorrected data expected from TFV. b. No data from Station 92 because of communication problem between Stations 92 and 7.
00:32	$T-240$ min	Range Safety Command (RSC) checks started.
00:45	$T-227$ min	RSC checks satisfactorily completed.
00:56	$T-216$ min	No-voltage checks satisfactorily completed.
01:07	$T-205$ min	Count picked up with spacecraft. Antenna reference hinge angle: 73.3°. Encounter parameter: 1215 counts.
01:12	$T-200$ min	Spacecraft power on: 38 v, 4.9 amp.
01:44	$T-168$ min	AZUSA tracking system checks satisfactorily completed.
02:05	$T-147$ min	Correct light indication not received when Atlas main-battery activation initiated. Battery believed to be OK, but will be replaced to gain additional assurance.
02:15	$T-137$ min	SRO report: Station 92 now in *green* condition.
02:42	$T-110$ min	Spacecraft report: Frequencies: a. 960.036718 at 02:25 GMT b. 890.037750 at 02:35 GMT c. 960.040722 at 02:38 GMT Case II temperature: 93° F D-deck sync: 0241:09
02:52	$T-100$ min	*Hold* for Atlas main-battery replacement, expected 30-min duration.
03:01	$T-100$ min	$T-12$ hr weather report: *Go* Bending moment: 24.5% Usable control: 18.4% Total effect: 52.5% $T-6$ hr weather report: *Go* Bending moment: 25.0% Usable control: 22.8% Total effect: 53.0%
03:02	$T-100$ min	Decision made to change Atlas telemetry "can" because of unsatisfactory channel 11 subcarrier.
03:09	$T-100$ min	Atlas main battery replaced and activated. Proper indication received.
03:20	$T-100$ min	*Hold* extended 15 min to complete installation of TV cameras on service tower (cameras required to monitor Agena acid tanking).
03:32	$T-100$ min	Count resumed.
03:35	$T-97$ min	DSIF in *green* condition with exception of voice communications with DSIF 4 and 5, not yet established.

[a] AMR test No. 3731, August 26–27, 1962.

Table 5-I.—Operations log for launch countdown 2—*Continued*

Time, GMT	Countdown time	Event
03:37	$T-95$ min	All spacecraft systems *Go*.
03:49	$T-83$ min	Difficulties experienced with Pasadena end of circuit GT131-69.
03:50	$T-82$ min	100% acid tanking started.
04:02	$T-70$ min	All spacecraft systems *Go*.
04:03	$T-69$ min	100% acid tanking completed.
04:04	$T-68$ min	Report received from Hangar AE Communications Center: circuit 69 checks out with CB toll office.
04:12	$T-60$ min	Built-in hold (BIH) started, expected duration 30 min. Intermittent trouble reported with data links between Communications Center and 7090 computer at IPP (may prevent transmission of acquisition message to Stations 12, 13, and TFV).
04:42	$T-60$ min	*Hold* extended by Mission Director to obtain verification of spacecraft battery life.
04:43	$T-60$ min	Count resumed.
04:48	$T-55$ min	DSIF *green* with exception of voice communication with DSIF 5. Trouble on voice line between London and Pretoria. Spacecraft, vehicle, and range all in *green* condition.
04:52	$T-51$ min	Radar 1.16 (Cape FPS-16) reported inoperative.
05:03	$T-40$ min	Spacecraft report: Frequencies: a. 960.036751 at 04:45 GMT b. 890.037600 at 04:51 GMT c. 960.040537 at 04.53 GMT d. 890.037750 at 04:49 GMT e. Minus 20 mv Case II temperature: 93° F D-deck sync: 0501:09
05:08	$T-35$ min	Loop test satisfactorily completed.
05:13	$T-30$ min	Radar 1.16 now reported *green*.
05:18	$T-25$ min	$T-2$ hr weather report: *Go* Bending moment: 20% Usable control: 16% Total effect: 49.7%
05:24	$T-19$ min	Voice communications with DSIF 5 now *green*.
05:31	$T-12$ min	Spacecraft report: Case II temperature: 93°F Encounter parameter: 1215 counts
05:36	$T-7$ min	Spacecraft station: all systems *Go*.
05:38	$T-5$ min	BIH started, expected duration 4 min. Launch plan: 27D Ready reports: Vehicle: *Go* Spacecraft: *Go* Range: *No-Go* GE guidance primary power lost. *Hold* extended for estimated 10 min.

Table 5-I.—Operations log for launch countdown 2—*Continued*

Time, GMT	Countdown time	Event
05:45	$T-5$ min	*Hold* extended for additional 5 min.
06:00	$T-5$ min	Launch plan: 27F Ready reports: Vehicle: *Go* Spacecraft: *Go* Range: *Go*
06:06	$T-5$ min	Count resumed.
06:10	$T-60$ sec	*Hold:* GE guidance experiencing fluctuations on return signal. Recycled to $T-5$ min.
06:22	$T-5$ min	Launch plan: 27H Ready reports: Vehicle: *Go* Spacecraft: *Go* Range: *Go*
06:26	$T-5$ min	Count resumed.
06:30	$T-50$ sec	*Hold:* GE guidance experiencing fluctuations on return signal. Recycled to $T-5$ min.
06:34	$T-5$ min	Voice communications with DSIF 5 out. RA–54 teletype line to DSIF 5 out.
06:41	$T-5$ min	Voice communications with DSIF 5 reinstated.
06:43	$T-5$ min	Remaining life (before launch) on Atlas main battery down to 3 min. When count resumed for next attempt, switch-over to internal power to be delayed until $T-60$ sec to help conserve battery life.
06:44	$T-5$ min	Launch plan: 27K. Ready reports: Vehicle: *Go* Spacecraft: *Go* Range: *Go*
06:48	$T-5$ min	Count resumed.
06:53	$T-0$	*Liftoff:* 06:53:13.927 GMT. DSIF 0 in one-way lock at liftoff. Lock maintained, with momentary dropouts during booster staging, until final loss of signal at $L+463$ sec. Signal level at launch: -85 dbm, gradually decreasing to -120 dbm just prior to dropout. Normal operation indicated in preliminary evaluation of spacecraft data. Event register reading subsequent to launch: 0-0-1-0. AMR inflight data transmission and computational operations all performing close to nominal times. Following general evaluations yielded by real-time monitoring of AMR data: Station 91: Approximately 30% of data badly garbled. Corrected when Station 91 switched frequencies. Station 12: Data generally of good quality.

Table 5-I.—Operations log for launch countdown 2—*Concluded*

Time, GMT	Countdown time	Event
		TFV: All yaw data uncorrected on board ship because of inoperative computer. Real-time utilization of data prevented by data-handling problem at AMR.
		Station 13: Data not time-labeled, preventing real-time utilization of information.
07:24	$L+1865$ sec	Spacecraft acquired by DSIF 1 at signal level of -100 dbm.
07:32	$L+2325$ sec	Reports received that DSIF 5 acquired spacecraft at 07:24 GMT.
08:28	$L+95$ min	Sun acquisition at 07:58:54 GMT confirmed by evaluation of spacecraft telemetry data at Hangar AE.

The altitude at BECO was somewhat high and the vehicle also had an attitude error of approximately 10° in pitch. During the period of uncontrolled roll, the Atlas was unable to respond effectively to guidance commands.

The Atlas-Agena separation sequence prior to Agena first-burn was executed satisfactorily, although the attitude error described above caused the shroud to be ejected into a position closer to the Agena flight path than was desired. As an additional result of the attitude error, the Agena was pitched down 2° at first ignition, and the horizon sensors did not complete correction of this error until 15 sec later. The improper altitude of the Atlas caused the Agena timer-start signal to be sent 8 sec early. However, the Agena successfully terminated its first burn when the preset velocity increment was sensed by the velocity meter.

At the termination of Agena first burn, the Agena-Mariner was in its parking orbit with a nominal altitude of 185 km (115 miles). The vehicle coasted in this orbit from an Earth-referenced point 64° west longitude and 22° north latitude to a point 9° west and 12° south, arriving about 980 sec later. At this point, Agena second burn was successfully initiated and cut off by the velocity meter. The Agena-Mariner separation was also successful and the spacecraft was injected into a geocentric escape hyperbola which would carry it to the vicinity of Venus. The Agena, by performing a programmed 140° yaw maneuver and expelling its unused propellant, reduced its speed and minimized the probability of impact with Venus. Injection occurred over the South Atlantic Ocean at $-14.8°$ latitude and $+357.9°$ longitude.

Figure 5–II.—Sequence of significant flight events for Mariner II

No.	Event	Date, 1962	Nominal time (a)	Predicted time, GMT (b)	Estimated time, GMT (c)
1	Inhibit on CC&S counter released	Aug. 27	*A*		06:50:07
2	CC&S relays cleared	Aug. 27			06:52:07
3	Lift-off	Aug. 27	*L*		06:53:14
4	Atlas-Agena separation	Aug. 27	*L*+300 sec	06:58:14	[d] 06:58:14
5	First Agena ignition	Aug. 27	L+349 sec	06:59:03	
6	First Agena burnout	Aug. 27	L+500 sec	07:10:34	
7	Second Agena ignition	Aug. 27	L+1302 sec to *L*+1736 sec	07:14–07:22	
8	Second Agena burnout	Aug. 27	*L*+1400 sec to *I* to *L*+1834 sec	07:16–07:23	
9	Spacecraft-Agena separation	Aug. 27	*I*+156 sec	07:21:53	07:21:53
	a. CC&S enabled		*I*+156 sec	07:21:53	07:21:53
	b. Pyrotechnics armed		*I*+156 sec	07:21:53	07:21:53
	c. Transmitter power up		*I*+156 sec	07:21:53	07:21:53
10	Command issued to unfold solar panels and unlatch radiometer	Aug. 27	*L*+44 min	07:37:07	07:37:04
11	Solar panels unfolded	Aug. 27			07:38:07
12	Initial Sun acquisition	Aug. 27	*L*+60 min	07:53:07	07:53:07
	a. Attitude control power on		*L*+60 min	07:53:07	07:53:07
	b. Sun sensor and gas-jet system activated		*L*+60 min	07:53:07	07:53:07
	c. Directional antenna extended		*L*+60 min	07:53:07	07:53:07
	d. Sun-acquisition sequence begun		*L*+60 min	07:53:07	07:53:07
13	Sun acquired	Aug. 27	*L*+60 min to *L*+90 min	07:53–08:23	07:55:35
	a. Gyros turned off		*L*+60 min to *L*+90 min	07:53–08:23	07:58:35
14	First antenna reference update, AC21F	Aug. 27	*A*+1000 min	23:30:07	23:30:02
15	RTC–8 transmitted (cruise science on)	Aug. 29			16:13:00
16	Initial Earth acquisition	Sept. 3	*A*+10 000 min	05:30:07	05:29:14
	a. Inhibit on automatic Earth acquisition removed		*A*+10 000 min	05:30:07	05:29:14

See footnotes at end of table.

Figure 5–11.—Sequence of significant flight events for Mariner II—*Continued*

No.	Event	Date, 1962	Nominal time (a)	Predicted time, GMT (b)	Estimated time, GMT (c)
16	Initial Earth acquisition—Continued	Sept. 3			
	b. Earth sensor power turned on		A+10 000 min	05:30:07	05:29:14
	c. Gyros turned on		A+10 000 min	05:30:07	05:29:14
	d. Cruise science turned off		A+10 000 min	05:30:07	05:29:14
	e. L-band switched to directional antenna [e]		A+10 000 min	05:30:07	05:29:14
	f. Roll search initiated		A+10 000 min	05:30:07	05:29:14
17	Earth acquired	Sept. 3	Event 16+0 to 30 min	05:30–06:00	05:58:58
	a. Roll search stopped		Event 16+0 to 30 min	05:30–06:00	05:58:58
	b. Gyros turned off		Event 16+0 to 30 min	05:30–06:00	05:58:58
	c. Cruise science turned on		Event 16+0 to 30 min	05:30–06:00	05:58:58
18	Preparation for midcourse maneuver	Sept. 4			21:30–
	a. SC-1 transmitted (roll-turn duration)				21:30–
	b. SC-2 transmitted twice (pitch-turn duration)				21:35–
	c. SC-3 transmitted twice (velocity increment)				22:23–
19	RTC-4 transmitted (directional to omniantenna)	Sept. 4			22:39–
20	RTC-6 transmitted (initiation of midcourse maneuver sequence)	Sept. 4	M		22:49:42
	a. Accelerometer turned on				22:49:42
	b. Gyros turned on				22:49:42
	c. Cruise science turned off				
21	Roll-turn sequence begun	Sept. 4	M+60 min	23:49:42	23:49:00
	a. Earth sensor turned off		M+60 min	23:49:42	23:49:00
	b. Roll gyro capacitor connected		M+60 min	23:49:42	23:49:00
	c. Roll-turn polarity set		M+60 min	23:49:42	23:49:00
	d. Directional antenna extended to 118°		M+60 min	23:49:42	23:49:00
	e. Roll turn started		M+60 min	23:49:42	23:49:00
	f. Roll turn stopped		Event 21+51 sec	23:50:33	23:49:51

See footnotes at end of table.

Figure 5–11.—Sequence of significant flight events for Mariner II—*Continued*

No.	Event	Date, 1962	Nominal time (a)	Predicted time, GMT (b)	Estimated time, GMT (c)
22	Pitch-turn sequence begun	Sept. 5	$M+72$ min	00:01:42	00:01:00
	a. Autopilot turned on		$M+72$ min	00:01:42	00:01:00
	b. Sun sensor error signals switched out		$M+72$ min	00:01:42	00:01:00
	c. Pitch and yaw gyro capacitors connected		$M+72$ min	00:01:42	00:01:00
	d. Pitch-turn polarity set		$M+72$ min	00:01:42	00:01:00
	e. Pitch turn started		$M+72$ min	00:01:42	00:01:00
	f. Pitch turn stopped		$M+85$ min, 15 sec	00:14:57	00:14:10
23	Motor-burn sequence begun	Sept. 5	$M+94$ min	00:23:42	00:23:00
	a. Motor ignition commanded		$M+94$ min	00:23:42	00:23:00
	b. Motor shutoff commanded		Event 23+0 to 2.5 min	00:23–00:25	00:23:31
24	Sun reacquisition	Sept. 5	$M+98$ min	00:27:42	00:27:00
	a. Autopilot turned off		$M+98$ min	00:27:42	00:27:00
	b. Gyro capacitors switched out		$M+98$ min	00:27:42	00:27:00
	c. Antenna extended to re-acquisition position		$M+98$ min	00:27:42	00:27:00
	d. Sun sensor signals switched in		$M+98$ min	00:27:42	00:27:00
	e. Sun reacquisition begun		$M+98$ min	00:27:42	00:27:00
25	Sun reacquired	Sept. 5	Event 24+0 to 30 min	00:27–00:57	00:34–
	a. Gyros turned off		Event 24+0 to 30 min	00:27–00:57	00:34–
	b. Cruise science turned on		Event 24+0 to 30 min	00:27–00:57	00:34–
26	Earth-reacquisition sequence started	Sept. 5	$M+200$ min	02:09:42	02:07:59
	a. Inhibit on Earth acquisition removed		$M+200$ min	02:09:42	02:07:59
	b. Earth sensor power turned on		$M+200$ min	02:09:42	02:07:59
	c. Gyros turned on		$M+200$ min	02:09:42	02:07:59
	d. Cruise science turned off		$M+200$ min	02:09:42	02:07:59
	e. L-band switched to directional antenna		$M+200$ min	02:09:42	02:07:59
	f. Roll search initiated		$M+200$ min	02:09:42	02:07:59
27	Earth reacquired	Sept. 5	Event 26+0 to 30 min	02:09–02:39	02:34–
	a. Roll search stopped		Event 26+0 to 30 min	02:09–02:39	02:34–
	b. Gyros turned off		Event 26+0 to 30 min	02:09–02:39	02:34–
	c. Cruise science turned on		Event 26+0 to 30 min	02:09–02:39	02:34–

See footnotes at end of table.

Figure 5-II.—Sequence of significant flight events for Mariner II—*Continued*

No.	Event	Date, 1962	Nominal time (a)	Predicted time, GMT (b)	Estimated time, GMT (c)
28	Earth-gate actuation	Sept. 8	Abnormal		12:50–
	a. Gyros turned on				12:50–
	b. Cruise science turned off				12:50–
29	Earth-gate actuation	Sept. 29	Abnormal		14:34–
	a. Gyros turned on				14:34–
	b. Cruise science turned off				14:34–
	c. Earth sensor indicating correct value				14:34–
30	Power system malfunction	Oct. 31	Abnormal		05:30–
	a. RTC-10 transmitted (cruise science off)				20:28–
31	Power system operating normally	Nov. 8			01:00–
	a. RTC-8 transmitted (cruise science on)				21:26–
32	Power system malfunction	Nov. 15	Abnormal		12:22–
33	Data encoder malfunction	Dec. 9	Abnormal		23:20–
34	CC&S malfunction	Dec. 12	Abnormal		20:01–
35	Encounter-phase sequence	Dec. 14			
	a. RTC-7 transmitted (encounter telemetry mode)				13:35–
	b. RTC-8 transmitted (cruise science on)				20:39–
36	Reference hinge angle updated				
	a. 4 RTC-2's transmitted	Dec. 15			
	b. 6 RTC-2's transmitted	Dec. 20			
	c. Failure to lock up command loop	Dec. 28			
37	CC&S or power system malfunction	Dec. 30	Abnormal		17:28–
	a. Frequency shift: data rate, 7.59 bps				17:28–

See footnotes at end of table.

Figure 5–II.—Sequence of significant flight events for Mariner II—*Concluded*

No.	Event	Date, 1962	Nominal time (a)	Predicted time, GMT (b)	Estimated time, GMT (c)
38	Final communication with spacecraft	Jan. 3, 1963			07:00–

[a] Letters in this column are defined as follows:
A, time at which launch counter starts counting; it controls all events from launch until cruise mode is established
I, time of injection
L, time of lift-off
M, time at which input decoder was to accept signals from spacecraft command system and start maneuver clock, which, in turn, was to provide signals to initiate midcourse maneuver events

[b] Predicted time is that at which event should occur, without reference to clock error.

[c] Estimated time is that at which event is believed to have occurred.

[d] Time announced by AMR.

[e] Switching from omniantenna to directional antenna should not have occurred before Earth acquisition; under the circumstances, however, this should not be regarded as abnormal behavior.

Coverage of the flight during the Atlas boost phase with both optical and electronic tracking devices was, in general, satisfactory. Tracking was provided by AMR stations 0 and 1 (at Cape Canaveral), 3 (Grand Bahama Island), and 5 (San Salvador). Telemetry coverage was supplied by station 1 tel 2 and station 1 tel 3 (Cape Canaveral), and stations 3 and 5 at Grand Bahama Island and San Salvador, respectively. The JPL launch-checkout tracking station at Cape Canaveral provided spacecraft coverage until loss of signal at the horizon. This station was in one-way lock at lift-off and maintained lock, with only a few momentary dropouts, for approximately 7½ min. The signal level at launch was −85 dbm, gradually decreasing as expected to −120 dbm immediately prior to reaching the horizon. Telemetry data indicated that all subsystems were performing satisfactorily.

At Agena first-burn cutoff, tracking coverage was provided by AMR stations 5 (San Salvador) and 91 (Antigua). However, systematic errors in the station 91 data prevented their use in real time. In addition, station 92 (Puerto Rico) was reported inoperative a few minutes prior to launch because of equipment failure. Telemetry data for Agena first burn was recovered at stations 3 (Grand Bahama Island), 5, and 91.

Telemetry coverage for Agena second burn, Agena-Mariner separation, and Agena retromaneuver was obtained from AMR, station 12 (Ascension Island), station 13 (Pretoria, South Africa), and three ships, ORV 1851 (*Whiskey*), ORV 1852 (*Yankee*), and ORV 1886 (*Uniform*, or the *Twin Falls Victory Ship*). Tracking coverage was provided during this time from stations 12 and 13, and ORV 1886.

The major events (nominal) during the Atlas-Agena boost phases are summarized in table 5–III and illustrated in figure 5–10. The altitude profile of the space vehicle during this period is shown in figure 5–11, and two concepts of the Earth-track record are presented in figures 5–12 and 5–13.

Table 5–III.—Launch-vehicle events

Event	Time, sec after lift-off (nominal)
Lift-off	L
Agena restart D-timer	L+267.5
Agena primary timer	L+288.8
Shroud jettison	L+296.8
Atlas-Agena separation	L+299.8
Agena first ignition	L+337.8
Agena first cutoff	L+484.9
Agena second ignition	L+1468.3
Agena second cutoff	L+1565.6
Agena-spacecraft separation	L+1722.3
Agena retromaneuver	L+1932.3

Flight Period From Injection Through Encounter

Mariner II was injected into interplanetary trajectory at lift-off + 26 min 3 sec. The NASA DSIF tracking station at Johannesburg, South Africa, acquired the spacecraft approximately 31 min after launch. The DSIF maintained virtually continuous contact with the spacecraft from this time until the end of the mission.

Approximately 18 min after injection (L+44 min), the solar panels had extended; the time required for full-extension was nominal, within 5 min after CC&S command. Initial telemetry data indicated that the Sun-acquisition

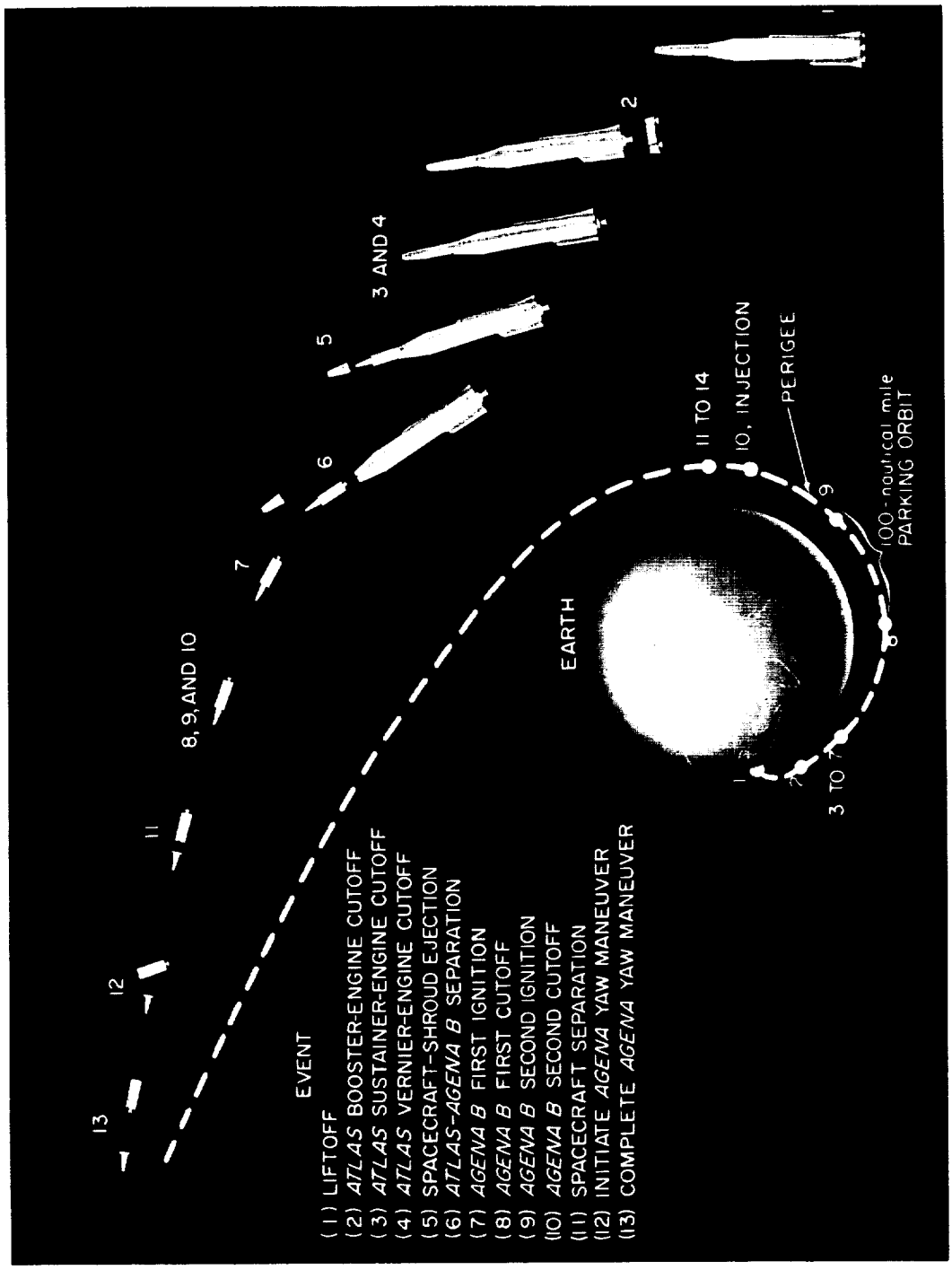

FIGURE 5–10.—Major events in booster phase of Mariner II flight.

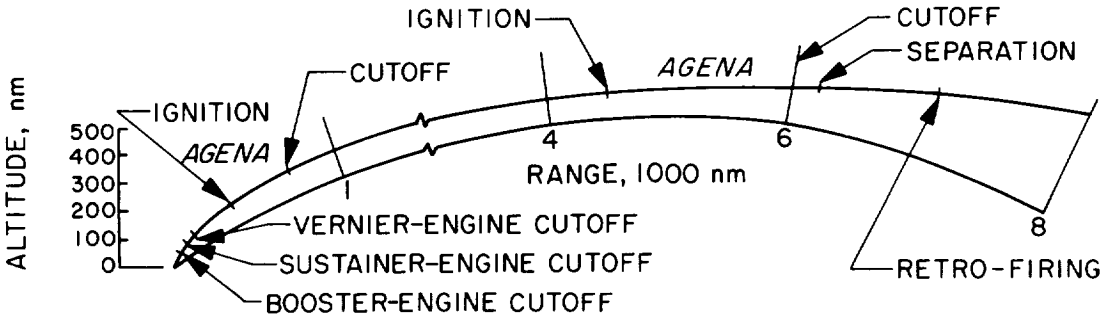

FIGURE 5–11.—Altitude profile of space vehicle during boost phase.

sequence was normal and was completed approximately 2½ min after command from the CC&S. The high-gain directional antenna was extended to its preset acquisition angle of 72°. The solar panel output of 195 w was slightly above the predicted output and represented an excess of 43 w over the spacecraft requirements for this period. Although temperatures were somewhat higher than expected for the cruise mode, after Sun acquisition most of the temperatures slowly decreased and 6 hours later showed an essentially stabilized average temperature of 84° F over the entire hexagonal structure.

With all subsystems performing normally, the battery fully charged, and the solar panels providing adequate power, the decision was made on August 29 to turn on the cruise science experiments. The first real-time command (RTC–8, see table 5–IV) was transmitted to the spacecraft from DSIF–5 (Johannesburg). Cruise science experiments were turned on, and the data rate decreased from 33⅓ to 8⅓ bits per second (BPS). The science data conditioning system (DCS) operated normally in all respects, and the science power switching unit associated with cruise operation functioned properly; however, approximately 75% of the components in this unit were inoperative until planetary encounter.

By August 31, temperatures had become stable within the tolerance limits, tracking had been continuously maintained with two-way lock, telemetry data were good, and all subsystems had operated as intended.

On September 3, 167 hours after launch, the Earth-acquisition sequence was initiated by the CC&S. The Earth sensor and the gyros were turned on, cruise science was turned off, and roll search was initiated. The spacecraft at that time was rolling at a rate of about −720 deg/hr, having steadily accelerated to that value from +235 deg/hr following first gyro turnoff. The directional antenna and Earth sensor were pointed 72° below the Earth-spacecraft plane,

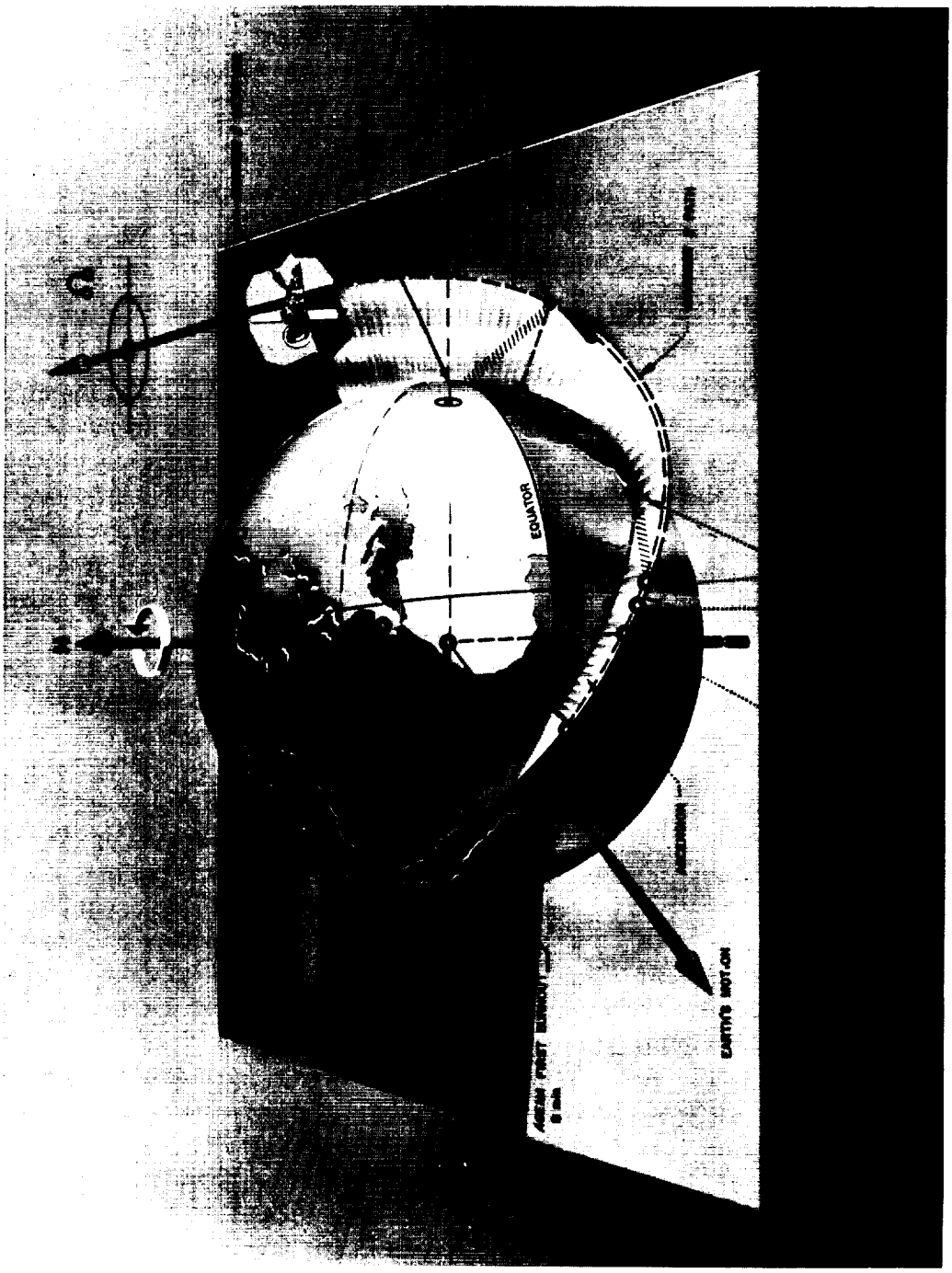

FIGURE 5–12.—Early flight of Mariner II as viewed from space.

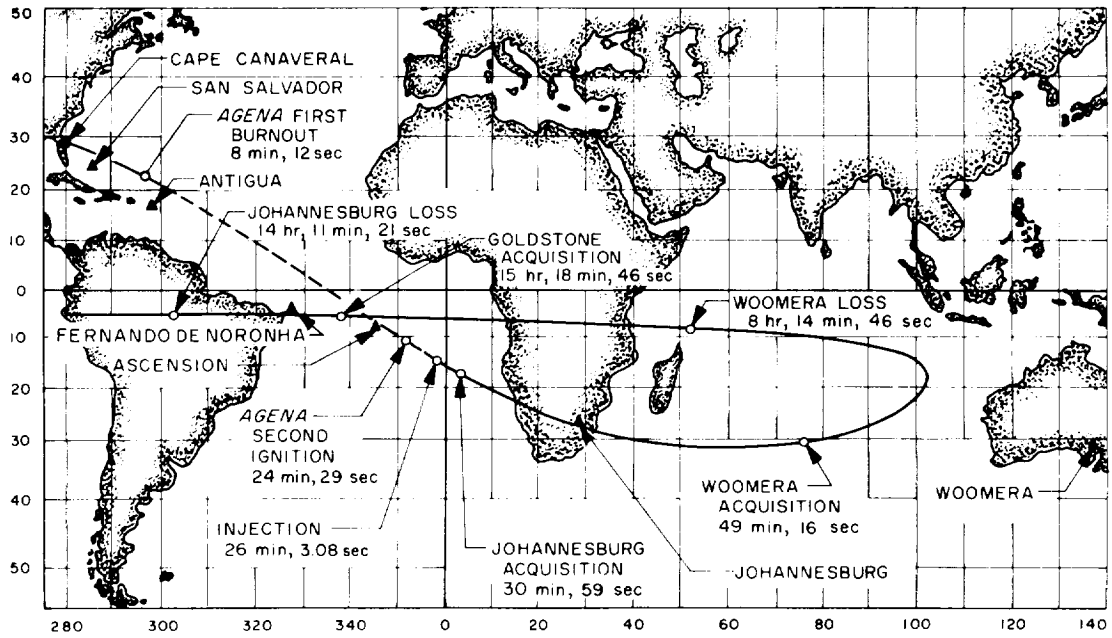

FIGURE 5–13.—Earth track of Mariner II, showing DSIF acquisition times and "turnaround" effect caused by Earth's rotation.

apparently caused by a switch from the omniantenna to the directional antenna, and data were lost until Earth lock was established 29 min later.

Telemetry data after acquisition indicated an Earth-brightness intensity measurement significantly lower than expected and comparable to that which would have resulted if the Earth sensor had been viewing the Moon. There was, therefore, a possibility that the Moon had been acquired, implying a malfunction in the antenna hinge servo. As a result, execution of the midcourse maneuver sequence (required to correct the dispersions in the original orbit) was postponed until the following day, when it could be determined that the antenna actuator had actually performed properly and that the directional antenna was pointing at the Earth.

Normal dispersions in launch-vehicle performance require inclusion of a midcourse maneuver capability in the spacecraft to provide the necessary orbit correction after the actual spacecraft trajectory is known. This capability in Mariner II was adequate to correct the original orbit.

The midcourse maneuver was initiated at 22:49:00 (GMT), September 4,

and completed at 02:45:25, September 5, with the spacecraft at a distance of 2 408 740 km (1 496 762 miles) from Earth. The maneuver sequence required five commands: three stored commands (SC–1, SC–2, and SC–3) and two real-time commands (RTC–4 and RTC–6). The stored commands contained the roll- and pitch-turn duration and polarity and the velocity increments.

Table 5–IV.—Real-time commands (RTC's)

Command number	*Command title*
RTC–1	Roll override
RTC–2	Clockwise hinge override
RTC–3	Counterclockwise hinge override
RTC–4	Command to omniantenna
RTC–5	Command to directional antenna
RTC–6	Initiate midcourse maneuver
RTC–7	A. Command planet science on B. Command planet telemetry mode
RTC–8	A. Command planet science off B. Command cruise telemetry mode C. Command cruise science on D. Command 8.3 BPS data rate
RTC–9	A. Command Sun acquisition (backup) B. Command solar panel unlatch (backup)
RTC–10	Command cruise science off
RTC–11	Spare
RTC–12	Command Earth acquisition (backup)

Commands SC–2 and SC–3 (stored commands) were transmitted twice because the station lost ground sync during transmission; however, the event registers indicated that all transmitted commands were received by the spacecraft. Mariner's receipt of the RTC–4 command switched the output of the spacecraft's transmitter from the directional antenna to the omniantenna, so that telemetry data could be recovered during the maneuver. The RTC–6 command initiated the maneuver sequence. One hour after receipt of the RTC–6 command, the Earth sensor was turned off, the directional antenna extended to 118° (nominally 120°), and the roll turn began. Exact times for the beginning and end of turns, as well as for the motor burn, could not be verified by telemetry because of the time resolution of the data; apparently, however, the roll and pitch turns and motor burn occurred normally. The entire maneuver took approximately 34 min. Telemetry data were lost for approximately 11 min because the spacecraft pitched into a partial null in the propagation pattern of the omniantenna.

Postmidcourse trajectory computations indicated that a projected miss distance of approximately 41 000 km (25 476 miles) and a flight time of 109.546 days had been achieved. Comparison of the desired and achieved encounter parameters indicated that the maneuver was accomplished with about a 10σ deviation from nominal performance. A number of possible explanations for this out-of-tolerance condition have been offered, but the telemetry data could provide no clear clues that could isolate the cause in this case.

Initial telemetry data received after the midcourse maneuver indicated that all subsystems were still operating normally. In the Sun-reacquisition sequence initiated by the CC&S at the nominal time following the maneuver, the autopilot was turned off and the directional antenna moved to the reacquisition position of 70°. The reacquisition sequence was normal and took approximately 7 min.

The Earth-reacquisition sequence was also initiated by the CC&S at the nominal time following the maneuver and, again, required approximately 30 min, the spacecraft rolling approximately 351° before Earth lock was established. The transmitter was switched to the high-gain antenna at the start of the sequence, just as in the initial Earth-acquisition sequence, causing severe fading and a loss of signal for approximately 6 min. With the exception of the propulsion subsystem, the spacecraft returned to the normal cruise mode of operation, as observed prior to the maneuver.

The first nonstandard flight event was experienced by the midcourse propulsion system. Apparently, the normally open nitrogen-shutoff valve did not close at the commanded motor shutoff, and nitrogen gas leaked slowly into the propellant tank. It was calculated that the equilibrium pressure, when reached, would be well below the burst pressure of the propellant tank and associated components; accordingly, no further complications were expected or observed.

The louvers, employed to assist in maintaining temperatures within specified bounds, caused some concern in the early stages of the cruise mode in that they appeared to be open 30° when the louver-position measurement indicated that they were closed. However, they performed satisfactorily throughout the flight and reduced the average hex temperature by 12° to 15° F.

On September 8, the gyros were automatically turned on and the cruise science experiments were automatically turned off, possibly because of an Earth-sensor malfunction or an impact with an unidentified object which temporarily caused the spacecraft to lose Sun lock. All attitude sensors were back to normal before the telemetry measurements could be sampled to determine whether or not an axis had lost lock. A similar occurrence was experienced three weeks

later, on September 29, when the gyros were again turned on and the cruise science experiments were automatically turned off. Here, again, all sensors were back to normal before it could be determined which axis had lost lock. By this date, the Earth sensor brightness indication had essentially gone to zero. The significant difference between the two events was that, in the second case, telemetry data indicated that the Earth-brightness measurement had increased to the nominal value for that point on the trajectory.

On October 31, the power subsystem began to operate abnormally with loss of power from the 4A11 solar panel (with solar sail attached), a malfunction diagnosed as a partial short circuit in the panel. As a precaution against the spacecraft's going into a power-sharing mode, an RTC–10 command was transmitted from Goldstone Tracking Station, turning off the cruise science experiments and, thereby, reducing power consumption.

Eight days later, telemetry data indicated that the panel was again operating normally; an RTC–8 command was, therefore, transmitted from Goldstone to reactivate the cruise science experiments. Science telemetry data remained essentially the same as before the experiments had been turned off; however, engineering telemetry data indicated that most temperatures increased shortly after the science experiments were reactivated, because of the increased power requirements of the spacecraft. A recurrence of the panel short was experienced on November 15. However, with the spacecraft nearer the Sun, power supplied by the one operative panel was adequate to meet the spacecraft's demands, and the cruise science experiments were permitted to remain active.

At this time, the magnetometer evidenced a high offset caused by current redistribution when the power failure occurred. This made readings difficult to interpret, but the data recorded indicated reasonably steady magnetic fields. Other occasional unscheduled magnetometer calibrations occurred throughout the flight.

Radiometer calibration data received during the cruise phase predicted a probable nonstandard operation of that instrument at the time of encounter, and it was considered possible that, upon initiation of mode III,[1] the radiometer would be in permanent slow scan, and that no scan-rate change or automatic scan reversal would occur. The data also indicated that only one of the two microwave radiometer channels would have the desired sensitivity. In actuality,

[1] Mode I was the launch phase, when only engineering data were transmitted. Mode II (cruise) provided both engineering and scientific data. Mode III (encounter) transmitted only scientific data from the immediate vicinity of Venus.

however, both the microwave radiometer and the infrared radiometer channels had acceptable sensitivities at encounter, and one scan-rate change occurred which allowed three scans of the planet.

The calibration data for the cosmic dust experiment indicated that, by November 27, either the instrument sensitivity or the amplitude of the calibration pulse had decreased by 10%; by December 14, a further decrease by a factor of 10 had occurred.

In the Deep Space Instrumentation Facility, occasional minor problems arose, such as a commercial power failure at Goldstone during the September 22–23 view period, when changeover to local generators was delayed because of an inoperable automatic-transfer switch. In this particular case, about 1½ hours of data were lost.

During the week ending November 21, an occasional out-of-sync condition in the telemetry data was diagnosed as a telemetry-demodulator problem at the stations; the spacecraft was not at fault. No real-time telemetry was transmitted from Goldstone and Johannesburg to Pasadena during the November 26 view period. The information was not lost, however, since all data were recorded on magnetic tape at these stations and later sent to the Space Flight Operations Center.

Except for problems of this nature, the DSIF stations covered the Mariner II operation continuously and successfully. In taking two-way Doppler data for orbit determination, DSIF 3 (Echo Station, Goldstone) transmitted to the spacecraft and DSIF 2 (Pioneer Station, Goldstone) received the signals from the spacecraft.

On November 14, the reference hinge angle changed by one data number (DN), an event which should normally have occurred only at cyclic update times. This phenomenon had occurred several times during preflight system tests. With the exception of this anomaly and the Earth sensor abnormalities previously noted, the attitude-control system performed without fault through December.

Spacecraft temperatures became a cause for concern in mid-November, since they had been higher than the predicted values. On November 16, the temperature of the lower thermal shield reached its telemetry limit: a "pegged" DN of 126, which corresponds roughly to 95° F. Seven out of eighteen temperature measurements were "pegged" before the encounter phase, and these temperatures were subsequently estimated by extrapolation.

On December 9, a failure in the data encoder circuitry disabled four telemetry measurements: Antenna hinge angle, propellant-tank pressure, midcourse-motor

pressure, and attitude-control nitrogen pressure. Loss of these four measurements did not affect the outcome of the mission.

The CC&S was designed to perform various functions, one of which was to provide the attitude-control subsystem with a timing, or cyclic update, pulse every 1000 min to update the antenna reference hinge angle. Each cyclic update pulse was evidenced by the fact that event register 3 stepped one count. Until December 12, the pulses occurred with predictable regularity. On that date, however, only 2 days before the encounter phase, the CC&S failed to issue the 155th (or any subsequent) cyclic pulse. As a result of this malfunction, the spacecraft was switched to the encounter mode of operation by a prearranged backup ground command (RTC–7), transmitted from Goldstone Tracking Station on December 14.

On December 14, prior to transmission of RTC–7, seven spacecraft temperature sensors had reached their upper limits. The Earth-sensor brightness data number had dropped to 3. Approximately 149 w of power was being consumed by the spacecraft (165 w was available from the 4A12 solar panel). About 16 w from the 4A12 panel were being dissipated in the 4A11 panel. All science experiments were operating and coverage by the DSIF remained continuous and virtually normal. Signals were clear and data quality was good.

Sixteen orbit computations were made during the interplanetary phase of the flight, covering the period from the midcourse maneuver on September 5 to December 7, when the mass of Venus caused the first detectable perturbation in the Mariner II trajectory. During the encounter phase (fig. 5–14), which, for purpose of trajectory computation, covered the period December 8 to 18, fourteen computations were run. Of these, eight preceded Venus encounter and six followed. On the basis of these fourteen computations, it was determined that the closest approach to the surface of the planet was 34 854 km (21 645 miles) occurring at 19:59:28, December 14, 1962. Spacecraft velocity at the time was 6.743 km/sec (4.19 miles/sec) relative to Venus. The elapsed time from injection to closest approach was 109.546 days (fig. 5–15). Additional pertinent data regarding the encounter trajectory and Venus scan are given in chapter 4.

During the encounter phase, only scientific telemetry data were transmitted by the spacecraft. The operation of all science experiments was essentially successful, except for the sensitivity decrease in the cosmic dust experiment.

The encounter mode lasted approximately 7 hours, being terminated by a ground command (RTC–8) transmitted from Goldstone. The spacecraft was returned to the cruise mode at 20:40:00 GMT on December 14, 1962.

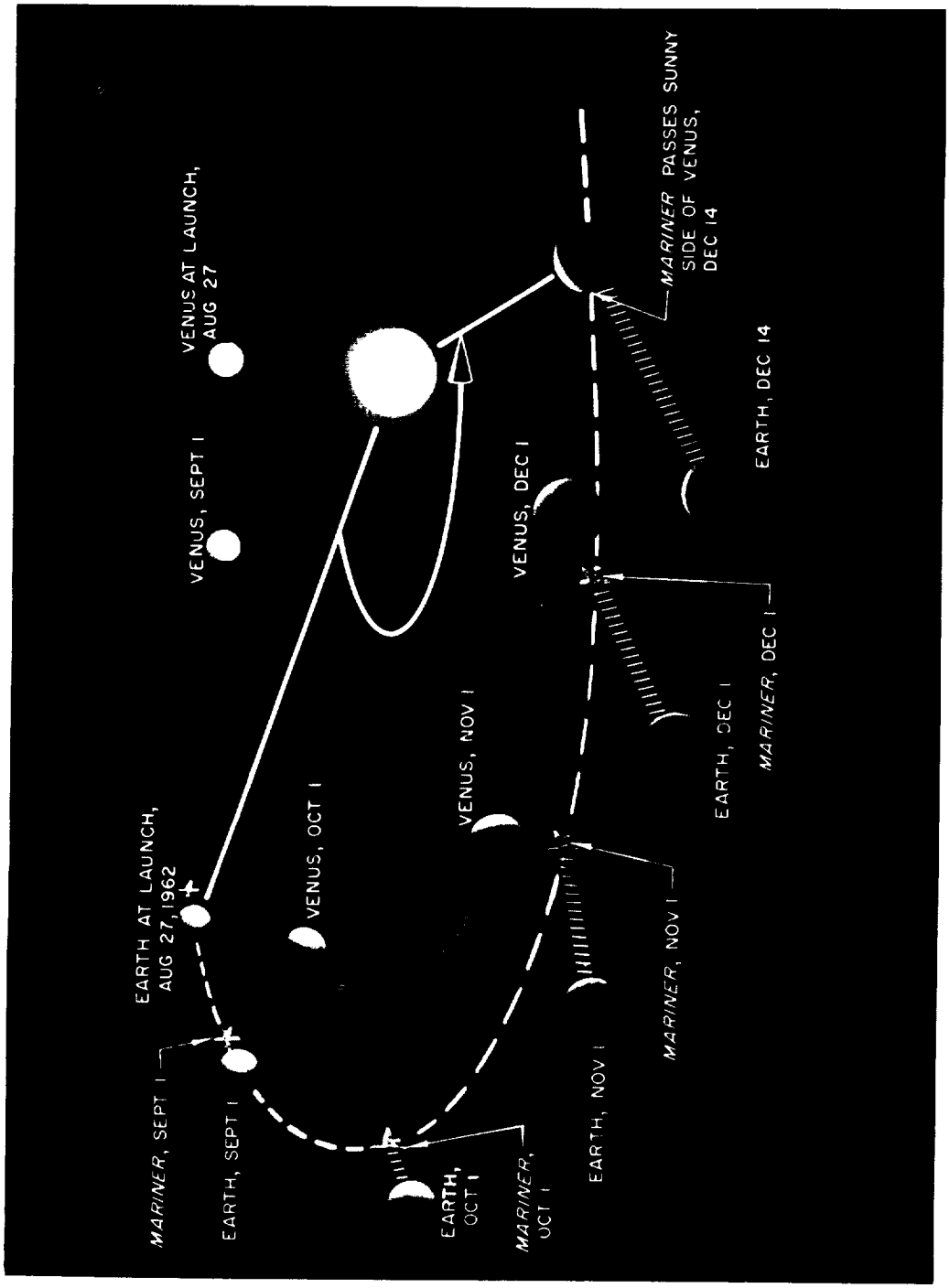

FIGURE 5-14.—Relative orbital positions of Earth, Venus, and Mariner II during 109-day flight.

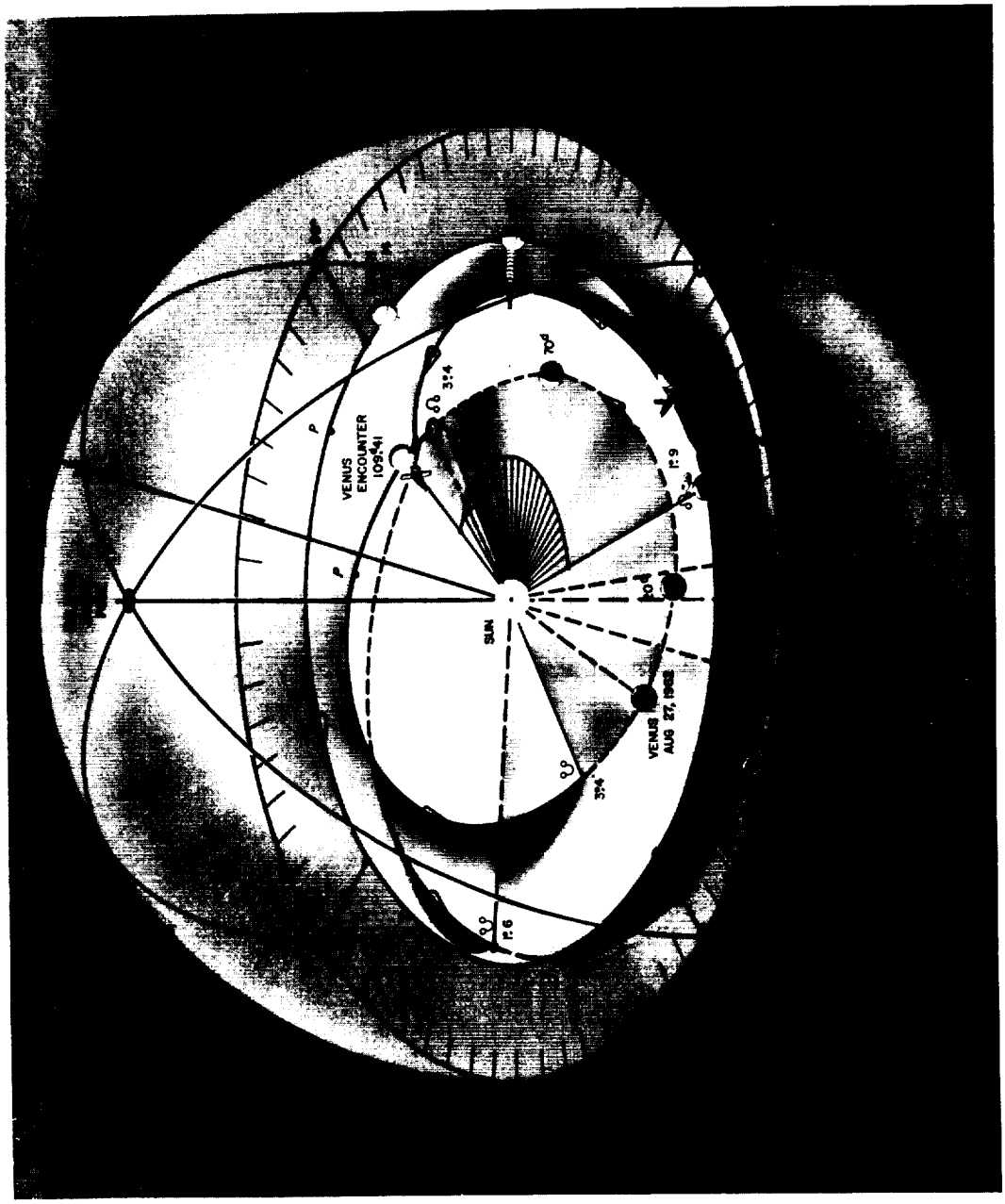

FIGURE 5–15.—Orientation of Mariner II trajectory in celestial sphere.

Postencounter Flight

In the postencounter flight of Mariner II, engineering telemetry data indicated that all subsystems performed essentially as before the encounter phase. Temperatures still rose and were not expected to decrease until after the attainment of perihelion (point closest to the Sun) on December 28.

As a result of the CC&S malfunction, the antenna reference hinge angle had not been updated since December 12. In the event that the spacecraft lost Earth lock, and to prevent the directional antenna from moving to the last antenna reference hinge-angle setting, two series of commands (RTC–2) were transmitted from Goldstone, once on December 15, and again on December 20, increasing and updating the reference hinge angle. Five of these commands were accepted by the spacecraft and the effective reference angle change was believed to be 8°.

On December 16, the Earth-sensor brightness data number dropped to 1, the telemetry threshold. Nevertheless, negative data-number values were extrapolated to a value of about −20 by January 3, 1963, when communication with the spacecraft ceased. Continuous DSIF coverage was changed on December 17 to approximately 10-hour coverage per day to provide relief to the stations.

Perihelion was reached at 05:15 on December 28. On this date, an attempt was again made to command the reference hinge angle to update, but Goldstone verified through its inability to lock up the command loop that command threshold had been reached, as previously predicted.

At 17:28:00 GMT December 30, a reference-frequency circuit failure in the CC&S countdown chain resulted in temporary loss of the telemetry signal; however, RF lock was maintained. When the telemetry signal was again locked up, 1½ hours later, the telemetry bit rate had changed from the nominal 8.33 BPS to approximately 7.59 BPS. Simultaneously, internal-temperature readings increased due to inefficiency of power subsystem design at lower frequencies.

The spacecraft was tracked for the last time at 07:00:00 (GMT) on January 3, 1963, by the Johannesburg DSIF. During this pass, about 30 min of real-time telemetry data was received. Although the demodulator went out of lock at 05:21 and remained out for the balance of the tracking period, good RF lock was maintained throughout the tracking period from 03:54 to 07:00. Examination of the recorded data showed that the spacecraft was still performing normally, with a power consumption of 151 w and available power of 163 w from the 4A12 solar panel. Spacecraft trajectory data during the final tracking period were as follows.

Distance from Earth	86.677 million km (53.860 million miles)
Distance from Sun	105.857 million km (65.778 million miles)
Distance from Venus	8.994 million km (5.588 million miles)
Velocity relative to Earth	21.980 km/sec (13.658 miles/sec)

Further search for the spacecraft was unsuccessful, as expected. Fifty commands were sent from Goldstone on January 8, 1963, but the spacecraft did not respond. On May 28, the Goldstone antenna was positioned according to the expected ephemeris data and a frequency search was conducted during the calculated view period, with negative results. A similar attempt on August 16, 1963, was also unsuccessful.

CHAPTER 6

Performance of Mariner II Subsystems

Although several of the spacecraft subsystems experienced adverse anomalies, the primary objectives of the Mariner mission were met successfully, and the flight provided a large quantity of valuable data relating to interplanetary and near-Venus space, and the nature of the planet's exosphere and surface temperature. Useful information concerning spacecraft performance and design was gained from the engineering telemetry—data that will be most useful in future spacecraft design.

Simplification of the alinement-control philosophy apparently had no adverse effects on the critical spacecraft alinements or midcourse maneuver accuracy. As an alternative to optical alinement of the assembled components, tight tolerances were held on individual mechanical components. Other design features confirmed by the successful completion of the mission were: The methods used for center-of-gravity determination, the midcourse-motor location, and the use of adequate view angles at the primary and secondary Sun sensor locations. The Earth sensor mirror and light baffles apparently performed as intended and did not affect the sensor's pointing accuracy, despite the early confusion about the validity of the initial Earth lock.

As the flight progressed, it became evident that spacecraft temperatures reached levels higher than predicted, although the flight transducers indicated that the upper thermal shield was performing as designed and that thermal energy was being adequately distributed throughout the basic hex structure, minimizing case-temperature differences. The louvers performed their function of lowering temperature excursions of the attitude-control case, and thereby indicated the operability of the louver bearings in a vacuum environment. The attempt to balance the solar torque on the spacecraft about the yaw axis by means of the solar sail was considered satisfactory.

ENGINEERING MECHANICS SUBSYSTEMS

On Mariner II, the major subsystems included in the engineering mechanics category were: (1) structures, (2) temperature control devices, (3) pyrotechnics (pin-pullers and squibs), (4) solar-panel actuators and radiometer scan actuators,

and (5) cabling. Analysis of spacecraft data indicates that nonstandard flight behavior occurred in the temperature control and pyrotechnics sybsystems. Since the performance of the temperature control subsystem, with the resulting effects on other subsystems, caused considerable anxiety during the later stages of the mission, it is discussed here in detail. Possible failure modes of the mid-course-motor shutoff squib, which may have caused the propellant-tank pressure rise, are reviewed in conjunction with the pyrotechnics subsystem.

Direct telemetry data were received on the performance of the temperature control subsystem, the electrical pyrotechnic pin-puller and valve-actuation subsystem, and the radiometer scan actuator. The behavior of the other engineering mechanics subsystems could only be deduced, directly or indirectly, from these telemetry data. Where applicable, this information has been interpreted as an indication of successful performance.

Structures

The primary purpose of a spacecraft structure was physical support of all subsystems in an optimum configuration. The Mariner II spacecraft structure was designed for compatibility and proper function with the booster. This included separation, shroud clearance, and boost-environment survival. Figure 6–1 is a photograph of the Mariner II basic hexagonal structure (or "bus").

As noted above, the configuration was apparently adequate. Although no instrumentation was included to measure the vibration environment, the spacecraft performance appeared to indicate that no failures resulted from unanticipated vibration levels. Had measurements been included to determine the boost environments, the weight penalty incurred by conservation in the design and test vibration levels could have been evaluated.

The damper system, which was added to limit Earth sensor excursions, apparently reduced the sensor vibration environment to an acceptable value. During the Mariner II launch, the abnormal rolling of the Atlas booster just after booster-engine cutoff apparently did not overload the spacecraft. The maximum centrifugal acceleration of any spacecraft component was less than 3g. This, however, was coupled with a 2g axial acceleration, plus some unknown vibration. The shroud was apparently ejected without spacecraft damage.

Agena-Mariner separation apparently occurred normally. On the basis of tumbling-rate information deduced from telemetry of the spacecraft gyro outputs, the yaw and roll rates before solar panel extension were below the

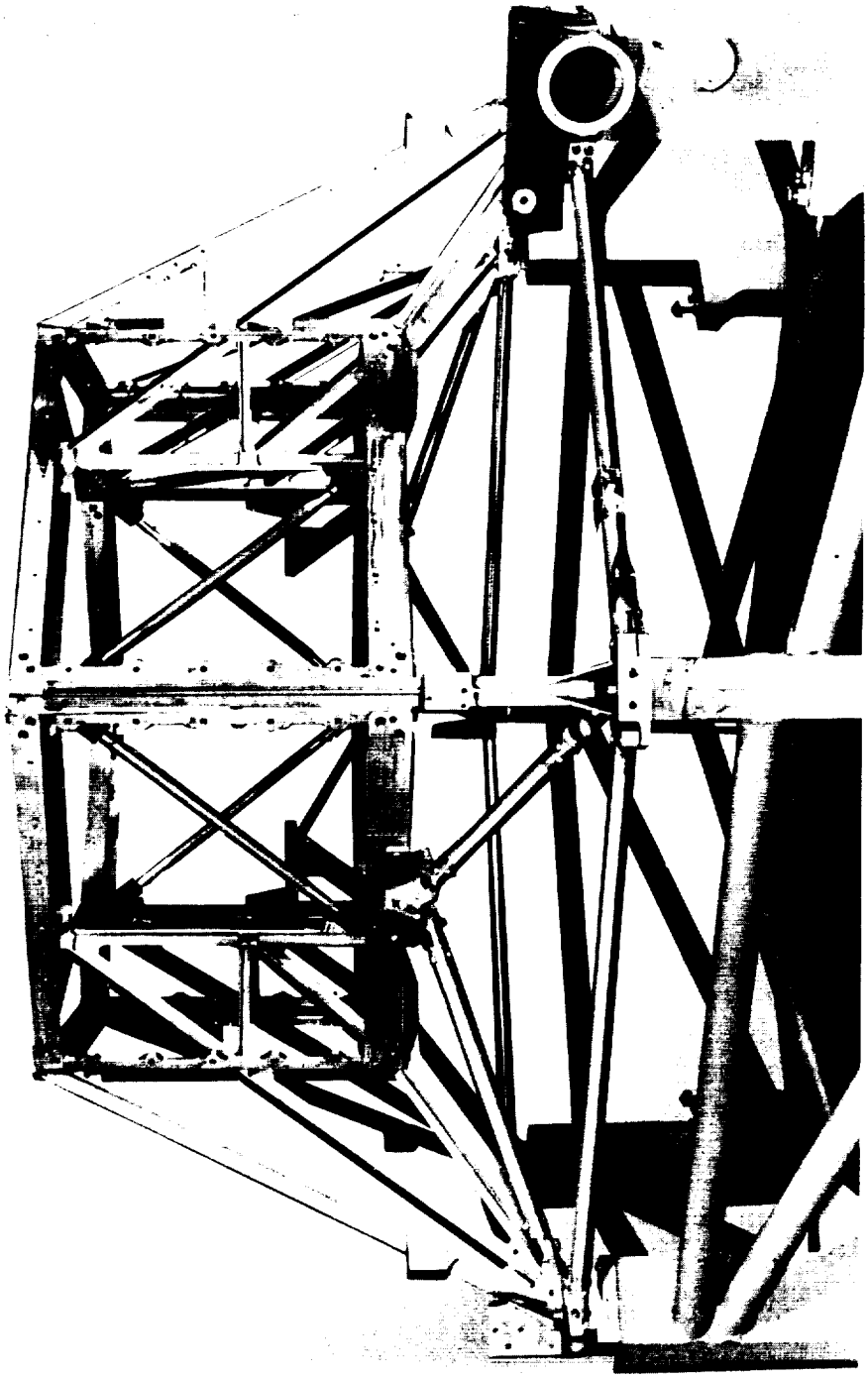

FIGURE 6-1.—Spacecraft hexagonal structure.

maximum measurable value and the pitch rate exceeded it. Later, as the product of inertia coupling and the opening of the solar panels, the yaw rate exceeded that value, whereas the pitch rate fell back within this maximum value. On the basis of this information, all separation rates were deduced to have been well within the specified maximum, indicating a normal separation.

Temperature Control

The basic features of the Mariner II temperature control system, shown in figure 6–2, are the upper and lower thermal shields, the louvers, and the various coatings and finishes.

At AMR, the prelaunch activity pertinent to temperature control of Mariner II involved final thermal preparation and the monitoring of spacecraft temperatures during final tests. Basically, final thermal preparation consisted of insuring that all spacecraft surfaces conformed to the temperature control design. All surfaces were meticulously cleaned where possible; however, repainting of some assemblies was required. Spacecraft temperatures were monitored during the various electrical tests, and checks were made to insure that no out-of-tolerance temperature conditions existed. A continuous log of spacecraft and environment temperatures was maintained; in this way, a normal thermal condition was established, against which spacecraft temperatures were checked during countdown as an aid in detecting any abnormal condition.

Prior to launch, Mariner II temperatures had stabilized at predicted levels, consistent with previous countdowns and tests. The environment within the shroud was maintained at 70° F by means of the air-conditioned shroud-cooling blanket. Spacecraft temperatures during launch changed from 70° to 109° F.

Although the immediate postlaunch environment caused temperatures to rise, they were slowly decreasing at 2 hours after launch. At 8 hours after launch, temperatures had stabilized, with an average hex temperature of 84° F.

From this time until initiation of the midcourse maneuver, all temperatures remained essentially constant. At that time, because of increased internal power, a significant heat input from the propulsion system, and the loss of Sun orientation as required by the maneuver, the spacecraft hex experienced an average rise of 20° F. Within 10 hours after midcourse, temperature had decreased to premaneuver values. The maximum and minimum temperatures measured during the midcourse maneuver were, respectively, 130° F on the midcourse-motor nitrogen tank and 72° F on the upper thermal shield.

During the cruise phase and through encounter, Mariner II temperatures

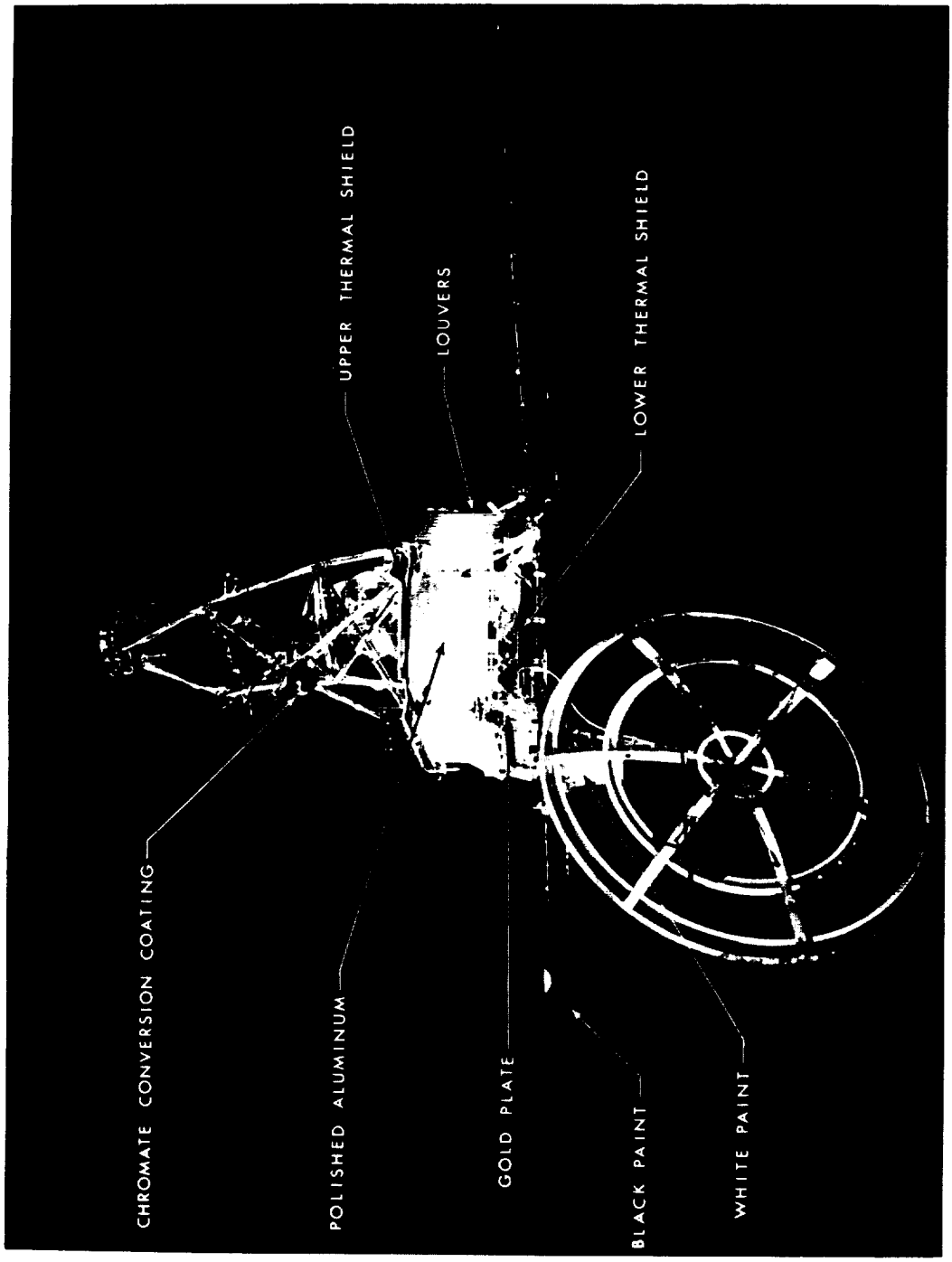

FIGURE 6-2.—Mariner R temperature control system.

steadily increased, except in the Earth sensor and the antenna yoke, which cooled to 85° F on October 27 and then again increased in temperature. This variation occurred because these components were shaded by the spacecraft structure as the antenna hinge angle changed.

On October 31, a solar-panel malfunction, followed by an off-science condition, resulted in a temperature decrease of 5° F in the hex. Particularly affected were the booster regulator, the battery, and a science electronics assembly, which dropped 9°, 5°, and 8° F, respectively. The temperature drops were a direct result of a decrease in the power dissipated within the hex. Eight days later the solar panel returned to normal operation and cruise science was reactivated. Within 8 hours temperatures had regained the increment dropped after the malfunction. On November 15, when the second solar-panel malfunction occurred, cruise science was not commanded off and temperatures were only slightly affected.

Although temperature measurements were not telemetered during the encounter mode, measurements made before and after encounter were compared to determine the thermal influence of Venus on the spacecraft. Both the battery and the power assembly indicated a 2° F temperature rise when the cruise mode was resumed. Both of these assemblies faced Venus during encounter; however, part of the temperature rise resulted from increased internal power dissipation.

After encounter, spacecraft temperatures continued to rise slowly until December 28, when the spacecraft had reached the point of closest approach to the Sun. Before the slowly decreasing solar intensity could result in lower temperatures, the CC&S failure on December 30 caused a lowering of electrical efficiency within the spacecraft. The result was a sharp rise in internal-power dissipation, which caused hex temperatures to rise gradually over the following 3 days. By January 2, 1963, the following temperature rises had occurred: Booster regulator, 9° F; midcourse-motor nitrogen tank, 8° F; propellant tank, 5° F; battery, 7° F; case I, 3° F; case II, 3° F; case III, 3° F; case IV, 5° F; case V, 17° F; upper thermal shield, 2° F.

During flight, the Mariner II temperatures near Earth exceeded expectations by as much as 40° F; those near encounter were higher than anticipated by as much as 75° F. The only monitored temperatures which behaved as expected were those of the solar panels. A summary of predicted and actual temperatures is presented in table 6–I.

There are four general categories into which possible causes for the high-temperature condition can be grouped:

Table 6-I.—Predicted and actual flight temperatures for Mariner II (typical)

Component	Temperature, °F					
	Earth (stabilized)		Venus		Maximum (Jan. 2, 1963)	Desired operating limits
	Actual	Predicted	Actual	Predicted		
Power booster regulator	80	78	129	114	143	32–140
Midcourse-motor nitrogen	78	55	139	84	151	35–165
Propellant tank	76	55	138	84	148	35–165
Earth sensor	78	40	• 165	90	• 171	0–95
Battery	70	55	• 130	91	141	50–120
Attitude control nitrogen	68	59	• 160	115		32–140
Solar panel front	126	132	• 250–254	262		As cold as possible
Case I	73	50	152	92	160	14–149
Case II	85	60	152	90	159	0–140
Case III	86	62	149	89	157	0–149
Case IV	74	60	124	80	134	50–130
Case V	86	52	135	84	158	32–140
Lower thermal shield	58	32	• 122	58		
Upper thermal shield	59	80	153	215	162	
Solar plasma experiment (case I)	78	50	155	92		14–158

• Extrapolated data.

1. High internal-power dissipation. Although erroneous predictions for individual components may have been made, it is believed that no great overall disparity between expected and actual power dissipation existed.

2. High solar-heat input. The fact that the temperature rise between Earth and Venus was substantially higher than expected suggests that excessive solar inputs were partially to blame. These inputs could have been caused by either or both of the following conditions:

a. Reflected solar irradiation. For example, the energy incident on hex faces which was reflected from intercostals and legs could not be simulated in preflight tests by the heater-pad approach. Direct solar inputs were simulated by applying the appropriate heat to sunlit areas, but any similar treatment of reflected sunlight was too difficult to implement properly.

b. Conduction of heat to the hex from sunlit structural members. This source resulted from the degradation of white paints and the upper shield

because of ultraviolet irradiation, which may have been caused by an increase in total spacecraft solar absorptivity.

3. Lowered emissivities. Any contamination of polished surfaces by oil, dirt, and so forth, causes an increase in emissivity and, hence, in heat-radiating capability. The exact nature and degree of contamination of spacecraft surfaces in vacuum chambers has proved difficult to assess, although oil contamination is known to occur from time to time. In any case, it is possible that the "cleaning" action of the hard vacuum of space may have lowered spacecraft emissivities, with resulting higher temperatures.

4. Inadequate thermal-test mockup. Some of the difficulties encountered in preflight thermal tests have been mentioned above. An additional source of error was the localizing (in heater pads) of distributed solar inputs and the possibility that heaters used in the test separated from the spacecraft surface. Both of these factors could have caused local hot spots which radiated heat at high temperatures, thereby creating artificially low temperatures within the spacecraft during preflight tests.

Despite the high temperatures of the spacecraft, the thermal design proved adequate. The louvers performed well, decreasing the average hex temperature excursions by 12° to 15° F. All temperatures stayed within limits during the critical midcourse maneuver. The large store of flight data which have been collected should prove invaluable in temperature control studies for future generations of spacecraft.

Pyrotechnics

The pyrotechnics subsystem (figs. 6–3 and 6–4) was designed to unlatch the solar panels and radiometer; open the nitrogen, fuel, and oxidizer valves to start the midcourse motor; and close the nitrogen and fuel valves to stop the motor at CC&S commands. All functions were performed as designed, with the exception of midcourse-motor nitrogen-pressure shutoff.

The failure of the midcourse-motor nitrogen-pressure shutoff has led to speculation that the firing relays in the pyrotechnic control assembly (PCA) may have failed to operate. In the following paragraphs, this speculation is discussed. As an aid in the analysis, a simplified schematic of the portion of the subsystem necessary for nitrogen-pressure shutoff is presented in figure 6–5.

Telemetered event register information indicated that the PCA was armed at spacecraft-Agena separation and supplied squib-firing voltage to primary

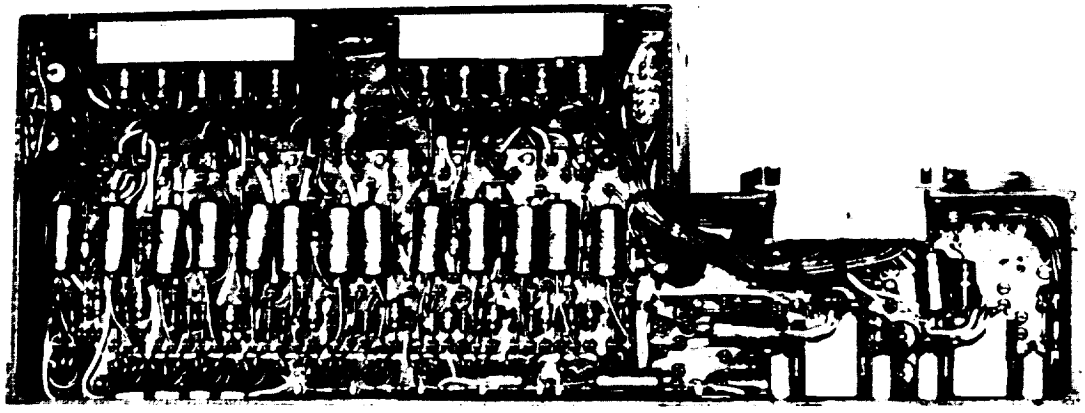

FIGURE 6–3.—Pyrotechnics control assembly.

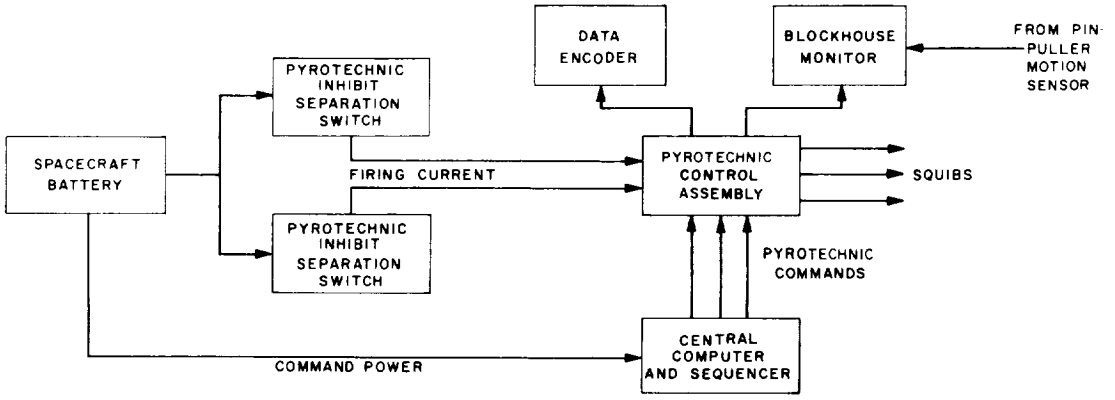

FIGURE 6–4.—Block diagram of pyrotechnics system.

solar panel and radiometer pin-pullers at command. Opening of the solar panels was verified by event register counts received when the solar panels were fully extended.

Necessary functions of the subsystem for midcourse-motor shutoff were: (1) receipt of the CC&S command, (2) delivery of firing current by the PCA to the dual bridgewire squibs, (3) maintenance of the continuity and integrity of the firing lines, (4) proper operation of the squibs, and (5) complete closure of the normally open fuel- and nitrogen-pressure explosive valves.

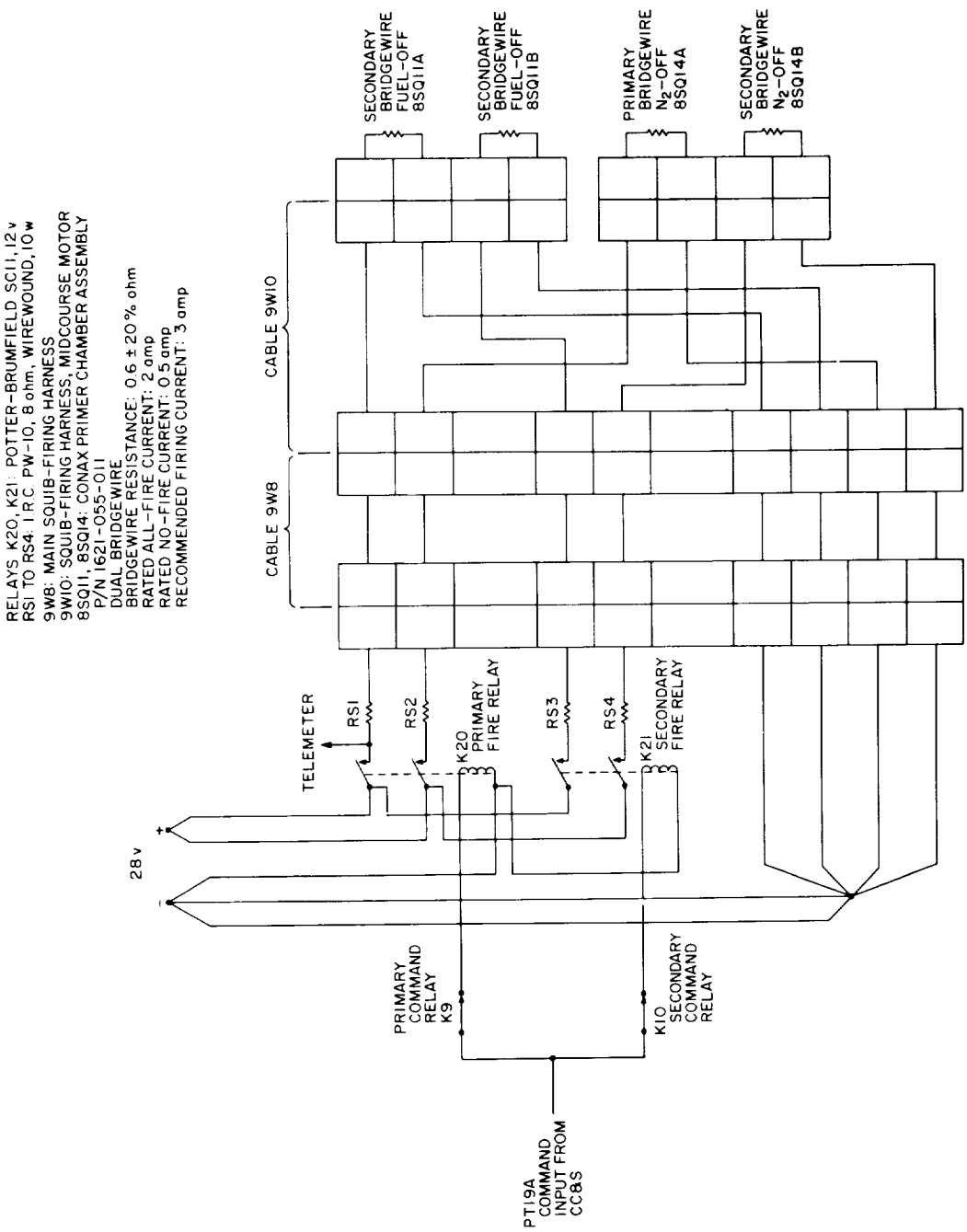

FIGURE 6–5.—Schematic diagram of nitrogen-pressure shutoff system.

The following facts are known from flight information received from the spacecraft:

1. After midcourse-motor firing, pressure on the nitrogen tank decreased, whereas pressure on the fuel tank increased, indicating an open or leaking nitrogen-shutoff valve.

2. The CC&S command was given as indicated by one count on event register 3.

3. Firing voltage was supplied by the PCA through relay K20 to the primary firing line to fuel-off squib bridgewire 8SQ11A, as indicated by one count on event register 1.

4. Squib 8SQ11 fired through relay K20, and the midcourse-motor fuel-supply valve was closed, causing the motor shutoff. This event was indicated by the end of Doppler variation. Firing voltage to the nitrogen-pressure-off squib 8SQ14A was not telemetered. However, relay K20 also supplies firing voltage to the primary bridgewire on the nitrogen-pressure-off squib through the other pole of the two-pole relay. The redundant firing circuit to squibs 8SQ11 and 8SQ14 is a duplicate circuit, with the exception that neither fuel-off nor nitrogen-pressure-off firing voltage is telemetered.

Cabling integrity and bridgewire resistance to the midcourse-motor squibs were verified prior to installation of the midcourse motor in the spacecraft. After midcourse-motor installation, the checks were repeated; measured resistances were recorded and all firing lines and bridgewires were checked for continuity. In all tests prior to flight, the PCA had never once failed to fire both primary and secondary squib simulators. Central recorder data taken during systems tests showed a minimum current of 2.6 amp delivered to nitrogen-pressure-off simulators. All squibs in the midcourse-motor valves fired normally during the dummy test run conducted at JPL on April 13, 1962. The probability of failure in the supply of firing current to the nitrogen-pressure-off squib was remote, since two failures would have had to occur in the PCA and/or the firing harness.

The theory has been advanced that a previously fired squib (nitrogen-pressure-on) may have fragmented and severed or damaged the firing leads to the nitrogen-pressure-off squib. While this is a possibility, the routing of cable 9W10 on the motor frame and the placement of the explosive valves and squibs also indicated that this type of failure was not likely (refer to fig. 6–6).

A more plausible explanation of the malfunction is failure of the squib itself, or failure of the valve to close completely. Squib testing indicated a high degree of firing reliability at the 2.6 amp minimum current mentioned above.

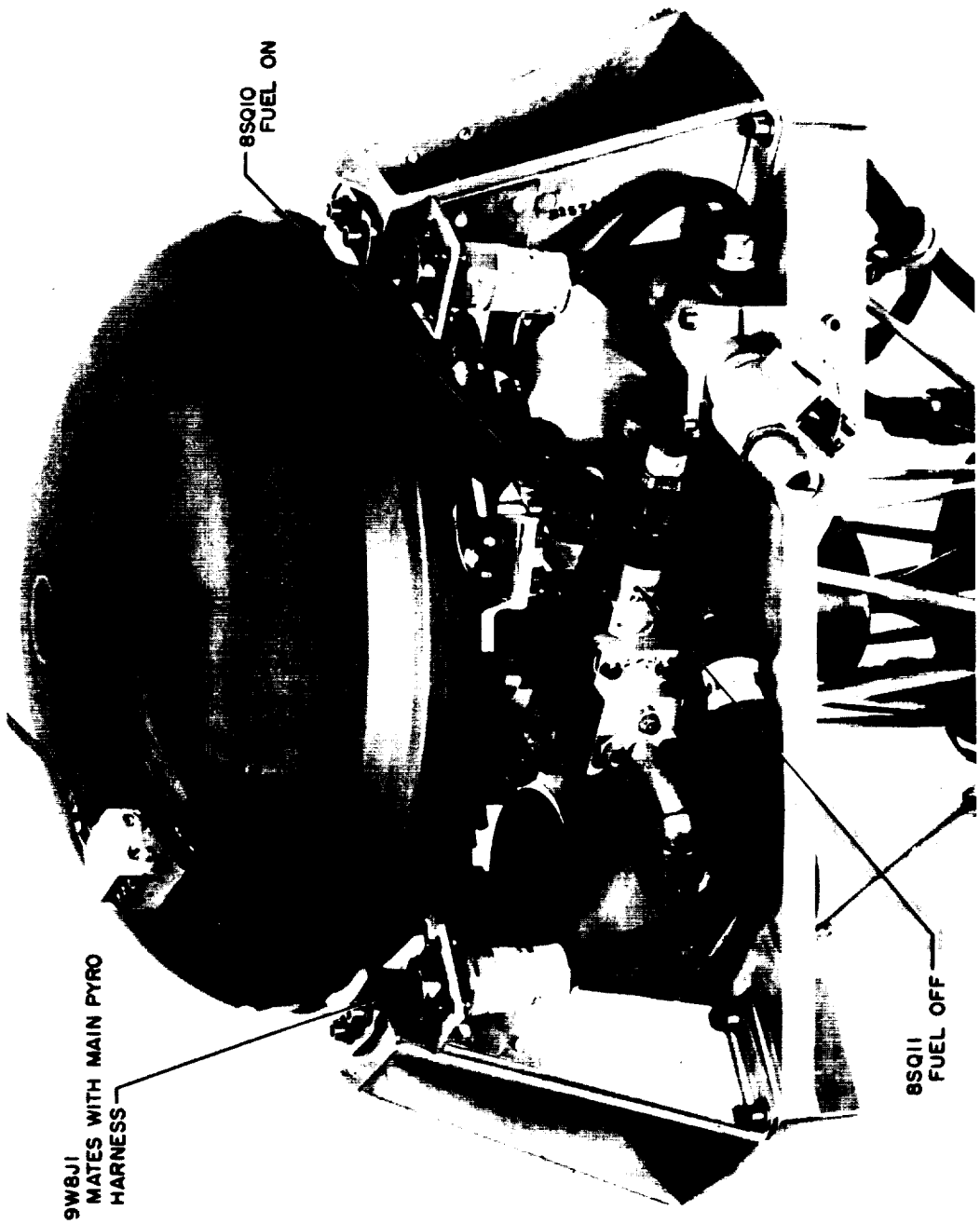

FIGURE 6–6.—Midcourse-maneuver-motor frame.

Valve test history indicated that the nitrogen valve operated reliably with the associated squib. There is reason to believe, however, that the squib charge may have been slightly high. Thus, any supposed squib-valve failure was probably not due to inadequate charge (degraded squib or welded valve) but was probably associated with an overcharge (fractured piston, or prior venting of on squibs, resulting in cable damage). Analysis testing was concentrated on the squib-valve overcharge concept, and also on the possibility of squib degradation due to space environment. It should be noted that the squibs were hermetically sealed, and that tests were run for seal verification.

Actuators

The radiometer scan actuator was designed to scan at either of two rates. During the planet-search phase, the actuator operated at the higher rate (1 deg/sec), with a fixed amplitude of $\pm 60°$. When the planet was located, the DCS changed the scan actuator to its low-speed scan (0.1 deg/sec) and controlled its amplitude to keep the radiometer correctly oriented on the planet. The only telemetry on the actuator was the position potentiometer on the output end, designed to correlate pointing position with radiometer data; thus, the position information was returned through the science system. On the basis of data analysis, it appears that the actuator functioned as commanded by the DCS.

During the flight, the actuator started in fast scan as designed; however, because of a malfunction in the radiometer system, it switched to slow scan 60 sec later and before planet encounter. The amplitude of the scan remained at $\pm 60°$ as controlled by the limit switches. At planet encounter, the actuator continued to scan at 0.1 deg/sec, but did not properly reverse at the planet limb because it was not commanded to do so. The first scan across the planet was on the dark side, and the second crossed the terminator onto the sunlit side. As the radiometer crossed the limb at the completion of the second scan, the actuator switched to fast scan. Shortly after the scan direction reversed at the 60° limit, the scan rate again switched back to the lower speed, and a third and final planet scan was made across the lighted side of the planet.

The actuator was designed, within schedule and state-of-the-art limitations, so that it would function over the required encounter phase without benefit of an artificial atmospheric environment. However, as a backup device, the actuator housing was sealed by O-rings and pressurized to 1 atm with clean dry air. The unit survived the 108 days of space-environment storage, as indicated

788-025 O—65——10

by the fact that it operated for the full encounter period; whether pressure was maintained is not known.

In addition to confirming the actuator design, the operation indicated that selection of the radiometer support bearing, cabling design, and material had been satisfactory.

Flight data from the pyrotechnics subsystem indicated that the solar-panel actuators opened the panels to within 5° of their cruise position in approximately 1 min. The panels are presumed to have extended and locked in the cruise position.

Cabling

The Mariner II cabling apparently did not deteriorate enough during the flight to impair spacecraft operation. Minor malfunctions in the spacecraft which might be attributed to deterioration of cabling components were studied, and laboratory tests under high temperature and vacuum were conducted on the wire insulation, connector inserts, abrasion-protective tubing, and potting-compound materials. No indication of inadequacy in the cabling system was uncovered by these efforts, and the successful performance of the mission tended to confirm this conclusion.

GROUND HANDLING EQUIPMENT

In general, the ground handling equipment for the Mariner R spacecraft was similar to Ranger and Mariner A equipment.

The hoisting assembly consisted of an upper sling, spreader frame, lower sling, and lifting bars. All lifting of the spacecraft by overhead cranes was performed with this equipment.

The support and JPL adapter were used with either the shop dolly or the transport trailer for assembly and local transport of the spacecraft (fig. 6–7). The upper portion of this assembly also served to position the high-gain antenna dish for installation and alinement. The lower part provided a mount for the Agena adapter. The height of the two-part assembly was designed to protect the antenna feed from damage. Thus, the JPL adapter and support were never separated during normal use.

The dolly was used with the support and adapter for convenience during assembly of the spacecraft and operations within the assembly building.

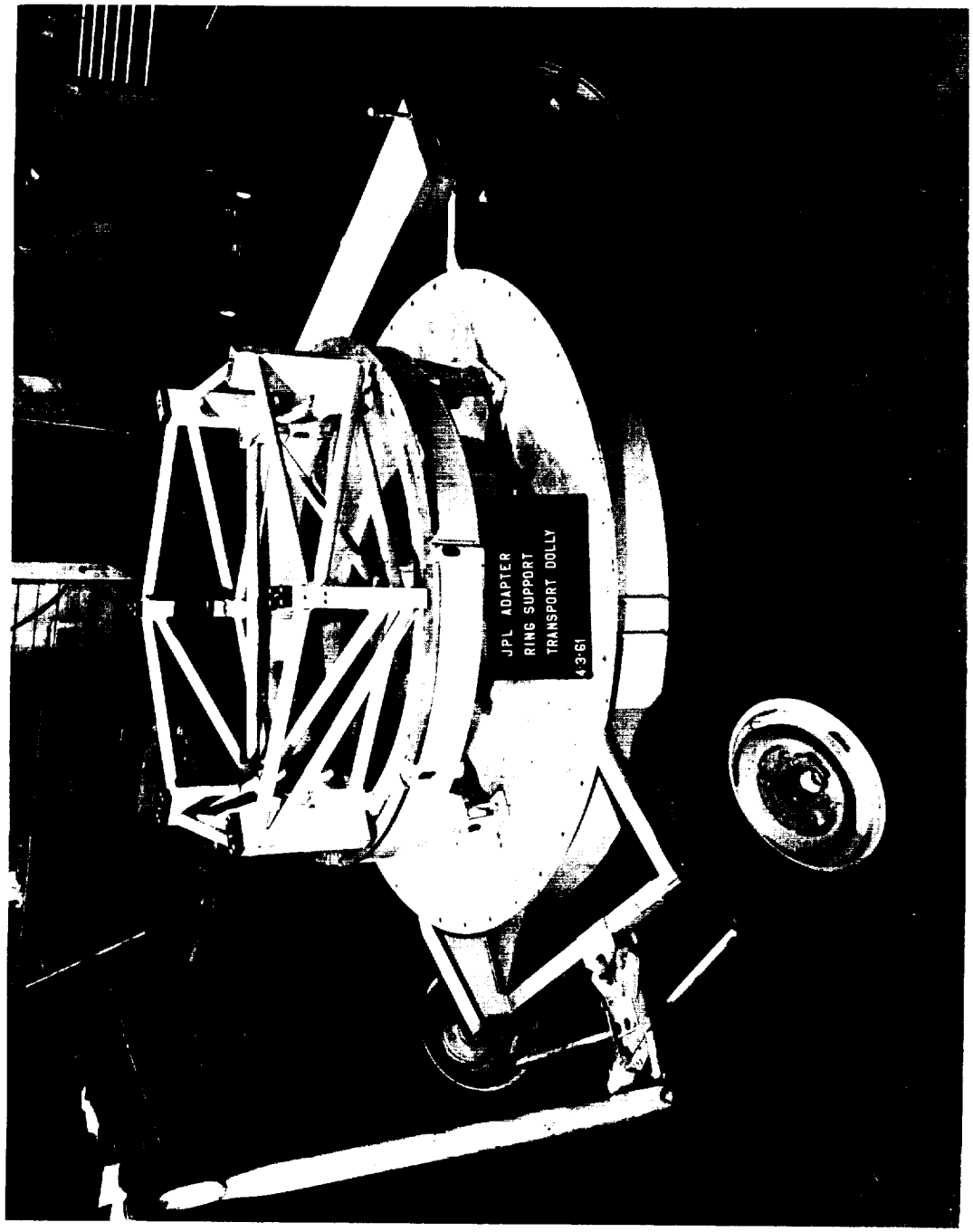

FIGURE 6-7.—Adapter and ring support on transport dolly.

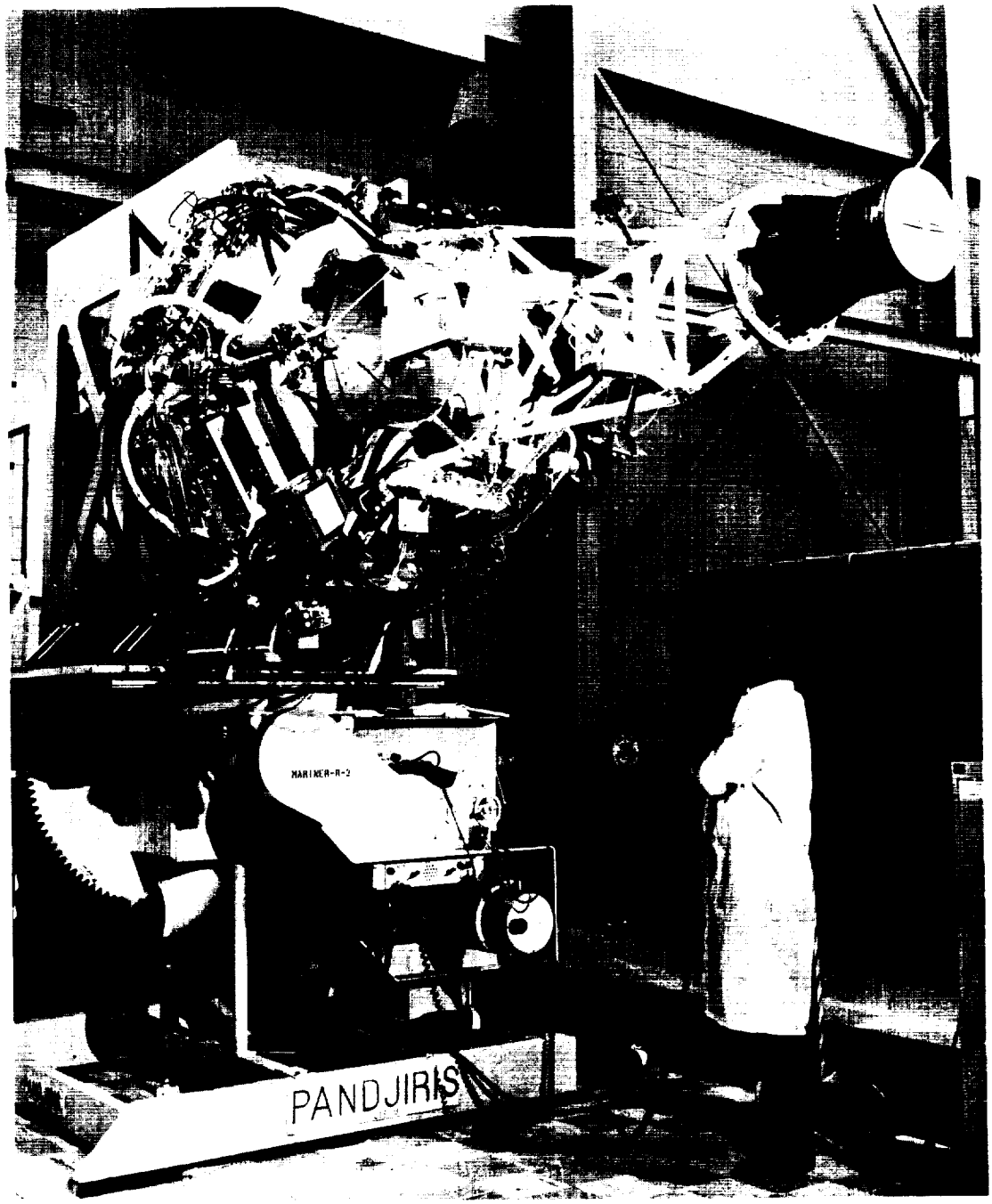

FIGURE 6–8.—System test stand with Mariner R–2 mounted.

The system test stand was the same as that designed for Mariner A. The test stand was capable of holding the spacecraft in an upright position, then swinging it 90° to a horizontal position so that the hinge axis of the high-gain antenna was vertical for operation of the antenna through its entire range of travel (fig. 6–8). The stand could then rotate the spacecraft to place the hinge axis of the solar panels in a vertical position for the operation of their actuation system. The stand consisted of two principal assemblies: (1) a commercial welding positioner and (2) a fixture to adapt the spacecraft to the welding positioner.

The motor loading stand was required to hold the spacecraft in the vertical position approximately 5 feet from the floor to allow the high-gain antenna to swing down for installation of the midcourse motor. The stand was also used for the general assembly work when it was necessary to have access beneath the spacecraft. Figure 6–9 shows the motor loading stand, with the system test stand in the background.

Two aluminum magnetometer-mapping fixtures were used to rotate the spacecraft about the magnetometer's X- and Z-axis. For 360° mapping about the magnetometer Z-axis, the spacecraft was attached to the vertical support fixture and mounted on an oil table. Using the system test stand, the spacecraft was then mounted on the X-axis mapping fixture and magnetometer calibrations were performed by rotating the spacecraft 360° about the magnetometer's X-axis (fig. 6–10).

ATTITUDE-CONTROL SUBSYSTEM

The attitude-control subsystem maintained the orientation of the spacecraft solar panels on the Sun and the directional antenna on the Earth throughout the mission from the time of initiation of attitude-control power. Two general modes of operation were necessary, a cruise mode and a midcourse-maneuver thrust mode. In the cruise mode, a cold-gas system was utilized as the propellant; in the thrust mode, the spacecraft attitude was controlled by deflecting vanes in the propelling stream of the midcourse motor. The functional mechanization of the Mariner II attitude-control system is shown in figure 6–11.

The attitude-control subsystem flight data obtained from telemetry were sampled, and comparisons were made, where possible, between the predicted nominal and the actual flight parameters. In many instances the attitude-control subsystem parameters have large uncertainties, due to two factors: (1) the difficulties involved in obtaining accurate measurements from a failure-mode telemetry

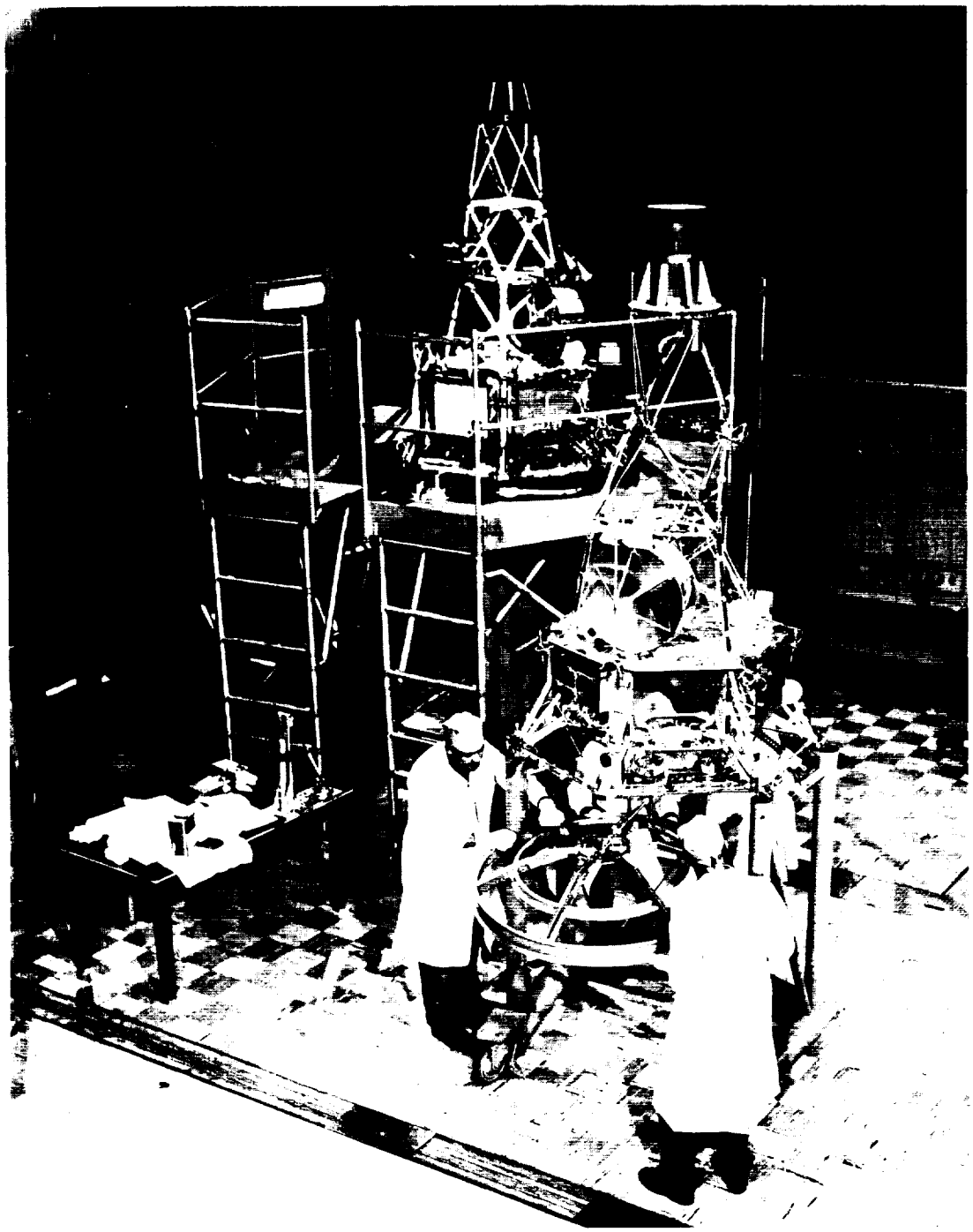

FIGURE 6–9.—Spacecraft on motor loading stand.

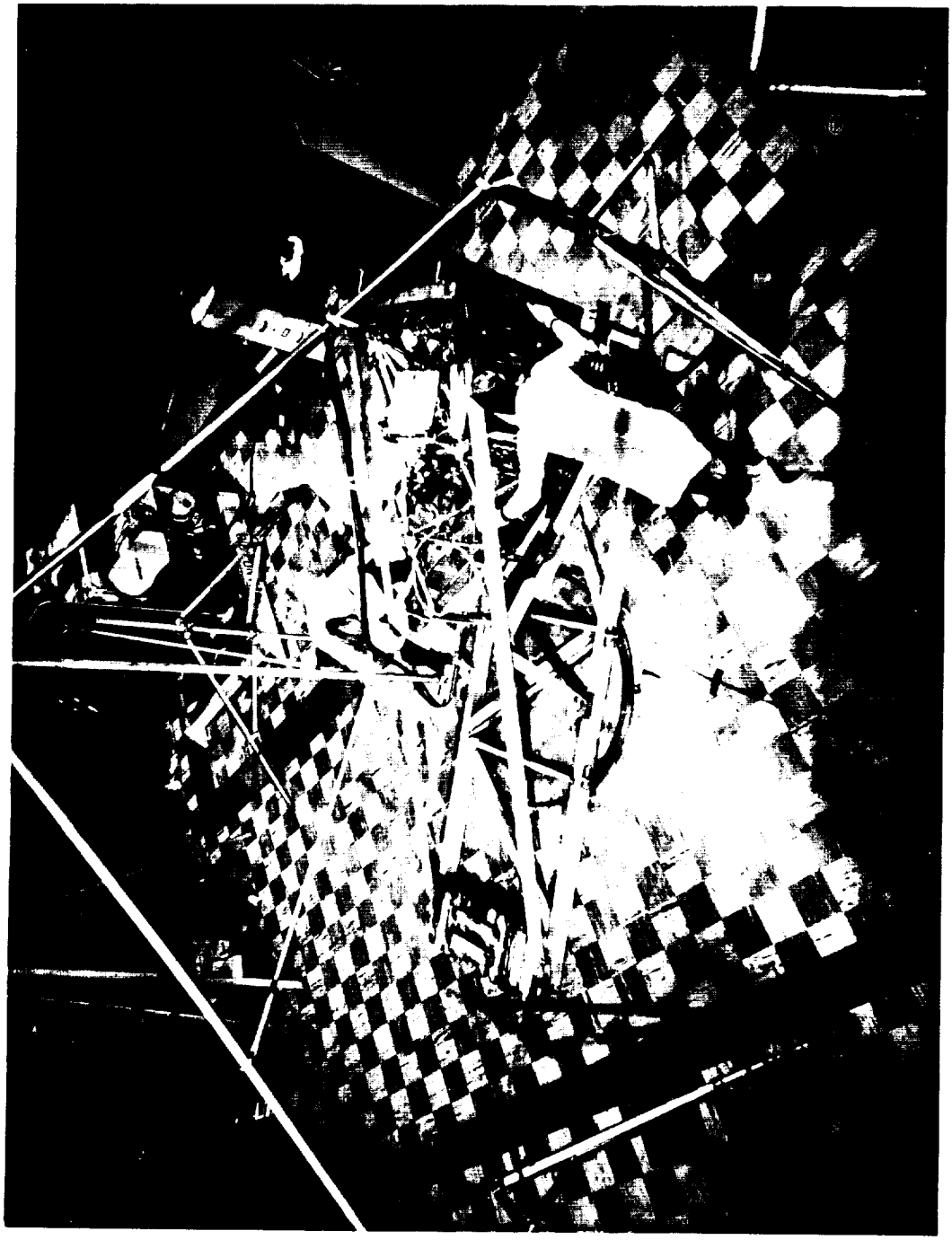

FIGURE 6-10.—Magnetometer-mapping stand.

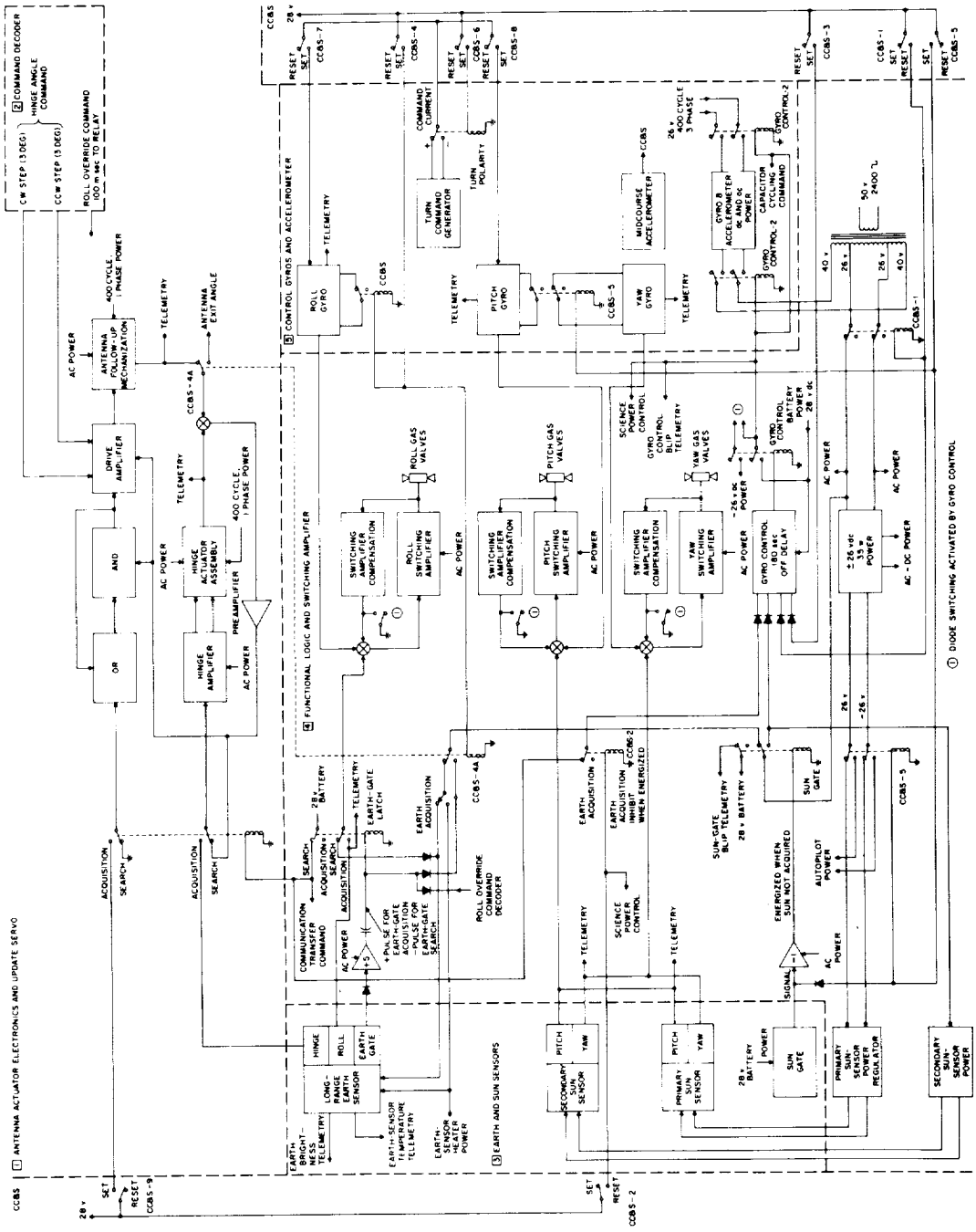

FIGURE 6–11.—Attitude-control system mechanization.

system, and (2) the low data rate of the telemetry system in the cruise portion of flight. It is, therefore, not possible to determine whether the discrepancies between the nominal predicted values and the flight performance values are the results of actual system deviations or of the measurement inaccuracies in the flight telemetry data.

The data were presented in four basic attitude-control modes: (1) Sun or Earth acquisition and reacquisition, (2) Sun-acquired cruise, (3) midcourse maneuver, and (4) Sun- and Earth-acquired cruise.

Sun Acquisition and Reacquisition

Yaw Sun acquisition was initiated at 07:53:07 GMT on August 27, 1962. The rate about the yaw axis at injection was greater than 1800 deg/hr. Since data were lost between 07:42 and 07:58, all rate information was lost. The estimated angular offset about the yaw axis was −280 mrad at the time of the Sun-acquisition command. Gas consumption for the yaw acquisition and injection-rate removal was estimated at 0.011 pound, compared with an estimated worst-case consumption of 0.07 pound. The acceleration constant calculated from the data was 0.226 mrad/sec^2, which was within 0.5% of the nominal 0.225 mrad/sec^2.

The yaw reacquisition after midcourse occurred at 00:27:00 on September 5. The yaw axis had a motion of approximately 85° during this sequence. This large angular change was investigated and appeared to be a result of normal attitude-control behavior at the end of the midcourse maneuver.

At spacecraft injection, the rate about the pitch axis was +675 deg/hr. The estimated angular offset in pitch at the time of the Sun-acquisition command was 130°. The acquisition rate was 1050 deg/hr versus a nominal rate of 1010 deg/hr. Gas consumption for the pitch acquisition and injection-rate removal was estimated at 0.006 pound, as compared with the worst-case estimate of 0.0503 pound. The acceleration constant calculated from the data was 0.303 mrad/sec^2, which was within 34% of the nominal 0.225 mrad/sec^2.

The pitch reacquisition after midcourse appeared to be normal. The approximate angular offset in pitch was −130°, which was within the telemetry-data time resolution.

Earth Acquisition and Reacquisition

The rate about the roll axis was greater than −400 deg/hr at spacecraft injection and was reduced to approximately 120 deg/hr at the time of gyro

turnoff (Sun acquisition). Momentum interchange during gyro rundown increased the vehicle roll rate to approximately +235 deg/hr. A gradual increase to −720 deg/hr was observed during the 167-hour Sun-acquired cruise period to Earth acquisition. This rate change corresponds to a roll torque of approximately 6 dyne-cm.

The initial Earth-acquisition command occurred at 05:29:14 on September 3. The roll search rate was observed to be nominal, and the angular offset in roll was approximately 285°. At the time of initial Earth acquisition, a transfer to high-gain antenna was observed, which was probably due to a power transient. The acceleration constant in roll was not obtained from telemetry data because of the low sampling rate at Earth acquisition. The gas consumption in roll for acquisition was estimated to be 0.019 pound, which was the preflight estimate.

Earth reacquisition after midcourse occurred at 02:07:59 on September 5. The reacquisition was similar to the initial Earth-acquisition sequence.

During the prelaunch period, the hinge reference or update servo was set at 72° (verified by telemetry), as compared with the nominal reference angle of 73.3°. At the initiation of the Sun-acquisition command at 07:53:07 on August 27, the antenna extended to the acquisition angle of 72°. The antenna slewing rate was 0.155 deg/sec, as compared with the nominal rate of 0.16 deg/sec.

During the initial Earth acquisition, the hinge servo telemetry indicated no motion, which verified the hinge angle setting prior to Earth acquisition. During the Earth-acquired time interval before midcourse, the hinge servo indicated normal tracking of the Earth, and the reference servo indicated the proper followup action.

At the initiation of the roll-turn sequence during midcourse, the antenna extended to 118° versus a nominal value of 120°. At the end of the midcourse sequence, the antenna returned to the original reference angle of 70°.

Sun-Acquired Cruise

During the Sun-acquired cruise mode, the roll axis was uncontrolled. As indicated above, the roll rate during this period changed from a maximum positive value of approximately 235 deg/hr to a maximum negative value of approximately 720 deg/hr at the Earth-acquisition command. The effect of the cross-coupled torques due to the roll rate was observed in the pitch- and yaw-axis limit cycles. Typical curves of Sun-acquired cruise operation in yaw and pitch are presented in figures 6–12 and 6–13, respectively.

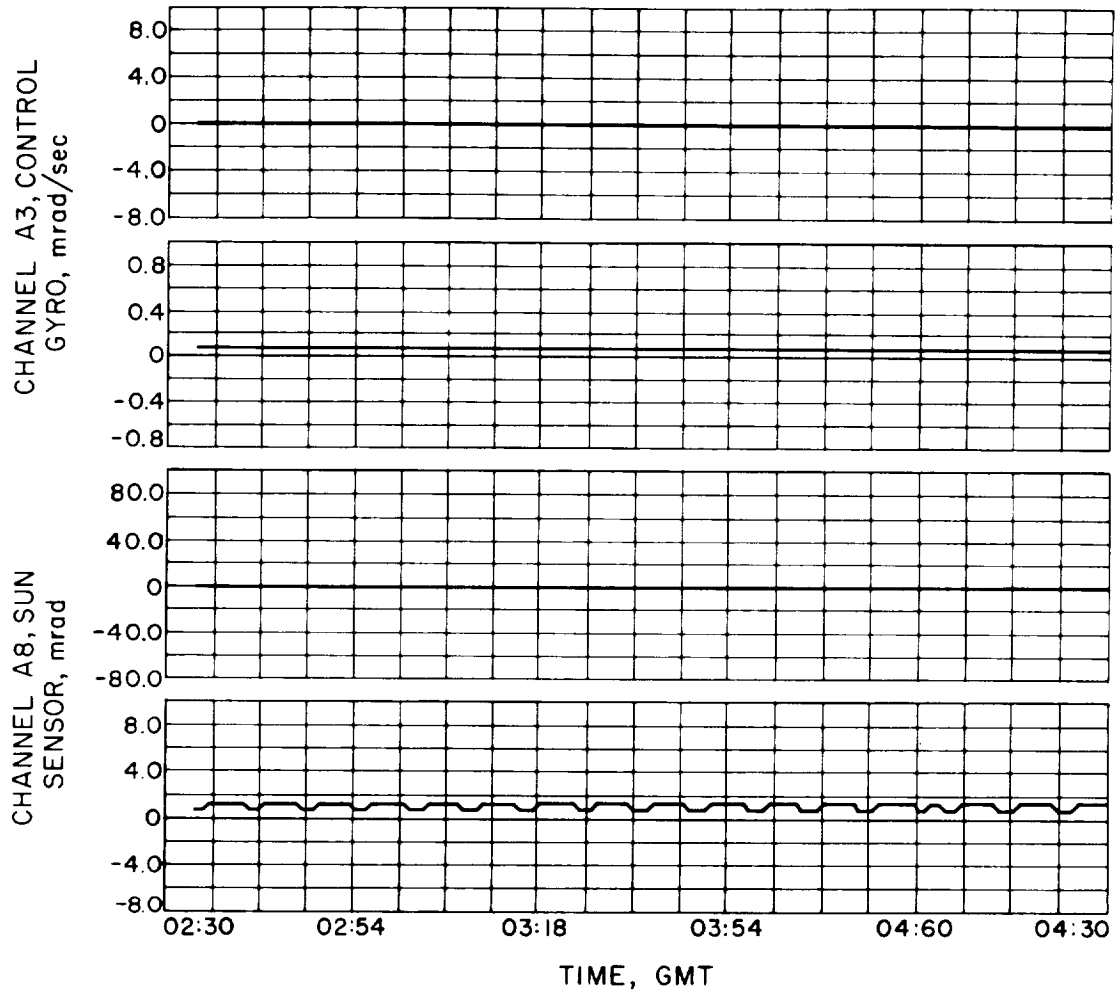

FIGURE 6–12.—Yaw attitude control in Sun-acquired cruise, typical curves for August 31.

Midcourse Maneuver

As the midcourse maneuver sequence began on September 4 the gyros were activated and, approximately 1 hour later, the roll-turn sequence was initiated. The only telemetry data available show the stop transient of the roll turn and verify the negative or counterclockwise-turn polarity. The pitch-turn polarity was verified by the reacquisition sequence of pitch and by a 1-point pitch-rate sample at the beginning of the pitch-turn sequence. The autopilot performance

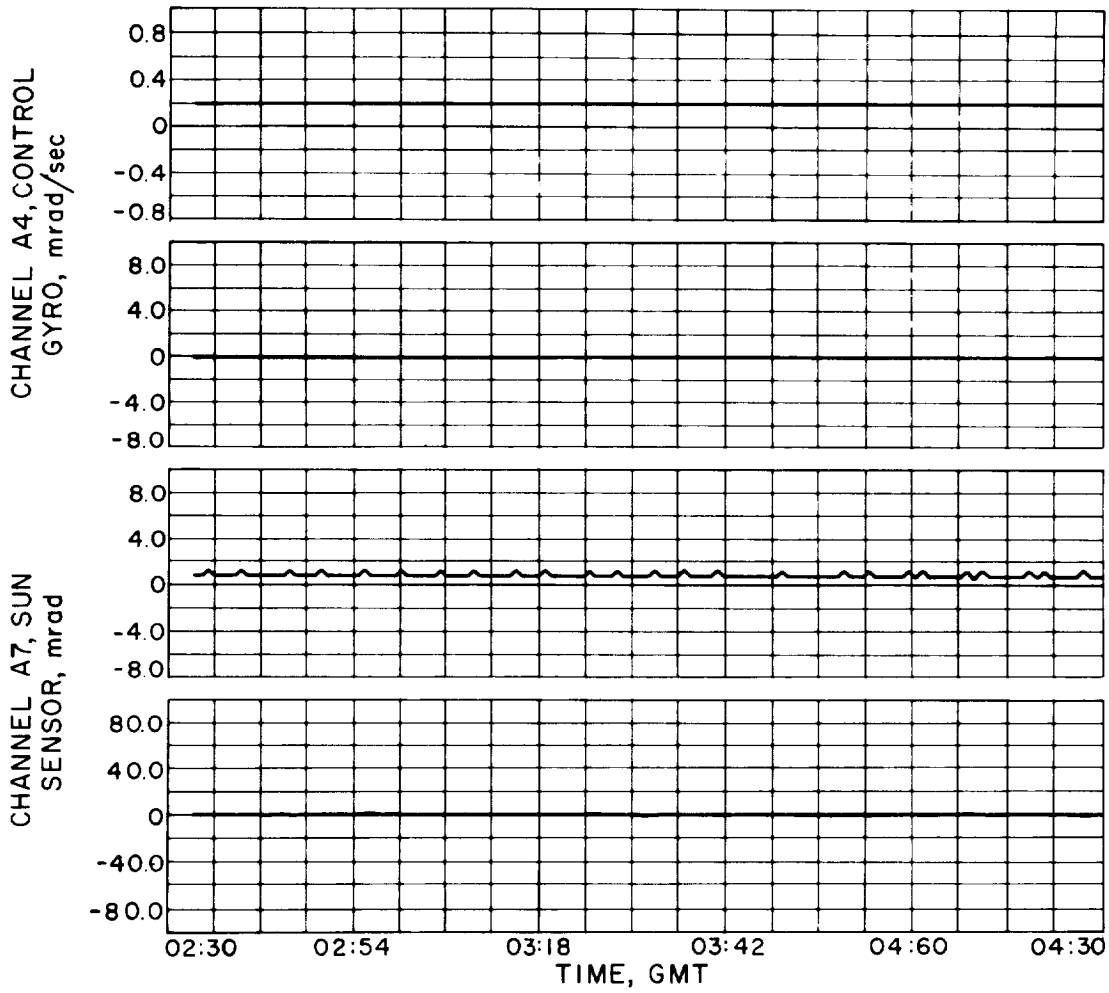

FIGURE 6-13.—Pitch attitude control in Sun-acquired cruise, typical curves for August 31.

could not be verified by telemetry because of the time resolution of the data; it was, however, verified by the trajectory analysis. One data point at motor ignition indicated that the yaw gyro saturated, which was verified by the pre-flight simulation. The trajectory analysis indicated that the pointing error (i.e., the angle between the commanded and the calculated maneuver vectors) was 54.3 mrad. This may be compared to the allowable 3σ error of 80 mrad. This error is a measure of attitude control and autopilot performance.

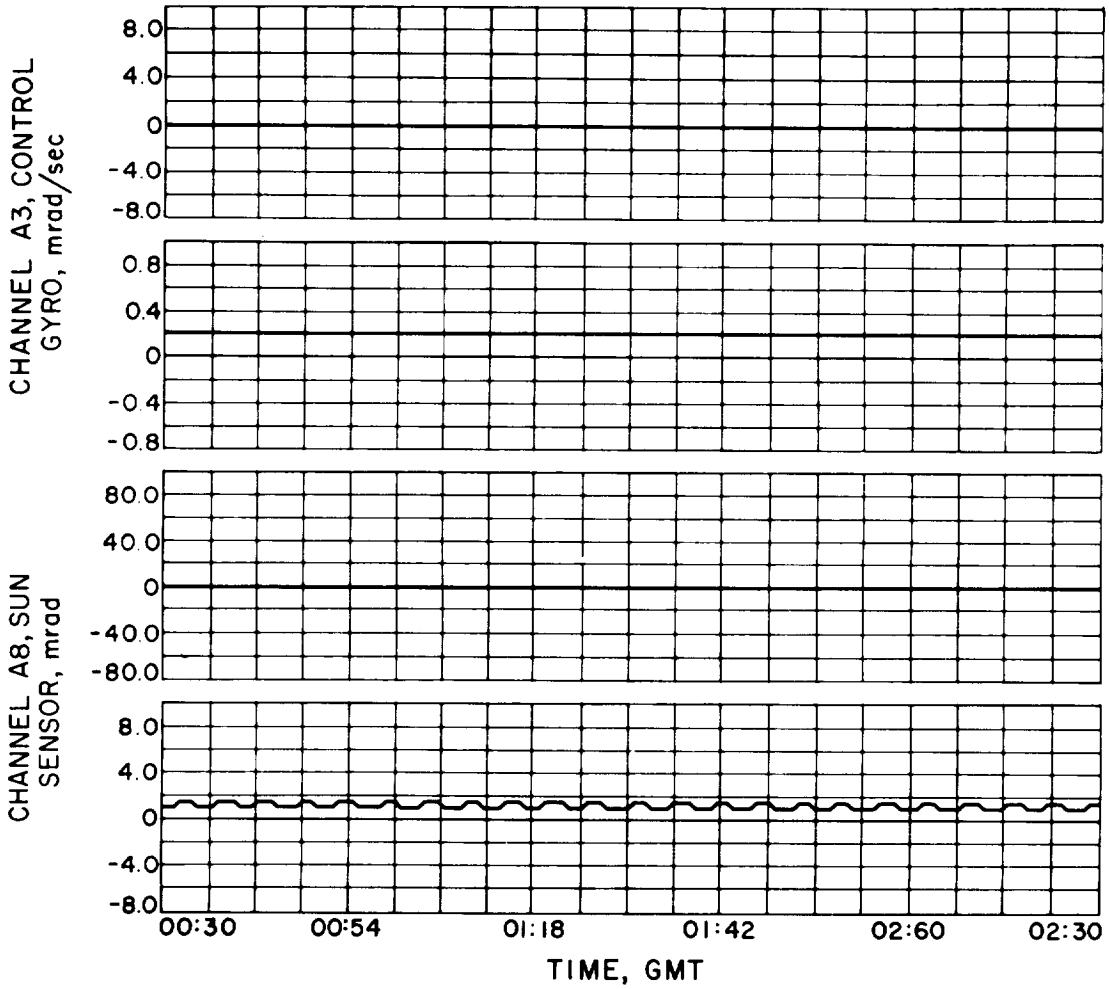

FIGURE 6–14.—Yaw attitude control in Sun- and Earth-acquired cruise, typical curves for September 4.

Sun- and Earth-Acquired Cruise

The yaw cruise performance was essentially normal; however, the disturbance torque experienced was approximately 28 dyne-cm, considerably higher than the preflight estimate of approximately 0 dyne-cm. The gas consumption in yaw was approximately 0.0028 lb/day, as compared with the preflight estimate of 0.0005 lb/day. Typical curves of cruise operation for this parameter are shown in figures 6–14, 6–15, and 6–16.

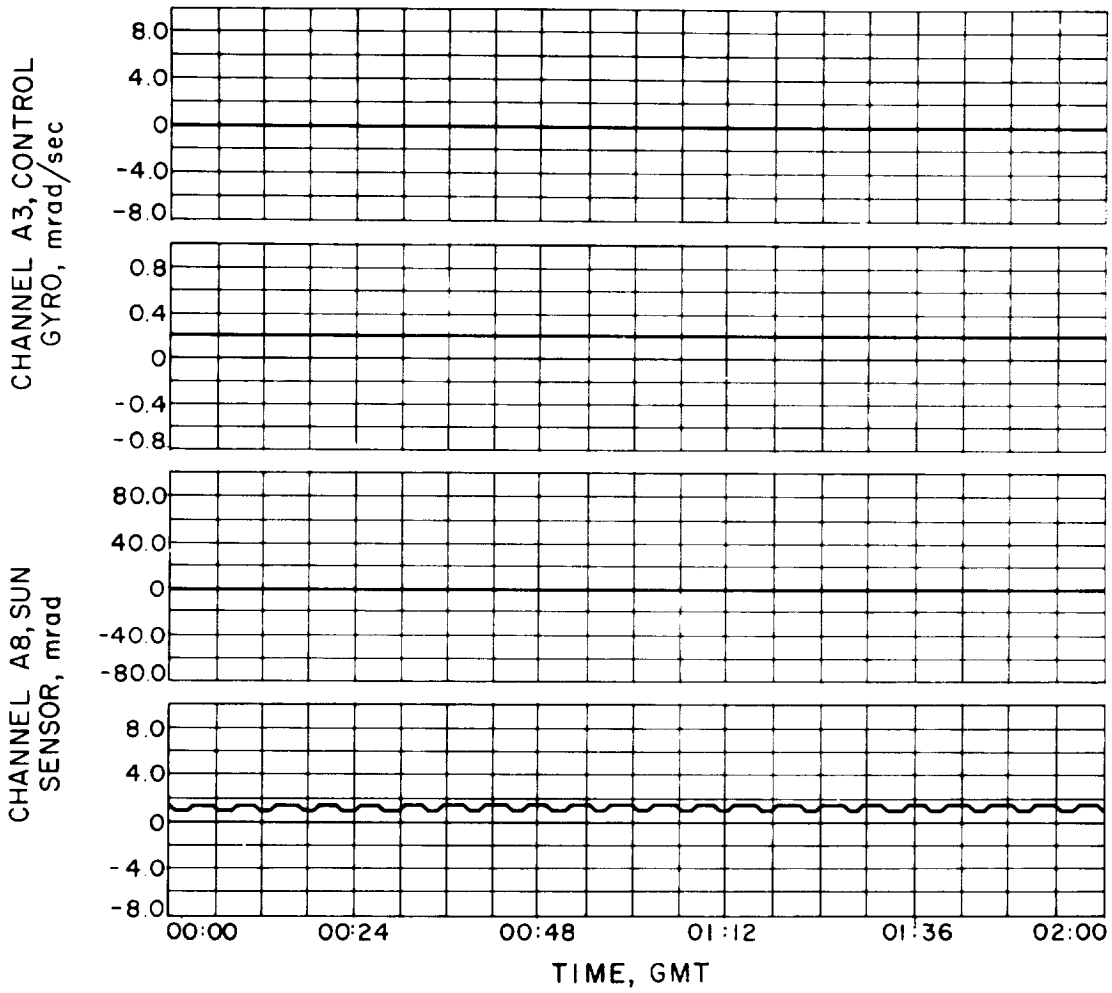

FIGURE 6–15.—Yaw attitude control in Sun- and Earth-acquired cruise, typical curves for September 15.

The pitch cruise performance was normal except for a 1-mrad offset of the negative switching level. The estimate of pitch disturbance torque observed was approximately 44 dyne-cm. The gas consumption in pitch was approximately 0.0042 lb/day, as compared with the preflight estimate of 0.00114 lb/day. Typical curves of pitch cruise operation are presented in figures 6–17 and 6–18.

After initial Earth acquisition on September 3, the roll system indicated a disturbance torque of approximately 11 dyne-cm. This disturbance continued to

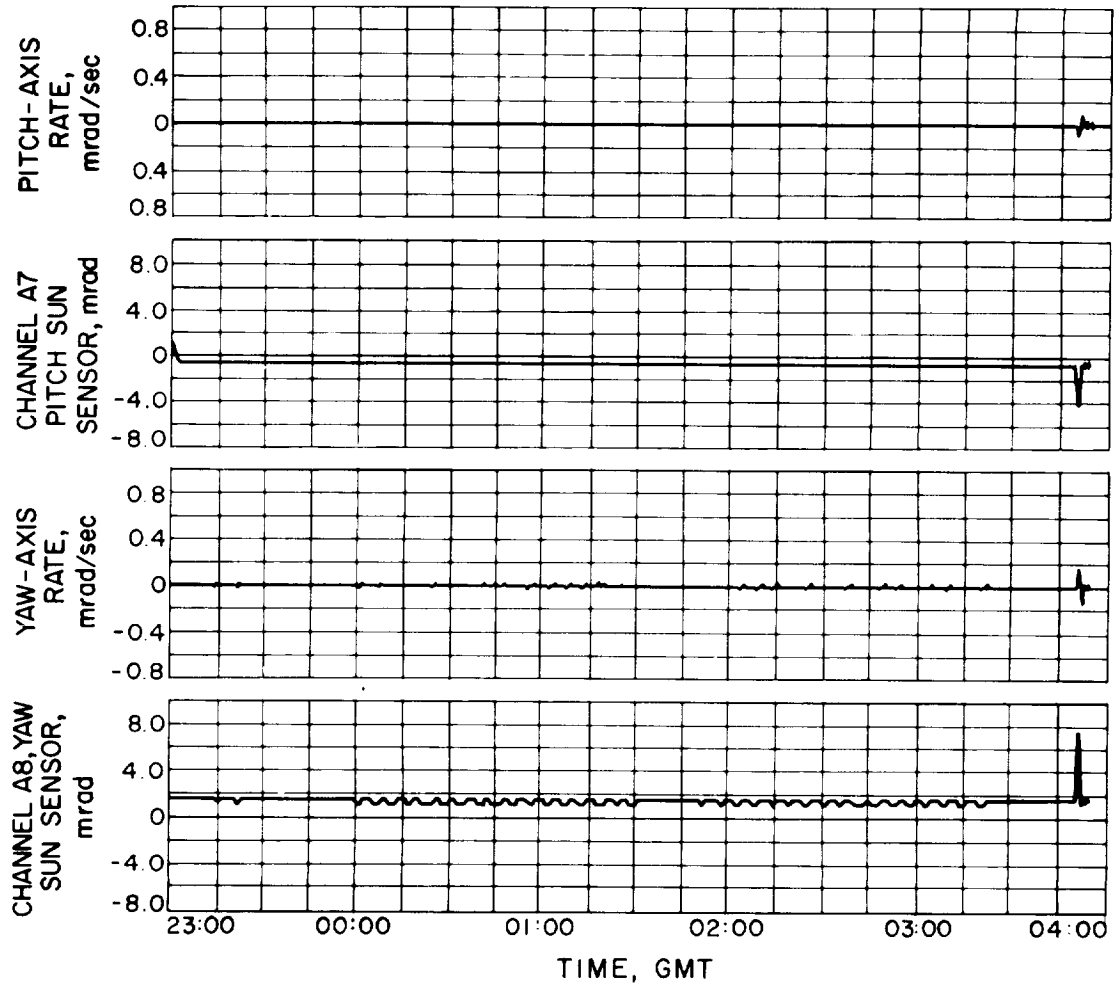

FIGURE 6-16.—Pitch and yaw attitude control in Sun- and Earth-acquired cruise, typical curves for December 5 and 6.

decrease, and on September 4 the roll system operated in the normal limit-cycle manner; however, the roll axis still exhibited a slight torque of 6 dyne-cm. The roll positional dead-band, as verified by telemetry, was $\pm 0.250°$, as compared with the nominal value of $\pm 0.229°$. Typical curves of cruise operations are shown in figures 6-19 and 6-20. The effects of yaw-axis cross-coupling into the roll axis as a result of the Earth-probe-Sun angle are presented graphically in figures 6-21 and 6-22.

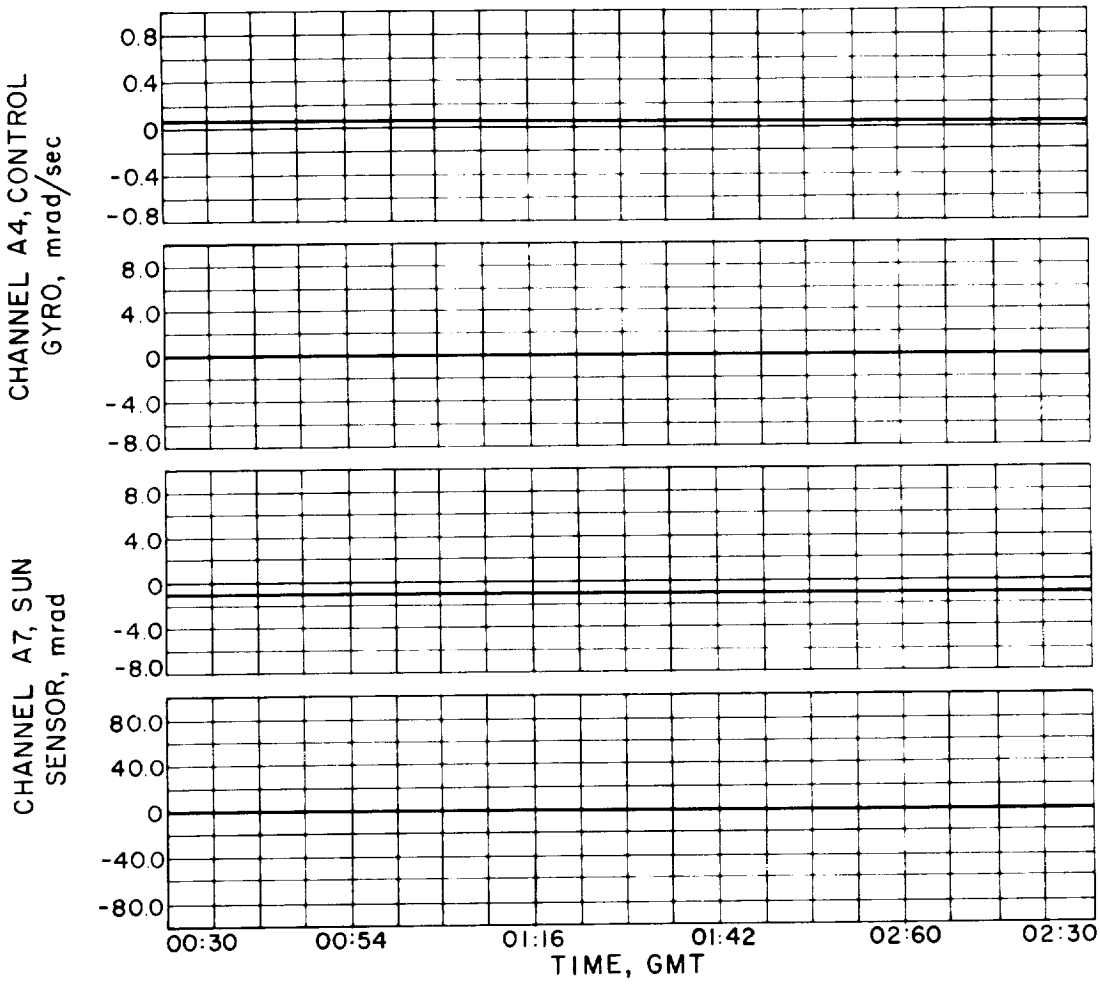

FIGURE 6–17.—Pitch attitude control in Sun- and Earth-acquired cruise, typical curves for September 4.

Nonstandard Events

In the coasting mode, the attitude-control system consistently maintained the orientation of the spacecraft in the presence of disturbance torques considerably higher than the preflight estimates. From a careful study of the limit-cycle performance (which was severely limited by the granularity of the telemetered angle information), the disturbance torques were estimated as follows:

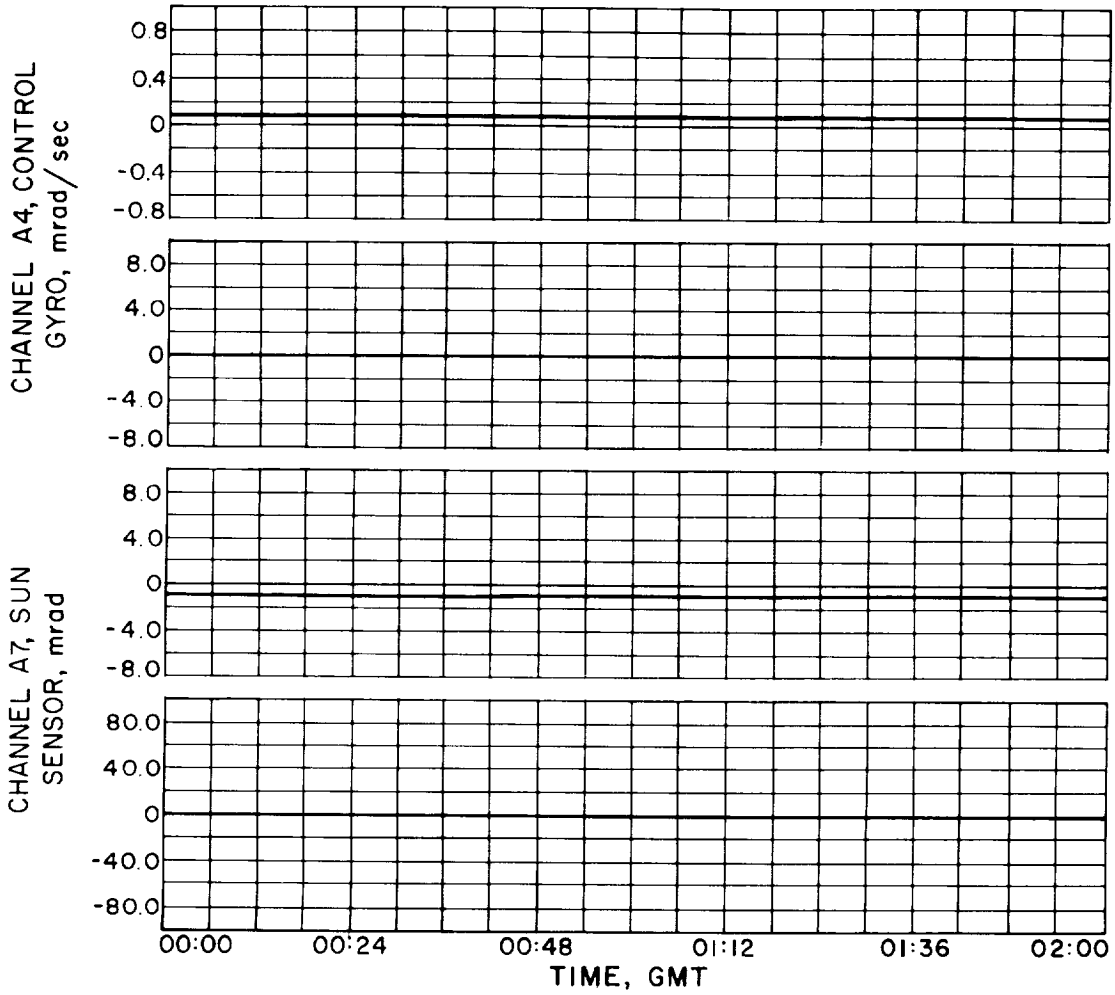

FIGURE 6–18.—Pitch attitude control in Sun- and Earth-acquired cruise, typical curves for September 15.

	Preflight estimate	*Flight-analysis estimate*
Pitch, dyne-cm	11	44
Yaw, dyne-cm	0	30
Roll, dyne-cm	0	3

Among the suspected possible causes of these disturbance torques are: (1) magnetic moment (the product of the distance between the poles of a magnet and the strength of either pole), (2) solar-pressure unbalance, and (3) gas-system

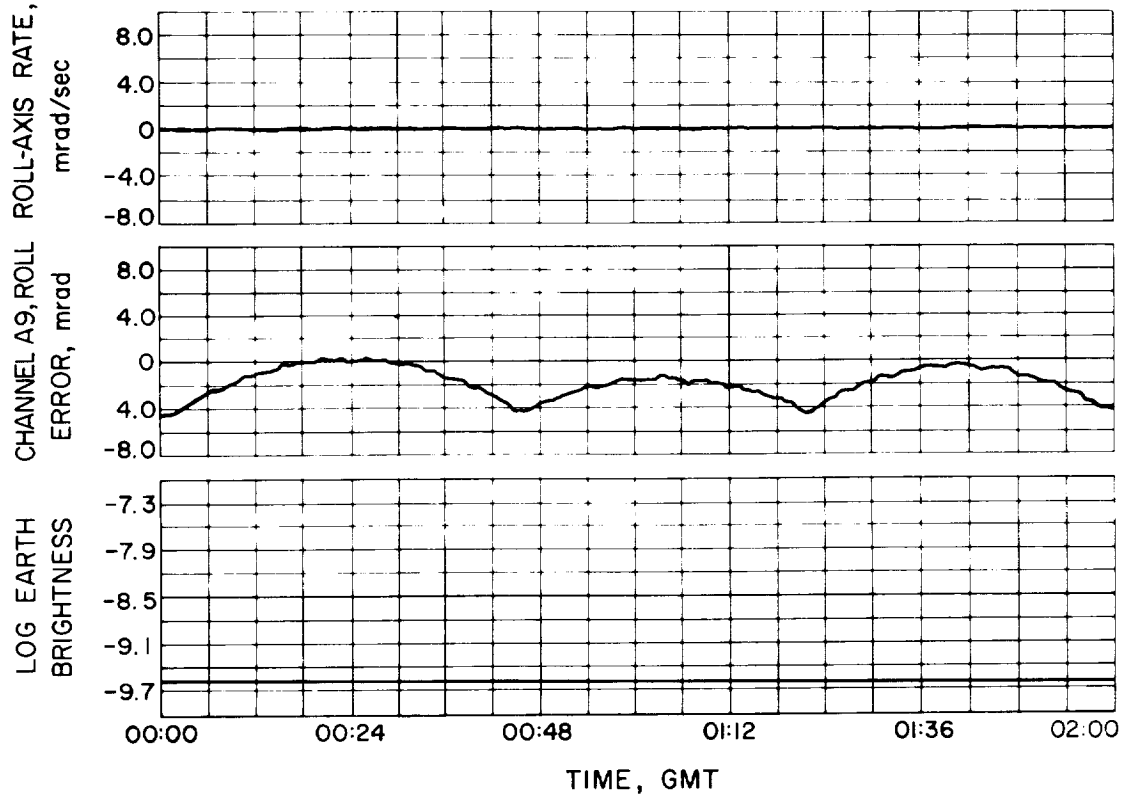

FIGURE 6–19.—Roll attitude control in Sun- and Earth-acquired cruise, typical curves for September 15.

leakage. As a result of the disturbance torques present on the spacecraft, gas consumption was directly proportional to the torque-time product. In figures 6–23 to 6–25, which are graphs of gas consumption as a function of time, the solid line shows actual consumption. The fact that, during cruise, the rate of consumption was higher than estimated corroborates the data indicating higher disturbance torques than anticipated. The allowance for contingency was such that the remaining gas was adequate to maintain the attitude of the spacecraft for approximately 100 days beyond encounter if no change in the attitude-control requirements occurred.

The attitude-control system responded to an unidentified impact at 12:50 on September 8. The disturbance, which probably centered about the pitch and yaw axes of the spacecraft, was of sufficient magnitude to require gyro activation

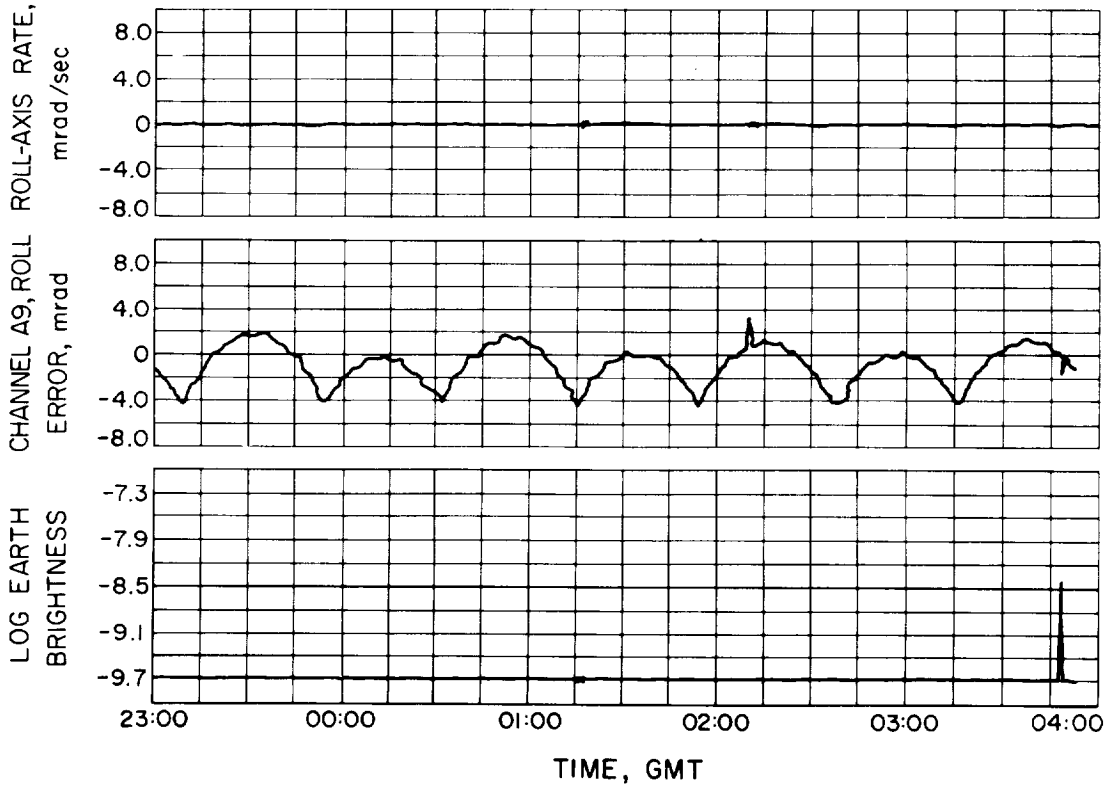

FIGURE 6–20.—Roll attitude control in Sun- and Earth-acquired cruise, typical curves for December 5 and 6.

to damp the control-system reacquisition. The attitude-control system functioned perfectly during this disturbance and, after removing the transient produced, returned to the cruise mode (i. e., gyros off).

The hinge reference servo telemetry measurement began to deviate from nominal performance as the antenna moved out after attainment of the maximum Earth-probe-Sun angle. Its deviation continued, and the telemetered measurement varied widely when commands were sent to reset the reference hinge angle. The best explanation for this discrepancy is that the telemetry potentiometer had a leakage path to the spacecraft frame, thus generating a variable impedance across the potentiometer. A graph of hinge angle, Earth-probe-Sun angle, and hinge reference angle is presented in figure 6–26.

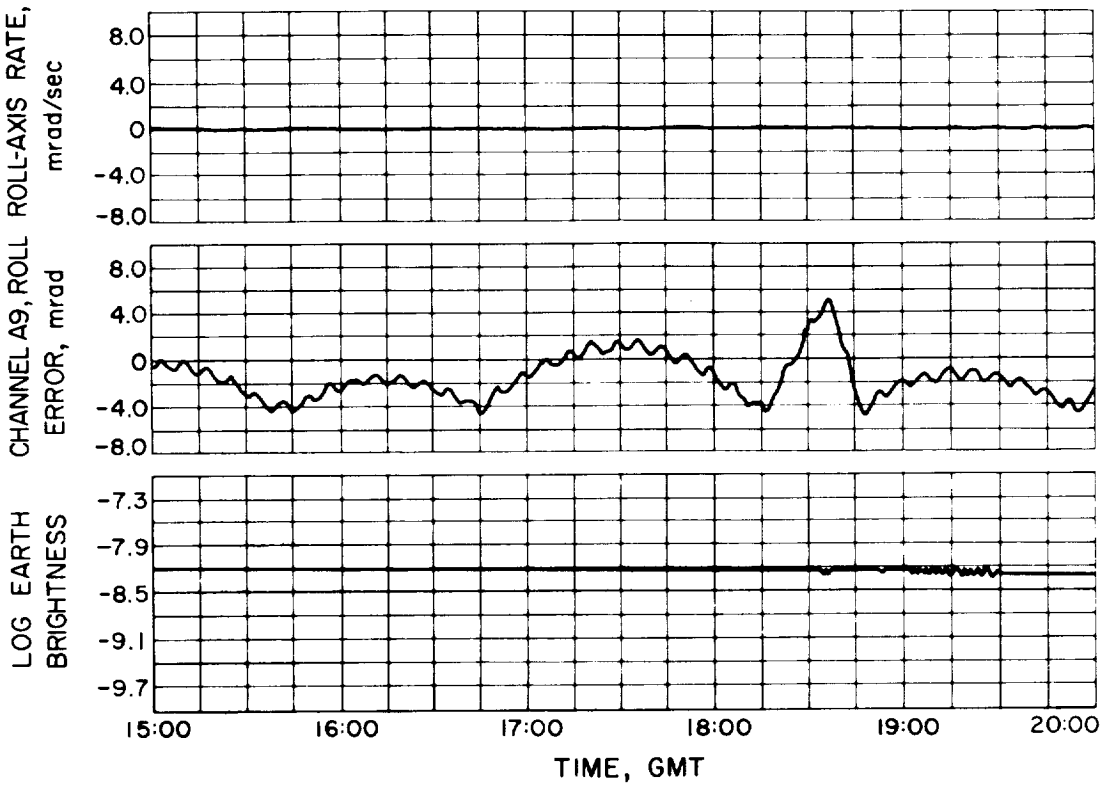

FIGURE 6–21.—Roll attitude control showing effects of yaw-axis cross-coupling, typical curves for October 28 (afternoon hours).

During the first 35 days of flight, the telemetered indication of Earth brightness registered an intensity several orders of magnitude below the expected value. At 14:34 on September 29, the Earth sensor telemetry measurement of intensity indicated a step change from a DN of 6 to a DN of 63. Postmission analysis to date has not determined the cause. Also, at this time, the gyros came on for 3 min, probably because this transient in the Earth sensor resulted in a momentary loss of the Earth-acquisition signal. After this event, the Earth sensor performed normally, although some degradation was apparent during the last 10 days of flight because the temperature of the component was above design specifications. A curve of the actual Earth-intensity measurements versus the predicted level is shown in figure 6–27.

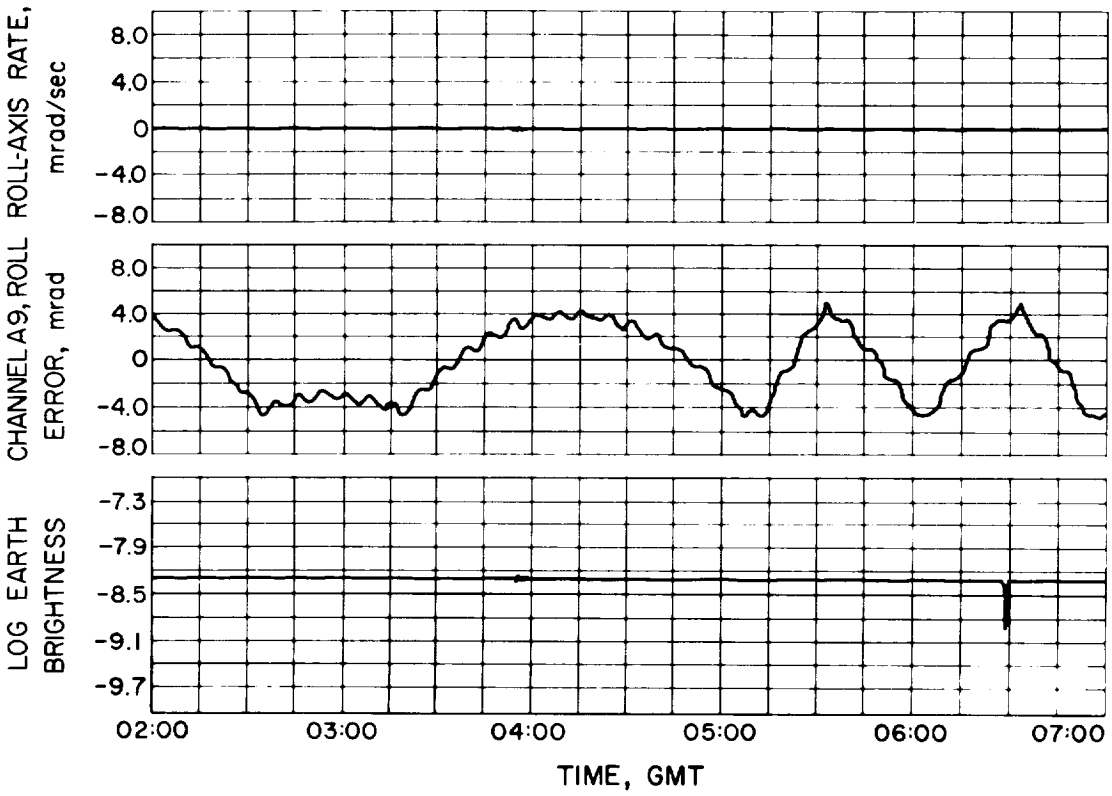

FIGURE 6–22.—Roll attitude control showing effects of yaw-axis cross-coupling, typical curves for October 28 (morning hours).

POWER SUBSYSTEM

The Mariner R power subsystem was designed to provide a central supply of electrical energy to operate the equipment on board the spacecraft. Power was derived from two solar panels and a rechargeable (secondary) battery. These sources fed a power switching and logic circuit which, in turn, fed a booster regulator. The booster regulator drove a 2400-cps square-wave power amplifier and a 400-cps sinusoidal power amplifier. Users provided transformer-rectifier units, utilizing the 2400-cps square-wave power to produce their dc requirements. The 400-cps power source principally supplied the ac motors, as shown in figure 6–28. The battery could be recharged when solar power was available. Power to operate the pyrotechnic devices was supplied directly from the battery.

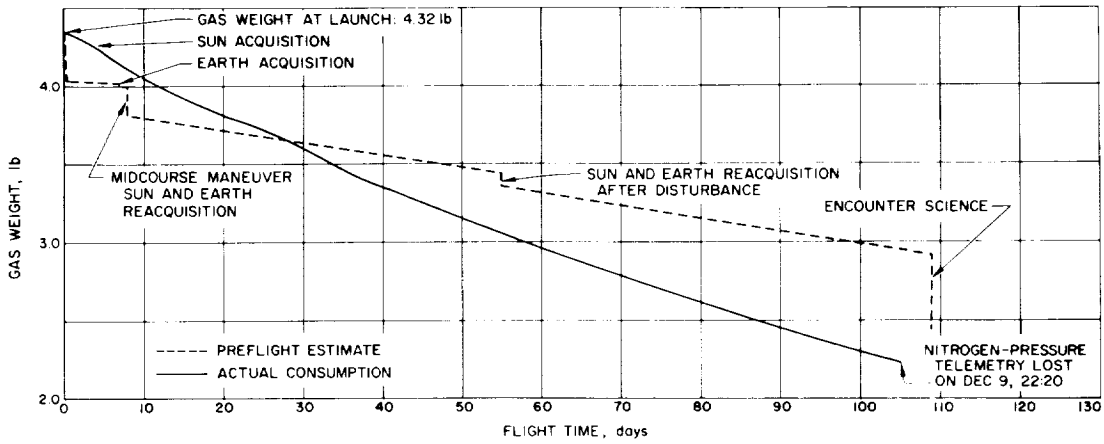

FIGURE 6–23.—Attitude-control system gas consumption vs time.

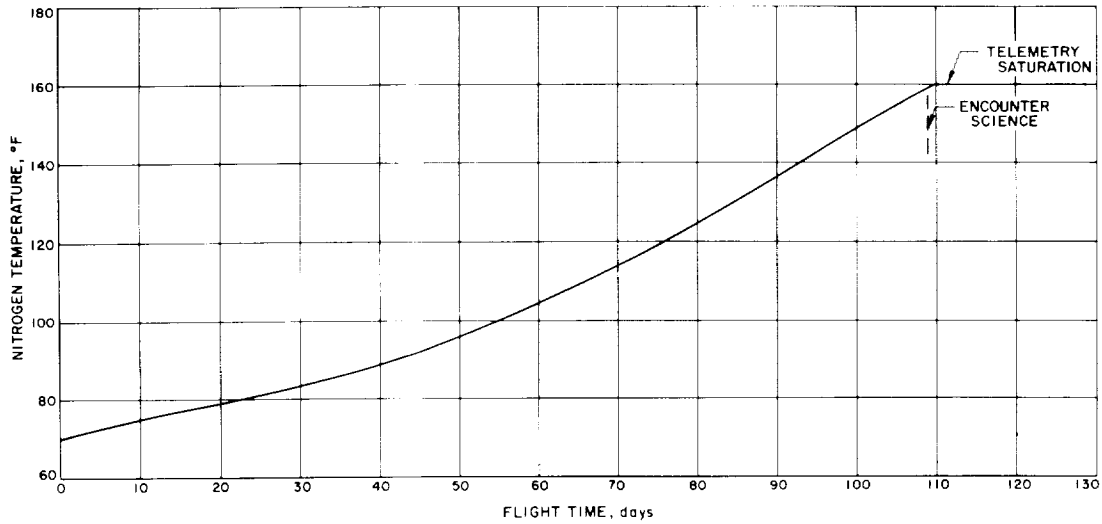

FIGURE 6–24.—Attitude-control system nitrogen temperature vs time.

The power system was sensitive to the orientation of the spacecraft and to the required electrical loads. During the launch phase the battery supplied all the power, since the spacecraft was not oriented to face the solar panels toward the Sun. When the spacecraft was Sun oriented, the solar panels assumed the

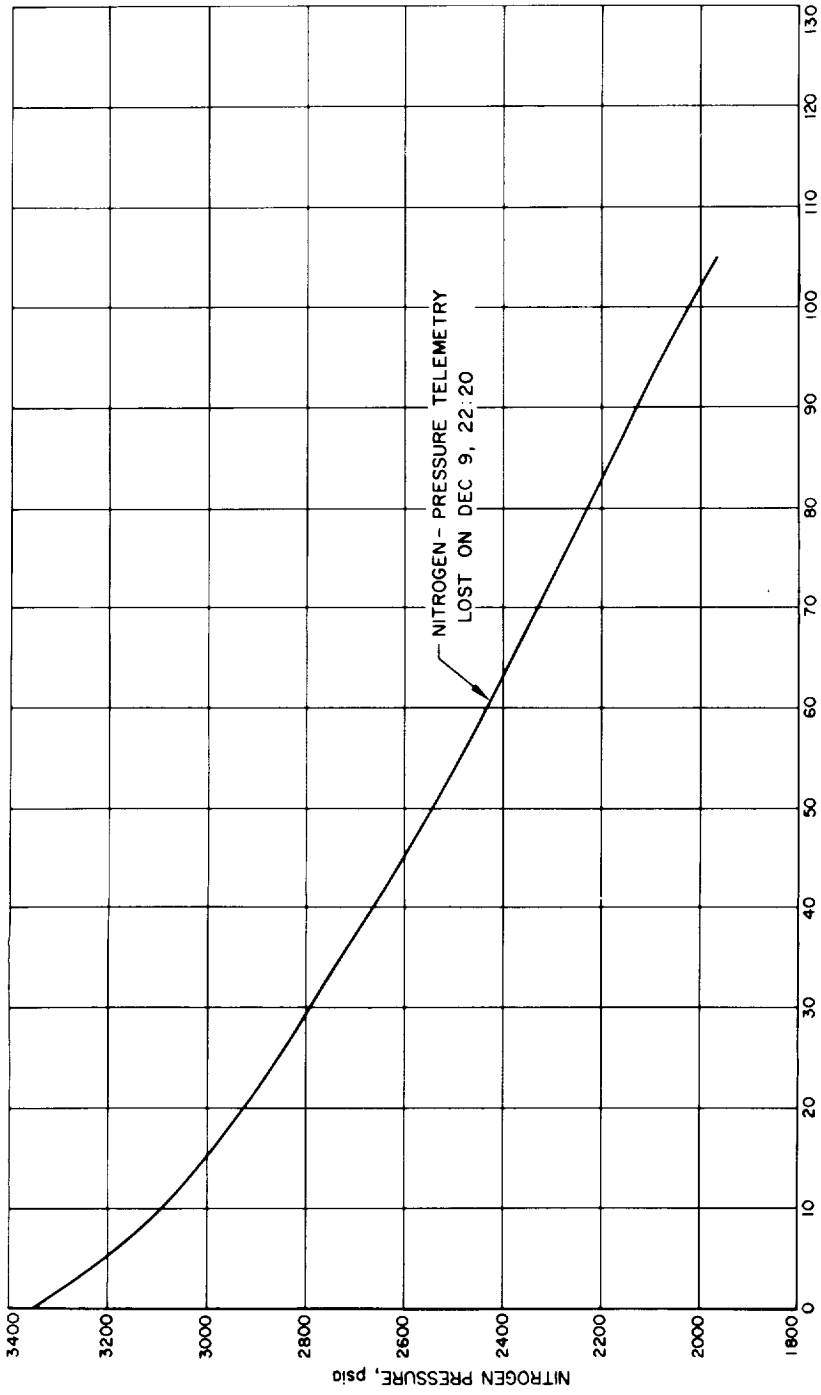

FIGURE 6-25.—Attitude-control system nitrogen pressure vs time.

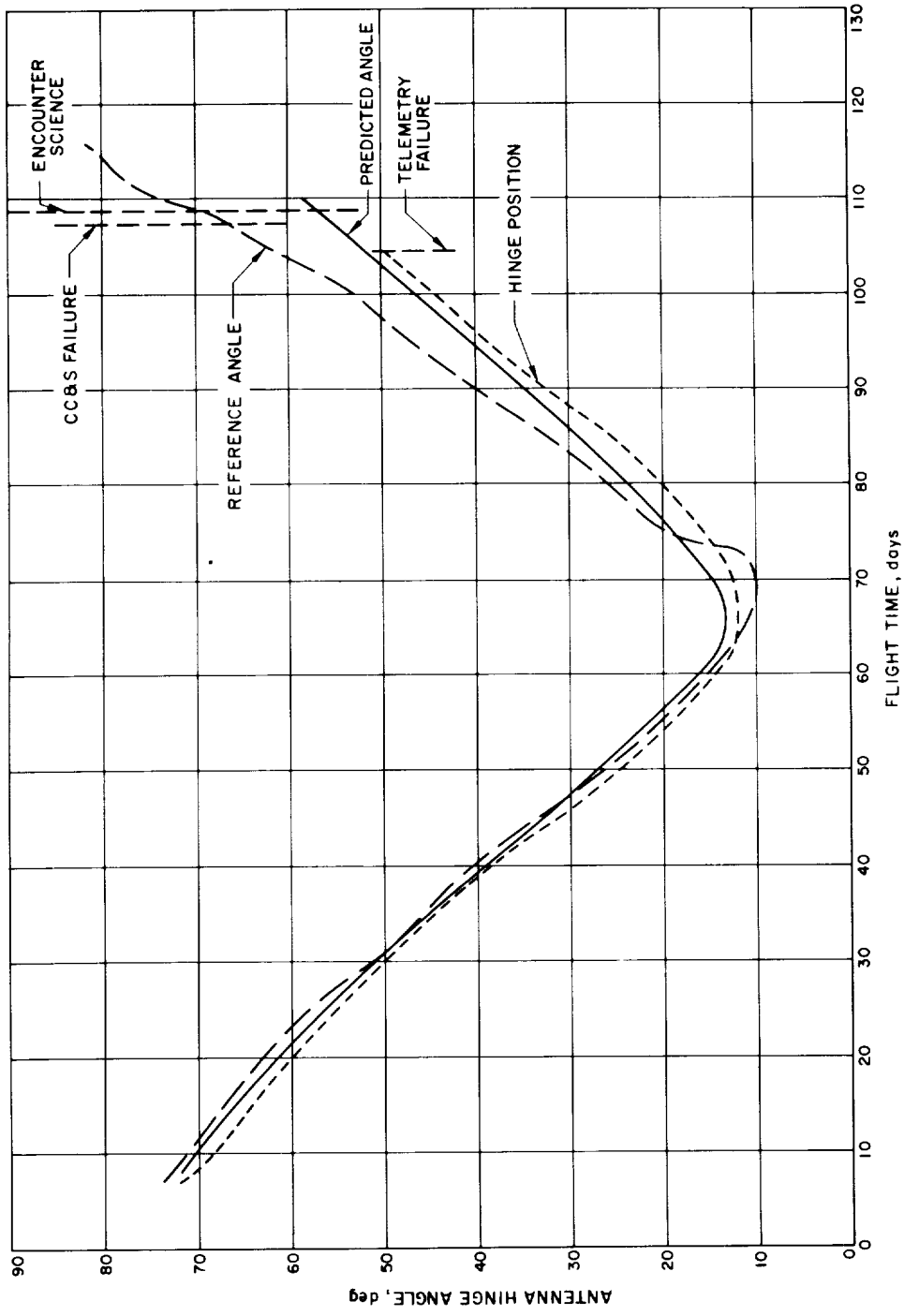

FIGURE 6–26.—Antenna hinge angle vs time.

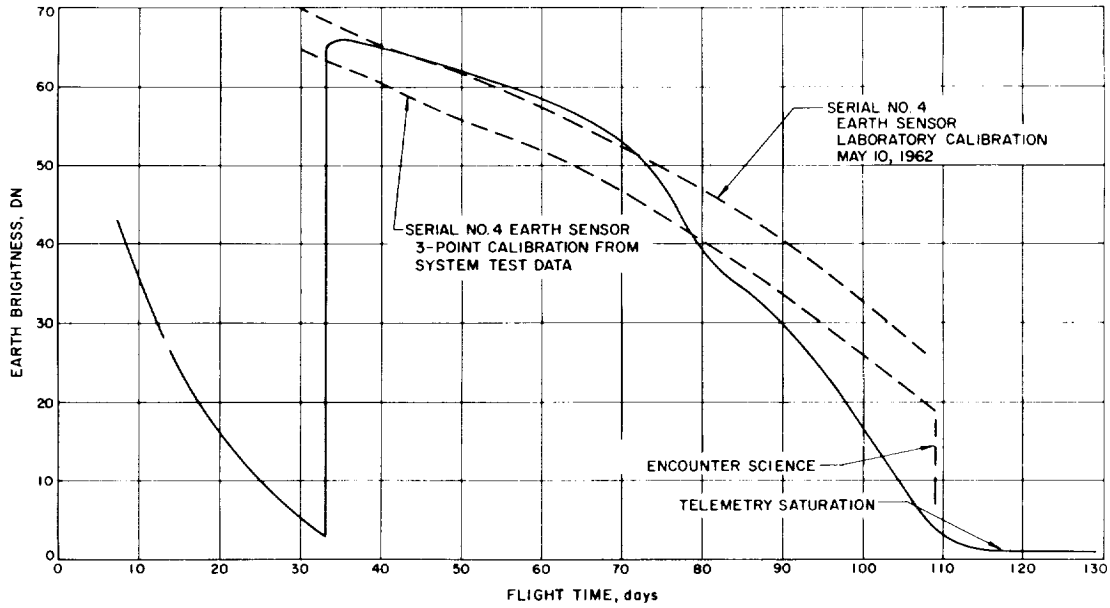

FIGURE 6–27.—Earth sensor intensity vs time.

load and recharged the battery. Again, during midcourse maneuver, scheduled to occur 7 to 10 days after launch, the anticipated orientation of the spacecraft provided that the load would be carried or, at best, shared by the battery. At encounter, it was expected that additional science loads would be imposed upon the system.

Launch

The spacecraft power system operated normally during launch, starting at 06:53 GMT on August 27; the solar panels were extended at 07:37, and Sun acquisition occurred at 07:53 on the same day. After that time, the solar panels provided power to the spacecraft until the end of the mission on January 3, 1963. Analysis of solar-source characteristics after launch revealed that the power output of the panels was sufficient to support the science load. When the science experiments were activated on August 29, an increase of 13 w in power demand was noted. The battery, which was discharged by approximately 179 w during launch, was completely recharged within 3.5 days at the estimated rate of charge. Up to the time of Earth acquisition the power demand of the spacecraft remained at 150 w, as expected, and the battery charger in parallel with the battery supplied

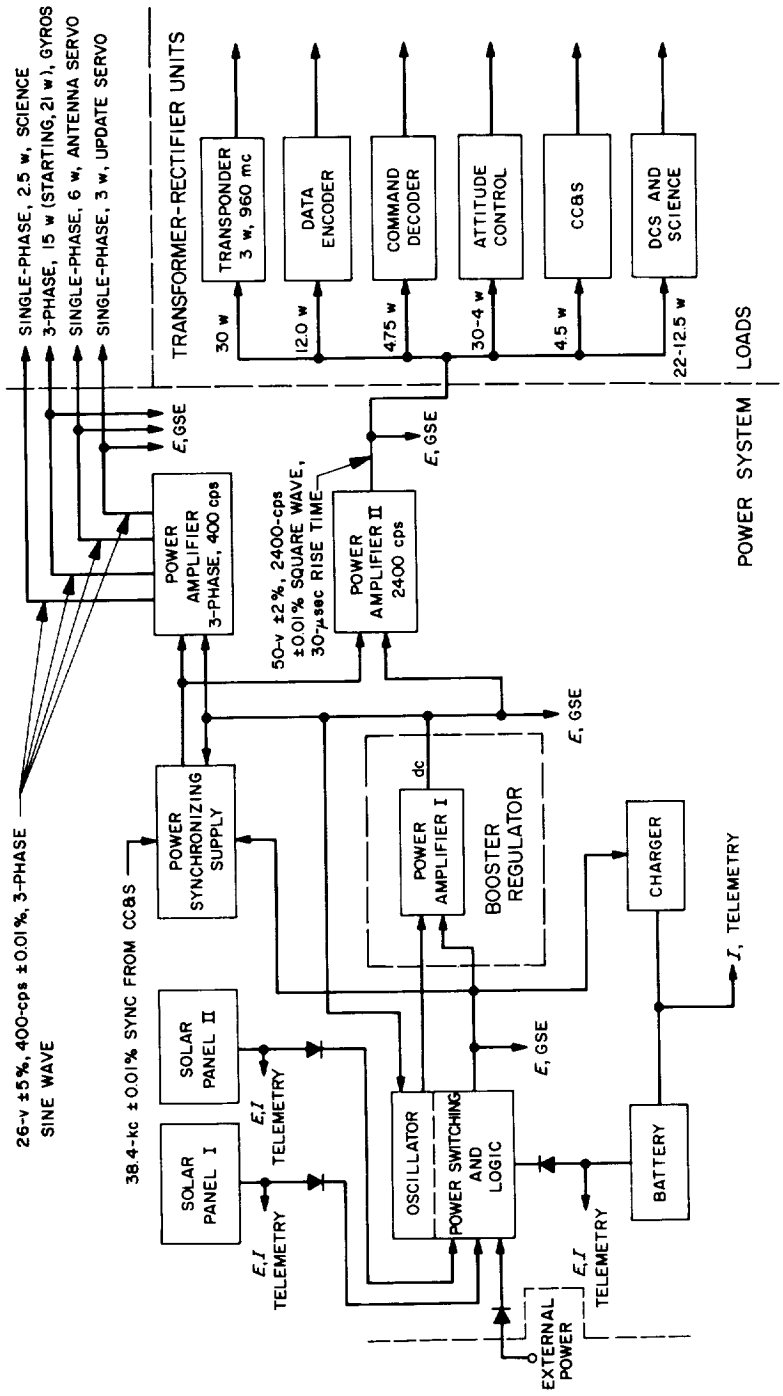

FIGURE 6–28.—Functional block diagram of power subsystem.

the direct battery loads. When the Earth-acquisition command was properly executed on September 3, the power system provided the required output of 3-phase power to operate the gyros. The power demand of the spacecraft system was normal; no battery sharing occurred, because the solar panels were able to support the peak power demand.

Midcourse

During the midcourse maneuver, executed on September 4, the power system performed properly, all power demands were normal, and the solar panels provided sufficient power to operate the gyros. Sharing with the battery occurred after the pitch turn was initiated. The battery power during the sharing phase and motor firing was approximately 1.67 amp-hr. The solar panels assumed the spacecraft load after Sun orientation and supported the spacecraft demand during the Earth-acquisition period of the midcourse maneuver.

Cruise

After midcourse maneuver the power demand returned to the cruise-mode level of 151.5 w; the battery was completely recharged in approximately 14 hours and remained fully charged, reducing the charging rate to a "trickle" value of approximately 2 ma. On October 31, the telemetry indicated that the panel voltage had dropped approximately 8.4 v from its previous operating level of 46.2 v. The current of panel 4A12 increased to 3.9 amp from the previous operating value of 1.92 amp, while the current of panel 4A11 read approximately zero. These new readings indicated that panel 4A11 had stopped providing solar power to the spacecraft.

On the assumption that only one panel was functioning, calculation of the available power indicated that the spacecraft was operating close to the maximum-power point of panel 4A12 (the panel with the solar cell extension). It was feared that sharing with the battery might occur if a load transient should appear. On the basis of this analysis, it was decided to transmit RTC turning off the cruise science instruments in order to relieve panel 4A12 of a 13 w demand, thus enabling it to operate below its maximum-power point. After the command was given, the data received showed that panel 4A11 was accepting power from 4A12 and that the operating point of panel 4A12 remained approximately the same. From these results, it was theorized that a short circuit had developed on panel 4A11, causing it to receive power and clamp panel 4A12 at about its maximum-power

point. Postflight analysis of the flight data showed that the short circuit was in one of the small sections of the solar-cell array located near the spacecraft frame (fig. 6–29). With the loss of one small section on panel 4A11, the solar-power output of both panels was clamped near the open-circuit voltage produced by the remaining series-connected section of panel 4A11. This voltage level forced panel 4A12 to operate at about its maximum-power point.

On November 8, panel 4A11 output returned to normal. All voltage and current telemetry data indicated normal readings for the temperature, trajectory, and load conditions. Science was turned on shortly thereafter with satisfactory results. On November 14, the panel telemetry readings again changed to the condition indicating a shorted section on panel 4A11. The lowering of panel voltage because of the short circuit had caused the battery charger to become inoperative. The battery voltage dropped slowly, since there was a small continuous load of approximately 20 ma on the battery.

Encounter

During encounter on December 14, the power system performed adequately despite the short circuit in panel 4A11. Although engineering data were not telemetered during the encounter phase, there were strong indications that the total encounter-mode load was being supplied by the solar panels.

Postencounter

On December 30 the 2400-cps power-supply frequency shifted to 2195 cps, the free-running frequency of the power-system magnetic oscillator. This indicated loss of the synchronizing signal, which should have been counted down from 38.4 kc to 2400 cps in the power synchronizer. At this new operating frequency the power requirements of the spacecraft increased by approximately 16 w. The power dissipation of the booster power inverter and the transformer-rectifier unit increased, as noted by the temperature rise. A stable condition was reached on January 2, 1963, however, and all the temperatures remained constant for approximately 24 hours, up to the time at which the last RF signal from the spacecraft was recorded.

PROPULSION SUBSYSTEM

The Mariner R midcourse propulsion system was designed to remove or reduce dispersion errors resulting from Agena injection, so that a Venus flyby

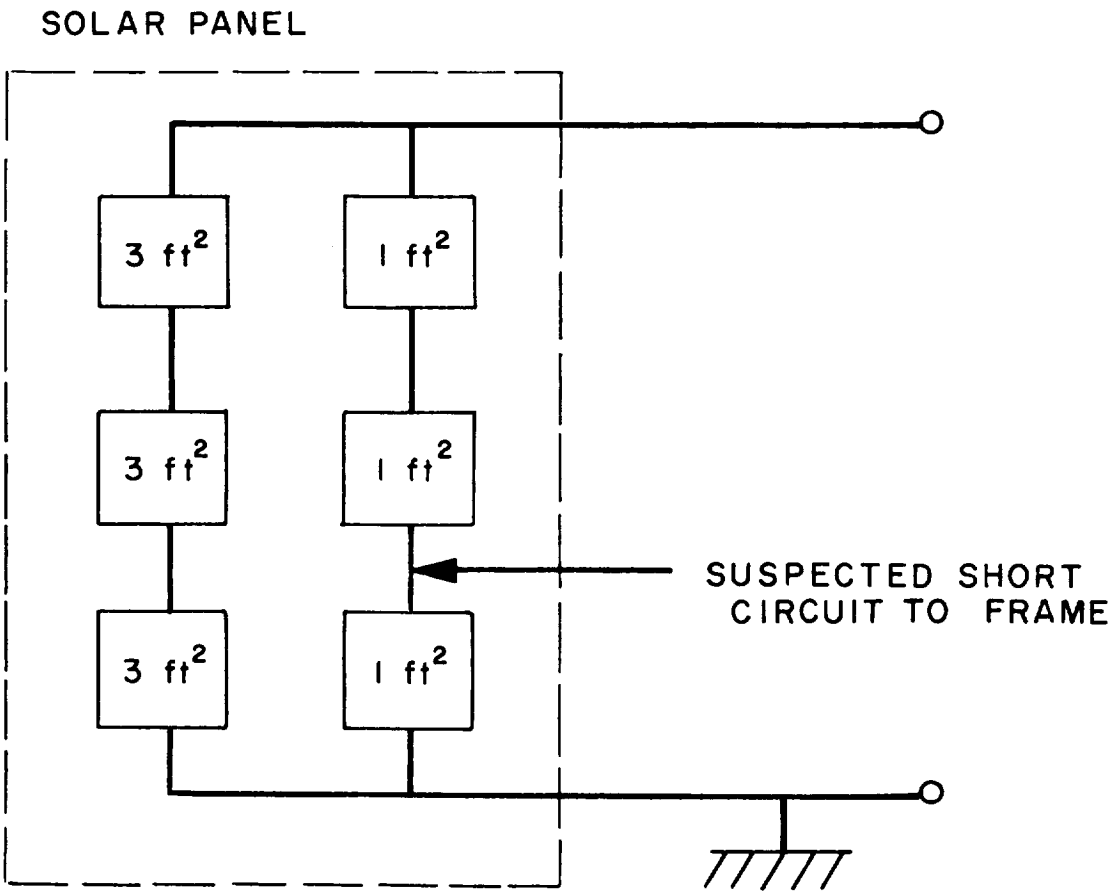

FIGURE 6–29.—Solar-panel connections.

with a sufficiently small miss distance could be reasonably assured. Nominally, this function was to be performed during a single midcourse maneuver, executed 7 to 10 days after launch, during which the spacecraft would turn to a prescribed attitude in space and respond to a corrective impulse provided by the midcourse propulsion system. In the Mariner II mission, this maneuver was delayed 1 day in order to insure that the spacecraft's Earth sensor was locked on the Earth and not on the Moon. On September 4, the eighth day after launch, the Mariner II spacecraft successfully executed the commanded roll and pitch turns, and the midcourse propulsion system imparted a velocity increment of approximately 31 m/sec to the spacecraft. This maneuver reduced the predicted Venus miss-

distance of some 386 232 km (240 000 miles) to approximately 32 186 km (20 000 miles).

A schematic of the midcourse propulsion subsystem is presented in figure 6–30, and figure 6–31 is a photograph of the subassembly. The subsystem utilized a liquid monopropellant, anhydrous hydrazine, as the propellant. The midcourse motor was, functionally, a constant-thrust rocket engine, fed by regulated gas pressure. The principal system components were a high-pressure nitrogen-gas reservoir, a gas-pressure regulator, a propellant tank and bladder, and a rocket engine. The rocket engine contained a quantity of catalyst to accelerate the decomposition of hydrazine. Explosively actuated valves were used throughout the system. Normally closed explosively actuated valves were activated to initiate nitrogen pressurization of the propellant tank, to start propellant flow to the rocket engine, and to release nitrogen tetroxide from the engine ignition cartridge. Normally open explosively actuated valves were activated to terminate nitrogen pressurization of the propellant tank and propellant flow to the rocket engine.

In order to avoid electrical or mechanical sequencing, the propellant tank was prepressurized with nitrogen during the preflight operation so that engine ignition and regulated nitrogen pressurization of the propellant tank could occur simultaneously through one signal from the CC&S; similarly, one signal is necessary for thrust termination. A summary of engine performance is given in table 6–II, and nominal system pressures and temperatures are shown in table 6–III.

The firing of the midcourse propulsion engine was controlled by the CC&S, which received the time, direction, and magnitude of the midcourse-motor firing through the ground communication link. After the spacecraft had assumed the correct firing attitude, the midcourse propulsion subsystem was ignited (at the prescribed time) through an electrical signal which was originated in the CC&S. After the specified velocity increment had been attained, as computed by the spacecraft integrating accelerometer, thrust termination was controlled by the CC&S by means of an electrical signal. During the rocket-engine firing, spacecraft attitude was maintained by the autopilot-controlled jet-vane actuators.

The four telemetry measurements for the midcourse propulsion subsystem were nitrogen-tank temperature and pressure and propellant-tank temperature and pressure. The reduced data for these four parameters, covering the period from launch to mission termination, are plotted in figures 6–32 to 6–34.

As depicted in figure 6–32, nitrogen-tank pressure remained constant up to the time of the midcourse correction, indicating a leak-tight system through

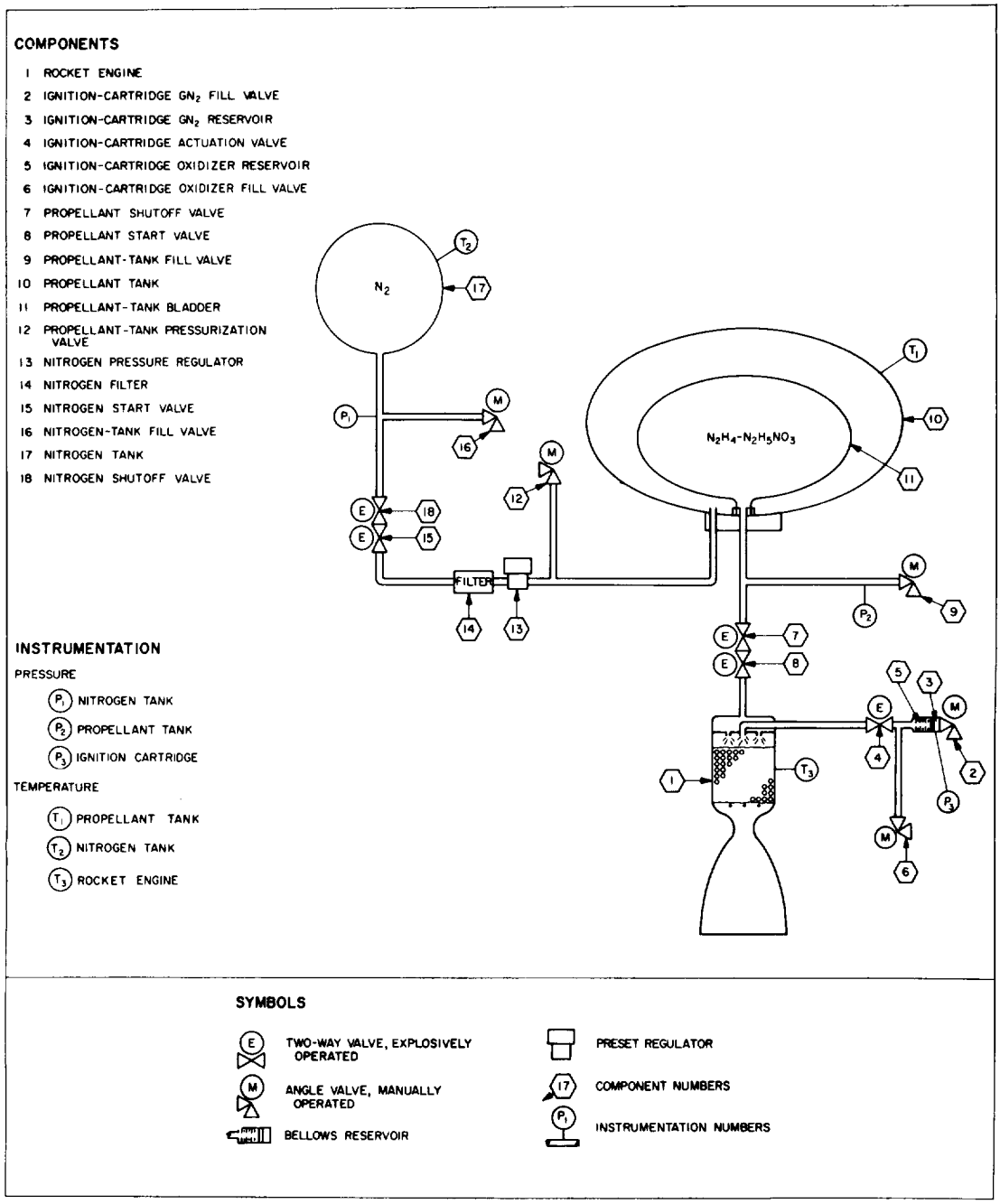

FIGURE 6–30.—Schematic diagram of Mariner R midcourse propulsion system.

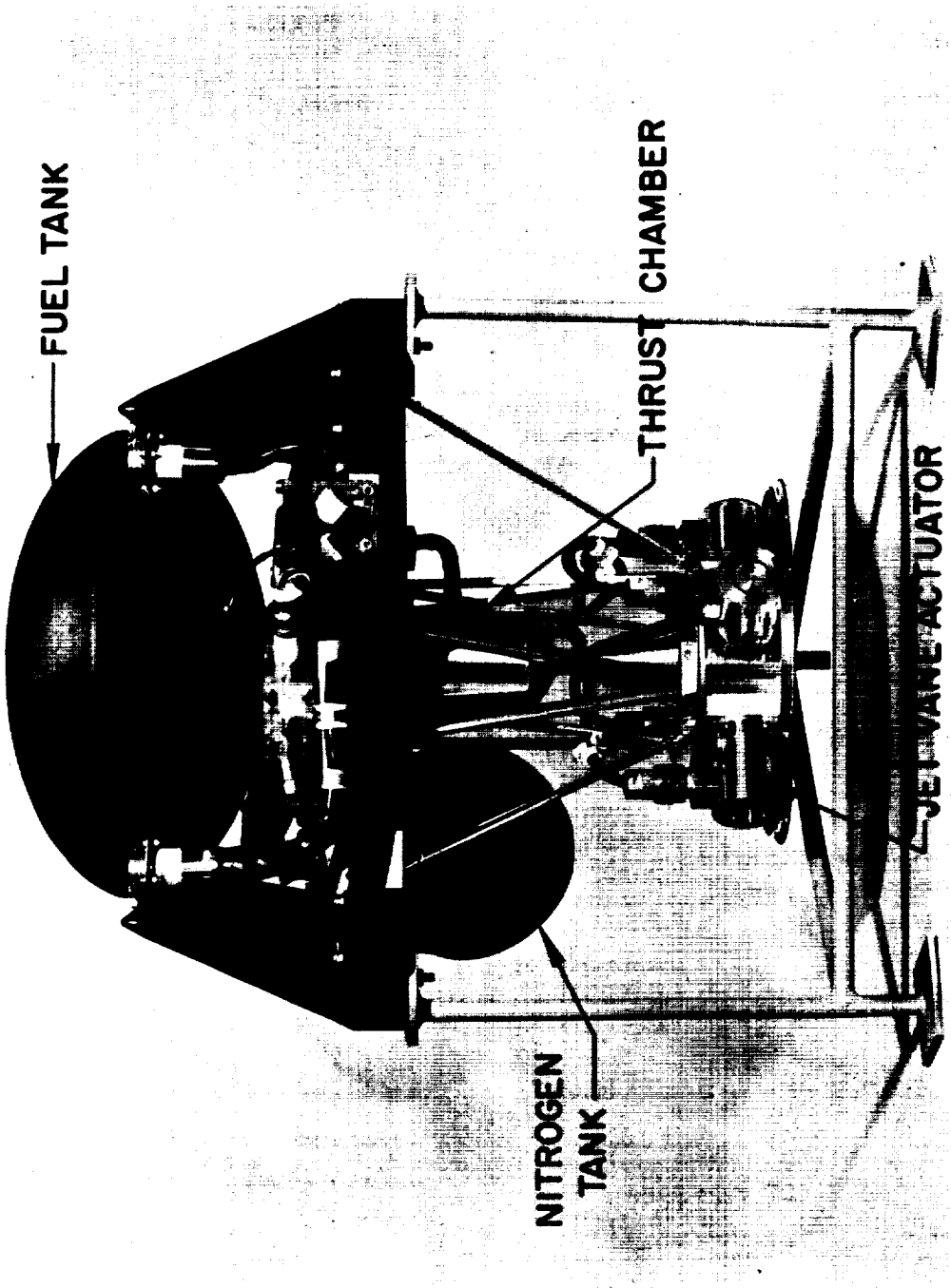

FIGURE 6–31.—Mariner R flight propulsion system.

boost and during the 8-day coast period. The near-nominal and constant nitrogen-tank pressure would have supported a maximum midcourse correction (as limited by the propellant load) and resulted in the maximum predicted velocity-increment capability of 61.05 m/sec.

Table 6–II.—Nominal performance (without jet vanes) for midcourse propulsion system

Vacuum thrust, lbf	50.7
Vacuum specific impulse, lbf-sec/lbm	235.05
Vacuum thrust coefficient (based on hot throat area)	1.7558
Propellant flow rate, lbm/sec	0.21574
Ambient throat area, in^2	0.15
Hot throat area, in^2	0.1527
Stagnation chamber pressure (based on hot throat area), psia	189.1
Characteristic velocity (based on hot throat area), fps	4306
Engine expansion ratio	44:1

Table 6–III.—Nominal pressures and temperatures for midcourse propulsion system

Component	Nominal pressure, psia	Nominal temp., ° F
Nitrogen reservoir, at ignition	3000	70
Nitrogen reservoir, at termination (maximum duration run)	940	−20
Propellant tank	.....	70
Propellant tank, prepressurization	300	.....
Propellant tank, operating	310	.....
N_2O_4 ignition cartridge, at ignition	350	.....
N_2O_4 ignition cartridge, at termination	210	.....
Thrust-chamber wall	.....	1800–1900
Chamber pressure, operating (represents stagnation pressure at entrance to nozzle convergent section)	189	.....

The propellant-tank pressure (fig. 6–33) maintained the rising characteristic noted prior to launch and up to the time of the midcourse maneuver. This rate of rise was roughly 3 to 4 psi/day; no pressure rise appears in figure 6–33 for the first several days after launch because of the compensating effect of a decreasing propellant-tank temperature. Tests indicate that the tank-pressure rise was due to hydrazine decomposition resulting from incompatibility with the expulsion bladder containing the propellant. At the time of the maneuver, the

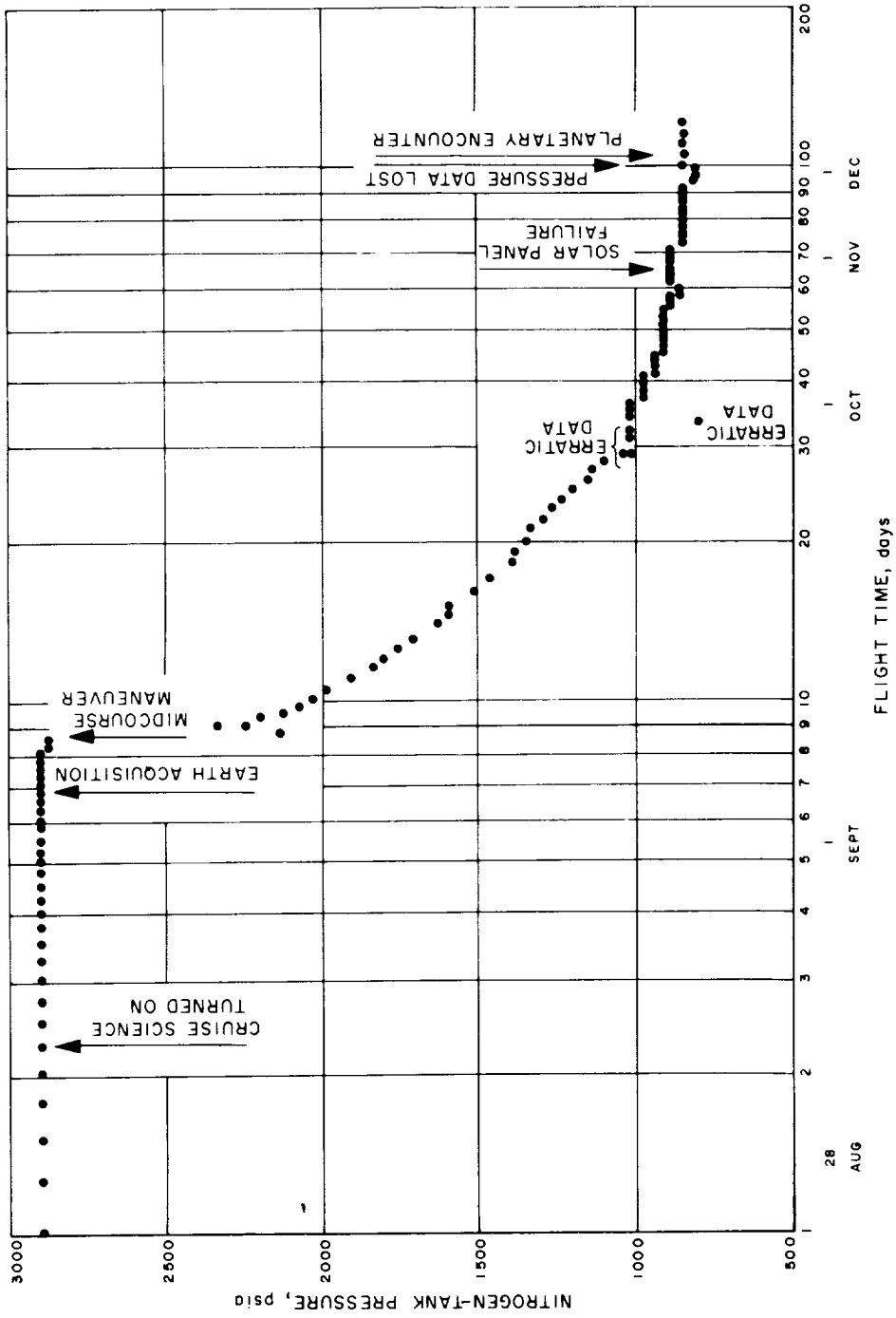

FIGURE 6–32.—Midcourse-motor nitrogen-tank pressure vs flight time.

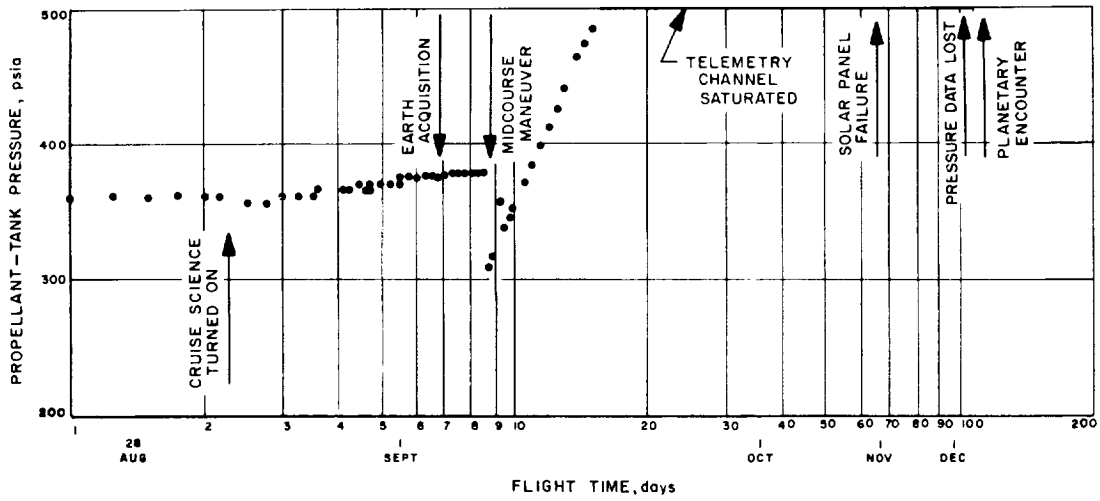

Figure 6–33.—Midcourse-motor propellant-tank pressure vs flight time.

propellant-tank pressure was 378 psia, roughly 70 psi above nominal for an 80° F propellant-tank temperature. This higher-than-nominal initial propellant-tank pressure resulted in a nonstandard starting transient for an 80° F firing; however, no difficulties were predicted or, apparently, encountered as a result of this transient. During the course of system type-approval testing, engine ignitions with initial propellant-tank pressures as high as 550 psig were successfully conducted, and, on the basis of these tests, the thrust transient shown in figure 6–35 was predicted.

On the basis of the pressure-regulator setting, characteristics of the Mariner II propulsion system, and nominal engine performance at a 10° jet-vane deflection, an engine steady-state vacuum thrust of 50.54 pounds was predicted. This steady-state thrust level, together with the predicted starting transient of figure 6–35, the velocity-increment requirement of 31.16 m/sec, and the spacecraft mass of 447.67 pounds, resulted in a predicted midcourse-correction burn time of 28.3 sec. From the Doppler-shift data acquired during the midcourse maneuver, motor ignition and thrust termination were verified, the burning time being roughly as predicted. Event-register blips indicating initiation of the fuel- and oxidizer-valve start signals and the fuel-valve shutoff signal were recorded during the midcourse maneuver. Also, the event blips for the CC&S motor-start and shutoff commands were recorded at the appropriate times. Further verification of normal propulsion-system operation during the midcourse maneuver is

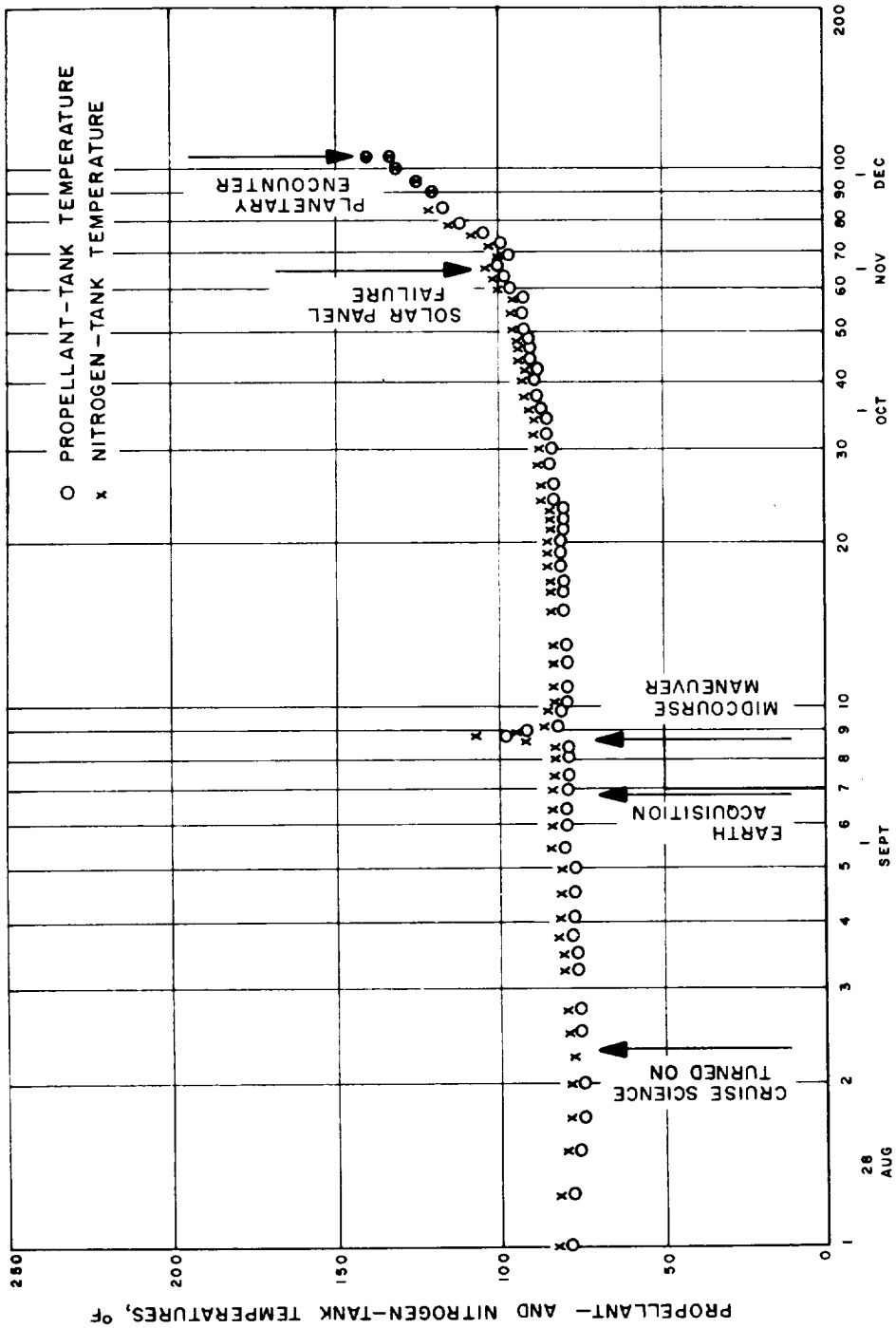

FIGURE 6–34.—Midcourse-motor propellant- and nitrogen-tank temperature vs flight time.

provided by the postmaneuver propellant-tank and nitrogen-tank pressures and temperatures. By using these pressures and temperatures after temperature stabilization had occurred, together with the premaneuver nitrogen- and propellant-tank pressures and temperatures and the nominal predicted engine performance at a 10° jet-vane deflection, a delivered velocity increment of 37. 5 m/sec was calculated.

Subsequent to the midcourse maneuver, the nitrogen-tank pressure steadily decreased, and the propellant-tank pressure steadily increased, as indicated in figures 6–32 and 6–33. This nonstandard situation was the result of a failure of the normally open nitrogen-shutoff valve to close at the motor-shutoff command. This failure permitted the remaining high-pressure nitrogen in the tank to leak slowly past the seat of the pneumatic regulator into the propellant tank. On the basis of the volumes of the two tanks involved and the pressures and temperatures in these tanks after the midcourse maneuver, an equilibrium pressure of approximately 850 psia in the two tanks was predicted at a temperature of 110° F. It appeared that the tank pressures were nearly equalized by the 80th or 90th day after launch, as indicated in figure 6–32, and that the predicted value of 850 psia at 110° F was roughly verified. Note that 850 psia was well below the burst pressure of the propellant tank and associated components, and no difficulties were expected or observed as a result of the failure.

It is essentially impossible to determine what component failed: a relay in the pyrotechnic control subsystem, the valve squib, or the valve itself. It is known, however, that a design weakness existed in the squib, as a result of which the connector, on occasion, had been blown from the squib upon actuation. It is conjectured, therefore, that the normally closed squib underwent such a failure at midcourse ignition, damaging the neighboring, normally open squib and/or connector and rendering the nitrogen-shutoff valve inoperative.

As noted in figures 6–32 and 6–33, the measurements of nitrogen-tank pressure and propellant-tank pressure were lost on December 9. In addition, the measurements of attitude-control nitrogen pressure and antenna hinge angle were lost. It is believed that these malfunctions were caused by a failure in the transducer circuit associated with, and common to, these four measurements.

The propellant-tank and nitrogen-tank temperatures followed closely the spacecraft temperature history throughout the flight. The temperature "spike" shown in figure 6–34 at the time of the midcourse maneuver was anticipated as a result of radiative heating of the nitrogen tank from the engine during the engine

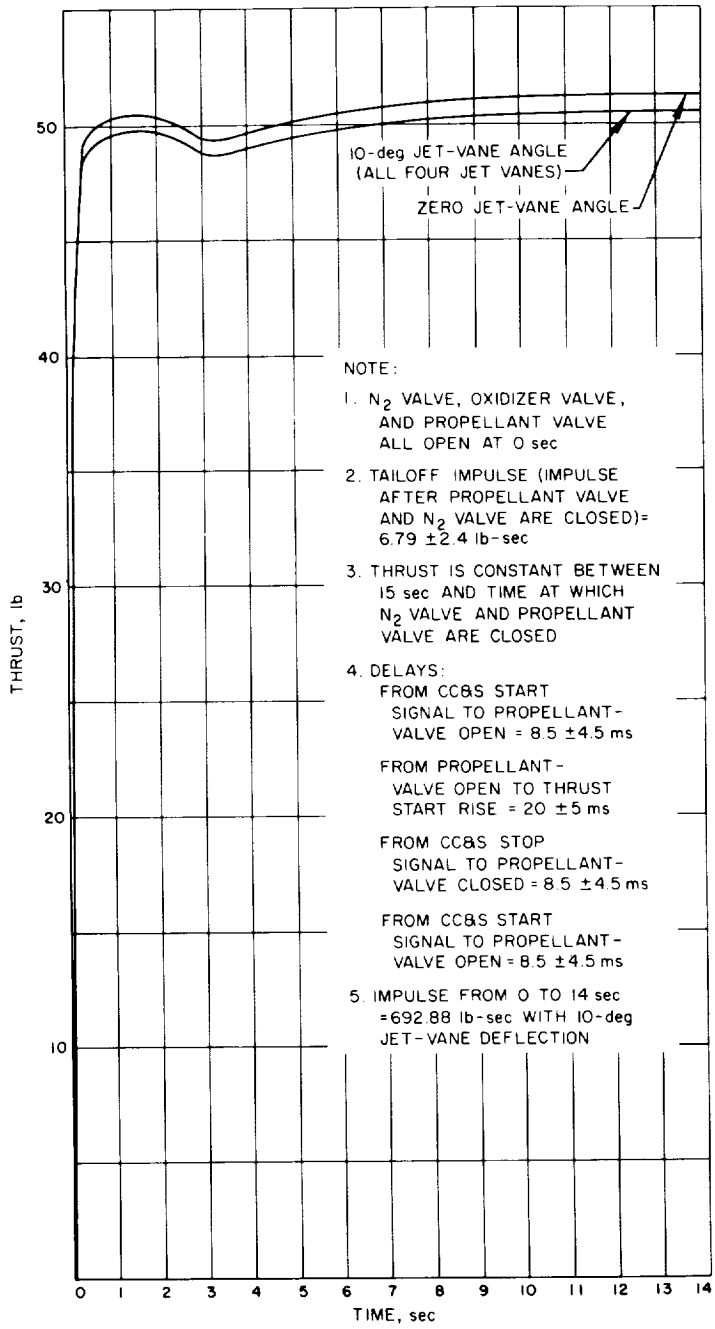

FIGURE 6–35.—Midcourse-motor predicted thrust vs time.

burn and of heat soak from the engine to the nitrogen and propellant tanks following engine shutdown.

CENTRAL COMPUTER AND SEQUENCER

In the Mariner R spacecraft, the computation and command of all time-sequenced events (except the science experiments) were performed by the digital central computer and sequencer. All events of the spacecraft were activated in three CC&S sequences: (1) The launch sequence, which controls events from launch through the cruise mode; (2) the midcourse propulsion sequence, which controls the midcourse trajectory-correction maneuver; and (3) the encounter sequence, which provides required commands for data collection in the vicinity of Venus.

The CC&S also provides the basic timing for the spacecraft subsystems. This time base was supplied by a crystal-controlled oscillator in the CC&S operating at 307.2 kc. This frequency is divided down to 38.4 kc for timing in the power subsystem and is divided down again to 2400 and 400 cps for use by the various subsystems. The control oscillator provides the basic counting rate by which the CC&S determines the issuance of commands at the right time in the three sequences. Figures 6–36 and 6–37 present, respectively, a block diagram and a photograph of the central computer and sequencer.

The discussion of CC&S performance during the Mariner II flight to Venus has been separated into four flight phases: Launch, midcourse, cruise, and postencounter.

Launch

At approximately launch minus 12 min, 1215 update pulses were inserted from the blockhouse in the CC&S, in order to set the encounter start time at approximately 12 hours prior to the closest approach to Venus. The CC&S clock began counting with the release of the inhibit current in the blockhouse 3 min prior to launch. Two minutes later, the clear-release command was observed as programmed, and the CC&S was declared in a go condition. At approximately 44 min after launch, the solar-panel-extension command was initiated correctly, as was the attitude-control power-up command at 60 min after launch. The antenna reference-angle update pulse was initiated as programmed at 16⅔ hours and was repeated every 16⅔ hours thereafter. At 166⅔ hours, the

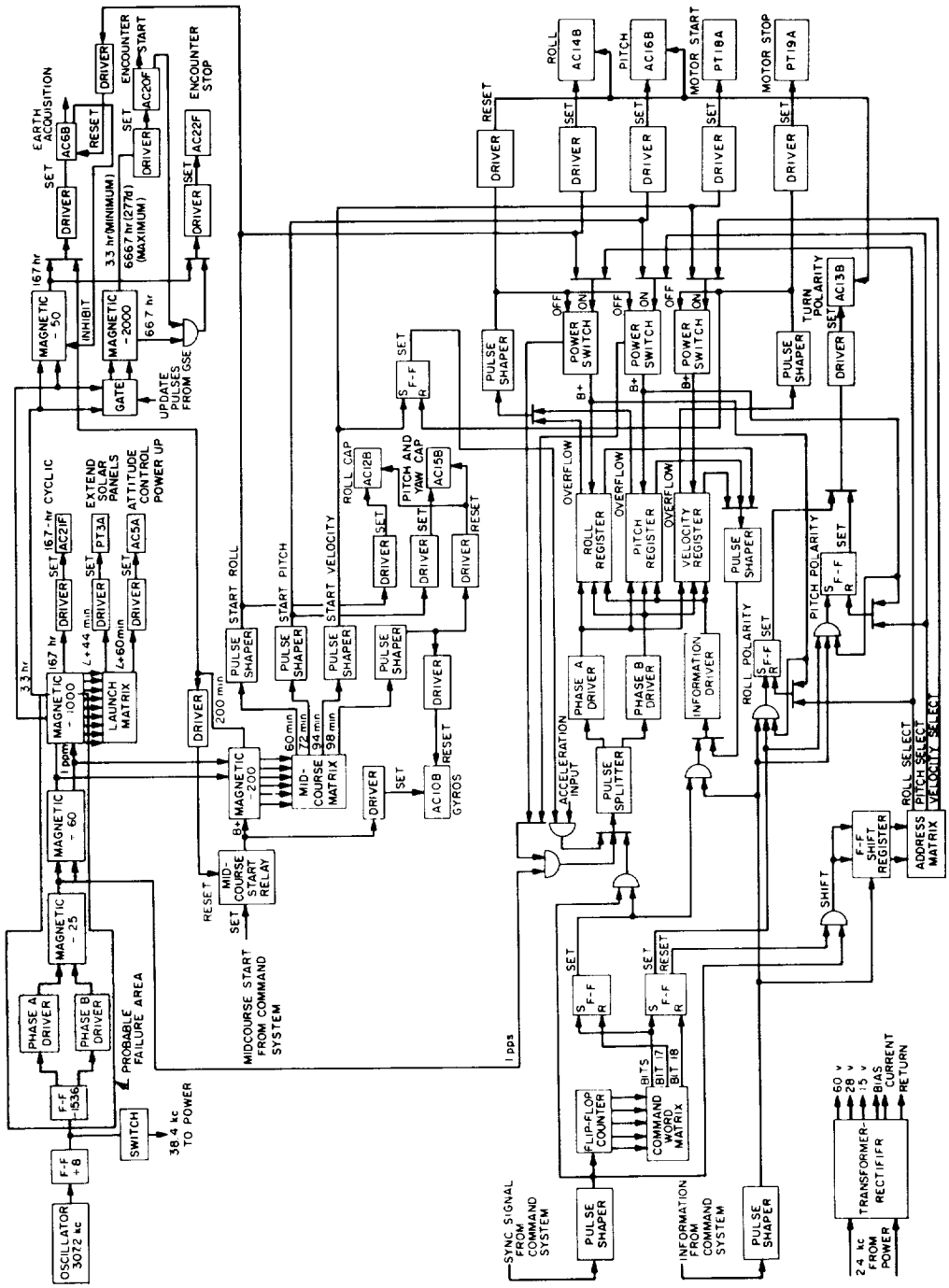

FIGURE 6–36.—Block diagram of central computer and sequencer.

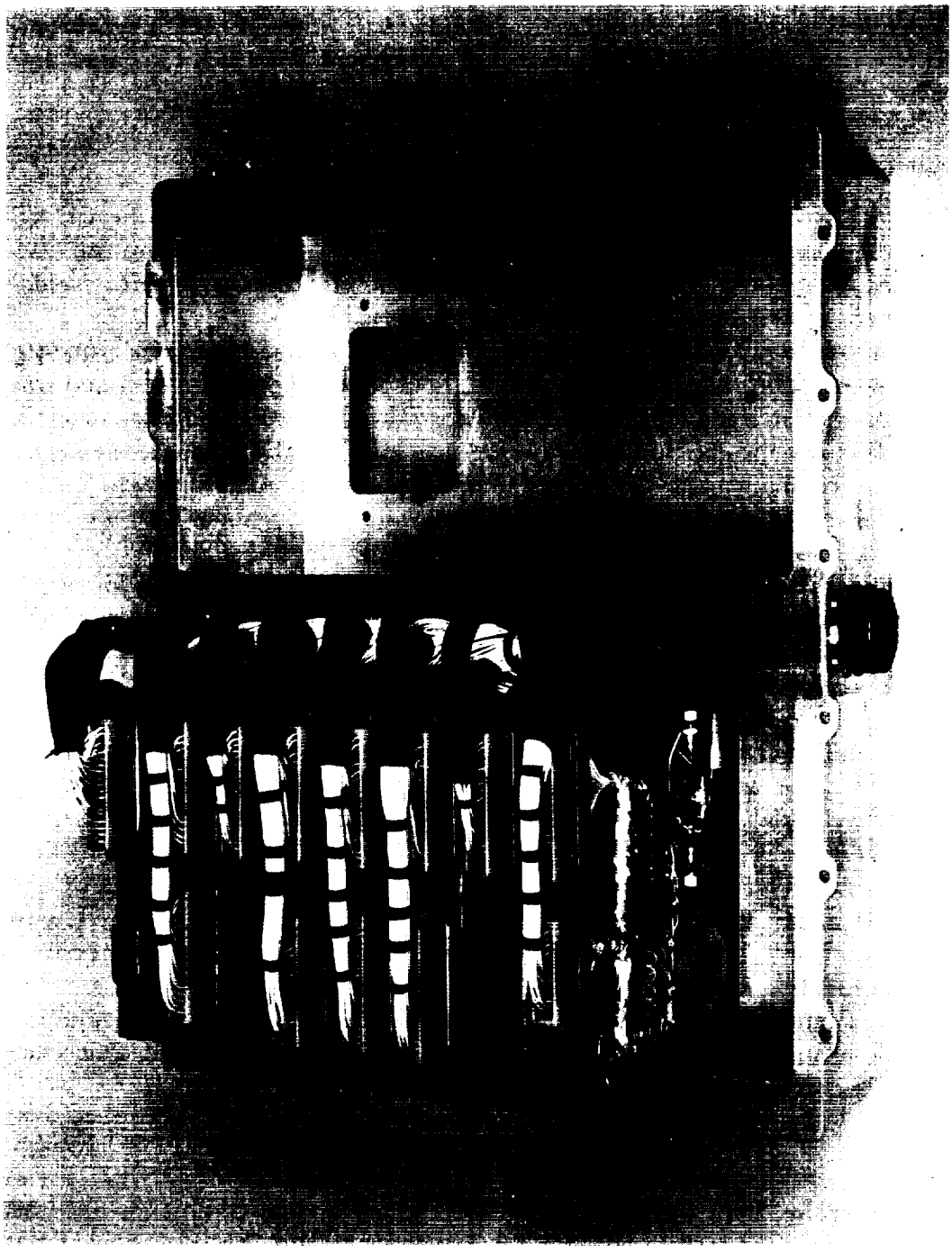

FIGURE 6-37.—Central computer and sequencer before encapsulation.

Earth-acquire command was initiated. Monitoring of the DO (data synchronization reference point) sync times prior and subsequent to launch indicated that the boost phase did not noticeably affect the stability of the clock frequency.

Midcourse

The following midcourse maneuver parameters were inserted in the CC&S by ground command prior to the start of the maneuver: 51 sec of minus roll, 795 sec of minus pitch, and 1033 accelerometer pulses to give the spacecraft a velocity increment of 31.16 m/sec.

At approximately 22:44 on September 4, the midcourse maneuver sequence was activated. The roll maneuver began 1 hour later, as programmed, and was followed by the pitch maneuver and the motor burn. At 00:27 on September 5, the CC&S command for Sun reacquisition was given, and the spacecraft began its reacquisition maneuver. The cruise mode was again established with Earth-reacquisition command by the CC&S, as programmed, 3⅓ hours after the start of the midcourse maneuver.

The designed resolution of the telemetry data was not fine enough for determination of the accuracy of the turn durations or computation of the motor-burn duration; only the occurrence was indicated. However, the turn and motor-burn durations, as indicated by telemetry and within telemetry resolution, were as commanded. Doppler data compiled by the DSIF tracking stations during the midcourse manuever indicated that the motor-burn duration was longer than commanded. The long burn could have been caused by a number of errors outside, as well as within, the CC&S subsystem. Within the CC&S, a contribution to this error might have been made by one or both of the following anomalies: (1) The possibility that all of the accelerometer pulses were not sensed by the CC&S; (2) a momentary malfunction of the feedback circuit associated with the velocity register in the CC&S. The first explanation appears more probable, since a malfunction of the register feedback circuit would normally be evident in the roll- and pitch-turn durations, as well as in the motor burn. No explanation is available as to why the CC&S might momentarily not have accepted accelerometer pulses, especially if the pulse characteristic did not change.

Cruise

During cruise, both the antenna reference-angle update commands and the DO sync times were monitored as a continuous check on the operation of the

CC&S. Figures 6–38 to 6–41 present graphs of CC&S antenna update command limits and DO sync times, as observed in telemetry data. On October 13 and again on December 28, the data encoder C-deck counter picked up an extra count resulting from noise generated by a radiometer calibration sequence. This caused the C-deck counter to overflow one frame too soon and resulted in a 37-sec shift in the observed DO sync times. The dashed curves in figures 6–39 to 6–41 represent the sync times which would have been observed if the calibration noise had not affected the C-deck counter. The solid and dashed curves of normal DO sync times in figures 6–38 to 6–41 fall between the respective antenna reference update limits, except for update number 82. Update number 82 should also have bracketed the DO sync curve because, under normal operation, the DO sync time should be the same as the errors in the antenna reference update command which were due to the CC&S clock-frequency error. No reason is known for the fact that this event did not appear to occur with the same error as the DO sync, which occurred a few minutes later. The CC&S counter which provides the cyclic timing for the update command could not have overflowed late because all subsequent commands would have been displaced by the same amount of time (11 to 48 sec).

The DO sync-time curve was used to calculate the CC&S frequency error during the flight, which is plotted in figure 6–42 versus the day of flight. Appearing on the same graph is a curve of case IV temperature. It is apparent from the graph that the CC&S frequency error was proportional to temperature. A graph of frequency error versus temperature for the Mariner II flight is presented in figure 6–43. Here, the dashed line represents a straight-line approximation of two temperature measurements made on the Mariner II CC&S assembly at a time prior to the flight. The differences between the curves could possibly be explained as follows:

1. There was some aging of the CC&S oscillator crystal between the time at which the static measurements were made and the flight, which could have contributed slightly to the difference.

2. Some error was, perhaps, introduced by the graphical analysis used to obtain the CC&S frequency error.

On December 12, the antenna reference-angle update command ceased to be generated by the CC&S. Two days later, on December 14, the encounter-start command, which was set for this date prior to launch, also failed to occur. It is possible, and quite probable, that these failures were attributable to the same cause within the CC&S.

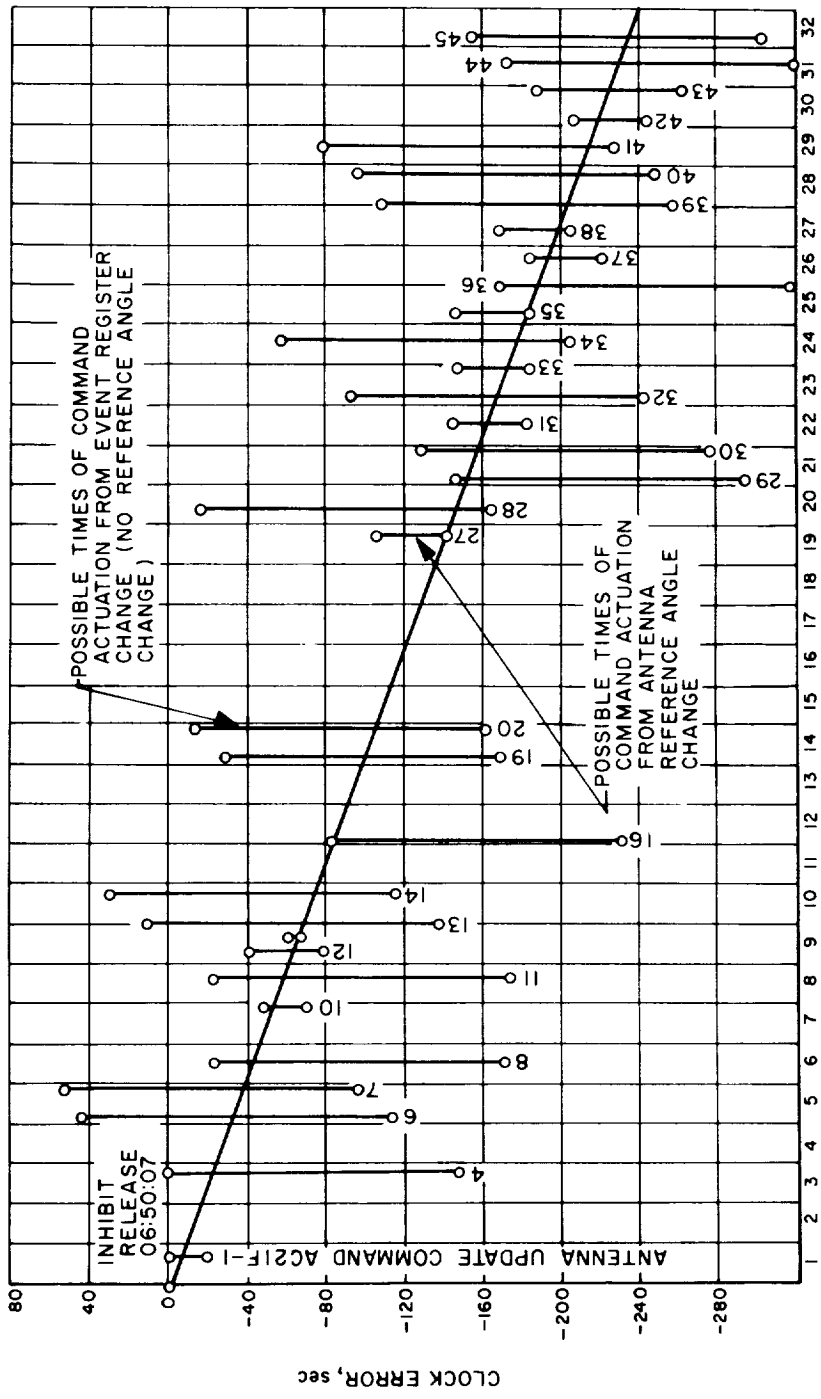

FIGURE 6–38.—Graph of antenna update commands and DO sync times, August 27 to September 27, 1962.

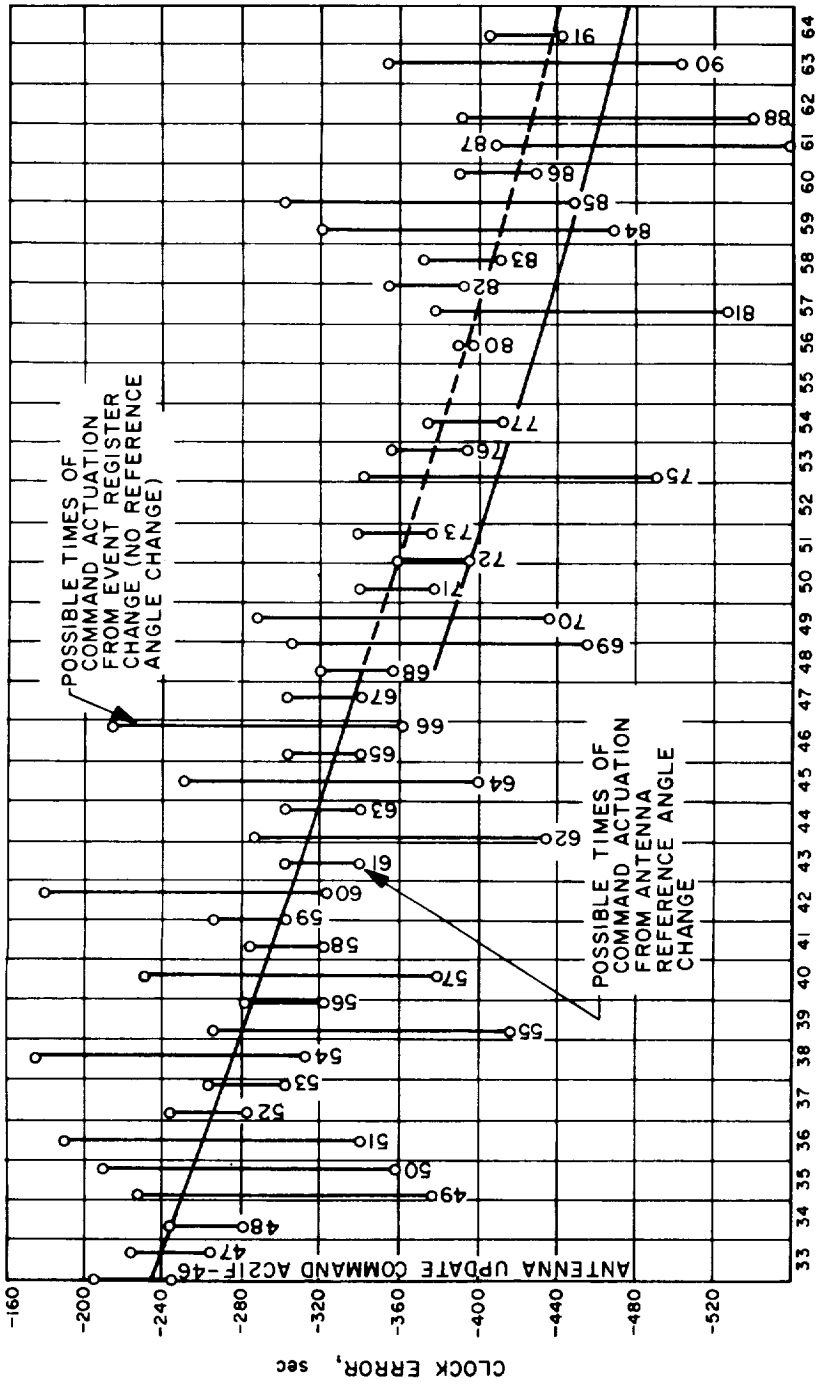

FIGURE 6-39.—Graph of antenna update commands and DO sync times, September 28 to October 29, 1962.

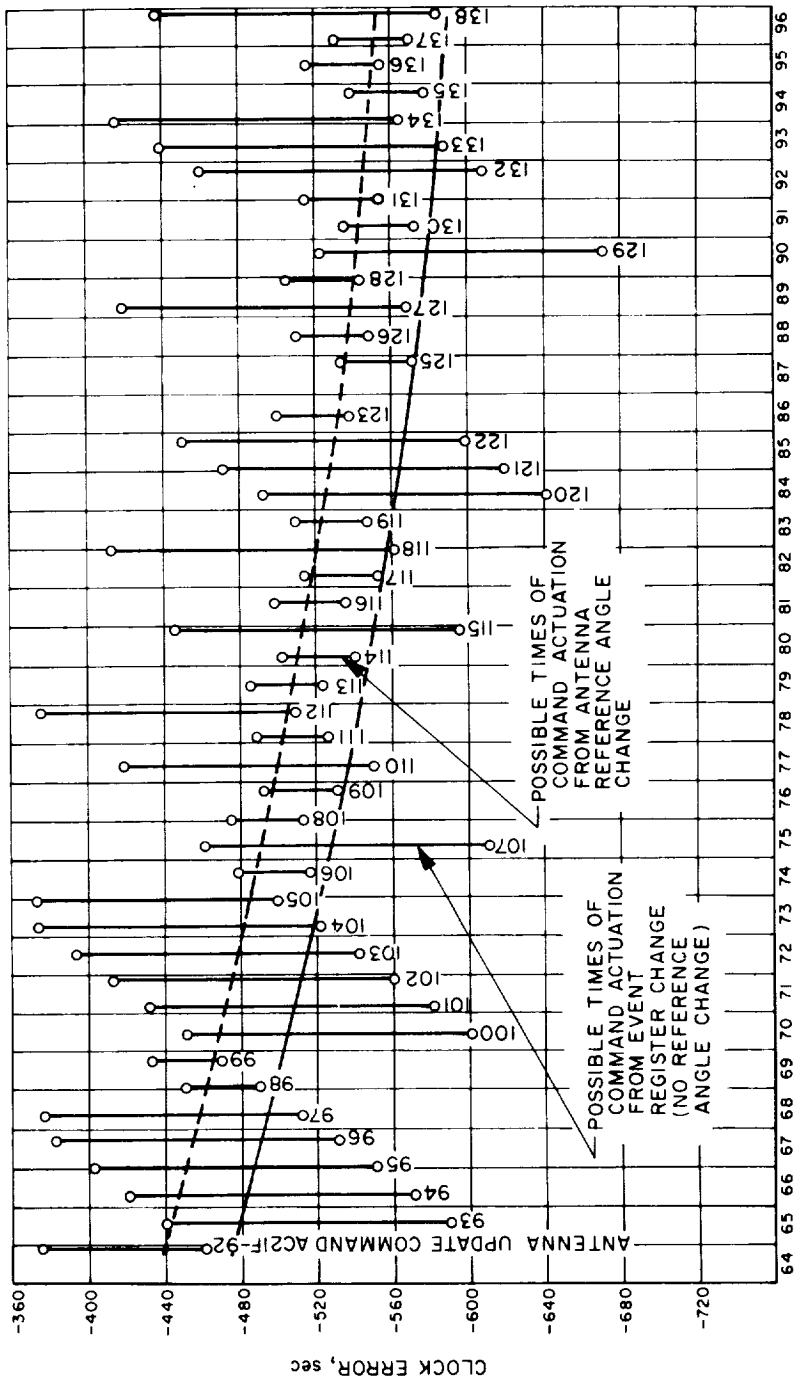

FIGURE 6–40.—Graph of antenna update commands and DO sync times, October 30 to November 30, 1962.

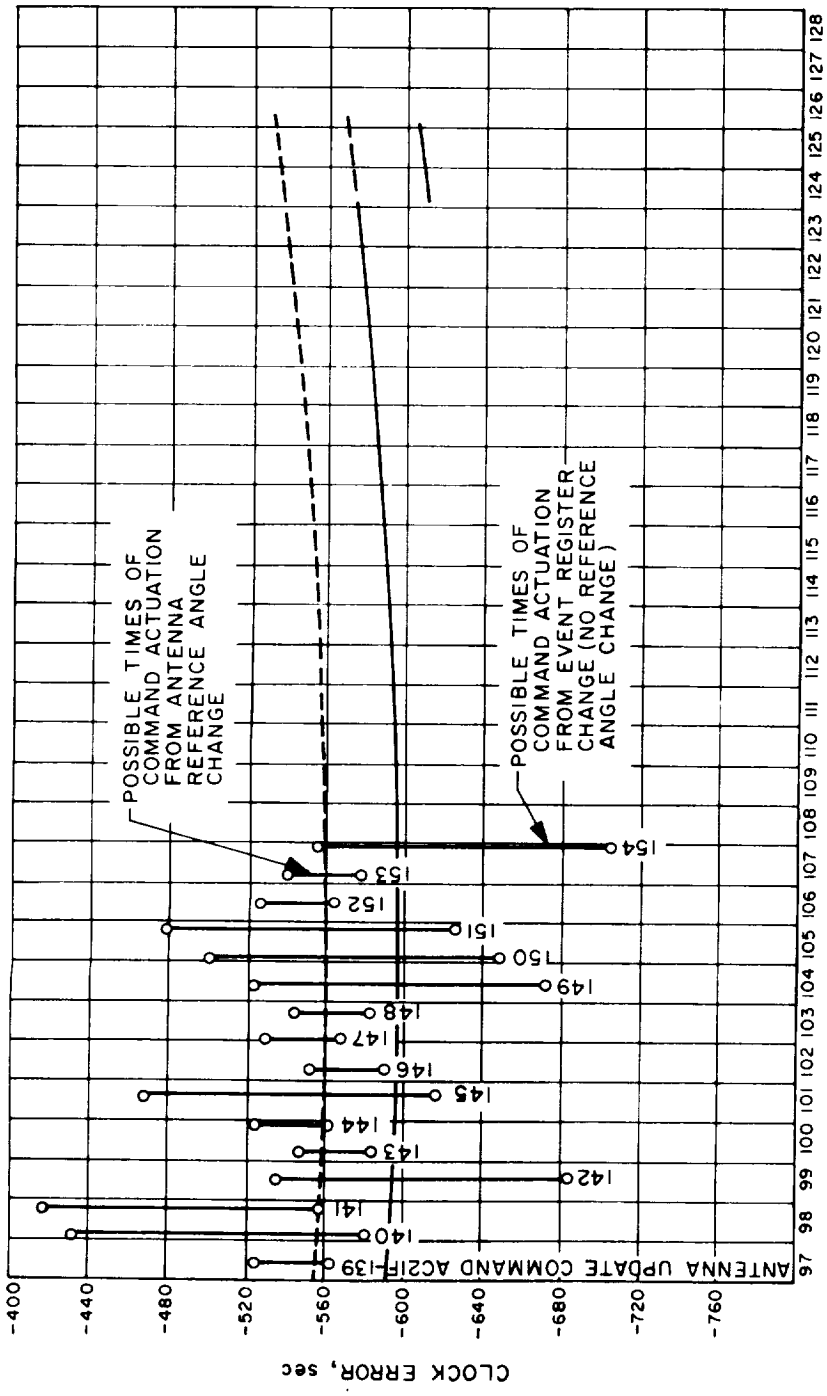

FIGURE 6-41.—Graph of antenna update commands and DO sync times, December 1 to 31, 1962.

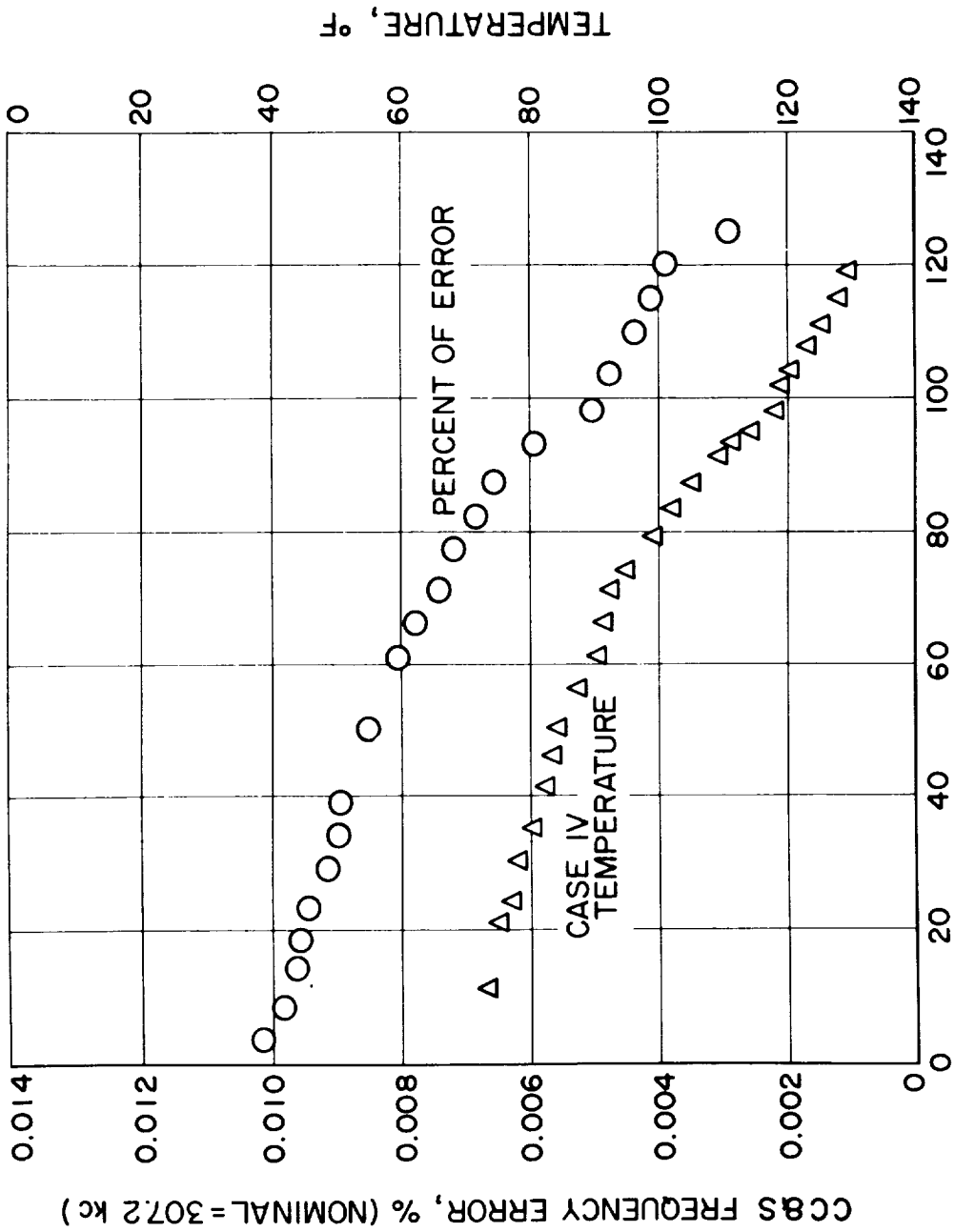

FIGURE 6–42.—CC &S frequency error and Case IV temperature vs flight time.

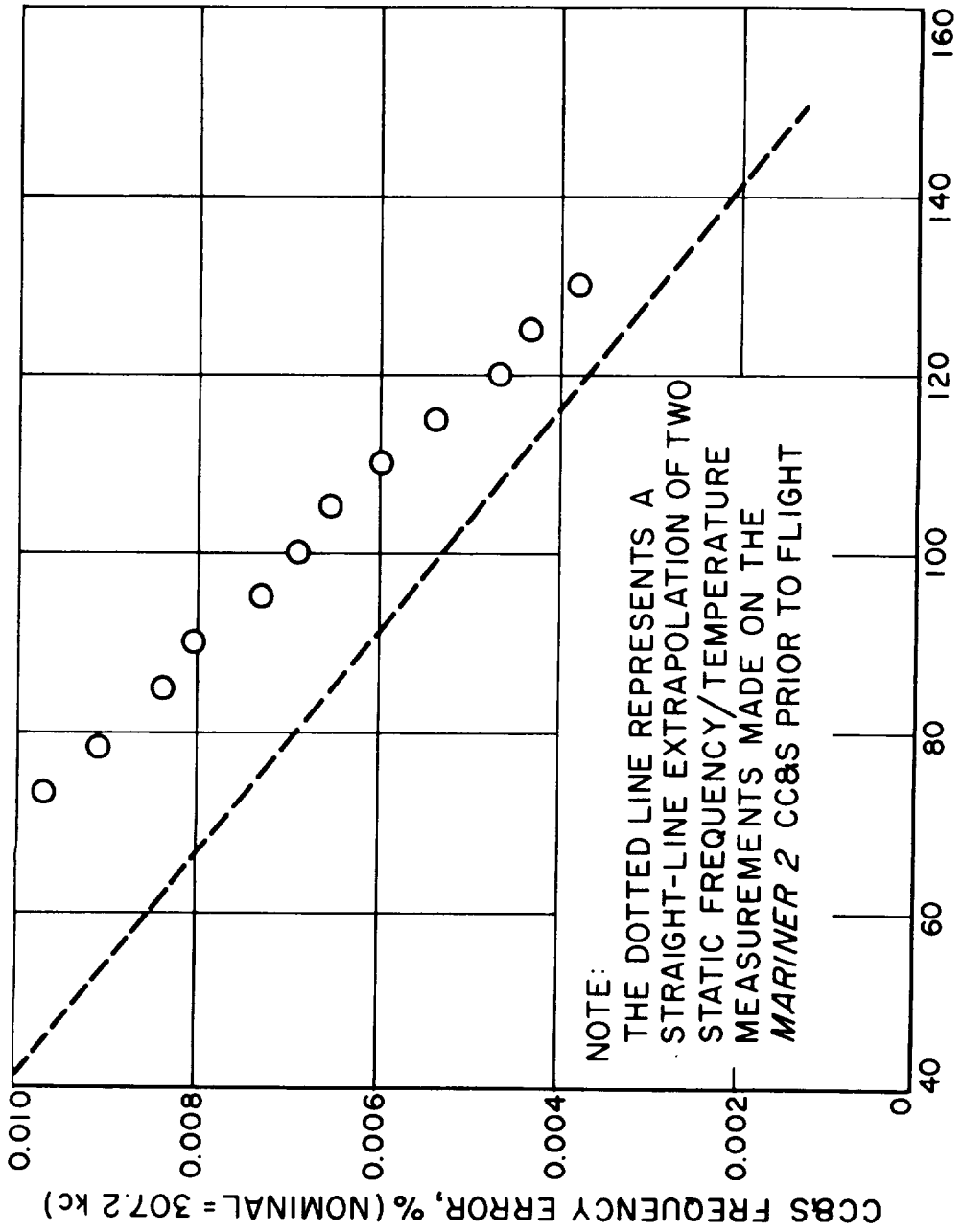

FIGURE 6-43.—CC &S frequency error vs Case IV temperature.

If such a single failure is assumed, then it must have occurred somewhere between the 38.4-kc signal (since it was still present at that point) and the 3⅓-hr/pulse point in the counter chain. The 3⅓-hr signal is the last counter pulse common to both the cyclic-update and encounter-start commands. The most probable cause would be a component failure. Included within the suspected area of malfunction are the following components: 160 resistors, 51 transistors, 50 cores, 40 diodes, 25 glass capacitors, 21 temperature-sensitive resistors, and 4 tantalum capacitors.

It is most unlikely that a resistor or a glass capacitor opened, shorted, or changed value enough to cause the malfunction, since the average power and voltage levels at which these components normally operate is quite low in comparison with their maximum ratings. Magnetic cores are generally considered reliable, but a change in core characteristics cannot be ruled out. The temperature-sensitive resistors, semiconductors, and tantalum capacitors are the most likely causes of failure. No data received by telemetry and analyzed to date have given any hint as to the exact nature of the CC&S failure. Because no CC&S signals, except the event pulses, are directly telemetered back to Earth, use of the telemetry data for failure analysis is limited.

Postencounter

At 17:28 on December 30, the 2.4-kc power frequency went out of sync. One possible cause, among others, could have been the loss of the 38.4-kc sync signal from the CC&S. As before, the more probable cause would be a component failure of the type discussed above, with the addition of a crystal and a transformer as possible sources of malfunction.

No further events or changes were noted in the CC&S up to the time of final communication with the spacecraft on January 3, 1963.

TELECOMMUNICATIONS SUBSYSTEMS

The telecommunications subsystems were designed to provide (1) two-way Doppler capability, (2) automatic angle tracking, (3) command capability, and (4) scientific and engineering data from the spacecraft. The limited bandwidth available on an interplanetary mission implied the capability of adding or deleting measurements as a function of specific flight phases, thus transmitting some data

only when needed and accommodating the scientific data and engineering measurements required for system evaluation in a reliable yet flexible manner.

A study of the possible Earth-Venus trajectories revealed that the telecommunications subsystems would have to be capable of operating over a distance of 6×10^7 km (37 282 million miles). A prediction of the maximum available communications system capacity at this distance showed that a telemetry system with a variable data-transmission rate was required.

At launch and until such time as attitude control was achieved, communications could not depend on the high-gain directional antenna; it was, therefore, necessary to provide an omnidirectional antenna system, which was also required to transmit information on spacecraft performance during the midcourse maneuver.

A further requirement for the telecommunications system was that it must be compatible with, and utilize to the fullest possible extent, the existing Deep Space Instrumentation Facility. Compatibility with the DSIF required that the RF carrier be phase-modulated, that the modulation spectrum be confined within certain limits, and that the modulation not completely suppress the carrier. The latter requirement was necessary to insure automatic angle tracking and receipt of the required two-way Doppler.

Within the bounds of the foregoing requirements, the telecommunications system was implemented. The flight system consisted of a data encoder, a transponder, a command assembly, antennas, transducers, and the associated ground support equipment used to verify proper operation of flight components. Figure 6–44 shows the functional block diagram of the spacecraft telecommunications system and ground support components.

Data Encoder Subsystem

The data encoder was designed to accept approximately 50 analog and digital signals from the spacecraft, in addition to accepting and keeping a cumulative count of an unspecified number of uncorrelated event pulses. It then conditioned and encoded these signals to a common 7-bit digital format, added unique codes into the data for identification purposes, and performed time-sequential biphase modulation of a sine-wave subcarrier with the 7-bit data words. The pseudo-noise generator generated a unique pattern of pulses during each work period in addition to word and bit sync, and these were also placed on a separate subcarrier. Proper combination of the two binary signals on the ground enabled reconstruction of the data words. Figures 6–45 and 6–46,

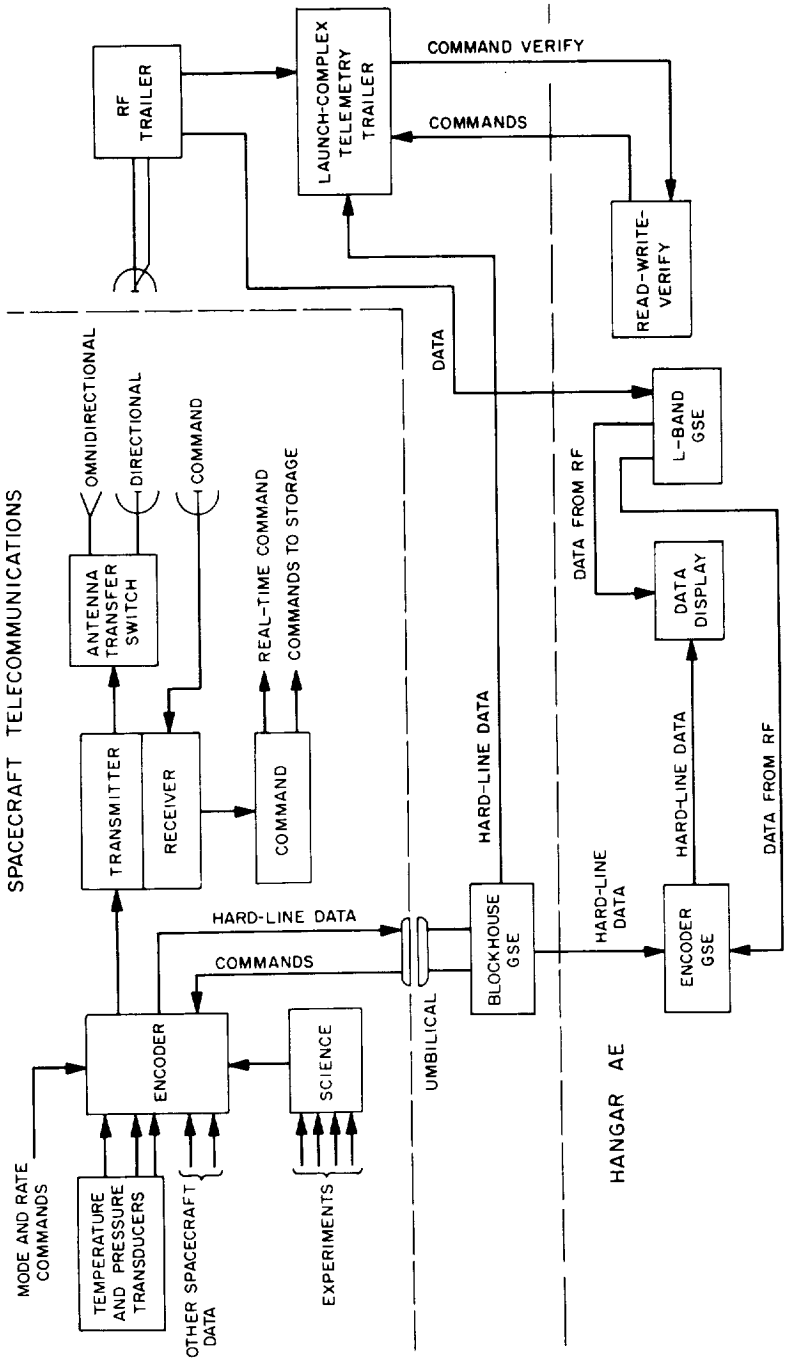

FIGURE 6–44.—Block diagram of telecommunications system, launch communication.

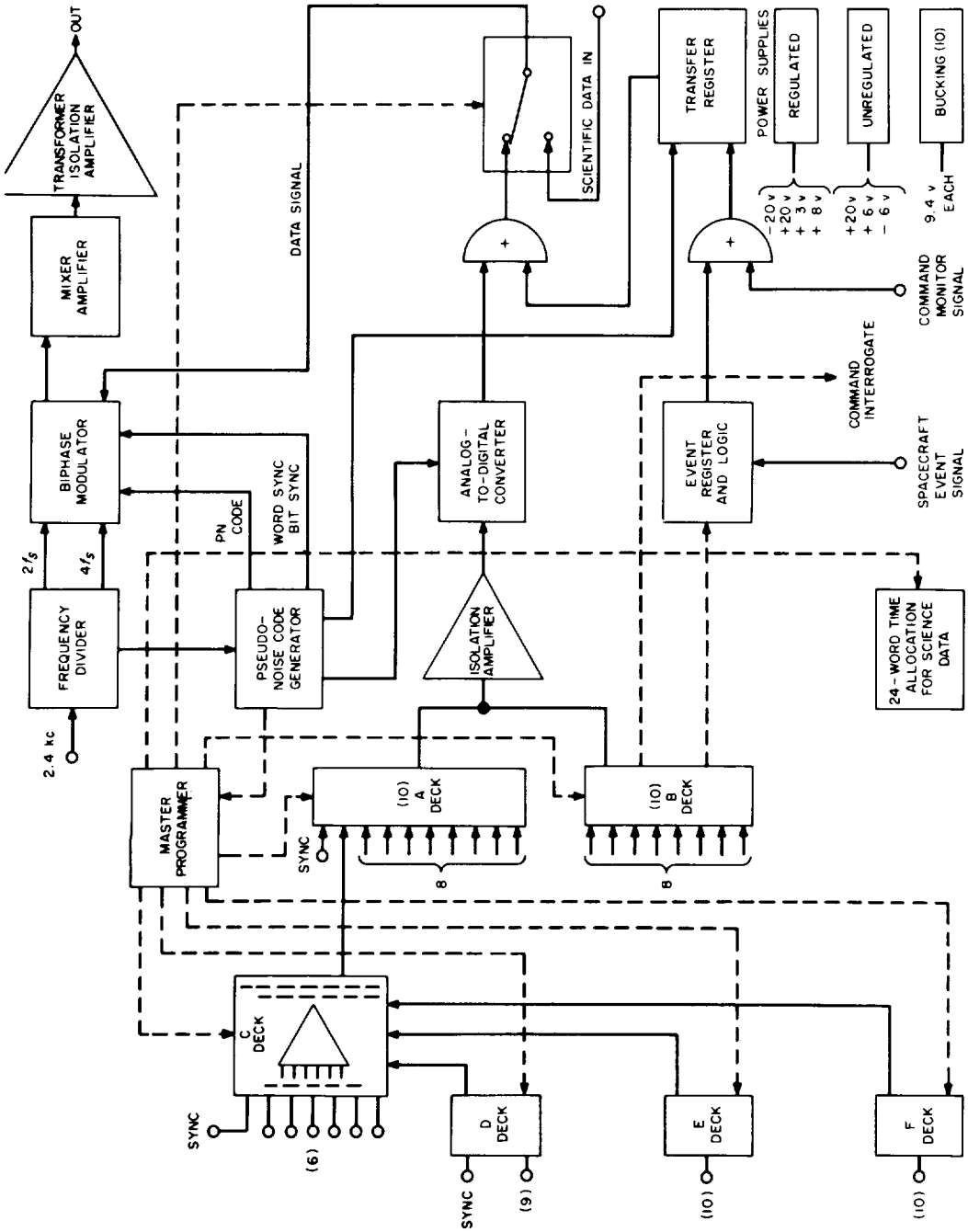

FIGURE 6–45.—Block diagram of data encoder.

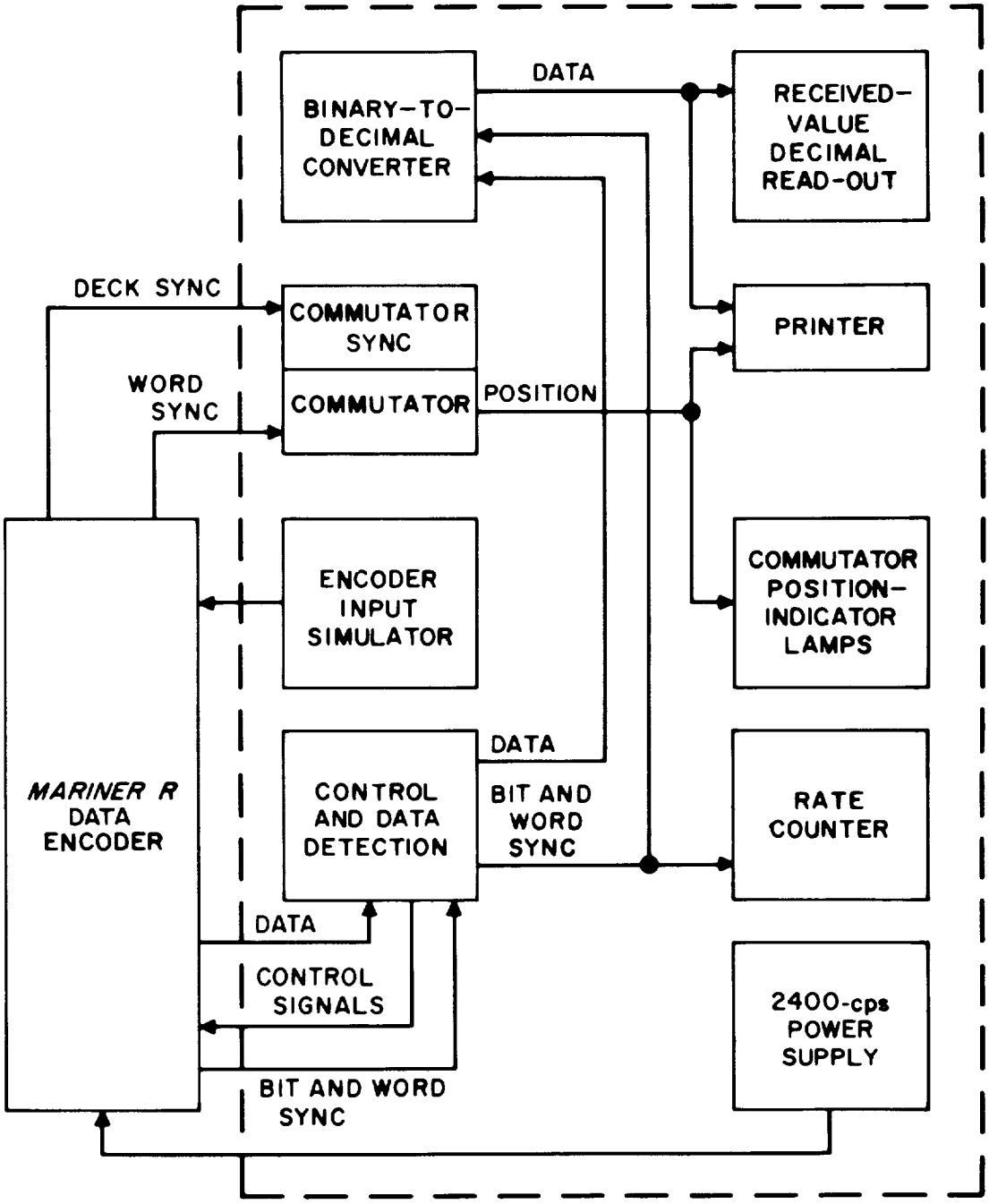

FIGURE 6–46.—Block diagram of data encoder ground support equipment.

respectively, present block diagrams of the data encoder and its ground support equipment.

The flight operation of the data encoder was for the most part normal. Anomalous events did not prevent successful completion of the mission.

A total of 18 nonstandard events were registered in the event counters during the flight. Of the 18 events, 14 can be correlated with radiometer calibration sequences. One event occurred at the time of Sun acquisition, with the remaining three events unexplained.

Since the primary source of these anomalies seems to be the injection of noise into the data encoder, it is informative to study the events leading to a malfunction that apparently originated from circuit noise. The data encoder used a differentiator as an input-signal conditioning circuit for the event registers; consequently, noise in the input lines could have triggered the event counter. During the testing of the spacecraft, it was found that the event registers were sensitive to most transients and would react in a manner similar to that encountered in flight. Rearrangement and elimination of the noisiest inputs, together with added filtering, improved the operation of the counters; however, this did not eliminate the occurrence of false counts. System-test records show that these nonstandard events were occurring prior to launch.

Noise, probably on the 2.4-kc power circuit to the data encoder, caused the "skipping" of the commutator decks. When this phenomenon occurred it could, like most of the nonstandard events, be traced to a radiometer calibration cycle. In figure 6–45, decks A, B, and C are shift registers which are clocked at the word rate and 1/20 of the word rate. The master programmer controls the insertion of a 1 into the shift registers in such a manner that no two input switches of the commutator can be closed simultaneously.

When a deck was skipped (the commutation cycle remaining unchanged, but with no output for any input) the 1 from the master counter was not inserted into the shift register of that deck, or was inserted and reset by noise. The exact process causing this abnormality was under investigation at the time of this report. However, it is generally believed that transients in the 2.4-kc power lines affected the data encoder's +6-volt dc unregulated supply, which is the collector supply for the flip-flops. The induced transient in the +6-volt power supply leads to an uncertainty concerning the operation of the master programmer, as well as the shift registers. This abnormality was also present during testing prior to launch. In addition, there was anomalous behavior in the data encoder that could not be linked to noise.

On December 9, four telemetry channels exhibited an apparent data-encoder failure, causing these channels to read a DN of 1. Channel D4, attitude-control nitrogen pressure, was also lost; however, the sample rate for this measurement was approximately 1 hour, making explanation of this failure more difficult. The indications from telemetry were that a transducer shorted sometime during the second 37-sec cycle period shown, causing a loading of channels B4 and B7. With the transducer completely shorted, the fuse in the spacecraft-excitation 3-v supply in the data encoder failed, resulting in a loss of all pressure and position channels except B3 (antenna reference), which was supplied from a different source (fig. 6–47). This failure could explain the previous erratic behavior of channel B9 on September 26 and 29. Refer to figure 6–45 for the spacecraft mechanization of these channels.

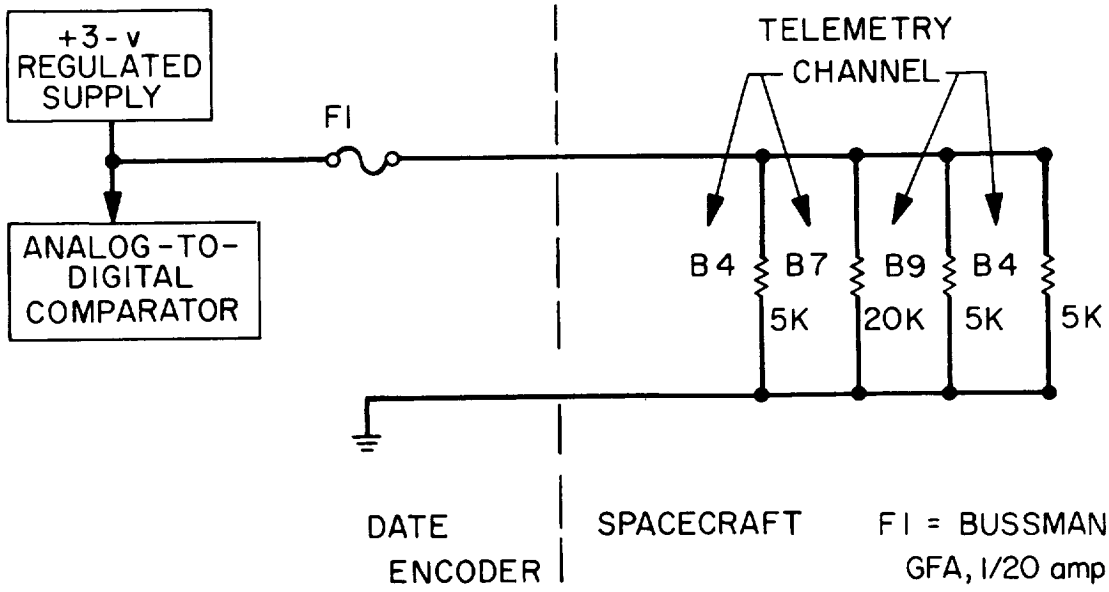

FIGURE 6–47.—Data encoder failure area.

The event register and logic block in figure 6–45 incorporates five counters, four of which are count-of-16, the fifth being a two-stage unit for a count-of-4. The two-stage counter develops the address for the event counters and controls all the sampling gates for these counters.

The CC&S update event that was expected to occur on November 20 filled

register 10/3, for a total count in all registers of 6–1–15–14. Normally, this would not have created a problem; however, after continuous operation at elevated temperatures for 85 days, some degradation was to be expected. The result was excessive loading of the address counter through the sampling gates. This loading would not allow the most significant digit of the address counter to toggle; consequently, the counter operated as a count-of-2, allowing only two registers to be sampled. This condition prevailed for approximately 12 hours, when a nonstandard event occurred, as previously described, resetting register 10/3 for a readout of 6–1–0–14. The new count unloaded the gates, and normal operation was resumed. The changes in data number received on November 23 and December 2 are believed to have been due to a change in the resistance values of components used in the signal-generating circuits for the reference channels. A change anywhere else would have caused a change in all the signals, which did not occur.

Seven temperatures had exceeded the design range, based on original estimates, at the time of Venus encounter, resulting in saturated output from the data encoder. These channels, with the dates on which the saturated output occurred, were as follows:

Lower thermal shield	November 18
Antenna yoke	November 25
Earth sensor	December 2
$-X$ solar panel (front)	December 9
$+X$ solar panel (front)	December 11
Plasma experiment	December 12
Attitude-control nitrogen	December 13

Radio Subsystem

The radio subsystem incorporated a phase-coherent transponder, cavity RF power amplifier, a low-gain transmitting antenna, a high-gain directional antenna, a command-receiving antenna, and associated control and monitoring circuits, arranged as shown in figure 6–48.

The purpose of the spacecraft radio (RF) system was to receive coherently a phase-modulated signal transmitted from an Earth-located transmitter and to transmit back to Earth a phase-modulated signal which was either phase-coherent with the received signal or derived from a crystal-controlled oscillator. The transmitter's phase-coherent mode of operation was automatically selected

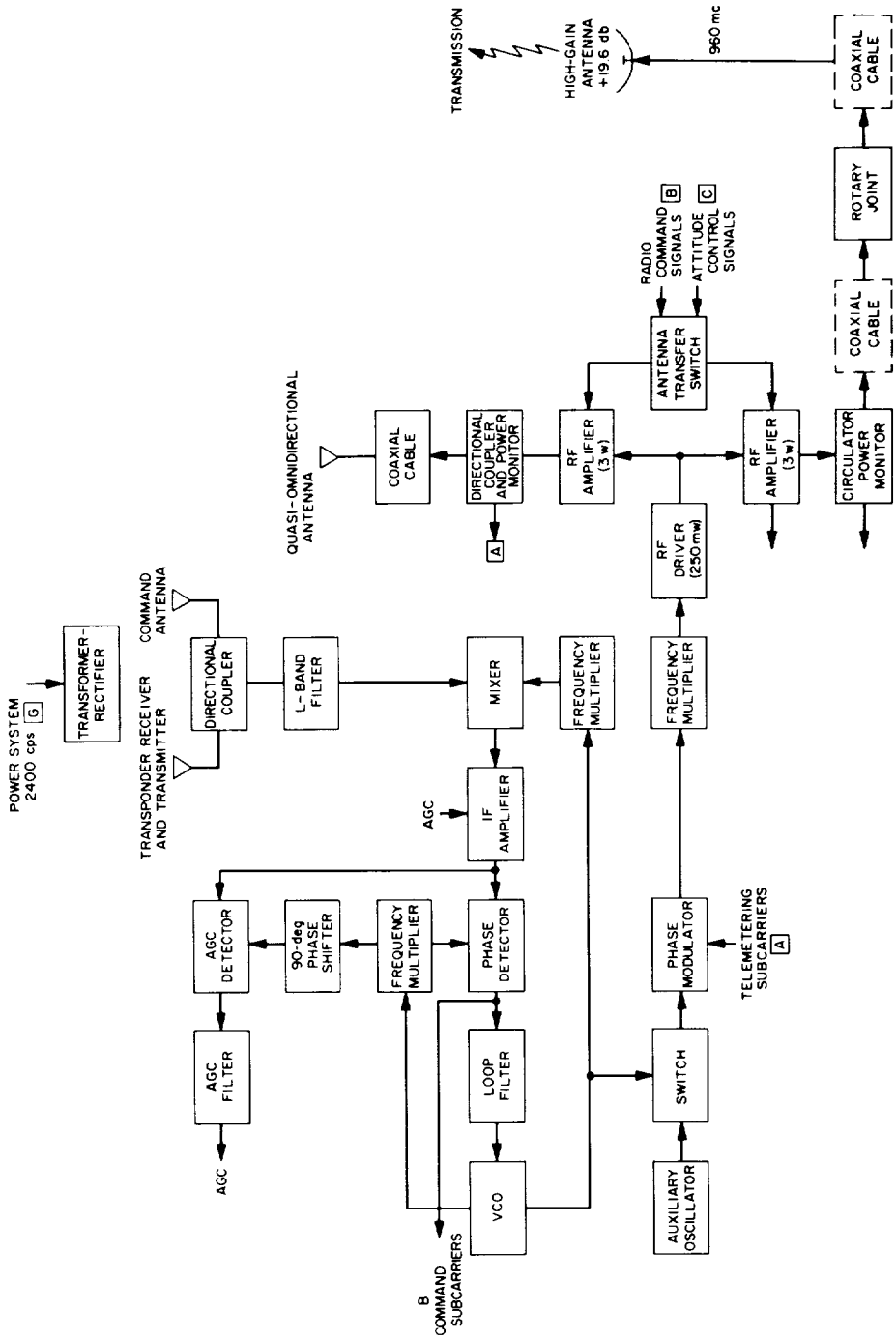

FIGURE 6-48.—Block diagram of radio subsystem.

whenever the transponder receiver acquired lock with the Earth-transmitted 890-mc signal. If the transponder receiver lost lock with the 890-mc signal, the crystal oscillator was turned on automatically, and the transmitted signal was then referenced to the crystal oscillator.

The demodulated signal from the transponder receiver was routed to the spacecraft command decoder system for decoding and subsequent issuance of spacecraft commands. The transponder modulation signal was received from the spacecraft data encoder system. This signal modulated the transponder transmitter carrier and, via this link, the spacecraft scientific and engineering measurements were then transmitted to Earth.

The RF subsystem operated normally throughout the Mariner II flight. The temperature of case II increased from 85° F at launch to 152° F at Venus encounter. Telemetry data indicated that the 960-mc transmitted power decreased approximately 1 db, possibly as a result of the temperature increase; however, this 1-db decrease was within the design tolerance of the system. Telemetry data also indicated that the automatic-gain-control voltage decreased 0.2 v dc. This AGC voltage shift was the amount estimated for the temperature increase. All other functions were normal.

The events of interest, as far as the overall communications system was concerned, are those indicating agreement or disagreement between the theoretical and the actually received signal strength for both the Earth-to-spacecraft and the spacecraft-to-Earth links.

For spacecraft-Earth communication, a comparison between the actual and the theoretical received-signal strength demonstrates good agreement, at least within the cumulative tolerance applied to the theoretical numbers. The only time at which the signal-power predictions really fell outside these bounds occurred during the pitch turn of the midcourse maneuver, when RF lock was lost. Since this maneuver took the spacecraft-Earth vector into one of the nulls of the low-gain transmitting antenna, this event demonstrates the relative indeterminacy with which the antenna characteristics were known in the null regions. During Earth reacquisition, RF lock was again lost; however, it is believed that this resulted from premature switching by the spacecraft from the low-gain to the high-gain transmitting antenna. This loss presented no problem, because the spacecraft signal was reacquired a few minutes later when the roll search was terminated with the complete reacquisition of Earth.

Command Subsystem

The command subsystem received command information from the transponder in the form of a phase-shift-keyed (PSK) subcarrier and a coded reference frequency, detected the serial binary bits, recovered the bit timing pulses, and decoded the commands. These commands were then presented to the appropriate subsystems by means of isolated solid-state-switch closures. All dc voltages required by the command subsystem were derived from a transformer-rectifier powered from the central spacecraft power unit.

The command subsystem was divided functionally into three units: (1) A command detector, which filtered and demodulated the PSK subcarrier and extracted the bit timing pulses; (2) a command decoder, which decoded the commands and supplied both the commands and appropriate timing pulses to the command users; and (3) a transformer-rectifier. The command detector also housed the command telemetry circuit, which conditioned the detector parameters to be telemetered to Earth. Block diagrams of the command detector and decoder are presented in figures 6–49 and 6–50, respectively, and a list of available commands is given in table 6–IV.

Table 6–IV.—Available Mariner R ground commands

Designation (a)	Command
RTC–1	Roll override
RTC–2	Clockwise hinge override
RTC–3	Counterclockwise hinge override
RTC–4	L-band to low-gain antenna
RTC–5	L-band to directional antenna
RTC–6	Initiation of midcourse maneuver
RTC–7	Encounter mode
RTC–8	Cruise mode
RTC–9	Sun acquisition; unlatch solar panel and radiometer; unlatch/reset Earth-acquisition relay
RTC–10	Cruise science off
RTC–11	Unused spare
RTC–12	Earth acquisition
SC–1	Midcourse maneuver roll turn, duration, and polarity
SC–2	Midcourse maneuver pitch turn, duration, and polarity
SC–3	Midcourse maneuver velocity increment

(a) RTC denotes *real-time command;* SC denotes *stored command.*

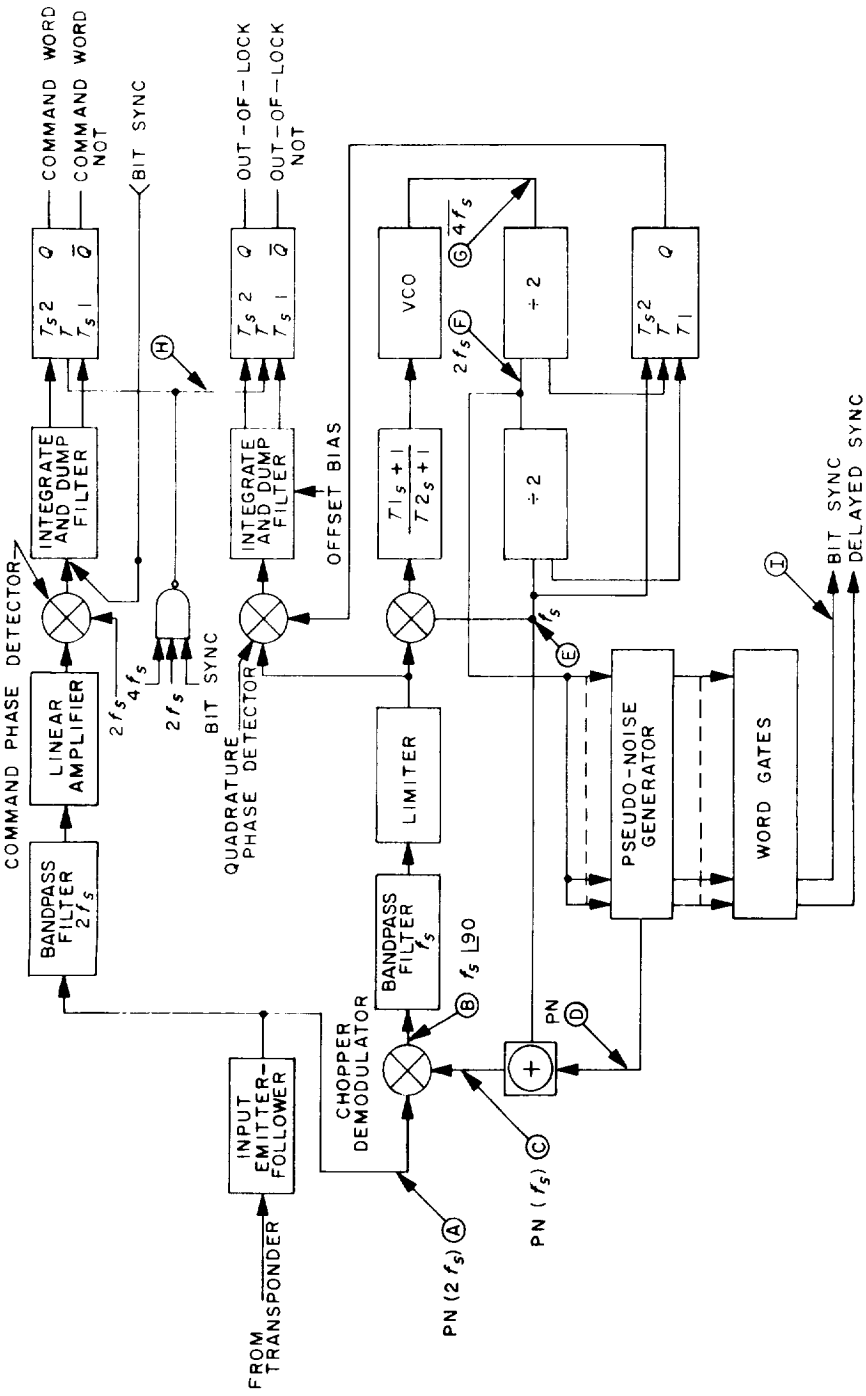

FIGURE 6–49.—Functional block diagram of command detector.

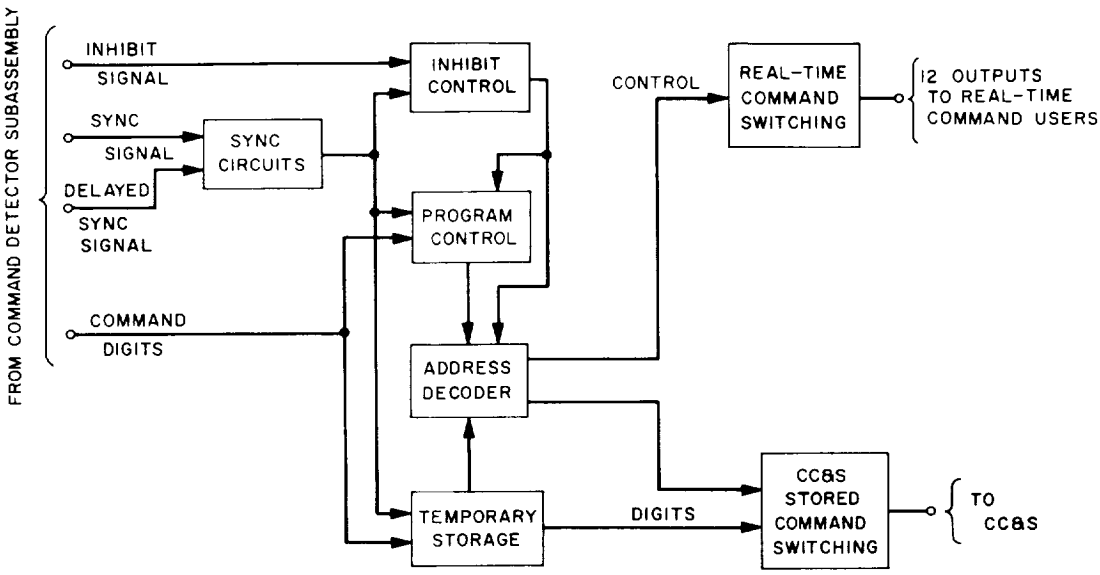

FIGURE 6–50.—Simplified block diagram of command decoder subassembly.

Basic to an understanding of the command subsystem operation was the fact that any command transmitted to the spacecraft was inhibited unless the command detector was in lock. However, command detector lock could be attained only if command modulation was applied to the radio signal which was transmitted to the spacecraft. To minimize the probability of a false command, command modulation was applied only if command transmission was anticipated, or if a checkout of the command detector was desired. Since commands were infrequently required during the Mariner II flight, the command subsystem was in an energized standby state for the greater portion of the flight.

The performance of the command link involved several items of equipment in addition to the command subsystem proper. The most important items are illustrated in the command flow diagram shown in figure 6–51. The overall command subsystem completed the entire flight with no indication of a hardware malfunction. Although its temperature exceeded the type-approval test temperature limit before encounter, no degradation in subsystem performance was observed.

The analysis of the command subsystem reveals that there were no discernible failures and that the performance adhered closely to the nominal case.

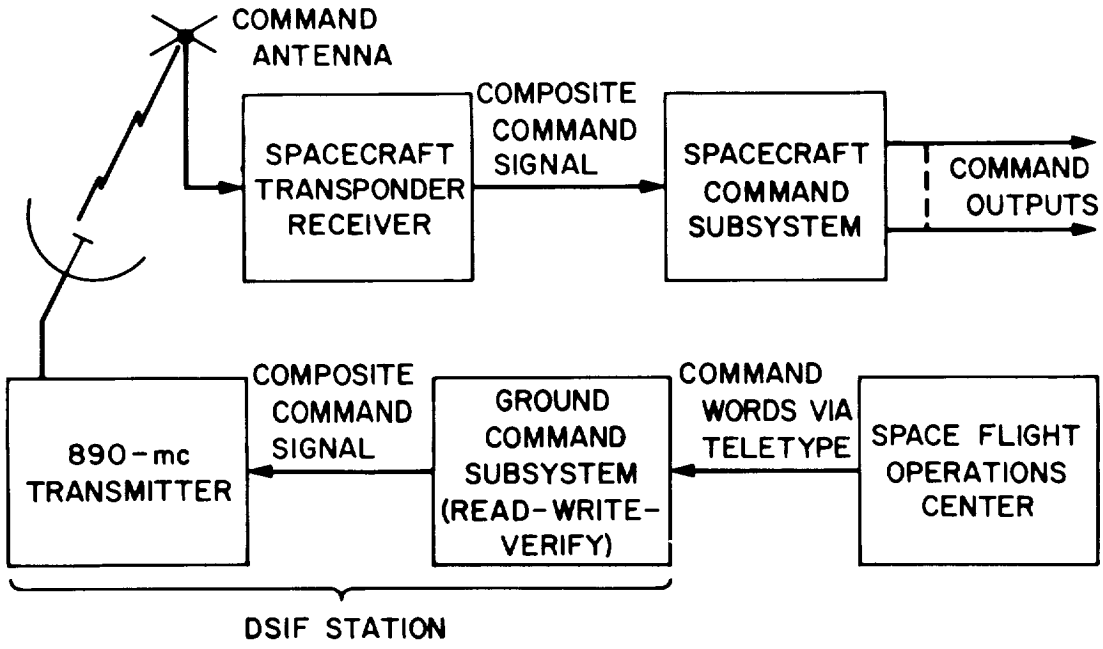

FIGURE 6–51.—Mariner R command flow diagram.

SCIENTIFIC EXPERIMENTS

Mariner II carried six scientific experiments representing the efforts of scientists at nine institutions.

One of the important considerations in choosing these experiments was the compromise between what scientists would have liked to measure during the 1962 mission and what was technologically possible. For example, of the original 460-pound total weight which could be placed in a Venus trajectory, only about 40 pounds could be allocated to scientific experiments.

Data Conditioning System

The data conditioning system (DCS) was a solid-state electronic system designed to gather information from the scientific instruments on board the Mariner II spacecraft and prepare the information for presentation to telemetry for transmission. The four basic functions performed by the DCS for the scientific instrumentation were: Analog-to-digital (A-to-D) conversion, digital-to-digital

(D-to-D) conversion, sampling and instrument-calibration timing, and planetary acquisition.

The transformed data were loaded into an eight-stage shift register, which was the center of the DCS data-handling section. This register acted as (1) a counter for the A-to-D conversions, (2) a PN generator for subframing and framing the data, (3) buffer storage for the digital-to-digital conversion, and (4) the comparator for the planet-acquisition function. Data formats and timing provided within the data conditioning system appear in figure 6–52. The analog voltages sampled were from the three magnetometer sensors, the solar plasma experiment, the infrared and microwave radiometers, and three temperature sensors.

The digital information sampled by the DCS was received (1) by transfer of data from the magnetometer scale-indication circuitry, the cosmic dust experiment, and the solar plasma power-on indicator, in parallel with the shift register; (2) by time-interval measurement between pulses from the ionization chamber; and (3) by counting of pulse data from the particle detectors plus the ionization chamber, during three different time intervals.

Sampling intervals, reset commands, and calibration of the scientific instruments were generated by a binary clock and associated matrix logic. A bit-synchronization pulse from the spacecraft data encoder was used for the binary-clock signal.

Detection of the planet by the microwave radiometer was performed by comparing the digital reading of the analog signal from the instrument with the digital equivalent of two voltages. If the analog voltages went above 1.5 v the scan speed was switched to a lower rate. When the voltage went above 2.25 v and then dropped below 1.5 v for more than 20 sec, the scan direction was reversed. If the analog voltage remained below 1.5 v for more than 160 sec, the scan was switched back to high speed.

The data conditioning system employed approximately 325 transistors, had a total of 3200 components, and required 2.5 w of raw power.

The DCS appeared to operate satisfactorily throughout the mission and accomplished its mission objectives; however, two types of anomalies were noted in the data. The first anomaly observed was the apparent "cross talk" between analog channels, particularly those from the radiometer subsystem. Basically, the problem appeared to be related to a grounding effect of some kind. The second anomaly was the occasional skip in the clock monitor, a phenomenon which appeared to be connected with the postulated grounding problem.

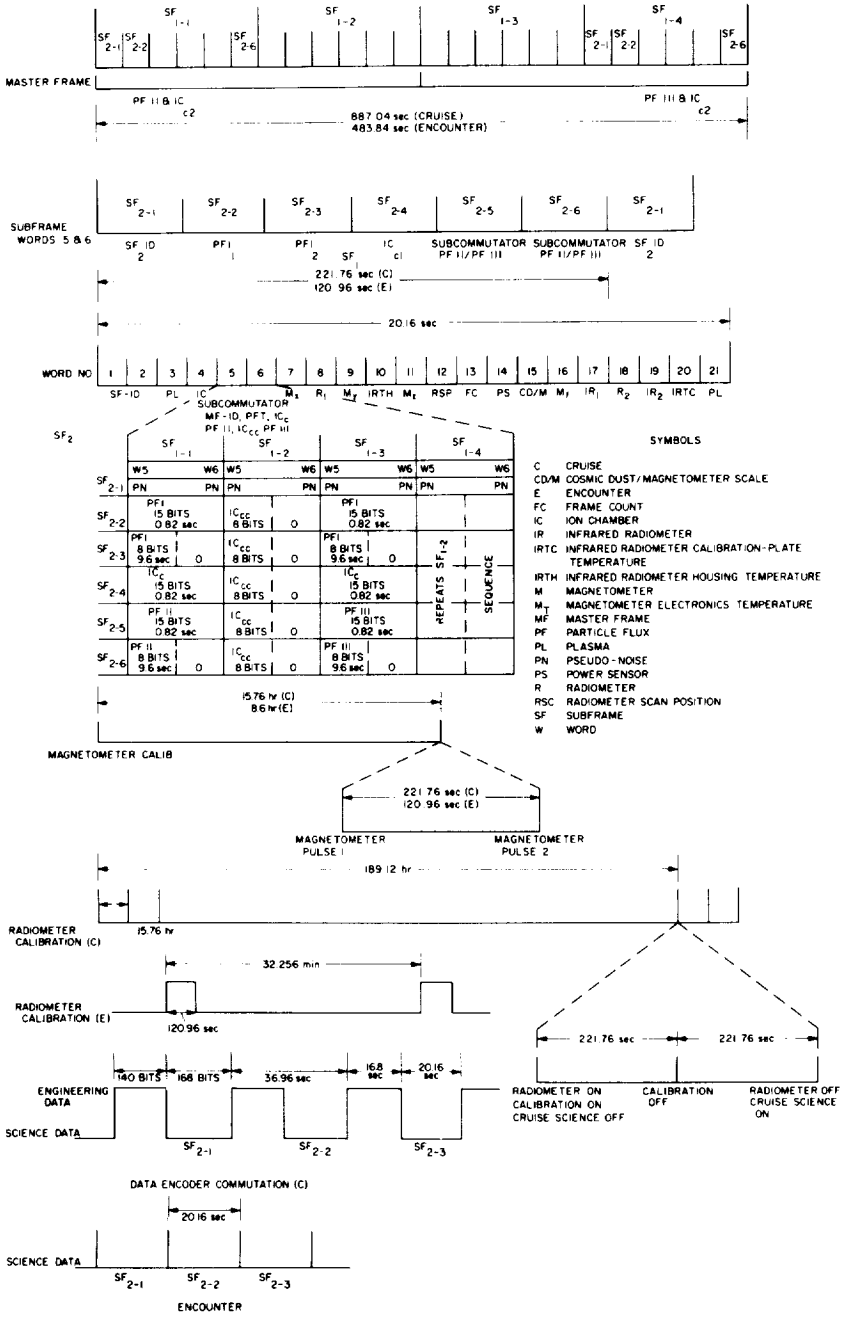

FIGURE 6–52.—Data conditioning system format and timing.

Power Switching to Science Experiments

The scientific power switching (SPS) unit was designed to perform the following functions:

1. Control of the application of ac spacecraft power to appropriate portions of the science subsystem in accordance with signals received from the attitude-control system, the CC&S, and the command decoder.
2. Application of power to the microwave and infrared radiometers and removal of power from the cruise instruments during the radiometer calibration periods commanded by the DCS.
3. Control of the speed and direction of radiometer scans according to signals received from the DCS during the encounter mode of operation.

Since this unit was a series element in obtaining scientific data, it was considered necessary to utilize some device inherently more reliable than the standard crystal-can relay for the task of switching the 50-v, 2400-cps square-wave power. Accordingly, the unique magnetic-ball relay was selected for this purpose. The properly mounted ball relay is capable of performing 4 times as many operations as most crystal-can relays; it also withstands more severe shock and vibration environments and utilizes a double hermetic seal to isolate the electrical contacts from the case and minimize the possibility of contact-to-case arcing. Therefore, although redundancy was effected by providing for either CC&S or command decoder actuation of the planetary instruments through the SPS unit, complete switching redundancy was not incorporated because of this utilization of the rugged ball relay.

During the Mariner II mission, cruise science power was switched 3 times by the command decoder, 6 times by attitude control (when the gyros were operated), and 25 times when the DCS commanded a cruise calibration of the radiometers. Power to the latter instruments was also switched 25 times by the DCS and, through separate relays, twice by the command decoder, at the beginning and end of the encounter mode. In addition, the scan-reversal relay operated 21 times during encounter. The data received from Mariner II indicated that the SPS unit performed as designed throughout the entire mission.

Microwave Radiometer

The microwave radiometer was designed to detect and measure the absolute temperature of Venus through its microwave-radiation characteristics. Measurements were performed simultaneously in two bands, centered at wavelengths of

19 mm (15.8 Gc) and 13.5 mm (22.2 Gc). The instrument was designed for an input dynamic range of approximately 1000° K, corresponding to a dc output range of 5.0 v. The output varied from 1.0 to 6.0 v, linearly with input temperature. The analog output voltage of each channel was converted to digital form in the data conditioning system.

The instrument consisted of a parabolic dish antenna 48.9 cm (19.25 inches) in diameter with a 19.3-cm focal length (fig. 6–53). The dish also constituted the frame on which all the waveguide runs and electronic packages were mounted. These components were mounted on the back (convex) surface and were covered by a sheet-metal thermal shield. A reference-horn assembly and a diplexer-feed assembly were mounted on the top and front of the dish, respectively. All metal components were aluminum, including the integral dish frame. The frame was entirely machined from a solid billet; the other components were machined (electronic chassis), extruded (waveguides), or dip-brazed (reference horns, waveguides). All the outside surfaces of the components covered by the thermal shield were painted flat black, and the outside surfaces of the instrument were of polished metal for temperature control purposes. In addition, some outside surfaces were painted to provide the proper reflection/absorption characteristics, for the same purpose. Small steps were machined into the concave surface of the dish to prevent dangerous concentration of infrared energy at the feed when the instrument looked at the Sun; however, the steps were so designed that they did not impair the focusing properties of the parabola at the much-longer wavelengths. The radiometer was mounted on the spacecraft at two points, one a bearing allowing rotation perpendicular to the instrument axis, and the other through the scan actuator, a mechanism consisting of motors and gears. The actuator drove the instrument through a $\pm 60°$ maximum scan angle.

A block diagram of the radiometer appears in figure 6–54. The microwave energy collected by the antenna was separated into the two frequency bands by the diplexer and propagated down the waveguides of the feed toward the video detectors. A ferrite switch alternately switched the detector between the antenna energy and the energy from a comparison horn which was always looking at empty space (near 0° K). The detected signal, at the modulation frequency of the switch (near 1 kc), was amplified by a two-stage, low-noise amplifier and rectified in a phase-sensitive detector. The signal was then integrated and further amplified before being delivered to the DCS. A tuning-fork oscillator provided the reference frequency for each channel. Since the microwave energy radiated by a hot body

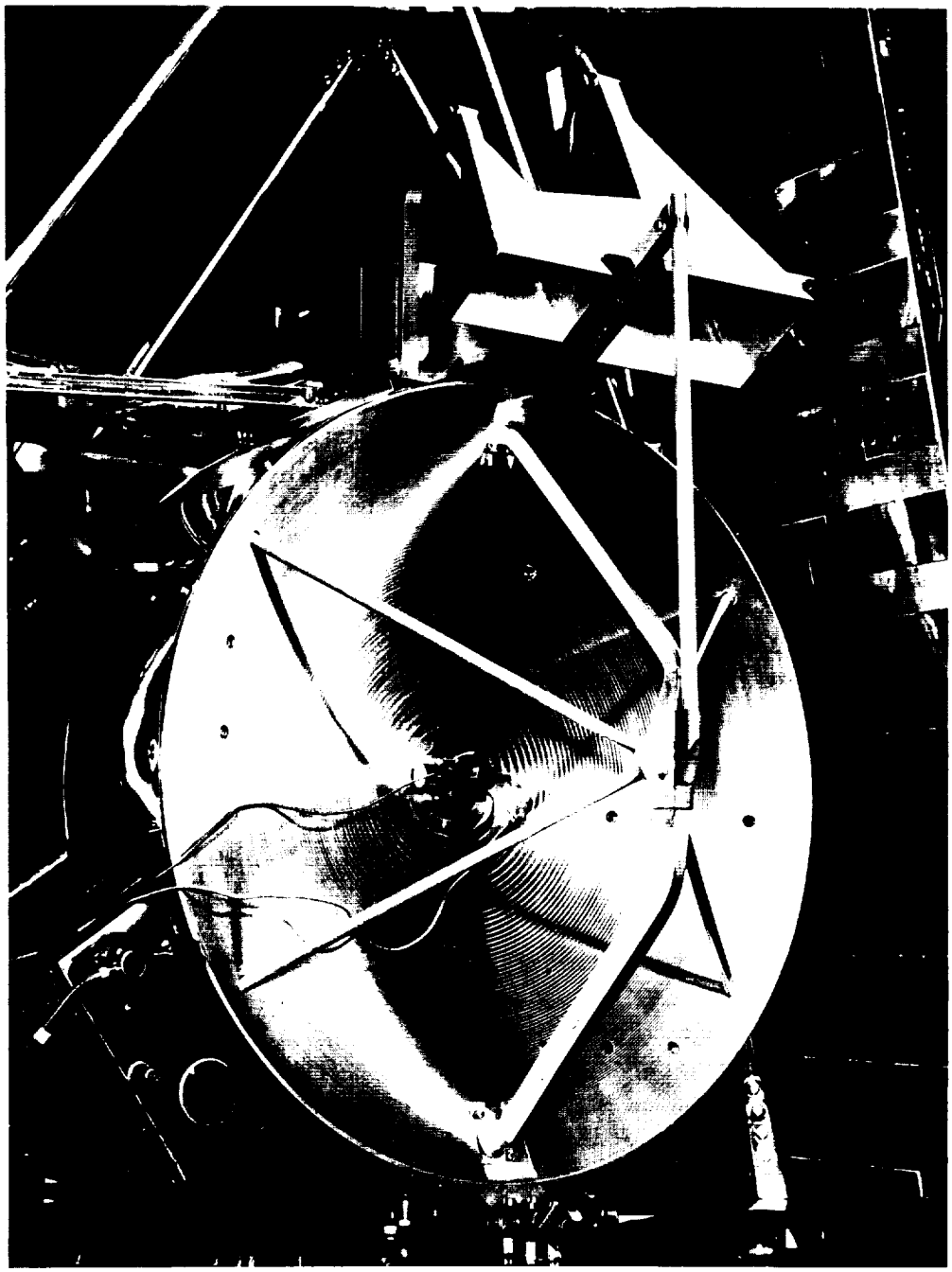

FIGURE 6–53.—Microwave radiometer, showing dish-antenna structure.

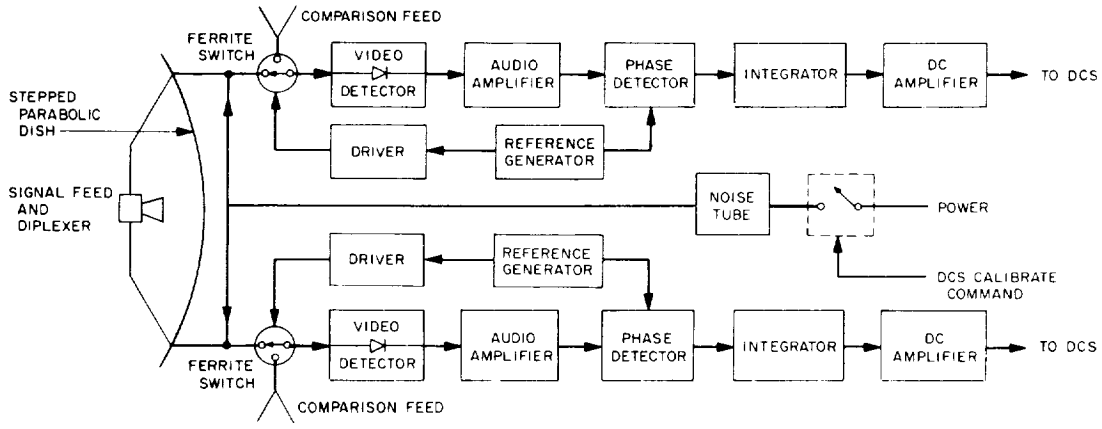

FIGURE 6–54.—Block diagram of microwave radiometer.

is proportional to its temperature and the reference was very near 0° K, the output of the radiometer was directly proportional to the absolute temperature of the body at which the instrument was pointed. The radiometer had a built-in calibration system, consisting of a dual-output gas-discharge noise tube and two 10-db directional couplers, one in each channel. A fixed calibrated amount of signal could thus be injected into the instrument whenever desired.

The scan-mechanism speed and direction of rotation were determined by the radiometer output-voltage levels. When one or both channels exceeded 1.5 v, the scan speed went from 1 to 0.1 deg/sec. The purpose of this feature was to allow maximum time on the planet and reduce the search time to a minimum. One or both radiometer outputs had to exceed 2.25 v in order to arm a scan-direction-reversal command. This command was to be generated when the planet signal was lost, or when both outputs went below 1.5 v. Thus, normally, the radiometer was to scan at low speed back and forth across the planet disk.

In prelaunch operations the mechanical accuracy of the radiometer frame and components was found to be excellent, and no difficulty was encountered in the assembly and feed-boresighting operations. The maximum warpage of the paraboloids was 0.051 cm (0.020 inch), the maximum allowable. No problem was encountered under flight-approval vibration testing, except in the area where the 22.2-Gc waveguide joined the diplexer feed, where fatigue cracks developed after repeated test runs. All units were rebrazed or reinforced with Devcon F in this area.

The radiometers were repeatedly tested over the temperature range of 0° to 55° C. Some output variations were present in all units, especially from ambient temperature "going hot," in which case the output of the instrument increased with temperature by as much as 15% at the 55° C limit. These variations were mainly due to the fact that the detector-crystal impedance changed as a function of temperature, as did the gain and phase shift of the audio amplifiers. These variations were not thought to be serious because of the self-calibrating feature of the instrument.

More serious, however, was the effect of certain factors on the absolute value of the zero-signal offset of the outputs (baselines). These factors were the mechanical layout, the grounding points of the amplifiers, and the physical locations of some cables and of the thermal shield. It was found that these effects were picked up in the highly sensitive crystal detectors and preamplifiers. Interference was picked up from the switch-drive amplifiers and ferrite switches, from the 2400-cps spacecraft power supply, and from various other sources. These pickup and interference effects, which varied in magnitude with the location and orientation of the various components with respect to each other, normally amounted to several tenths of a volt. In several instances, the stray signal amounted to more than 1 v, as measured at the output. To reduce these effects, it was necessary to isolate the preamplifiers and crystal detectors from the chassis ground and to change the layout significantly. More extensive shielding was not possible, since it would have involved complete redesign of several components.

During the flight of the spacecraft, the radiometer was periodically commanded on for a 2-min baseline and a 2-min calibration sequence. Figure 6–55 shows the baseline and calibration output values as functions of time; the channel 1 (19-mm) data appear on the upper half of the graph, and the channel 2 (13.5-mm) data on the lower half. During launch, the baseline of channel 1 shifted down by approximately 2 v, and the baseline of channel 2 shifted up by 1.5 v. The prelaunch values were +1.0 v. The only way in which shifts of this magnitude could be duplicated in the laboratory was by removing the screws securing the thermal shield to the rim of the radiometer and permanently distorting the shield. Thus, it is thought that the observed baseline shifts were possibly due to launch vibrations considerably exceeding the flight-approval levels and resulting in the thermal shield being torn from the screws securing its edge to the radiometer.

The gradual changes of the baseline and calibration amplitude (i.e., sensitivity) of channel 1 stemmed mainly from the basic design of the audio-amplifier

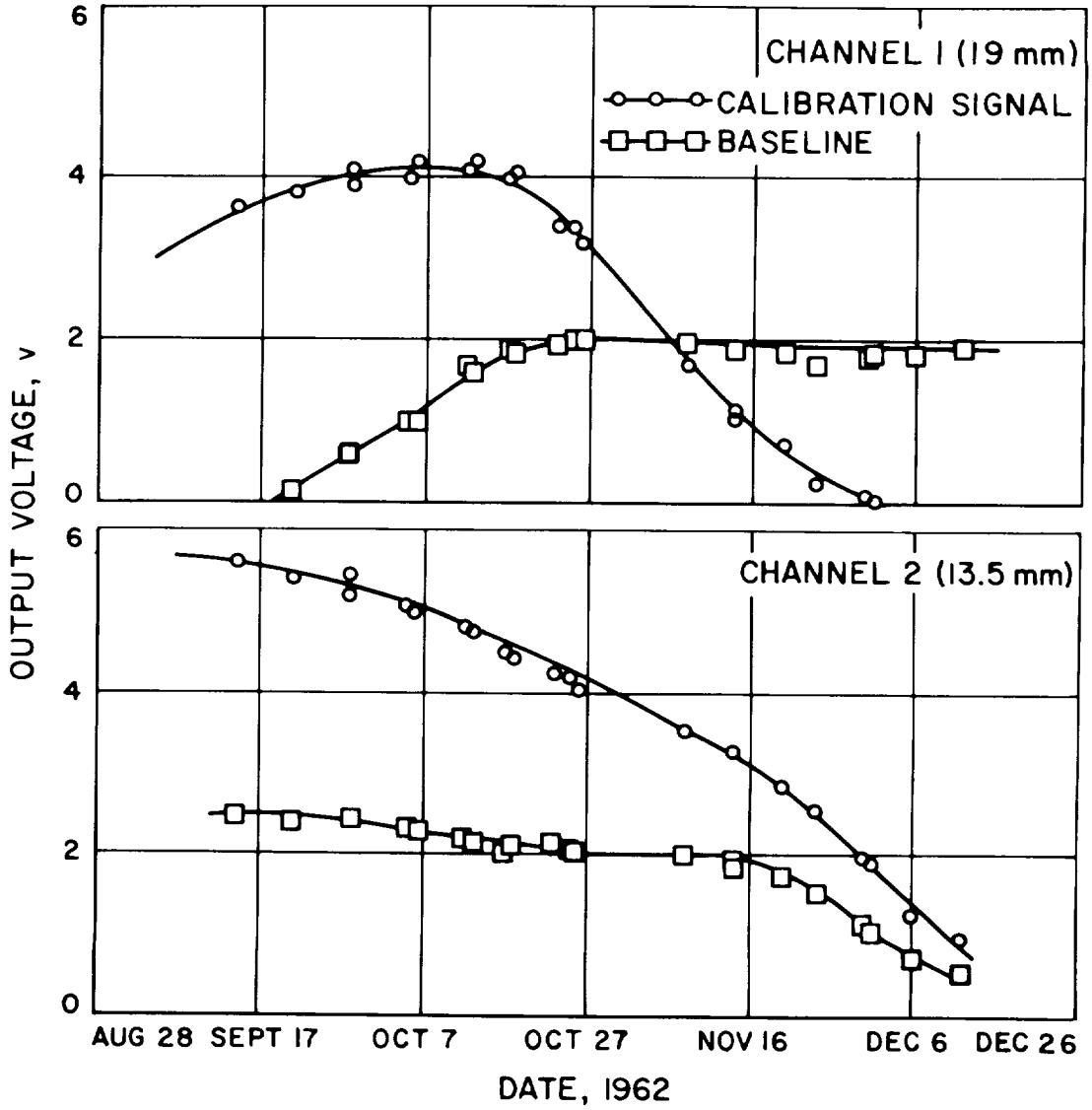

FIGURE 6–55.—Microwave radiometer calibration history.

chain. This chain consisted of two amplifiers in cascade, each with a narrow 20-cps passband centered at the ferrite-switch frequency. Furthermore, the phase-shift characteristics of these amplifiers were quite sensitive to passband-signal frequency variations. These factors rendered the design dependent, to a

certain extent, on component stability in the reference oscillator, passband, and gain-determining elements. Although the components used were of high quality, and no phase-passband shifts of sufficient magnitude to cause substantial output variations were observed in the laboratory, it appears that one, or possibly several, components slowly degraded under the extended vacuum and heat conditions of the flight. Enough phase shift was observed in channel 1 to cause actual phase reversal, resulting in a negative, rather than a positive, output for a given input signal. Channel 2 also experienced some phase shift, but its gradually decreasing sensitivity was basically due to a deteriorating video crystal, as evidenced by the proportionally decreasing signal-to-noise ratio of the calibration signal.

The temperature control of the radiometer was designed to provide a temperature at encounter of 35° ±10° C. Figure 6–56 shows actual performance: the nominal temperature of 35° C was exceeded on November 13; at encounter, on December 14, the temperature was estimated to be 58° C. This came dangerously close to the maximum permissible operating temperature (65° C) of the video-detector crystals. The microwave radiometer temperatures were based on the temperature values of the infrared radiometer housing, since no sensor was carried on the microwave instrument itself; the infrared-microwave temperature relation was based on ground calibrations.

During the cruise calibration periods, starting about October 12 and varying in magnitude, differences were noted in the microwave radiometer scan-position readout, as well as in the outputs of the infrared radiometer, plasma experiments, and magnetometer, and in the infrared radiometer temperature readouts with the calibration noise source on and off (see fig. 6–54). Differences in readout as high as 11 digital steps were noted on outputs known to be steady. They did not appear to be internal to the radiometers but, rather, related to interactions between the various instruments, possible through spurious grounding loops.

The most important net effect of the radiometer's internal functioning was that the channel 1 baseline was positioned above the 1.5-v slow-scan trigger level during encounter. This produced a slow-scan condition during initial planet search and no scan reversal upon loss of planet signal, resulting in a less efficient planetary scan pattern and corresponding loss of data. However, the data obtained by the radiometer on its three scans across the planet were of high quality. The baselines obtained before and after the planetary scans were quite stable and free of noise, and the signal-to-noise ratios, especially in channel 1, were high during the recording of the planetary data.

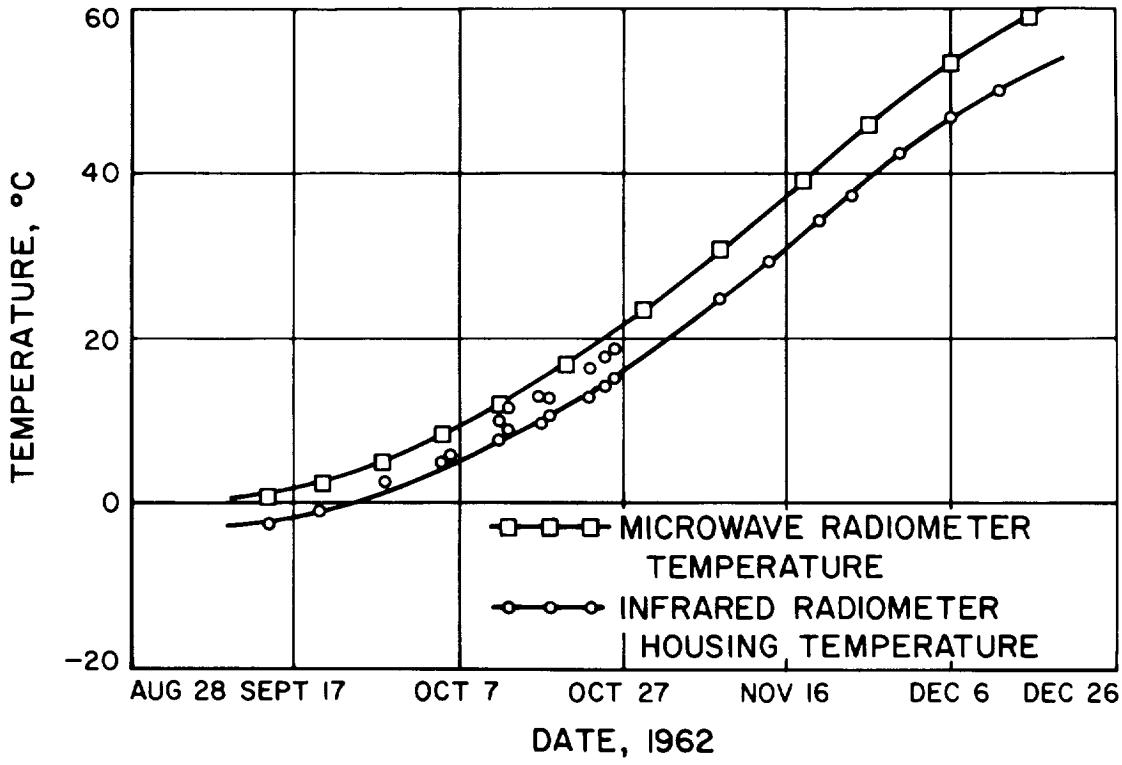

FIGURE 6-56.—Microwave radiometer temperature history.

Infrared Radiometer

The two-channel infrared (IR) radiometer for Mariner II was designed to measure the effective temperatures of small areas of Venus, thus complementing the radiation-temperature measurements made by the microwave radiometer. The radiation to be received by the IR radiometer might originate on the planetary surface, clouds in the atmosphere, the atmosphere itself, or a combination of these. This radiation was recieved in two spectral ranges: 8μ to 9μ and 10μ to 10.8μ.

As illustrated in figure 6-57, two mounting flanges permitted "hard" mounting to the microwave radiometer frame. The alinement was such that the lens having its axis normal to the front face of the instrument was boresighted with the microwave radiometer beams. The other lens was used as a chopping reference and viewed dark space at an angle of 45° with respect to the first lens.

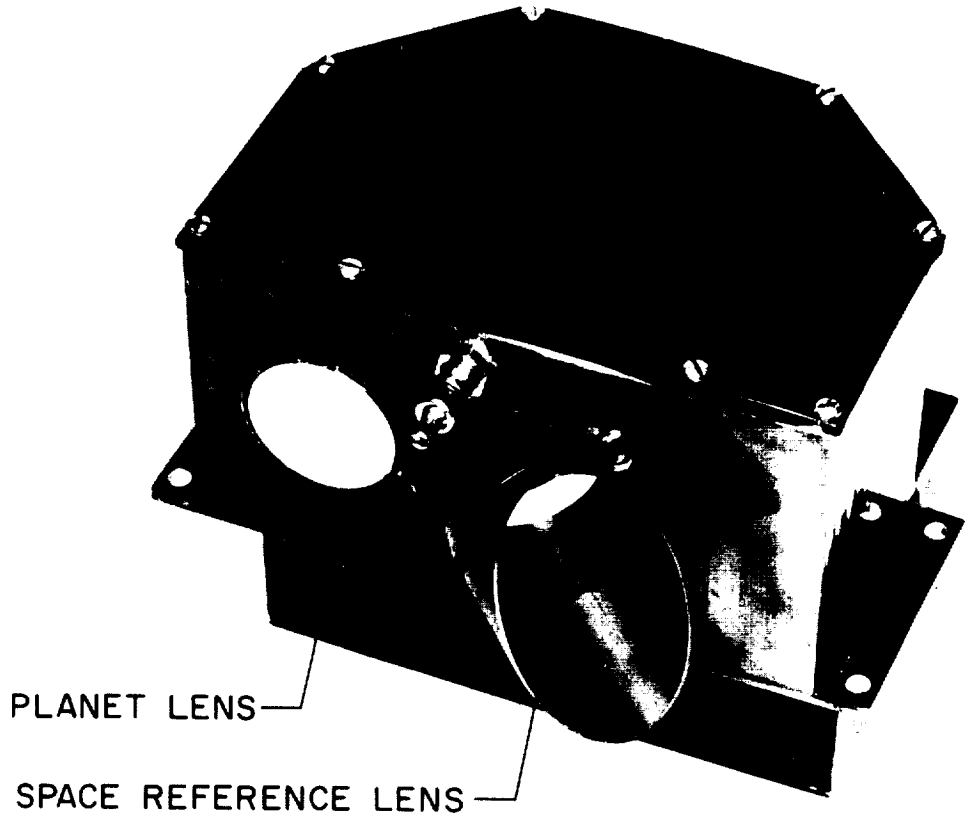

FIGURE 6–57.—Infrared radiometer in case.

The chopper disk is driven on its edge by a 400-cps synchronous motor and rotates at 600 rpm. It has alternate quadrants gold plated and cut out so that the radiation transmitted through the system comes alternately from one lens and then the other. The dichroic filter serves as a beam splitter; that is, about 90% of the radiation having wavelengths longer than 9.5μ is transmitted, while 90% of the radiation of wavelengths shorter than 9.5μ is reflected.

Since the expected dynamic range of planet radiant energy is greater than that of the data system, it was necessary to provide compression of the data output. Accordingly, a logarithmic amplifier is employed so that one digitizing level of 23 mv corresponds to a temperature increment of about 1.0° C in the 200° to 250° K range, while at 600° K the smallest resolvable temperature is 7° C.

A synchronous demodulator and low-pass filter were used as a relatively simple way to get narrow noise bandwidth (0.1 cps) and still have the output voltage insensitive to fluctuations in chopper speed.

One of the firm requirements of the system was an in-flight calibration check. This was accomplished by mounting a small plate on the superstructure of the spacecraft in such a way that the space reference lens views the plate when the radiometer scan is near one end of its travel in the fast scan mode. The planet lens views space during this check.

Since the instrument is sensitive to the phase of the input radiation (one lens system compared with the other), the output voltage would be negative during calibration were it not for the output selector and calibration demodulator circuit. These circuits maintain a positive output voltage regardless of the sense of the input radiation. Emitter-followers are used at the output to obtain low output impedance.

A block diagram of the infrared radiometer functions is presented in figure 6–58.

Figure 6–59 presents a flight temperature history of the IR radiometer housing and calibration plate, together with the 8μ and 10μ channels, IR1 and IR2. Two points are plotted for each data day: the upper points taken when the microwave radiometer noise source was on, and the lower points when the source was off. The lower points show less variation with time and are considered the more valid data. The cause of the fluctuation is unknown.

Except for the effects of cross-talk, which first appeared on October 27, both the plate and the housing temperatures followed the curves predicted on the basis of distance from the Sun. It had been thought that there would be an increase in instrument temperature of about 8° F when the chopper motor was turned on, resulting from the 1.5-w motor dissipation. The predicted rise did not occur, however, and the housing temperature was within the range of calibration throughout the encounter sequence (between 50° and 55° C). Although no particular meaning can be attached to the IR1 and IR2 data during cruise, since the chopper was off, large changes would have indicated anomalous behavior and, perhaps, catastrophic failure. A large drop in IR1 and IR2 data did occur on October 27. This drop was unexpected but can be explained in the following manner: During normal operation, with the chopper energized, a photodiode pickoff drove a Schmitt trigger circuit which, in turn, switched the synchronous demodulator on and off in synchronism with the chopping rate. Following the demodulator was an intregrating circuit and an output driver.

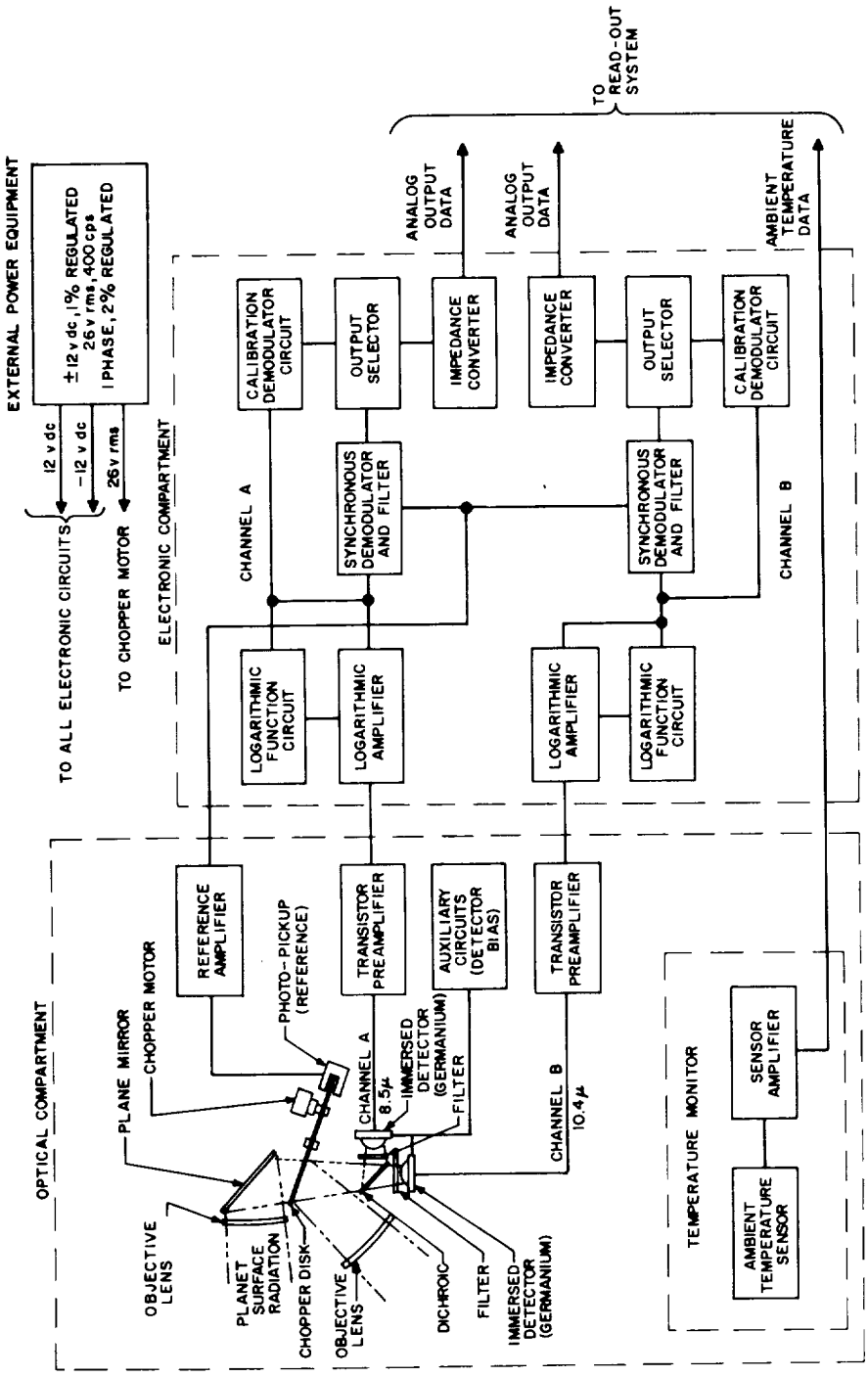

FIGURE 6–58.—Block diagram of two-channel infrared radiometer.

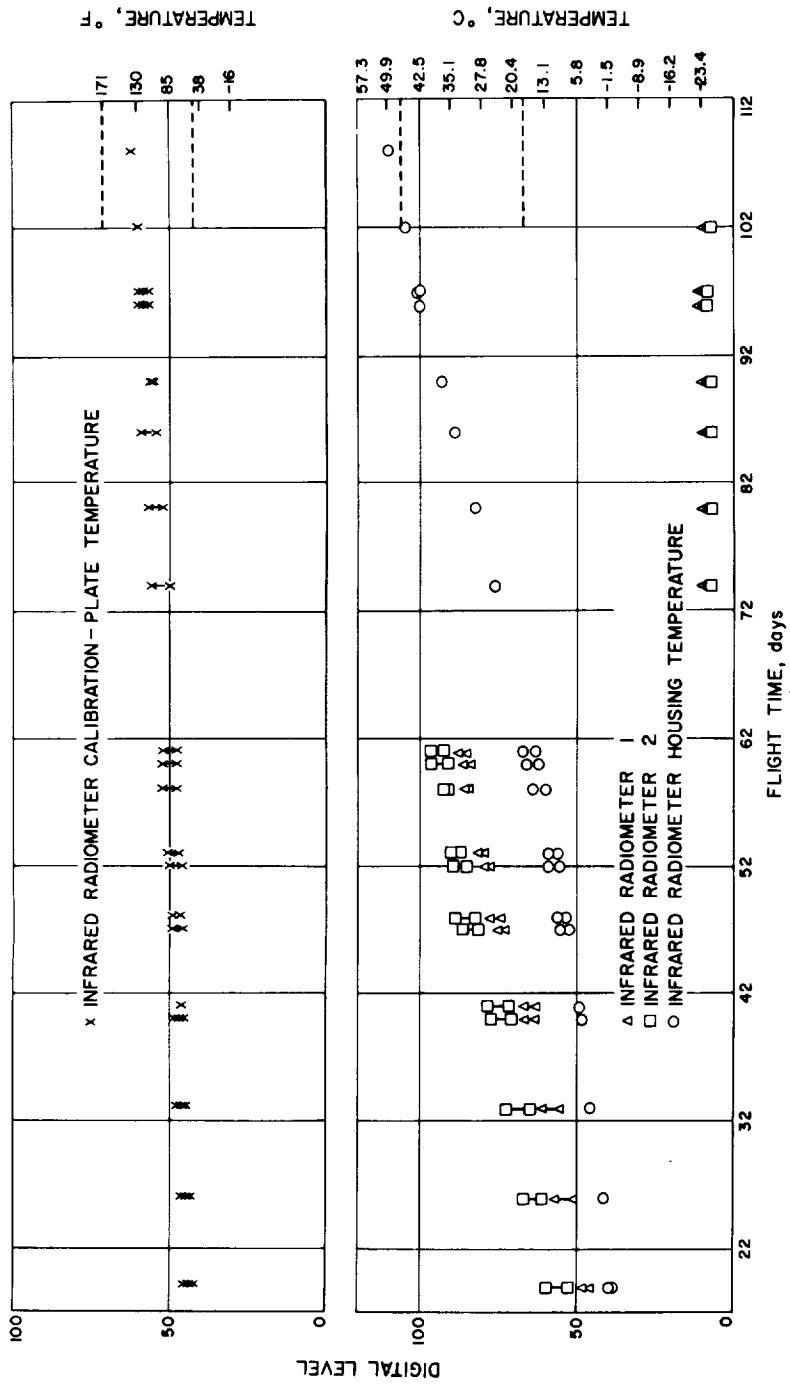

FIGURE 6–59.—Infrared radiometer temperature history.

In the absence of radiation to either lens, a null determined by optical balance and system noise was obtained. In the cruise mode, when the chopper was off, a higher-than-baseline output arose from base current flowing from the output driver into the integrating capacitors.

With the chopper off, the Schmitt trigger circuit became increasingly sensitive to noise pulses with increasing temperature. When this happened the integrating capacitors were discharged, and an output much lower than normal was obtained. Normal operation prevailed with the chopper running, however, since the photodiode signal overrides the noise. This effect had been observed in tests with a breadboard and the spare radiometer, but it was less pronounced than the apparent effect on the spacecraft. That is, in the laboratory, the Schmitt circuits would not trigger spuriously at a temperature below about 60° C. On the spacecraft, the effect was observed at a temperature around 20° C.

Two typical calibration sequences are shown in figure 6–60 between frame counts 162 and 165, and 19 and 21. Note that there is a discontinuity in the frame-count numbering on the graph. At this point, there is a discrepancy of 7 sec between the time scale and the frame count, which is ignored on the curve. Each small division represents one subframe of 20.16 sec duration. The dip in the center of the calibration was the result of the radiometer scanning past the calibration plate just before direction reversal. The difference in the calibration amplitudes on each side of the dip arose because the calibration plate was at different temperatures at these times, as shown in figure 6–61. The calibration plate was 9° F warmer when the scan direction was clockwise than when it was counterclockwise. This effect was apparently caused by variations in the reflected sunlight from the hex thermal shield as the radiometer scanned. The changes in calibration-plate temperature can be accounted for on the basis of changes in channels IR1 and IR2 and in the calibration curves. A similar, but less pronounced, effect was observed in the housing data.

Comparison of the in-flight calibration data received at encounter with that taken in the laboratory indicates a decrease in sensitivity of approximately 50%. The large dips before and after calibration (fig. 6–60) result from a phase reversal in the electronics when the instrument switched from the normal to the calibration mode.

Data taken on the planet are also shown in figure 6–60. The first pass occurred at frame-count 159/4, the second at 167, and the third at 17. Figure 6–62 shows three passes taken on the planet with the reference lens, prior to actual planet encounter. The maximum points on the curves represent the

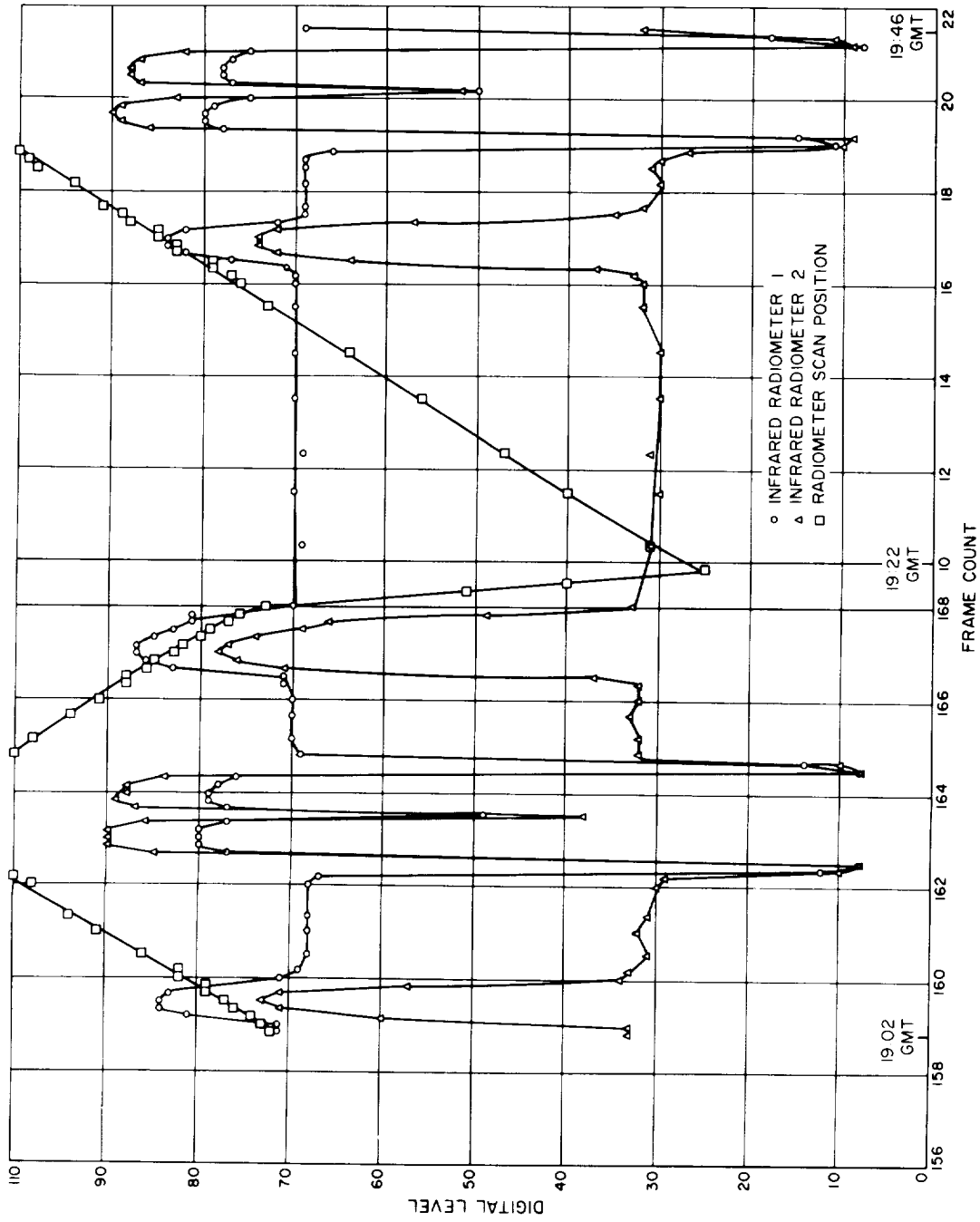

FIGURE 6-60.—Infrared radio scan position and data received during encounter.

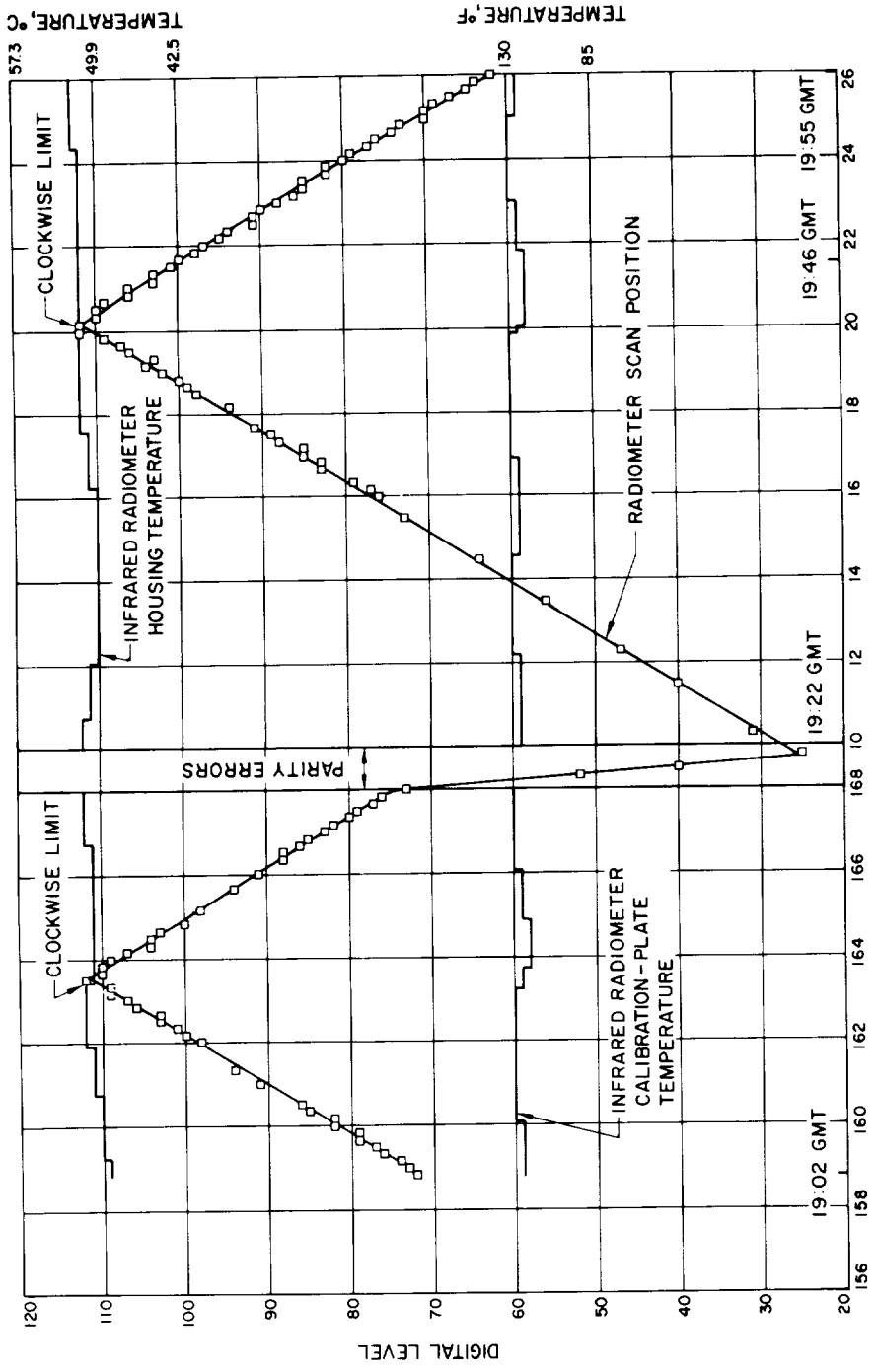

FIGURE 6-61.—Infrared radiometer temperature and scan-position data.

normal baseline values; the two minimums are data points on the planet. Since the planet was "seen" by the reference lens, the radiometer should have switched to the calibration mode as it does when viewing the calibrate plate. Unfortunately, however, the radiance of the planet was insufficient to cause this transition, and the electronics remained in the normal mode with a depressed baseline. No meaning can be attached to these curves, since no prior calibrations were run under these conditions.

Radiometer scan-position data are shown in figures 6–60 and 6–61. The break in the curve at frame-count indicates switching into the fast-scan mode. Slow scan was resumed after reversal. Positive slope indicates clockwise rotation, as seen looking down from the omniantenna.

Magnetometer

The triaxial fluxgate magnetometer was designed to measure the magnetic-field intensity in the vicinity of the sensor, which was mounted immediately inboard of the omniantenna. Three probes were incorporated in the sensors to obtain three mutually orthogonal components of the field vector. The three analog outputs had two sensitivity scales each: $\pm 64\gamma$ and $\pm 320\gamma$ ($1\gamma = 10^{-5}$ gauss). The scales were switched automatically within the instrument, and the scale-switch position for each axis was indicated by a voltage on an additional data line. The instrument had provisions for in-flight calibration, performed periodically on command from the science data conditioning system. On receipt of a command pulse, a preadjusted current, nominally equivalent to 30γ, was switched into auxiliary coils on each of the three probes. The resulting Δ-value, or change in the outputs, allowed determination of instrument sensitivity. The calibration current was switched off after six subframes (six readouts) by a command pulse on a separate line. Figures 6–63 and 6–64, respectively, present a block diagram of the magnetometer and a photograph of its electronics package.

The design specifications called for an uncertainty in the zero-field output (set at +3.5 volts in a 0- to +6-volt range) of $\pm 2\gamma$ long-term, and a noise level of 0.25γ. Some causes of possible offset, or the difference between 3.5 v and true zero-field output, are: (1) Second-harmonic distortion in the probe-excitation waveform, (2) pickup or circuit cross-talk, and (3) detector-bias drift.

The following anomalies in magnetometer performance and their effect on data quality during flight were noted in the flight record:

1. The total zero offset (including instrument- and spacecraft-field contribu-

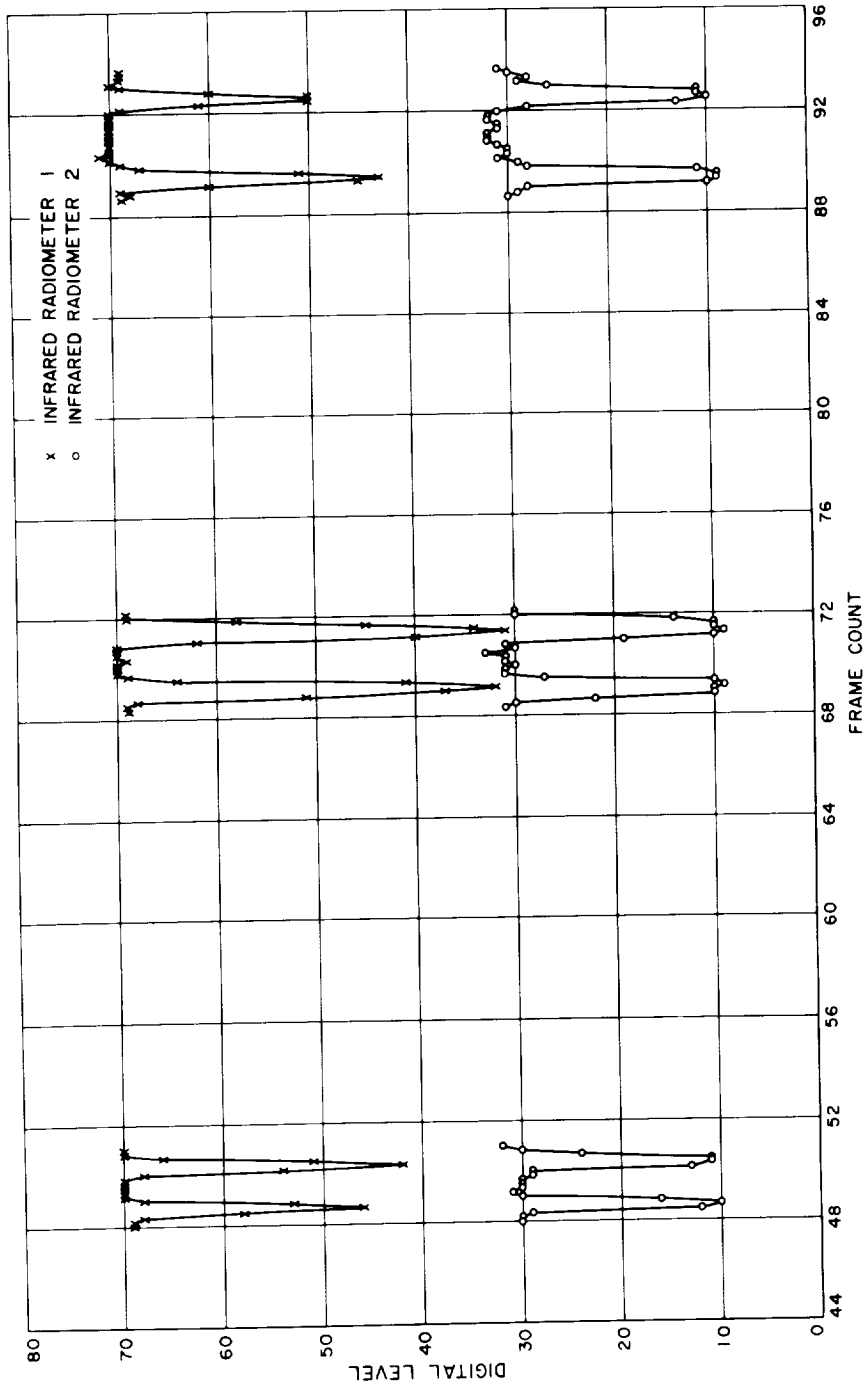

FIGURE 6–62.—Infrared radiometer data taken with reference lens.

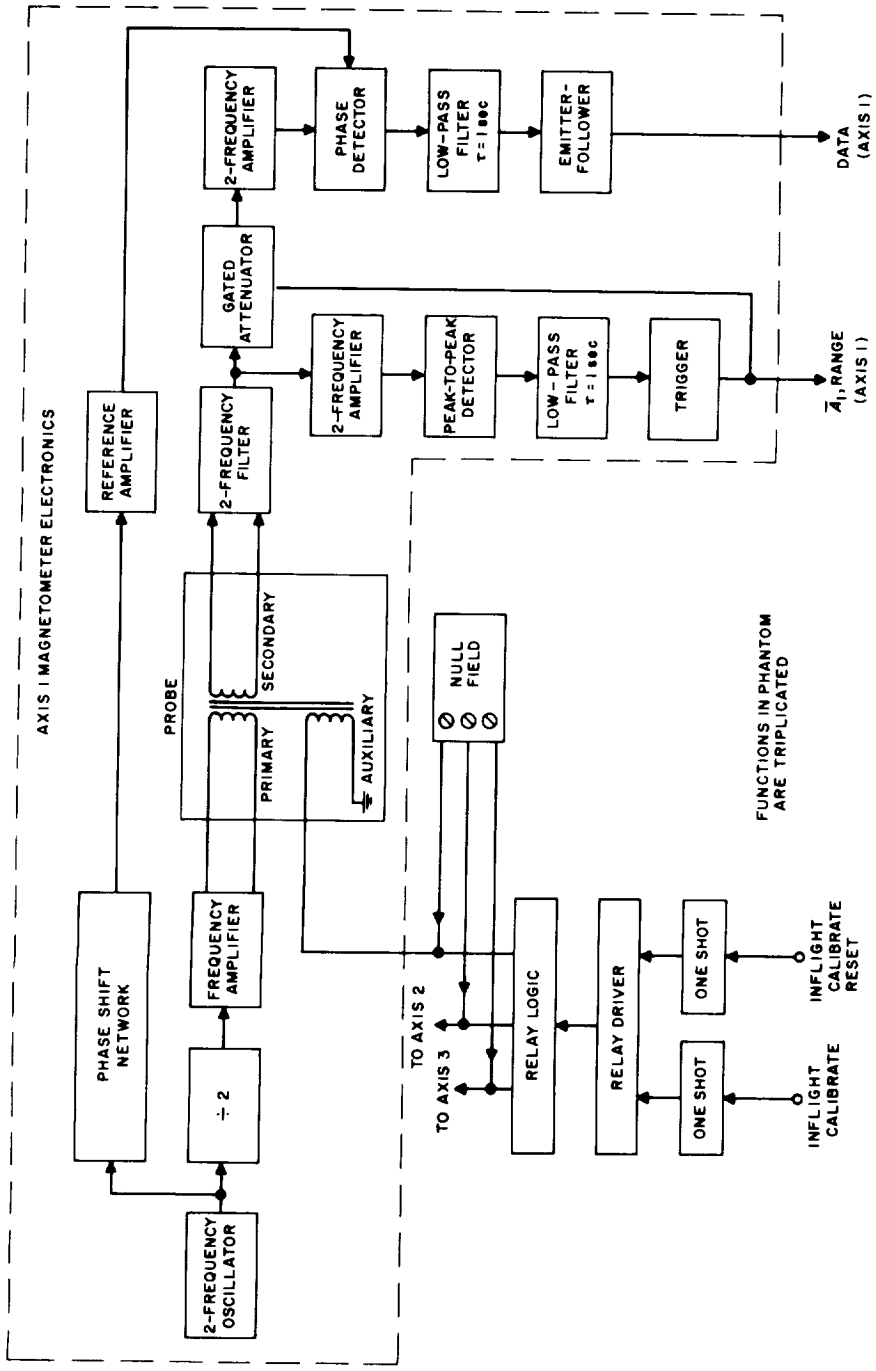

FIGURE 6–63.—Block diagram of triaxial fluxgate magnetometer.

tion) measured during the time between Sun acquisition and Earth acquisition, while the spacecraft rotated, differed from prelaunch estimates (based on prelaunch measurements) by 32γ along the $+X$ spacecraft axis, 55γ along the $-Y$ axis, and 7γ along the $-Z$ axis. A second shift of approximately 105γ in the total offset, having roughly the same direction cosines, occurred during solar-panel failure on October 31, but this offset disappeared on November 8 when the panel failure corrected itself. The offset again appeared with the second panel failure and, of course, continued, since the panel failure mode remained in force until transmission termination.

The initial or launch-mode offset did not materially degrade data quality beyond the uncertainties predicted for offset stability. However, the second or panel-failure offset placed all three axes on the low-sensitivity scale, resulting in a loss of resolution from 0.7γ to 4γ.

A number of possibilities exist to explain the launch-mode shift, but available data do not permit the singling out of any one factor. Instrument stability is a possible cause, although rather unlikely; prelaunch testing did not indicate reasonable grounds for expecting two axes to undergo large shifts during vibration or temperature cycling. Spacecraft field measurement methods were checked at the Malibu (Calif.) low-field facility and were found valid, although the effects on residual fields of launch-phase vibration and temperature were not well known. Other possibilities are (1) magnetic contamination of the spacecraft structure very near the sensor prior to launch and (2) current-loop fields resulting either from partial power-system failures not materially affecting system operation or from current configurations not present during simulated conditions without actual panel illumination.

2. The inflight calibration system began malfunctioning after September 20, exhibiting random switching between the normal and calibration modes. However, the periods in either mode were usually hours or, at worst, minutes in duration and, therefore, were not of a noisy nature. Data quality did not suffer appreciably, since the observed steps or changes in output checked reasonably well with prelaunch calibration data.

3. A few brief periods of complete data loss occurred after September 20. The noise- and low-level outputs during these periods were caused by an unexplainable drop in the value of regulated dc voltage from the magnetometer power supply. The drop was detected by observing the temperature behavior, which is a direct function of the power supply voltage at any given temperature. The time pattern of this failure mode was such that less than 1% of received data was

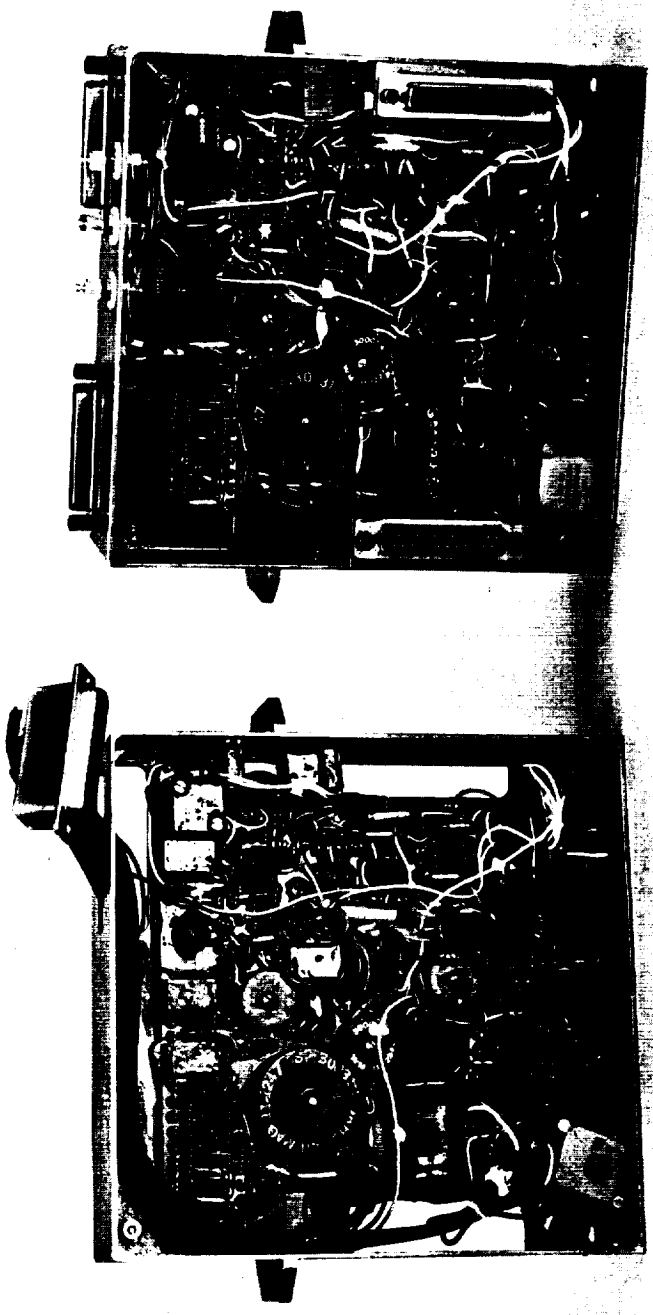

FIGURE 6–64.—Magnetometer electronics.

lost up to the postencounter phase. This failure mode became more frequent a few days after encounter.

4. On November 15, the scale-switching circuit for the X-axis began malfunctioning in a manner similar to that of the calibration anomaly mentioned in paragraph 2. For periods of minutes to hours, the X-axis scale switched from the normal low-sensitivity scale (solar-panel failure had occurred previously) to the high-sensitivity scale. During these periods, the X-axis output did not exceed the full-scale voltage range, and calibrations were obtained for the abnormal scale condition. The sensitivity was much lower than normal in the high-sensitivity scale at these times, since the operating point on the detector curve was well into the "knee" of the characteristic curve. The data resolution in this condition, as indicated by the calibration steps, remained at least as good as that obtained during normal low-sensitivity-scale operation.

5. During the in-flight calibration mode, the output change on the Z-axis was larger than the change predicted from the prelaunch calibration data. Since a shift in Z-axis sensitivity is far more likely than a shift in the calibration current, the new sensitivity measurement can be confidently accepted as valid.

In summary, it may be stated that, except for brief periods which constitute less than 1% of the data transmission time, no complete loss of instrument output data occurred throughout the flight. Accurate absolute values of the low interplanetary fields were obtained only for the X- and Y-axes prior to Earth acquisition when the spacecraft was rolling. Otherwise, an estimated $\pm 10\gamma$ long-term zero-field stability of the instrument, together with shifts in total offset during launch and at solar-panel failure, introduced uncertainties larger than the interplanetary "quiet-field" value. Changes in the interplanetary field should be detectable over periods of a few hours (occasionally a few days) to within $\pm 2\gamma$, except during panel failure, when the resolution of the instrument was degraded to approximately 4γ on all axes, with unknown stability. In these estimates, correction is assumed for previously calibrated current-loop fields.

At planet encounter, the stability of the instrument was estimated to have been sufficient for detection of a planetary-field component of 4γ to 8γ, and no instrument malfunctions occurred throughout the encounter mode which would result in loss of data for any period of time.

Ionization Chamber

The ionization chamber was a gas-filled sphere with a 0.2-g/cm^2 stainless steel wall. As illustrated in figure 6–65, an ion-collection and pulsing mechanism

was placed within the sphere. Protons, electrons, and heavier particles with sufficient energies to penetrate the wall ionized the gas, and the ions thus formed were collected. When the collector had lost a predetermined amount of its charge through this ionizing action, the pulsing mechanism simultaneously recharged the collector and transmitted a pulse to a preamplifier associated with the experiment. The amplified pulse was further shaped for transmission to the data conditioning system, where the information was stored until the proper time for transmission to Earth through the telemetry link. The instrument output represented the integrated rate of ionization and, as such, could vary in frequency over a wide range. In order to accommodate this wide range, the instrument was designed to operate with a 5-decade bandpass. Output pulse rates (intervals between pulses) of 1000 to 0.01 sec were possible with the Mariner II configuration. The pulse amplifier was designed specifically to exhibit stability over an extremely wide temperature range and to be insensitive to extraneous interference. The resulting assembly was capable of repeatable operation at any temperature from $-50°$ to $150°$ C. The complete assembly weighed less than 1 lb and consumed 100 mw of raw power.

The nominal interval between pulses during flight was 500 sec, corresponding to an ionization rate of 670 ion pairs per cm^3 sec atm of STP air. This rate was expected of the galactic cosmic radiation and, with the exception of data for October 23 and 24, varied no more than 10%. Following a class 2 flare on October 23, the interval between pulses decreased to a minimum of 10 sec in a period of 2.5 hours. The radiation decayed in an approximately exponential manner after this increase and, in a few days, returned to nominal. The relationship between the dynamic-range capability of the ionization chamber and the range through which the assembly operated during the mission is shown in figure 6-66. It was evident that had a trapped radiation belt around Venus been encountered, the ionization chamber would have been able to accept the reduced interval between pulses without extrapolation. That is, the rates would probably have remained within the dynamic-range capability of the instrument.

In summary, the ionization chamber performed as anticipated throughout the Mariner II flight. It has been concluded that all facets of the design were suited to the task performed.

Particle Flux Detector

The particle flux detector was designed (1) to obtain data complementary to the results of the ionization chamber experiment and (2) to detect and measure

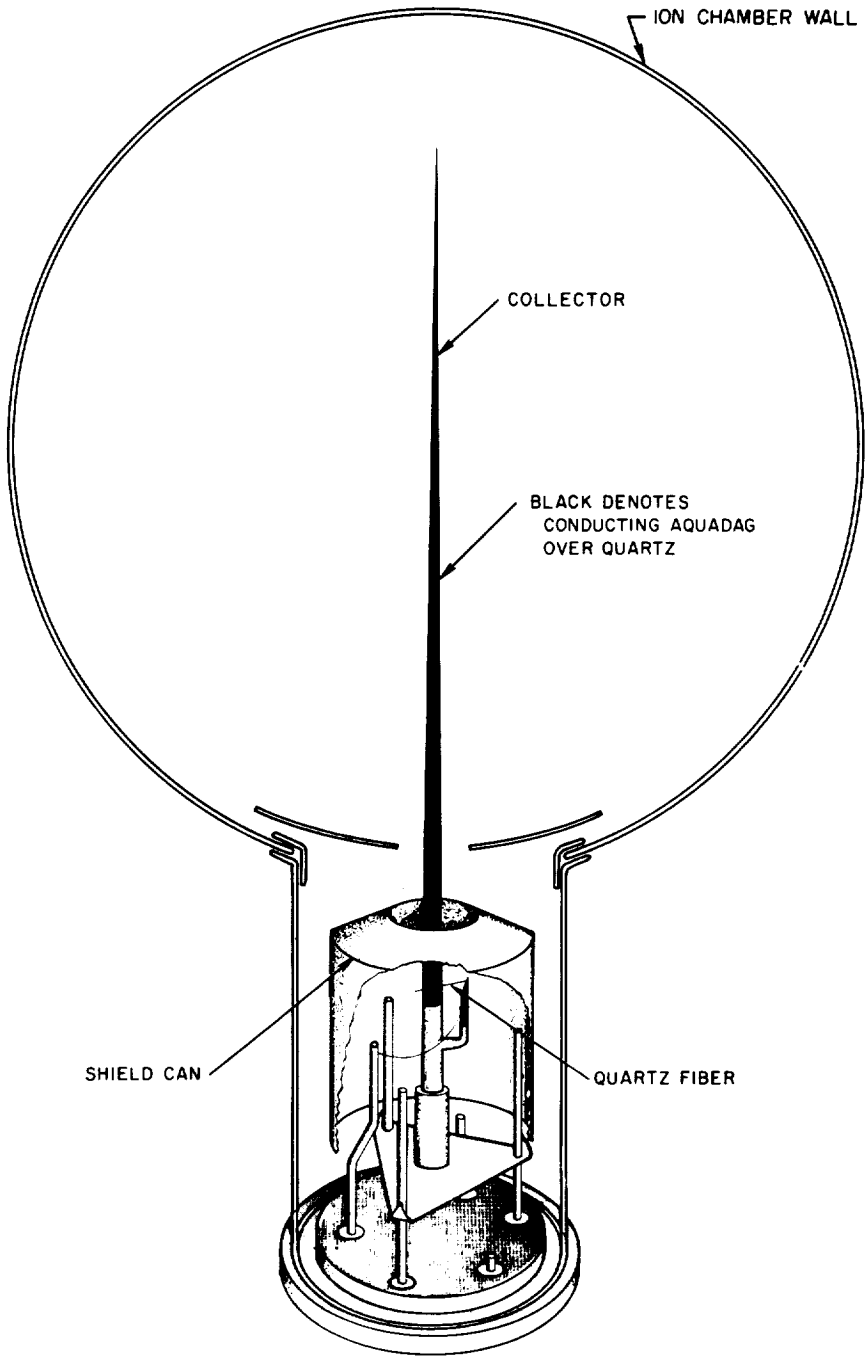

FIGURE 6–65.—Cross section of ionization chamber.

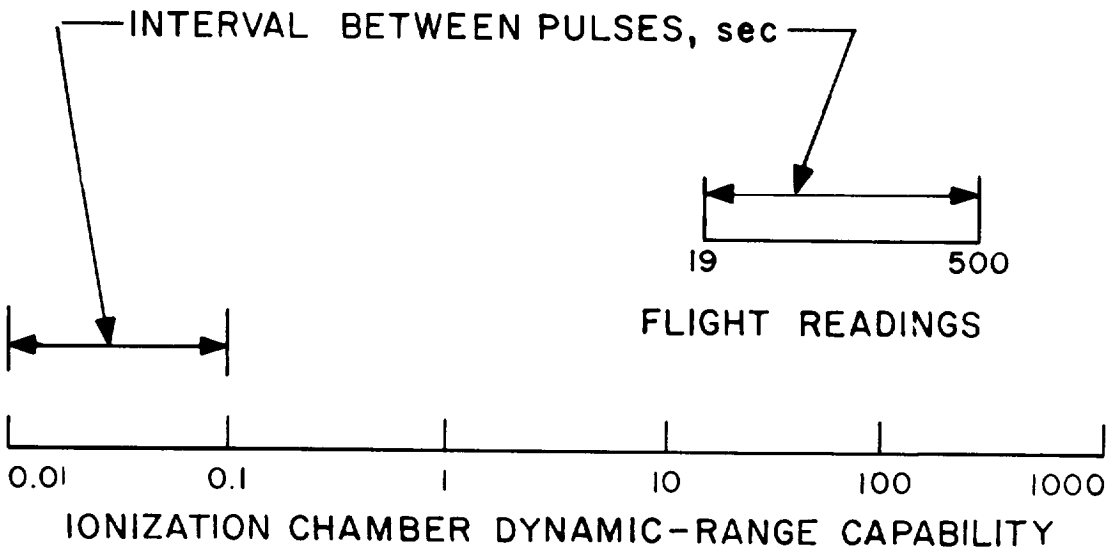

FIGURE 6–66.—Comparison of ionization chamber dynamic-range capability with actual flight readings.

trapped corpuscular radiation in the vicinity of Venus. Since development time was short, and weight and power constraints were rigorous, the two complementary instruments were consolidated.

The ionization measured in the chamber was proportional to the rate of energy dissipation per unit volume of gas, but did not depend uniquely on the flux of ionization radiation. It was decided, therefore, to measure this flux by means of an instrument matched to the ionization chamber in such a way that both would respond to particles of similar energies. Figure 6–67 shows the two instruments mounted on the spacecraft.

The particle flux detector incorporated three Geiger-Mueller tubes, supported in shields of various configurations, and three electronic amplifiers, all housed in a single chassis. One of the Geiger tubes, of a special end-window type, was supplied in flyable condition from the State University of Iowa. The other two were commercial glass counters, surrounded by metallic shields. The shields determined the energy which a proton, electron, or heavier particle had to possess in order to penetrate and be counted. The amplifiers served many functions, such as converting charge energy to a voltage pulse, inverting and shaping this pulse, and matching the Geiger-tube and transmission-equipment impedances. The design of the amplifiers optimized temperature stability and

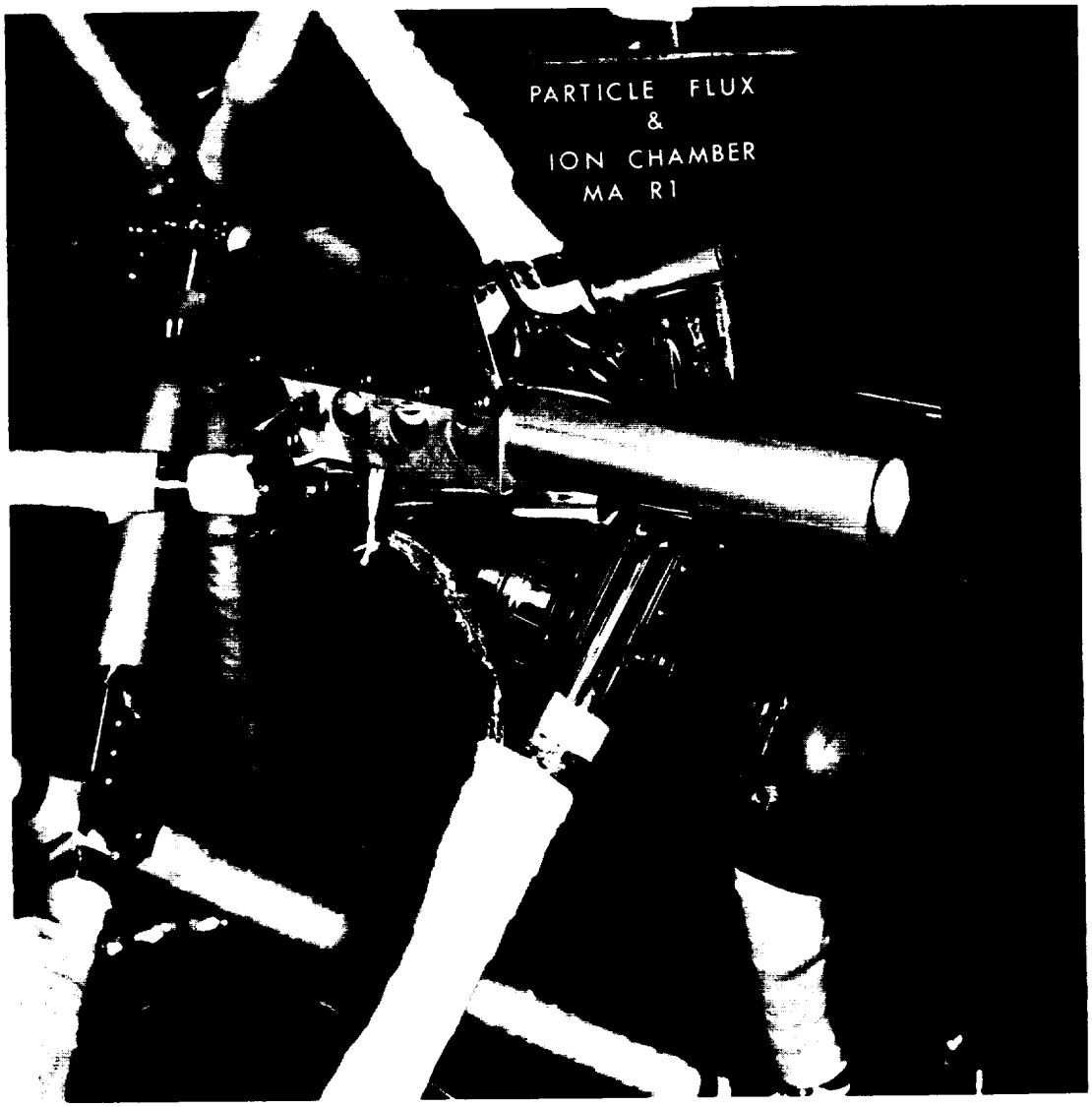

FIGURE 6–67.—Ionization chamber and particle flux detector mounted on spacecraft.

low-noise operation of very-low-level signals. The particular selection of parameters permitted an extension of the normal dynamic range of the tube by at least one order of magnitude. The instrument weighed 1.85 pounds complete and required 300 mw of raw power to operate.

The performance of the particle flux detector was normal throughout the Mariner II mission. A high degree of confidence has been placed in the data received from this instrument.

The average counting rate of the two larger tubes during flight was 20 counts/sec, which corresponds to an omnidirectional flux of 2.95 particles/cm^2 sec. The rates agree with expected galactic cosmic radiation. With the exception of a period beginning on October 23 and lasting several days, the rates varied no more than 10%. Following a class 2 flare on October 23, the average rates increased to 200 counts/sec, and then gradually declined. Had the rates increased by an additional factor of 100, the particle flux detector would have been able to respond with a small and accurately known counting-rate correction.

The average rate of the end-window tube was 0.6 count/sec. Increases in its counting rate were larger and more frequent than for the larger tube, since it was sensitive to particles of lower energy. It is estimated that the end-window-tube rate would have increased by 10^4 had Mariner II passed through a radiation belt at Venus similar to that of the Earth.

Cosmic Dust Detector

The primary objective of the cosmic dust experiment carried aboard Mariner II was to obtain the first direct measurement of the interplanetary dust flux as a function of time, and also of distance from the Sun, the Earth, and Venus.

Because of the short development time permitted, the Mariner II instrument employed much of the Ranger I circuitry and hardware (fig. 6–68). Measurements in flight were obtained by means of a two-channel pulse-height analysis of a microphone momentum sensor. When data readout occurred once per frame by parallel "dumping" into the data conditioning system, a delayed data-reset command signal was received for the purpose of resetting the data binaries and initiating an electrical calibration pulse in the input of the microphone amplifier, across the sensor crystal. The calibration-voltage amplitude was preset for 10% above the threshold of the less sensitive channel.

Two weeks prior to Venus encounter, a degradation became apparent in the performance of the cosmic dust detector. The less sensitive data channel began missing calibration and 45 min later no longer displayed calibration. At Venus encounter, the calibration signal began missing in the more sensitive channel and within a 45-min period stopped showing calibration altogether.

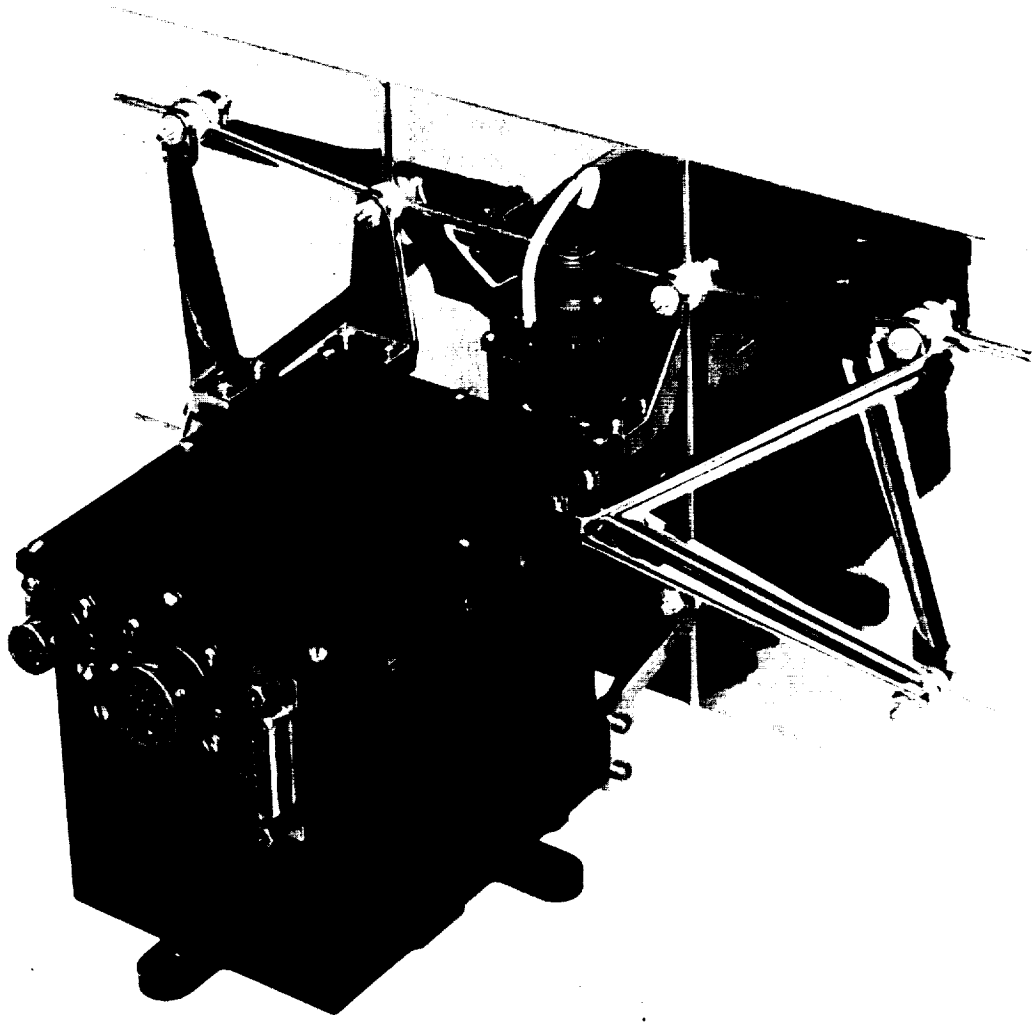

FIGURE 6–68.—Cosmic dust detector.

It is believed that overheating of the sensor crystal caused a change in its impedance, degrading the calibration amplitude, but the electronics were not degraded.

Solar Plasma Analyzer

The solar plasma analyzer was designed to measure the flux and energy spectrum of the positively charged component of the plasma emitted from the

Sun, commonly called the solar wind. Specifically, the instrument measured those positive ions falling into the energy range of 240 to 8400 ev that are of sufficient flux density to produce a current of 10^{-13} amp or greater.

Figure 6–69 shows, in block-diagram form, the following subsystems of the instrument: (1) The programmer, (2) the sweep amplifier, (3) the curved electrostatic-analyzer plates, and (4) the electrometer amplifier. The programmer commutated different inputs to the sweep amplifier, where these inputs were amplified and two outputs of equal magnitude and opposite polarity were generated. These outputs were connected to the electrostatic deflection plates, the positive output going to the outer plate and the negative output to the inner plate. Because of the geometry of the plates, the electrostatic field produced by these voltages allowed positive ions in a narrow energy range to be deflected into the collector cup. The electrometer measured the rate at which these ions were collected. The electrometer had a logarithmic feedback element, so that the dynamic range of the output was within the measurement capability of the analog-to-digital converter of the data conditioning system. This logarithmic feedback enabled the instrument to measure currents from 10^{-13} to 10^{-6} amp. Also included in the instrument was an inflight calibration current to make data analysis more accurate.

The Mariner II solar plasma analyzer operated successfully during the entire flight, in both the cruise and the encounter mode. Two anomalies, however, were noted in its performance.

First, a downward shift in the electrometer-current calibration occurred on September 5 (see table 6–V). On October 8, another downward shift of 2 DCS

Table 6–V.—Calibration history for solar plasma analyzer electrometer

Date, 1962	Temperature range, °F	Calibration	Duration of calibration
Aug. 30–Sept. 5	85–89	120	6 days
Sep. 5–Oct. 8	89–100	119	33 days
Oct. 8	100	118	11 hours
Oct. 8–Nov. 11	100–122	117	34 days
Nov. 11–21	122–133	118	10 days
Nov. 21–Dec. 3	133–146	119	12 days
Dec. 3–26	[a]146–160	120	23 days

[a] Estimated temperature.

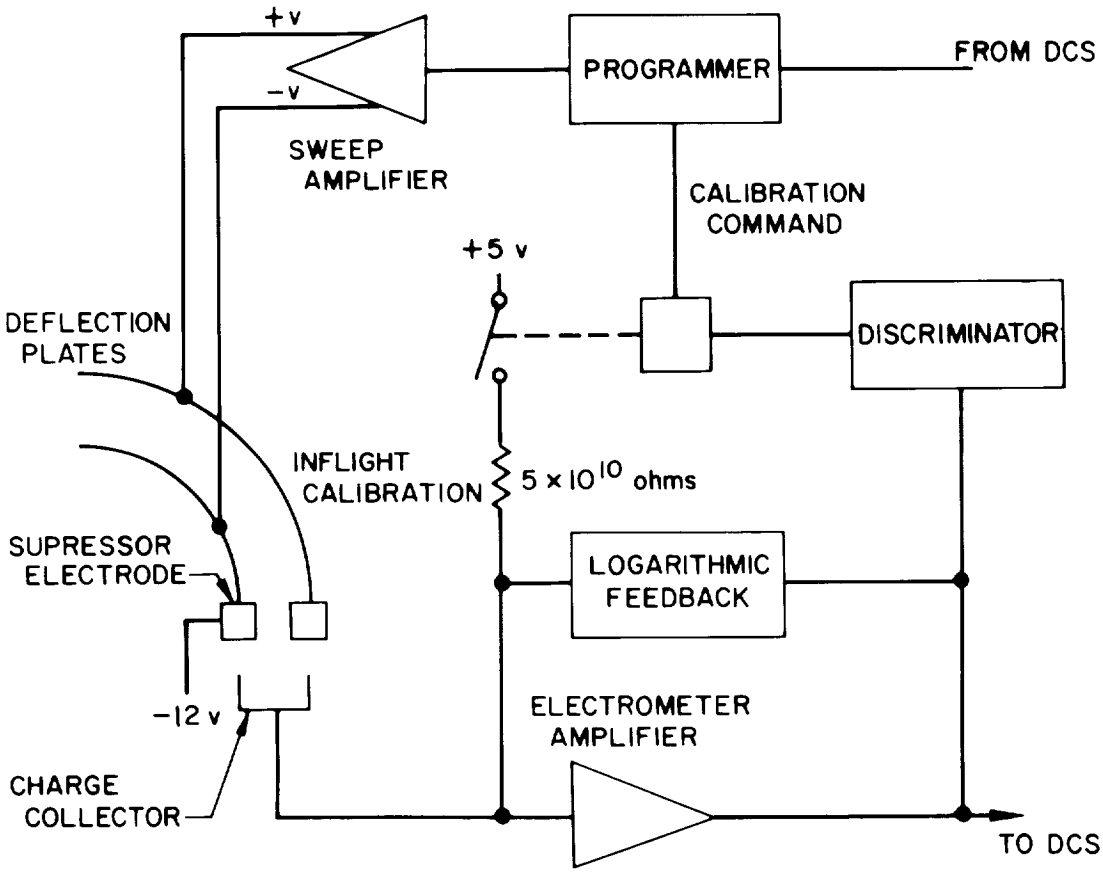

FIGURE 6–69.—Block diagram of solar plasma analyzer.

steps occurred. On November 11, the calibration began increasing, and at encounter it had returned to 120. The expected shift for the flight was a minimum increase of 2 steps and a maximum of 3 steps. Therefore, at least part of the increase in calibration after November 11 can be explained by the normal temperature-induced changes.

In comparing these shifts with other spacecraft events, it was noted that the science temperature measurement for the magnetometer shifted about 1.2 DCS steps on October 8. The engineering temperature measurements near the magnetometer did not record a similar shift. Since the magnetometer uses a 7-bit channel, this shift, if attributable to a common circuit such as the staircase generator, would correspond to a 2.4-step decrease on the 8-bit plasma channel The electrometer-output shifts in the laboratory vacuum-temperature chamber

had indicated that the plasma data should be increased by 2 to 3 DCS steps at encounter. The simultaneous downward shifts of the plasma analyzer calibration, discriminator threshold, and magnetometer temperature data on October 8 indicated that the correction should be made for all data from this date to flight termination. The magnetometer temperature shift indicated that a 2.4-step correction should be added to the plasma data, and the plasma analyzer preflight temperature tests verified that a 2- to 3-step correction should be made.

The second problem which arose in the flight performance of the plasma analyzer was that of ambiguity in the very-low-current portions of the spectrum. A reed switch was used to apply the calibration current to the electrometer and to prevent the electrometer from saturating if negative transients or background currents in excess of positive currents should occur. Negative background current might have been caused by sunlight reflecting down the analyzer plates and liberating electrons from the suppresssor electrode. It might also have been caused by energetic electrons reaching the collector cup after having been scattered at least twice from the walls of the analyzer deflecting plates. This background current fluctuated throughout the flight and, on occasion, was observed to be as high as -10^{-13} amp. The minimum net positive current needed to charge the electrometer-compressor capacitance from the discriminator threshold to the proper point on the static characteristic has been calculated as 3×10^{-13} amp, where the voltage excursion is 1.5 v, the time interval is 20 sec, and the diode capacitance is 4 pf. All net positive currents above 3×10^{-13} amp may be taken from the static electrometer characteristics. An electrostatic transient caused by the reed-switch coil in sequencing from calibration to energy level 1 usually leaves the electrometer near the discriminator threshold at the end of step 1. The ability of a 3×10^{-13} amp current to restore the output to its steady-state value within 20 sec is illustrated in the transient record plotted in figure 6–70. An integration calculation may be used for average currents of less than 3×10^{-13} amp when the electrometer feedback capacitance is in a highly discharged state. Under this condition, the integration scale factor is 6×10^{-15} amp per DCS step per measurement time interval. Negative background current must then be added to arrive at a value for positive ion current.

During the encounter mode, off-step sampling intervals were reduced to 3 sec, or 1/6 of the cruise intervals. In this condition, the minimum current required to charge the electrometer to its correct static characteristic in odd steps, when the electrometer feedback capacitance was in the maximum discharge state, was 6 times the cruise threshold, or 1.8×10^{-12} amp. Most odd-

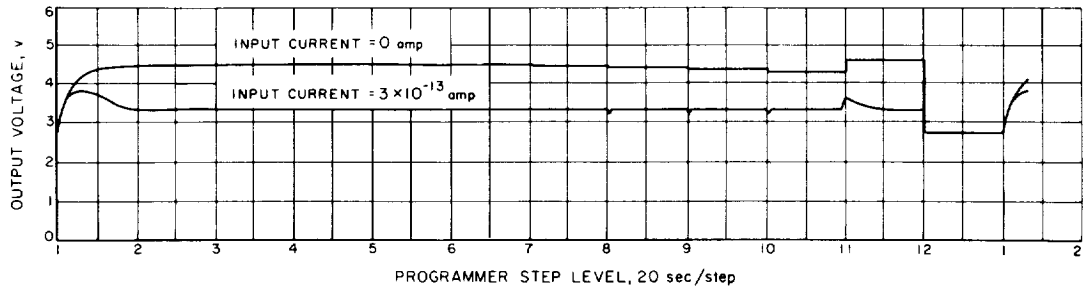

FIGURE 6–70.—Electrometer time response.

step encounter data were directly usable, with no corrections required. Step 1 readings were different because of the switch-coil transient, but even in this area the results were quite predictable.

The solar plasma analyzer had a highly reliable preflight history and accomplished its mission without any detectable deterioration in performance. In addition to the wealth of scientific information which accrued during the thousands of hours of operation, valuable engineering experience was obtained, in both components and techniques.

CHAPTER 7

Tracking and Data Acquisition Operations

The Space Flight Operations Complex (SFOC) comprised the Earth-based facilities and personnel required for the conduct of space-flight operations, which covered the phase from injection of the spacecraft into a Venus transfer trajectory through termination of the mission. For the Mariner II flight, the complex included the Space Flight Operations Center, the Launch Control Center, the Communications Center, the Central Computing Facility (CCF), the Deep Space Instrumentation Facility (DSIF), and certain Atlantic Missile Range (AMR) facilities. The Mariner II Complex was operational 24 hours a day from launch through the encounter phase.

The Space Flight Operations Center at the Jet Propulsion Laboratory in Pasadena, Calif., was the coordinating focal point for activities associated with the mission. Within the Space Flight Operations Center, the following activities were in progress throughout the flight of Mariner II:

1. Information pertaining to the flight path and to spacecraft performance was analyzed by the Spacecraft Data Analysis Team (SDAT), the Scientific Data Group, the Tracking Data Analysis Group, the Orbit Determination Group, and the Midcourse Maneuver Commands Group.
2. Control was exercised over DSIF tracking operations.
3. All spacecraft commands were originated.
4. Current overall status of the operation was displayed on the status display boards.

The Launch Control Center, located at Cape Canaveral, provided coordination of countdown and launch activities involving the spacecraft and AMR facilities.

The Communications Center (fig. 7–1) controlled all communication lines over which data flowed throughout the SFOC, except for the high-speed data line between Goldstone and the CCF. The center was the terminus for all communications associated with the Mariner operation.

The Central Computing Facility incorporated a Primary Computing Facility, a Secondary Computing Facility, and a Telemetry Processing Station (TPS). The CCF processed and reduced tracking and telemetry data to forms required

FIGURE 7–1.—Communications Center at JPL–Pasadena.

by the users for analysis of spacecraft performance, flight-path information, and command generation.

The Deep Space Instrumentation Facility was made up of four permanent station installations, one mobile tracking station, and a launch station. The DSIF obtained angle and Doppler data, and also received scientific and engineering telemetry. Data received by the DSIF was transmitted to JPL in real and near-real time. Ground-computed commands were transmitted to the spacecraft by the DSIF.

ATLANTIC MISSILE RANGE SUPPORT

The Atlantic Missile Range (AMR) supplied JPL with real-time tracking data on the Agena parking orbit from the Antigua and Ascension stations.

The Antigua data covered that part of the trajectory from first Agena cutoff to the horizon. Data prior to this time were concerned with powered flight and were, therefore, not usable in the parking-orbit-determination program. Good data were received at low elevation angles but, because of the uncertainty of refraction effects in the atmosphere, no data below 3.7° elevation were used for precision orbit determination. Between first Agena cutoff and the horizon, a maximum of 37 data triplets could have been received, but, because of radio-frequency transmission problems, only 16 of the data triplets were received at AMR in real time. In addition, some of these 16 triplets were not intact. Of the 48 total measurements, only 39 were usable in the final orbit determination; these consisted of 16 range points, 13 of 16 azimuth points, and 10 of 16 elevation points.

The Ascension Tracking Station sent a full pass of data, ranging from an initial elevation angle of 5° to a maximum angle of 73° and back down to 12°. Range at the peak elevation angle was 190 km. Agena second ignition occurred toward the end of the pass at the 12° elevation angle. No data were accepted after this, because powered-flight data are not applicable in the parking-orbit-determination program. All data were of excellent quality.

A relatively new tracking station at Pretoria, South Africa, equipped with an FPS–16 radar set, tracked the Agena after second burnout. However, an equipment malfunction caused a loss of the time-word in the data message. Approximately 10 hours later, when sufficient DSIF tracking data had been received to give a good orbit determination, the Pretoria data were compared with this orbit and time correlation was obtained. The Pretoria data covered the time

period from 9 min 25 sec to 34 min 30 sec after second Agena burnout. At the end of the tracking period, the Agena was approximately 14 000 km (8699 miles) from Pretoria. These data were subsequently compared with five optical fixes of the Agena obtained from the Mount Palomar Observatory. The Mount Palomar data were partially reduced, yielding an accuracy on the order of 0.2 min of arc. The two data sources were found to be statistically consistent. The transfer orbit thus determined for the Agena indicated that it was not on a collision course with Venus. A final transfer-orbit determination and data evaluation were conducted when a reduction to 1 sec of arc in accuracy was completed on the Mount Palomar data.

Because of an equipment failure in the 4101 computer on board the *Twin Falls Victory Ship*, no tracking data were available from this source. The computer's function was to remove the ship's motion in pitch, roll, and heading from the tracking data obtained by the shipboard radar. Useful range data were taken, but were not used in real time because of the availability of the Pretoria data.

DEEP SPACE INSTRUMENTATION FACILITY

Six stations of the Deep Space Instrumentation Facility (DSIF) were used for the Mariner Mission. These stations were located and designated as follows:

Launch Station: Cape Canaveral, Fla	DSIF 0
Mobile Tracking Station (MTS): South Africa	DSIF 1
Pioneer Station: Goldstone, Calif	DSIF 2
Echo Station: Goldstone, Calif	DSIF 3
Woomera Station: Australia	DSIF 4
Johannesburg Station: South Africa	DSIF 5

The DSIF stations obtained angular position, Doppler, and telemetry data during postinjection phases of the trajectory, and transmitted ground-computed commands to the spacecraft. Tracking operations were carried on by the DSIF on a 24-hr/day schedule during virtually the entire mission.

The telemetry data were transmitted to the Space Flight Operations Center in near-real time throughout the mission. The tracking data were transmitted in near-real time during the launch, midcourse, and encounter periods, and also 1 day a week when precision tracking data were obtained. During the remainder of the period, tracking data were forwarded in nonreal time. Tracking summaries were supplied to the Operations Center on a daily and weekly basis, so that tracking and station conditions could be included in the data analysis.

To maintain 24-hour contact with the Mariner spacecraft from the rotating Earth required the operation of at least three deep-space tracking and communications stations, which were located approximately 120° apart: at Johannesburg, South Africa; Woomera, Australia; and Goldstone, Calif.

Before escaping the Earth, the Mariner spent some very crucial minutes in initial launch ascent and low Earth orbit. Tracking and radio acquisition during these periods required two additional Earth stations. The first was a Spacecraft Monitoring Station located at Cape Canaveral, Fla., and used both for prelaunch checkout of the spacecraft system and early spacecraft telemetry from above the launch pad to the Cape horizon. A second station, the Mobile Tracking Station located near the Johannesburg Station in South Africa, provided early spacecraft tracking while the Agena stage and Mariner II were still in Earth-parking orbit.

Deep Space Communication Station, Goldstone

North of Barstow, Calif., some 100 miles from the Jet Propulsion Laboratory, lie the Goldstone Stations of the DSIF. (See figs. 7–2 to 7–8.) The two DSIF sites (Echo and Pioneer) were equipped with precision antenna systems which were capable of continuous communications with spacecraft. The location had to be remote from population centers and large industrial areas to overcome noise interference to the receivers; yet proximity to the Jet Propulsion Laboratory was essential because the Goldstone facilities, apart from DSIF activities, are also used for advanced research and development in space communications.

The site of the Goldstone DSIF covers 68 square miles and includes Goldstone Dry Lake, which is used as an airstrip for light aircraft. Offices for technical and administrative personnel are situated at the Echo site, the headquarters for Goldstone operations.

The Pioneer and Echo sites are both equipped with a steerable 85-ft-diameter paraboloidal reflector antenna, each with its associated drive system, radio tracking, transmitting and receiving, and data-recording and transmitting systems (figs. 7–9 and 7–10). The antennas are polar-mounted (moving parallel in hour-angle and perpendicular in declination to the Earth's equatorial plane) and have a pointing accuracy of better than 0.02°. The tracking system at the Echo site consisted of the antenna, an antenna feed system, a master parametric amplifier subsystem, a phase-coherent receiving subsystem, and a digital data handling subsystem. The receiving subsystem detected a signal transmitted from the

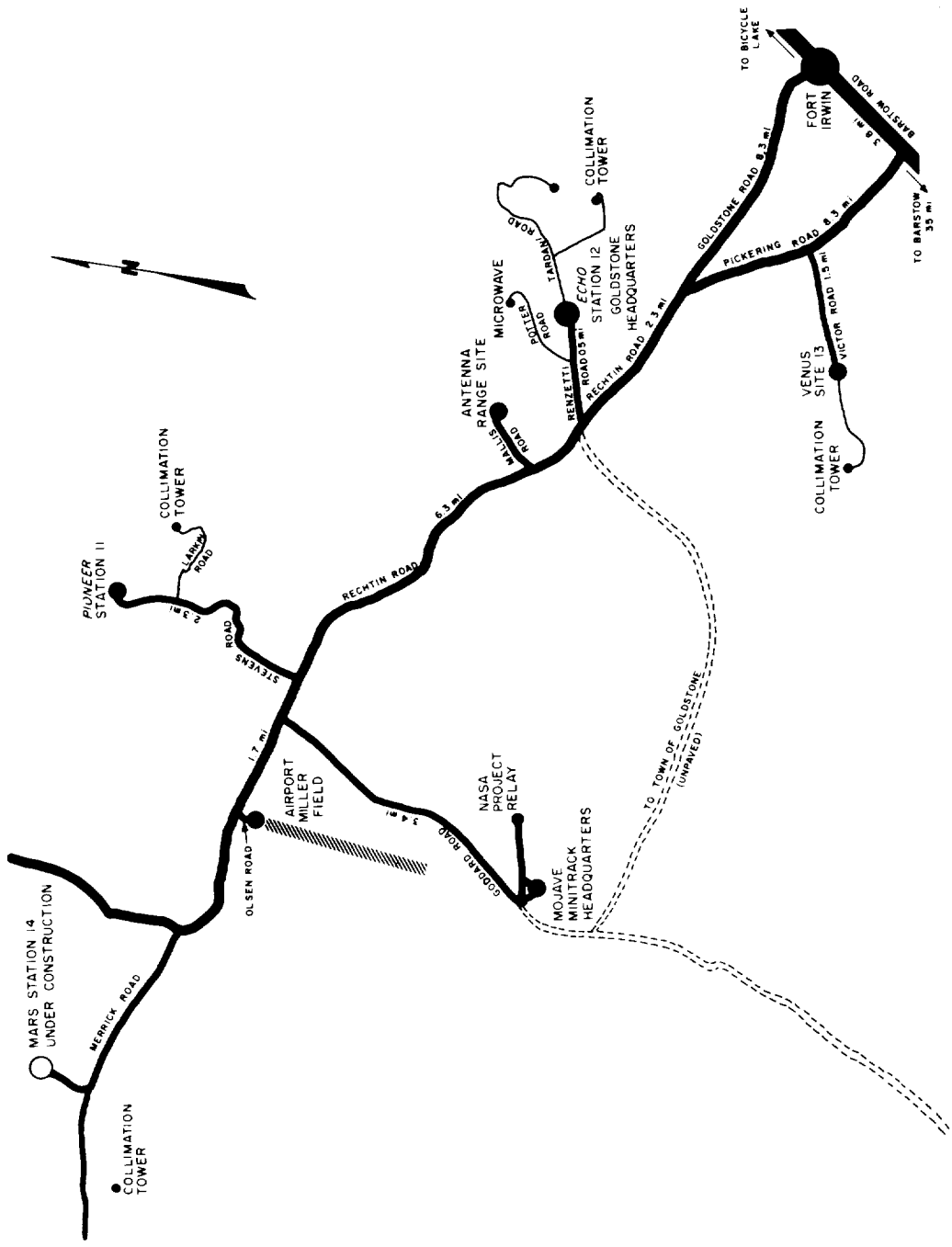

FIGURE 7–2.—Area map of Goldstone Stations.

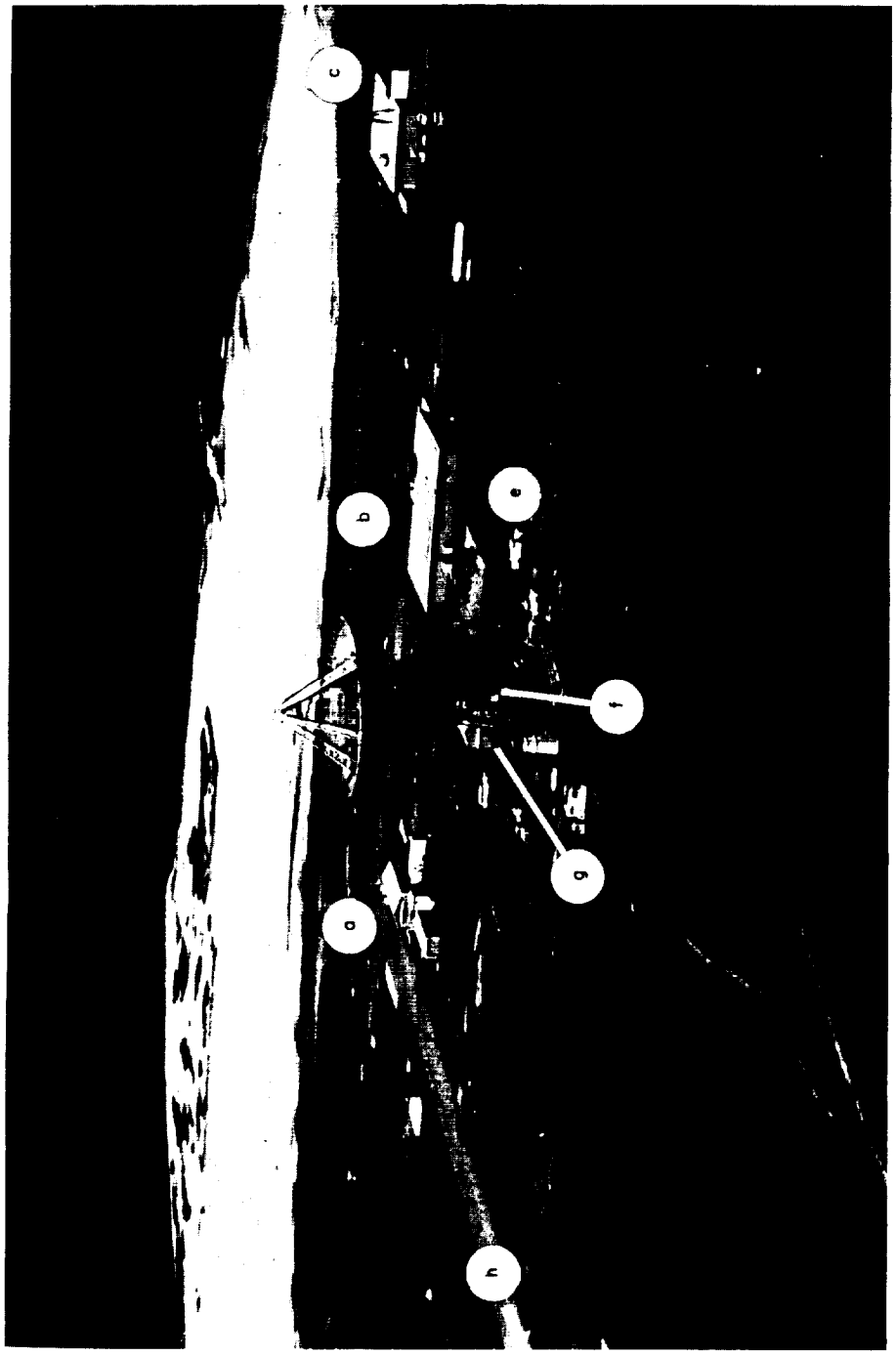

FIGURE 7-3.—Goldstone Pioneer Station. (a) Generator building, (b) control building, (c) laboratory building, (d) antenna, (e) hydro-mechanical building, (f) maser and parametric amplifier building, (g) antenna field storage building, (h) guard house.

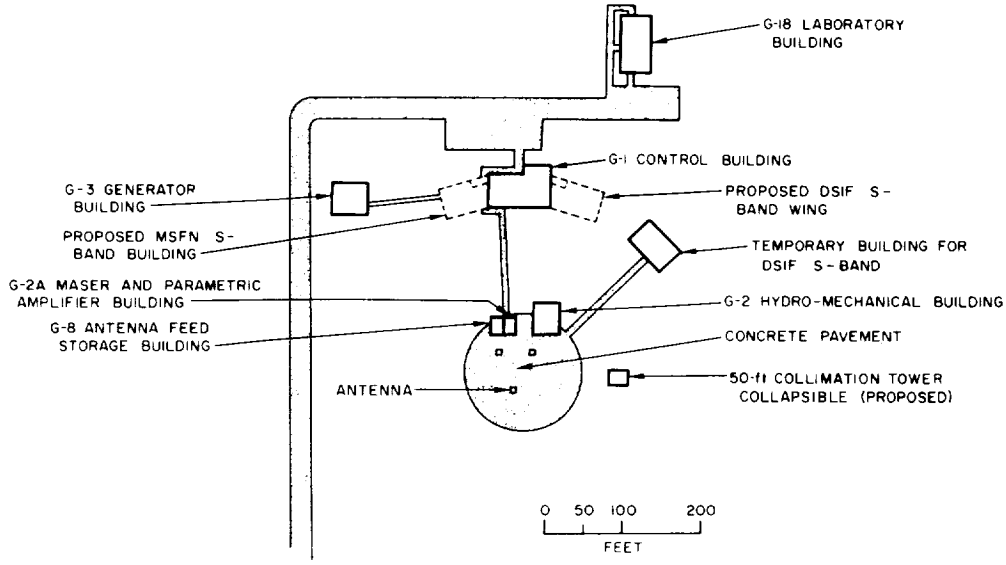

a. STATION MAP

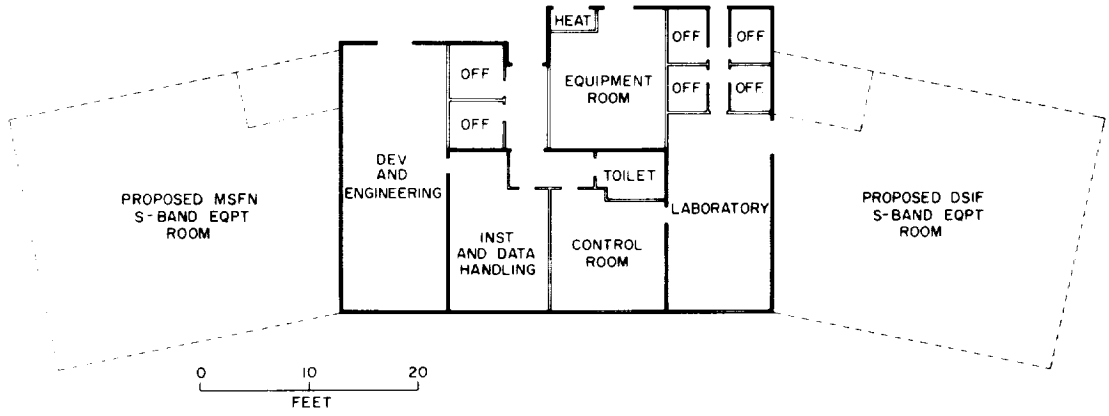

b. CONTROL BUILDING

FIGURE 7–4.—Goldstone Pioneer Station.

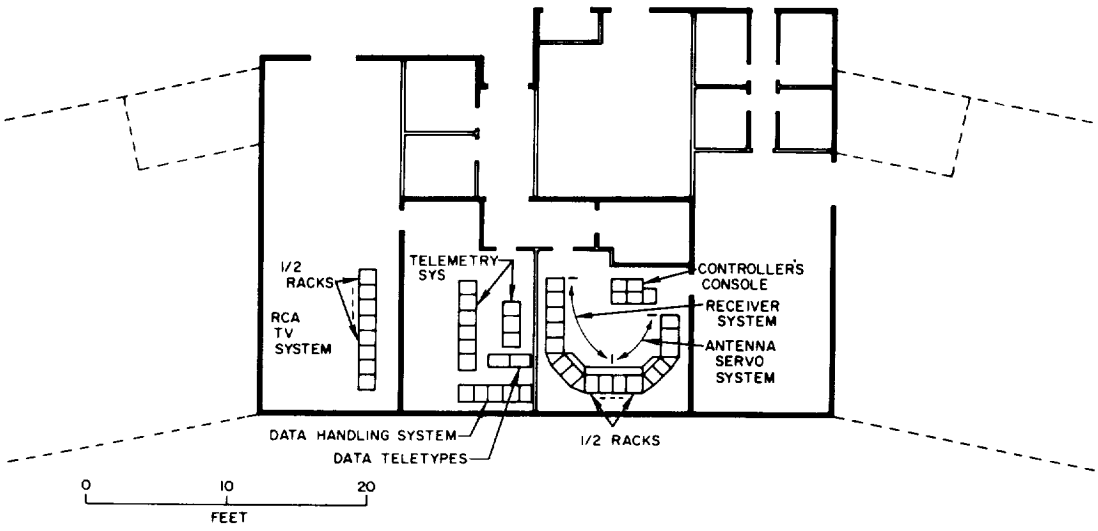

a. CONTROL AND INSTRUMENTATION ROOMS

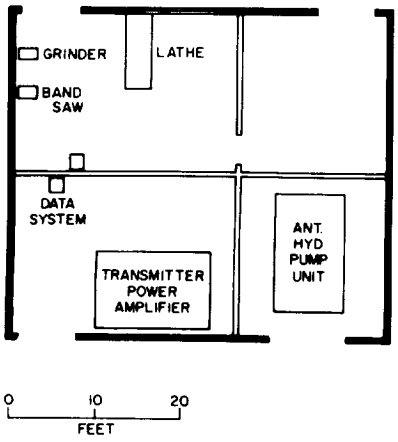

b. HYDRO-MECH. BUILDING

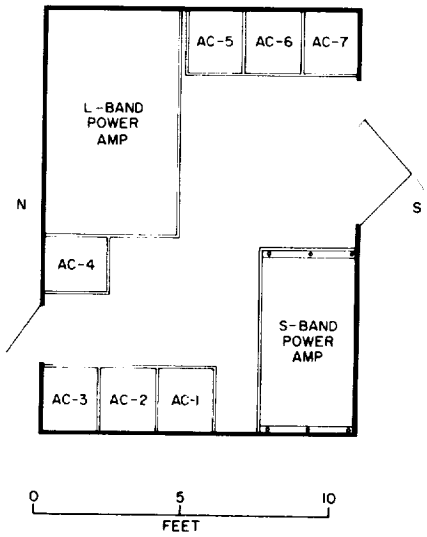

c. ANTENNA CAGE

FIGURE 7–5.—Goldstone Pioneer Station.

FIGURE 7–6.—Goldstone Echo Station. (a) Guard house, (b) dormitory, (c) water storage tank, (d) system engineering, administration, and cafeteria building, (e) transportation building, (f) generator building, (g) control building, (h) storage building and future machine shop, (i) hydro-mechanical building, (j) communications and operations building.

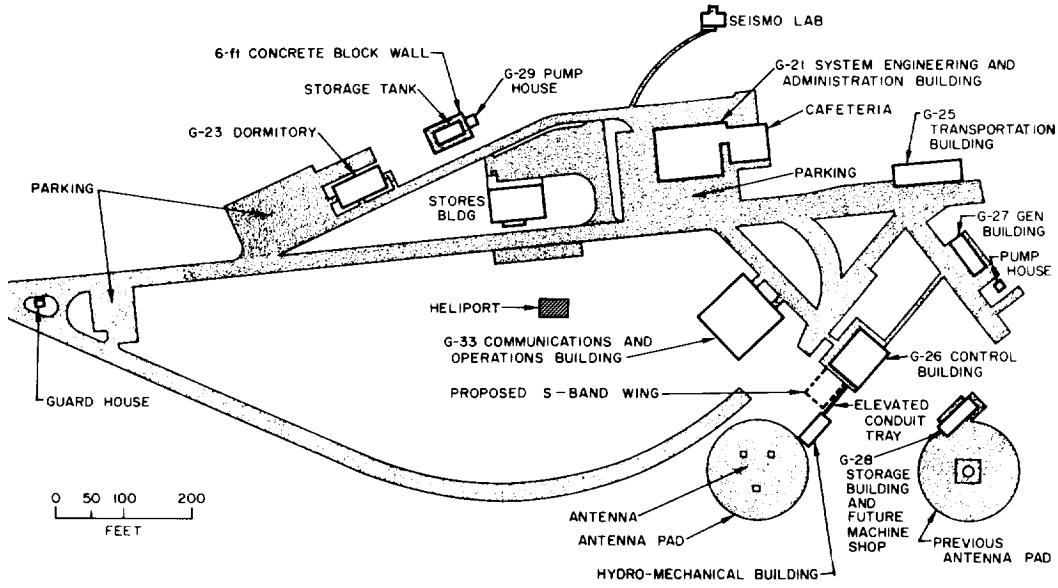

a. STATION MAP

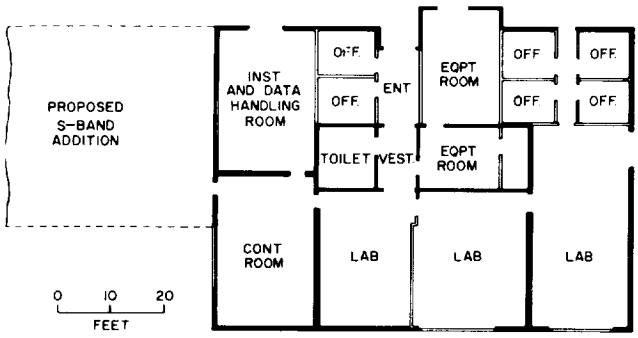

b. G-26 CONTROL BUILDING

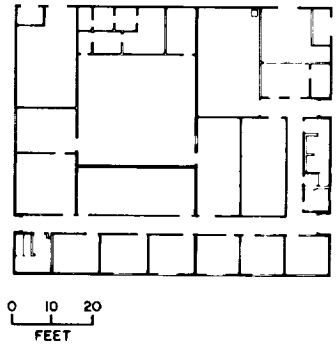

c. G-33 COMMUNICATIONS AND OPERATION BUILDING

FIGURE 7-7.—Goldstone Echo Station.

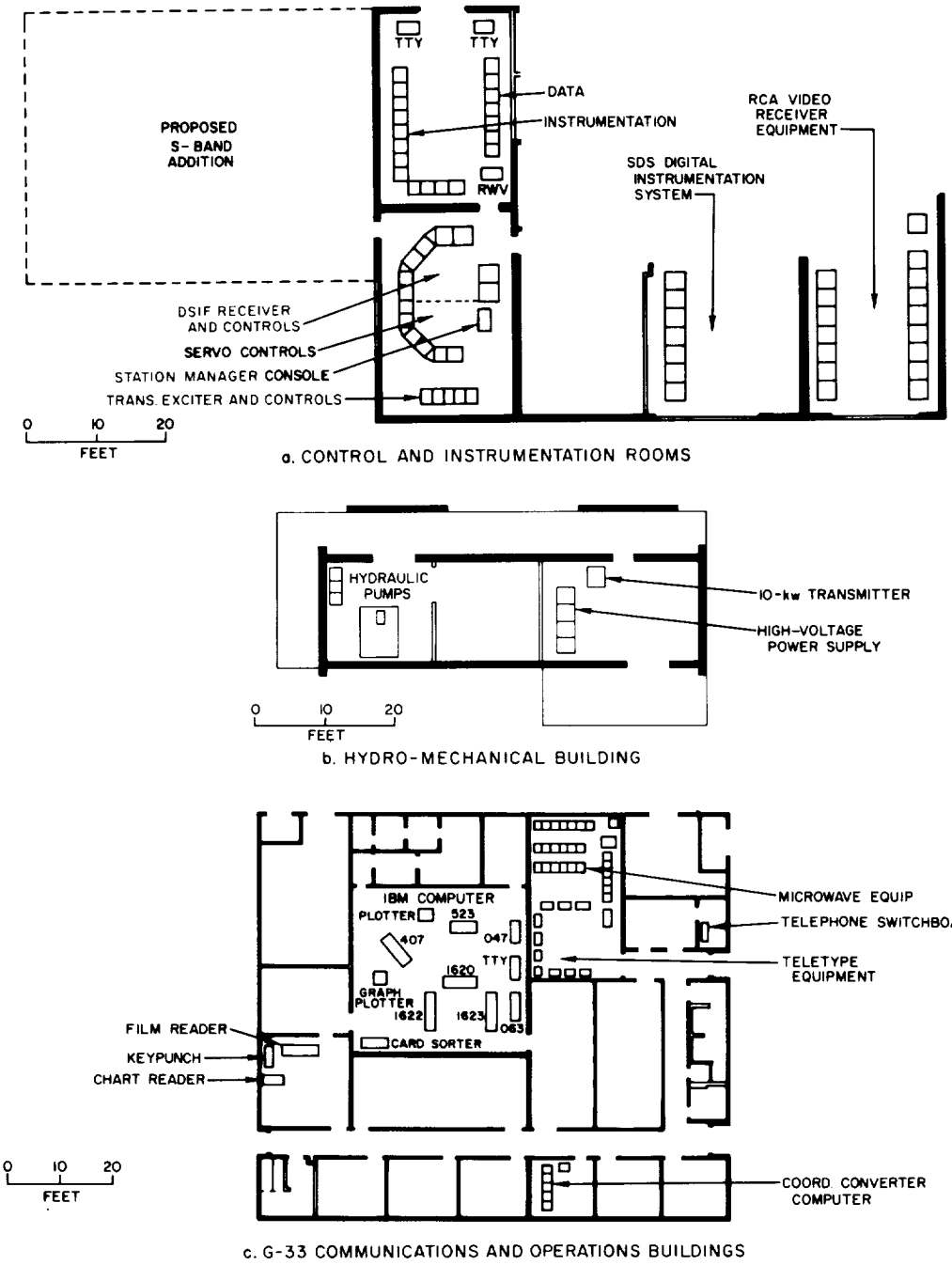

FIGURE 7–8.—Goldstone Echo Station.

Mariner spacecraft and, from a combination of the antenna feed signals, provided a pointing error signal which was used to position the antenna. The Echo site had the added capability of tracking with a precision two-way Doppler system, and of transmitting commands to space vehicles.

The Echo and Pioneer sites at the Goldstone Station were both equipped with a three-channel 960-mc superheterodyne receiver designed for reception of a continuous-wave signal in a narrow frequency band in the 960-mc range. These receivers used phase-lock techniques to achieve a very narrow noise bandwidth and to track the signal over the frequency region it occupied during the mission. The inputs to the receiver channels consisted of three signals from the antenna feed: a sum of reference signal and two angular error signals. The sum channel provided telemetered spacecraft information for recording. The angular error channels provided the dc-error signals for the antenna servosystem.

The transmitter at the Echo site was a 10-kw 890-mc unit which could be used with a diplexer to allow simultaneous operation of the transmitter and the receiver. Simultaneous operation of the receiver and transmitter and the use of a spacecraft transponder (communication equipment that receives a transmitted signal, frequency converts it, and retransmits it) enabled accurate Doppler (radial velocity) measurements to be made. The Echo transmitter also provided command transmission capability for the site.

Instrumentation and data-handling systems at the Echo and Pioneer sites recorded tracking data for computer analysis to determine accurately the Mariner position and to record spacecraft telemetery. The data-handling system recorded the time-labeled tracking data—antenna pointing angles, Doppler data, and a quality code on paper tape in teletype code. The tracking data were then transmitted via teletype to the Central Computing Facility at the Jet Propulsion Laboratory. The instrumentation system at each site consisted of the phase-lock discriminators and the recording equipment necessary to record the telemetry signal from the receiver supplementary wideband telemetry channel. At each site, the recording equipment consisted of two seven-track magnetic-tape recorders, an ultraviolet oscillograph, and a hot-stylus recorder. These instruments also recorded site performance information. The magnetic-tape records were used for subsequent detailed analysis of the data, while the oscillograph records provided data for quick-look analysis.

At the Echo and Pioneer sites, the antenna was positioned by an electro-hydraulic servosystem which used the error signals from the receiver to position the antenna so that the error signals were nulled. Hydraulic drive systems were

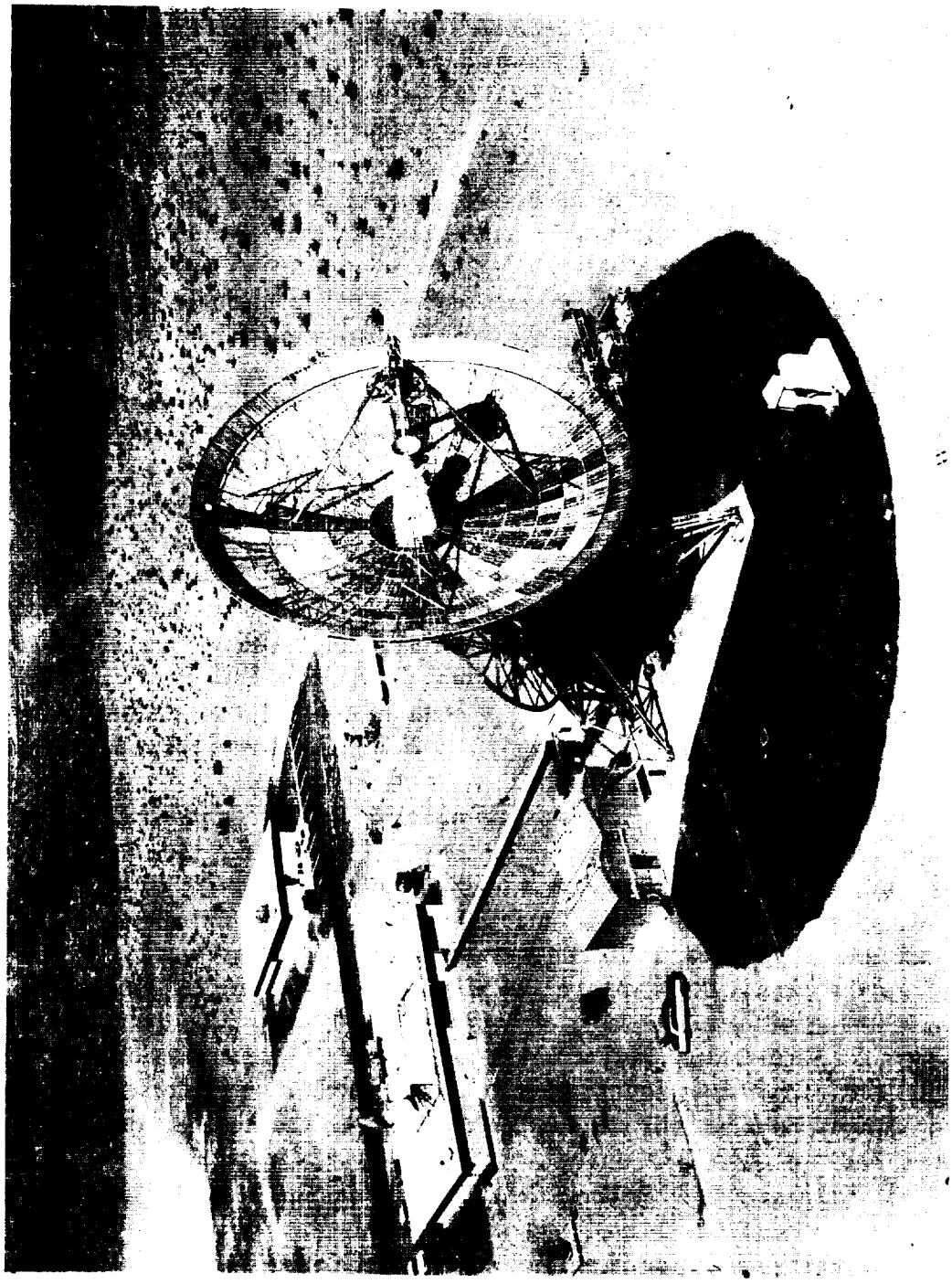

FIGURE 7–9.—DSIF Tracking Station at Goldstone (Pioneer site).

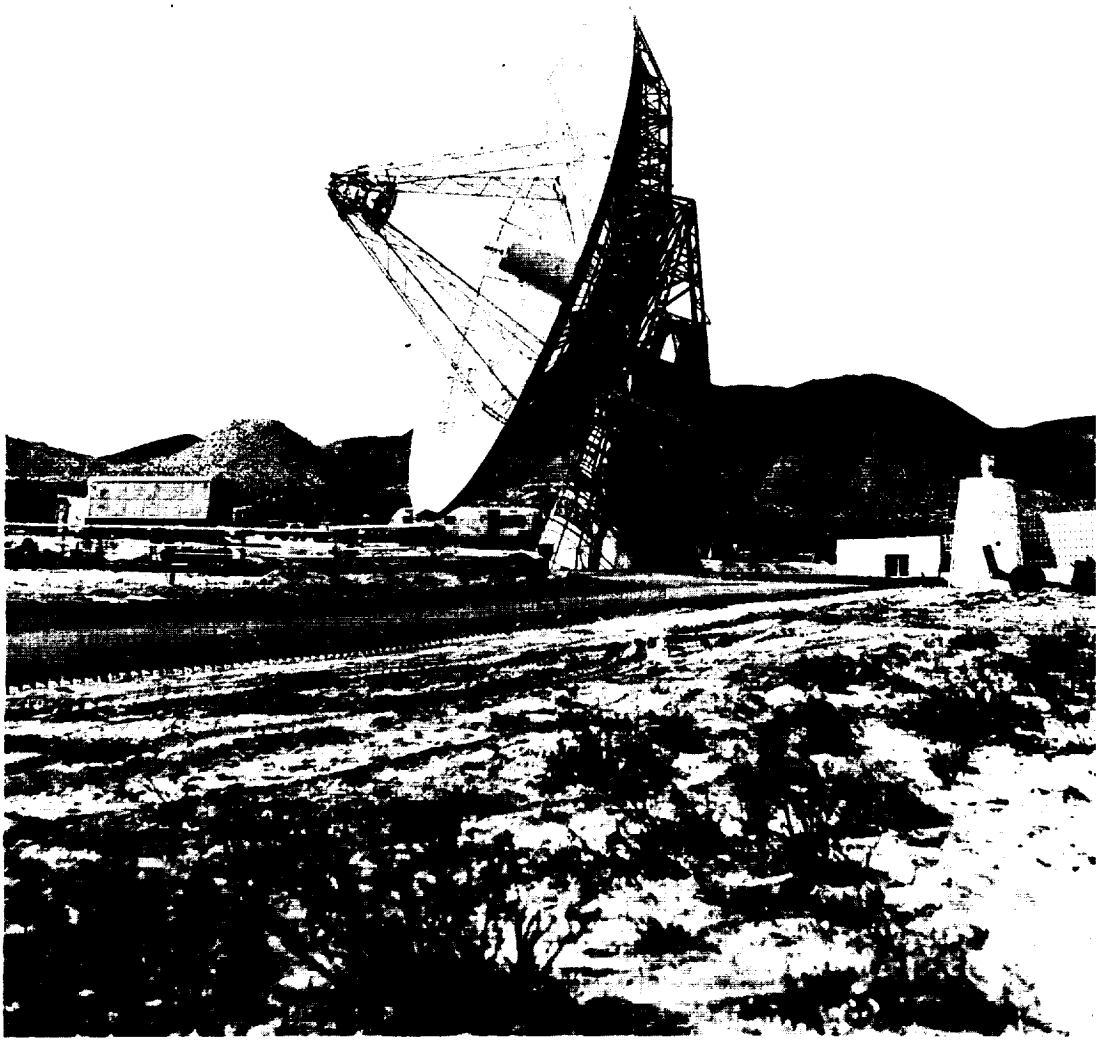

FIGURE 7–10.—DSIF Tracking Station at Goldstone (Echo site).

used because they produced no electrical interference and had a high stiffness. Two-speed drive systems were employed at each site to provide the speed capability required for tracking spacecraft or an orbiting satellite. The low-speed antenna rates were 0.001 to 0.030 deg/sec for both axes. The high-speed rates ranged from 0.020 to 1 deg/sec for hour-angle and from 0.20 to 0.8 deg/sec for declination. The antennas can be operated in winds up to 45 mph and can be driven to the stowed (minimum wind load) position in winds up to 60 mph. In the stowed position, the antennas can withstand winds of 120 mph.

Launch Station, Cape Canaveral

The Launch Station was located at Cape Canaveral, Fla., near Launch Complex 12. (See fig. 7–11.) The station had two trailers, one for the transmitter and receiver and the other for test equipment, recording equipment, and equipment for processing portions of the received signal for real-time display on strip charts; a 6-ft-diameter dish antenna for receiving and transmitting; and a collimation tower for calibrating and checking station equipment. The tower simulated the spacecraft for checkout procedures, transmitting on the frequencies used by Mariner.

Mobile Tracking Station, Johannesburg

During the Mariner mission, the mobile station was located approximately 1 mile east of the DSIF station at Johannesburg, South Africa. The Mobile Tracking Station was used primarily to obtain data near the Mariner II injection point. The station had a 10-ft parabolic antenna reflector that was capable of tracking 10 deg/sec. (See fig. 7–12.) A circular polarized tracking antenna feed was mounted at the antenna reflector focal point. In addition to the standard receiving equipment, a 25-w, 890-mc/s transmitter was diplexed on the antenna for the purpose of obtaining precision two-way Doppler data. Angle and precision Doppler data were transmitted to JPL by teletype in real time.

Adequate support equipment is an important logistic factor in maintaining the Mobile Tracking Station in remote areas. An office van provided administrative space and also a central location for site documentation. Master patch panels were located in this van for the tactical intervan intercom system, a paging system, a five-key telephone system, and a full duplex teletype terminal. Backup communications equipment consisted of a teletype converter and an S-line communications receiver and 2-kw transmitter. Power for the MTS was provided by four 75-kw diesel-driven generators and two 400-cps converters.

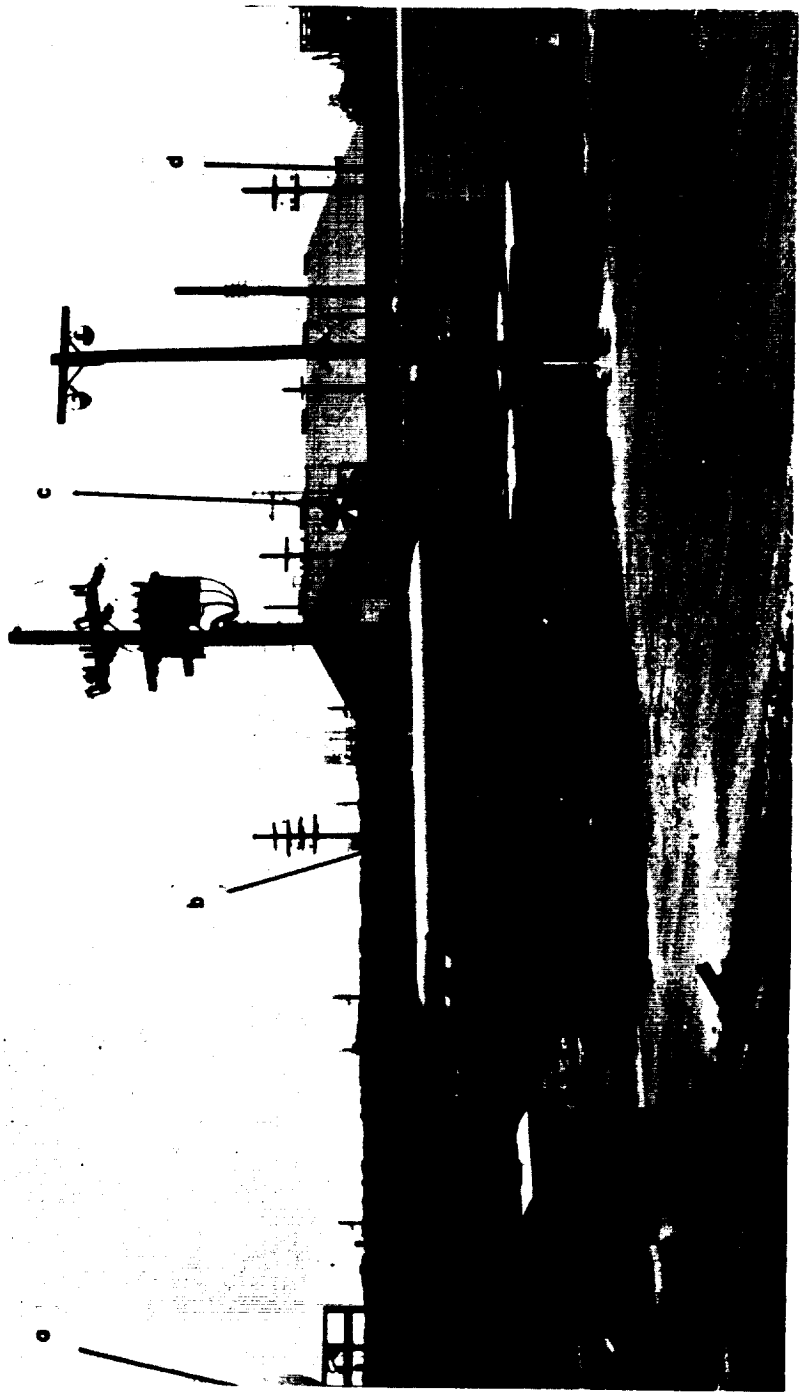

FIGURE 7-11.—Spacecraft Monitoring Station, Cape Canaveral. (a) Receiving and transmitting antenna, (b) transmitter and receiver trailer, (c) checkout antenna (collimation), (d) telemetry trailer.

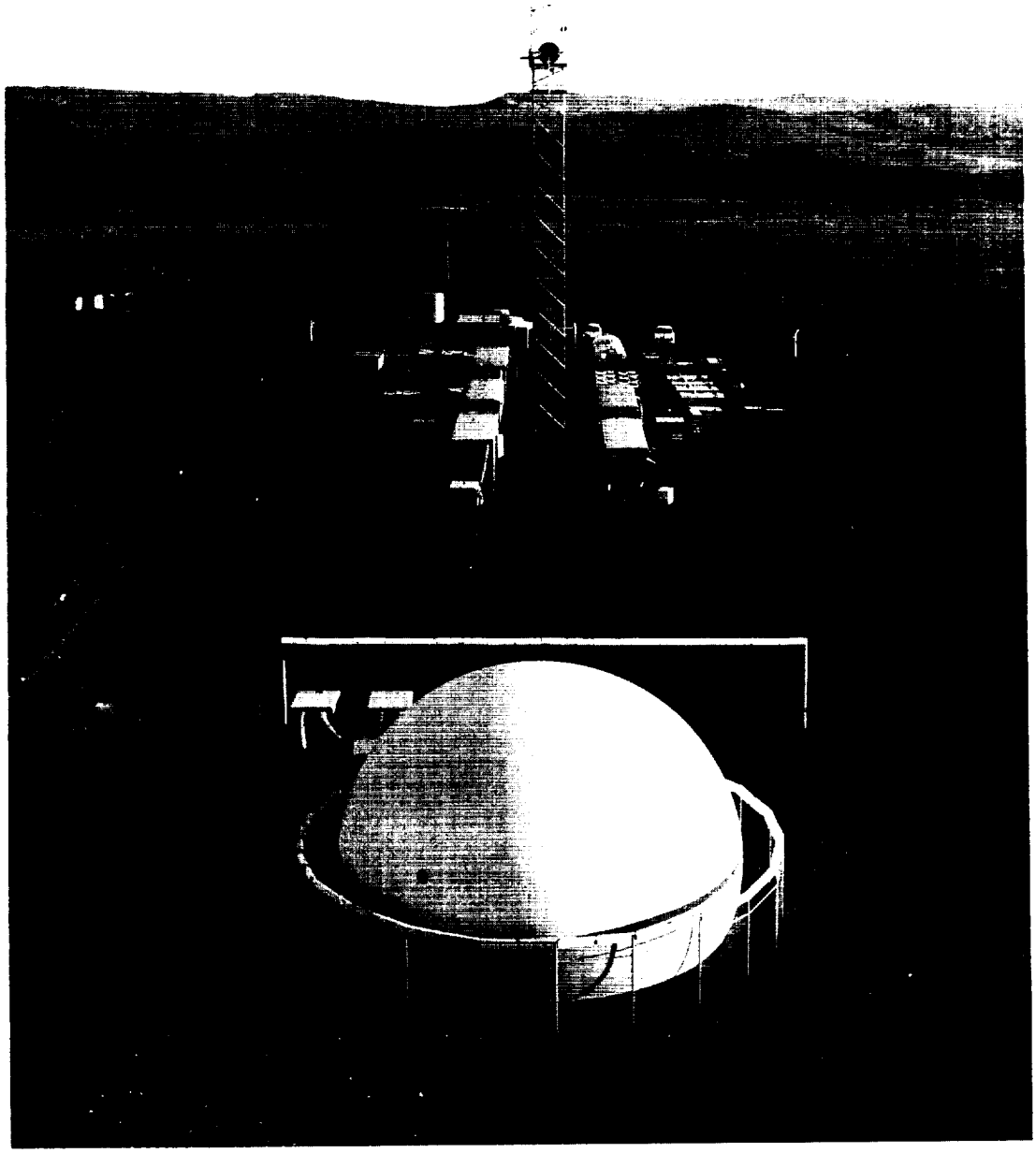

FIGURE 7–12.—DSIF Mobile Tracking Station, South Africa.

Magnetic switches allowed for instantaneous transfer to load in the event of failure of either generators or converters. Diesel fuel was stored in a 4000-gallon fuel tanker. The rear of this tanker held spares for the air-conditioning equipment (provided for each van) and for power generation equipment. A spare-parts van held spare modules, test equipment, and miscellaneous hardware and tools.

Deep Space Communication Station, Johannesburg

The Johannesburg Deep Space Station was staffed by personnel from the National Institute of Telecommunications Research (NITR) of the South African Council for Scientific and Industrial Research and was sponsored by NASA and technically directed by JPL as part of the Deep Space Instrumentation Facility.

The South African station is located in a bowl-shaped valley, approximately 40 miles northwest of Johannesburg (figs. 7–13 to 7–17). Its facilities included a steerable, 85-ft-diameter, parabolic reflector antenna and associated drive system, radio-tracking and receiving equipment, and data recording and transmitting equipment. The antenna-reflector surface was polar mounted (moving parallel in hour-angle and perpendicular in declination to the Earth's equatorial plane) and had a pointing accuracy of better than 0.1°. The tracking system comprised a simultaneous lobing antenna feed supported at the focus of the reflector by a quadripod, a parametric low-noise amplifier, a phase-coherent receiving system, and an electrohydraulic servosystem. The receiver system detected a signal transmitted from the spacecraft and, from a combination of the antenna feed signals, provided a pointing error signal which was used by the servosystem to position the antenna. This station had a phase-locked 960-mc/s receiver diplexed with a 10-kw 890-mc/s transmitter to provide both precision two-way Doppler and spacecraft command capability. The station provided telemetry angle and precision Doppler data readouts for real-time data transmission to JPL by teletype.

Deep Space Communication Station, Woomera

The Woomera Deep Space Station was operated by the Australian Department of Supply and is also sponsored by NASA and technically directed by JPL as part of the Deep Space Instrumentation Facility capable of tracking, commanding, and receiving telemetry from deep space vehicles. Geographically the Australian Station is located 15 miles from Woomera village in south central Australia (fig. 7–18). The facilities were almost identical to those at Johannesburg, South Africa. (See figs. 7–19 to 7–22.)

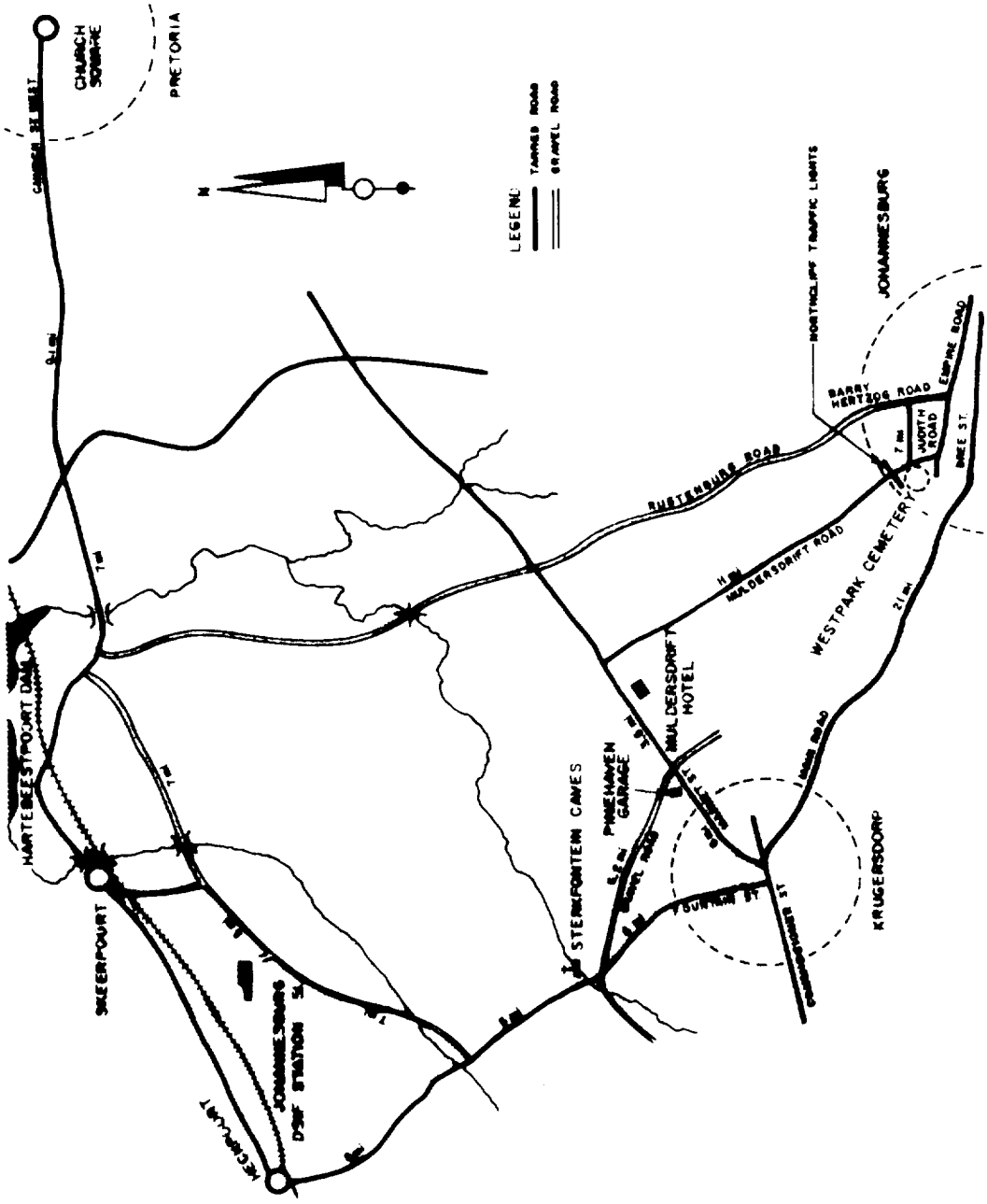

FIGURE 7–13.—Area map of Johannesburg Station.

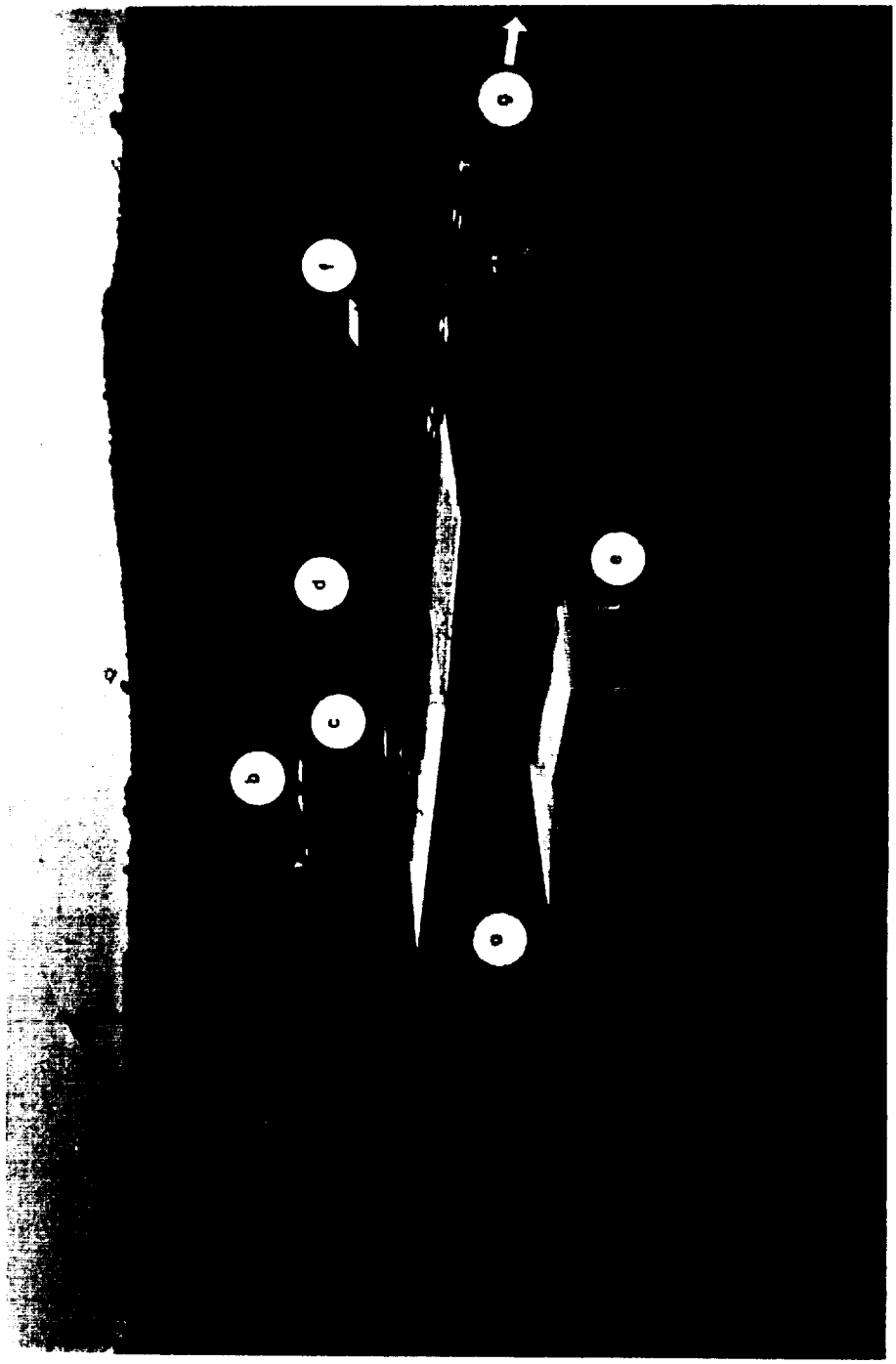

FIGURE 7–14.—Johannesburg Station. (a) Control building, (b) station personnel housing, (c) guard house, (d) mess and recreation building, (e) hydro-mechanical building, (f) dormitory, (g) to transport and generator building.

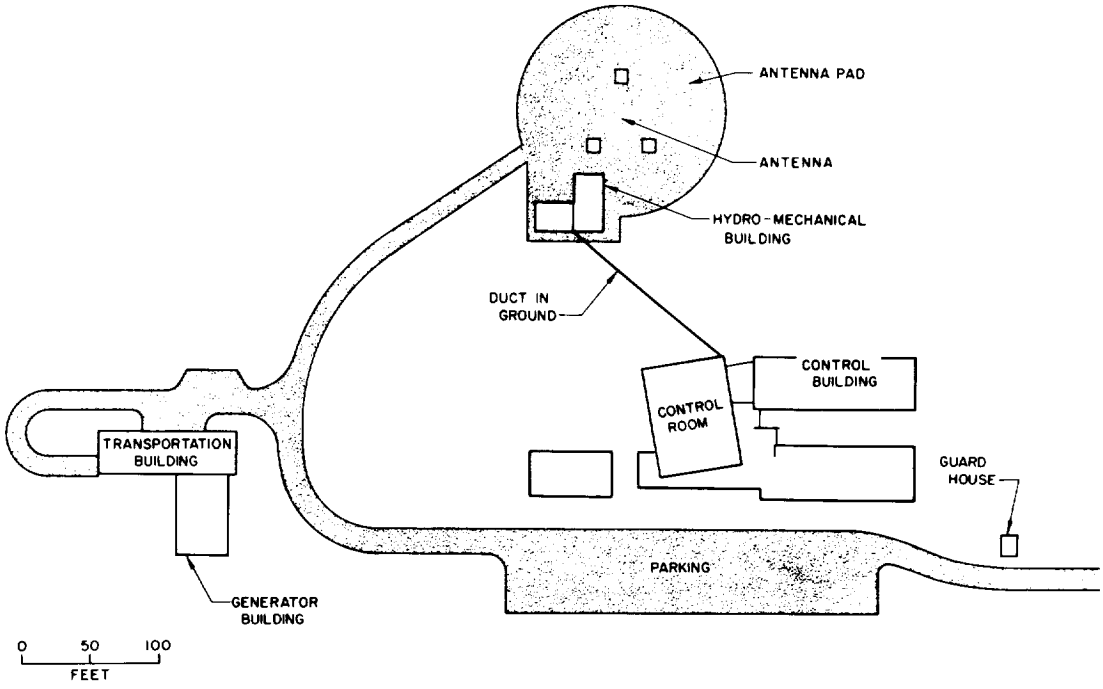

a. STATION MAP

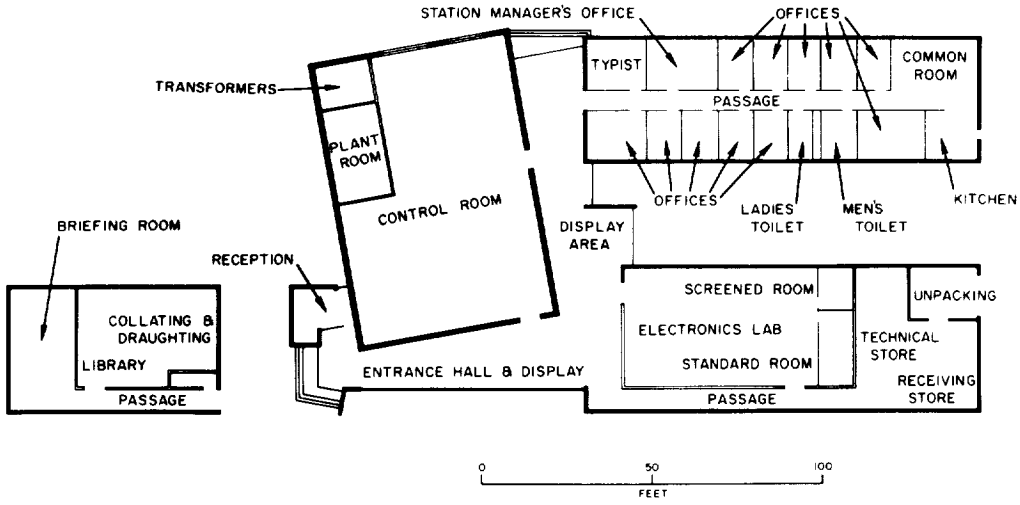

b. CONTROL BUILDING

FIGURE 7–15.—Johannesburg Station.

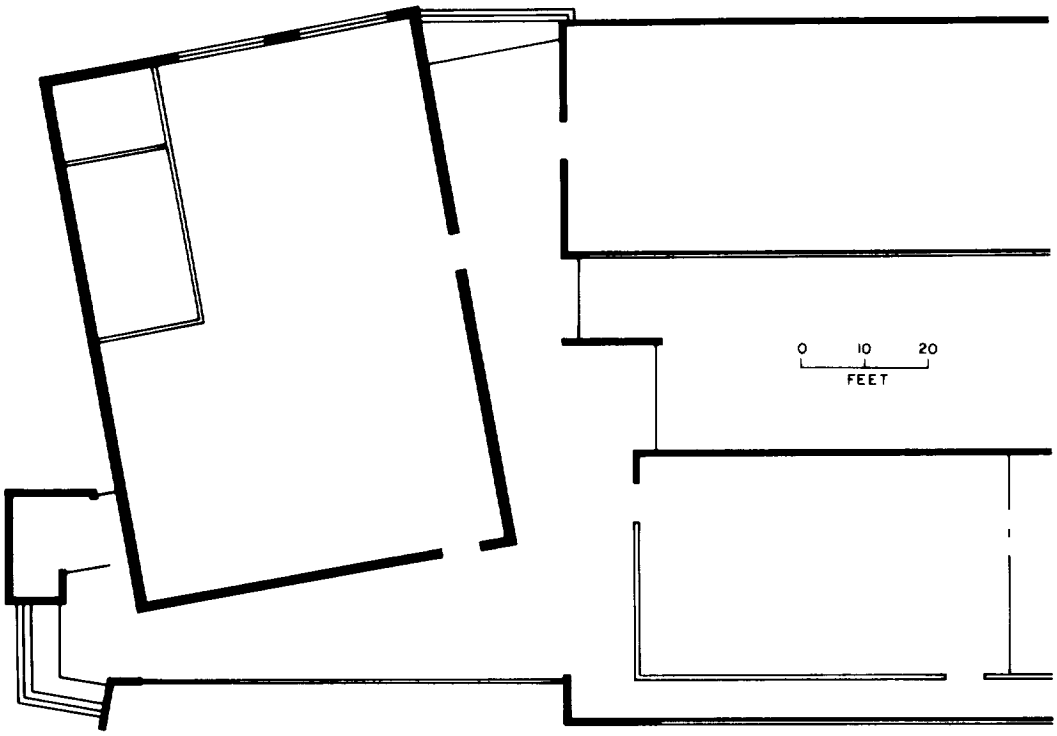

a. CONTROL ROOM

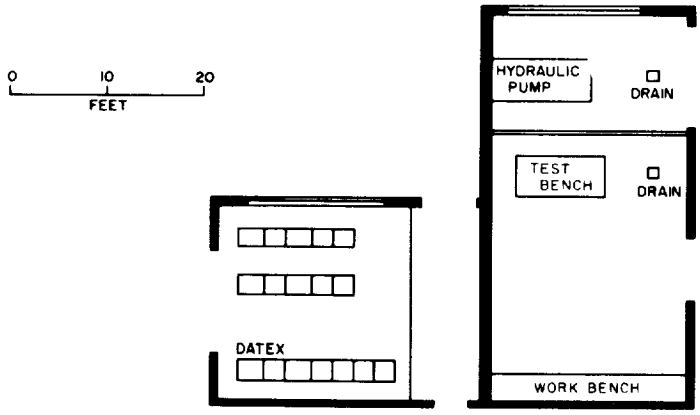

b. HYDRO-MECHANICAL BUILDING

FIGURE 7–16.—Johannesburg Station.

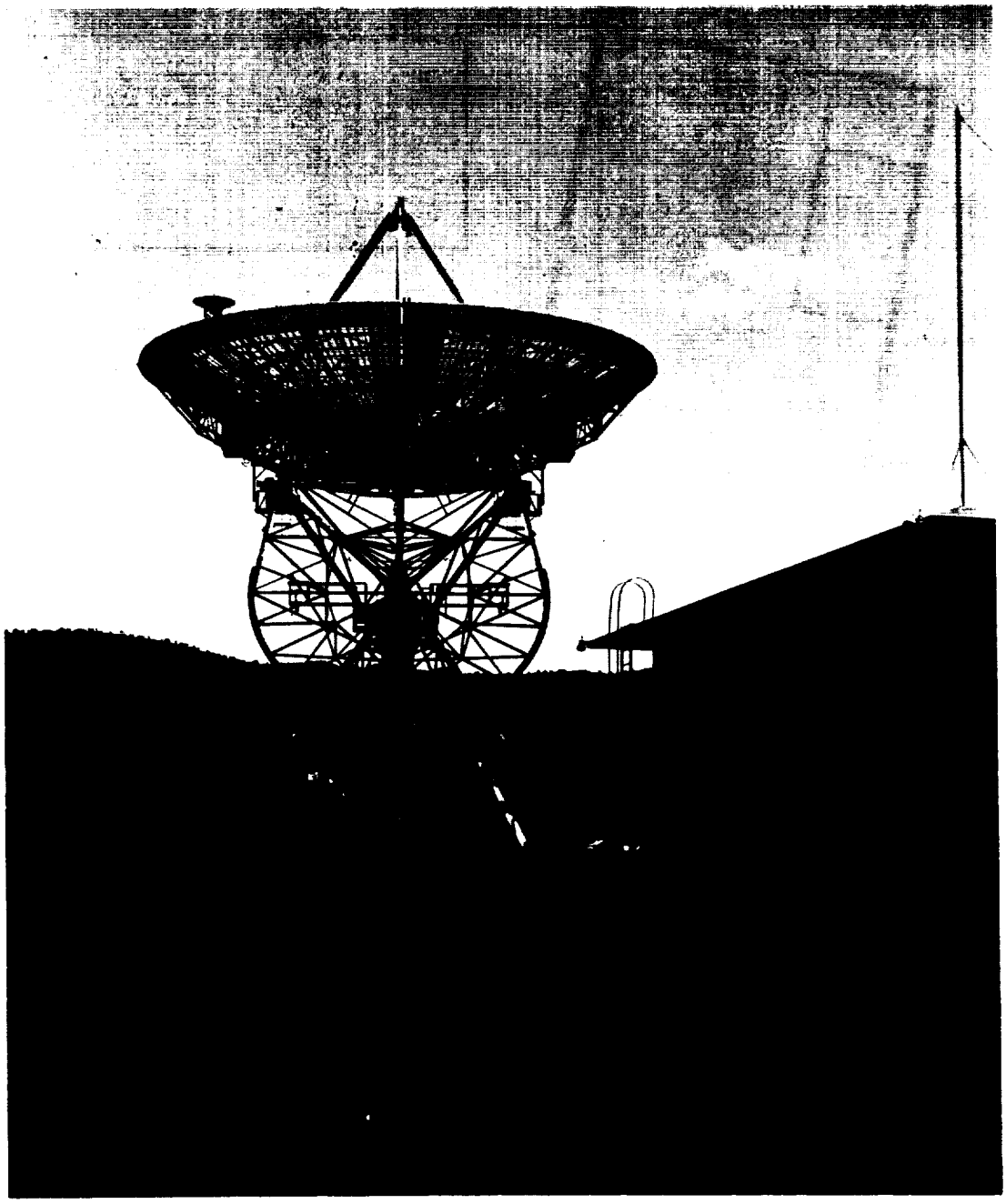

FIGURE 7–17.—DSIF Tracking Station at Johannesburg.

The station provided angle and two-way Doppler data readouts on Mariner II for real-time transmission to JPL by teletype. The telemetry demodulator output was encoded in a suitable format and transmitted to JPL in near-real time.

DSIF Operations

The DSIF operations manager occupied a console beside the test director in the main operations room, which was also shared by the DSIF advisers. The DSIF Net Control, which functioned for the first time in this mission as an integral portion of the Space Flight Operations Center, was located in a room adjacent to and behind the main operations room. Net Control advised the operations manager of the current status of each station over a private phone line. In turn, the operations manager advised Net Control of changes in the test plan, so that Net Control might then advise the DSIF stations. During critical portions of the mission, long-distance telephone contact was established with the overseas DSIF stations; teletype communications were maintained almost continuously.

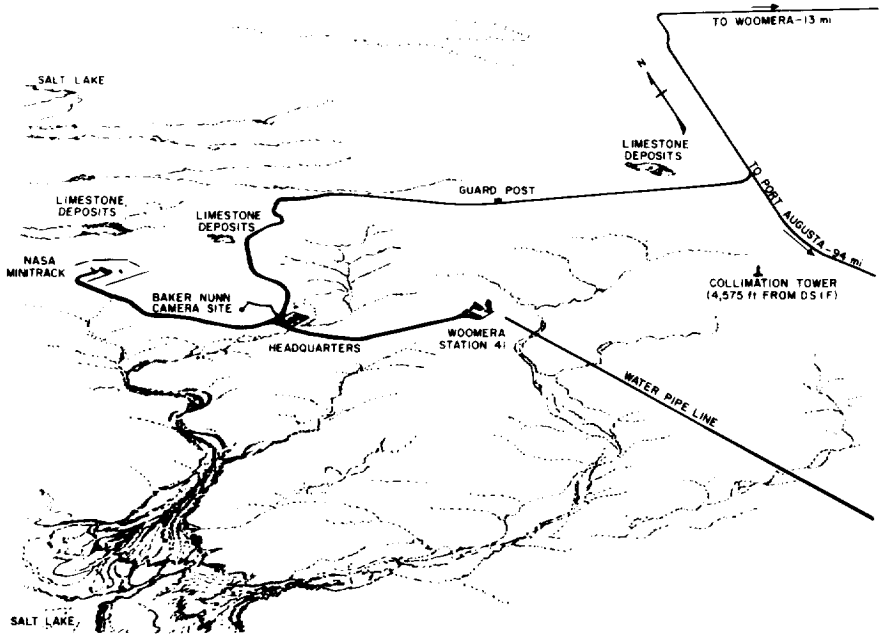

FIGURE 7–18.—Area map of Woomera Station.

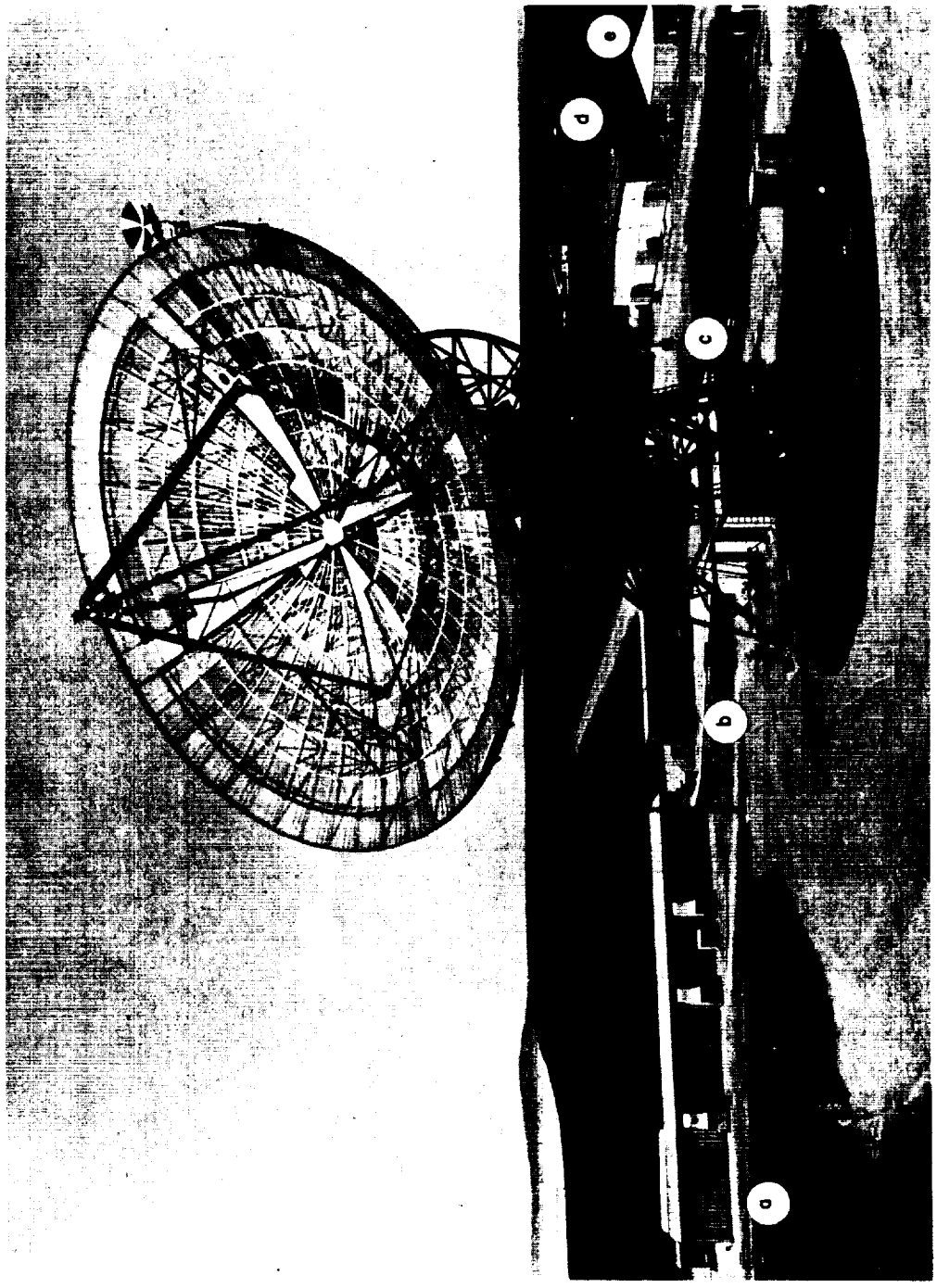

FIGURE 7–19.—Woomera Station. (a) Control building, (b) trailer shed, (c) hydro-mechanical building, (d) generator building, (e) water tank.

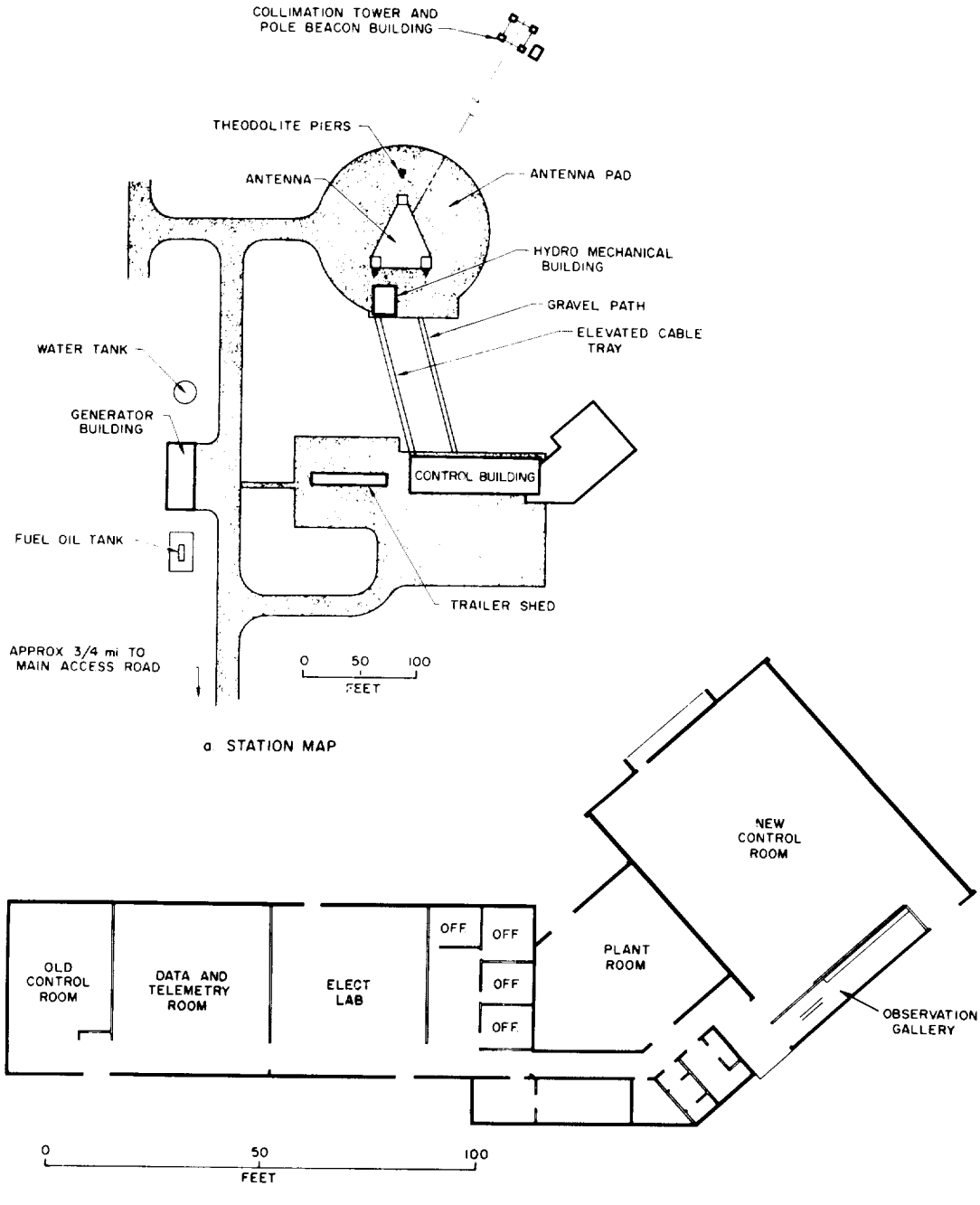

FIGURE 7–20.—Woomera Station.

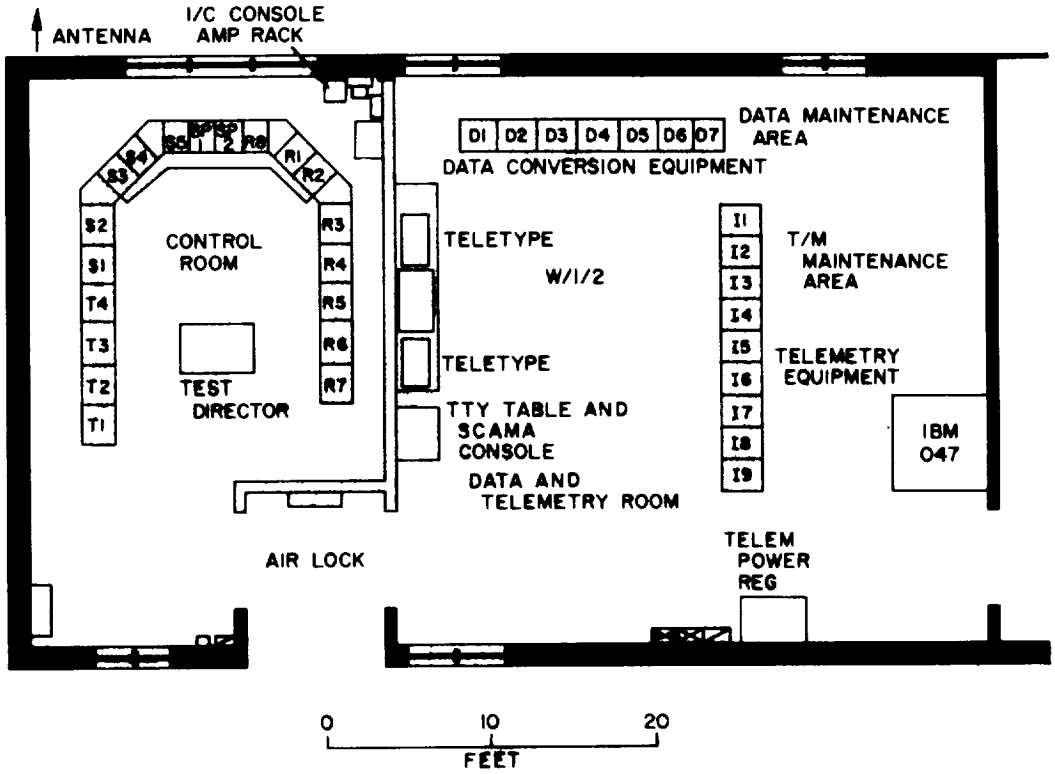

a. CONTROL AND INSTRUMENTATION ROOMS

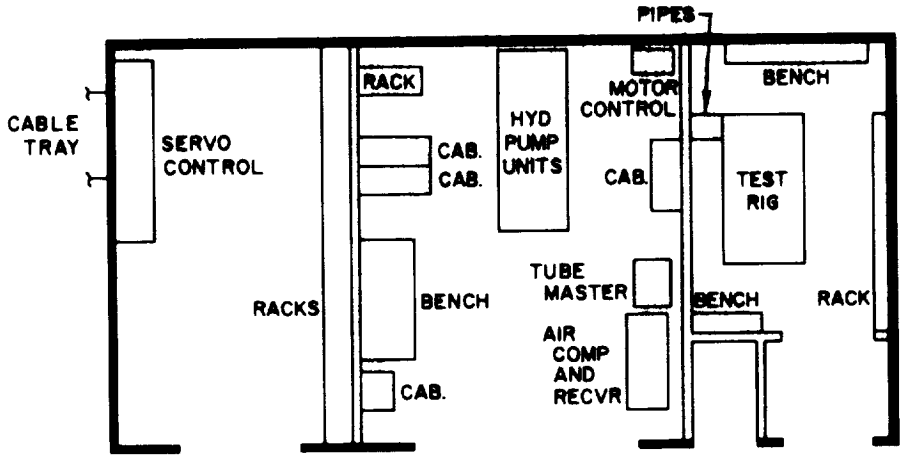

b. HYDRO-MECHANICAL BUILDING

FIGURE 7–21.—Woomera Station.

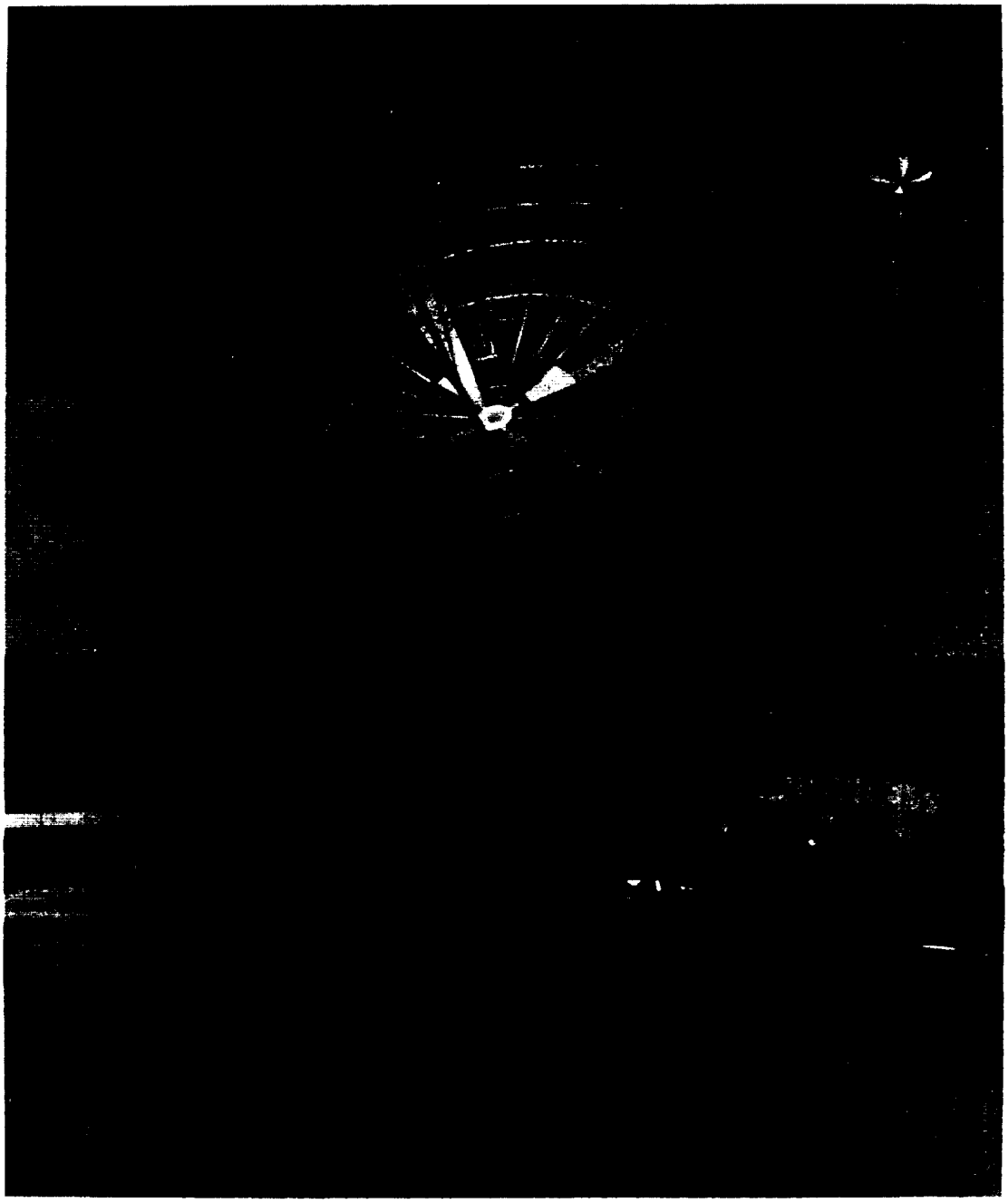

FIGURE 7–22.—DSIF Tracking Station at Woomera.

The following paragraphs outline, in chronological sequence, the major features of the DSIF operation during the Mariner II flight. Figure 7–23 shows the locations and ranges of the major DSIF installations throughout the world.

Following lift-off at 06:53:14 on August 27, DSIF 0 (at AMR) was in lock and maintained lock with the spacecraft until 07:00:56. The received-signal level varied between −80 and −125 dbm. After the signal was lost over the horizon of DSIF 0, various AMR stations tracked the space vehicle and, at 07:21:37, DSIF 1 (the mobile tracking station) acquired Mariner II in one-way lock; 3 min later, DSIF 5 (Johannesburg) had also acquired the spacecraft in one-way lock.

After this initial acquisition, DSIF 1 achieved two-way lock at 07:30:20. The DSIF 1 transmitter was turned off at 07:48:00, since DSIF was having difficulty maintaining pseudo-two-way lock. DSIF 5 turned on its transmitter at 08:12:00 and began radiating 200 w, attempting to obtain two-way lock until 08:39:00, when it was instructed to turn its transmitter off. During the period in which DSIF 5 was trying to acquire two-way lock, both DSIF 1 and DSIF 4 (Woomera) were tracking the spacecraft, with intermittent loss of lock. DSIF 4 acquired the spacecraft at 07:37:00 in one-way lock, with a received-signal level of −110 dbm. At 08:44:32, DSIF 4 acquired two-way lock with a radiated power of 58 w. After this initial period, there were few problems in obtaining two-way lock. The initial difficulties were those attributable to tracking an unstabilized spacecraft using a very narrow bandwidth transponder.

The first command was sent to the spacecraft on August 29 from DSIF 5: RTC–8, transmitted at 16:13:00 and verified at 16:13:57. This command changed the telemetry to the cruise mode, switched on cruise science, and reduced the telemetry-transmission bit rate from 33⅓ to 8⅓ BPS. This command transmission was a deviation from the operations plan, in that the telemetry mode change was to have been effected by an internal command in the spacecraft. After this time, the DSIF continued to track the spacecraft on a 24-hr/day basis, as outlined in table 7–I.

The midcourse maneuver command sequence was performed completely from the Goldstone stations; DSIF 2 functioned as the receiving station and DSIF 3 as the transmitting station. The command loop was locked up by DSIF 3 at 21:01:00, after which the transmission of commands was as shown in table 7–II. The received-signal level at DSIF 2 was −129 dbm before the spacecraft started the midcourse maneuver. During the maneuver, the received-signal level dropped as low as −162 dbm. Several momentary out-of-lock

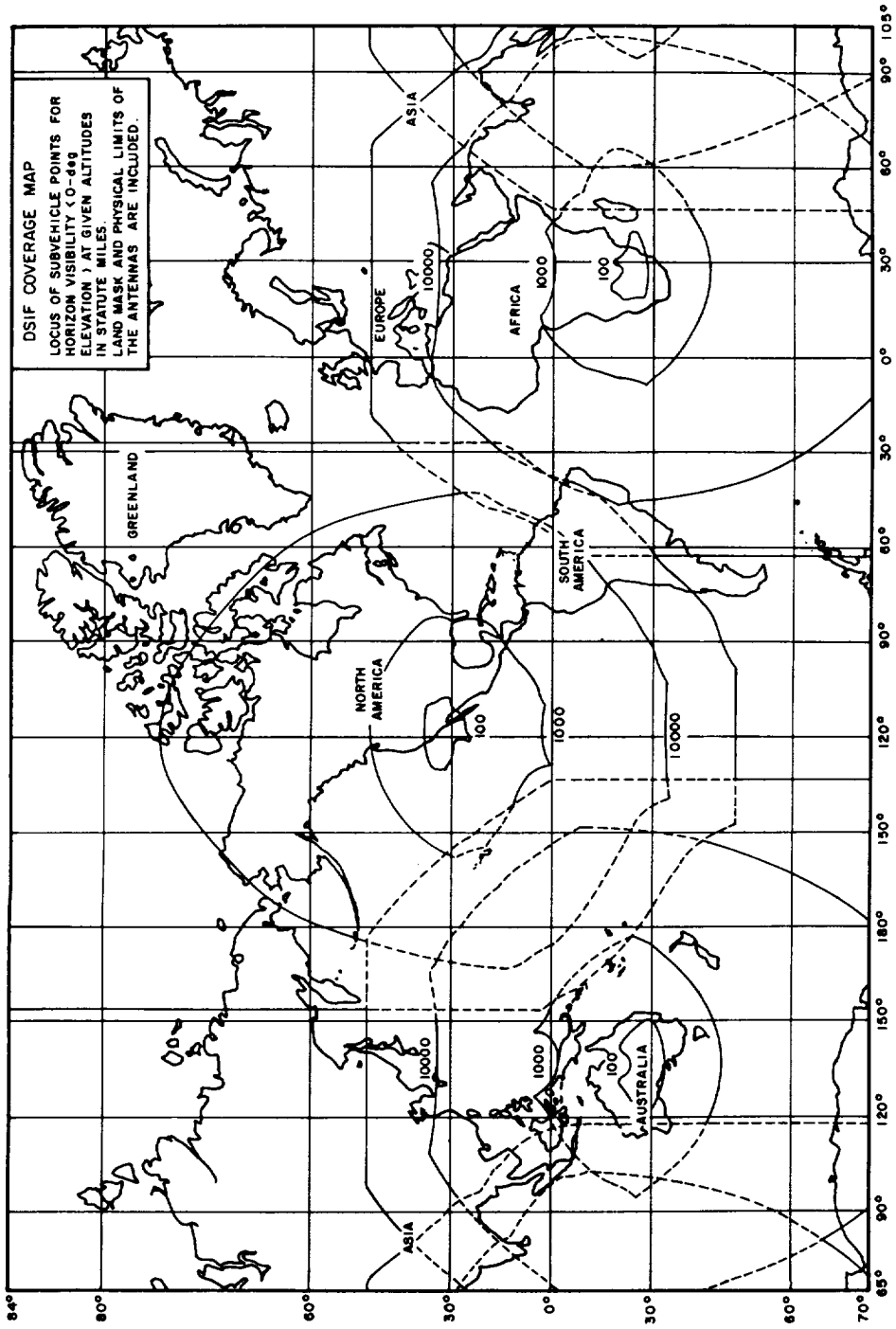

FIGURE 7-23.—Station locations and ranges for worldwide Deep Space Instrumentation Facility.

Table 7-I.—Summary of DSIF operations, launch to midcourse

DSIF station	Pass	Date, 1962	Time of acquisition, GMT	Time of loss, GMT	Maximum received-signal strength, dbm	Remarks
1	1	Aug. 27	07:21:37	21:08:46	−100	Two-way lock at 07:30:38. Trouble at DSIF 1 in maintaining two-way lock. Also, trouble in data system, resulting in loss of approximately 2 hr of data.
5	1		07:31:45	21:04:35	−82	Initial attempts to obtain two-way lock not successful. Two-way lock acquired at 10:02.
4	1		07:37:30	13:18:00	−110	Two-way lock at 08:44:43. Receiver in- and out-of-lock between 08:14 and 08:44 while DSIF 5 was attempting two-way lock.
2	1		19:34:05	03:31:20	−122	Variations of 12 db in received signal noted, caused by MASER and PARAMP drift. Two-way lock at 20:12.
3	1		20:12:15	03:31:20		Transmitter power, 7 kw.
4	2	Aug. 28	01:48:00	13:52:00	−128	Two-way lock at 03:01:13.
5	2		09:35:48	21:10:35	−132.5	No telemetry data sent by teletype until 11:27 because of telemetry demodulator difficulties.
2	2		19:37:30	06:09:00	−132	MASER bypassed for this tracking period. Two-way lock at 20:26:23.
3	2		20:00:35	06:09:00		
4	3	Aug. 29	01:51:10	13:58:00	−134.5	Two-way lock at 06:10.
5	3		09:34:34	21:06:40	−126	Two-way lock from 11:51 to 20:18. RTC–8 transmitted at 16:13:00.
2	3		19:41:00	06:25:45	−138.2	Two-way lock at 20:01:49.
3	3		20:01:49	05:48:00		
4	4	Aug. 30	01:51:30	13:57:00	−138	Two-way lock at 05:53.
5	4		09:40:20	21:02:20	−142	Two-way lock at 13:20:50.
2	4		19:32:00	06:27:48	−137	Two-way lock at 21:05:45; MASER back in operation.
3	4		20:05:00	06:27:00		

Table 7-I.—Summary of DSIF operations, launch to midcourse—*Concluded*

DSIF station	Pass	Date, 1962	Time of acquisition, GMT	Time of loss, GMT	Maximum received-signal strength, dbm	Remarks
4	5	Aug. 31	01:46:00	13:53:06	−140	50-w transmitter at DSIF 4 not used after Aug. 30.
5	5		09:32:05	21:01:01	−140.5	Two-way lock at 09:33:15. Scheduled transmitter-power decrease from 400 w to 20 w to determine transponder threshold.
2	5		19:28:15	06:21:40	−138	Two-way lock at 19:30:25.
3	5		19:20:00	06:20:00		
4	6	Sept. 1	01:53:00	13:50:00	−142.5	
5	6		09:30:00	20:56:35	−142	Listening feed installed before this track.
2	6		19:23:00	06:20:21	−142	Considerable variation in received-signal level because of MASER and PARAMP gain variation.
3	6		19:25:00	06:20:00		
4	7	Sept. 2	01:44:00	13:41:00	−144	
5	7		11:58:15	19:56:00		Attempt for two-way lock prevented by noise problem in transmitter.
2	7		19:20:30	06:16:00	−128	Received-signal level, −145 dbm before Earth acquisition. Two-way lock at 19:20:30.
3	7		19:20:00	06:15:00		
4	8	Sept. 3	01:41:00	13:38:00	−124	Decrease in received-signal level to −161 dbm and lock-drop by receiver before Earth acquisition.
5	8		13:45:00	20:51:34	−125	
2	8		19:15:50	06:14:00		Two-way lock at 19:27:00.
3	8		19:27:00	06:15:00		
4	9	Sept. 4	01:40:00	13:42:00	−125	
5	9		09:15:62	20:47:40		Two-way lock at 09:18:27.
2	9		19:09:00	06:00:29	−129	Decrease in signal level to −156 dbm during midcourse maneuver.
3	9		19:09:00	06:00:00		Commands transmitted for midcourse maneuver.

Table 7–II.—Midcourse maneuver command sequence

Command	Time initiated, GMT	Time transmitted, GMT	Time verified, GMT
SC–1	21:30:00	21:30:32	21:30:57
SC–2	21:32:00	21:32:31	[a] Inhibited
SC–2	21:35:00	21:35:30	21:35:57
SC–3	21:37:00	21:37:28	[a] Inhibited
SC–3	22:23:00	22:23:28	22:23:56
RTC–4	22:39:00	22:39:31	22:39:58
RTC–6	22:49:00	22:49:29	22:49:57

[a] When SC–2 was inhibited, the cause was assumed to be a momentary loss of sync between the *read-write-verify* (RWV) modulator and detector. When SC–3 was inhibited, a thorough investigation showed the temperature in the modulator compartment of the RWV system to be much lower than normal. The compartment was left open, allowing the temperature to rise, and the system then functioned normally throughout the remainder of the command sequence.

periods were experienced by DSIF 2 during this time. At the completion of the maneuver, the received signal returned to −130 dbm at 02:34:45.

At 01:30:23, DSIF 4 acquired with a received-signal level of −152 dbm, and was in- and out-of-lock until 02:34:27, at which time the received-signal level increased to −130 dbm. Good data were obtained throughout the remainder of the tracking period.

The DSIF was originally committed to provide 24-hr/day coverage from launch (L) through $L+10$ days, 10-hr/day tracking during the cruise phase, and 24-hr/day coverage through September 9, after which date its coverage was reduced to approximately 12 hr/day. On September 16 the DSIF returned to the 24-hr/day schedule and remained on that basis until the encounter phase was completed (table 7–III).

Mariner II was programmed to encounter Venus during a Goldstone view period. Telemetry data obtained prior to the encounter data indicated that it would be necessary to transmit RTC–7 to command the spacecraft to the encounter mode. DSIF 2 acquired the spacecraft signal in one-way lock at 12:16 on December 14, and two-way lock was obtained at 12:24. DSIF 3 turned on command modulation at 12:42 and obtained command-loop lock and vehicle

sync at 12:56. RTC–7 was initiated at 13:35:00 and verified by the spacecraft at 13:35:57. At 13:46, DSIF 2 confirmed that the spacecraft was in the encounter mode, and DSIF 3 turned off command modulation at 13:51. At 20:20, DSIF 3 turned on command modulation; RTC–8, the command to end the encounter mode and return to cruise mode, was initiated at 20:32:00 and verified at 20:32:57. Command modulation was turned off at 20:43, and DSIF 3 turned off the transmitter at 22:10. DSIF 4 acquired the spacecraft signal at 18:10; therefore, two DSIF stations were receiving the spacecraft telemetry during the planet scan. Both DSIF 2 and DSIF 3 were secured at 22:11. DSIF 3 radiated 10 kw throughout the encounter phase. The received-signal level at DSIF 2 was approximately −150.5 dbm throughout the period.

Table 7–III.—Summary of DSIF operations, midcourse to end of mission

DSIF station	Pass	Date, 1962	Time of acquisition, GMT	Time of loss, GMT	Maximum received-signal strength, dbm	Remarks
4	10	Sept. 5	01:30	13:31	−125	
5	10		09:19	20:43	−126	Two-way lock from 09:56–18:50.
2	10		19:04	06:00	−127	Two-way lock at 19:15.
3	10		19:15	06:00		
4	11	Sept. 6	01:40	13:34	−128	
5	11		09:07	19:14	−125.5	Two-way lock from 09:22–18:50.
2	11		19:00	06:10	−127	Two-way lock at 19:40.
3	11					
4	12	Sept. 7	01:20	13:31	−127.5	
5	12		09:00	20:36	−126.5	Two-way lock from 09:36–18:50.
2	12		18:57	06:05	−128.5	Two-way lock at 18:59.
3	12		18:59	06:00		
4	13	Sept. 8	01:15	13:27	−126	
5	13		09:02	19:50	−127.5	Two-way lock from 09:28–18:45.
2	13		18:53	06:01	−130	Two-way lock at 18:53.
3	13		18:53	06:00		
4	14	Sept. 9	03:52	10:00	−128	
5	14		08:54	20:28	−128.5	One-way lock.
2	14		18:48	05:55	−126.5	One-way lock.
3	14					Not scheduled.

Table 7–III.—Summary of DSIF operations, midcourse to end of mission—*Continued*

DSIF station	Pass	Date, 1962	Time of acquisition, GMT	Time of loss, GMT	Maximum received-signal strength, dbm	Remarks
4	15	Sept. 10				Not scheduled.
5	15		08:50	20:20	−129.5	One-way lock.
2	15		18:39	05:48	−131	One-way lock.
3	15					Not scheduled.
4	16	Sept. 11	01:04	13:15	−130	
5	16					Not scheduled.
2	16					Not scheduled.
3	16					Not scheduled.
4	17	Sept. 12				Not scheduled.
5	17		09:01	20:13	−132	One-way lock.
2	17					Not scheduled.
3	17					Not scheduled.
4	18	Sept. 13	00:55	13:05	−132.5	
5	18		00:	00:		Not scheduled.
2	18		18:31	05:40	−133	One-way lock.
3	18					Not scheduled.
4	19	Sept. 14				Not scheduled.
5	19		08:48	20:06	−131.5	
2	19		18:28	05:27	−132	Two-way lock at 18:38.
3	19		18:37	05:20		
4	20	Sept. 15	00:55	09:00	−131	
5	20		08:29	20:01	−132.5	
2	20					Not scheduled.
3	20					Not scheduled.
4	21	Sept. 16	00:42	12:52	−131.5	
5	21					Not scheduled.
2	21		18:20	03:15	−132	One-way lock.
3	21					Not scheduled.
4	22	Sept. 17	02:38	11:00	−131.5	
5	22		10:30	19:15	−132	
2	22		18:30	04:00	−132	One-way lock.
3	22					Not scheduled.

Table 7-III.—Summary of DSIF operations, midcourse to end of mission—*Continued*

DSIF station	Pass	Date, 1962	Time of acquisition, GMT	Time of loss, GMT	Maximum received-signal strength, dbm	Remarks
4	23	Sept. 18	03:20	12:30	−131.5	
5	23		11:45	19.00	−132	
2	23		18:30	03:00	−132.5	One-way lock.
3	23					Not scheduled.
4	24	Sept. 19	02:26	11:00	−134	
5	24		10.33	19:00	−132.5	
2	24		18:30	03:00	−132.5	One-way lock.
3	24					Not scheduled.
4	25	Sept. 20	02:13	11:00	−134. 5	
5	25		10:30	18:45	−133. 5	
2	25		18:15	02:45	−134	One-way lock.
3	25					Not scheduled.
4	26	Sept. 21	02:11	10:45	−134. 7	
5	26		10:08	18:46	−133	
2	26		18:15	02:45	−130	One-way lock.
4	27	Sept. 22	02:05	10:45	−133. 8	
5	27		10:15	18:45	−134	
2	27		18:08	04:45	−135	Two-way lock at 18:08.
3	27		17:58	04:45		
4	28	Sept. 23	02:08	10:45	−134	
5	28		10:12	18:57	−133. 5	
2	28		17:47	04:33	−135	Two-way lock at 17:57.
3	28		17:52	04:30		
4	29	Sept. 24	01:45	10:30	−135	
5	29		09:31	18:30	−134	
2	29		18:00	02:30	−134	One-way lock.
4	30	Sept. 25	01:57	10:30	−135	
5	30		09:45	18:30	−134	
2	30		17:40	03:00	−137	One-way lock.
4	31	Sept. 26	01:54	10:30	−135. 4	
5	31		10:02	18:30	−134. 5	
2	31		17:38	04:35	−135. 5	One-way lock.

Table 7-III.—Summary of DSIF operations, midcourse to end of mission—*Continued*

DSIF station	Pass	Date, 1962	Time of acquisition, GMT	Time of loss, GMT	Maximum received-signal strength, dbm	Remarks
4	32	Sept. 27	01:52	10:30	−136	
5	32		09:46	18:15	−135	
2	32		17:29	03:00	−135.5	One-way lock.
4	33	Sept. 28	01:46	10:15	−136.3	
5	33		09:45	18:15	−135	
2	33		18:07	02:45	−134.5	
4	34	Sept. 29	01:39	10:15	−135.7	
5	34		09:44	18:45	−135.1	
2	34		17:19	04:01	−136.3	Two-way lock at 17:19.
3	34		17:04	04:00		
4	35		23:51	10:00	−137.4	
5	35	Sept. 30	09:28	18:00	−136.1	
2	35		17:24	02:30	−136.5	One-way lock.
4	36	Oct. 1	01:25	11:00	−137.9	
5	36		09:30	18:00	−136.3	
2	36		17:08	02:30	−136.2	One-way lock.
4	37	Oct. 2	01:15	09:45	−137.8	
5	37		09:07	17:45	−136.4	
2	37		17:04	02:15	−136.5	One-way lock.
4	38	Oct. 3	01:11	09:45	−136.5	
5	38		09:06	17:45	−136	
2	38		16:58	02:15	−137.5	One-way lock.
4	39	Oct. 4	01:15	09:45	−138	
5	39		09:09	17:30	−136	
2	39		17:13	02:00	−137.5	One-way lock.
4	40	Oct. 5	01:00	09:30	−138.2	
5	40		08:58	17:30	−136.8	
2	40		16:51	02:00	−136.4	One-way lock.
4	41	Oct. 6	01:03	09:30	−138.1	
5	41		08:52	17:30	−137.7	
2	41		16:43	03:30	−136.4	One-way lock.
4	42	Oct. 7	00:42	09:15	−138.4	
5	42		08:45	17:15	−136	
2	42		16:50	02:00	−137.5	One-way lock.

Table 7-III.—Summary of DSIF operations, midcourse to end of mission—*Continued*

DSIF station	Pass	Date, 1962	Time of acquisition, GMT	Time of loss, GMT	Maximum received-signal strength, dbm	Remarks
4	43	Oct. 8	00:42	09:15	−139.1	
5	43		08:26	17:00	−137.7	
2	43		16:35	01:45	−139	One-way lock.
4	44	Oct. 9	00:26	09:00	−139.1	
5	44		08:51	17:00	−138.4	
2	44		16:25	01:45	−141.5	One-way lock.
4	45	Oct. 10	00:33	09:00		No signal strength due to AGC trouble.
5	45		09:01	16:15	−138.3	
2	45		16:28	23:15	−139.5	One-way lock.
4	46		23:00	08:15	−143.4	
5	46	Oct. 11	08:07	17:00	−134	
2	46		16:26	01:30	−139.2	One-way lock.
4	47	Oct. 12	00:23	09:00	−143.6	
5	47		08:11	17:02	−140.1	
2	47		16:17	01:30	−139	One-way lock.
4	48	Oct. 13	00:12	08:45	−143.4	
5	48		08:19	16:15	−139	
2	48		16:06	23:12	−139	
4	49		22:38	08:30	−149.9	
5	49	Oct. 14	08:09	17:15	−139.4	
2	49		16:16	03:00	−139.2	Two-way lock at 16:16.
3	49		15:30	02:50		
4	50		22:20	08:30	−144.6	
5	50	Oct. 15	07:59	16:50	−139.3	
2	50		15:54	01:30	−138.5	One-way lock.
4	51	Oct. 16	00:28	08:32	−139.4	
5	51		08:26	16:45	−139.4	
2	51		15:50	01:30	−139.5	One-way lock.
4	52	Oct. 17	00:45	09:00	−140	
5	52		08:00	16:30	−139.3	
2	52		16:03	01:17	−141	One-way lock.

Table 7–III.—Summary of DSIF operations, midcourse to end of mission—*Continued*

DSIF station	Pass	Date, 1962	Time of acquisition, GMT	Time of loss, GMT	Maximum received-signal strength, dbm	Remarks
4	53	Oct. 18	00:15	00:45	−140.5	
5	53		08:12	15:30	−142.1	
2	53		15:38	02:40	−140.3	One-way lock.
4	54	Oct. 19	04:35	09:58	−141	Late acquisition due to RA–5 tracking.
5	54		11:20	15:36	−141	
2	54		16:33	02:34	−140	One-way lock.
4	55	Oct. 20	03:46	09:52	−141.1	Late acquisition due to RA–5 tracking.
5	55		11:09	17:03	−141.1	
2	55		16:07	02:33	−141	One-way lock.
4	56	Oct. 21	03:46	00:48	−138.2	Late acquisition due to RA–5 tracking.
5	56		11:02	16:59	−141	
2	56		20:54	02:26	−142.5	One-way lock.
4	57	Oct. 22	03:42	09:41	−140.8	Late acquisition due to RA–5 tracking.
5	57		08:26	16:54	−143.1	
2	57		15:26	01:00	−142.5	One-way lock.
4	58		23:59	08:30	−139	
5	58	Oct. 23	08:00	16:30	−141.5	
2	58		15:21	01:00	−141.9	One-way lock.
4	59		23:38	08:15	−137.6	
5	59	Oct. 24	07:45	16:42	−141.7	
2	59		14:31	01:50	−141.5	Two-way lock at 14:38.
3	59		14:38	01:50		
4	60		22:42	08:11	−142.1	
5	60	Oct. 25	06:53	16:00	−142.5	
2	60		14:59	00:27	−141	One-way lock.
4	61		23:21	07:45		No signal level recorded because of paramp trouble.
5	61	Oct. 26	06:49	15:45		No AGC calibration.
2	61		14:56	00:15	−142	One-way lock.
4	62		23:16	07:45	−145.6	

Table 7–III.—Summary of DSIF operations, midcourse to end of mission—*Continued*

DSIF station	Pass	Date, 1962	Time of acquisition, GMT	Time of loss, GMT	Maximum received-signal strength, dbm	Remarks
5	62	Oct. 27	06:49	16:15	−142	
2	62		14:52	01:32	−142. 5	Two-way lock at 15:37.
3	62		14:52	01:32		
4	63		22:25	07:30	−146. 8	
5	63	Oct. 28	06:22	15:30	−143. 9	
2	63		14:47	23:10	−142. 1	One-way lock.
4	64		22:45	07:30	−145. 9	
5	64	Oct. 29	06:27	15:30	−142	
2	64		14:41	23:51	−142. 4	One-way lock.
4	65		22:57	07:30	−145. 6	
5	65	Oct. 30	06:30	15:30	−142. 2	
2	65		14:35	00:00	−143. 8	One-way lock.
4	66		22:59	07:30	−146. 7	
5	66	Oct. 31	06:20	15:30	−144. 5	Horn feed installed after this tracking period.
2	66		14:47	23:45	−145	Two-way lock 20:00 to 20:42.
3	66		19:57	20:42		RTC–10 initiated at 20:25:30 and verified at 20:26:27.
4	67		22:30	07:15	−147. 1	
5	67	Nov. 1	06:20	15:15	−142. 4	
2	67		14:34	23:45	−143	One-way lock.
4	68		22:41	06:53	−147. 1	
5	68	Nov. 2	06:19	15:15	−142. 4	
2	68		14:23	01:13	−146	One-way lock.
4	69	Nov. 3	00:26	07:15	−147. 4	
5	69		06:10	15:15	−143. 6	
2	69		14:17	01:08	−143. 5	One-way lock.
4	70	Nov. 4	01:12	07:00	−144. 4	
5	70		06:07	15:00	−143. 4	
2	70		14:12	23:30	−143. 5	One-way lock.
4	71		21:45	07:00	−145. 5	
5	71	Nov. 5	06:04	15:30	−143	
2	71		14:07	00:32	−143. 5	Two-way lock at 14:07.
3	71		00:30	13:55		
4	72		21:15	07:32	−144. 2	

Table 7-III.—Summary of DSIF operations, midcourse to end of mission—*Continued*

DSIF station	Pass	Date, 1962	Time of acquisition, GMT	Time of loss, GMT	Maximum received-signal strength, dbm	Remarks
5	72	Nov. 6	05:39	14:45	−144.7	
2	72		14:03	23:15	−144	One-way lock.
4	73		21:59	06:45	−144.9	
5	73	Nov. 7	05:39	14:45	−144	
2	73		13:58	23:00	−144.5	One-way lock.
4	74		21:36	06:30	−145.4	
5	74	Nov. 8	05:22	14:30	−143.2	
2	74		13:54	23:00	−144.7	Two-way lock at 20:46–22:32.
3	74		20:45	22:32		RTC-8 initiated at 21:25:00 and verified at 21:26:00.
4	75		21:42	06:30	−145.1	
5	75	Nov. 9	05:30	15:20	−143.7	
2	75		13:50	22:08	−144	One-way lock.
4	76		21:17	06:30	−147.3	
5	76	Nov. 10	05:28	15:30	−144	
2	76		13:45	00:32	−145.5	Two-way lock at 13:45.
3	76		13:43	00:35		
4	77		20:24	06:15	−146.8	
5	77	Nov. 11	05:14	14:15	−143.4	
2	77		13:40	22:45	−146	One-way lock.
4	78		21:22	06:00	−145.6	
5	78	Nov. 12	05:10	14:15	−145.3	
2	78		13:36	23:30	−145.5	One-way lock.
4	79		21:05	06:00	−146.8	
5	79	Nov. 13	04:59	14:00	−145	
2	79		13:33	22:30	−145	One-way lock.
4	80		21:06	06:00	−146.7	
5	80	Nov. 14	05:02	14:00	−146	
2	80		13:28	22:30	−145	One-way lock.
4	81		21:15	06:00	−147.2	
5	81	Nov. 15	04:54	14:00	−145.2	
2	81		13:24	22:30	−145.5	One-way lock.
4	82		21:19	06:59	−146	

Table 7-III.—Summary of DSIF operations, midcourse to end of mission—*Continued*

DSIF station	Pass	Date, 1962	Time of acquisition, GMT	Time of loss, GMT	Maximum received-signal strength, dbm	Remarks
5	82	Nov. 16	05:48	14:00	−147.1	
2	82		13:22	21:55	−146	One-way lock.
4	83		21:16	06:00	−146.2	
5	83	Nov. 17	05:00	14:40	−146	
2	83		13:20	23:58	−146	Two-way lock at 13:20.
3	83		13:13	24:00		
4	84		21:01	05:45	−148.2	
5	84	Nov. 18	04:52	13:45	−146.6	
2	84		13:14	22:15	−146	One-way lock.
4	85		20:56	05:46	−146.9	
5	85	Nov. 19	04:51	13:45	−147.1	
2	85		13:15	22:15	−146	One-way lock.
4	86		21:14	05:45	−148.8	
5	86	Nov. 20	04:46	13:45	−146.4	
2	86		13:13	22:00	−146.5	One-way lock.
4	87		20:43	05:30	−148.7	
5	87	Nov. 21	04:36	13:30	−146.7	
2	87		13:05	22:00	−146	One-way lock.
4	88		20:37	06:56	−148.7	
5	88	Nov. 22	04:44	14:00	−148.3	Very little telemetry data by teletype because of demodulator trouble.
2	88		12:57	22:00	−146.5	One-way lock.
4	89		20:44	05:30	−149.1	
5	89	Nov. 23	04:34	13:30	−148.2	
2	89		12:57	21:45	−146.5	One-way lock.
4	90		20:30	05:15	−148.7	
5	90	Nov. 24	04:15	13:15	−149	
2	90		12:56	21:45	−146.5	One-way lock.
4	91		20:27	05:15	−149.2	
5	91	Nov. 25	04:01	13:15	−149.3	
2	91		12:54	21:45	−147.5	One-way lock.
4	92		20:16	05:15	−148.2	

Table 7-III.—Summary of DSIF operations, midcourse to end of mission—*Continued*

DSIF station	Pass	Date, 1962	Time of acquisition, GMT	Time of loss, GMT	Maximum received-signal strength, dbm	Remarks
5	92	Nov. 26	04:17	14:00	−148. 6	
2	92		12:46	23:11	−147. 5	Two-way lock at 13:13.
3	92		13:13	23:15		
4	93		20:31	05:15	−148. 8	
5	93	Nov. 27	04:09	13:15	−148. 8	
2	93		12:45	21:45	−147. 5	One-way lock.
4	94		20:13	05:15	−149. 3	
5	94	Nov. 28	04:02	13:15	−149	
2	94					Not scheduled.
3	94		12:57	21:45	−148	Functional as *receive only* station.
4	95		20:39	06:15	−150	
5	95	Nov. 29	05:49	13:15	−151. 9	Paramp trouble during most of this period.
2	95					Not scheduled.
3	95		12:12	21:46	−148. 4	*Receive only.*
4	96		20:27	05:15	−148. 4	
5	96	Nov. 30	04:11	13:15	−148. 5	
2	96					Not scheduled.
3	96		12:08	21:40	−148. 3	
4	97		20:39	05:15	−150. 6	
5	97	Dec. 1	04:21	13:45	−150. 5	
2	97		12:35	20:55	−147. 8	Two-way lock at 12:35.
3	97		12:25	21:45		*Transmit* only.
4	98		20:15	06:43	−150. 5	
5	98	Dec. 2	05:27	13:00	−148. 7	
2	98		12:36	21:30	−148. 8	One-way lock.
4	99		19:57	05:00	−150. 9	
5	99	Dec. 3	03:56	13:00	−150. 3	
2	99		12:30	21:30	−149. 2	One-way lock.
4	100		20:30	05:30	−149. 7	
5	100	Dec. 4	03:56	13:00	−150. 3	
2	100		12:27	21:30	−148	One-way lock.
4	101		19:53	05:30	−151. 5	

Table 7-III.—Summary of DSIF operations, midcourse to end of mission—*Continued*

DSIF station	Pass	Date, 1962	Time of acquisition, GMT	Time of loss, GMT	Maximum received-signal strength, dbm	Remarks
5	101	Dec. 5	03:55	13:00	−150.1	
2	101		12:41	21:30	−148.1	One-way lock.
4	102		20:01	05:00	−151	
5	102	Dec. 6	03:49	13:00	−146.1	Sudden gain change during calibrations.
2	102		12:23	21:30	−149.4	One-way lock.
4	103		20:17	05:00	−150.6	
5	103	Dec. 7	03:48	13:00	−152.3	
2	103		12:24	21:30	−148.7	Two-way lock at 12:24.
3	103		12:14	21:30		
4	104		20:08	05:30	−151.1	
5	104	Dec. 8	04:44	13:00	−150	
2	104		12:24	22:30	−149.5	Two-way lock at 12:24.
3	104		12:12	22:30		Command-modulation tests conducted during this period.
4	105		19:44	05:10	−150.4	
5	105	Dec. 9	03:50	13:00	−150	
2	105		12:20	21:30	−149.2	One-way lock.
3	105		14:01	21:30	−151	*Receive only.*
4	106		19:38	05:00	−150.5	
5	106	Dec. 10	03:47	13:01	−150.8	
2	106		12:18	22:30	−149.2	One-way lock.
3	106		13:03	20:15	−152.5	*Receive only.* Tests conducted to determine telemetry threshold.
4	107		22:16	04:45	−149.7	Listening feed installed before this period.
5	107	Dec. 11	03:45	12:45	−152.1	
2	107		12:17	22:26	−149	Two-way lock at 12:17.
3	107		12:08	22:20		*Transmit only.*
4	108		18:28	05:00	−148	
5	108		03:45	13:28	−151.9	
2	108	Dec. 12	12:20	22:23	−150.5	Two-way lock at 12:31.
3	108		12:31	22:20		*Transmit only.*
4	109		18:32	05:00	−149.3	

Table 7–III.—Summary of DSIF operations, midcourse to end of mission—*Continued*

DSIF station	Pass	Date, 1962	Time of acquisition, GMT	Time of loss, GMT	Maximum received-signal strength, dbm	Remarks
5	109	Dec. 13	03:49	13:31	−151.5	
2	109		12:13	22:20	−150.6	Two-way lock from 12:13–13:06, 17:06–17:43, 19:30–22:10.
3	109		12:04	22:10		Command-loop tests conducted.
4	110		18:15	05:00	−149.5	
5	110	Dec. 14	01:36	13:31	−152.3	
2	110		12:16	22:16	−150.6	Two-way lock at 12:27. Routine Venus encounter.
3	110		12:24			RTC–7 initiated at 13:35 and verified at 13:35:57. RTC–8 initiated at 20:32:00 and verified at 20:32:57.
4	111		18:10	05:00	−149.7	
5	111	Dec. 15	01:37	13:27	−152	
2	111		12:17	22:12	−151.4	Two-way lock at 12:17. Tests conducted on telemetry demodulator threshold.
3	111		12:07	22:10		RTC–2 initiated at 13:25 and verified at 13:25:56; again initiated at 13:40 and verified at 13:40:56. Between 13:50 and 22:06:30, a total of 165 RTC–0 commands transmitted.
4	112		18:29	04:30	−149.1	
5	112	Dec. 16	03:00	13:26	−152.2	
2	112		12:12	22:15	−151	Two-way lock at 12:34.
3	112		12:34	21:50		Between 13:08 and 13:50, a total of 25 RTC–0 commands transmitted.
4	113		18:31	04:00	−150.6	
5	113	Dec. 17				Not scheduled.
2	113		12:08	22:08	−151	Two-way lock at 12:34.
3	113		12:02	21:55		
4	114					Not scheduled.

Table 7-III.—Summary of DSIF operations, midcourse to end of mission—*Continued*

DSIF station	Pass	Date, 1962	Time of acquisition, GMT	Time of loss, GMT	Maximum received-signal strength, dbm	Remarks
5	114	Dec. 18				
2	114		13:20	22:06	−151.5	Two-way lock at 17:39. Acquisition delayed because of water in feed line.
3	114		17:39	21:55		Total of 7 RTC-0 commands transmitted between 21:02 and 21:08. Spacecraft transponder threshold tests conducted.
4	115					Not scheduled.
5	115	Dec. 19				Not scheduled.
2	115		12:07	22:05	−150.6	Two-way lock at 12:07.
3	115		11:59	21:45		
4	116					Not scheduled.
5	116	Dec. 20				Not scheduled.
2	116		12:27	22:01	−152.4	Two-way lock at 12:27.
3	116		11:58	21:50		Total of 6 RTC-2 commands transmitted between 16:05 and 17:20.
4	117					Not scheduled.
5	117	Dec. 21	02:09	12:00	−154.2	
2	117					Not scheduled.
4	118					Not scheduled.
5	118	Dec. 22	02:06	12:00	−156	
2	118					Not scheduled.
4	119		19:00	05:00	−153.8	
5	119	Dec. 23				Not scheduled.
2	119					Not scheduled.
4	120		18:58	05:00	−153.7	
5	120	Dec. 24				Not scheduled.
2	120					Not scheduled.
4	121					Not scheduled.
5	121	Dec. 25				Not scheduled.
2	121					Not scheduled.
4	122					Not scheduled.

Table 7–III.—Summary of DSIF operations, midcourse to end of mission—*Continued*

DSIF station	Pass	Date, 1962	Time of acquisition, GMT	Time of loss, GMT	Maximum received-signal strength, dbm	Remarks
5	122	Dec. 26	01:54	12:00	−154.5	
2	122					Not scheduled.
4	123		18:48	05:00	−153.9	
5	123	Dec. 27				Not scheduled.
2	123					Not scheduled.
4	124		18:53	05:30	−155	
5	124	Dec. 28				Not scheduled.
2	124		12:00	21:30	−154.2	Two-way lock at 12:10.
3	124		12:10	21:30		In and out of two-way lock several times because of synthesizer. Unable to obtain vehicle sync for transmission of RTC–2.
4	125	Dec. 29				Not scheduled.
5	125		04:41	08:22	−156	
2	125					Not scheduled.
4	126		17:52	02:00	−155.3	
5	126	Dec. 30				Not scheduled.
2	126		12:01	21:35	−155.5	Two-way lock at 12:30.
3	126		12:30	21:35		Demodulator and decommutator continuously dropping lock; determination made that spacecraft 4Fs had dropped by 13cps.
4	127					Not scheduled.
5	127	Dec. 31	02:45	12:00	−156.6	
2	127					Not scheduled.
4	128		23:15	02:00	−157.1	
5	128	Jan. 1				Not scheduled.
2	128		19:10	20:00		One-way lock.
4	129					Not scheduled.
5	129	Jan. 2	09:51	13:02	−156. 4	
2	129					Not scheduled.
4	130					Not scheduled.

Table 7–III.—Summary of DSIF operations, midcourse to end of mission—*Concluded*

DSIF station	Pass	Date, 1963	Time of acquisition, GMT	Time of loss, GMT	Maximum received-signal strength, dbm	Remarks
5	130	Jan. 3	03:54	07:00	−157	Last signal received from spacecraft.
2	130					Not scheduled.
4	131					Spacecraft signal searched for from 20:58 through 03:15 with no success.
5	131	Jan. 4				Secured from mission.
2	131					Spacecraft signal searched for from 12:00 to 20:46 with no success.
4	132					Secured from mission.
2	132	Jan. 5				Not scheduled.
2	133	Jan. 6				Not scheduled.
2	134	Jan. 7				Not scheduled.
2	135	Jan. 8				Spacecraft signal searched for from 17:10 to 21:00. No signal received.
3	135					Starting at 18:30, total of 40 RTC–2 commands sent. Starting at 19:12, total of 10 RTC–1 commands sent.
2	136	Jan. 9				Station relieved of tracking and placed on standby until later date.

The DSIF continued to track on a reduced-time basis after December 16, as indicated in table 7–III. After December 30, the DSIF schedule was planned around the spacecraft radiometer calibration periods, in an attempt to obtain a calibration. DSIF 5 completed its scheduled tracking period at 07:00 on January 3, 1963, the received-signal level at that time being −157 dbm. DSIF 4 started its scheduled track at 20:58 on January 3 and searched until 03:15, January 4, without success. The last signal from the spacecraft, therefore, was

received by DSIF 5 at 07:00, January 3, 1963. DSIF 2 searched for the signal from 12:00 through 20:46 on January 4, again with no success. On January 5, DSIF 4 and 5 were secured. On January 8, DSIF 2 searched for the signal from 17:10 until 21:00 without success. During the same period, DSIF 3 transmitted 40 RTC–2 (clockwise hinge override) commands and 10 RTC–1 (roll override) commands in an attempt to update the spacecraft antenna hinge angle. There were no indications that any of the commands were received or acted upon by the spacecraft. On January 9, the Goldstone stations were placed on standby status which for all practical purposes terminated the mission.

CENTRAL COMPUTING FACILITY

The Central Computing Facility (fig. 7–24) located at JPL, Pasadena, Calif., was composed of three installations:

1. The Primary Computing Facility, Station C, located in Building 125.
2. The Secondary Computing Facility, Station D, located in Building 202.
3. The Telemetry-Processing Station, located in Building 125.

It was the function of the CCF to reduce the tracking and telemetry data from Mariner II so that the required orbital calculations and command decisions could be made. After the teletype and magnetic tapes of telemetry data acquired and recorded by the DSIF had been received at JPL, the CCF processed the raw data into the form required by the user. All real-time data processing and normal non-real-time data were processed in the CCF.

Primary Computing Facility, Station C

Tracking and telemetry data received from the DSIF were processed in Station C, which included both real- and non-real-time data (fig. 7–25). The processing equipment at Station C included:

1. *IBM 7090 computer (and associated card handling equipment).* The IBM 7090 is a large, high-speed, general-purpose, digital computer. The JPL installation had a 32 168-word core memory, and was equipped with two input-output channels with each channel containing seven 729 IV tape units.

2. *Telemetry to magnetic tape translator.* This data translator accepted up to seven channels of digital data (asynchronously), converted these data into blocked IBM format, and recorded them on magnetic tape for entry into the IBM 7090 computer.

3. *Teletype tape to magnetic tape translator.* This device took the bit configura-

tion of a five-level teletype character and put it into channels A, 8, 4, 2, and 1 of an IBM magnetic tape character. One magnetic tape record comprised 1026 of these characters. The normal rate in this mode was 300 characters/sec and the maximum rate was 600 characters/sec. The device was also capable of punching paper tape from IBM magnetic tape. The rate in this mode was 60 characters/sec.

4. *IBM 1401 computer (two units).* This computer acted as a satellite to the IBM 7090. It was primarily a bookkeeping and input-output processing unit which would relieve the 7090 of these time-consuming functions. It was equipped with a 600-line/min printer, a card punch, a card reader, and two magnetic tape handlers. The 1401 communicated with the 7090 by magnetic tape, thereby eliminating card punching, card reading, and listing as on-line functions of the 7090.

5. *Stromberg Carlson 4020 printer-plotter.* The SC 4020 was a high-speed microfilm recorder. It was intended to record on microfilm real-time information supplied by the 7090 computer. Standard options extended its capabilities as a plotter and printer, and permitted off-line operation from magnetic tape. "Quick-look" was available in the form of a hard-copy camera option which provided one copy, 7.5 by 7.5 inches, of each frame of information generated by the SC 4020. The copy was developed at the site in the F85 oscillogram processor. The quick-look copy was available within 30 min of processing the raw data.

6. *Paper-tape-to-card (IBM 047) and card-to-paper-tape (IBM 063).* These devices were used for the tracking operation of Mariner II. For the initial orbit determination, the data points were entered into the computer as quickly as possible. By putting these points on cards, human checking of transmission errors was made possible.

7. *Digital Equipment Corporation PDP–1 computer.* The computer handling of telemetered data for Mariner II was accomplished with the PDP–1 as the prime data handling equipment. The IBM 7090 was still used to perform complex reduction and analysis, but was relieved of bookkeeping, quick-look, and near-real-time monitoring. The PDP–1 was a small, fast computer designed specifically for data processing. It was equipped with 4096 18-bit words of core storage, two Plotter 906 II tape units connected through a high-speed tape channel, a paper-tape reader and punch, a typewriter, and a word buffer to accept data from a telephone line. Generally, the PDP–1 was able to perform the following functions simultaneously:

a. Prepare a magnetic tape file of all telemetered measurements, which were

FIGURE 7-24.—Central Computing Facility, JPL-Pasadena.

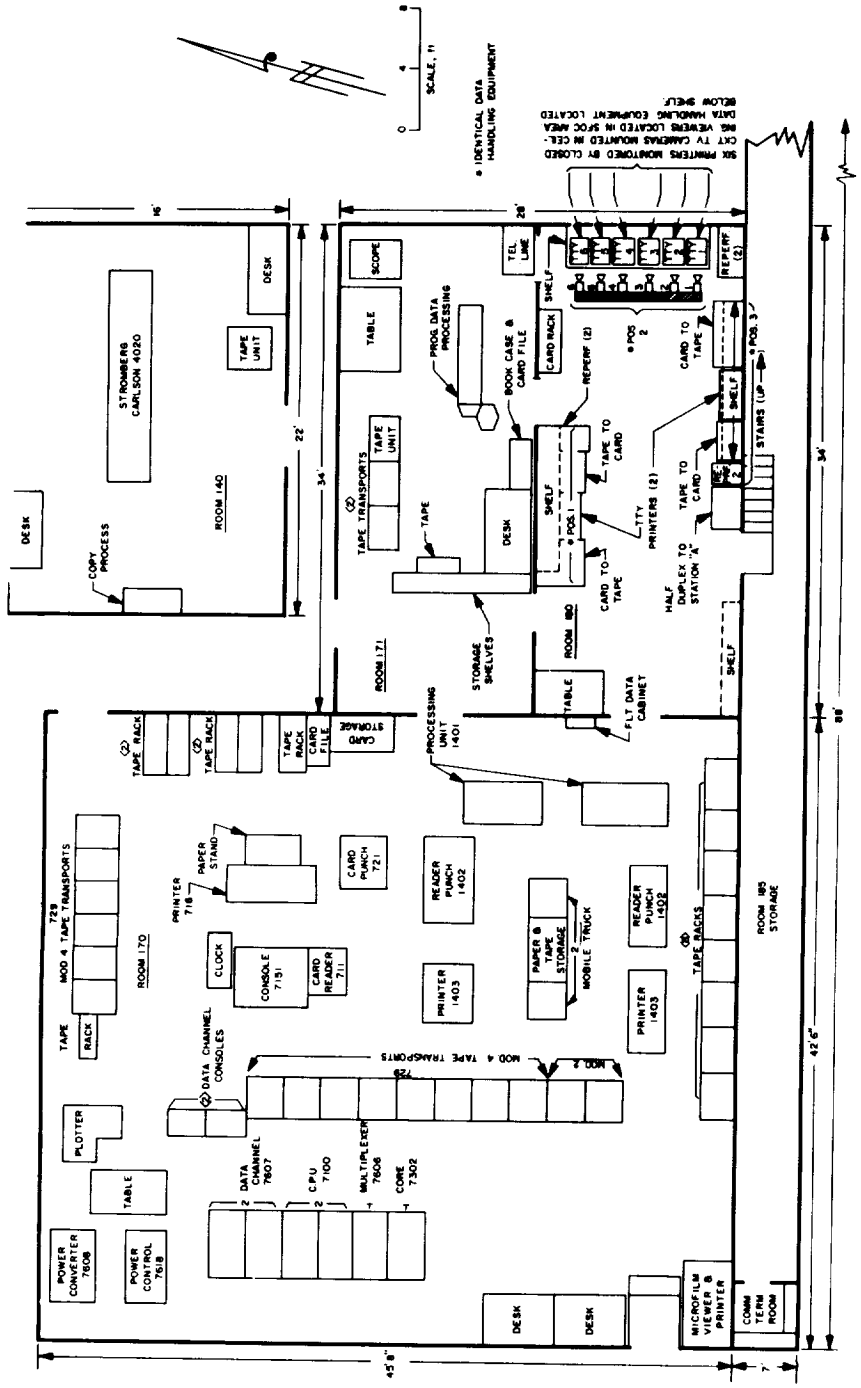

FIGURE 7–25.—Primary Computing Facility, Station C.

used as input to the IBM 7090 for analysis, and for preparing a final report.

b. Prepare magnetic tapes to drive the IBM 1401 printer.

8. *Sending and receiving teletype equipment.*

Secondary Computing Facility, Station D

The basic function of Station D (fig. 7–26) was to provide backup computational facilities in case of a failure in Station C. The normal mode of operation for this backup facility was to parallel the effort of Station C during the critical phase of flight—launch and initial orbit determination. Station D was used for processing other data as needed. The processing equipment at Station D duplicated that of Station C.

Telemetry Processing Station (TPS)

It was the responsibility of the TPS (fig. 7–27) to process telemetry magnetic tapes recorded at the DSIF sites. All signals recorded on the tape (including DSIF station functions) were processed by the TPS except the spacecraft telemetry composite signal. The decoded spacecraft telemetry composite signal was recorded on this tape by the DSIF for processing by the TPS.

Ground Communications Net

The ground communication net which was used during the Mariner II mission, is shown in figure 7–28. Teletype lines were the primary communication links for the mission and were used for transmitting data from the DSIF stations to the Central Computing Facility and for passing command, acquisition, prediction, and administrative information to the stations. The voice circuits were available for high-priority real-time communications during the launch and any other critical phase of the Mariner operation. All these communications links were monitored and controlled by DSIF Net Control. All messages pertaining to the mission passed through or originated from Net Control.

Data Circuits Communication Links

The Communications Center had three half-duplex teletype circuits available for data transmission to or from the Echo Station. There were two half-duplex

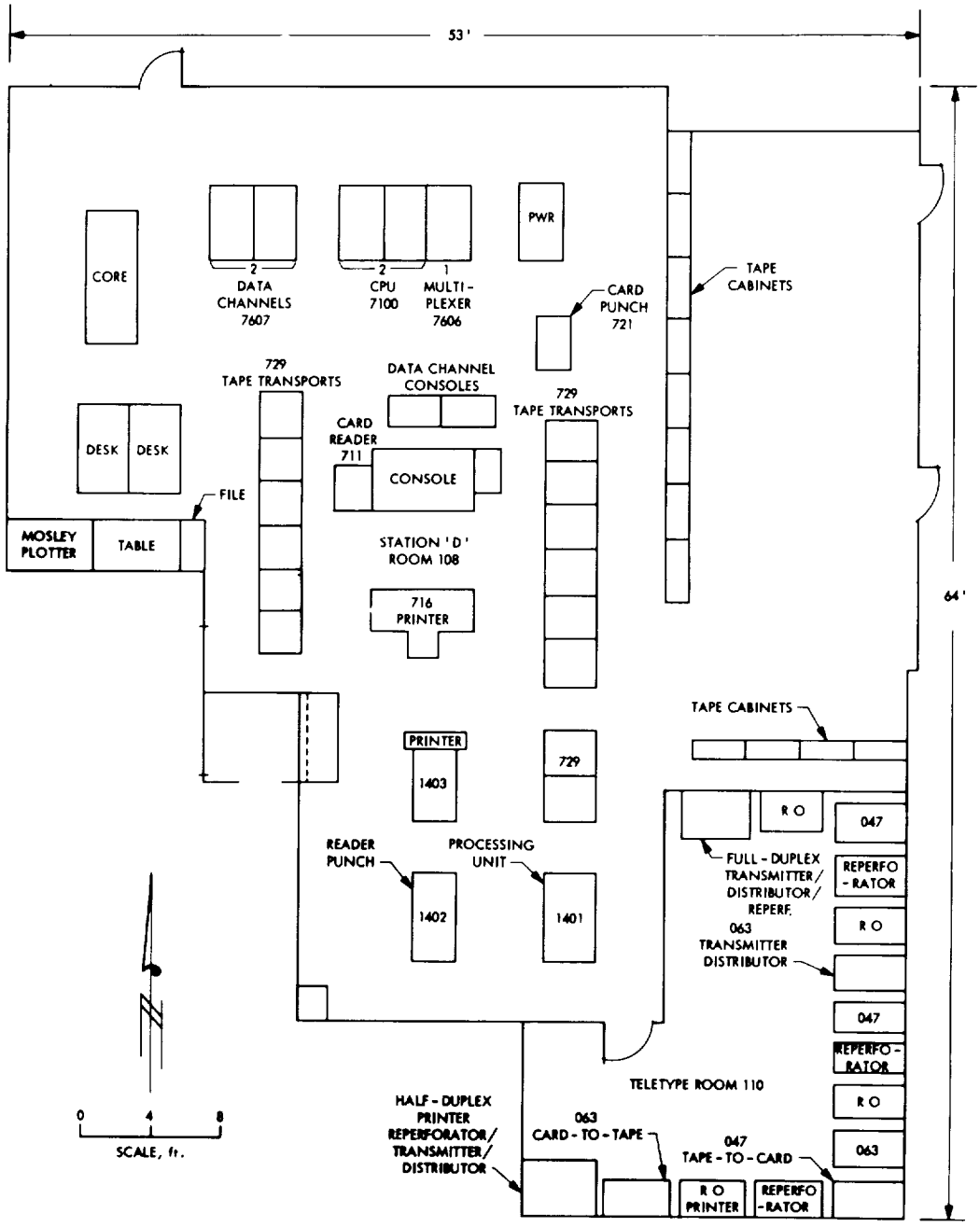

FIGURE 7–26.—Secondary Computing Facility, Station D.

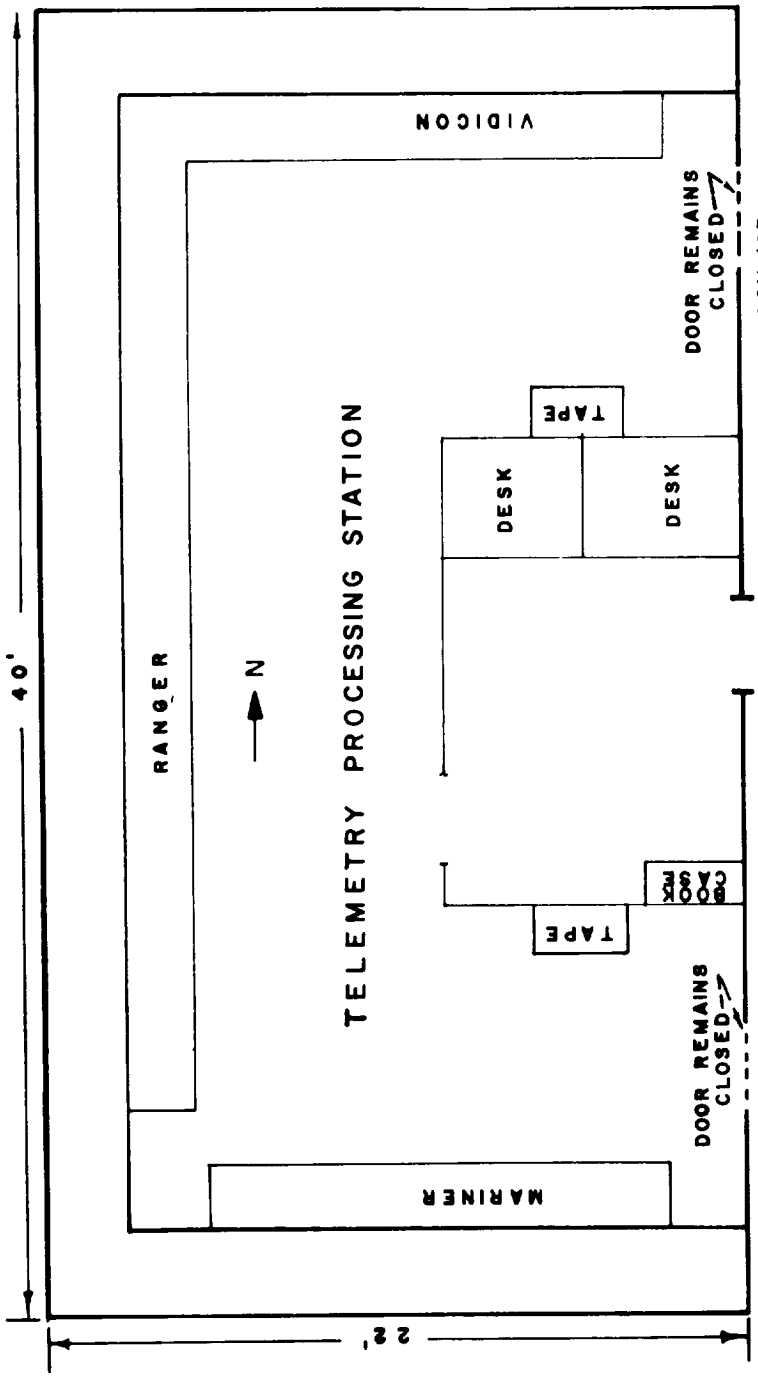

FIGURE 7-27.—Telemetry Processing Station (TPS).

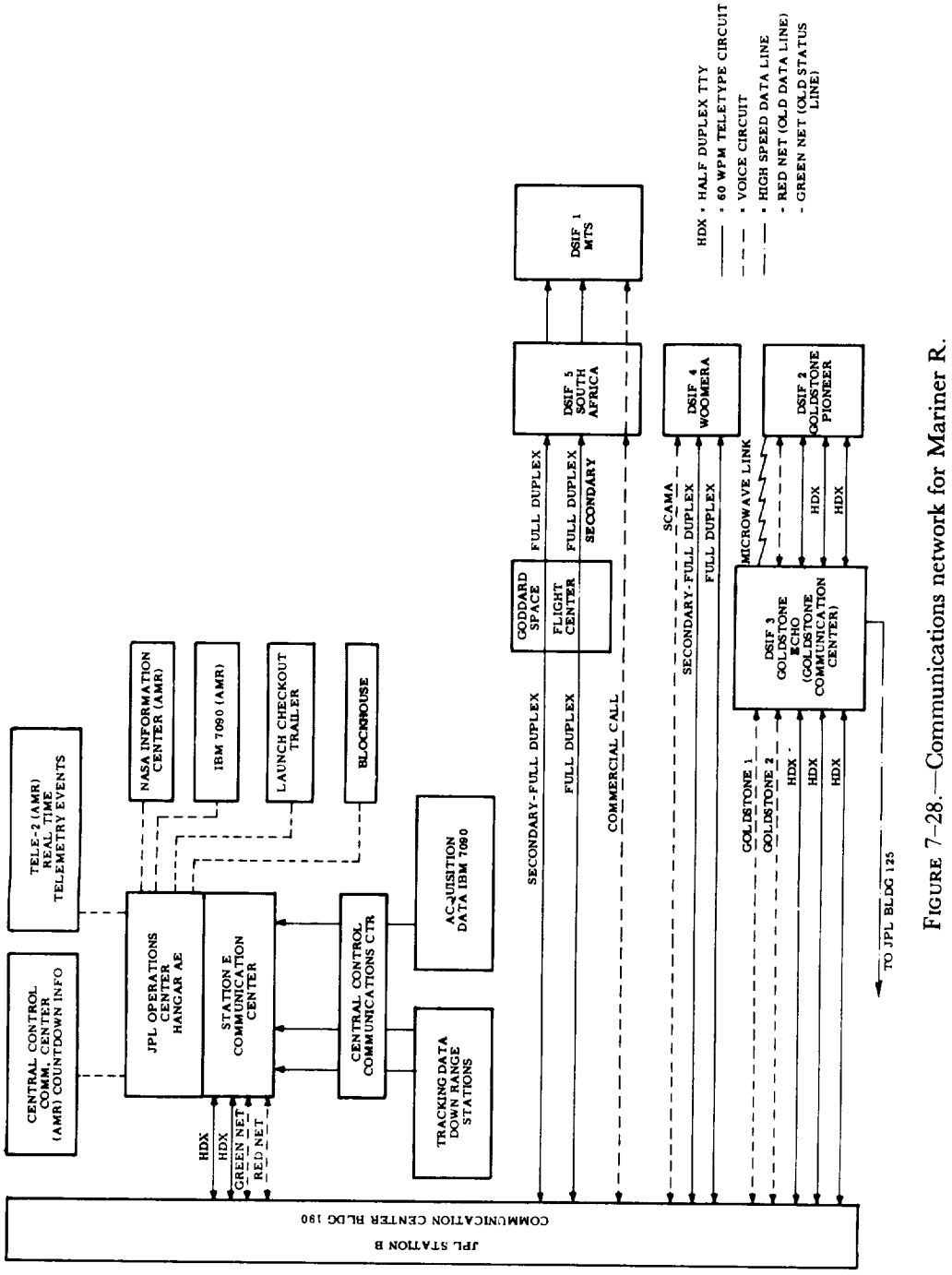

FIGURE 7–28.—Communications network for Mariner R.

circuits between the Pioneer and Echo Stations, and one wideband telephone data circuit available for one-way transmission from Goldstone to JPL. These circuits were available for full-time usage as required. Data transmissions were restricted on any one circuit to transmission in one direction only.

One full-duplex circuit was available to each of the overseas stations (Woomera and Johannesburg) on a full-time basis. A second circuit was available to each station on a limited basis during critical periods or when primary circuits failed. Due to the necessity of utilizing radio teletype over a significant portion of the transmission path, both circuits were not 100-percent reliable during periods of poor high-frequency radio propagation. Therefore, to gain a measure of redundancy, the primary and secondary circuits were routed over different paths. Data transmission over these circuits took place simultaneously in both directions.

The Mobile Tracking Station utilized the same teletype circuits as the Johannesburg Station.

Two half-duplex circuits were available to Cape Canaveral during the Mariner II launch period. These circuits were available two weeks prior to the mission and were used for data flow between the launch complex and the JPL Communications Center at Pasadena, Calif.

Voice Circuits

Two voice circuits were available to Goldstone. These circuits consisted of four-wire telephone circuits capable of being conferenced at JPL Building 125 (SFOC) with other voice circuits that were used as part of the DSIF operations.

A commercial toll call was placed to Johannesburg prior to each Mariner operation. Voice communications to Woomera used either the Mercury Net on a noninterference basis or a commercial toll call. These circuits were used as required for the first three operating days after launch of Mariner II and were not available on a full-time basis.

The Mobile Tracking Station used the same voice circuits as the Johannesburg Station.

Two voice circuits were available during the launch period for communications with the launch complex. One circuit connected the Central Computing Facility with the Cape Canaveral Computing Facility, and the second was used to coordinate the DSIF and launch activities (data and status lines).

Numerous circuits interconnected the DSIF Net Control (JPL Building 125) with the test director and other personnel within the Building 125 Space Flight

Operations Center, and with the Communications Center in JPL Building 190. These circuits included two four-wire hot lines, an intercom system, and a conventional telephone system.

Four-wire conference circuits and an intercom system connected the Building 125 computer to the SFOC and the JPL Building 202 computer facility.

SPACE FLIGHT OPERATIONS

Tracking Data Analysis Group

In preparation for the Mariner II mission, precalibration testing was performed at all DSIF stations, including star tracks and boresight-vs-polarization tests. The calibration data obtained from these tests contained angle systematic-error corrections and boresight-shift information.

The monitoring of raw data assumed major importance on several occasions whenever there was a question of the validity of the tracking data. Because monitoring procedures as conceived before the flight proved to be inadequate in providing the sensitivity and speed of monitoring required, the IBM 1620 computer at Goldstone Tracking Station was utilized to provide such monitoring in near-real time. This form of monitoring became a standard procedure when DSIF 3 was taking precision two-way Doppler data every 8 days, and provided invaluable assistance to both the Tracking Data Analysis Group and the Orbit Determination Group.

Monitoring of reduced data proceeded according to preflight planning, except that somewhat closer teamwork than had been envisioned proved necessary between the Tracking Data Analysis Group and the Orbit Determination Group in the interpretation of tracking-data residuals. This need resulted, in large measure, from the complexity and newness of the orbit determination program and from the variety of options available within the program. Correlation of supplementary data, including VCO frequencies, transmitter on-times, and so forth, was quickly recognized as a full-time job.

Spacecraft Data Analysis Team

The Spacecraft Data Analysis Team (SDAT) was composed of the director and one or more cognizant engineers for each subsystem of the spacecraft. The SDAT director's primary function was to coordinate, from analysis of the telemetry

data received, the efforts of the SDAT in determining the performance of the spacecraft in flight.

It was initially planned that the SDAT would convene daily during cruise-mode periods to examine and evaluate all data received since the previous session, and that the Central Computing Facility would monitor all incoming data during nonstandard working hours and notify the cognizant engineer in the event that an alarm situation developed. This method of monitoring, however, proved inadequate early in the operation, since it was not mechanized to operate in an on-line fashion. The computer's failure to identify low-rate measurements was primarily due to discontinuous transmission, characteristic of most of the data as received by teletype from the overseas tracking stations. The inability of the computer to identify low-rate data hampered the SDAT in evaluating the spacecraft's performance and necessitated a change in the method of operation, with a simultaneous effort to improve the computer's capability of processing noisy data.

Rather than rely on computer-generated tabulated listings for low-rate measurements, the SDAT assigned a technician to the task of monitoring the teletype page printers to identify these subcommutated measurements. Printed data were supplied by the teletype page printers in commutated form; therefore, in effect, the technician assumed one of the computer's initial functions of decommutating the data.

In addition, an engineer was made available 24 hours a day, 7 days a week, to examine and evaluate the data identified and decommutated by the technician. This arrangement worked satisfactorily and was continued for the remainder of the mission.

Orbit and Trajectory Determination Group

The spacecraft's path with respect to the Sun, the Earth, and the target planet was computed by the Orbit and Trajectory Determination Group. Determinations were made at least once a day during the encounter phase, which encompassed the period from December 8 to 18. Up-to-date information was supplied to the other operational groups on orbital elements, target parameters, and spacecraft trajectory and attitude, for purposes of data analysis and emergency-action planning. An important contribution of the Orbit and Trajectory Determination Group was establishment of the target-miss parameters, both prior and subsequent to the midcourse maneuver.

Midcourse Maneuver Commands Group

In order to fulfill its responsibility for generating the commands for the midcours maneuver, the Midcourse Maneuver Commands Group, during that portion of the flight preceding the maneuver, maintained liaison with the Spacecraft Data Analysis Team, the Scientific Data Group, and the Communications Coordinator. Information obtained from these sources pertaining to spacecraft status and scientific objectives was coordinated with additional information developed by the group itself; this, in turn, was correlated with an analysis of the operational situation. The resulting study was presented to the test director in the form of a recommended midcourse maneuver and a detailed analysis of the effect of such a maneuver on the accomplishment of the mission objectives.

Scientific Data Group

The Scientific Data Group was composed of the project scientist and certain of the JPL cognizant scientists for data handling. As the occasion demanded, the remaining JPL cognizant scientists served in a consulting capacity. Throughout the Mariner II operation, the group translated the scientific aspects of the mission into a format permitting their utilization by the space flight test director.

The group began to function early in May 1962 and was active in the formulation of the scientific requirements of the mission, as reflected in the Space Flight Operations Plan. This effort served, primarily, to establish the scientific data requirements, and to bring to the determination of the planet aiming point the optimal correction permitted by the constraints imposed on the trajectory by the scientific instrumentation. Procedures to be followed during nonstandard modes of operation were also formulated.

The first cruise-science telemetry was received about 16:14:00 on August 29. The telemetry was analyzed by the Scientific Data Group, and all cruise-science instrumentation was found to be performing as expected. The first magnetometer calibration occurred at 00:06:00 on August 30. Since the spacecraft was rotating about its roll axis, important magnetometer information was obtained and an independent check was made on the roll rate.

The first radiometer calibration sequence occurred at 10:49:00 on September 14. The times of possible recurrence were predicted and supplied to the test director for circulation among the DSIF stations in order to assure coverage of these events. Until encounter, 130 scheduled magnetometer calibrations and 23

radiometer calibrations were obtained, all but two of the latter occurring at predicted times. These calibrations were carefully followed, since they were of great importance in the assessment of the extrapolated operational status of this primary planetary experiment. The microwave radiometer calibration sequence occurred, on the average, every 5 to 6 days, and the scheduled magnetometer calibrations every 15 hr 46 min.

On September 27, the magnetometer evidenced nonstandard operation, in that certain calibration sequences began at unscheduled times and extended for longer than normal intervals. Scale changes occurred on one or more axes, usually at the beginning and end of these unscheduled sequences. Certain minor nonstandard aspects of operation were observed in the solar plasma experiment, and the cosmic dust experiment suffered a decrease in sensitivity, starting on November 26 and degrading further on December 14. No science telemetry was obtained from October 31 to November 8 because of the necessity of conserving electrical power during the first solar-panel power failure. At the time of this power failure, the three magnetometer axes changed to the high scale because of the larger change in the spacecraft magnetic signature occasioned by the redistribution of electrical current from the solar panels.

During encounter (mode III), liaison was maintained with the associate experimenters, some of whom were at the Jet Propulsion Laboratory for the operation. An extensive series of spacecraft science reports were provided to the information coordinator. Science telemetry in modes II and III was analyzed as nearly in real-time as the availability of printouts permitted. Through a telephone link with Goldstone Echo Station, the cognizant scientist for data handling maintained a real-time surveillance of the scientific data translator printout. An analysis of this printout was furnished to the test director, constituting his only real-time information relative to the planetary scan. One approximately diametrical scan and two chordal scans of the planetary disk were obtained, with corresponding changes in the readings on both channels of both radiometers. No changes which could be correlated with the radiometer experiments were observed in the readings of the other scientific experiments.

Immediately after return to mode II operation at 20:43:00 on December 14, a radiometer calibration sequence occurred. During the period of telemetry degradation just mentioned, nine additional magnetometer calibrations were observed, and one final radiometer calibration, which occurred on December 28. Science telemetry gradually degraded, slowly at first, then more rapidly, until the spacecraft signal was finally lost at 07:00 on January 3. The quality of the

telemetry at the end of the mission was such as to render any analysis practically meaningless.

During the mission, close liaison was maintained with the SDAT scientific team. The AGIWARN service of the North Atlantic Radio Warning Service was closely followed. (This is a world-wide reporting service on solar activity and associated geophysical phenomena, administered by the U.S. National Bureau of Standards.) No class 3 or larger solar flares occurred during the mission; only one of the several class 2 flares was reported through the AGIWARN Alert Program. The purpose of following the AGIWARN alert was to enable the DSIF stations to be alerted for continuous coverage should a significant solar event occur.

CENTRAL COMPUTING FACILITY OPERATIONS

The data-processing operation, as presented here, is divided into three modes of data acquisition, patterned after the three modes (or types) of telemetry data: Mode I (launch), mode II (cruise), and mode III (encounter). Figures 7–29 and 7–30 illustrate the flow of telemetry and tracking data.

Mode I (L to L+2 Days)

Tracking-data processing at both Station C and Station D closely followed the sequence of events specified in the SFOP. Computer-time sharing with telemetry data imposed no constraints on meeting the initial mission requirements. However, because of operational pressure at Station C, predictions for the DSIF, generated at Station D, were used for the first view periods. From L to $L+12$ hr, Station D performed parallel tracking computations for complete Station C backup. At $L+12$ hr, Station D discontinued flight operations until start of the midcourse maneuver. The processing of tracking data was accomplished twice daily from $L+12$ hr through $L+2$ days at Station C, with no operational difficulty.

Telemetry teletype data from AMR were processed on-line from $L-180$ min to $L-5$ min; processing was in quick-look format, using the PDP–1 computer. After acquisition by South Africa, telemetry was processed on-line in both quick-look and full-reduction formats at the intervals specified in the SFOP. Because of the inability of teletype to transmit the 33-BPS telemetry-data rate in real time, the wideband data-phone link from Goldstone, with on-line PDP–1 processing, was used with positive and significant results in this mode.

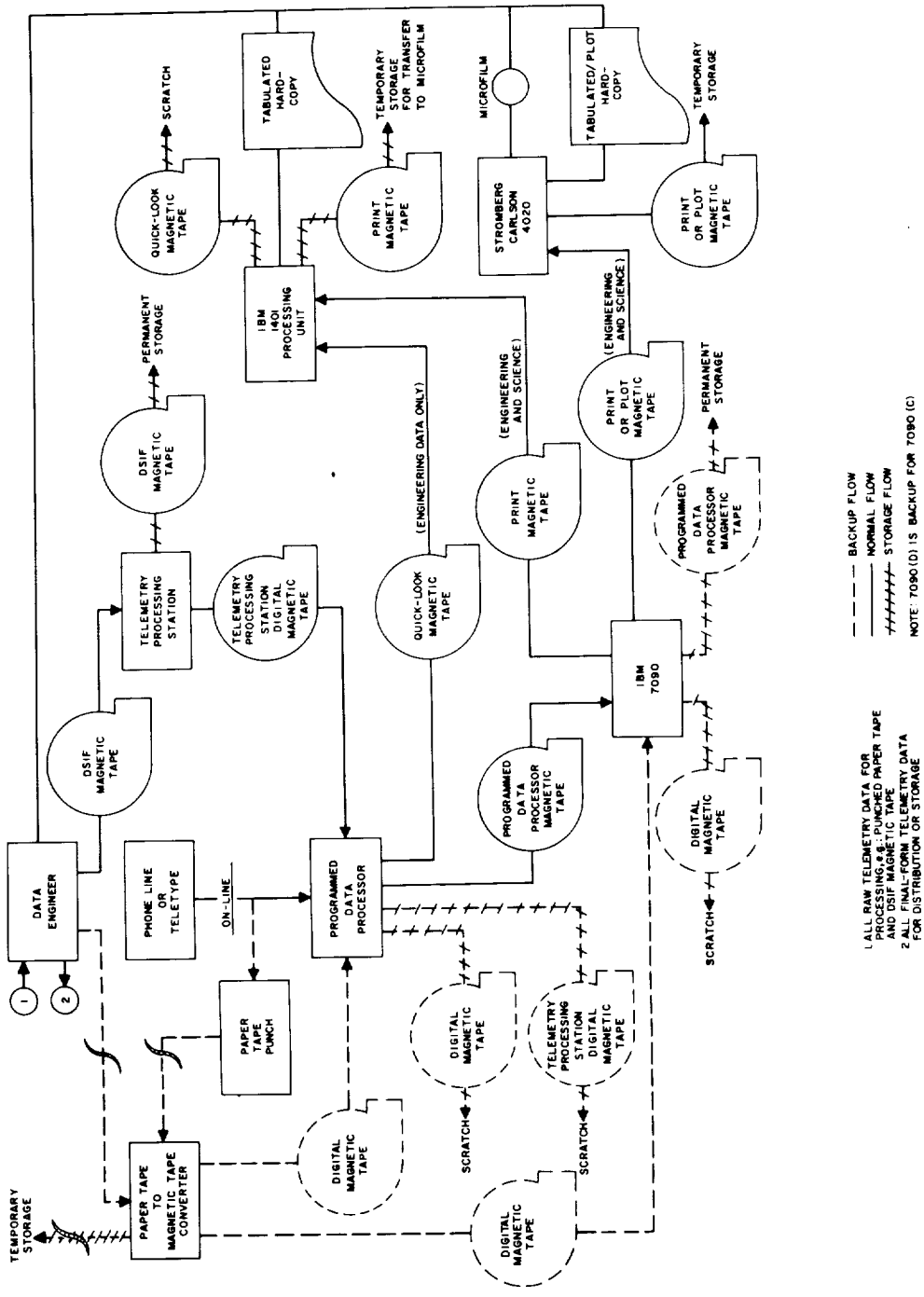

FIGURE 7-29.—Telemetry-data flow chart.

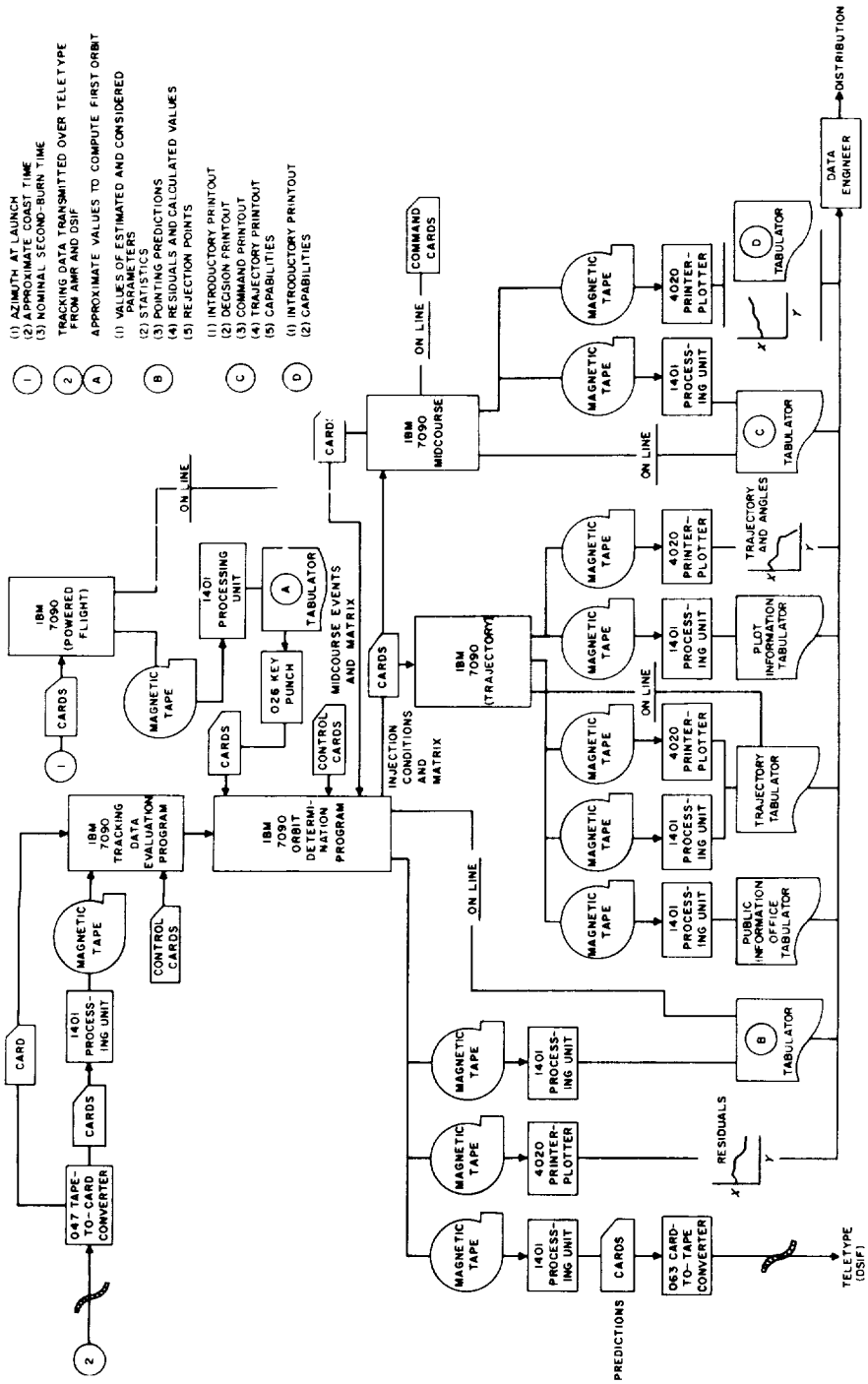

FIGURE 7–30.—Tracking-data flow chart.

Mode II (L+2 Days to L+108 Days)

Tracking-data processing and midcourse maneuver studies were conducted on a daily basis until occurrence of the midcourse maneuver at $L+8$ days. Thereafter, tracking data were processed once each week until encounter $(E)-3$ days ($L+105$ days), and DSIF predictions were generated for periods of 10 days. Public information pertaining to the spacecraft trajectory was also released on a weekly basis. Beginning at $E-3$ days, tracking data were processed daily until encounter.

Telemetry-data processing in mode II consisted of quick-look on-line processing, by means of the PDP–1 computer, every 3 hours, 24 hours a day. Until encounter, full processing and analysis of engineering and scientific data were performed daily, 7 days a week, on the IBM 7090 computer.

Mode III (Encounter, L+109 Days)

Tracking-data processing was conducted in near-real time at Station D throughout the Goldstone pass on encounter day, December 14, and daily thereafter until $L+2$ days. After this time, processing was done every sixth day until mission termination.

During the Goldstone pass on encounter day, telemetry data were processed on-line by the PDP–1 computer, using the wideband data-phone line. Quick-look data were not available in this mode. However, magnetic tapes generated by the PDP–1 computer and containing scientific encounter data were processed by the IBM 7090 computer every 30 min. The processing and delivery of data in this mode required from 4½ to 7 min. After mode III until mission termination, telemetry-data processing was similar to that for mode II.

Major Problem Areas in Flight Data Processing

Down times on the two IBM 7090 computers and the PDP–1 computer were negligible. Never during the mission were all three machines inoperative at the same time. During September, and again during December, power fluctuations resulted in the loss of both IBM 7090's for several hours, but the PDP–1 was not affected. Had this event occurred during a critical phase of the mission, such as launch, the capability of performing the necessary functions in a timely fashion would have been seriously jeopardized. This possibility pointed to a definite need for an auxiliary power source. Maintenance of the PDP–1 and associated

equipment was difficult to schedule under the 24 hr/day postlaunch-operation requirement without disrupting normal data flow. Fortunately, adequate backup modes were available to permit minimum maintenance.

DATA-HANDLING PROCESSES

Recovery of telemetry data comprises those procedures and processes required to place useful data from the spacecraft in the hands of the final users. Recovery begins at the DSIF tracking stations and ends when the data have been as exhaustively analyzed as is practicable. In the Mariner II operation, the DSIF station sent data to the laboratory in both raw and demodulated form. The raw form was stored on magnetic tape and served as a backup to the demodulated form sent via teletype in near-real time. Data received at the laboratory were presented to the operations personnel in a commutated but readable form, printed on a modified teletype page printer, and also in the form of decommutated computer printouts from operational programs. Analytical computer programs, particularly in the area of science telemetry, were used to obtain more meaning from the received data.

The DSIF, prior to launch, was scheduled to give continuous telemetry coverage for only part of the mission. However, in an effort to get as much telemetry as possible from the spacecraft, continuous coverage was provided until after encounter. It has been conservatively estimated that 95% of the total data transmitted from the spacecraft during this time was recovered; more than 85% was processed in real time via teletype and was available to analysts within an hour of transmission from the spacecraft.

Engineering Telemetry

The telemetry system on board the Mariner II was the first all-digital system utilized by JPL. The system encompassed three data modes of operation, one for each of the three phases of the flight, defined as follows:

Mode I—Launch. This mode was used for the first 57.3 hours of flight and provided only engineering data, transmitted at the rate of 33⅓ BPS.

Mode II—Cruise. This mode was used for the major portion of the 129-day flight. It furnished both science and engineering data, transmitted at the rate of 8⅓ BPS.

Mode III—Encounter. This mode was used for approximately 7 hours at planet

788-025 O—65 --21

encounter. It yielded only science data, transmitted at the rate of 8⅓ BPS.

Mariner II engineering telemetry data consisted of 44 parameters or measurements and the contents of the four event registers. Engineering measurements were in analog form and were read as variable dc voltages, whereas data from the event counters were in binary form. The spacecraft's data encoder (A through F) sampled, encoded, and prepared each measurement for transmission by converting it into a continuous binary signal that modulated one subcarrier of the transmitted signal. The pseudo-noise generator in the data encoder generated a unique pattern of pulses during each word period, in addition to word and bit sync, and this was also transmitted on a separate subcarrier. Proper combination of the two binary signals on the ground by the DSIF tracking stations enabled the reconstruction of data words. The words were then identified and decommutated by locating certain data words containing unique bit patterns. The data were then converted into a suitable format for telephone or teletype transmission by the teletype data encoder.

The teletype encoder was designed to punch the standard Baudot five-level paper tape with an engineering word consisting of seven bits in a format containing the commutated data in binary form. The engineering word was accommodated in two five-level columns on the paper tape. The first level of the first column was a word-sync indicator; the fifth level of both columns was an even-parity bit. The seven remaining positions contained the data word in binary form with the most significant bit in the second level of the first column. In this manner, two teletype characters were used to designate one engineering-data word. The encoder also inserted a time tag in the data at approximately 5-min intervals.

Telemetry-data decommutation was accomplished at the CCF by using a Digital Equipment Corporation PDP–1 computer. The PDP–1 was normally used on-line to receive real-time transmission of telemetry data from the DSIF by means of a high-speed paper-tape reader that had been adapted to read the five-level tape. The PDP–1 generated two types of outputs: (1) a tabular listing (quick-look) by address of the decimal number equivalent of the received binary number, and (2) a magnetic tape to be used as an input of the engineering reduction program in the IBM 7090 computer. The IBM 7090 computer also generated two outputs: (1) a tabulated listing similar to that of the PDP–1, but also containing the engineering equivalent of the decimal number with interpolated time tags, and (2) a magnetic tape to be used as an input to the Stromberg-Carlson 4020 plotter: The output of the 4020 plotter was a series of curves of specified measurements, grouped by subsystems.

In addition to the two computers, two teletype page printers were modified and used on-line to provide immediate access to the commutated data received from the DSIF. The modification of the page printer resulted in the printing of lower-case characters for each of the 64 characters in a given teletype line. These page prints became the primary source of the subcommutated data until it became evident that the computers frequently did not adequately identify the low-rate data. It also became apparent early in the flight that most of the personnel involved preferred to work directly with the decimal numbers, rather than with the equivalent engineering unit. The decommutated listing of decimal numbers (quick-look) became the most widely used form of reduced data for user analysis.

Figures 7–31 to 7–37 are representative of the formats used for data presentation during the Mariner II mission.

MA R-II ENGINEERING F/M QUICK LOOK MEASUREMENTS TELEMODE 2 STATION 4 DATE 331 S/C 2

HRMNSC	A1	A2	A3	A4	A5	A6	A7	A8	A9	B0	B1	B2	B3	B4	B5	B6	B7	B8	B9
034745	C3=126	63	63	63	63	4	66	63	48	1 6	13	28	88	32	1	66	125	4	27
034745	C4= 91	63	63	63	63	4	66	63	49	2 1	25	28	88	32	1	66	125	4	27
034745	C5=106	63	63	63	63	4	66	63	50	3 10	13	28	88	32	1	66	125	4	27
034745	C6= 90	63	63	63	63	4	66	63	49	4 0	11	28	88	32	1	66	125	4	27
034745	C7= 72	63	63	63	63	4	66	63	50	1 6	11	28	88	32	1	65	125	4	27
034745	C8= 52	63	63	63	63	4	66	63	50	2 1	25	28	88	32	1	67	125	4	27
034745	C9= 44	63	63	63	63	4	66	63	50	3 10	9	28	88	32	1	65	125	4	27
035303	C0= 0	63	63	63	63	4	66	63	50	4 0	9	28	88	32	1	67	125	4	27
035303	C1= 46	63	63	63	63	4	66	63	52	1 6	21	28	88	32	1	65	125	4	27
035303	C2=106	63	63	63	63	4	66	63	53	2 1	9	28	88	32	1	64	125	4	27
035303	C3= 60	63	63	63	63	4	66	63	54	3 10	21	28	88	32	1	65	125	4	27
035303	C4= 68	63	63	63	63	4	66	61	55	4 0	5	28	88	32	1	54	125	4	27
035303	C5=106	63	63	63	63	4	66	63	56	1 6	30	28	88	32	1	65	125	4	27
035303	C6= 89	63	63	63	63	4	66	63	57	2 1	21	28	88	32	1	65	125	4	27
035303	C7= 72	63	63	63	63	4	66	63	56	3 10	13	28	88	32	1	66	125	4	27
035753	C8= 51	63	63	63	63	4	66	63	58	4 0	30	28	88	32	1	65	125	4	27
035753	C9= 44	63	63	63	63	4	66	63	58	1 6	30	28	88	32	1	66	125	4	27
035753	C0= 0	63	63	63	63	4	66	63	59	2 1	5	28	88	32	1	54	125	4	27
035753	C1= 55	63	63	63	63	4	66	63	60	3 10	17	28	88	32	1	66	125	4	27
035753	C2=110	63	63	63	63	4	66	63	62	4 0	13	28	88	32	1	66	125	4	27
035753	C3=113	63	63	63	63	4	66	63	64	1 6	17	28	88	32	1	66	125	4	27
035753	C4= 76	63	63	63	63	4	66	63	66	2 1	5	28	88	32	1	66	125	4	27
035753	C5=106	63	63	63	63	4	66	63	67	3 10	25	28	88	32	1	66	125	4	27
040244	C6= 90	63	63	63	63	4	66	63	67	4 0	5	28	88	32	1	65	125	4	27
040244	C7= 72	63	63	63	63	4	66	63	67	1 6	25	28	88	32	1	66	125	4	27
040244	C8= 52	63	63	63	63	4	66	63	68	2 1	5	28	88	32	1	67	125	4	27

FIGURE 7–31.—Example of quick-look engineering data.

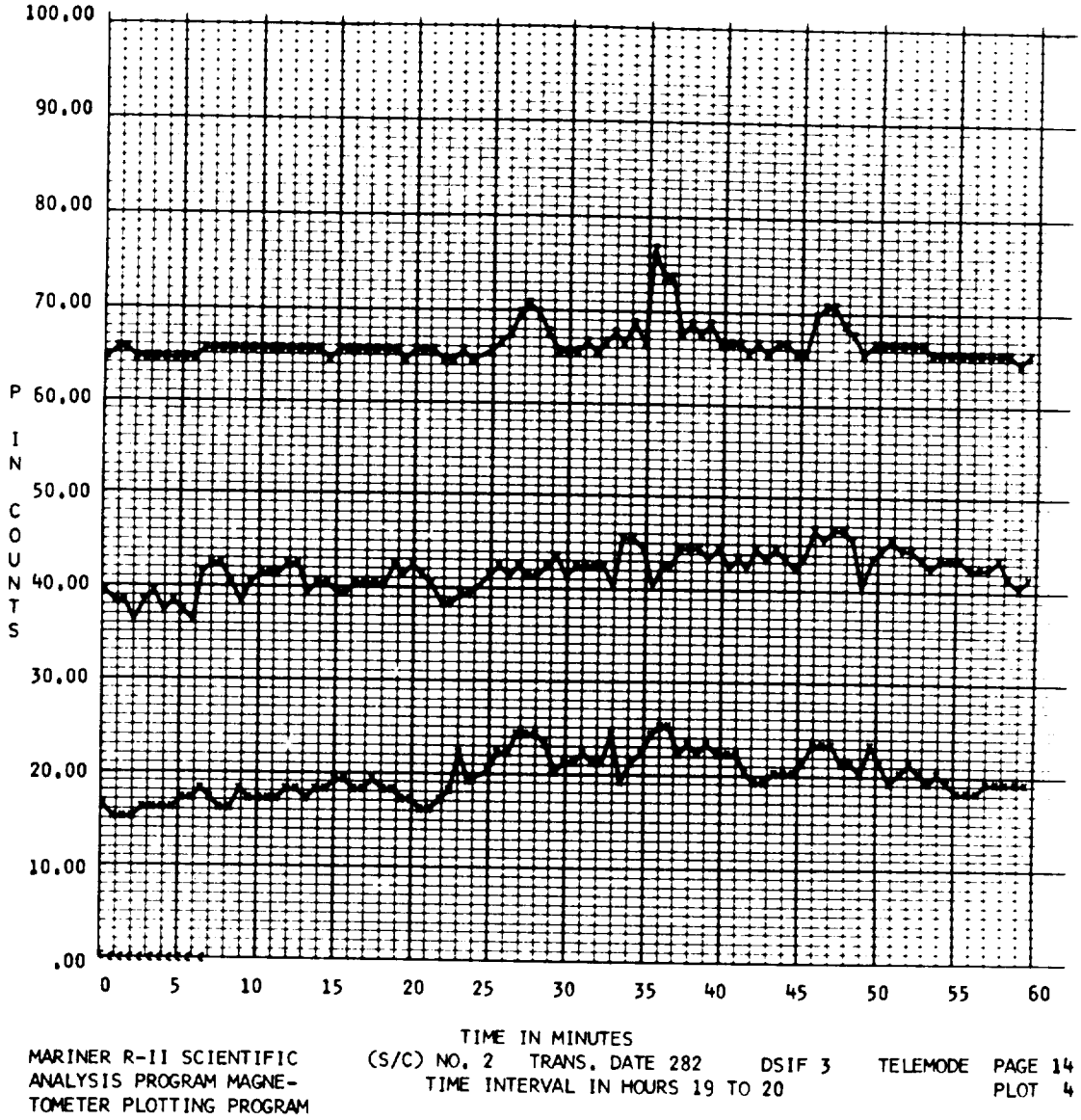

FIGURE 7–32.—Typical graph of analyzed science data produced by Stromberg-Carlson 4020 plotter.

MA R-II SCIENCE T/M QUICK LOOK MEASUREMENTS STATION 3 DATE 274

HRMNSC	PL	IT	EV SIX	MX	RI	MY	IRTH	MZ	RSC	FC	PS	CO	M	MT	IR1	R2	IR2	IRTC	PL
200341	161	42	2	187	0	180	0	135	0	99	1	0-0	1-1-1	44	0	0	0	0	119
200341	238	42	25870	186	0	179	0	131	0	100	1	0-0	1-1-1	44	0	0	0	0	242
200341	155	42	16	185	0	183	0	137	0	100	1	0-0	1-1-1	44	0	0	0	0	161
200341	164	42	171	185	0	183	0	136	0	100	1	0-0	1-1-1	44	0	0	0	0	144
200341	132	42	1	186	0	182	0	135	0	100	1	0-0	1-1-1	44	0	0	0	0	138
200341	154	43	20	185	0	182	0	135	0	100	1	0-0	1-1-1	44	0	0	0	0	156
200341	161	42	203	186	0	180	0	135	0	100	1	0-0	1-1-1	44	0	0	0	0	119
200832	237	42	25870	186	0	180	0	133	0	101	1	0-0	1-1-1	44	0	0	0	0	243
200832	156	42	0	188	0	180	0	136	0	101	1	0-0	1-1-1	44	0	0	0	0	162
200832	166	42	0	182	0	186	0	132	0	101	1	0-0	1-1-1	44	0	0	0	0	150
200832	134	42	0	183	0	184	0	132	0	101	1	0-0	1-1-1	44	0	0	0	0	135
200832	154	19	1	183	0	184	0	134	0	101	1	0-0	1-1-1	44		0	0	0	156
200832	163	42	2	186	0	180	0	131	0	101	1	0-0	1-1-1	44	0	0	0	0	119
200832	238	42	25870	183	0	181	0	129	0	102	1	0-0	1-1-1	44	0	0	0	0	243
200832	159	42	22	183	0	184	0	127	0	102	1	0-0	1-1-1	44	0	0	0	0	163
200832	166	42	155	189	0	179	0	135	0	102	1	0-0	1-1-1	44	0	0	0	0	145
201349	132	42	1	192	0	181	0	136	0	102	1	0-0	1-1-1	44	0	0	0	0	144
201349	153	43	1	190	0	180	0	136	0	102	1	0-0	1-1-1	44	0	0	0	0	155
201349	161	42	6	189	0	181	0	137	0	102	1	0-0	1-1-1	44	0	0	0	0	119
201349	238	42	25870	187	0	182	0	137	0	103	1	0-0	1-1-1	44	0	0	0	0	242
201349	147	42	0	187	0	182	0	138	0	103	1	0-0	1-1-1	44	0	0	0	0	159
201349	162	42	0	183	0	184	0	135	0	103	1	0-0	1-1-1	44	0	0	0	0	145
201349	131	42	0	186	0	180	0	136	0	103	1	0-0	1-1-1	44	0	0	0	0	142
201349	153	43	0	186	0	180	0	135	0	103	1	0-0	1-1-1	44	0	0	0	0	155
201840	161	42	1	186	0	181	0	136	0	103	1	0-0	1-1-1	44	0	0	0	0	119
201840	238	38	25870	186	0	181	0	136	0	104	1	0-0	1-1-1	44	0	0	0	0	242

FIGURE 7–33.—Example of quick-look science data.

```
CASE 1                                  SPACE TRAJECTORIES                                  1

                        MA R-II    ORBIT VEMV-8D  POST ENC DEC 7,1962      2  12/15/62
     EPHEMERIDES WITH V NUS VELOCITIES

  GME  .39860320 06     J  .16234500-02     H -.57499999-05     D  .78749999-05     RE  .63781650 04    REM  .63781650 04
    G  .66709998-19     A  .88745998 29     B  .88763998 29     C  .88800998 29    OME  .41780741-02     AU  .14959930 09
  GMM  .49007589 04   SMS  .13271544 12   SMV  .32480830 06   GMA  .42977799 05    GMB  .00000000 00    GMJ  .12671060 09
  ARA  .38300000 01    G8  .38300000 00   MAS  .19822000 03   GB1  .00000000 00    GB2  .00000000 00     SC -.10200000 09

INJECTION CONDITIONS              VENUS              JULIAN DATE 2438005.50000000              DEC. 7,1962   00 00 00.000

GEOCENTRIC          X0-.36494777 08   Y0-.29910862 08   Z0-.94549110 07 DX0-.73400789 01 DY0-.10825428 02 DZ0-.54160900 01
CARTESIAN         GMC .00000000 00 SGC .00000000 00   T0 .00000000 00 GHA .75283384 02 GH0 .75283984 02

   0 DAYS  0 HRS.  0 MIN.  0.000 SEC.              JULIAN DATE 2438005.50000000              DEC. 7,1962   00 00 00.000

GEOCENTRIC                                                                          EQUATORIAL COORDINATES

    X -.36494775 08      Y -.29910862 08      Z -.94549114 07     DX -.73400778 01     DY -.10825427 02     DZ -.54160899 01
    R  .46124043 08    DEC -.11330586 02     RA  .21933780 03      V  .14156293 02    PTH  .70676945 02     AZ  .12742878 03
    R  .46124042 08    LAT -.11330586 02    LON  .14405382 03     VF  .34371720 04    PTE  .22268551 00    AZE  .26995253 03
   XS -.39629461 08     YS -.13023531 09     ZS -.56473325 08    DXS  .29174320 02    DYS -.72396077 01    DZS -.31395477 01
   XM  .35299953 08     YM  .98256499 05     ZM  .81954999 04    DXM -.29592443 00    DYM  .95276982 00    DZM  .38660192 00
   XT -.37501211 08     YT -.32036233 08     ZT -.12382398 08    DXT -.59612937 01    DYT -.75810990 01    DZT -.10726709 01
   RS  .14734035 09     VS  .30222667 02     RM  .36651359 06     VM  .10699545 01     RT  .50852579 08     VT  .97036440 01
  GED -.11405734 02    ALT  .43117666 08    LUS  .17779147 03    RAS  .25307545 03    RAM  .15555987 02    LOM  .30027200 03
  DUT  .34000000 02     OT -.21600000 05     OR  .13358831 02    SHA -.26953946 08    DES -.22530851 02    DEM  .12812794 01
 BOARD UNITS
   UE  .20000000 01     VE  .20000000 01    ALF  .80000000 02     S1  .50000000 05     S2  .10000000 05
  UP1  .57346404 03    VP1 -.29082832 03    UM1 -.65207329 00    VM1  .56627338 01      S  .22162253 02      M  .13629542 03
  UP2  .26073204 04    VP2 -.14621416 04    UM2 -.11260366 02    VM2  .20313669 02     GM  .19513358 03

GEOCENTRIC                                        CONIC     CONVENTIONAL B.T AND B.R     EQUATORIAL COORDINATES

EPOCH OF PERICENTER PASSAGE                                JULIAN DATE 2437968.38064742              OCT. 30,1962   21 08 07.938
  SMA -.19341960 04     ECC  .50055959 04     INC  .38864489 02     LAN  .24940607 02     APF  .12756307 03     RCA  .15922710 08
   VH  .14155708 02      C3  .20038407 03      C1  .22542539 09     SLR  .12748671 12     APO  .00000000 00     TFP  .32071120 07
   TA  .70683596 02      SA  .10144381 03      HA  .13076478 07     DAD -.22494569 02     RAD  .23586150 03     MTA  .90007156 02
   WX  .26459511 00      WY -.56896514 00      WZ  .77863220 00      PX -.81304668 00      PY  .30258100 00      PZ  .49739303 00
   QX -.51859863 00      QY -.76467206 00      QZ -.38253374 00      RX  .21471095 00      RY  .31666829 00      RZ -.92391577 00
  SXO -.51849706 00     SYO -.76470985 00     SZO -.38259587 00      TX -.82768351 00      TY  .56119516 00      TZ  .00000000 00
   BX -.81311145 00      BY  .30248548 00      BZ  .49734525 00      MX  .59573288 00      MY -.53848931 00      MZ -.59592919 00
  B.T  .13420577 08     B.R -.85722890 07      B  .15924699 08     PER  .00000000 00     OMD  .14516053-12     NOD -.11128283-12

HELIOCENTRIC                                                                        ECLIPTIC COORDINATES

    X  .31346863 07      Y  .11074392 09      Z  .32253680 07     DX -.36514397 02     DY -.41955198 01     DZ -.66208677 00
    R  .11054021 09    LAT  .16674993 01    LON  .88378704 02      V  .36760603 02    PTH -.82013759 01     AZ  .90802670 02
   XE  .39629461 08     YE  .14195236 09     ZE  .41700000 03    DXE -.29174320 02    DYE  .78910505 01    DZE  .27152896-03
   XT  .21282497 07     YT  .10763434 09     ZT  .13850560 07    DXT -.35135613 02    DYT  .50896181 00    DZT  .20321334 01
  LTE  .16211347-03    LUE  .74401628 02    LTT  .73710632 00    LOT  .88867239 02    RST  .10766428 09    VST  .35198010 02
  EPS  .13186355 03    ESP  .14074205 02    SEP  .34062239 02    EPM  .18754147 00    EMP  .25466829 02    MEP  .15434553 03
  MPS  .13167606 03    MSP  .14197056 02    SMP  .34126875 02    SEM  .12029609 03    EMS  .59581031 02    ESM  .12294532 00
  EPT  .13509013 03    ETP  .41421536 02    TEP  .29882662 01    TPS  .31723024 02    TSP  .10507857 01    STP  .14722617 03
  SET  .31973511 02    STE  .13354251 03    EST  .14483971 02    RPM  .48454687 08    RPT  .37550361 07    SPN  .13185595 03
  SAC -.22185995-04
  GCE  .87303390 02    GCT  .33626744 03    SIP  .31628421 02    CPT  .72848451 02    SIN  .72753847 02
  REP  .49124043 08    VEP  .14156293 02
```

FIGURE 7–34.—Example of processed tracking data for trajectory program.

MA R-II SCIENTIFIC ANALYSIS PROGRAM (S/C) NO. 2 TRANS. DATE 364 DSIF STAT. 2 TELEMODE 2 PAGE174
IC CHAMBE EXPERIMENT PAGE 24

FC	TIME	IT	F	CON	CON	START-TME	END-TME	DEL-TME	ION-RT	INT-MDPT	INT-2	RATE-2
---	DY HR MN SS	CTS	CTS	ONL	TMD	SECONDS	SECONDS	SECONDS		HR MN SC	SCNDS	
225	13 02 12	42	0	NO	NO							
225	13 02 49	42	0	NO	NO							
225	13 03 26	42	0	NO	NO							
225	13 04 03	42	0	NO	NO							
226	13 04 40	42										
226	13 05 17	42										
226	13 05 53	42										
226	13 06 30	42										
226	13 07 07	31				5217.96	47220.24	42002.28	8.15	07 16 59	41997.47	8.15
226	13 07 44	42										
227	13 08 21	42										
227	13 08 58	42										
227	13 09 35	42	0	NO	NO							
227	13 10 12	42	0	NO	NO							
227	13 10 50	42	0	NO	NO							
227	13 11 26	42	0	NO	NO							
228	13 12 03	42										
228	13 12 40	42										
228	13 13 17	42										
228	13 13 54	42										
228	13 14 31	43										
228	13 15 08	42										
229	13 15 45	2				47220.24	47713.88	493.64	693.03	13 11 07	493.04	693.88
229	13 16 22	42										
229	13 16 58	42	0	NO	NO							
229	13 17 35	42	0	NO	NO							
229	13 18 12	42	0	NO	NO							
229	13 18 49	42	0	NO	NO							
230	13 19 26	42										
230	13 20 03	42										
230	13 20 41	42										
230	13 21 18	42										
230	13 21 55	43										
230	13 22 31	42										
231	13 23 08	42										
231	13 23 45	7				47713.88	48198.08	484.20	706.54	13 19 15	484.64	705.90
231	13 24 22	42	0	NO	NO							
231	13 24 59	42	0	NO	NO							
231	13 25 36	42	0	NO	NO							
231	13 26 13	42	0	NO	NO							

FIGURE 7–35.—Typical page of analyzed science data.

ENGINEERING TELEMETRY MEASUREMENTS TELEMODE 2 STATION 000004 DATE 361 1962 S/C 2 PAGE 4

HIGH RATE

GMTIM.	A0 ACC DN	A1 C-DECK UNILENT DN	A2 BATTERY VOLTAGE DN	VOLT	A3 YAW CNTRL GYRO DN	MR/S	A4 PITCH CTRL GYRO DN	MR/S	A5 ROLL CNTRL GYRO DN	MR/S	A6 BATTERY CUR DRAIN DN	AMPS	A7 PITCH SUN SENSOR DN	MR	A8 YAW SUN SENSOR DN	MR	A9 ROLL ERROR DN	MR
193757			51	31.1	63	.22	63	.21	63	.21	4	-.1	66-1.119		60	1.298	82-2.841	
193834			51	31.1	63	.22	63	.21	63	.21	4	-.1	66-1.119		60	1.298	84-3.165	
193911			51	31.1	63	.22	63	.21	63	.21	4	-.1	66-1.119		60	1.298	86-3.490	
193948			51	31.1	63	.22	63	.21	63	.21	4	-.1	66-1.119		60	1.298	88-3.815	
194025			51	31.1	63	.22	63	.21	63	.21	4	-.1	66-1.119		60	1.298	90-4.139	
194102			51	31.1	63	.22	63	.21	63	.21	4	-.1	66-1.119		60	1.298	92-4.464	
194139			51	31.1	63	.22	63	.21	63	.21	4	-.1	66-1.119		60	1.298	92-4.464	
194216			51	31.1	63	.22	63	.21	63	.21	4	-.1	66-1.119		60	1.298	90-4.139	
194253			51	31.1	63	.22	63	.21	63	.21	4	-.1	66-1.119		59	1.639	88-3.815	
194330			51	31.1	63	.22	63	.21	63	.21	4	-.1	66-1.119		60	1.298	86-3.490	
194407			51	31.1	63	.22	63	.21	63	.21	4	-.1	66-1.119		60	1.298	84-3.165	
194444			51	31.1	63	.22	63	.21	63	.21	4	-.1	66-1.119		60	1.298	83-3.003	
194521			51	31.1	63	.22	63	.21	63	.21	4	-.1	66-1.119		60	1.298	81-2.678	
194558			51	31.1	63	.22	63	.21	63	.21	4	-.1	66-1.119		60	1.298	80-2.516	
194635			51	31.1	63	.22	63	.21	63	.21	4	-.1	66-1.119		60	1.298	78-2.191	
194712			51	31.1	63	.22	63	.21	63	.21	4	-.1	66-1.119		59	1.639	76-1.867	
194749			51	31.1	63	.22	63	.21	63	.21	4	-.1	66-1.119		60	1.298	75-1.704	
194826			51	31.1	63	.22	63	.21	63	.21	4	-.1	66-1.119		60	1.298	74-1.542	
194903			51	31.1	63	.22	63	.21	63	.21	4	-.1	66-1.119		60	1.298	72-1.218	
194939			51	31.1	63	.22	63	.21	63	.21	4	-.1	66-1.119		60	1.298	72-1.218	
195016			51	31.1	63	.22	63	.21	63	.21	4	-.1	66-1.119		60	1.298	70 -.893	
195053			51	31.1	63	.22	63	.21	63	.21	4	-.1	66-1.119		60	1.298	68 -.568	
195130			51	31.1	63	.22	63	.21	63	.21	4	-.1	66-1.119		60	1.298	67 -.406	
195207			51	31.1	63	.22	63	.21	63	.21	4	-.1	66-1.119		60	1.298	67 -.406	
195244			51	31.1	63	.22	63	.21	63	.21	4	-.1	66-1.119		60	1.298	66 -.244	
195321			51	31.1	63	.22	63	.21	63	.21	4	-.1	66-1.119		60	1.298	64 .081	
195358			51	31.1	63	.22	63	.21	63	.21	4	-.1	66-1.119		60	1.298	63 .243	
195435			51	31.1	63	.22	63	.21	63	.21	4	-.1	66-1.119		60	1.298	63 .243	
195512			51	31.1	63	.22	63	.21	63	.21	4	-.1	66-1.119		59	1.639	62 .406	
195549			51	31.1	63	.22	63	.21	63	.21	4	-.1	66-1.119		60	1.298	62 .406	
195626			51	31.1	63	.22	63	.21	63	.21	4	-.1	66-1.119		60	1.298	61 .568	
195703			51	31.1	63	.22	63	.21	63	.21	4	-.1	66-1.119		60	1.298	61 .568	
195740			51	31.1	63	.22	63	.21	63	.21	4	-.1	66-1.119		60	1.298	61 .568	
195817			51	31.1	63	.22	63	.21	63	.21	4	-.1	66-1.119		60	1.298	60 .730	
195854			51	31.1	63	.22	63	.21	63	.21	4	-.1	66-1.119		60	1.298	60 .730	
195931			51	31.1	63	.22	63	.21	63	.21	4	-.1	66-1.119		59	1.639	59 .893	
200008			51	31.1	63	.22	63	.21	63	.21	4	-.1	65 -.743		60	1.298	59 .893	
200045			51	31.1	63	.22	63	.21	63	.21	4	-.1	66-1.119		60	1.298	59 .893	
200122			51	31.1	63	.22	63	.21	63	.21	4	-.1	66-1.119		60	1.298	59 .893	
200159			51	31.1	63	.22	63	.21	63	.21	4	-.1	66-1.119		59	1.639	59 .893	
200236			51	31.1	63	.22	63	.21	63	.21	4	-.1	66-1.119		60	1.298	59 .893	
200313			51	31.1	63	.22	63	.21	63	.21	4	-.1	66-1.119		60	1.298	60 .730	
200349			51	31.1	63	.22	63	.21	63	.21	4	-.1	66-1.119		59	1.639	59 .893	
200426			51	31.1	63	.22	63	.21	63	.21	4	-.1	66-1.119		60	1.298	60 .730	
200503			51	31.1	63	.22	63	.21	63	.21	4	-.1	66-1.119		60	1.298	61 .568	
200540			51	31.1	63	.22	63	.21	63	.21	4	-.1	66-1.119		60	1.298	61 .568	
200617			51	31.1	63	.22	63	.21	63	.21	4	-.1	66-1.119		59	1.639	61 .568	
200654			51	31.1	63	.22	63	.21	63	.21	4	-.1	66-1.119		60	1.298	62 .406	
200731			51	31.1	63	.22	63	.21	63	.21	4	-.1	66-1.119		60	1.298	63 .243	
200809			51	31.1	63	.22	63	.21	63	.21	4	-.1	66-1.119		60	1.298	63 .243	

FIGURE 7–36.—Example of processed engineering data.

BATTERY DATA AND INTERNAL TEMPERATURES — CRAFT 2 — STATION 4 DATE 12/27 1962 — PAGE 004

TIME FAT. CURRENT H M S	CHARGER CURRENT AMPS	BATTERY CURRENT AMPS	CHARGE STATE AMPHOUR	BATTERY VOLTAGE VOLTS	BATTERY TEMP. DEG. F	BOOSTER TEMP. DEG. F	PS AND L TEMP. DEG. F	INVERTER TEMP. DEG. F
205643	-.01	-.11	40.21	31.06C	133.5B	136.5	155.C	130.0
205118	-.01	-.11	40.21	31.06C	133.5B	136.5	155.C	130.0
205155	-.01	-.11	40.21	31.06C	133.5B	136.5	155.C	130.0
205232	-.01	-.11	40.21	31.06C	133.5B	136.5	155.C	130.0
2053 9	-.01	-.11	40.22	31.06C	133.5B	136.5	155.C	130.0
205346	-.01	-.11	40.22	31.06C	133.5B	136.5	155.C	130.0
205423	-.01	-.11	40.22	31.06C	133.5B	136.5	155.C	130.0
2055 0	-.01	-.11	40.22	31.06C	133.5B	136.5	155.C	130.0
205537	-.01	-.11	40.22	31.06C	133.5B	136.5	155.C	130.0
205615	-.01	-.11	40.22	31.06C	133.5B	136.5	155.C	130.0
205652	-.01	-.11	40.22	31.06C	133.5B	136.5	155.C	130.0
205729	-.01	-.11	40.22	31.06C	133.5B	136.5	155.C	130.0
205E 6	-.01	-.11	40.23	31.06C	133.5B	136.5	155.C	130.0
205843	-.01	-.11	40.23	31.06C	133.5B	136.5	155.C	130.0
205920	-.01	-.11	40.23	31.06C	133.5B	136.5	155.C	130.0
205956	-.01	-.11	40.23	31.06C	133.5B	136.5	155.C	130.0
21 033	-.01	-.11	40.23	31.06C	133.5B	136.5	155.C	130.0
21 1 9	-.01	-.11	40.23	31.06C	133.5B	136.5	155.C	130.0
21 146	-.01	-.11	40.23	31.06C	133.5B	136.5	155.C	130.0
21 223	-.01	-.11	40.23	31.06C	133.5B	136.5	155.C	130.0
21 3 1	-.01	-.11	40.24	31.06C	133.5B	136.5	155.C	130.0
21 33.	-.01	-.11	40.24	31.06C	133.5B	136.5	155.C	130.0
21 415	-.01	-.11	40.24	31.06C	133.5B	136.5	155.C	130.0
21 452	-.01	-.11	40.24	31.06C	133.5B	136.5	155.C	130.0
21 529	-.01	-.11	40.24	31.06C	133.5B	136.5	155.C	130.0
21 6 6	-.01	-.11	40.24	31.06C	133.5B	136.5	155.C	130.0
21 643	-.01	-.11	40.24	31.06C	133.5B	136.5	155.C	130.0
21 720	-.01	-.11	40.24	31.06C	133.5B	136.5	155.C	130.0
21 757	-.01	-.11	40.25	31.06C	133.5B	136.5	155.C	130.0
21 .33	-.01	-.11	40.25	31.06C	133.5B	136.5	155.C	130.0
21 910	-.01	-.11	40.25	31.06C	133.5B	136.5	155.C	130.0
21 947	-.01	-.11	40.25	31.06C	133.5B	136.5	155.C	130.0
211024	-.01	-.11	40.25	31.06C	133.5B	136.5	155.C	130.0
2111 1	-.01	-.11	40.25	31.06C	133.5B	136.5	155.C	130.0
211140	-.01	-.11	40.25	31.06C	133.5B	136.5	155.C	130.0
211217	-.01	-.11	40.26	31.06C	133.5B	136.5	155.C	130.0
211254	-.01	-.11	40.26	31.06C	133.5B	136.5	155.C	130.0
211331	-.01	-.11	40.26	31.06C	133.5B	136.5	155.C	130.0
2114 8	-.01	-.11	40.26	31.06C	133.5B	136.5	155.C	130.0
211445	-.01	-.11	40.26	31.06C	133.5B	136.5	155.C	130.0
211521	-.01	-.11	40.26	31.06C	133.5B	136.5	155.C	130.0
211558	-.01	-.11	40.26	31.06C	133.5B	136.5	155.C	130.0
211634	-.01	-.11	40.26	31.06C	133.5B	136.5	155.C	130.0
211711	-.01	-.11	40.27	31.06C	133.5B	136.5	155.C	130.0
211748	-.01	-.11	40.27	31.06C	133.5B	136.5	155.C	130.0
211826	-.01	-.11	40.27	31.06C	133.5B	136.5	155.C	130.0
2119 3	-.01	-.11	40.27	31.06C	133.5B	136.5	155.C	130.0
211940	-.01	-.11	40.27	31.06C	133.5B	136.5	155.C	130.0
212017	-.01	-.11	40.27	31.06C	133.5B	136.5	155.C	130.0
212054	-.01	-.11	40.27	31.06C	133.5B	136.5	155.C	130.0
212131	-.01	-.11	40.27	31.06C	133.5B	136.5	155.C	130.0
2122 8	-.01	-.11	40.28	31.06C	133.5B	136.5	155.C	130.0
212245	-.01	-.11	40.28	31.06C	133.5B	136.5	155.C	130.0
212321	-.01	-.11	40.28	31.06C	133.5B	136.5	155.C	130.0

FIGURE 7–37.—Typical page of analyzed engineering data.

Scientific Telemetry

The flow of information from the scientific instruments on board the spacecraft to the experimenters was described above under Data-Handling Processes. A first analysis was performed to determine the quality and quantity of science telemetry transmitted over teletype from the DSIF stations and over the phone line from Goldstone during the periods from August 30 to October 31 and November 8 to December 14. During this 100-day period, slightly more than 225 000 science subframes were generated on the spacecraft. (A subframe consists of the 168 bits of data that time-share the telemetry link with 140 bits of engineering data every 36 957 sec, at the rate of 8.334 BPS.)

Approximately 87.7% of the generated 37.8 million bits were processed in excellent condition through the DSIF demodulators, teletype encoders, transmitters, and JPL terminal computers (PDP–1 or IBM 7090). The daily pattern was reflected in figure 7–38. Data classified as missing were later partially recovered from DSIF station tapes, and the effort to reconstruct an optimal set of science computer tapes was continued. Errors were classified as significant if they affected the readout of any of the cruise science experiments or any of the 23 pre-encounter radiometer calibrations. No attempt was made to distinguish between error sources; these may have existed anywhere between the spacecraft and the IBM 1403 printer. The periods considered were those during which the DSIF station concerned was actually committed to track Mariner. By using redundant decommutation and transmission equipment at Goldstone during mode III, 100% of the planetary data were recovered in excellent condition on the day of Venus encounter.

INFORMATION COORDINATION

SDAT Reports

Initial spacecraft-status information was provided by SDAT to the information coordinator at $L+2$ hr, $L+3$ hr, $L+12$ hr, $L+14$ hr, and $L+18$ hr. A preliminary flight summary for the first 24 hours of flight was provided at $L+1$ day. SDAT reports were made thereafter on each weekday until November 1; after that date, reports were provided twice each weekday (1600 and 2300) until Venus encounter. During the encounter phase, SDAT reports were provided at $E-25$ hr, $E-10$ hr, $E+4$ hr, and $E+23$ hr. (The symbol E, as used here, should be interpreted as encounter or time of closest approach to the planet.)

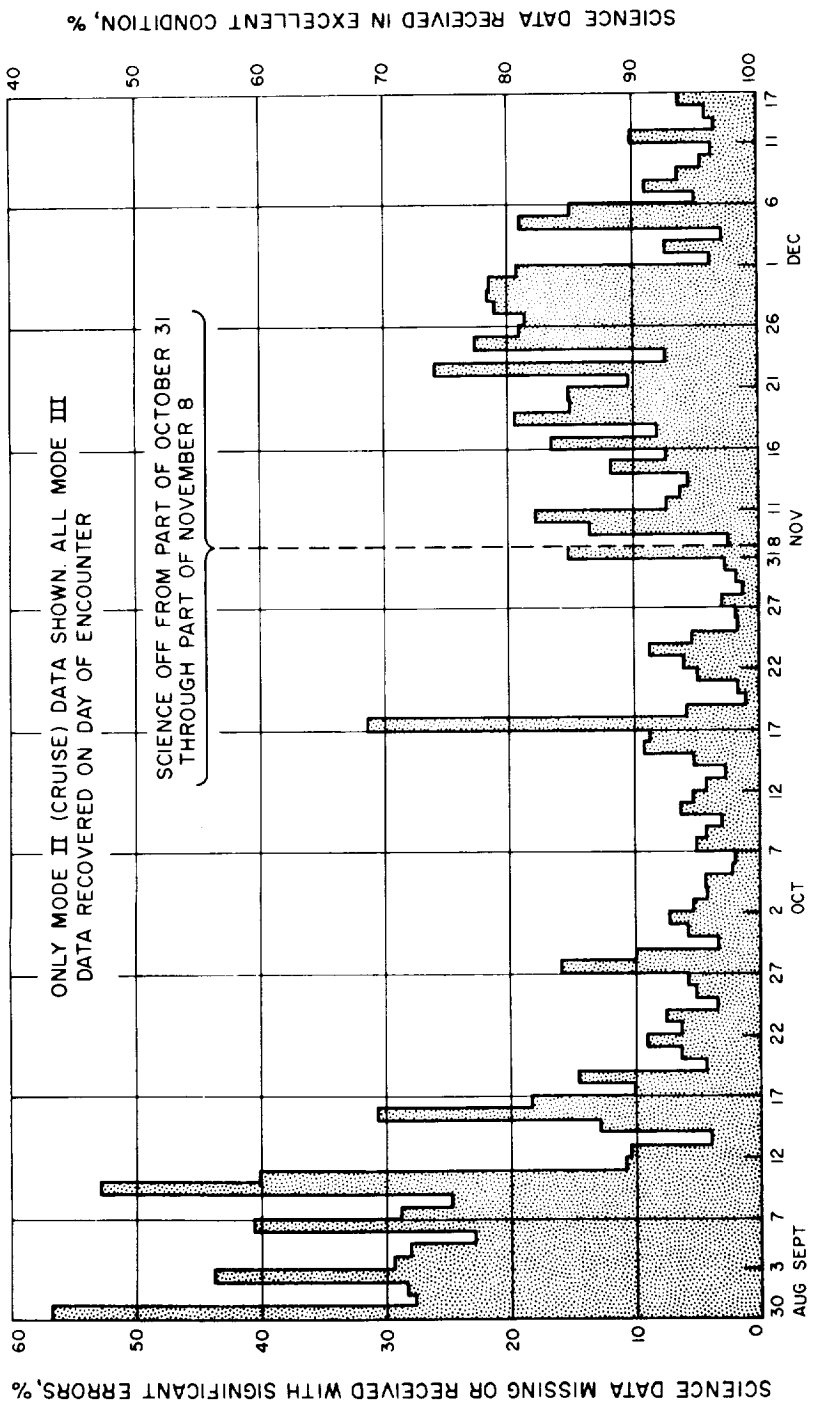

FIGURE 7–38.—Percentage of missing or significantly erroneous cruise science data received in real-time or near-real-time transmission by teletype or telephone.

Following encounter, SDAT provided reports twice each weekday until 24 hr/day DSIF coverage was discontinued. Thereafter, an SDAT report was made for each tracking period (approximately once per day) until the end of the mission.

The reports provided by SDAT between launch and September 18 indicated only that spacecraft-subsystem status was normal or abnormal; abnormal conditions were accompanied by short explanations of the situation. Beginning on September 18, however, the SDAT report form was changed to include specific spacecraft-subsystem measurements. The specific measurements given were CC&S pulse times, attitude-control nitrogen supply and usage, Earth-brightness data number, antenna hinge angle, hinge reference angle, battery voltage and current for each solar panel, spacecraft power consumption and available power, antenna RF power, telemetry mode and data rate, and temperatures at 18 locations on the spacecraft.

Trajectory Information

The initial spacecraft trajectory information provided was based on the nominal and first-through-sixth orbit computations run from launch to the period just prior to the midcourse maneuver. Predicted nominal midcourse-maneuver trajectory information was issued at midcourse. Postmidcourse trajectory information was reported on September 25 (fifth postmidcourse-orbit computation), on November 8 (twelfth postmidcourse-orbit computation), and weekly thereafter until Venus encounter. During encounter, trajectory-information reports were received at $E-25$ hr, $E-10$ hr, and $E+45$ min. This type of report was then no longer provided.

Trajectory-information reports received from launch through September 25 contained Earth-fixed spherical, Earth conic, and heliocentric conic coordinates. Beginning with trajectory information received on November 8, the report contained both Venus encounter and radiometer scan parameters.

The JPL Office of Public Education and Information (OPEI) was provided with data on August 29, September 4, 8, 24, November 28, and December 10. These data blocks contained information for updating display boards located at JPL, NASA, and AMR, and also contained spacecraft distances and speed. Specifically, the data blocks contained 6-hour increments, from launch to encounter, of spacecraft distance from Earth and Venus, spacecraft velocity relative to Earth and Sun, spacecraft latitude and longitude, and board coordinates.

DSIF Information

Every 20 min during the first day of flight, each station in the DSIF net transmitted real-time status information by teletype to the Net Control Room in the Space Flight Operations Center. The messages represented a complete record of the mission functions at each station, and their content was made available to the information coordinator.

Central Computing Facility Information

During the hours of launch, midcourse maneuver, and encounter, the CCF data processing project engineer reported equipment conditions over the voice communication system in the Space Flight Operations Center. During the encounter phase, these conditions were additionally presented on the computer-equipment status board located in the Space Flight Operations Center. During the remainder of the mission, CCF operations were directly coordinated with the test director, the DSIF operations manager, and CCF users.

Communications Status

Similarly, the status ot communications with the DSIF stations during the hours involving launch, midcourse maneuver, and encounter was reported by the communications coordinator over the voice communication system and was additionally reported during the encounter phase, via the DSIF communications status board. During the remainder of the mission, communications were coordinated directly with the test director and the DSIF operations manager.

Science Status

Reports were received from the Scientific Data Group each weekday from August 29, when science was first turned on, until October 19. From October 19 to Venus encounter, a report was received daily. During Venus encounter, scientific reports were received at E −25 hr, E −10 hr, E −2 hr, E +45 min, E +4 hr, and E +23 hr. Thereafter, until the end of the mission, scientific reports were received daily.

Each report received prior to October 19 contained a general statement regarding the condition of the scientific instruments. A short statement was also occasionally included to explain any unusual condition. Beginning on

October 19, the daily scientific status report contained a short statement concerning the condition of each experiment as well as the condition of the received data. Specific measurements produced by each experiment were included in reports received after November 10. Typical information reported was as follows:

Solar plasma:
- Plasma range, kev
- Calibration digital level
- Maximum discriminator level

Ion chamber:
- Recharging time, sec
- Milliroentgens, hr

Geiger-Mueller counters:
- Stainless steel, counts/sec
- Beryllium, counts/sec
- Anton 213, counts/sec

Magnetometer:
- Calibration times
- Temperature, ° F
- Interplanetary-field condition

Radiometers:
- Calibration times
- Microwave signal voltage, each channel
- Microwave baseline voltage, each channel
- Microwave scan position
- Infrared housing temperature, ° F
- Infrared calibration-plate temperature, ° F
- Voltage condition, both channels

Cosmic dust:
- Experiment condition
- Hits recorded, if any

COMMUNICATIONS COORDINATION

During the system tests and the flight of the Mariner II spacecraft, the Space Flight Operations Complex was provided with telephone, teletype, television, and high-speed data-communications support.

The long duration of the Mariner II mission provided a proving ground for the engineering concepts and hardware associated with communications. During this period, systems and subsystems underwent a proving-out process that confirmed the basic soundness of the engineering concepts, while revealing certain deficiencies in component subassemblies. As a result of these findings, an engineering study was initiated to provide for redesign and reconstruction of those units that had proved unsatisfactory.

The Mariner II operation also provided a testing ground for communications procedures. The concept of Communications Control as a central coordinating point for mission-dependent communications services was tested, modified, and found to be highly effective. Staffing requirements were evaluated for effective operation throughout the Complex during the course of a long mission and will be used in the procurement and training of personnel required for subsequent flights. The heavy and constant use of teletype equipment throughout the mission revealed deficiencies in maintenance procedures that have resulted in the procurement of additional maintenance equipment and the training of more maintenance personnel.

DISSEMINATION OF INFORMATION

The following paragraphs outline the manner in which information was disseminated to users and to the public throughout the mission.

Information Coodinator

Agency Status Reports were composed by the information coordinator. Their content was drawn from SDAT reports, trajectory information, science-status reports, and DSIF information. Each Agency Status Report was intended as a current summary of mission status, with emphasis on any abnormal or unusual events. Agency Status Reports were published, beginning immediately after launch, at 2400 each weekday and at 1600 each Monday. This routine continued until Venus encounter, when the reports were published at $E-24$ hr, $E-9$ hr, $E-6$ hr, $E-1$ hr, $E+1$ hr, and $E+6$ hr. Publication on each weekday was then resumed and continued until completion of the mission.

Technical Bulletins, prepared by the information coordinator, were based on the content of the SDAT reports, trajectory information, science-status reports, and DSIF information. The Technical Bulletins, which were more detailed than Agency Status Reports, were not published as frequently and had their

own distribution list at JPL. Off-lab distribution was the same as that for the Agency Status Reports. The bulletins were published each weekday from launch through the midcourse maneuver, weekly until Venus encounter, daily during encounter, and weekly thereafter, until the end of the mission.

Office of Public Education and Information

OPEI data were transmitted to cognizant personnel for the purpose of updating trajectory display boards. The frequency of these transmissions corresponded with receipt of the data blocks from the Orbit and Trajectory Determination Group.

All OPEI press releases were submitted to the information coordinator, and after final approval by the cognizant JPL and NASA management personnel the information was released to the press.

Display System

The Space Flight Operations status boards (fig. 7–39) in the Operations Center (Pasadena) were maintained in near-real time, 24 hr/day, from launch through midcourse maneuver and during Venus encounter. During the remainder of the mission, the boards were maintained during regular working hours. The trajectory-information, spacecraft, and scientific status boards were revised on the basis of each status report.

The DSIF and Communications status board was used to display, by means of lights, the DSIF station tracking the spacecraft, the ground mode existing at the station, the teletype lines being used to communicate with the DSIF stations, the use of each teletype line, and the condition of each teletype line. This board was remotely and indep ndently controlled; thus, the DSIF portion was controlled from the DSIF Net Control room and the communications-line status was controlled from the Communications Center.

The computer-equipment status board showed the condition and use of the equipment in the CCF. The control panel for this display was located in the CCF, so that computer personnel could remotely notify Space Flight Operations personnel of their local conditions.

The postlaunch-event board was maintained throughout the mission to display spacecraft events, relative distances and velocities, DSIF view and tracking periods, received-spacecraft-signal strength, and DSIF acquisition and loss times.

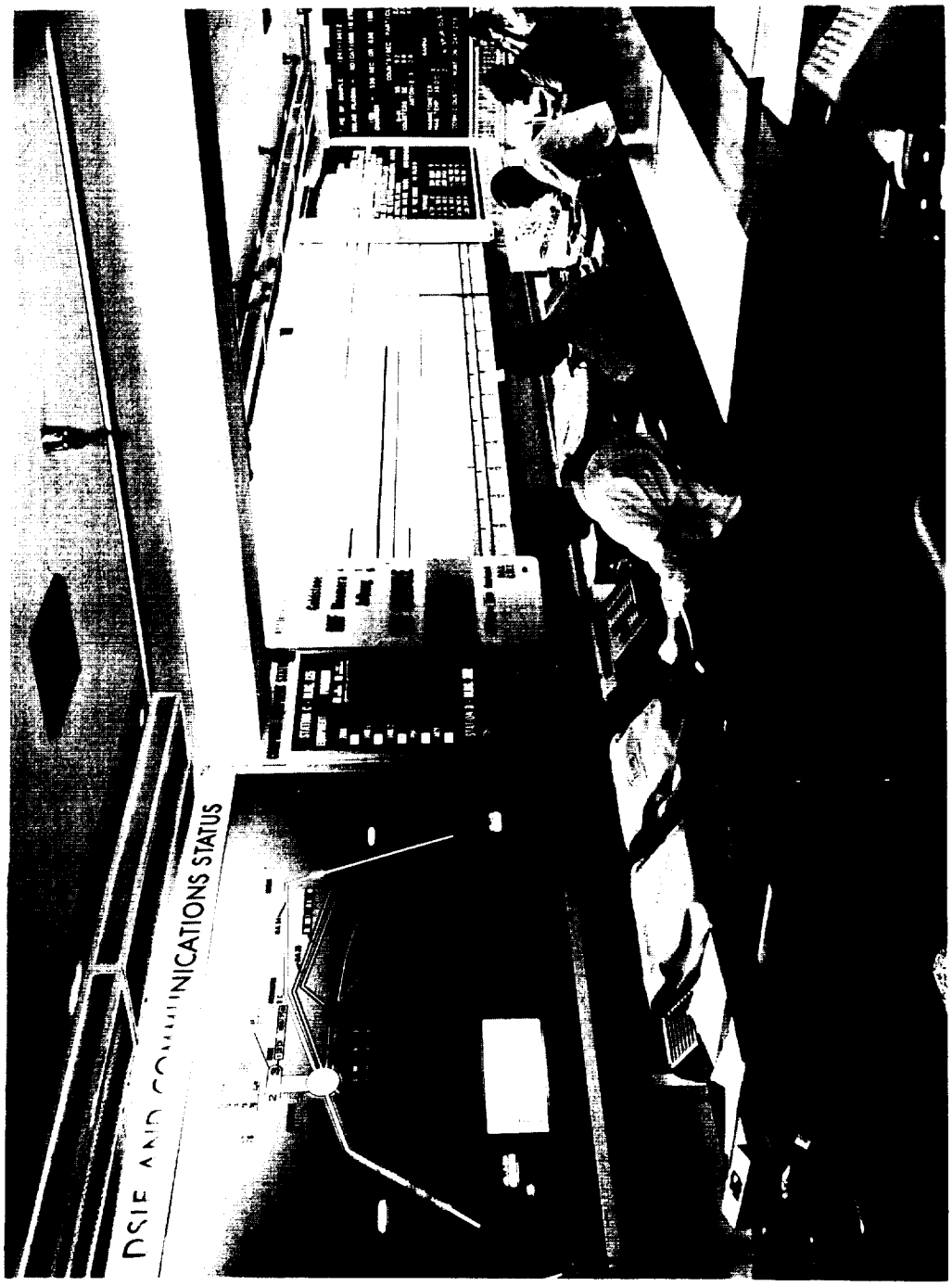

FIGURE 7-39.—Space Flight Operations status boards maintained at JPL-Pasadena through flight of Mariner II.

Current Greenwich mean time, Pacific standard time, and flight times were also shown.

A special-events board was also maintained, with entries made at the discretion of the test director. The board was used to display all significant spacecraft events, GMT and date of occurrence, and numbered day-of-the-year of occurrence.

Four digital clocks were maintained in the Space Flight Operations Center: (1) a GMT clock, (2) a countdown-countup clock, used during the launch, midcourse maneuver, and encounter periods, (3) a six-digit total-minutes-of-flight clock, used throughout the mission, and (4) a four-digit total-seconds-of-flight clock (days, hours, minutes, and seconds), used throughout the flight.

CHAPTER 8

Scientific Results

Several years will be required to analyze and fully evaluate all the scientific data derived from the Mariner II mission. In that sense, the measurements and results detailed in this chapter must be regarded as preliminary, although sufficiently definitive to establish a profile in each of the experimental areas.

INTERPLANETARY MEASUREMENTS

The Mariner II instruments were designed not only to provide observations in the vicinity of Venus but also to measure several properties of the interplanetary environment over the range of heliocentric distances between 1.5×10^8 and 1.1×10^8 km (9×10^7 and 7×10^7 miles).

The data recorded during the interplanetary flight of Mariner II indicated a persistent interplanetary magnetic field averaging about 4γ with rms fluctuations over 1 day of approximately 2γ. The interplanetary field appeared to lie mainly in the ecliptic plane and to have the expected spiral form, although there was a substantial fluctuating component. During the flight there was always a measurable flow of plasma from within 10° of the direction of the Sun. The plasma's bulk velocity was in the range of 320 to 770 km/sec (199 to 478 miles/sec). There were strong correlations between the plasma velocity and the level of terrestrial magnetic activity. Both of these quantities showed pronounced variations which displayed a 27-day recurrence tendency (equal to the Sun's rotation period). These variations (peaks) could not be identified with visible features on the Sun. The ion chamber reading did not change during the flight; however, terrestrial data indicated that the ionization level produced near the Earth by galactic cosmic rays increased. Figures indicated a gradient in galactic cosmic ray intensity of about 9% per astronomical unit. During this period there were several minor radiation-flux excursions and two major excursions associated with solar flares. The cosmic dust detector recorded only two definite impacts during the flight, indicating a flux of such particles of magnitude 10^{-4} times that near the Earth.

Magnetic Fields

The magnetic field observed by the triaxial fluxgate magnetometer was a superposition of the interplanetary field and a nearly constant spacecraft field. The two components of the spacecraft field perpendicular to the Sun-spacecraft direction were determined by examination of the magnetic readings at a time when the interplanetary field was fairly steady and the spacecraft was rolling about the Sun-spacecraft axis. A tentative estimate of the entire spacecraft field and its slow variation with time was made by combining the above data with plausibility arguments regarding the configuration of the interplanetary field averaged over long periods of time.

The results described here were obtained in interplanetary space during late August and September 1962, far enough from the Earth to be unaffected by the Earth's presence. No magnetic measurements were obtained either inside the geomagnetic field or in the region of the transition to interplanetary space.

Analysis of the data has verified a number of widely accepted beliefs and confirmed the main features of prior and less complete observations. One important result is the convincing evidence that interplanetary space is rarely empty or field-free. Magnetic fields of at least a few gamma were always observed, and transient nulls were too brief to be recorded as such. The fields varied irregularly with characteristic periods ranging from the observable lower limit (40 sec) to several hours. A typical average field strength was 4γ, and rms fluctuations over 1 day were approximately 2γ.

Figures 8–1 to 8–3 show the 1-day averages of the three interplanetary magnetic-field components with spacecraft fields subtracted in each case. The three figures depict, respectively, the radial component (positive in a direction outward from the Sun), the tangential component (in the ecliptic, positive in the direction opposite to planetary motion), and the normal component (perpendicular to the ecliptic, positive toward the north). The lower plot shows standard deviations for different time intervals: 3.7 min (bottom curve), 30 min (circles), 3 hr (crosses), 24 hr (top curve).

The long-time average field in the early portion of the flight (during which the spacecraft field was apparently constant) lay in the ecliptic and was directed in a manner corresponding to the spiral pattern expected for field lines immersed in solar-wind plasma flowing radially outward. Field fluctuations were large, however, with the tangential and normal components showing greater disturbance than the radial component. The radial and tangential components showed a

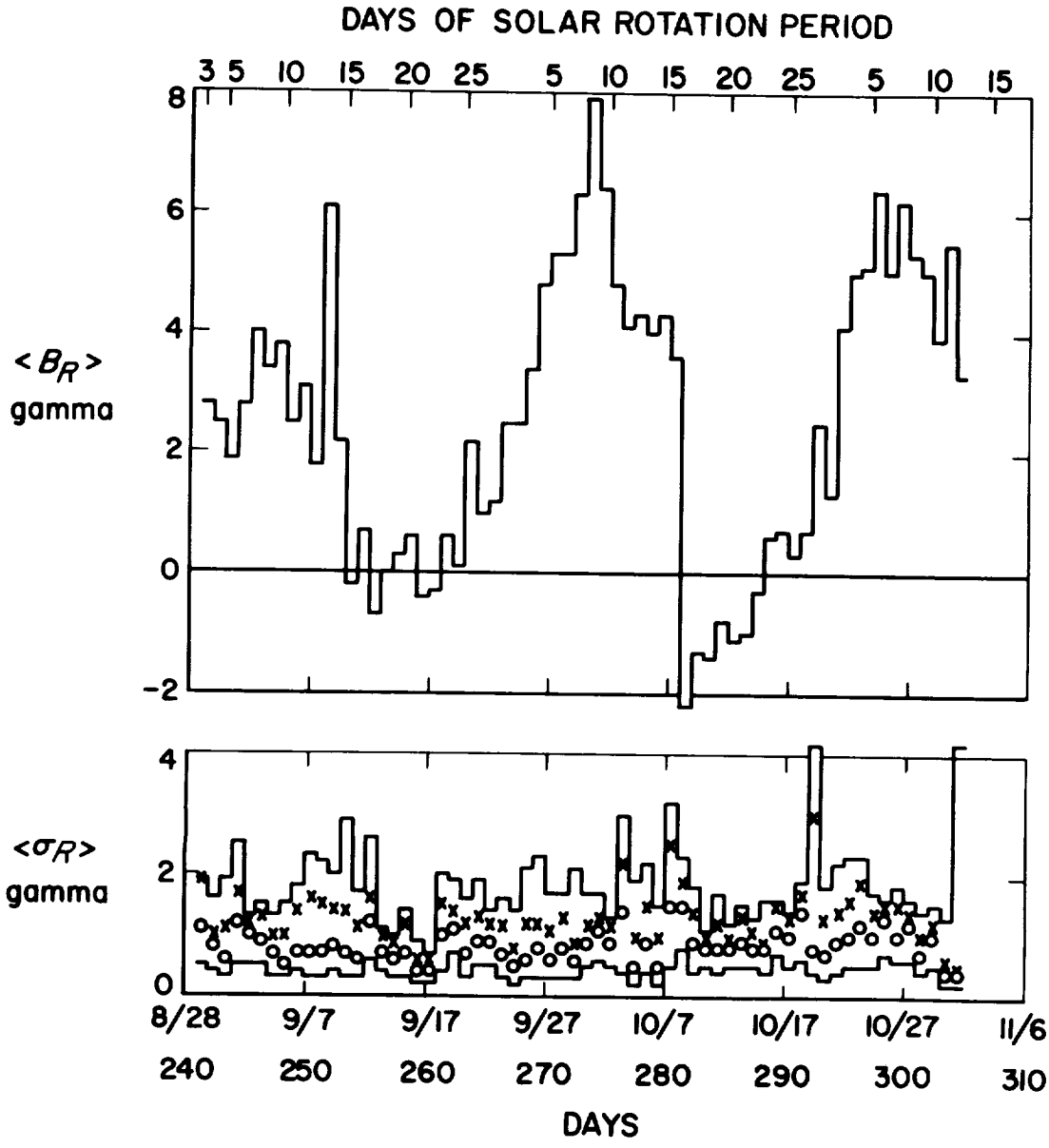

FIGURE 8–1.—Corrected interplanetary magnetic field, radial component, 1-day average.

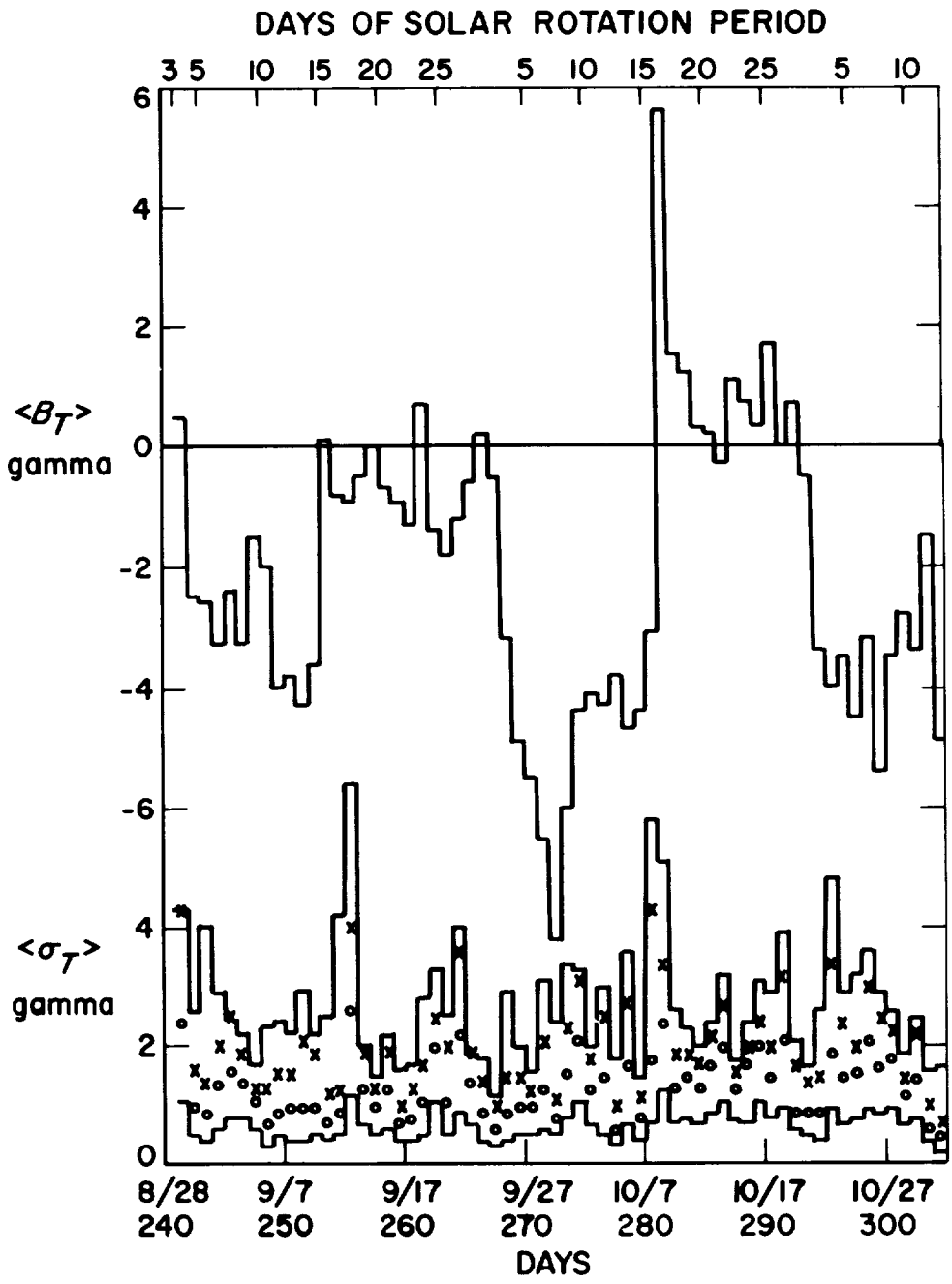

FIGURE 8–2.—Corrected interplanetary magnetic field, tangential component, 1-day average.

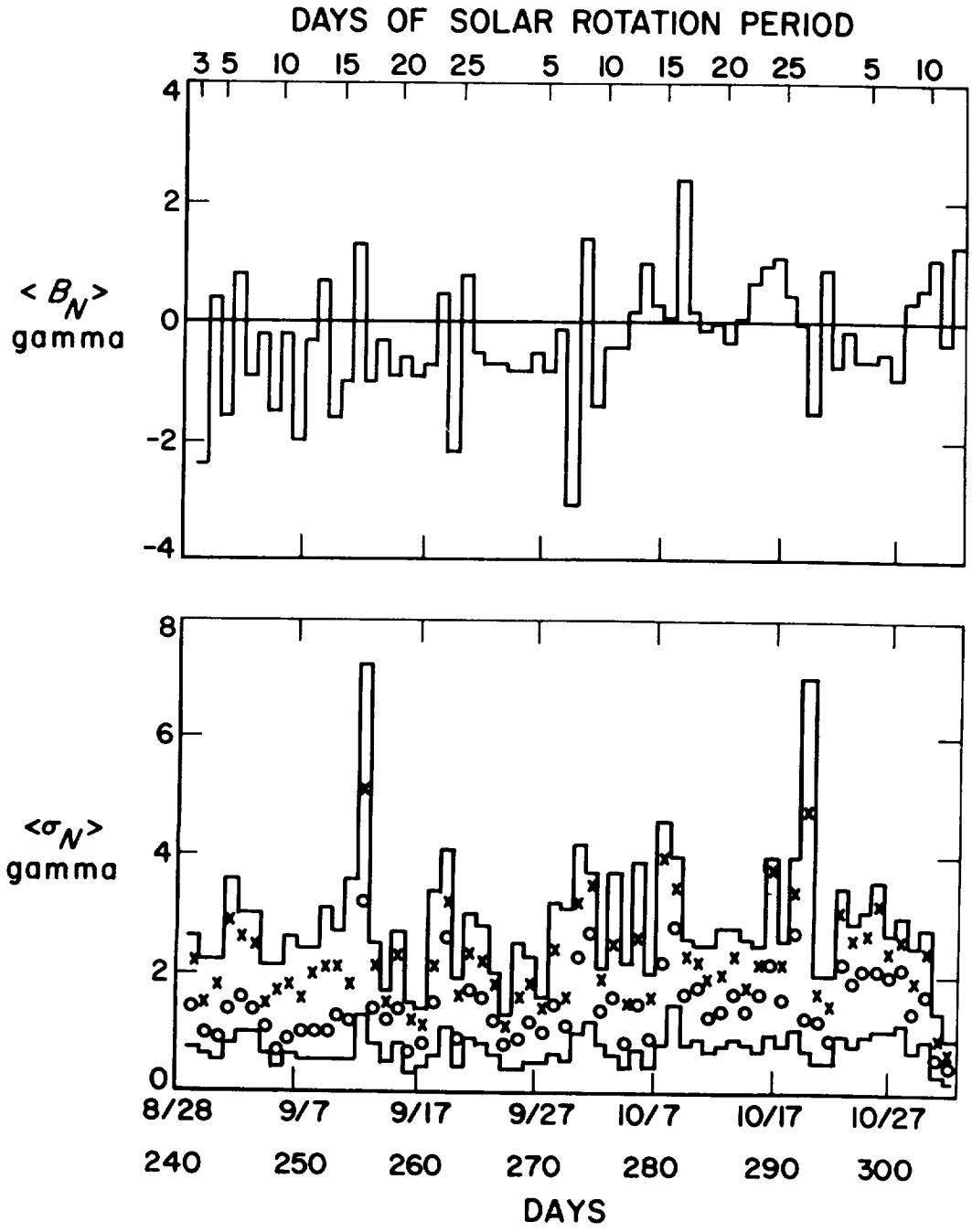

FIGURE 8-3.—Corrected interplanetary magnetic field, normal component, 1-day average.

recognizable 27-day recurrence pattern (associated with the rotation of the Sun). The normal component did not show such an effect. Peaks in the fluctuations of the magnetic field generally seemed to occur during periods of rapid increase in the solar wind velocity.

For approximately 1 month there was a definite southward component of the solar magnetic field with magnitude about 1γ; it seemed to vanish later on. The net flux observed throughout the flight was consistently outward from the Sun.

Solar Plasma

Approximately 40 000 spectra of the positive-ion component of the interplanetary plasma were obtained from the solar plasma instrument during the period August 29, 1962, through January 3, 1963. The data reception was practically continuous except for the period from November 1 through November 8, when all the scientific instruments were turned off, and the period from December 15 through January 3, when reception was intermittent.

During the period of observation, there was always a measurably large flow of plasma from the direction of the Sun. The instrument was pointing within 0.1° of the center of the Sun and had an acceptance angle of about $\pm 10°$.

The velocity of the positive ions in this plasma was not constant in time; it not only varied gradually over a period of days but occasionally changed so rapidly that the instrument, which requires 3.7 min to obtain a spectrum, observed an apparent discontinuity in velocity. Although there were times when distorted spectra were obtained because the plasma was changing rapidly, it is usually possible to find several consecutive readings that were essentially or exactly in agreement, so that the spectra obtained are physically meaningful.

The peak of the ion-energy spectrum was always between the third and the eighth energy channels of the spectrometer (out of a total of 10 channels). Table 8–I is a summary of the percentage of the time during which the peak of the measured spectrum fell within each of the channels; the numbers in this table are based on an analysis of approximately 88% of the total data received.

The width of the spectral peak was taken as indicative of a plasma "temperature," as would be measured in a frame of reference moving with the plasma. The mean velocity was always many times the "thermal" velocity; that is, the flow was supersonic. It was also supersonic in the sense that the mean velocity was many times the expected hydromagnetic wave velocity.

Table 8–I.—Energy distribution of peak of solar plasma spectrum

Channel number	Proton energy, ev	Proton velocity, km/sec	Percentage of time peak fell within channel
3	516	314	4.5
4	751	379	23.2
5	1124	464	27.9
6	1664	563	26.6
7	2476	690	16.9
8	3688	840	0.8

The mean velocity and the "temperature" are plotted as a function of time in figure 8–4. The plot shows 27-day recurrence peaks ("streams") of hot, high-velocity plasma. These peaks correlate quite well with 27-day recurrence peaks in the K_p index of terrestrial magnetic activity. The velocity varied between 320 and 770 km/sec, with an average of 505 km/sec. The "temperature" varied between 3×10^4 and 6×10^5 °K with an average of 1.5×10^5 °K. Figure 8-5 shows time variation of the velocity and the calculated proton density (assuming radial flow). The density was found to be highest between high-velocity streams or at the leading edge of a stream. The 3-hour average density varied between 0.2 and 70 protons/cm^3.

A detailed analysis of the plasma and magnetic parameters recorded in the leading edge of a stream observed on October 7 gives a consistent interpretation of this event as the passage of a collisionless shock front, a phenomenon of considerable interest and some controversy in plasma physics.

As expected, the plasma flux density varied inversely with the square of the radius from the Sun. The particle density showed approximately the same dependence, while the average plasma velocity between the orbits of Venus and the Earth was roughly constant.

The plasma spectra showed a secondary peak at a value of energy-per-unit-charge approximately twice the value at the principal peak. The most probable explanation of the two peaks is that the plasma contained two positive-ion components—protons and alpha particles—which had approximately the same bulk velocity. The detailed spectral shapes were most consistent with the hypothesis that the mean velocity spread of the alpha particles was equal to the mean velocity spread of the protons; that is, the alpha "temperature" was four

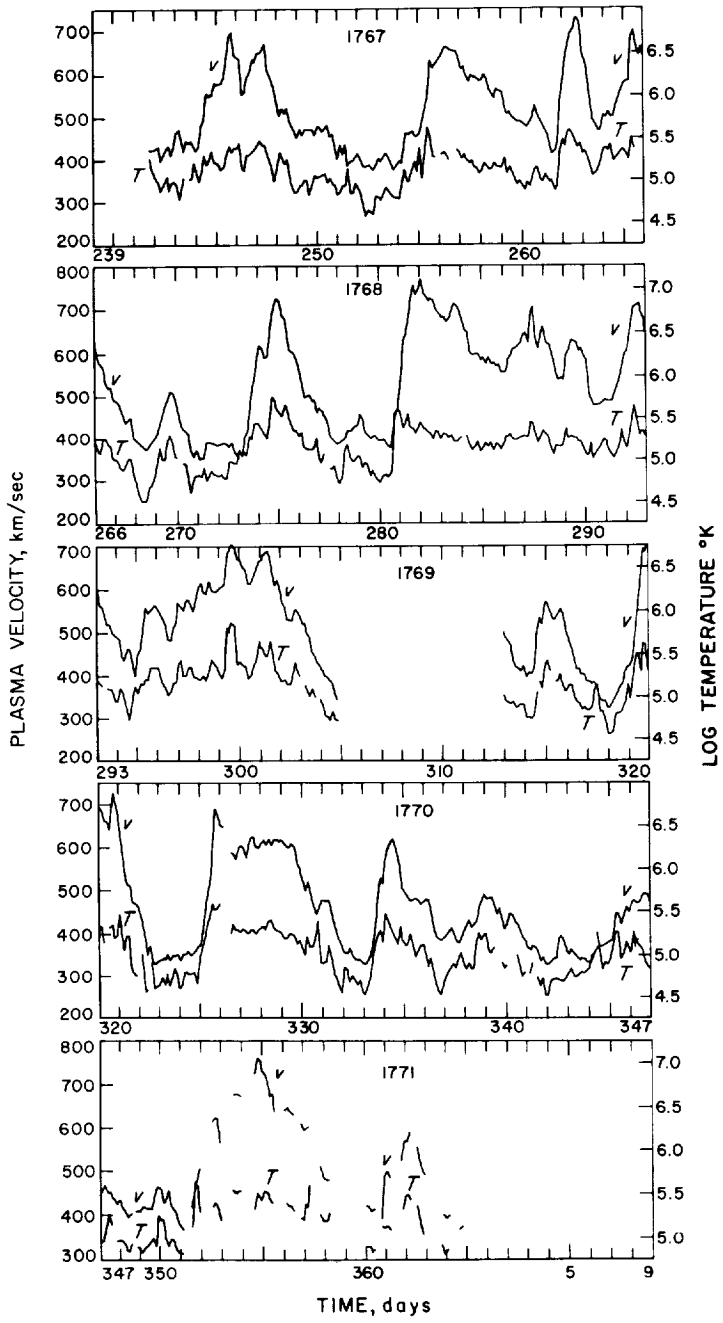

FIGURE 8–4.—Three-hour averages of the calculated proton velocity and "temperature."

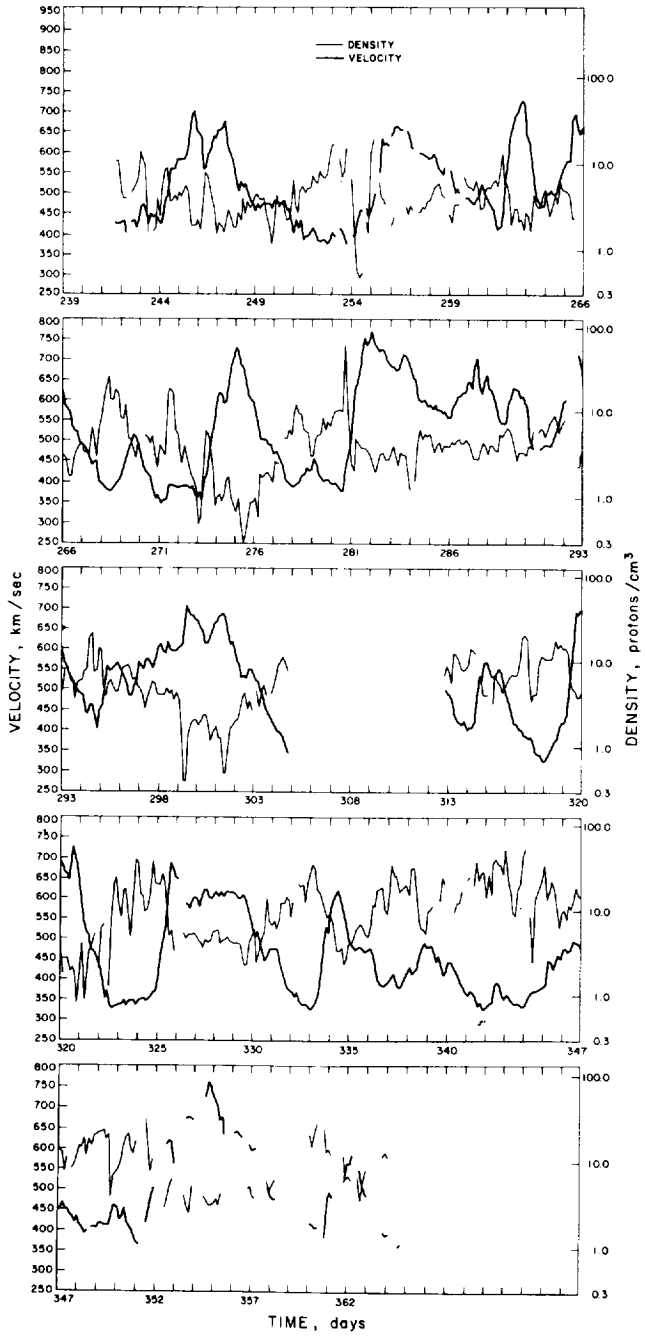

FIGURE 8–5.—Three-hour averages of the calculated proton velocity and density.

times the proton "temperature." Temperature equality was ruled out by the data. The indicated alpha particle density, according to preliminary calculations, was 4.6% of the proton density, independent of the drift velocity of the plasma.

A possible explanation of the equality of the alpha- and proton-velocity spreads is that these velocity spreads ("temperatures") are determined by interaction with the magnetic-field disturbances rather than by interparticle temperature relaxation. Comparison of the calculated proton thermal energy density with the indicated magnetic field energy density ($B^2/8\pi$) shows a rough equality, consistent with the speculation of equipartition of energy between plasma random motions and the magnetic field.

Attempts to extrapolate the velocity peaks back to recognizable features on the Sun were unsuccessful. The extrapolated points of departure (assuming constant velocity) generally appeared to be about 2 days away from the long-lived plage regions with which it would have been plausible to associate them.

Radiation

Four detectors were chosen for the high-energy radiation experiments: (1) a gas-filled integrating ionization chamber with a 0.2-g/cm^2 stainless steel wall; (2) a thin-walled cylindrical glass Geiger-Mueller (GM) tube (RCL 10311), shielded with stainless steel so that the total thickness of the wall matched that of the ionization chamber; (3) an identical glass GM tube, shielded with beryllium so that it admitted protons and heavier nuclei of the same energies ($E_p > 10$ Mev; $E_e > 0.5$ Mev) as did the stainless-shielded tube and the ion chamber; and (4) a thin-window GM tube (Anton Type 213) which responded to protons with energies above 0.5 Mev and electrons above 40 kev, and was baffled against solar X-rays. The two shielded GM tubes had different efficiencies for counting the X-rays produced in the wall by nonpenetrating electrons.

Figure 8–6 shows values of flux and ionization measured by the three high-energy-threshold detectors between the time the instruments were turned on and the encounter with Venus. The points are averages of individual data points taken over approximate 6-hour intervals. The statistical uncertainties of each point are shown on the graph at the left. The data have not been corrected for the presence of the spacecraft mass, but it has been estimated that the effect of this mass did not exceed a few percent.

Typical values of the ionization and flux were: 670 ion pairs/cm^3 sec/STP atmosphere of air, and 2.90 particles/cm^2 sec. The ratio of these values I/F gives

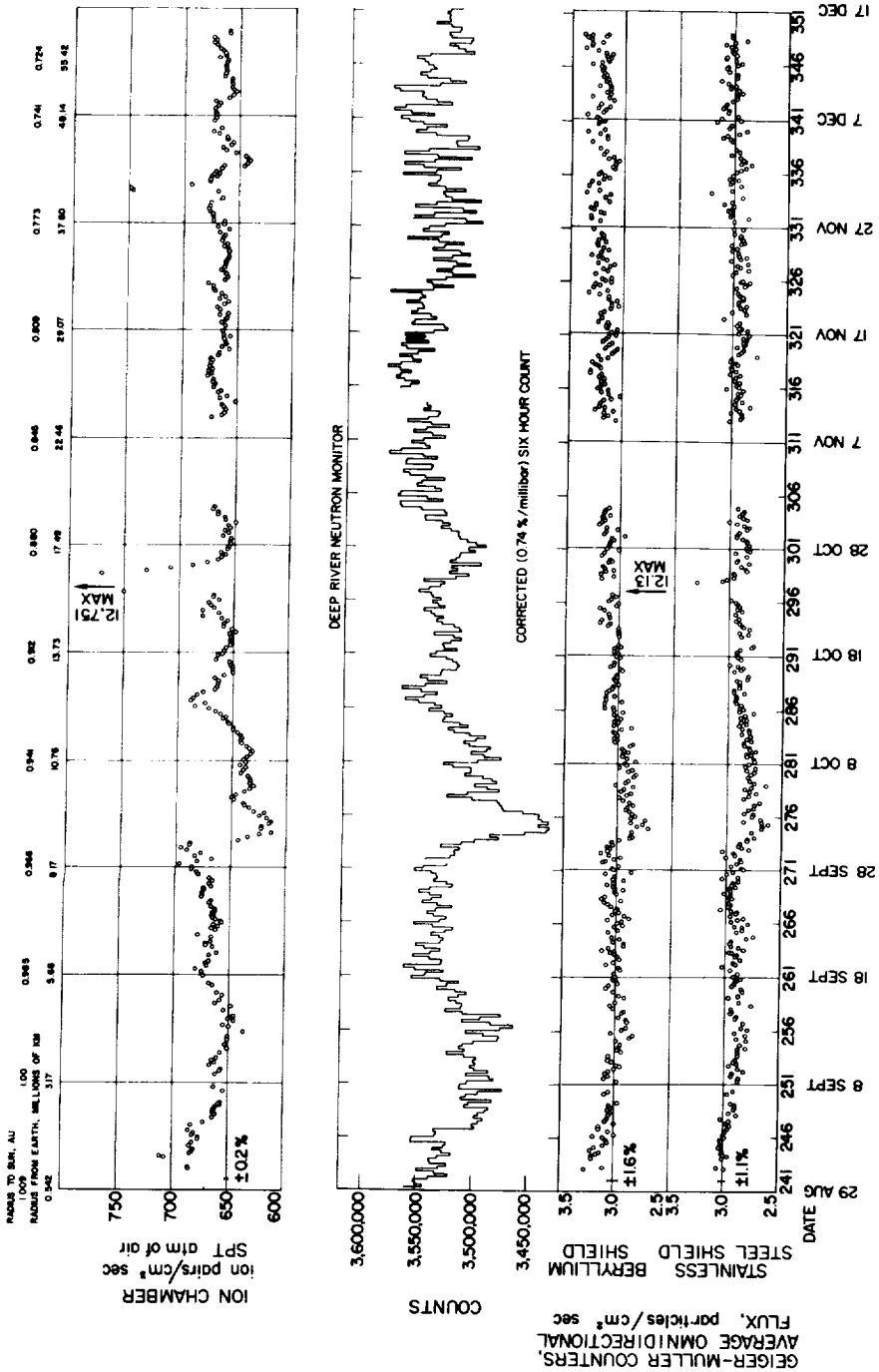

FIGURE 8–6.—Six-hour averages of ionization rate and flux between Earth and Venus.

an average specific ionization of 231 ion pairs per cm of STP air, which is 2.9 times the amount produced by a minimum ionizing proton in ionizing interactions.

The data are consistent with the known charge spectrum of relativistic particles and the energy spectrum of protons measured in 1961, if the flux of all particles is presumed to have increased, because of declining solar activity, from the value of 2.2 cm^2 sec measured in 1961 to the level of the 1962 results.

The data in figure 8–6 show an interesting variation with time. For comparison, the counting rate of the Deep River Neutron Monitor is shown for the same time period. It responds only to neutrons produced by primary cosmic rays with energies above 1 Bev. Comparison of the neutron-monitor rate with the ionization rate in a chamber (effectively identical to that on Mariner) at balloon altitudes near the north magnetic pole (taken as representing the ionization level in space around the Earth) shows that during 1961 and 1962 the variation in this ionization was 2.36 times the variation in the neutron count rate. Using this figure, it was possible to use the neutron count rate as a measure of the ion chamber rate that would be obtained near the Earth and compare it with that of the spacecraft. The Mariner ion chamber rate did not vary significantly (except during disturbed intervals) when averaged for the first four rotations of the Sun. During this time the increase in the neutron count rate was such as to indicate a solar system gradient in galactic cosmic-ray intensity of 9% per astronomical unit. During the last solar rotation, the ion chamber rate rose so that the apparent gradient became negative.

The correlation of the ion chamber reading with the neutron counter reading during a solar rotation showed a general decrease as the spacecraft became farther from the Earth. However, in the last rotation the correlation moved sharply upward again. This irregular behavior suggests that correlation of readings is not merely a matter of the size of "trapping zones" for cosmic ray particles but also depends on the magnetic interconnectedness between various regions of space.

The GM tube rates increased systematically by 3% and 10%. It seems likely, however, that the efficiency of the tubes drifted with increasing temperature, or that the length of time during which the data conditioning system sampled the tube counts changed enough during the mission to produce this apparent shift in flux.

The fluxes measured by the beryllium- and stainless-steel-shielded GM tubes did not differ significantly. It was concluded that there were not enough nonpenetrating electrons to be detected by these counters.

The thin-window GM tube measured a much more variable flux of particles than the ion chamber and the matched GM tubes. In figure 8–7, which shows data obtained in September and October, each point is the average of five data points, and the minimum counting rate of 0.6/sec corresponds to the omnidirectional flux (galactic cosmic rays) measured by the more heavily shielded GM tubes. Enhanced rates were observed at least seven times during this 2-month period. Assuming that these counts were caused by charged particles, the enhanced flux of particles varies from 0 to 30/cm^2 sec sterad.

It is not known whether this enhanced flux consisted of protons of energies between 0.5 and 10 Mev or of electrons between 0.040 and 0.5 Mev. It is also possible that X-rays produced the increases of counting rate, but the detector does not look at any known source of X-rays. The slow buildup and decay of the flux suggests that charged particles are trapped in the interplanetary magnetic field.

Figure 8–7 also shows the planetary magnetic A-index of geomagnetic disturbance. The data suggest that the increased counting rates coincide with disturbed periods at the Earth, but this correlation has not been firmly established.

Cosmic Dust

The objective of the cosmic dust experiment carried on Mariner II was to make a determination of the flux of dust particles in interplanetary space by direct-measurement techniques similar to those used in recent satellite experiments.

For the first 950 hours of data that were studied, all information indicated that the experiment functioned properly. During the portion of the flight represented by these data, the detector plate was approximately perpendicular to the ecliptic plane and facing in the direction of flight. Thus, it was primarily sensitive to particles in retrograde heliocentric orbits, although impacts from particles in direct heliocentric orbits with the proper relative collision velocities were a possibility. During this period, two definite hits were recorded on the more sensitive momentum channel. An estimate of the flux can be made by computing the flux necessary for a 0.9 probability of at least two impacts for the time of the measurement.

With an area-time product of 1.2×10^5 m^3 sec, a flux of 1.2×10^{-5} particles/m^2 sec sterad is obtained. If an average collision velocity of 55 km/sec for this retrograde flux is assumed, the mass of the minimum detected particle is $1.2\pm0.3\times10^{-10}$ g.

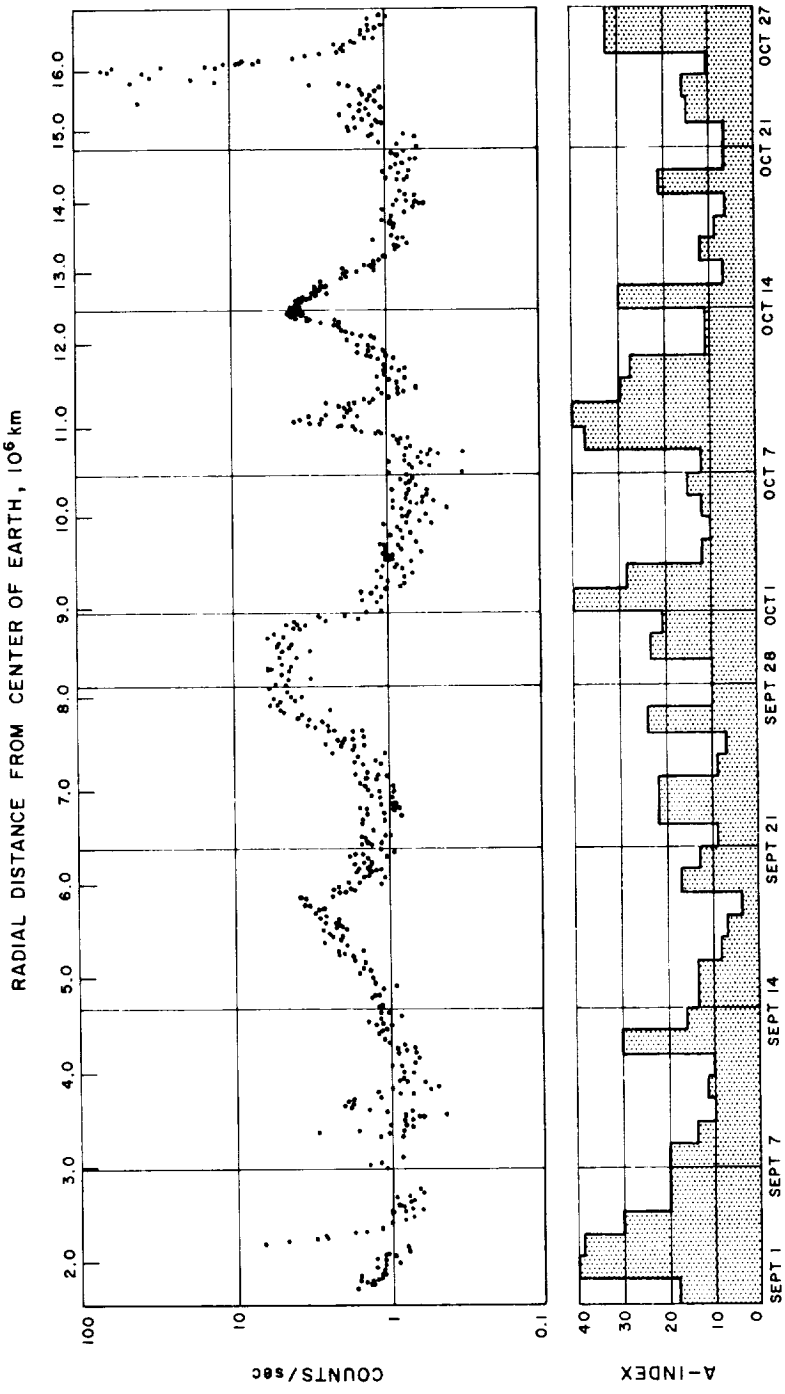

FIGURE 8–7.—Variable flux of particles measured by Anton 213 GM tube during September and October.

A few remarks can be made concerning the direct measurements from earlier satellites and the preliminary results from the cosmic dust experiment on Mariner II. If an assumption is made that the flux of the dust particles in interplanetary space is omnidirectional, the flux of dust particles measured by satellites near the Earth is found to be about 10^4 times greater than the preliminary measurement from the Mariner II experiment. From a similar experiment on Pioneer I, Dubin reported a measurement of dust particle flux in cislunar space. The flux obtained from this measurement is 10^2 times greater than the preliminary Mariner II flux value. These direct measurements suggest a concentration of small dust particles near the Earth.

After the scheduled 180° rotation of the spacecraft about the Sun-probe axis, the detector plate was primarily sensitive to particles in direct heliocentric orbits. During this period, which was somewhat shorter than that previous to the rotation, there were two possible hits but no definite impacts.

Near Venus, there was no indication of a concentration of particles similar to that near the Earth, and it was estimated that the density of such particles there is less than 2×10^{-4} of their density near the Earth.

VENUS MEASUREMENTS

During the Venus encounter phase of the Mariner II flight, the response of the 19-mm microwave radiometer indicated roughly equal temperatures on the light and dark sides of the planet; three scans (dark side, terminator, light side) indicated temperatures of 460°, 570°, and 400° K, respectively. Limb-darkening, observed with both microwave and infrared radiometers, is consistent with the high temperatures originating deep in the atmosphere or at the surface of the planet. In both the 8μ and 10μ channels of the infrared instrument, the central radiation temperature was of the order of 240° K. The apparent equality suggested that there was little carbon dioxide absorption in the light path, implying that the measured temperatures were those of thick clouds. Again, light- and dark-side temperatures were qualitatively the same. A region 10° K cooler than the rest was indicated on the southern part of the terminator scan. Near Venus, there was no indication of a magnetic field or of appreciable change in the solar plasma flux or the charged particle flux.

These data are consistent with the premise that Venus has no magnetic field. The charged-particle data, interpreted as indicating that the Venus magnetosphere did not extend out to the spacecraft orbit, suggest that its dipole moment

is less than 18% of that of the Earth. The magnetic field and solar plasma data, interpreted as showing that the spacecraft did not penetrate the transition region outside the Venus magnetosphere, indicate that its dipole moment is less than 10% of that of the Earth. No cosmic dust particles were detected, suggesting that their density near Venus is less than 2×10^{-4} of their density near Earth.

Microwave Radiometer

Earth-based measurements of the radio emission of Venus have indicated that the planet's temperature is approximately 600° K for wavelengths in excess of 3 cm. This temperature may be contrasted with infrared measurements of Venus which yield values somewhat less than half those obtained by radio. The radio data, which are critical to our understanding of the Venusian environment, rest on terrestrial observations which suffer from lack of spatial resolution and insufficient precision. Flyby planetary probes offer the possibility of precision and resolution with modest radiometers. Accordingly, the Mariner II spacecraft was instrumented with a two-channel microwave radiometer operating at wavelengths of 13.5 and 19.0 mm.

The pertinent equipment performance parameters are given in table 8–II. The effective antenna gain was calibrated by using a black disk of known temperature, whose angular size was designed to be approximately the size of Venus

Table 8–II.—Microwave radiometer characteristics

Parameter	Channel	
	1	2
Center wavelength, mm	19	13.5
Center frequency, Gc/sec	15.8	22.2
Predetection bandwidth, Gc/sec	1.5	2.0
Sensitivity, rms, °K	15	15
Calibration signals, °K	1500	800
Time constant, sec	40	40
Beamwidth, deg	2.5	2.2
Side lobes, db	−23	−23
Reference frequency, cps	950	1050

at encounter. This calibration was performed on Table Mountain near Wrightwood, Calif., in March 1962.

During the 109-day flight, 23 noise calibrations were made; thus, the gain, base-level, and time-constant performance of the radiometers could be monitored en route.

The radiometers were energized, and the antenna scan motion was activated about 6½ hours before encounter. The scan motion had an angular extent of 123.5° and a nominal scan rate of 0.1 deg/sec. The microwave radiometer first made contact with the planet Venus at 18:59 GMT (spacecraft time) on December 14, 1962. During the next 35 min, three scans across the planetary disk were obtained, as follows:

Scan	Approx. angular extent, deg	Alt. at mid-scan, km	Location
1	10	40 200	Dark side.
2	15	37 750	Near terminator.
3	10	35 850	Light side.

Telemetered digital data points constituted the basic data, which had to be corrected for a number of effects before they could be considered as yielding the microwave temperature distribution across the planet. Among these corrections were the more important effects of the post-detection time constant and a detailed consideration of the antenna pattern.

The noise tube calibrations obtained en route to Venus made it possible to determine the in-flight time constant and gain of the radiometers. The gain of both channels decreased during the cruise, and the zero levels had systematic variations. These effects were more serious in the 13.5-mm radiometer.

Preliminary estimates of the peak-brightness temperatures of the three scans were: Scan 1 (dark side), 460° K; scan 2 (near terminator), 570° K; scan 3 (light side), 400° K. The temperatures are based on calculations which account for the effects of the antenna beam and the postdetection time constant. The errors of the quoted temperatures are estimated to be 15%. The analysis of the preliminary results suggests that there is no significant difference in the microwave temperatures on the light and dark sides of the planet. The results suggest a limb-darkening, an effect which represents cooler temperatures near the edge of the planetary disk. The ionosphere model of the Venus atmosphere, which

permits Earth-like temperatures, appears to be ruled out by these observations. On the other hand, the observed limb-darkening is consistent with a model of the Venusian environment which has high temperatures originating deep in the atmosphere or at the surface of the planet.

Thus, Mariner II found an unquestionable limb-darkening and also found that there is little difference in temperature on the dark side compared with the sunlit side of the planet. On the basis of the radiometer scans, the surface of Venus, where the 19-mm radiation originates, appears to have a temperature of about 400° K.

Infrared Radiometer

The infrared radiometer which was flown on Mariner II in conjunction with the microwave radiometer was designed to measure, with high geographical resolution, the infrared radiation from Venus in two wavelength regions. One of these was centered on the 10.4μ carbon dioxide band, while the other was selected to correspond to an infrared window centered at 8.4μ. The infrared radiometer was mounted upon and boresighted with the microwave radiometer described in the preceding section. Both instruments, therefore, executed the same scan pattern caused by the combined effects of the probe motion and a rotation of the radiometers in a plane normal to the probe-Sun line. From the three scans of the planet, five pairs of radiation temperatures were obtained on the dark side, five on the sunlit side, and eight along the terminator.

The radiometer was calibrated at the Jet Propulsion Laboratory by using two cylindrical blackbodies; one was maintained at liquid nitrogen temperature, while the other was varied over the expected planetary temperature range. In addition, a one-point check was obtained during encounter by causing the radiometer to view a plate, located on the spacecraft structure, whose temperature was independently measured.

The data are consistent with an equality of the 8μ and 10μ radiation temperatures. This apparent equality would indicate that there was little carbon dioxide absorption in the light path. The implications are that the measured temperatures were cloud temperatures, that the clouds were quite thick, and that essentially no radiation was transmitted from the surface.

A definite limb-darkening was observed in both spectral channels; the radiation temperatures showed a monotonic decrease of approximately 20° K between the central region and the limbs. Central radiation temperatures are

estimated to be on the order of 240° K. The data do not show any clear-cut evidence of asymmetry in the limb-darkening, except for an anomaly on the southern part of the terminator scan. In particular, the light- and dark-side temperatures were qualitatively the same. The anomaly was about 10° K cooler than expected on the basis of symmetrical limb-darkening. One obvious interpretation of this temperature anomaly is that the clouds were locally higher, or more opaque, or both.

Magnetic Field

Magnetometer data obtained as Mariner II passed Venus gave no evidence of a Venusian magnetic field at any point on the trajectory. No rise in the average value of the magnetic field above the value of the interplanetary field was detected which could be attributed to the planet. The sensitivity of the magnetometer was such that a field change as large as about 4γ on any axis would have been detected ($1\gamma = 10^{-5}$ oersted; the magnitude of the Earth's field at the equator is about 30000γ). During encounter, a slow change no larger than about 10γ was observed. However, this change should be attributed to a temporal change in the interplanetary magnetic field, because it did not have the character of a planetary field. There was no detection of the continuous fluctuations, with periods from 1 sec to 1 min and amplitudes of the order of 3γ, that are characteristic of the transition region just outside the geomagnetic field. Simultaneous measurements by other Mariner experiments also failed to reveal any effect associated with a planetary field, such as trapped particles or a modification in the flow of solar plasma.

These results do not necessarily mean that Venus has no magnetic field, since the solar wind would confine a weak field to a limited region close to the planet. The observations indicate that the field does not extend out to the Mariner trajectory, for which the distance of closest approach from the center of Venus was approximately 41 000 km. The results are consistent, however, with the possibility that Venus has no magnetic field. Since the planetary field does not extend out to the Mariner trajectory, only an upper limit for the magnetic dipole moment of Venus can be estimated. Theoretical models of the interaction of the solar wind with a dipole magnetic field, including a crude estimate of the extent of the disturbed region outside the magnetosphere, indicate that the dipole moment of Venus, if it is approximately perpendicular to the Sun-Venus line, is less than 0.1 that of the Earth. Comparison of the measure-

ments made near Venus with those made by other spacecraft near the Earth leads to the conclusion that the dipole moment of Venus is less than 0.1 that of the Earth. If the dipole moment of Venus is the dominant field source, the magnitude of the surface field is less than 10% of the geomagnetic field. If Venus has a more complicated magnetic structure than the Earth so that higher-order multipoles are important, the surface field in places could be larger than the Earth's field without increasing the strength of the field along the Mariner trajectory to an observable value.

Phenomena associated with the geomagnetic field, such as the trapping of particles in radiation belts and the aurora, are likely to be greatly modified, less important, or completely absent on Venus because of its weaker field. The cosmic ray flux at the top of the Venus atmosphere may everywhere correspond to the high level found on Earth only in the polar regions.

Solar Plasma

The following conclusions have been drawn from the plasma data obtained near Venus:

(1) The plasma flux was not observed to vanish, as would be expected if the probe had entered the magnetosphere of Venus. This negative finding is in agreement with the results of the magnetic field measurement.

(2) There was no clear evidence of passage through a bow shock wave associated with Venus.

(3) There was a gradual increase and subsequent decrease of the plasma velocity as the spacecraft approached and later receded from Venus. Many such short-period variations were observed during Mariner's flight and it is believed unlikely that this one was associated with the proximity of Venus.

(4) The average momentum flux in the solar wind near Venus was 3.8×10^8 dyne cm^{-2}. Since this is not an unusually high value, the Venus magnetic field was probably not compressed an unusually large amount at the time of encounter.

Charged Particles

This experiment was designed to search for charged particles magnetically trapped in the vicinity of the planet Venus and, if such particles were found, to obtain measurements of their spatial distribution and intensity. The thin-window Geiger-Mueller tube (Anton 213) was the most sensitive of the radiation instru-

ments used for this purpose. Throughout the flight, including the planetary flyby, the axis of the detector's conical field of view (90° full angle) was directed at $70° \pm 1°$ to the spacecraft-Sun line, lay in the plane containing the Sun, Earth, and spacecraft, and was on the Earthward side of the spacecraft.

In the upper portion of figure 8–8, the true counting rate R of the detector is plotted as a function of universal time during the planetary encounter period, as well as during periods of about 30 hours before and after the time of closest approach. Also shown on the same time scale are the Sun-Venus-probe angle L_{svp} and the radial distance from the probe to the center of the planet R_v. During the interplanetary, or cruise, mode of operation of the spacecraft, the accumulated number of counts from the detector during a 9.60-sec interval was read out once each 887 sec. During the encounter mode, the accumulated number of counts during a 9.60-sec interval was read out once each 484 sec. Each plotted point in figure 8–8 represents a single sample and has, therefore, a statistical uncertainty of about 25%. The most striking feature of figure 8–8 is the absence of any discernible increase in counting rate during the passage by Venus.

This impression is made more quantitative by reference to table 8–III and to the following discussion. For the 50 samples obtained during the encounter mode, the observed root-mean-square deviation from the mean counting rate was 0.28 count sec^{-1}, and the statistically expected value was 0.33 count sec^{-1}.

Fifteen of the 50 sample rates differed from the mean rate of 1.125 counts sec^{-1} by an amount equal to or greater than σ, and none differed by as much as 2σ. This feature of the data was borne out by the ion chamber and shielded Geiger counters, which, although responsive only to particles of much higher energy than the Anton counter, had significantly better statistics overall. Of those which differed by as much as or more than σ, nine exceeded the mean and six were less than the mean. Both positive and negative deviations appeared to be randomly distributed through the period of the encounter mode. Thus, it appears that the absence of a discernible effect in the vicinity of the planet was as complete as was possible on statistical grounds.

The mean counting rate during the encounter mode was actually significantly less than that during either the prior period of flight or, to a lesser extent, the subsequent period. There are three conceivable explanations for this effect: (1) An instrumental effect peculiar to the encounter mode of spacecraft operation; (2) an incidental decrease in the intensity of low-energy particles in interplanetary space, such decrease having no relationship to the proximity to the planet; and (3) a geometric or magnetic "shadowing" effect by the planet.

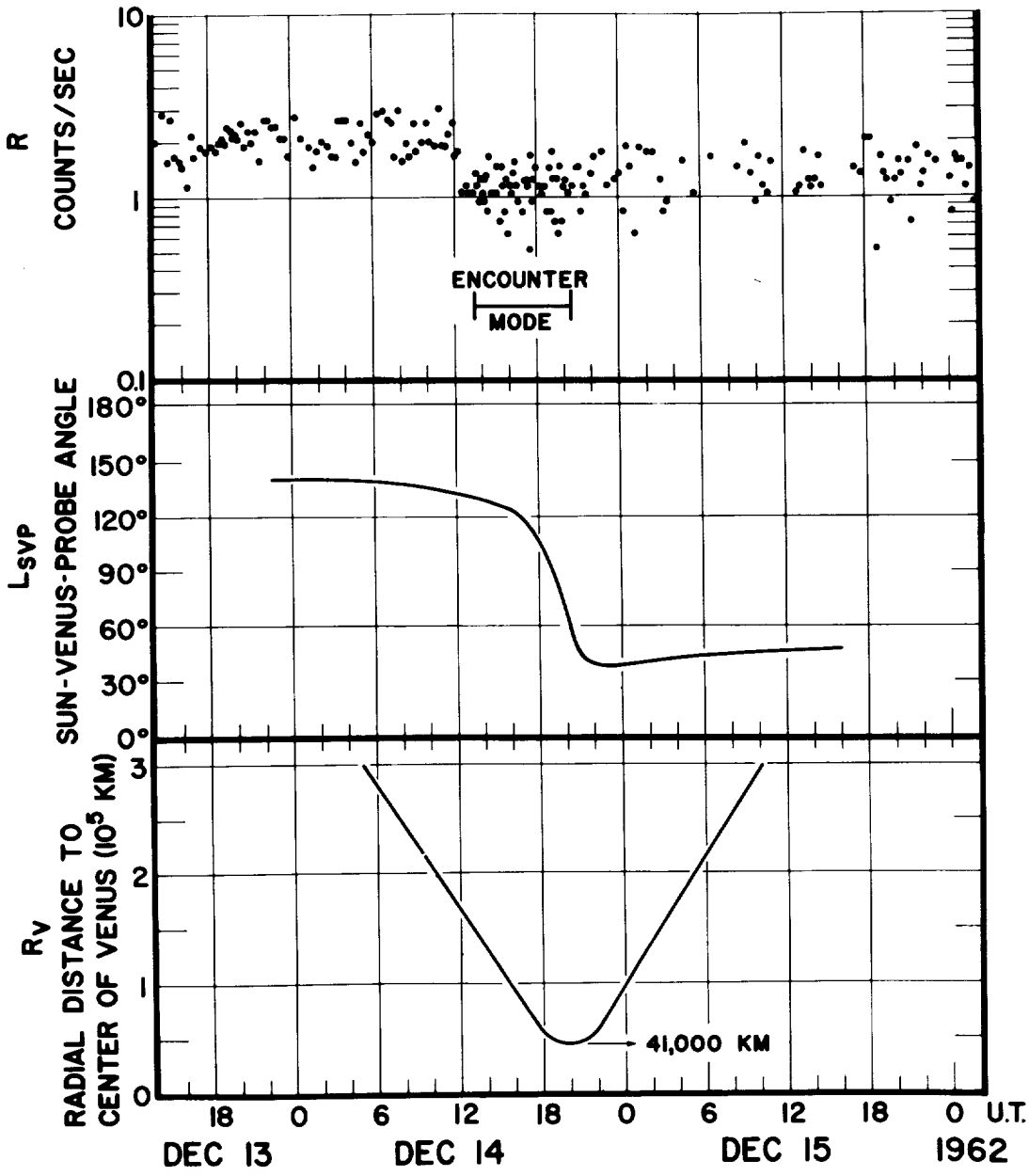

FIGURE 8–8.—Counting rate of the Anton 213 GM detector in the vicinity of Venus.

The first explanation has been examined with reference to the telemetered engineering data and other knowledge of the spacecraft's operation. No plausible foundation for this explanation has been found. Moreover, figure 8–8 and table 8–III show that the sharp drop in counting rate occurred at about 1220 UT during the cruise mode and over an hour before the encounter mode was actuated. No discontinuity in counting rate occurred at either the beginning or the end of the encounter mode. Hence, the first explanation has been rejected.

Table 8–III.—Summary of count-rate data in vicinity of Venus

Time period, UT (1962)	Radial distance range, 10^3 km	Mean counting rate and statistical uncertainty, count sec^{-1}	Spacecraft mode
16:03, Dec. 13, to 12:15, Dec. 14	569 to 167	2.097 ± 0.058	Cruise
12:33, Dec. 14, to 13:14, Dec. 14	161 to 147	1.15 ± 0.17	Cruise
13:35, Dec. 14, to 20:40, Dec. 14	140 to 41 to 45	1.125 ± 0.049	Encounter
20:55, Dec. 14, to 03:07, Dec. 15	48 to 160	1.366 ± 0.086	Cruise
03:19, Dec. 15, to 11:51, Dec. 16	163 to 809	1.329 ± 0.031	Cruise

For acceptance of the third explanation, that the planet had a geometrical or magnetic "shadowing" effect, some reasonable physical mechanism must be proposed. For example, one might expect a reduced intensity of particles in the solar wind within a region of finite dimensions on the leeward, or antisolar, side of a nonmagnetic planet. But the rapid reduction in the counting rate of the Mariner II detector occurred at a position 164 000 km (26.4 planetary radii) from the center of the planet at a Sun-Venus-probe angle of 133° and a planet-referenced declination of +19°. At this time, the detector's cone of acceptance was directed generally away from the planet. Thus, such a "shadowing" seems to be a most unlikely possibility, even if the planet were magnetic and had an effectively greater cross section. Moreover, there was no evidence for a subsequent return of the counting rate to its "unshadowed" value.

For the reasons cited, it is judged that only the second explanation—that there was an incidental decrease in the intensity of low-energy particles in interplanetary space—is acceptable. It is a matter of some reassurance that sharp changes in counting rate of similar magnitude were observed at several other times

during the 2½ months of interplanetary flight under constant operating conditions at positions very remote from either Earth or Venus. The counting rate due to galactic cosmic rays alone was 0.6 sec^{-1}.

It may be noted here that at no time during the planetary flyby did the planet fall within the conical field of the detector.

The absence of charged particles associated with the planet Venus at radial distances as small as 41 000 km on the Sunward side of the planet is taken to mean that the magnetosphere of Venus, if any, does not extend to that great a distance. The most plausible interpretation is that $M_V/M_E \leqq 0.18$, where M_V and M_E are the dipole magnetic moments of Venus and Earth, respectively. The results are consistent with $M_V/M_E = 0$. Certain qualifications prevent this interpretation from being a definitive one.

MASS OF VENUS AND OTHER SOLAR CONSTANTS

The orbit of the Mariner II spacecraft is unique in that it was dominated first by the Earth, then the Sun, and finally the planet Venus. On December 14, 1962, the spacecraft came within about 35 000 km (22 000 miles) of Venus, and its flight path was deflected by about 40° because of its close encounter. In addition, precise two-way Doppler data were obtained throughout the 129-day period from launch to January 3, 1963. Fortunately, prior to the launch of Mariner II an atomic reference had been installed at the Goldstone tracking station of the Deep Space Instrumentation Facility, and this piece of equipment allowed the transmitter frequency to be held to better than one part in 10^{11} over a period of an hour. Equivalently, the Doppler shift in the received signal was measured to an accuracy of about 0.03 cps. In terms of velocity units, the corresponding accuracy of the range rate between the probe and station was on the order of ½ cm/sec at a received frequency of 960 Mc and a cycle count time of 60 sec.

A combination of the aforementioned factors allows the determination of certain constants of the solar system to an accuracy that has been unobtainable in the past. In particular, at least an order of magnitude improvement in the mass of Venus appears possible because of the close approach to the planet. The same order of improvement should be obtained for the mass of the Moon because the periodic component in the data which results from the motion of the Earth about the center of mass or barycenter of the Earth-Moon system is appreciable. The astronomical unit can also be obtained from the data, and its accuracy should eventually be comparable to that of the recent NASA/JPL radar determinations from the tracking of Venus (149 591 412 ± 482 km).

Correlations of the mass of Venus with the position of the probe are fairly high. However, inaccuracy in the calculation of the trajectory near Venus is a serious matter, and the value of the mass determined with a Venus-centered integration could easily fall outside the probable error as computed from the normal equations associated with this solution.

The full scientific value of the Mariner II tracking data will not be realized until the heliocentric and encounter data are combined in one least-squares reduction. This is impossible at the present time because: (1) the low-thrust forces are neglected, (2) the calculation of the trajectory is inaccurate in the vicinity of Venus, and (3) the effects of uncertainties in the ephemerides of the Earth and Venus are unknown. It is unacceptable to be satisfied with the results without a detailed investigation of these three sources of error. It is expected that the final reduction will be accomplished with the inclusion of a physically reasonable low-thrust model, a Venus-centered integration of the equations of motion during encounter, and an inclusion of orbital elements of the Earth and Venus as additional free parameters in the solution.

Pending final reduction of data, a preliminary calculation of the mass of Venus is 0.81485 that of Earth, with an error probability of 0.015%. Since the Earth's mass is known to be approximately 5.977×10^{24} kg, Venus' mass becomes approximately 4.870×10^{24} kg.

APPENDIX A

Abbreviations

A-to-D	analog-to-digital
AFETR	Air Force Eastern Test Range
AFSSD	Air Force Space Systems Division
AGC	automatic gain control
AMR	Atlantic Missile Range
AU	astronomical unit
BECO	booster-engine cutoff
BPS	bits per second
CCF	Central Computing Facility
CC&S	central computer and sequencer
CW	clockwise
CCW	counterclockwise
DCS	data conditioning system
D-to-D	digital-to-digital
DN	data number
DSIF	Deep Space Instrumentation Facility
DO	data synchronization reference point
ECR	engineering change requirement
ESA	explosive safe area
GD/A	General Dynamics/Astronautics
GE	General Electric
GM	Geiger-Mueller
GMT	Greenwich mean time
GN_2	gaseous nitrogen
GSE	ground support equipment
IPP	impact prediction point
IR	infrared
J-FACT	joint flight acceptance composite test

JPL	Jet Propulsion Laboratory
L	launch
LOD	Launch Operations Directorate (later LOC)
LMSC	Lockheed Missiles and Space Company
MSFC	Marshall Space Flight Center
MTS	Mobile Tracking Station
NASA	National Aeronautics and Space Administration
NITR	National Institute of Telecommunications Research
ODP	orbit determination program
OPEI	Office of Public Education and Information
PCA	pyrotechnic control assembly
PN	pseudo noise
PSK	phase-shift key
PTM	proof test model
RF	radio frequency
RTC	real time command
SC	stored command
SDAT	Spacecraft Data Analysis Team
SFOC	Space Flight Operations Complex
SFOF	Space Flight Operations Facility
SPS	scientific power switching
SRO	superintendent of range operations
SSD	Space Systems Division
STC	Systems Test Complex
STP	standard temperature and pressure
TDEP	Tracking Data Editing Program
TFV	Twin Falls Victory Ship
TPS	Telemetry Processing Station
USAF	United States Air Force
VCO	voltage-controlled oscillator

APPENDIX B

Subcontractors

Thirty-four subcontractors to JPL provided instruments and other hardware for Mariner II:

Aeroflex Corporation, Long Island City, N.Y.	Jet vane actuators
American Electronics, Inc., Fullerton, Calif.	Transformer-rectifiers for flight telecommunications
Ampex Corporation, Instrumentation Div., Redwood City, Calif.	Tape recorders for ground telemetry and data-handling equipment
Applied Development Corporation, Monterey Park, Calif.	Decommutators and teletype encoders for ground telemetry equipment
Astrodata, Inc., Anaheim, Calif.	Time code translators, time code generators, and spacecraft signal simulators for ground telemetry equipment
Barnes Engineering Company, Stamford, Conn.	Infrared radiometers: planet simulator
Bell Aerospace Corporation, Bell Aerosystems Div., Cleveland, Ohio	Accelerometers and associated electronic modules
Computer Control Company, Inc., Framingham, Mass.	Data conditioning systems
Conax Corporation, Buffalo, N.Y.	Midcourse-propulsion explosive valves; squibs
Consolidated Electrodynamics Corp., Pasadena, Calif.	Oscillographs for data reduction
Consolidated Systems Corporation, Monrovia, Calif.	Scientific instruments; operational support equipment
Dynamics Instrumentation Company, Monterey Park, Calif.	Isolation amplifiers for telemetry; operational support equipment
Electric Storage Battery Company, Missile Battery Div., Raleigh, N.C.	Spacecraft batteries
Electro-Optical Systems, Inc., Pasadena, Calif.	Spacecraft power conversion equipment
Fargo Rubber Corporation, Los Angeles, Calif.	Midcourse-propulsion fuel-tank bladders
Glentronics, Inc., Glendora, Calif.	Power supplies for data conditioning system
Groen Associates, Sun Valley, Calif.	Actuators for solar panels

Houston Fearless Corporation, Torrance, Calif.	Pin pullers
Kearfott Division, General Precision, Inc., Los Angeles, Calif.	Gyroscopes
Marshall Laboratories, Torrance, Calif.	Magnetometers and associated operational support equipment
Matrix Research and Development Corporation, Nashua, N.H.	Power supplies for particle flux detectors
Menasco Manufacturing Company, Burbank, Calif.	Midcourse-propulsion fuel tanks and nitrogen tanks
Midwestern Instruments, Tulsa, Okla.	Oscillographs for data reduction
Mincom Div., Minnesota Mining & Manufacturing, Los Angeles, Calif.	Tape recorders for ground telemetry and data-handling equipment
Motorola, Inc., Military Electronics Div., Scottsdale, Ariz.	Spacecraft command subsystems, transponders, and associated operational support equipment
Nortronics, Div. of Northrop Corporation, Palos Verdes Estates, Calif.	Attitude-control gyro electronic, autopilot electronic, and antenna servo electronic modules; long-range Earth sensors and Sun sensors
Ransom Research, Div. of Wyle Laboratories, San Pedro, Calif.	Verification and ground command modulation equipment
Rantec Corporation, Calabasas, Calif.	Transponder circulators and monitors
Ryan Aeronautical Company, Aerospace Div., San Diego, Calif.	Solar-panel structures
Spectrolab, Div. of Textron Electronics, Inc., North Hollywood, Calif.	Solar cells and their installation and electrical connection on solar panels
State University of Iowa, Iowa City, Iowa	Calibrated Geiger counters
Sterer Engineering & Manufacturing Company, North Hollywood, Calif.	Valves and regulators for midcourse-propulsion and attitude-control systems
Texas Instruments, Inc., Apparatus Division, Dallas, Tex.	Spacecraft data encoders and associated operational support equipment; ground telemetry demodulators
Trans-Sonic, Inc., Burlington, Mass.	Transducers

In addition to these subcontractors, over 1000 other industrial firms contributed to the Mariner Project.

Bibliography

1. The Mariner R Project: Progress Report, September 1, 1961–August 31, 1962. Tech. Rept. No. 32–353, Jet Propulsion Laboratory, Jan. 1, 1963.
2. The Mariner R Project: Progress Report, September 1, 1962–January 3, 1963. Tech. Rept. No. 32–422, Jet Propulsion Laboratory, July 1, 1963.
3. Newell, Homer E.: Goals and Potentials of Scientific Research in Space, in Conference on Space, Science, and Urban Life. NASA SP–37, 1963, pp. 29–43.
4. Mariner Mission to Venus. Prepared for the National Aeronautics and Space Administration by the Staff, Jet Propulsion Laboratory. McGraw-Hill Book Co., Inc., 1963.
5. Moore, Patrick: "The Planet Venus," Faber and Faber Ltd. (London), 1959, pp. 17–23.
6. System Capabilities and Development Schedule of the Deep Space Instrumentation Facility, 1964–68. Tech. Memo. No. 33–83, Jet Propulsion Laboratory, Apr. 24, 1964.
7. Deep Space Instrumentation Facility Digest Series. Jet Propulsion Laboratory, Apr. 1963.
8. Wyckoff, R. C.: "Venus Mission—1962." Astronautics, vol. 7, July 1962.
9. Stubbs, P.: "Mariner's Flight to Venus: The Scientific Objectives." New Scientist, vol. 15, no. 301, Aug. 23, 1962.
10. Holahan, J.: "Mariner 2." Space/Aeronautics, vol. 38, No. 6, Nov. 1962.
11. Barnes, F. L.; Bollman, W. E.; Curkendall, D. W., and Thornton, T. H.: "Mariner 2 Flight to Venus." Astronautics, vol. 7, no. 12, Dec. 1962.
12. Barrett, A. H., and Lilley, E.: "Mariner 2 Microwave Observations of Venus." Sky and Telescope, vol. XXV, no. 4, Apr. 1963.
13. Goldstein, R. M., and Carpenter, R. L.: "Rotation of Venus Period Estimated from Radar Measurements." Science, vol. 139, no. 3558, Mar. 8, 1963. Also, Tech. Rept. No. 32–429, Jet Propulsion Laboratory, Mar. 1963.
14. Murray, B. C.; Willey, R. L., and Westphal, J. A.: "Venus: A Map of Its Brightness Temperature." Science, vol. 140, no. 3565, Apr. 26, 1963.
15. The Mariner Mission—1962. Jet Propulsion Laboratory, 1962.
16. Clarke, V. C., Jr.; Bollman, W. E.; Roth, R. Y., and Scholey, W. J.: Design Parameters for Ballistic Interplanetary Trajectories—Part 1.

One-way Transfer to Mars and Venus. Tech. Rept. No. 32–77, Jet Propulsion Laboratory, Jan. 16, 1963.

17. Clark, V. C., Jr.: Design of Lunar and Planetary Ascent Trajectories. Tech. Rept. No. 32–30, Rev. 1, Jet Propulsion Laboratory, Mar. 15, 1962.
18. Clarke, V. C., Jr.; Roth, R. Y.; Bollman, W. E.; Hamilton, T. W., and Pfeiffer, C. G.: Earth-Venus Trajectories. Vol. 1, 1964; Vol. 2, 1965–66; Vol. 3, 1967; Vol. 4, 1968–69; Vol. 5, 1970. Tech. Memo. No. 33–99, Jet Propulsion Laboratory.
19. Holdridge, D. B.: Space Trajectories Program for the IBM 7090 Computer. Tech. Rept. No. 32–223, Rev. 1, Jet Propulsion Laboratory, Sept. 15, 1962.
20. Anderson, J. D.; Null, G. W., and Thornton, C. T.: "The Evaluation of Certain Physical Constants from the Radio Tracking of Mariner 2." Tech. Rept. No. 32–476, Jet Propulsion Laboratory.
21. Noton, A. R. M.; Cutting, E., and Barnes, F. L.: Analysis of Radio Command Midcourse Guidance. Tech. Rept. No. 32–48, Jet Propulsion Laboratory, Sept. 8, 1960.
22. "The Mission of Mariner II: Preliminary Observations—Profile of Events." Neugebauer, M., and Snyder, C. W.: "Solar Plasma Experiment." Van Allen, J. A., and Frank, L. A.: "The Iowa Radiation Experiment." Alexander, W. M.: "Cosmic Dust." Coleman, P. J., Jr., et al.: "Interplanetary Magnetic Fields." Science, vol. 138, no. 3545, Dec. 7, 1962.
23. Anderson, H. R.: "Mariner II: High-Energy-Radiation Experiment." Science, vol. 139, no. 3549, Jan. 4, 1963.
24. "Mariner II: Preliminary Reports on Measurements of Venus." Frank, L. A.; Van Allen, J. A., and Hills, H. K.; "Charged Particles." Chase, S. C.; Kaplan, L. D., and Neugebauer, G.: "Infrared Radiometer." Smith, E. J., Davis, L., and Sonnett, C. P.: "Magnetic Fields." Science vol. 139, no. 3558, March 8, 1963. Also, Tech. Rept. No. 32–429, Jet Propulsion Laboratory, Mar. 1963.
25. Wyckoff, R. C. (ed.): Scientific Experiments for Mariner R–1 and R–2. Tech. Rept. No. 32–315, Jet Propulsion Laboratory, July 15, 1962.
26. Alexander, W. M.; McCracken, C. W.; Secretan, L., and Berg, O. E.: "Review of Direct Measurements of Interplanetary Dust From Satellites and Probes." Space Research III, Proceedings of the Third International Space Science Symposium, Washington, May 1962. John Wiley & Sons, Inc., 1963.

27. Sinton, W. M., and Strong, J.: "Radiometric Observations of Venus." The Astrophysical Journal, vol. 131, no. 2, 1960.
28. James, J. N.: "The Voyage of Mariner II." Scientific American, vol. 209, no. 1, July 1963.
29. "Voyage to Venus: The Story of Mariner II." National Geographic, vol. 123, no. 5, May 1963.
30. "Space Exploration—Voyage to the Morning Star." Time Magazine, vol. LXXXI, no. 10, Mar. 8, 1963.
31. National Academy of Sciences: "Results of the Mariner II Spaceflight to Venus." International Geophysics Bulletin, No. 73, July 1963.
32. "Mariner II Spaceflight to Venus." Cospar Information Bulletin, no. 14, Mar. 1963.
33. Afanas'yeva, V. I.: "Solar Corpuscular Streams and Geomagnetic Storm Families During the Flight of Mariner II." Geomagnetizm i Aeronomiya, vol. 3, no. 6, pp. 1126–7, Izd-vo Akad. Nauk SSSR, 1963.
34. Öpik, E. J.: "Venus and the Mariner." The Irish Astronomical Journal, vol. 6, no. 2, June 1963.
35. Sjogren, William J., and Trask, Donald W.: Astrodynamical Results From the Radio Tracking of the Mariner Venus and Ranger Missions. AIAA Paper No. 65–91.
36. Sonett, Charles P.: A Summary Review of the Scientific Findings of the Mariner Venus Mission. Space Science Reviews 2, D. Reidel Publishing Co., Dordrecht-Holland, 1963, pp. 751–777.
37. Barath, F. T.; Barrett, A. H.; Copeland, J.; Jones, D. E., and Lilley, A. E.: "Mariner 2 Microwave Radiometer Experiment and Results." Astronomical Journal, vol. 69, no. 1, Feb. 1964, pp. 49–58.
38. NASA Press Releases

62–182, Mariner II Prelaunch
62–187, Midcourse Maneuver
62–193, Progress Report
62–234, Mariner II Passes Earth
62–243, Experiments Turned On
62–246, Sets Record
62–253, Sets Record
62–260, News Venus
62–262, Dr. Newell's Statement
62–263, Experiments Turned On
62–270, Magnetometer
62–271, Radiation
62–272, Tracking
62–273, Solar Wind
63–36–1, Radiometer Results
63–36–2, Fields & Particles Results
63–36–3, Cosmic Dust Results
63–36–4, Tracking Results
63–36–5, Deep Space Telecommunications

U.S. GOVERNMENT PRINTING OFFICE: 1965 O—788–025